

**PROCEEDINGS,
CONFERENCE ON RESEARCH
IN TECTONICS**

(Kink Bands and Brittle Deformation)

Ottawa, March 1968

**MANUSCRIPT AND
CARTOGRAPHY**

MAR 7 1969

SECTION

**Edited by
A.J. BAER
D.K. NORRIS**

**NATIONAL ADVISORY COMMITTEE ON RESEARCH
IN THE GEOLOGICAL SCIENCES**

Published by the Geological Survey of Canada as GSC Paper 68-52

This document was produced
by scanning the original publication.

Ce document est le produit d'une
numérisation par balayage
de la publication originale.

GEOLOGICAL SURVEY
OF CANADA

PAPER 68-52

RESEARCH IN TECTONICS

Report of a workshop held in Ottawa 14-15
March, 1968, under the sponsorship of and
with financial assistance from the National
Advisory Committee on Research in the
Geological Sciences.

Edited by A. J. Baer and D. K. Norris

DEPARTMENT OF
ENERGY, MINES AND RESOURCES
CANADA

© Crown Copyrights reserved

Available by mail from the Queen's Printer, Ottawa,
from Geological Survey of Canada,
601 Booth St., Ottawa,

and at the following Canadian Government bookshops:

HALIFAX
1735 Barrington Street

MONTREAL
Æterna-Vie Building, 1182 St. Catherine St. West

OTTAWA
Daly Building, Corner Mackenzie and Rideau

TORONTO
221 Yonge Street

WINNIPEG
Mall Center Bldg., 499 Portage Avenue

VANCOUVER
657 Granville Street

or through your bookseller

Price \$5.00 Catalogue No. M44/68-52

Price subject to change without notice

Queen's Printer and Controller of Stationery
Ottawa, Canada
1969

CONTENTS

	Page
INTRODUCTION	v
OPENING REMARKS	
By Y.O. Fortier, Director, Geological Survey of Canada	1
MECHANICS OF NATURAL EXTENSION FRACTURING AT DEPTH IN THE EARTH'S CRUST	
By D. T. Secor	3
Discussion	48
A DYNAMIC MECHANISM FOR THE DEVELOPMENT OF SECOND-ORDER FAULTS AND RELATED STRUCTURES	
By N. J. Price	49
Discussion	72
Written comments by K. Barron	72
Reply to K. Barron by N. J. Price	75
Written comments by D. F. Coates	75
Reply to D. F. Coates by N. J. Price	77
FRACTURE AS A MECHANISM OF FLOW IN NATURALLY DEFORMED LAYERED ROCKS	
By D. W. Stearns	79
Discussion	91
Written comments by W. C. Brisbin	93
Written comments by J. J. Prucha	95
BRITTLE FRACTURE IN DIRECT SHEAR AND THE DEVELOPMENT OF SECOND-ORDER FAULTS AND TENSION GASHES	
By E. Z. Lajtai	96
Discussion	112
THE MECHANICAL EFFECTS OF PORE PRESSURE ON THE FRACTURING OF ROCKS	
By W. F. Brace	113
Discussion	124
Written comments by D. F. Coates	124
SOME OBSERVATIONS ON THE AGE OF JOINTING IN MACROSCOPICALLY FOLDED ROCKS	
By H. A. K. Charlesworth	125
Discussion	134

	Page
STRUCTURAL ANALYSIS OF FEATURES ON NATURAL AND ARTIFICIAL FAULTS	
By D.K. Norris and K. Barron	136
Discussion	167
Written comments by J.B. Currie	168
Reply to J.B. Currie by K. Barron and D.K. Norris	172
IMPLICATIONS OF SUB-CONTINENTAL SIZED FRACTURE SYSTEMS DETECTABLE BY TOPOGRAPHIC SHADOW TECHNIQUES	
By D. U. Wise	175
Discussion	198
THE GEOMETRY OF A NATURAL ORTHORHOMBIC SYSTEM OF KINK BANDS	
By T.B. Anderson	200
Discussion	220
Written comments by D.K. Norris	220
Written comments by H. Rondeel	226
KINK-BAND DEVELOPMENT IN THE LAKE ST. JOSEPH AREA, NORTHERN ONTARIO	
By P. Clifford	229
Discussion	241
PROFILE VARIATION IN A KINK SET	
By W.K. Fyson	243
Discussion - See General Session	254
EXPERIMENTAL STUDY OF KINK-BAND DEVELOPMENT IN STRONGLY ANISOTROPIC ROCK	
By F.A. Donath	255
Discussion	288
FLEXURAL SLIP FOLDING OF FOLIATED MODEL MATERIALS	
By L. E. Weiss	294
Discussion	358
GENERAL SESSION	
Discussion	360
Written comments by P. Clifford on papers by T.B. Anderson, P. Clifford, F.A. Donath and W.K. Fyson	362
On the nucleation of kink bands by H. Rondeel	363
APPENDIX I: Nomenclature of kink-band angles	366
APPENDIX II: List of participants	367
APPENDIX III: Program	372

INTRODUCTION

"Du choc des esprits jaillit la lumière"

The modern geologist tends to limit his activities to an ever narrower field of observations. This may be the price to pay to unravel the great complexity of our science, but by the same token, this creates insuperable obstacles between disciplines.

To obviate such obstacles in a modest and limited way, D.K. Norris conceived the idea of this conference. It was to bring together a dozen or so specialists in the field of brittle failure and of kink bands, and to choose these people about evenly among laboratory men and field men. By bringing these specialists together and leaving them ample time for discussions, it was hoped that cross-pollination would operate to everybody's advantage. Enthusiasm of the participants and promise of similar future meetings were to justify these hopes.

An organizing committee comprised of D.K. Norris, A.J. Baer, P. Clifford and W.K. Fyson was formed, and the National Advisory Committee on Research in the Geological Sciences in Canada accepted to sponsor the workshop. Canadian universities were invited to send discussants who would agree to read preprints of papers presented at the conference, and to participate in discussing them.

This volume follows fairly closely the program of the conference, which is contained in Appendix III. Discussions following individual papers are taken from taped records and, whenever possible, from written versions submitted by the participants. Questions raised about specific papers during periods of general discussions have been regrouped following papers to which they refer. Remarks have been edited to varying degrees and discussants have had an opportunity to examine the edited version.

The committee wishes to thank speakers, session chairmen and participants who were the 'raison d'être' of the meeting; the National Advisory Committee which supplied the financial backing; and the University of Ottawa and Dr. D.D. Hogarth, acting chairman of the Department of Geology. We are especially grateful to Dr. Y.O. Fortier, Director of the Geological Survey of Canada, for his support and participation, as well as for authorizing publication of these proceedings as a Survey report.

Dr. P. Harker, Chief Scientific Editor, acted as editorial consultant for the layout and design of the volume which was completed by Mrs. L.R. Mahoney and Miss D. Snowden; the final typescripts were prepared by Mrs. B. Richard and Mrs. H. Ainsworth.

Our gratitude goes also to all those who operated the equipment, tape recorders, slide projectors or copying machines so efficiently as to make themselves invisible.

The Organizing Committee.

CONFERENCE ON RESEARCH IN TECTONICS
KINK BANDS AND BRITTLE DEFORMATION

OPENING REMARKS

Y. O. Fortier
Director
Geological Survey of Canada

As Chairman of the National Advisory Committee on Research in the Geological Sciences and Director of the Geological Survey of Canada, I have the honour and pleasure of welcoming you to this workshop on "Brittle Deformation and Kink Folding in Rocks". My Canadian colleagues join me in extending friendly greetings to our visitors from the United States and the British Isles. You are most welcome in Ottawa which, especially for the occasion, greets you with a fresh mantle of snow.

Nearly 20 years ago several prominent Canadian geologists including the late Dr. J. E. Hawley of Queen's University, the late Dr. J. B. Mawdsley of the University of Saskatchewan, Dr. H. C. Gunning of the University of British Columbia and Dr. J. E. Gill of McGill University were instrumental in forming the National Advisory Committee on Research in the Geological Sciences. It was decided to associate the Committee with the Geological Survey, the focus of federal government geological activities. It was also decided to have as permanent Chairman, the Director of the Survey - perhaps mainly because it was thought at that time that through the Survey, funds might be obtained for more fundamental research in the geological sciences. At the Committee's urging, funds were made available by the Survey but once the need was shown the National Research Council stepped in and has become the main source of research grants to our universities.

We continue to experiment in ways and means by which the many disciplines of the geological sciences may be assisted in their development. For many years the various subcommittees of the National Advisory Committee assembled the material for their annual reports by correspondence instead of round-table discussions and workshops. Within the last few years it has become financially possible for the subcommittees to meet to discuss projects and suggested projects, and to prepare annual reports advising the main Committee on fruitful lines of research and the means of carrying them out. This workshop is a further development along this line; we are drawing on the best national and international talent to explore a highly specialized field of tectonics.

This workshop is not an exploration of the whole realm of structural geology but is confined to the discussion by a relatively small group of specialists of brittle failure and the mechanics of folding; it is a new venture and we expect much of it. The only stipulation we make is that the proceedings are published. The Geological Survey will be pleased to publish them on behalf of the National Advisory Committee, but you are free to publish them where you please as long as your findings are made available to scientists at large.

Last evening I had the good fortune to meet a number of you and could not help but be excited at learning of the barriers you are breaching. You are moving from observation of structural phenomena in the outcrop to mechanical and mathematical modelling in the laboratory, and back to the field to test your models and measurements.

You have two days to discuss and test your ideas against those of your colleagues; to sharpen your wits and to be stimulated by the clash of conflicting hypotheses. I hope this will prove enjoyable and profitable to each of you personally, and later, when the proceedings are published, to the scientific community at large.

I know you will want me to thank the originator and the organizers of this workshop. The concept shows originality; with such a gathering of talent so full of optimistic enthusiasm, the workshop cannot help but be a success. Good Luck!

Ottawa,
March, 1968.

MECHANICS OF NATURAL EXTENSION FRACTURING
AT DEPTH IN THE EARTH'S CRUST

Donald T. Secor, Jr.
University of South Carolina, Columbia

Abstract

In a previous paper (Secor, 1965) the writer proposed that some joints are natural hydraulic fractures developed perpendicular to the least principal stress direction. Mechanical considerations indicate that this kind of jointing can occur to depths of several thousand feet when the ratio of fluid pressure to overburden weight is hydrostatic. At greater depths abnormally high ratios of fluid pressure to overburden weight are required for jointing. The present paper is essentially an elaboration of this hydraulic fracturing hypothesis for jointing.

By using the results of Sneddon (1946) it is possible to calculate the volume of fluid contained in a crack or flaw just before it begins to propagate and develop into a joint. Energy considerations indicate that the formation of a macroscopic joint is a slow process consisting of numerous short quick episodes of fracture propagation interspersed with longer periods of quiescence during which pore fluid from the surrounding rock percolates into the crack and wedges it open. The growth rate of a joint is controlled by the rate that pore fluid seeps into the joint. The length of a single joint fracture is probably limited both by ductile behavior of the rock at the crack tip and by the development of other nearby joints.

The fluid volume needed to wedge open a systematic array of joints comes from both the elastic expansion of the ambient pore fluid and from the closure of other non-propagating cracks and flaws. Calculations indicate that most rocks contain sufficient pore fluid to produce the joints observed in them. The porosity necessary for the formation of a particular joint set of assumed geometry is fixed by selection of appropriate material parameters, but given a particular value of porosity it is not presently possible to determine which of the many possible joint geometries will actually develop. For example, a joint set containing a few long fractures may require the same porosity as another set of short closely spaced fractures. The geometry (fracture length, longitudinal and lateral separation) of a particular joint set is probably related to rock permeability and to the rate of decrease of the least effective principal stress at the time of fracturing. In a rock sequence of uniform porosity, a slow rate of stress decrease and high permeability would favor the development of a few long joints, whereas a rapid rate of stress decrease and low permeability would favor the development of numerous short joints.

INTRODUCTION

The ultimate objective of any science is to understand as thoroughly as possible the collective phenomena on which it is based. Scientific inquiry normally begins with the observation of some fundamental facts of either a natural or experimental nature and then proceeds to the development of a number of working hypotheses explaining the observations. These hypotheses in turn may suggest additional experiments or observations that ultimately result in the confirmation, modification or rejection of the original

ideas. The various working hypotheses are continually and impartially assessed and modified as the work progresses. The successful hypotheses which survive the final judgement are added to our general body of knowledge and may then be used to assist in the solution of related problems. However, even a successful hypothesis should remain tentative in the sense that it must periodically be evaluated in the light of new knowledge (Chamberlin, 1897). The sciences of chemistry and physics have made great progress in this manner because many of the fundamental laws are relatively simple and involve only a few variables. Geology has also made great progress, but it has been more difficult to establish reliable working hypotheses because of the complexity and inexact nature of its fundamental phenomena.

During the last two centuries, the majority of geologists have been concerned with collecting the basic facts of earth history. In structural geology one begins with data on the attitudes, ages and distribution of rock types, and then proceeds to determine the deformation pattern using the method of multiple working hypotheses along with geometric methods. It is now clear that the local deformation of a considerable portion of the earth's crust can be expressed in terms of a few simple types of geologic structures such as folds, faults, cleavage, joints, or their combinations, which have been repeatedly generated in time and space. It is apparent that an understanding of the physical processes responsible for generating geologic structures might be useful in establishing the environment of deformation. For this reason structural geologists have attempted to set up simple mechanical models (or working hypotheses) for the formation of geologic structures. In some instances the initial attempts to do this were unsuccessful, because the mechanical considerations indicated that it would be impossible to form the structures under the assumed conditions. Mechanics has therefore led us into such paradoxical problems as the movement of broad thin thrust plates (Hubbert and Rubey, 1959, pp. 122-129; Lawson, 1922; Longwell, 1945; Oldham, 1921), the generation of deep focus earthquakes (Reid, 1911; Orowan, 1960; Griggs and Handin, 1960) and the origin of slaty cleavage (Maxwell, 1962, pp. 281-311). In recent years there has been renewed interest in the mechanics of geologic structures coupled with laboratory experiments in rock physics, and some of the long standing problems have been resolved, at least in part, by the application of more rigorous methods of analysis using experimental data on the physical properties of rocks.

No completely satisfactory mechanical model has yet been proposed for the phenomenon of rock jointing, although considerable progress has been made in understanding certain aspects of the mechanics (Price, 1966, pp. 110-164). As used in this paper, the word "joint" is a field term applied to natural fractures which show little or no lateral displacement. Almost all consolidated rocks are jointed to some extent, and in some places joint sets are systematic over broad areas and through considerable thickness of strata. Because of the abundance, apparent simplicity, and systematic nature of joints, geologists have long sought to use them as indicators of the past stress and strain history of rock masses. Consequently, a great quantity of data on joint geometry and orientation from many parts of the world have accumulated. In some instances the interpretations made from this data are controversial and uncertain, because the physical processes responsible for jointing are not generally understood. The purpose of this paper is to propose a mechanical model which logically explains the origin of at least some kinds of joints. It is hoped that the interpretations of field data can thereby be made more reliable and useful.

In all likelihood the joints studied by field geologists have multiple origins (Price, 1966, p. 127). Some may be natural shear fractures of small lateral displacement (Parker, 1942; Muehlberger, 1961), whereas others may be natural extension fractures (Nickelsen and Hough, 1967). It may be possible for natural extension fractures to form normal to compressive least effective principal stresses, whereas others may form normal to tensile least effective principal stresses (Griggs and Handin, 1960, pp. 347-352). Natural tension fractures may form near the earth's surface where tensile total principal stresses are possible (Anderson, 1951, p. 159; Hubbert, 1951, p. 367), or they may form at depth where only effective tension is possible and where the pore fluid is important in fracture genesis (Secor, 1965). The mechanical model presented in this paper is applicable only to joints in this last category. It is presented in the spirit of a tentative working hypothesis which needs much testing by field and experimental geologists. The model does seem to explain many of the puzzling geometric characteristics of natural joint patterns.

GROWTH OF A TENSION FRACTURE AT DEPTH IN THE EARTH'S CRUST*

The Griffith Theory

One of the fundamental problems in engineering mechanics has been to understand the factors which control the strength of solid materials. Calculations based on the known strengths of molecular cohesive forces have indicated that solid materials ought to be 10 to 100 times stronger than they really are (Griffith, 1921; Cottrell, 1959). This discrepancy between the theoretical and actual strengths of materials led Griffith (1921) to postulate that solids are greatly weakened by the presence of internal or surface cracks, and that premature failure is caused by high stress concentrations at crack tips. Griffith (1925) derived expressions for the tensile strength and failure envelope of a two dimensional elastic material containing an array of randomly oriented cracks. In the terminology of the present paper the expressions for tensile strength are as follows:

$$-K = -\sqrt{\frac{2E\gamma}{\pi C}} \quad \text{(for plane stress),} \quad (1)$$
$$-K = -\sqrt{\frac{2E\gamma}{\pi C(1-\nu^2)}} \quad ** \text{ (for plane strain),} \quad (2)$$

where $-K$ is the tensile strength (tension considered negative), E is Young's Modulus, ν is Poisson's Ratio, γ is the specific surface energy of the material, and C is the half length of the cracks. Griffith also derived the following failure criteria for a two dimensional elastic material:

* A major revision was received after the text of this volume had been typed. These changes were best made by using the author's typescript. - The editors.

** This expression is incorrectly given as $-K = \sqrt{2E\gamma(1-\nu^2)/\pi C}$ by Griffith (1925). The correct expression shown above is taken from Sack (1946) and Sneddon (1946)

$$\text{if } S_1 \leq +3K, \quad S_3 = -K, \quad (3)$$

$$\text{if } S_1 \geq +3K, \quad (S_1 - S_3)^2 - 8K(S_1 + S_3) = 0, \quad (4)$$

where S_1 and S_3 are the greatest and least principal stresses respectively, with tension considered negative. The tensile strength of a brittle material is therefore a constant, as long as the greatest compressive principal stress (S_1) is less than three times the tensile strength as given in equations (1) or (2). When S_1 exceeds $+3K$, the strength of the material is a function of both S_1 and S_3 as specified by equation (4).

The Griffith theory has been extended to three dimensions by Sack (1946) and Sneddon (1946), both of whom derived the following equation:

$$-K = -\sqrt{\frac{\pi E \gamma}{2C(1-\nu^2)}}, \quad (5)$$

for the theoretical tensile strength of a three dimensional elastic solid containing a penny-shaped crack of radius C perpendicular to the tension direction.

In recent years there has been considerable research on the applicability of the Griffith theory to fracturing problems in rocks. Almost all rocks contain cleavage or grain boundary cracks that might be expected to behave as Griffith flaws during deformation. Most recent research has been directed toward the application of the Griffith theory to the phenomenon of shear fracture in response to compressive effective principal stresses (Brace, 1961, 1964; Brace, Paulding and Scholz, 1966). McClintock and Walsh (1962) presented a modification of the Griffith theory that included the effect of frictional stresses developed along the walls of cracks closed in compression. Brace and Bombolakis (1963) and Bombolakis (1964) found from photoelastic studies of uniaxial compression that a critically oriented crack will propagate out of its initial plane into a position of parallelism with the direction of compression. They concluded that a macroscopic shear fracture could develop

by the coalescence of special en echelon arrays of critically oriented cracks. The experiments of Brace, Paulding and Scholz (1966) have shown that crack opening and/or growth begins well below the stress necessary for the formation of a macroscopic shear fracture. The failure criterion for crack growth must therefore differ from the criterion for shear fracturing.

In the present paper the three dimensional Griffith theory is applied only to tension fracturing, and the difficulties encountered in applying the theory to compressive stress states are avoided. In tension fracturing the critically stressed cracks are oriented perpendicular to the tensile direction. At the point of incipient fracture the cracks are open, because the normal stress across them is tensile. Frictional stresses on crack walls are impossible both because the cracks are open and because they are in a principal plane. When the plane of an elliptical crack is perpendicular to a tensile principal stress direction, the point of greatest tensile stress concentration occurs on the major axis of the ellipse at the tip of the crack (Inglis, 1913). Tension cracks therefore propagate in their initial plane, and the failure criterion for crack growth and for macroscopic tension fracturing are identical.

A number of experimental studies have indicated that the presence of a pore fluid pressure in rock has a profound effect on strength. Hubbert and Willis (1957), Hubbert and Rubey (1959) and Jaeger (1962) have predicted on theoretical grounds that critical principal effective stresses should control rock strength, and this prediction is verified by the experiments of Handin, Hager, Friedman and Feather (1963), Jaeger (1963) and Brace (this conference). An effective principal stress is defined as the corresponding total principal stress less the pore pressure:

$$\sigma_{(1,3)} = S_{(1,3)} - p \quad (6)$$

The effective stress does not correspond to any physically tangible fraction of the total stress, however the theoretical and experimental studies cited above indicate that the failure criteria for rocks with pore pressure should be expressed in terms of critical effective stresses as defined by equation (6). Hence the failure criteria for tension fracturing of rocks with internal pore pressure is:

$$\sigma_3 = -K = - \sqrt{\frac{\pi E \gamma}{2C(1-\nu^2)}} \quad . \quad (7)$$

Volume Equations

Equations (6) and (7) indicate that a crack oriented normal to the least principal stress will become unstable and spread whenever the pressure of the pore fluid (p) exceeds the total least principal stress (S_3) by an amount equal to the tensile strength of the rock. Sneddon (1946) proved that the shape of a crack containing pressurized fluid in a three dimensional elastic medium is that of a oblate ellipsoid, and he found that the component of surface displacement at the center of the crack (ϵ , the semi-minor axis) was related to the elastic properties of the solid medium, the crack radius and the fluid pressure as follows:

$$\epsilon = \frac{4(1-\nu^2)pC}{\pi E} \quad (8)$$

Combining this result with the formula for the volume of an oblate ellipsoid:

$$V = \frac{4}{3} \pi \epsilon C^2 \quad , \quad (9)$$

an expression for the volume of fluid in the crack is obtained:

$$V = \frac{16}{3E} (1-\nu^2) p C^3 . \quad (10)$$

In deriving equation (8) Sneddon assumed that the stresses at infinity in the elastic medium were zero. Before Sneddon's results can be applied directly to the problem of tension fracturing in rocks, it is necessary to consider the effect of total external principal stresses on the volume of the crack. In general a crack will be closed ($V=0$) if the total compressive least principal stress (S_3), acting perpendicular to the crack, is greater than the pore pressure (p). Conversely the crack will be wedged open by the pore fluid if p exceeds S_3 . Only that fraction of p which exceeds S_3 will be effective in opening the crack. The quantity p in equation (10) should therefore be replaced by $(p-S_3)$:

$$V = \frac{16}{3E} (1-\nu^2) (p - S_3) C^3 . \quad (11)$$

Combining this result with equation (6):

$$V = - \frac{16}{3E} (1-\nu^2) \sigma_3 C^3 , \quad (12)$$

it is seen that the crack volume is directly proportional to the magnitude of the least effective principal stress. It is important to remember that it is not possible for a crack to have negative volume, and so the applicability of equation (12) is limited to the case where σ_3 is tensile and hence negative. The upper limit of applicability of equation (12) is governed by the tensile strength of the rock. When σ_3 reaches the critical limit specified by equation (7), the crack will begin to propagate, and the actual volume will be greater than that given by equation (12). Substituting equation (7) in (12), we obtain an expression for the critical crack volume just prior to propagation:

$$V = \frac{16}{3} \sqrt{\frac{\pi \gamma (1-\nu^2)}{2E}} \cdot C^{5/2} . \quad (13)$$

Crack Propagation

Introduction

Theory developed thus far does not predict how far a crack will propagate once the critical conditions specified by equations (7) and (13) are attained. The rapid propagation of a fracture can only occur when there is a net decrease in the various forms of potential energy stored in the rock. The potential energy lost during the fracturing process is converted into kinetic energy of rapid crack growth:

$$\text{Decrease in Potential Energy} = \text{Kinetic Energy} \quad (14)$$

There are four kinds of potential energy associated with fluid saturated rocks that could conceivably undergo major change during the fracturing process:

1. Potential of external forces.
2. Strain energy of the rock.
3. Compressional fluid energy.
4. Surface energy of the crack.

In order to determine the amount of crack propagation that is likely to occur in any particular case, it is necessary to estimate the changes in the four potential energy terms resulting from the introduction of a fluid filled crack into a stressed medium.

Potential of External Forces and Strain Energy

The change in the sum of the first two potential energy terms in the above list, resulting from the introduction of a fluid filled crack into a rock mass, can be calculated by determining the amount of work done on the crack walls by the pressurized fluid as the crack is opened up. Imagine a penny-shaped crack

of radius C , oriented perpendicular to the S_3 direction, which is opened up by an increase in internal fluid pressure so that the pressure and volume just before crack propagation are p_0 and V_0 respectively (Figure 1a). The work necessary to open the crack will be given by:

$$W_{(1+2)} = \int_0^{V_0} (p) dV \quad (15)$$

Solving equation (11) for p , and substituting the result in equation (15):

$$W_{(1+2)} = \int_0^{V_0} \frac{3EV}{16(1-\nu^2)C^3} dV + \int_0^{V_0} (S_3) dV \quad (16)$$

$$W_{(1+2)} = \frac{3E V_0^2}{32(1-\nu^2)C^3} + S_3 V_0 \quad (17)$$

The first term on the right side of equation (17) represents the change in rock strain energy, whereas the second term represents the increase in potential of the least principal stress (S_3). When V_0 reaches the critical limit specified by equation (13), the crack will become unstable and propagate distance ΔC (Figure 1b). After crack growth the final pressure (p_1) will be less than the original pressure (p_0), and the final volume (V_1) will be greater than the initial volume (V_0). The change in the sum of the first two potential energy terms that would result from the introduction of a fluid filled crack of radius $C_1 = C + \Delta C$ into the same rock mass can be calculated as before:

$$W'_{(1+2)} = \frac{3E V_1^2}{32(1-\nu^2)C_1^3} + S_3 V_1 \quad (18)$$

The net increase in the sum of the potential of external forces and the strain energy after propagation will be:

$$\Delta W_{(1+2)} = W'_{(1+2)} - W_{(1+2)} = \frac{3E}{32(1-\nu^2)} \left(\frac{V_1^2}{C_1^3} - \frac{V_0^2}{C^3} \right) + S_3 (V_1 - V_0) \quad (19)$$

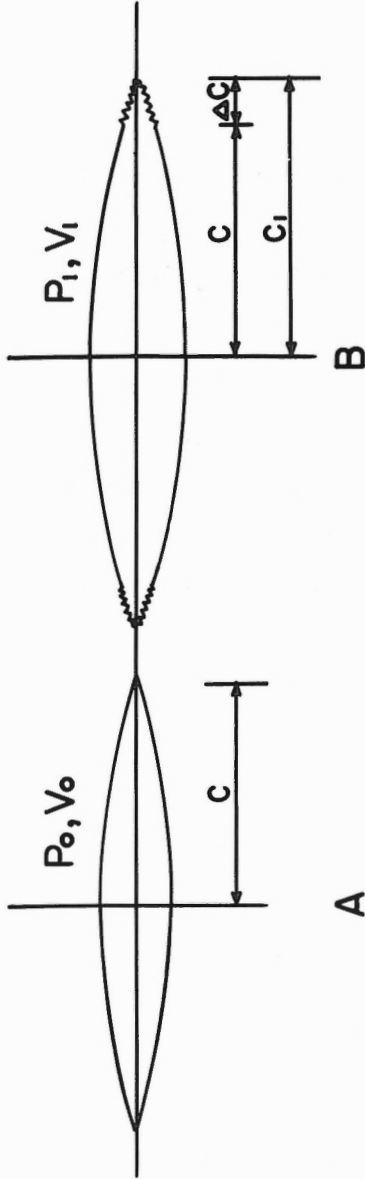


Figure 1. (A) Crack configuration just before an episode of propagation.
(B) Crack configuration just after an episode of propagation.

The first term on the right side of equation (19), representing the change in strain energy, could be either positive or negative depending on the sign of the quantity in parenthesis. The second term, representing the change in potential of the least principal stress, will be positive because $V_1 > V_0$. Energy release during fracturing could occur only if:

$$\frac{3EV_0^2}{32(1-\nu^2)C^3} > \frac{3EV_1^2}{32(1-\nu^2)C_1^3} + S_3(V_1 - V_0) \quad , \quad (20)$$

and the amount of energy released ($\Delta W_{(1+2)}$) must be less than the expression:

$$\Delta W_{(1+2)} < \frac{3EV_0^2}{32(1-\nu^2)C^3} \quad . \quad (21)$$

At the time of incipient propagation the volume of fluid in the crack (V_0) will be given by equation (13):

$$V_0 = \frac{16}{3} \sqrt{\frac{\pi \gamma (1-\nu^2)}{2E}} \cdot C^{5/2} \quad . \quad (13)$$

Substituting in expression (21):

$$\frac{3EV_0^2}{32(1-\nu^2)C^3} = 4/3 \pi \gamma C^2 > \Delta W_{(1+2)} \quad . \quad (22)$$

In the case of an ideal incompressible fluid:

$$V_1 = V_0 \quad , \quad (23)$$

and equation (19) reduces to:

$$\Delta W_{(1+2)} = \frac{3EV_0^2}{32(1-\nu^2)} \left(\frac{1}{C_1^3} - \frac{1}{C^3} \right) \quad . \quad (24)$$

It is apparent that strain energy would be released even in the case of an ideal incompressible fluid because $C_1 > C$.

Fluid Compressional Energy

As a crack propagates and opens up, the fluid inside the crack is permitted to expand, and the potential energy stored in the compressed fluid decreases. The energy released by fluid expansion inside the crack is available for conversion to the other kinds of potential energy or kinetic energy associated with crack growth. In most places the pressure and temperature of underground water are such that there is an approximate linear relationship between pressure difference (dp) and volumetric strain ($\frac{dV}{V}$):

$$dp = - \frac{1}{k} \left(\frac{dV}{V} \right) \cdot \tag{25}$$

where k is the fluid compressibility. Integrating we obtain:

$$p = - \frac{1}{k} \ln V + \phi \tag{26}$$

The constant of integration ϕ can be evaluated by applying the boundary condition:

$$\text{at } p = p_0, V = V_0 \cdot \tag{27}$$

Substituting in equation (26):

$$\phi = p_0 + \frac{1}{k} \ln V_0 \cdot \tag{28}$$

Therefore:

$$p = - \frac{1}{k} \ln V + \frac{1}{k} \ln V_0 + p_0 \cdot \tag{29}$$

The potential energy released by fluid expansion inside the crack as it grows will be given by:

$$\Delta W_s = \int_{V_0}^{V_1} (p) dV \cdot \tag{30}$$

or:

$$\Delta W_3 = \int_{V_0}^{V_1} \left(-\frac{1}{k} \ln V + \frac{1}{k} \ln V_0 + p_0 \right) dV \quad , \quad (31)$$

Where V_0 and V_1 are the fluid volumes before and after propagation respectively. If equation (30) is integrated, and if V_1 is expressed in terms of V_0 , p_0 and p_1 from equation (29), the equation for the released compressional energy becomes:

$$\Delta W_3 = e^{k(p_0 - p_1)} V_0 \left(p_1 + \frac{1}{k} \right) - V_0 \left(p_0 + \frac{1}{k} \right) \quad , \quad (32)$$

where e is the natural logarithmic base. The quantity (p_1) in equation (31) is not known, but it is unlikely that p_1 could decrease below the magnitude of the total least stress (S_3), because the crack would be completely closed under these stress conditions. Therefore an estimate of the maximum possible compressional energy available for crack propagation (ΔW_3) can be obtained by replacing p_1 by S_3 in equation (31):

$$\Delta W_3 < e^{k(p_0 - S_3)} V_0 \left(S_3 + \frac{1}{k} \right) - V_0 \left(p_0 + \frac{1}{k} \right) \quad . \quad (33)$$

Potential Surface Energy

The potential surface energy of a crack will be given by the product of the area of the crack times the specific surface energy (γ):

$$W_4 = 2\pi C^2 \gamma \quad . \quad (34)$$

If C is the crack radius prior to propagation and ΔC is the increase in length of the crack radius after propagation, then the increase in potential surface energy (ΔW_4) will be:

$$\Delta W_4 = 2\pi \gamma [(C + \Delta C)^2 - C^2] = 2\pi \gamma (2C\Delta C + \Delta C^2) \quad (35)$$

If ΔC is small:

$$\Delta W_4 = 4\pi\gamma C \Delta C \quad (36)$$

or:

$$\frac{\Delta C}{C} = \frac{\Delta W_4}{4\pi\gamma C^2} \quad (37)$$

The Energy Balance

The foregoing discussion has indicated that during the short period of time in which a crack is propagating, the potential of external forces and the potential surface energy both increase, whereas the potential strain energy in the rock around the crack and the potential compressional energy in the crack fluid both decrease. The net decrease in potential energy is converted into kinetic energy. If equations (21) and (33) are added, an equation for an energy quantity (ΔW) that must exceed the increase in surface energy potential (ΔW_4) is obtained:

$$\Delta W > \Delta W_4 \quad (38)$$

$$\Delta W = \frac{3E V_0^2}{32(1-\nu^2)C^3} + e^{k(p_0 - S_3)} V_0 \left(S_3 + \frac{1}{k} \right) - V_0 \left(p_0 + \frac{1}{k} \right) \quad (39)$$

In order to estimate the maximum amount of crack propagation that could occur from equation (39), it is necessary to assume some values for the physical parameters and constants which appear in equations (12), (13), (33) and (35):

$$k = 1.94 \times (10^{-8}) \text{ ft.}^2/\text{lb. at 10,000 ft. depth}$$

$$k = 1.72 \times (10^{-8}) \text{ ft.}^2/\text{lb. at 20,000 ft. depth}$$

$$k = 1.63 \times (10^{-8}) \text{ ft.}^2/\text{lb. at 30,000 ft. depth}$$

$$\gamma = .0687 \text{ lb./ft.}$$

$$E = 720 \times (10^6) \text{ lbs./ft.}^2$$

$$\gamma = .250$$

Three different depths (10,000, 20,000, and 30,000 feet), and six initial crack lengths (.001, .01, .1, 1, 10, 100 feet) at each depth were chosen for analysis. It was assumed that the original flaw lengths prior to the initiation of fracturing were .001 feet and that the original tensile strength of the rock containing the flaws was 288,000 lbs./ft.². The listed value of γ can be calculated from equation (7) assuming the above tensile strength and flaw length. This value of surface energy is near the upper limit measured for quartz (Brace and Walsh, 1962), but is less than the surface energies measured for sandstone by Perkins and Bartlett (1963). Average values of E and γ were chosen from data tabulated by Birch (1966). The initial fluid pressure in unfractured rock was taken as the minimum value necessary for tension fracturing at the depth considered (Secor, 1965), and S_3 was calculated from equation (6) assuming that σ_3 was -288,000 lbs./ft.². The internal pressure (p_0) in the longer cracks, that had undergone previous episodes of propagation, was assumed to exceed S_3 by an amount equal to the tensile strength of the rock containing flaws of the same length as the longer cracks. The fluid compressibility (k) was estimated from the data of Holser and Kennedy (1958) and Kennedy, Knight and Holser (1958) as tabulated in Sharp (1962), assuming a normal geothermal gradient (Birch, 1955). Crack volumes just prior to propagation (V_0) were calculated from equation (13).

Values for ΔW have been calculated from equation (39) for a variety of depths and initial crack lengths, using the physical constants and parameters previously listed. The results are shown in Figure 2a. For comparison purposes, equation (35) has been plotted in Figure 2b for a variety of initial crack lengths. Remembering that:

$$\Delta W > \Delta W_4$$

(38)

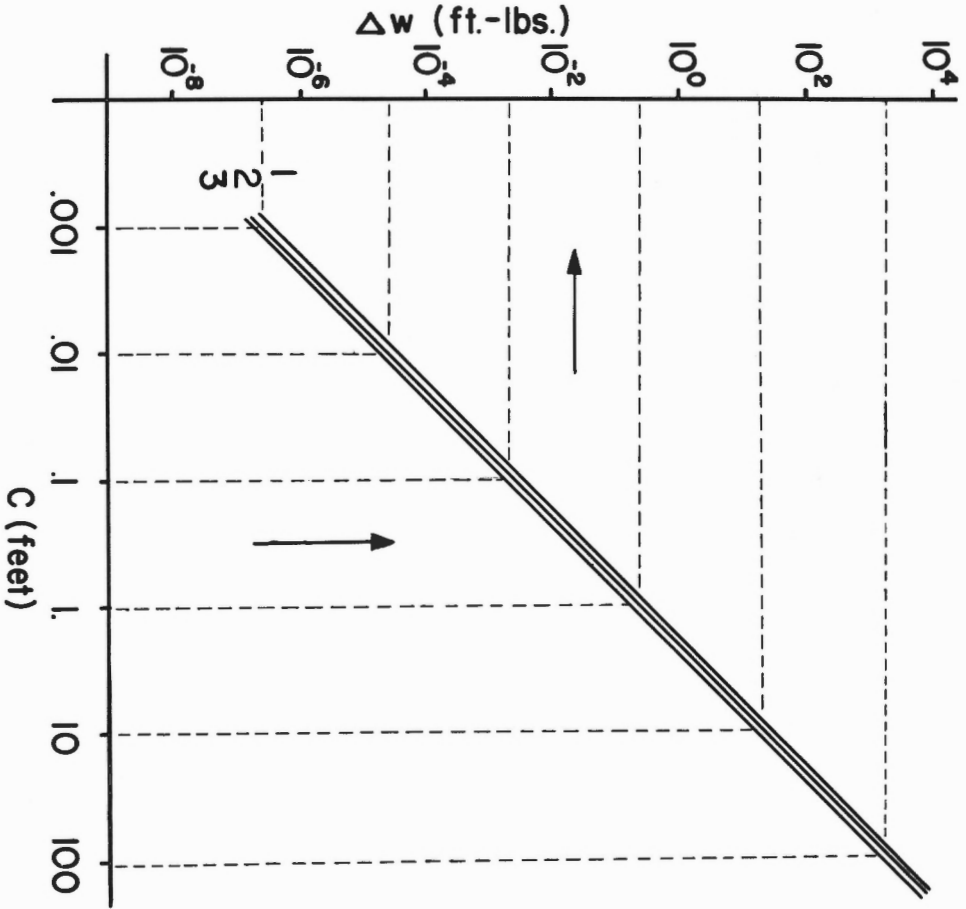


Figure 2. (A) A graph showing the relationship between an energy quantity (ΔW) that must exceed the energy available for crack propagation, and initial crack length. 1/ depth 30,000 feet, 2/ depth 20,000 feet, 3/ depth 10,000 feet.

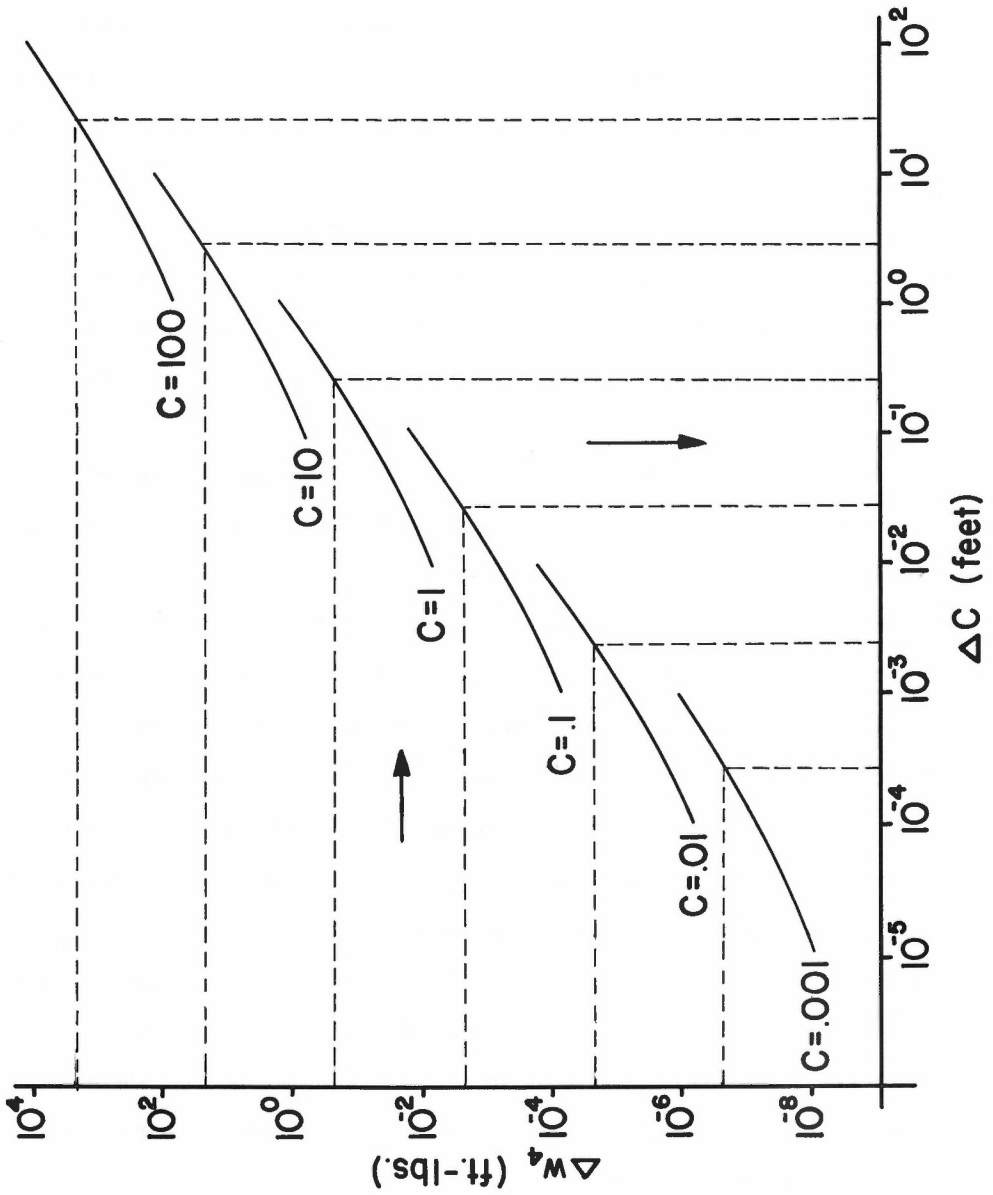


Figure 2. (B) A graph showing the increase in surface energy potential (ΔW_4) as a function of propagation distance (ΔC), for various initial crack lengths.

it is apparent from comparison of Figures 2a and 2b that the amount of energy available for crack propagation, during any single episode of propagation, will only be sufficient for the crack to be extended a small fraction of its initial length.

In light of this conclusion, one might wonder how it is possible for a single tension fracture ten or one hundred feet long to originate from the growth of a small grain boundary flaw. At the end of any particular episode of crack growth, the final pressure (p_1) is less than the initial pressure (p_0), because the crack volume has increased and the contained fluid has expanded. The crack fluid will therefore be at a lower potential than the fluid in the pore spaces of the surrounding rock, and the pore fluid will be driven down the potential gradient into the crack. The pressure of the fluid in the crack will therefore gradually increase and the crack will be wedged open. Eventually the critical volume specified by equation (13) will again be reached, and another episode of propagation will occur. The growth of a macroscopic tension fracture must be the result of numerous episodes of short propagation interspersed with longer periods of quiescence during which the pore fluid in the surrounding rock percolates into the crack. The macroscopic rate at which a natural tension fracture grows therefore depends on the porosity and permeability of the surrounding rock. The rate of growth must decrease rapidly as the crack becomes longer, because the volume of fluid needed to wedge the crack open increases as the 5/2 power of the radius, whereas the surface area of the crack, across which the incoming fluid must percolate, increases as the square of the radius.

Field observations have indicated that most joints are relatively short, extending for a few feet or yards before being replaced by another fracture of the same attitude in offset position. It is interesting to consider the question

of why a particular tension joint might stop propagating. It is theoretically possible for a tension fracture in an ideal elastic medium to continue propagating indefinitely, and given enough time it might attain a length of hundreds or thousands of feet. However two natural mechanisms operate to limit the extent of natural tension fractures. As a crack gets longer and as its growth rate decreases, a limit is eventually reached where the extreme tensile stresses at the crack tip are relieved by ductile creep more rapidly than they are increased by opening of the crack. This mechanism would tend to limit the extent of crack growth even in the absence of other factors. It is also unlikely that only one tension fracture would develop in a critically stressed rock mass. In all likelihood numerous tension cracks will begin to develop throughout the rock mass when a critical value of σ_3 is attained. Each crack will have only a limited amount of fluid available to it, and when the ambient pore pressure had decreased below the critical limit specified by equations (6) and (7), all of the cracks will cease propagating. Therefore, both ductile creep at crack tips and the development of multiple fractures in a rock mass, will limit the length of any one fracture.

Summary

The foregoing analysis has indicated that the growth of a tension fracture at depth in the earth's crust is macroscopically a slow process, consisting in detail of numerous short quick episodes of crack propagation interspersed with longer periods of quiescence during which the pore fluids from the surrounding rock percolate into the crack and wedge it open. Energy considerations have indicated that the increase in crack length, during any single episode of crack propagation, is a small fraction of the initial length. Equation (13) can therefore be used, with only small error, to calculate the volume of fluid in the crack during any stage of its growth.

RELATIONSHIP BETWEEN JOINT GEOMETRY AND POROSITY

Introduction

The model for natural tension fracturing proposed in the preceding section predicts that the fluid volume necessary for the development of a fracture of radius C_1 will be given by:

$$V = \frac{16}{3} \sqrt{\frac{\pi \delta (1-\nu^2) l}{2 E}} \cdot C_1^{5/2} \quad (13)$$

This fluid volume may originate from elastic expansion of the ambient pore fluid in the rock, or from compaction and porosity reduction during the fracturing episode, or from closure of other non-propagating cracks. The question of whether a particular rock can supply enough fluid to generate the joint pattern observed in it is a test which the proposed model must pass if it is to be generally accepted. In order to answer this critical question, it is first necessary to develop a quantitative way of expressing the geometry of a joint set.

Quantification of Joint Geometry

Imagine a rectangular block of rock with edge lengths X , Y and Z (Figure 3), containing an array of circular fractures parallel to the front face of the block. The fractures are assumed to occur in a series of planes separated by distance d . Within any one plane the fractures have diameter $2C_1$, and are separated from other fractures in the same plane by distances A and B (Figure 3). In a plane parallel to the front of the block there are L joints in each vertical row and N joints in each horizontal row. There are M plane

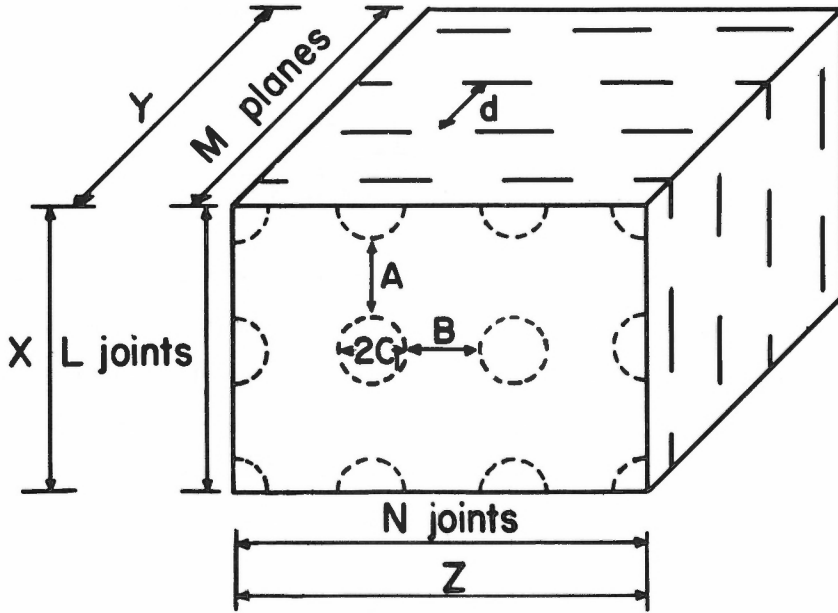


Figure 3. A block of rock containing a regular array of joint fractures.

groups of joints between the front and back of the block. From the geometry of the block:

$$X = L(2C_1 + A) \quad (39)$$

$$Y = dM \quad (40)$$

$$Z = N(2C_1 + B) \quad (41)$$

The total volume of the rock will be:

$$XYZ = LMN(2C_1 + A)(2C_1 + B)(d) \quad (42)$$

The total volume of fluid in all of the joints in the block will be equal to the number of joints (LMN) multiplied by the volume of one joint:

$$\text{Total volume of all joints} = LMN \frac{16}{3} \sqrt{\frac{\pi \gamma (1 - \nu^2)}{2E}} \cdot C_1^{5/2} \quad (43)$$

Dividing equation (43) by equation (42) we obtain an expression for the volume of fluid in the joints per unit volume of rock:

$$\frac{\text{Volume of fluid in Joints per unit Volume of rock}}{\text{Volume of rock}} = \frac{16 \sqrt{\frac{\pi \gamma (1-\nu^2)}{2E}} \cdot C_1^{5/2}}{(d)(2C_1 + A)(2C_1 + B)} \quad (44)$$

This result will be used subsequently in a comparison with the volumes of fluid available in rocks. It should be noted that there is nothing fundamental about the joint geometry illustrated in Figure 3. Other systematic fracture distributions could have been assumed. However, the present geometry has the virtue of simplicity and can be adjusted to approximate many natural joint patterns by appropriate choice of the parameters A, B, C₁ and d.

Amount of Fluid Available
For Jointing In Rocks

Introduction

The amount of fluid available for jointing in a particular rock mass is critically dependent on the amount and nature of porosity. If the pores are all spherical or tube-shaped, the porosity will remain constant during a jointing episode, and all of the fluid contained in joint cracks must come from elastic expansion of the pore fluid. Conversely, if the pores are all crack-shaped, the fluid contained in joint fractures could come from both elastic expansion of the pore fluid and from the closure of other non-propagating cracks or flaws. Most rocks probably contain both spherical pores and crack shaped pores, and it is impossible to make a single generally applicable assumption about the nature of the porosity. Therefore, two porosity models are assumed here, representing the end extremes of all spherical pores (constant porosity) and all crack-shaped pores (variable porosity).

The Constant Porosity Model

Let f , the fractional porosity, represent the amount of fluid in a unit volume of rock. During an episode of jointing, the increase in fluid volume per unit volume of rock (ΔV) will be given by:

$$\Delta V = -k V_0 \Delta p \quad (45)$$

where k is the fluid compressibility, V_0 is the initial fluid volume and $-\Delta p$ is the pressure decrease. The initial volume of fluid will be equal to the fractional porosity, and equation (45) reduces to:

$$\Delta V = -k f \Delta p \quad (46)$$

At any stage in the period of joint growth the relationship between the total least stress (S_3), the effective least stress (σ_3) and the pore pressure (p) will be given by equation (6):

$$S_3 = \sigma_3 + p \quad (6)$$

The change in the magnitude of the pore pressure (Δp), during an episode of jointing, must be balanced by the changes in S_3 and σ_3 :

$$\Delta p = \Delta S_3 - \Delta \sigma_3 \quad (47)$$

In an environment where the earth's crust is extending in the S_3 direction (the "constant stress case"), S_3 might remain constant so that:

$$\Delta S_3 = 0 \quad (48)$$

and equation (47) reduces to:

$$\Delta p = -\Delta \sigma_3 \quad (49)$$

Just prior to the initiation of a jointing episode, σ_3 will be given by equation (7):

$$\sigma_3 = - \sqrt{\frac{\pi E \gamma}{2C(1-\nu^2)}} \quad (7)$$

where C is the initial flaw radius. At the end of an episode of jointing σ_3 will be just slightly less than the critical magnitude necessary for additional joint growth:

$$\sigma_3 = - \sqrt{\frac{\pi E \gamma}{2C_1(1-\nu^2)}} \quad (7)$$

where C_1 is the final radius of the joints. The change in σ_3 must therefore be:

$$\Delta \sigma_3 = - \sqrt{\frac{\pi E \gamma}{2(1-\nu^2)}} \left(\frac{1}{\sqrt{C_1}} - \frac{1}{\sqrt{C}} \right) \quad (50)$$

Substituting in equation (49):

$$\Delta p = \sqrt{\frac{\pi E \gamma}{2(1-\nu^2)}} \left(\frac{1}{\sqrt{C_1}} - \frac{1}{\sqrt{C}} \right) . \quad (51)$$

Substituting in equation (46):

$$\Delta V = -kf \Delta p = kf \sqrt{\frac{\pi E \gamma}{2(1-\nu^2)}} \left(\frac{1}{\sqrt{C}} - \frac{1}{\sqrt{C_1}} \right) . \quad (52)$$

The volume of fluid accommodated within the joint fractures must be equal to the volume of fluid resulting from elastic expansion of the pore fluid.

Equating equations (52) and (44):

$$kf \sqrt{\frac{\pi E \gamma}{2(1-\nu^2)}} \left(\frac{1}{\sqrt{C}} - \frac{1}{\sqrt{C_1}} \right) = \frac{16}{3} \sqrt{\frac{\pi \gamma (1-\nu^2)}{2E}} \cdot C_1^{5/2} \quad (53)$$

Solving for f :

$$f = \frac{16}{3k} \left(\frac{1-\nu^2}{E} \right) \left(\frac{\sqrt{C} C_1}{\sqrt{C_1} - \sqrt{C}} \right) \cdot C_1^{5/2} \quad (54)$$

Equation (54) can be used to calculate the original constant porosity (f) necessary for the formation of any joint pattern of assumed geometry, in an environment where the total least stress (S_3) remains constant during the jointing episode. In Figure 4, the required porosity is plotted as a function of fracture spacing (d) for a variety of fracture geometry and initial crack lengths (C), assuming the following rock and fluid properties:

$$k = 1.72 (10^{-8}) \text{ ft. }^2 / \text{ lb.}$$

$$E = 720 (10^6) \text{ lb. } / \text{ ft.}^2$$

$$\nu = .250$$

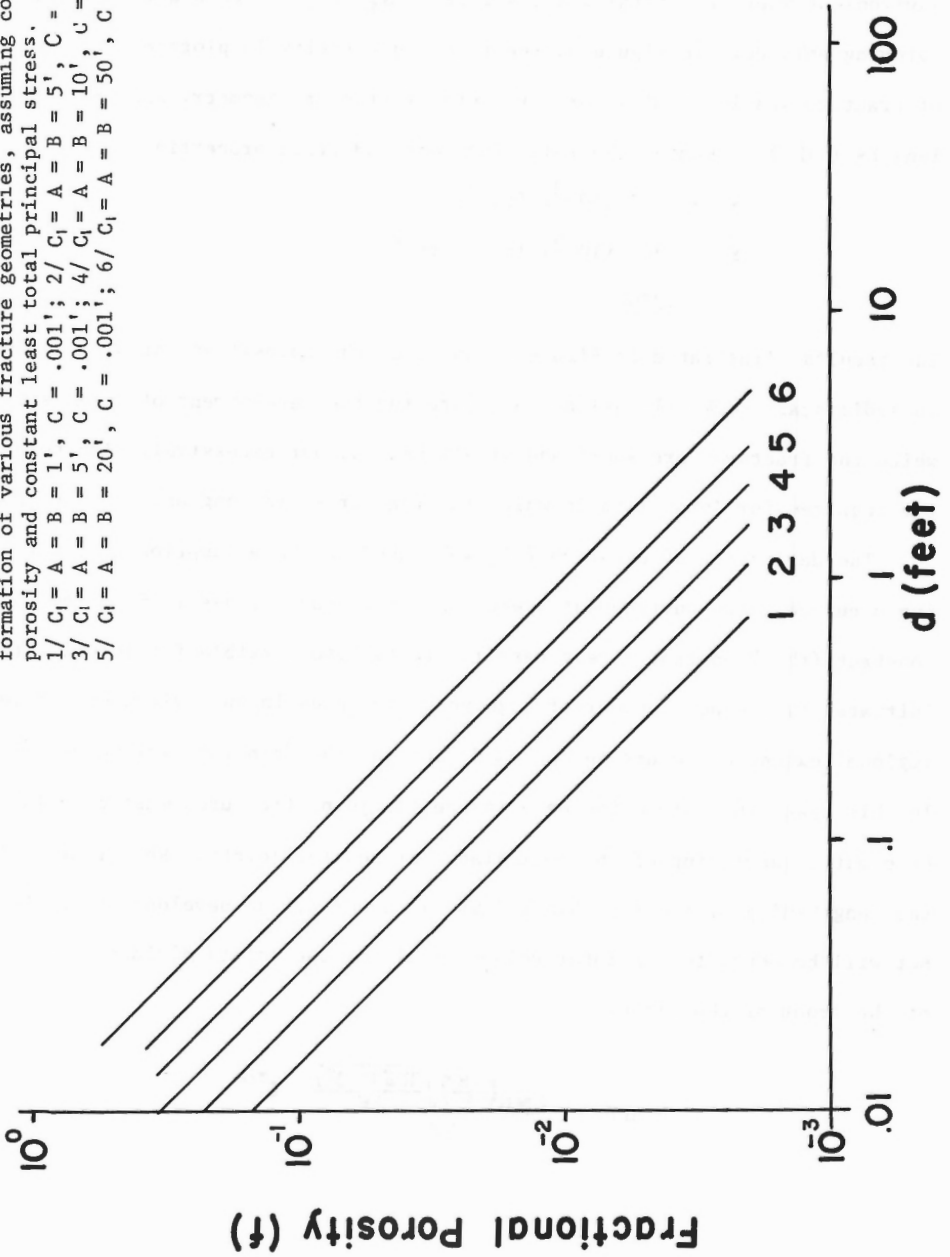
The results illustrated in Figure 4 show that the porosities normally encountered in sedimentary rocks (1-10%) are adequate for the development of joint sets in which the fractures are short and widely spaced, but excessively high porosities are required for joint sets in which the fractures are long and closely spaced.

The derivation of equation (54) was based on the assumption that the jointing occurred in an environment where the total least stress (S_3) remained constant (the "constant stress case"). It is also possible for jointing to be initiated by the development of high pore pressures in an environment where no regional extension occurs in the S_3 direction (the "constant volume case"). In this case, the volume increase inside the joint fractures must be balanced by elastic shortening of the rock slabs between the joints. Referring to Figure 3, the lengthening of the rock block (ΔY) caused by the development of the joint set will be equal to the total volume of all of the joints divided by the area of the front of the block.

$$\Delta Y = \frac{LMN \left(\frac{16}{3} \right) \sqrt{\frac{\pi d (1-\nu)^2}{2E}} C_1^{5/2}}{XZ} \quad (55)$$

Figure 4. A graph showing the fractional porosity (f) required for the formation of various fracture geometries, assuming constant porosity and constant least total principal stress.

- 1/ $C_1 = A = B = 1'$, $C = .001'$; 2/ $C_1 = A = B = 5'$, $C = .0005'$;
- 3/ $C_1 = A = B = 5'$, $C = .001'$; 4/ $C_1 = A = B = 10'$, $C = .001'$;
- 5/ $C_1 = A = B = 20'$, $C = .001'$; 6/ $C_1 = A = B = 50'$, $C = .001'$.



If the Poisson effect is neglected, this lengthening caused by the development of the joints must be balanced by the elastic shortening of the block due to an increase in S_3 :

$$\Delta Y = \frac{(\Delta S_3) Y}{E} \quad (56)$$

where E is Young's Modulus, and ΔS_3 is the increase in the total least principal stress. Equating equations (55) and (56) and solving for ΔS_3 :

$$\Delta S_3 = \frac{(E)LMN \left(\frac{16}{3}\right) \sqrt{\frac{\pi \gamma (1-\nu)^2}{2E}} C_1^{5/2}}{XYZ} \quad (57)$$

Substituting equations (39), (40) and (41):

$$\Delta S_3 = \frac{E \left(\frac{16}{3}\right) \sqrt{\frac{\pi \gamma (1-\nu)^2}{2E}} \cdot C_1^{5/2}}{d(2C_1+A)(2C_1+B)} \quad (58)$$

An expression for the change in pore pressure, during jointing in an environment where no crustal extension can occur, is obtained by substituting the expressions for ΔS_3 and $\Delta \sigma_3$ from equations (58) and (50) respectively into equation (47):

$$\Delta p = \frac{E \left(\frac{16}{3}\right) \sqrt{\frac{\pi \gamma (1-\nu)^2}{2E}} \cdot C_1^{5/2}}{d(2C_1+A)(2C_1+B)} + \sqrt{\frac{\pi E \gamma}{2(1-\nu)^2}} \left(\frac{1}{\sqrt{C_1}} - \frac{1}{\sqrt{C}} \right) \quad (59)$$

When equations (59), (46) and (44) are combined an expression involving porosity (f') as the only unknown is obtained:

$$f' = \left(\frac{\frac{16}{3k} \left(\frac{1-\nu^2}{E}\right) \frac{\sqrt{C_1 C}}{\sqrt{C_1 - \sqrt{C}}}}{d(2C_1+A)(2C_1+B)} \cdot C_1^{5/2} \right) (1 + kE f') \quad (60)$$

Comparison of equation (60) with equation (54) reveals that the bracketed term is the expression for the porosity in the constant stress case. Therefore the

original porosity required to produce a particular joint geometry in the constant volume case (f') is a simple function of the original porosity required to produce the same geometry in the constant stress case (f):

$$f' = f(1 + kEf') \quad (61)$$

Solving for f' :

$$f' = \frac{f}{1 - kEf} \quad (62)$$

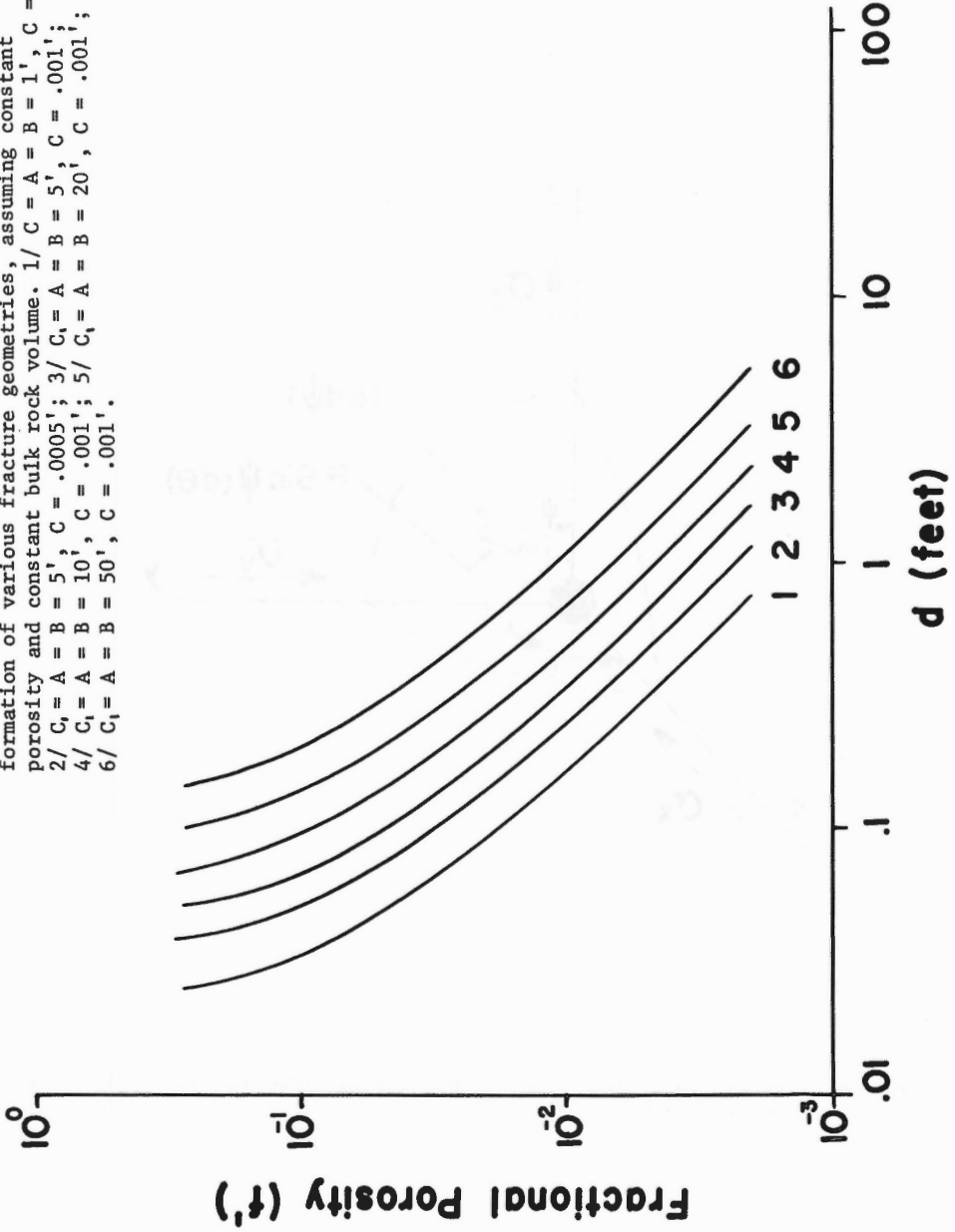
Equations (62) and (54) can be used to calculate the required porosity for any desired joint geometry, assuming constant bulk volume of the rock during the jointing episode. The results of such calculations are shown in Figure 5. Apparently, very closely spaced joints are impossible under the assumed conditions in rocks of normal porosity.

The Variable Porosity Model

Most rocks contain some crack-shaped pores and in crystalline rocks of low porosity almost all of the fluid is contained in grain boundary and cleavage cracks. It has been shown that a tensile least effective principal stress of considerable magnitude (equation 5) is necessary for the initiation of a macroscopic tension fracture from a small pre-existing flaw. At the time of fracturing there must therefore be a considerable range of directions, sub-parallel to the σ_3 direction, along which the effective stress is tensile. If a flaw is perpendicular to the σ_3 direction, equation (12) can be used to calculate its volume:

$$V = - \frac{16}{3E} (1 - \nu^2) \sigma_3 C^3 \quad (12)$$

Figure 5. A graph showing the fractional porosity (f') required for the formation of various fracture geometries, assuming constant porosity and constant bulk rock volume. 1/ $C = A = B = 1'$, $C = .001'$;
2/ $C_1 = A = B = 5'$, $C = .0005'$; 3/ $C_1 = A = B = 5'$, $C = .001'$;
4/ $C_1 = A = B = 10'$, $C = .001'$; 5/ $C_1 = A = B = 20'$, $C = .001'$;
6/ $C_1 = A = B = 50'$, $C = .001'$.



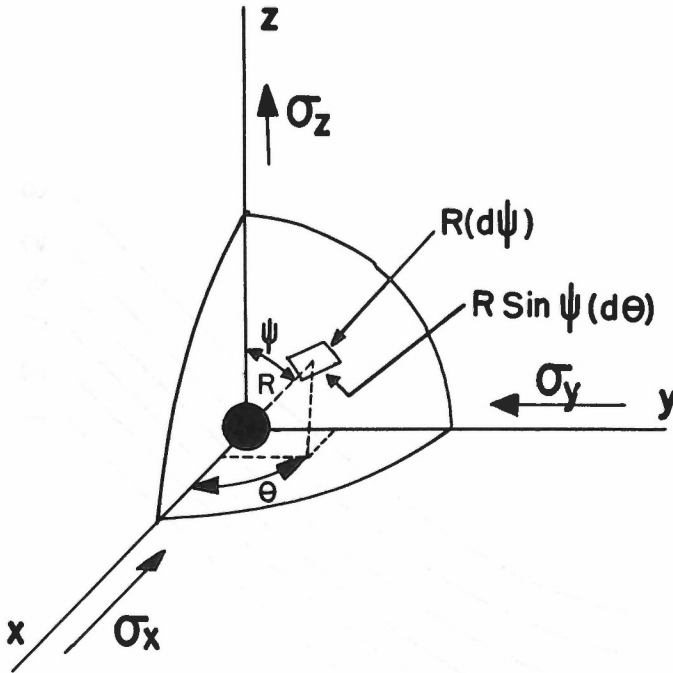


Figure 6. Coordinate systems used in projecting poles of cracks to a reference sphere of radius (R).

If the crack is not perpendicular to the σ_3 direction, equation (12) can still be used to calculate its volume providing:

1. That the term (σ_3) in equation (12) is replaced by (σ), the component of effective stress perpendicular to the plane of interest:

$$V = - \frac{16}{3E} (1-\nu) \sigma C \quad (63)$$

2. That this normal effective stress is tensile.
3. That the component of shear stress parallel to the plane of interest does not have a major effect on the volume of the crack.

Recent compression experiments on rocks with pore pressure by Brace (this conference) have indicated that rocks become dilatant when the differential stress is about one half the value necessary for the formation of a shear fracture. Apparently crack opening can be caused by high shear stress even when the macroscopic effective principal stresses are all compressive. The experimental results of Brace suggest that shear stress will tend to increase the volume of cracks, and so crack volumes calculated from equation (63) will be too low because the shear effect is neglected. The use equation (63) to estimate crack porosity changes during jointing will therefore give a conservative estimate of the amount of fluid available for the jointing process.

Imagine a spherical element of rock of unit volume located at the center of an x, y, z coordinate system (Figure 6). The radius of the element is assumed to be large with respect to the flaw length (C), but small with respect to the radius (R) of an enclosing reference sphere. The orientation of the radius (R) of the reference sphere is fixed by the angular spherical coordinates θ and ψ . If infinitesimally small variations ($d\theta, d\psi$) are permitted in θ and ψ , the radius R will scribe an infinitesimal area on the reference sphere having edge lengths $R(d\psi)$ and $R \sin \psi (d\theta)$. If the spherical element of rock at the center of the coordinate system contain n randomly oriented

cracks, a small fraction of the cracks will have poles located inside the infinitesimal area on the reference sphere. This fraction will be given by:

$$\text{Total number of cracks with poles in element} = n \left(\frac{\text{Area of element}}{\text{Half area of sphere}} \right) = \frac{n \sin \psi d\psi d\theta}{2\pi} \quad (64)$$

The volume of fluid (dV) contained in the cracks that have poles in the infinitesimal area will be given by:

$$dV = - \left(\frac{n \sin \psi d\psi d\theta}{2\pi} \right) \left(\frac{16}{3E} (1-\nu^2) \sigma c^3 \right) \quad (65)$$

$$dV = - \frac{8n(1-\nu^2) c^3}{3\pi E} \cdot \sigma \sin \psi d\psi d\theta \quad (66)$$

The component of effective normal stress in the direction of R will be given by:

$$\sigma = \sin^2 \psi \cos^2 \theta \sigma_x + \sin^2 \psi \sin^2 \theta \sigma_y + \cos^2 \psi \sigma_z, \quad (67)$$

where σ_x , σ_y , and σ_z are the principal stresses in the x , y , and z directions respectively. Substituting in equation (66) and integrating:

$$V = - \frac{8n(1-\nu^2) c^3}{3\pi E} \int_{\psi} \int_{\theta} (\sin^3 \psi \cos^2 \theta \sigma_x + \sin^3 \psi \sin^2 \theta \sigma_y + \sin \psi \cos^2 \theta \sigma_z) d\theta d\psi \quad (68)$$

In performing this integration it is important to permit the direction of the radius R to vary only in those directions where the normal stress is tensile, because the applicability of equation (63) is limited to the case where σ is tensile. In the special case where σ_x , σ_y and σ_z are all tensile, the limits on θ and ψ are $(2\pi, 0)$ and $(\pi/2, 0)$ respectively, and equation (68) reduces to:

$$V = \frac{-16n(1-\nu^2) c^3}{9E} (\sigma_x + \sigma_y + \sigma_z) \quad (69)$$

In the special case where σ_x and σ_y are equal and compressive, the limits on θ and ψ will be:

$$(2\pi, 0), (\text{Arccos} \sqrt{\frac{\sigma_x}{\sigma_x - \sigma_z}}, 0)$$

respectively, and equation (68) reduces to:

$$V = - \frac{16n(1-\nu^2)C^3}{9E} \left(\sqrt{\frac{\sigma_x}{\sigma_x - \sigma_z}} (-2\sigma_x) + 2\sigma_x + \sigma_z \right) \quad (70)$$

In the special case where σ_z is compressive and where σ_x and σ_y are equal and tensile, the limits on θ and ψ will be:

$$(2\pi, 0), (\pi/2, \text{Arccos} \sqrt{\frac{\sigma_x}{\sigma_x - \sigma_z}})$$

respectively, and equation (68) reduces to:

$$V = - \frac{16n(1-\nu^2)C^3}{9E} (2\sigma_x) \sqrt{\frac{\sigma_x}{\sigma_x - \sigma_z}} \quad (71)$$

Equations (69), (70) are mutually compatible in the sense that they both converge to the same result:

$$V = - \frac{16n(1-\nu^2)C^3}{9E} (\sigma_z) \quad (72)$$

when $\sigma_x = \sigma_y = 0$. Likewise equations (69) and (71) converge to the result:

$$V = - \frac{16n(1-\nu^2)C^3}{9E} (2\sigma_x) \quad (73)$$

when $\sigma_z \rightarrow 0$ and when $\sigma_x = \sigma_y$. Mathematical difficulties have so far precluded the derivation of a general equation for the case where the principal stresses all have different magnitudes, and where at least one of the principal stresses is compressive. The fluid volumes calculated from equations (69), (70), and (71) are equal to the fractional crack porosity if the small spherical rock element in Figure 6 is considered a unit volume.

Equations (69), (70) and (71) comprise a theoretical model for the fractional crack porosity of a rock, and can be used to estimate porosity changes induced by changes in the effective principal stresses. In the present paper these equations will be used to estimate the quantity of fluid squeezed out of crack shaped pores into opening joint cracks, during an episode of jointing.

In a rock with crack porosity:

$$\begin{array}{l} \text{Fluid volume} \\ \text{occupying joints} \end{array} = \begin{array}{l} \text{Volume from elastic} \\ \text{expansion of the} \\ \text{pore fluid.} \end{array} + \begin{array}{l} \text{Volume from porosity} \\ \text{reduction of the} \\ \text{rock.} \end{array} \quad (74)$$

The fluid volume occupying joints can be calculated from equation (44):

$$\text{Fluid volume occupying joints} = \frac{16 \sqrt{\frac{\pi \gamma (1-\nu^2)}{2E}} C_1^{5/2}}{d(2C_1+A)(2C_1+B)} \quad (44)$$

In an environment where the least total principal stress remains constant during the jointing episode, equation (52) will give the fluid volume available from elastic expansion of the pore fluid:

$$\begin{array}{l} \text{Volume from elastic} \\ \text{expansion of the pore} \\ \text{fluid} \end{array} = k f'' \sqrt{\frac{\pi E \gamma}{2(1-\nu^2)}} \left(\frac{1}{\sqrt{C}} - \frac{1}{\sqrt{C_1}} \right) \quad (52)$$

Just before the beginning of a jointing episode, the fractional porosity (f'') will be given by equations (69), (70) or (71). If the jointing is occurring in an environment where σ_1 and σ_2 are compressive and equal:

$$f'' = - \frac{16n(1-\nu^2) C^3}{9E} \left(\sqrt{\frac{\sigma_x}{\sigma_x - \sigma_z}} (-2\sigma_x) + 2\sigma_x + \sigma_z \right) \quad (70)$$

solving for n :

$$n = \frac{f''}{- \frac{16(1-\nu^2) C^3}{9E} \left(\sqrt{\frac{\sigma_x}{\sigma_x - \sigma_z}} (-2\sigma_x) + 2\sigma_x + \sigma_z \right)} \quad (75)$$

The fractional porosity (f_1'') of the rock after the jointing episode has been completed will be given by:

$$f_1'' = - \frac{16n(1-\nu^2) C^3}{9E} \left(\sqrt{\frac{\sigma_x'}{\sigma_x' - \sigma_z'}} (2\sigma_x') + 2\sigma_x' + \sigma_z' \right) \quad (76)$$

where σ_x' , σ_y' and σ_z' are the new values of effective principal stress. The volume of fluid available from porosity reduction of the rock will be given by:

$$\begin{array}{l} \text{Volume from porosity} \\ \text{reduction of the rock} \end{array} = f'' - f_1'' \quad (77)$$

Substituting equation (75) and (76) into (77):

$$\text{Volume from porosity reduction of the rock} = f'' - f'' \left(\frac{\left(\sqrt{\frac{\sigma_x'}{\sigma_x' - \sigma_z'}} (-2\sigma_x') + 2\sigma_x' + \sigma_z' \right)}{\left(\sqrt{\frac{\sigma_x}{\sigma_x - \sigma_z}} (-2\sigma_x) + 2\sigma_x + \sigma_z \right)} \right) \quad (78)$$

Sample calculations for typical jointing episodes has indicated that there is very little residual tensile stress left in the rocks after fracturing has occurred:

$$\sigma_z' \rightarrow 0 \quad (79)$$

When equation (79) is substituted in equation (78), the bracketed term in (78) approaches zero:

$$\left(\frac{\left(\sqrt{\frac{\sigma_x'}{\sigma_x' - \sigma_z'}} (-2\sigma_x') + 2\sigma_x' + \sigma_z' \right)}{\left(\sqrt{\frac{\sigma_x}{\sigma_x - \sigma_z}} (-2\sigma_x) + 2\sigma_x + \sigma_z \right)} \right) \rightarrow 0 \quad (80)$$

and equation (78) reduces to:

$$\text{Volume from porosity reduction of the rock} = f'' \quad (81)$$

Apparently the near elimination of effective tensile stress from a rock mass during a jointing episode results in the closure of all non propagating flaws, so that all of the original fluid contained in grain boundary cracks is available for jointing.

When equations (44), (52), and (81) are substituted in equation (74), we obtain:

$$\frac{\frac{16}{3} \sqrt{\frac{\pi \gamma (1-\nu^2)}{2E}} C_1^{5/2}}{d(2C_1+A)(2C_1+B)} = f'' \left(\left[k \sqrt{\frac{\pi E \gamma}{2(1-\nu^2)}} \left(\sqrt{\frac{1}{C}} - \sqrt{\frac{1}{C_1}} \right) \right] + 1 \right) \quad (82)$$

The bracketed term on the right side of (82) may be neglected because it is a small fraction much less than one. Therefore:

$$f'' = \frac{\frac{16}{3} \sqrt{\frac{\pi \gamma (1-\nu^2)}{2E}} C_1^{5/2}}{d(2C_1+A)(2C_1+B)} \quad (83)$$

The initial crack porosity (f'') necessary for the formation of a joint pattern of any assumed geometry can be calculated from equation (83). In Figure 7, the required porosity is plotted as a function of fracture spacing (d) for a variety of fracture geometries, assuming the following parameters:

$$k = 1.72 (10^{-8}) \text{ ft. }^2 / \text{ lb.}$$

$$E = 720 (10^6) \text{ lbs./ ft.}^2$$

$$\nu = .250$$

$$\gamma = .0687 \text{ lbs. / ft.}$$

The results show that an extremely small initial crack porosity could produce most commonly observed joint patterns.

In the constant volume case:

$$\Delta p = \Delta S_3 - \Delta \sigma_3 \quad (47)$$

where:

$$\Delta \sigma_3 = \sqrt{\frac{\pi E \gamma}{2(1-\nu^2)}} \left(\frac{1}{\sqrt{C_1}} - \frac{1}{\sqrt{C}} \right) \quad (50)$$

and where:

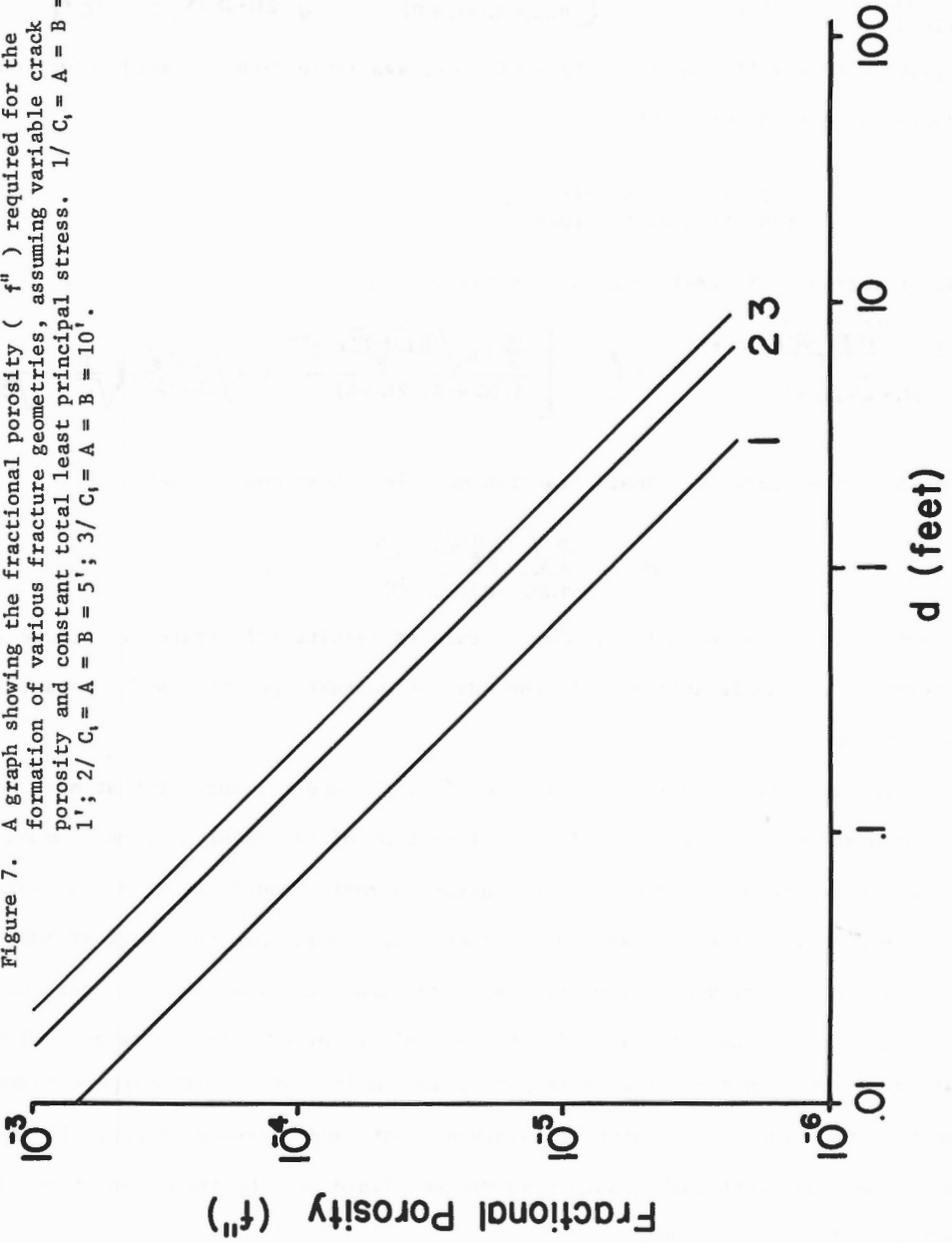
$$\Delta S_3 = \frac{\frac{16}{3} (E) \sqrt{\frac{\pi \gamma (1-\nu^2)}{2 E}} C_1^{5/2}}{d(2C_1+A)(2C_1+B)} \quad (58)$$

The volume of fluid available from elastic expansion of the pore fluid will be given by:

$$\begin{array}{l} \text{Volume from elastic} \\ \text{expansion of the} \\ \text{pore fluid} \end{array} = -k f''' \Delta p = -k f''' (\Delta S_3 - \Delta \sigma_3), \quad (46)$$

where (f''') is the initial crack porosity of the rock. Substituting equations (50) and (58) in (46):

Figure 7. A graph showing the fractional porosity (f'') required for the formation of various fracture geometries, assuming variable crack porosity and constant total least principal stress. $1/ C_1 = A = B = 1'$; $2/ C_1 = A = B = 5'$; $3/ C_1 = A = B = 10'$.



Volume from elastic expansion of the pore fluid = $-k f''' \left[\frac{16}{3} (E) \sqrt{\frac{\pi \gamma (1-\nu^2)}{2E}} C_1^{5/2} + \sqrt{\frac{\pi E \gamma}{2(1-\nu^2)}} \left(\frac{1}{\sqrt{C_1}} - \frac{1}{\sqrt{C}} \right) \right]$ (84)

Equation (81) will give the volume of fluid available from porosity reduction during an episode of jointing:

Volume from porosity reduction of the rock = f''' (81)

Substituting (81), (84), and (44) in (74):

$$\frac{16}{3} \sqrt{\frac{\pi \gamma (1-\nu^2)}{2E}} C_1^{5/2} = f''' \left(1 - \left[\frac{16}{3} k E \sqrt{\frac{\pi \gamma (1-\nu^2)}{2E}} C_1^{5/2} + k \sqrt{\frac{\pi E \gamma}{2(1-\nu^2)}} \left(\frac{1}{\sqrt{C_1}} - \frac{1}{\sqrt{C}} \right) \right] \right) \quad (85)$$

The bracketed term is a small fraction much less than one so that:

$$f''' = \frac{16}{3} \sqrt{\frac{\pi \gamma (1-\nu^2)}{2E}} C_1^{5/2} \quad ,$$

which is identical with (83). The calculated results illustrated in figure 7 therefore are applicable also in the case of variable porosity and constant bulk volume.

The results illustrated in figures (4), (5) and (7) suggest that most rocks contain sufficient pore fluid for the formation of the joint patterns commonly reported by field geologists. The constant porosity model predicts that joints one hundred feet long and spaced one foot apart could form in a rock of 10% porosity. The crack porosity model predicts that porosities much less than one percent will be required for the formation of most commonly observed joint patterns. Almost all rocks contain some crack-like pores, and in igneous and metamorphic rocks most of the fluid is contained in grain-boundary and cleavage cracks. It is concluded that most rocks contain sufficient fluid for the formation of the joint patterns observed in them.

DISCUSSION

When a geologic phenomenon is analyzed using the methods of physics and mathematics, the results tend to have an aura of precision and elegance which is not justified. It must be remembered that rocks are extremely complicated systems, and the application of physical equations to characterize rock behavior is at best a crude approximation and a poor substitute for empirical data on the behavior of rocks in the environment of interest. However, theoretical consideration of jointing mechanics is presently justifiable, because the results will be useful in guiding future field and laboratory investigations. The numerical results presented in the preceding section are only crude approximations to reality and should not be taken seriously beyond the first significant figure. However, even with this qualification in mind, the following conclusions seem justified:

1. When natural tension fracturing occurs at depth in the earth's crust, in the presence of high pore pressures, macroscopic fracture growth in a slow process consisting in detail of numerous short, quick episodes of fracture propagation interspersed with longer periods of quiescence during which pore fluid from the surrounding rock percolates into the crack and wedges it open.
2. Both ductile creep of rock at crack tips, and the development of multiple fractures in the same rock mass will tend to limit the length of any one joint fracture.
3. Most rocks appear to have porosities adequate for the development of the joint patterns observed in them.

The development of equations relating porosity and fracture geometry has revealed that tension fracturing at depth in the earth's crust is an incredibly complicated process. Inspection of equations (44), (52), (78), (79), and (83) indicated that the porosity required to produce a particular fracture geometry is functionally dependent on the following parameters: E , ν , γ , k , C , σ_1 , σ_2 , and σ_3 . Moreover the required porosity depends on whether the pores

are spherical or crack-shaped, and whether the fracturing is occurring in a "constant stress" or a "constant volume" environment. The variety of rocks and pore fluids available in nature permit considerable latitude in the choice of E , γ , C and k , and this could result in an order of magnitude variation in the calculated porosity. Variations in pore geometry and stress environment have an even greater effect on calculated porosity. An obvious extension and improvement of the work presented here would result from machine computation of required porosities over a wider range of values for the environmental stresses and rock and fluid properties.

The volume of fluid available for jointing is fixed by selection of appropriate material and environmental parameters. However, inspection of equation (54) reveals that an infinity of different fracture geometries are possible from any given fluid volume. It is possible to calculate the porosity needed for the formation of a fracture set of assumed geometry, but given a particular value of porosity, it presently is not presently possible to determine which of the many possible fracture geometries will actually develop.

Some qualitative considerations may be useful in understanding natural fracture geometries. Equation (13) indicates that the fluid volume needed for the growth of a particular fracture is proportional to the $5/2$ power of the crack radius. The final length of a fracture is dependent on how easy it is for pore fluids from the surrounding rock to move into the fracture. In an environment where subjacent permeable and impermeable rock masses are being jointed under identical stress conditions, one would predict that fractures in the impermeable rocks would be short and closely spaced, whereas the fractures in the permeable rock would be long and widely spaced. This may explain the commonly observed wide spacing of joint fractures in massive sandstones as compared with the close spacing in enclosing shales and siltstones. The rate at which the least effective principal stress changes during the beginning of an episode of fracturing may also be important in controlling fracture geometry. If the critical stress condition

for jointing results from a very slow decrease in the least effective principal stress, tension fractures would be initiated at a few particularly long flaws before the stress became small enough for the initiation of fractures at more numerous shorter flaws. However, if the stress decrease was rapid, numerous tension fractures would be initiated at about the same time throughout the rock mass. Changes in the magnitude of the least effective principal stress could result from either changes in the pore pressure or changes in the total least principal stress. The rate at which σ_3 changes will therefore depend on the rate at which S_3 and p change in the local environment. A slow decrease in σ_3 would result in a few long joints, whereas a rapid decrease in σ_3 would result in more numerous short joints.

It is important to remember that the mechanical model proposed in this paper is applicable only to joints that originate as natural tension fractures in rocks with pressurized pore fluid. The model is not applicable to joints forming near the earth's surface where tensile total stresses are possible, nor is it applicable to the development of "shear" joints (if shear joints do indeed exist).

Field observations in metamorphic terranes often indicate that the joint pattern is symmetrically oriented with respect to fold axes and linear structures. This symmetry may be a consequence of rock anisotropy; it may also be a consequence of residual stresses remaining in the rock after the main phase of the deformation. These facts are not basically incompatible with the hydraulic fracturing hypothesis proposed here. The present model could be extended to include a degree of anisotropy and/or residual stress in a rock mass undergoing jointing.

Studies of field examples of jointing have always been handicapped by the lack of adequate criteria for recognizing the various kinds of joints. How can tension joints formed in a surficial environment be differentiated from natural hydraulic fractures formed at depth in the earth's crust? The presence of

mineral druses indicative of metamorphic conditions might be useful but such fillings are relatively rare and indicate only that the fracture was open at depth. How can natural tension fractures be distinguished from natural shear fractures of small lateral displacement? The presence of two acutely intersecting fracture directions have often been used as a criterion for a shear origin. However, a pair of acutely intersecting fracture directions could have originated as two sets of tension fractures formed at different times. Slickensides are indicative of shear, and yet a set of tension fractures could suffer shear displacement during a later deformation. It is also very difficult to establish the relative ages of a number of intersecting joint sets because such sets often indiscriminately cut each other without apparent lateral displacement.

It appears that we have made a beginning in understanding the origin of some kinds of joints, but the traditional goal of using joints in structural interpretation seems as elusive as ever.

ACKNOWLEDGMENTS

This work was done during the tenure of National Science Foundation Grant # GP 5533. Discussions with W. F. Brace, W. E. Sharp and J. L. Boal contributed to the formulation of the ideas expressed here. W. R. Muehlberger pointed out several relevant papers on hydraulic fracturing that were originally unknown to the writer.

REFERENCES

- Anderson, E.M.
1951: The dynamics of faulting and dyke formation, with applications to Britain; Second Edition, Edinburgh, Oliver and Boyd.
- Birch, F.
1955: Physics of the crust; in Crust of the earth, A. Poldervaart, editor; Geol. Soc. Am., Spec. Paper 62, pp. 101-117.
1966: Compressibility; elastic constants; in Handbook of physical constants, S.P. Clark, Jr., editor; Geol. Soc. Am., Mem. 97, pp. 97-173.
- Bombolakis, E.G.
1964: Photoelastic investigation of brittle crack growth within a field of uniaxial compression; Tectonophysics, vol. 1, pp. 343-351.
- Brace, W.F.
1961: Dependence of fracture strength of rocks on grain size; Bull. Mineral Ind. Expt. Sta., Penn. State Univ., No. 76, pp. 99-103.
1964: Brittle fracture of rocks; in State of stress in the earth's crust, W.R. Judd, editor; New York, Elsevier, pp. 110-178.
- Brace, W.F., and Bombolakis, E.G.
1963: A note on brittle crack growth in compression; J. Geophys. Res., vol. 68, pp. 3709-3713.
- Brace, W.F., and Paulding, B.W., Jr., and Scholz, C.H.
1966: Dilatancy in the fracture of crystalline rocks; J. Geophys. Res., vol. 71, pp. 3939-3953.
- Brace, W.F., and Walsh, J.B.
1962: Some direct measurements of the surface energy of quartz and orthoclase; Am. Mineralogist, vol. 47, pp. 1111-1122.
- Chamberlin, T.C.
1897: The method of multiple working hypotheses; J. Geol., vol. 5, pp. 837-848.
- Cottrell, A.H.
1959: Theoretical aspects of fracture; in Fracture, B.L. Averbach, et al., editors, Cambridge Technology Press.
- Griffith, A.A.
1921: The phenomena of rupture and flow in solids; Phil. Trans. Roy. Soc. London, Ser. A, vol. 221, pp. 163-198.
1925: The theory of rupture; Proc. 1st. Internat. Cong. Applied Mechanics, Delft, 1924; pp. 55-63.

- Griggs, D., and Handin, J.
1960: Observations on fracture and a hypothesis of earthquakes; in Rock deformation, D. Griggs and J. Handin, editors; Geol. Soc. Am., Mem. 79, pp. 347-364.
- Handin, J., Hager, R.V. Jr., Friedman, M., and Feather, J.N.
1963: Experimental deformation of sedimentary rocks under confining pressure; pore pressure tests; Bull. Am. Assoc. Petrol. Geologists, vol. 47, pp. 717-755.
- Holser, W.T., and Kennedy, G.C.
1958: Properties of water, Pt. IV, Pressure-volume-temperature relations of water in the range 100-400C and 100-1400 bars; Am J. Sci., vol. 256, pp. 744-754.
- Hubbert, M.K.
1951: Mechanical bases for certain familiar geologic structures; Bull. Geol. Soc. Am., vol. 62, pp. 355-372.
- Hubbert, M.K., and Rubey, W.W.
1959: Role of fluid pressure in mechanics of overthrust faulting. I Mechanics of fluid-filled porous solids and its application to overthrust faulting; Bull. Geol. Soc. Am., vol. 70, pp. 115-166.
- Hubbert, M.K., and Willis, D.G.
1957: Mechanics of hydraulic fracturing; Petroleum Trans. AIME, vol. 210, pp. 153-166.
- Inglis, C.E.
1913: Stresses in a plate due to the presence of cracks and sharp corners; Trans. Inst. Naval Architects, vol. 55, pp. 219-230.
- Jaeger, J.C.
1962: Elasticity, fracture and flow; New York, John Wiley and Sons.
1963: Extension failures in rocks subject to fluid pressure; J. Geophys. Res., vol. 68, pp. 6066-6067.
- Kennedy, G.C., Knight, W.L., and Holser, W.T.
1958: Properties of water, Pt. III, Specific volume of liquid water to 100C and 1400 bars; Am. J. Sci., vol. 256, pp. 590-595.
- Lawson, A.C.
1922: Isostatic compensation considered as a cause of thrusting; Bull. Geol. Soc. Am., vol. 33, pp. 337-351.
- Longwell, C.R.
1945: The mechanics of orogeny; Am. J. Sci., Daly Volume, vol. 243A, pp. 417-447.
- Maxwell, J.C.
1962: Origin of slaty and fracture cleavage in the Delaware water gap area, New Jersey and Pennsylvania; in Petrologic studies, A.E.J. Engel, H.L. James, and B.F. Leonard, editors; Geol. Soc. Am., Buddington Volume, pp. 281-311.

- McClintock, F.A., and Walsh, J.B.
1962: Friction on Griffith cracks in rocks under pressure; Proc. 4th Natl. Cong. Applied Mechanics, Berkeley, California, 1962, pp. 1015-1021.
- Muehlberger, W.R.
1961: Conjugate joint sets of small dihedral angle; J. Geol., vol. 69, pp. 211-219.
- Nickelsen, R.P., and Hough, V.N.D.
1967: Jointing in the Appalachian Plateau of Pennsylvania; Bull. Geol. Soc. Am., vol. 78, pp. 609-629.
- Oldham, R.D.
1921: 'Know your faults' (Presidential address); Quart. J. Geol. Soc. London, vol. 77, Pt. I, pp. lxxvii-xcii.
- Orowan, E.
1960: Mechanism of seismic faulting; in Rock deformation, D. Griggs, and J. Handin, editors; Geol. Soc. Am., Mem. 79, pp. 323-345.
- Parker, J.M., III.
1942: Regional systematic jointing in slightly deformed sedimentary rocks; Bull. Geol. Soc. Am., vol. 53, pp. 381-408.
- Perkins, T.K., and Bartlett, L.E.
1963: Surface energies of rocks measured during cleavage; Soc. Petrol. Engrs. J., vol. 3, pp. 307-313.
- Price, N.J.
1966: Fault and joint development in brittle and semi-brittle rock; New York, Pergamon Press.
- Reid, H.F.
1911: The elastic-rebound theory of earthquakes, Univ. Calif. Pub; Dept. Geol. Sci., vol. 6, pp. 413-444.
- Sack, R.A.
1946: Extension of Griffith's theory of rupture to three dimensions; Proc. Phys. Soc. London, vol. 58, pp. 729-736.
- Secor, D.T., Jr.
1965: Role of fluid pressure in jointing; Am. J. Sci., vol. 263, pp. 633-646.
- Sharp, W.E.
1962: The thermodynamic functions for water in the range -10 to 1000C and 1 to 250,000 bars. University of California Lawrence Radiation Laboratory Pub. 7118, 50 p.
- Sneddon, I.N.
1946: The distribution of stress in the neighborhood of a crack in an elastic solid; Proc. Roy. Soc. London. Ser. A, vol. 187, pp. 229-260.

DISCUSSION

D. F. Coates asked the speaker to elaborate somewhat on basic criteria concerning the necessary condition of his theory, and asked in particular what the limitations on the principal stresses were.

The author replied that one has of course to consider a brittle material containing some type of cracks. The value of the tensile strength can be figured out mathematically. As to limitations on the principal stresses, if tension fractures are to form, the least effective stress has to equal the tensile strength and the greatest effective compressive stress cannot be greater than three times the tensile strength or else the work will fail in shear. This is a consequence of the Griffith theory of brittle fracture, and has been demonstrated experimentally by W. F. Brace.

P. S. Simony asked for some more details concerning the second model developed by the author, and in particular about the walls of the cracks which, at one time appeared impermeable, and at another time appeared permeable.

The author explained that if a crack propagates, its volume increases and therefore the fluid pressure inside the crack decreases. As a consequence, fluid in the rock around the crack will tend to flow into the crack again. The wall of the crack is probably permeable at all times but the difference between the rate of propagation of the crack (possibly the speed of sound) and the rate of seepage of fluid into the crack (possibly measured in tens or hundreds of years) explains that during crack propagation, effects of seepage are negligible.

G. R. Stevens asked if solubility of the rock in the pore fluid might play any role.

The author said that he had always felt that when a fluid flows from a higher pressure environment into a lower pressure environment, some of the matters in solution in the fluid might precipitate and that one often finds joints filled with mineral matter.

J. B. Currie asked what would be critical field relationships that could help to test the theory developed by the author.

The author suggested that investigations of joint geometry including a large number of joints in rocks of different permeabilities might be useful, but he also warned that there might not be enough geometric variables to determine the origin of joints. The difficulty was, he said in the large number of variables on which joint geometry depends, namely Young's modulus, Poisson's ratio, the surface energy, σ_1 , σ_2 , σ_3 , the nature of the porosity, permeability, and the way the stress field changes during jointing.

A DYNAMIC MECHANISM FOR THE DEVELOPMENT OF
SECOND ORDER FAULTS

N. J. Price

Department of Geology, Imperial College
University of London, England

Abstract

The initiation and development of second order faults cannot satisfactorily be explained by analyses based on a study of the static stress fields before and after movement along a first order, strike-slip fault. However, increments of displacement on faults commonly occur so abruptly that vibrations of the rock masses are generated. In certain circumstances, the frequency and amplitude of the shock waves and the stresses associated with these vibrations can so alter the static stress field that the orientation and intensities of the principal stresses are momentarily such that small second order fractures may develop. These small fractures, it is suggested, propagate and extend with the passing of every shock wave and during subsequent increments of movement of the first order fault, until these small fractures eventually attain the magnitude of second order faults. The angle which the second order fault makes with the first order structure, and whether the movement on the secondary fractures is strike slip or dip slip, depends upon a number of factors which include the value of the vertical principal stress, the pore-water pressure and the intensities of the inertial stresses associated with the rock vibrations.

INTRODUCTION

Relatively small scale shear structures which are associated with main, or 'first order', faults in the manner indicated in Figure 1 have been termed secondary or 'second order' faults. When these subsidiary fractures occur near the end of the first order structures they are sometimes referred to as splay faults. The movement sense along the second order fault is such that they are obviously not complementary to the first order structure.

The possible origin of these second order shears has been discussed by a number of authors. Anderson (1951) presented an analysis of stress distribution around a vertical, strike-slip fault which, in the analysis, was represented in plan as an open, elliptical fracture. He concluded that although, in general, fault movement reduced the stress intensities in the vicinity of the fault plane, in small areas near the ends of the fault, the stresses actually increased. Moreover, the orientation of the principal stresses changed so that splay faults with the orientation and movement sense indicated in Figure 1 might in fact develop near the ends of first order faults. Elsewhere along the first order fault, according to this analysis, stress levels are insufficient to promote second order shears.

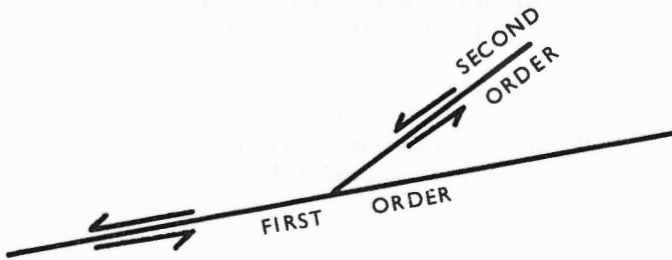


Figure 1. Showing typical angular relationship and movement sense of first order and second order faults

Anderson's physical model and his analysis of stresses around a fault may be criticised from a number of viewpoints. However, the most obvious one is that the faults are not open structures. Consequently, it is imperative to include in an analysis the influence of frictional effects along the surface of the fault.

McKinstry (1953) carried out just such an analysis and concluded that if the axis of maximum principal stress (σ_1) originally makes an angle of 30° with the first order fault, then, after movement, the principal stress takes up a new position and makes an angle of 60° with the main fault plane, so that second order faults may then form at 30° or 90° to the main fault.

Chinnery (1966) has recently criticised McKinstry's argument and has shown that the maximum principal stress, after faulting, rotates in the opposite sense from that suggested by McKinstry. Such a reorientation of the stresses is completely unable to give rise to second order faults with the orientation and movement sense shown in Figure 1.

Chinnery also presented an analysis of the stresses before and after faulting along a first order, strike-slip fault and also showed that splay development is possible in the vicinity of the ends of the first order fault. However, the pattern of second order fractures is, he predicts, much more complicated than that suggested by Anderson. He does, however, support Anderson's other main conclusion, that the stress levels in the vicinity of the central portion of first order faults, which develop in homogeneous and isotropic material, are too low to propagate second order fractures.

In all these analyses, the stress change after fault displacement has been considered from the static viewpoint, that is, two separate states are considered; the first is the system of stresses which initiates fault movement and the second, which develops after some unspecified time-lapse when the displacement and stress changes are completed. However, analyses using this approach are unable to explain the development of second order faults in regions which are remote from the ends of the first order structures. Nevertheless, despite the conclusions of both Anderson and Chinnery, second order faults which are remote from first order fault-ends are commonly observed in the field.

It is known from earthquake data and from theoretical considerations that increments of displacement along a fault are frequently accomplished in a very short time and that before the final static displacement is attained the system undergoes a period of transient oscillations. Stresses are generated during these oscillations which, it is suggested, momentarily modify the orientation and magnitude of the static stress field to such an extent that, in favourable circumstances, second order faults may develop. The mechanism envisaged is outlined in the following sections.

PHYSICAL MODEL

For the sake of analytical simplicity, we will follow Anderson, McKinstry and Chinnery and assume the primary, or first order, structure to be a vertical, strike-slip fault which develops as a brittle fracture in an unlimited, homogeneous and isotropic layer and we will consider only one layer within the medium.

Two conditions of the initial static stress will be considered, namely, (1) it will be assumed that these stresses are sufficient to initiate first order movement and (2) the first order fault is assumed to be in existence and the stress system is sufficient to cause fresh movement along the first order fault.

Prior to failure, the homogeneous and isotropic rock mass on either side of the actual, or incipient, fault plane is in a state of elastic strain, represented in Figure 2 by line AA', which on failure is translated to AA". Failure is assumed to be initiated at some small source and to propagate at high velocity. Thus, for the two conditions postulated, the thick line in Figure 2 represents in the one instance the developing fracture while the thin line is its path and indicates the future position of the first order fault, or alternatively, in the case of reshearing, the thin line represents the existing first order fault while the thick line indicates the developing zone of reshear along the first order fault.

It is assumed that the unshered rock fails according to the Navier-Coulomb criterion of brittle failure, so that the stresses at failure are given by

$$\tau = C_o + \sigma_n \cdot \tan \phi \quad (1)$$

where τ is the shearing stress along and σ_n is the stress acting normal to the plane which is to become the first order fault, C_o is the cohesive strength of the rock material and ϕ is its angle of friction. However, if a fault plane already exists, the shearing stress necessary to initiate reshearing is given by

$$\tau = \sigma_n \cdot \tan \phi \quad (2)$$

Failure is assumed to take place progressively, but rapidly. The resulting sudden displacement (e.g. from AA' to AA") gives rise to vibrations of the rock mass adjacent to the fault which, in turn, results in the propagation of elastic waves. It will be noted that when fracture propagation is rapid there is an accompanying fall in stress at the instant of failure to some relatively low level. Of course, in the case

of reshearing, there must be a subsequent increase in the stress level before further movement along the first order fault can take place.

From the equations of motion of an elastic solid it can be shown (Jaeger, 1964) that the vibrations take the form of longitudinal (P) waves or transversal (S) waves which propagate at the velocities V_p and V_s respectively, where V_s is approximately one-half the value of V_p . The displacement of the type represented in Figure 2 will give rise to a near planar wave front which propagates parallel to the fault trace $A'A''Q$. At some distance from the fault this simple model will not hold. Nevertheless, near the fault plane at point Q (which we assume is sufficiently distant from the propagating fracture so that the stresses at the tip of the moving 'crack' and associated effects can be neglected) one may apply the theory of plane waves to the model. That is, one assumes that the stress conditions in any plane perpendicular to the first order fault, at any instant in time, are uniform. The longitudinal wave is one of dilation. Hence, movement occurs only in the direction of propagation of the wave front, i. e. parallel to the fault, which in this analysis is chosen as the x direction, whereas the

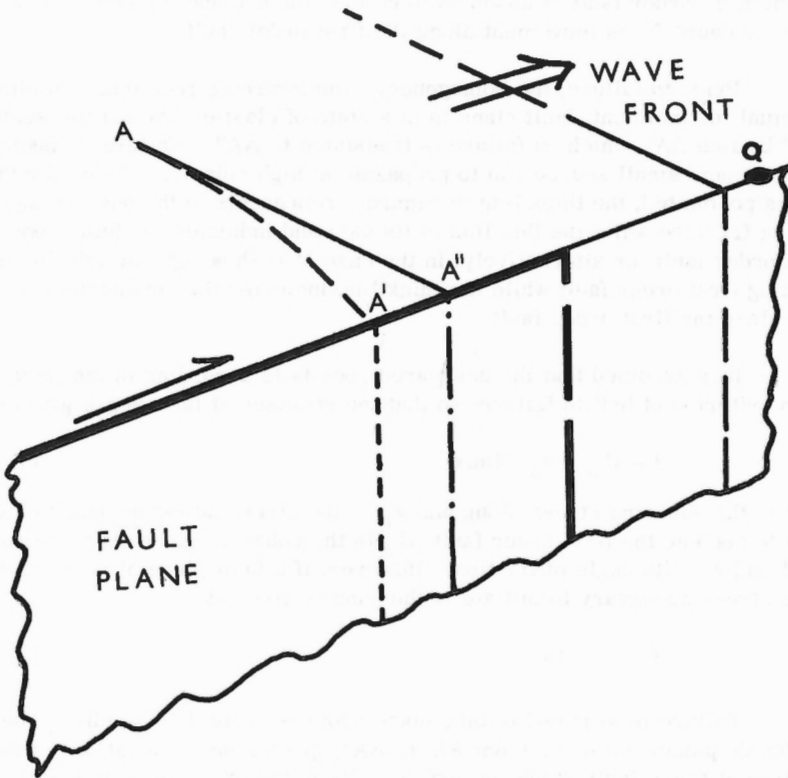


Figure 2. Diagrammatic representation of a wave front generated by sudden displacement along the fault from A' to A''

wave front of the shear waves travels in the x direction, but movement of elements occurs only in the y direction (normal to the first order fault).

Assuming that viscous damping is insignificant in the early cycles of vibration and that the movement of the elements, with time, is sinusoidal, then inertial stresses (σ_{In}) are generated parallel to the direction of element vibration which are given by

$$\sigma_{In} = K.f^2.u \quad (3)$$

where f is the frequency of vibration, u is the amplitude of vibration and K is a constant. These inertial stresses, for the conditions postulated, will act parallel to the fault when they are generated by P waves and normal to the fault when they are associated with S waves.

At this stage of the analysis it will be assumed that these inertial stresses may attain high magnitudes. A discussion of the values of f and u and the corresponding values of the inertial stresses which are likely to develop during fault movement will be presented later.

Because the P wave velocity is so much higher than that of the corresponding S wave, P waves will reach an element (Q) adjacent to the fault (see Fig. 2) before the S wave. Therefore, during the early wave lengths of the P waves reaching point Q, only the stress component parallel to the first order fault will be affected by inertial stresses, so that the momentary stress (σ_x') is given by

$$\sigma_x' = \sigma_x \pm \sigma_{In} \quad (4)$$

where σ_{In} is the inertial stress given by equation 3 (and is tensile, i. e., negative, in the extension phase of the oscillation) and σ_x is the component of stress parallel to the fault due to the static principal stresses σ_1 and σ_3 . For any specific value and orientation of these principal stresses, the stresses parallel (σ_x) and normal (σ_y) to the fault can be obtained from the expression

$$\sigma_x \text{ or } \sigma_y = \frac{\sigma_1 + \sigma_3}{2} \pm \frac{\sigma_1 - \sigma_3}{2} \cos 2\theta \quad (5)$$

where θ is the angle that the greatest principal stress makes with the first order fault plane. When the fault is being initiated, θ is given by

$$\theta = 45^\circ - \phi/2 \quad (6)$$

The value of the shearing stress (τ) on the fault plane is given by equation 1 or 2, depending upon the circumstances, and also by

$$\tau = \frac{\sigma_1 - \sigma_3}{2} \sin 2\theta \quad (7)$$

Because σ_x , σ_y and τ are uniquely determined by the magnitude and orientation of σ_1 and σ_3 , it follows that if σ_x is momentarily changed to σ_x' , there must be a corresponding change in the orientation and magnitude of the principal

stresses. The momentary magnitudes (σ_1' and σ_3') and orientation Θ' of the momentary principal stresses can be obtained from the expressions

$$\sigma_1' \text{ and } \sigma_3' = \frac{1}{2} \left\{ (\sigma_x' + \sigma_y) \pm \sqrt{(\sigma_x' - \sigma_y)^2 - 4\tau^2} \right\} \quad (8)$$

and

$$\tan \Theta' = (\sigma_1' - \sigma_x') / \tau \quad (9)$$

Once the values of the momentary principal stresses have been determined it is necessary to ascertain whether they satisfy the failure conditions.

It can be shown (Price, 1966) that the Navier-Coulomb criterion (equation (1)) can be expressed in terms of principal stresses at failure as

$$\sigma_1 = \sigma_0 + k \cdot \sigma_3 \quad (10)$$

where σ_0 is the uniaxial compressive strength, and

$$k = (1 + \sin \phi) / (1 - \sin \phi) \quad (11)$$

If, when specific values are assigned to σ_0 and ϕ , the values of σ_1' and σ_3' satisfy equation (10), then fresh shear fractures may develop and the orientation of these possible second order fractures can be ascertained from a knowledge of Θ' and ϕ , see equation (6).

It is now of interest to consider specific examples to illustrate the use of these equations in determining whether, during a phase of vibration, the new orientations and intensities of the momentary principal stresses are capable of initiating second order fractures with the disposition and movement sense given in Figure 1. To do this it is necessary to attribute certain physical values to the rock in which the second order fracture may develop. Let the uniaxial compressive strength of the unfractured rock be 10,000 lb. in². and the angle of friction (ϕ) be 30°. From these data and from equations (10) and (11), the relationship between principal stresses which must be satisfied if second order fractures are to develop is given by

$$\sigma_1 = 10,000 + 3 \cdot \sigma_3 \quad (12)$$

Let it further be assumed that the first order fault is in existence and that the greatest and least principal stresses which cause reactivation of this structure are 30,000 lb. in². and 10,000 lb. in². respectively and that σ_1 acts at an angle (Θ) of 30° to the first order fault.

From equation (5) it follows that $\sigma_x = 25,000$ lb. in². and $\sigma_y = 15,000$ lb. in². The shear stress is given by equation (7) and equals 8,660 lb. in².

Let the inertial stress due to the passage of a P wave momentarily attain a value of -14,500 lb. in²., then from equation (4), $\sigma_x' = 10,500$ lb. in². Putting these values of σ_x' , σ_y and τ in equation (8), the values of the instantaneous greatest and least principal stresses (σ_1' and σ_3') which are obtained are 21,700 and 3,900 lb. in². respectively¹. From reference to equation (12) it will be seen that these values of

¹ Calculations presented in this paper were carried out using a slide rule, so that calculated values given in this paper are approximate beyond the third place.

principal stresses can give rise to the development of second-order shears in the unfractured rock flanking the first order fault. From equation (9) it can be shown that the axis of the greatest principal stress (σ'_1) at this moment makes an angle with the first order fault of 50° . Consequently, from equation (6), it follows that a second order, strike-slip fracture could develop at an angle of 20° to the first order fault (provided, of course, that the vertical stress falls in the range 10,000 to 21,700 lb. in²). The movement along the potential, complementary, second order fracture would be almost perpendicular to the general movement along the main fault and this might mitigate against its development.

As will be seen later, it is more apposite to refer to the second order structures, at this stage of development, as fractures rather than faults.

Consider now a second example in which the greatest and least principal stresses initiating reshear along the first order fault are 15,000 and 5,000 lb. in². respectively and, as before, $\Theta = 30^\circ$, $\phi = 30^\circ$ and $\sigma_0 = 10,000$ lb. in². If the inertial stress reaches a value of $-10,000$ lb. in². the instantaneous principal stresses have the values of 10,000 and zero lb. in². At this instant $\Theta = 61^\circ$. Thus, it is again possible for a second order strike-slip fracture to develop. However, it should be noted that a further requirement must be met before such strike-slip movement can take place, which is that the vertical stress must be the intermediate principal stress, i. e., for this specific example the vertical stress must fall in the range between 5,000 and 10,000 lb. in². However, if, as is possible in this example, the vertical stress falls in the range 10,000 to 15,000 lb. in². it will momentarily be the greatest principal stress, so that the second order shear will be a normal, dip-slip fracture and such a fracture could develop even if the inertial stresses are somewhat lower than the figure quoted.

Thus, depending upon the values of the least and intermediate principal stresses, this mechanism can give rise to either strike-slip or dip-slip second order fractures. The strike of the latter type of fracture will, of course, be parallel to the axis of the larger of the two instantaneous horizontal principal stresses, so that the types of fracture will have the orientations indicated in Figure 3. Such orientations are in agreement with field observations (e. g., Dead Sea Area).

From the calculations presented in this section it follows that, provided large inertial stresses are generated during faulting, second order fractures of one type or another may form. In the following sections a more general study of the conditions which may give rise to such fracturing is carried out. The data which are presented were obtained by repeated calculations of the type used in the preceding paragraphs.

INITIATION OF FIRST ORDER FAULTS

In this section it will be assumed that the regional static stresses are able to initiate first order faults. As in the previous section we will consider a specific example in which the angle of friction of the rock (ϕ) equals 30° and its uniaxial strength is 10,000 lb. in². Consider an example when the least principal stress (σ_3)

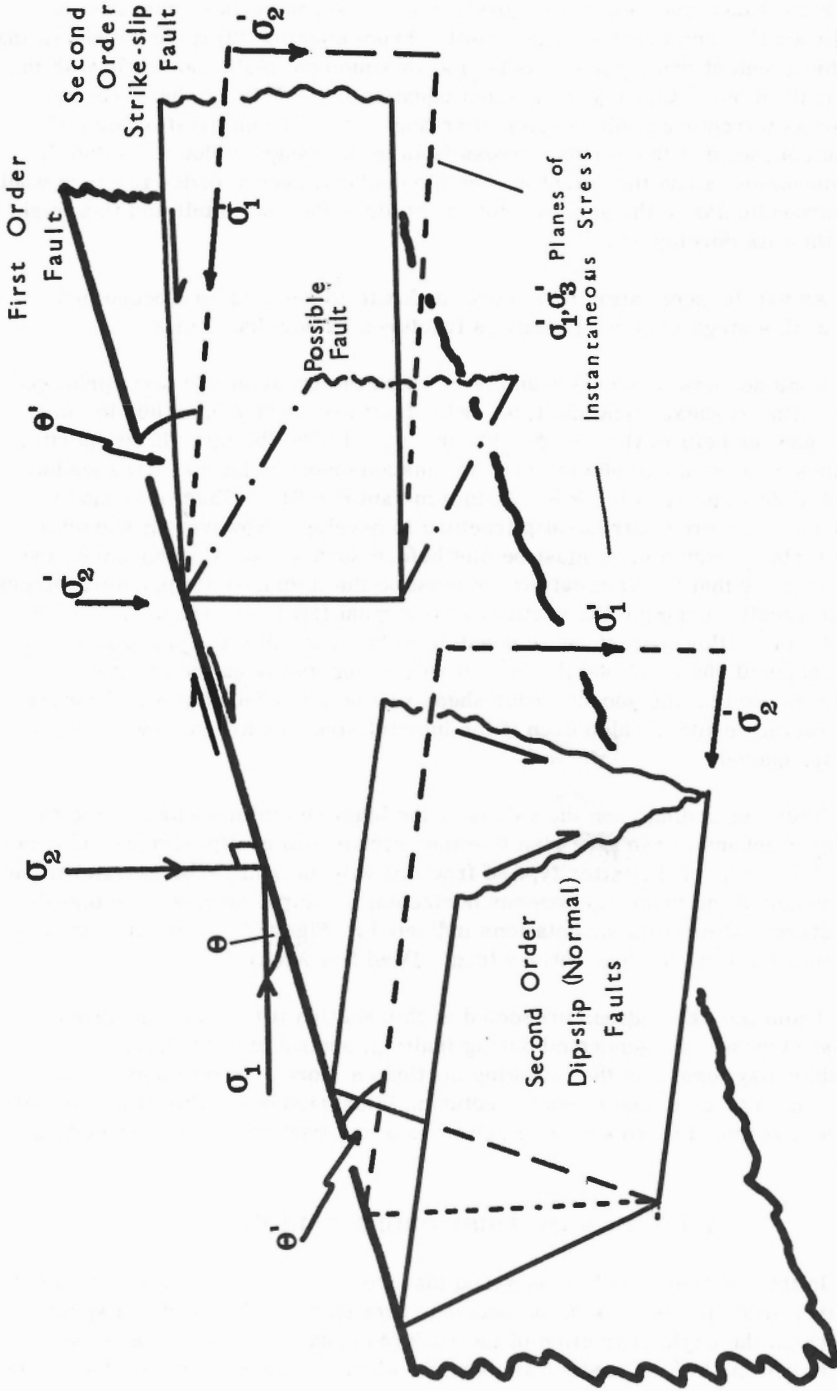


Figure 3. Showing the orientation of (a) second order, strike-slip fractures when the vertical stress is the intermediate principal stress throughout the phase of oscillation and (b) second order dip-slip fracture which may develop when the vertical stress is momentarily the greatest principal stress

is 10,000 lb. in²., then from equation (12), σ_1 at failure is 40,000 lb. in². and from equation (6) the angle between the axis of maximum principal stress and the first order shear plane which will be initiated is 30°. The values of these static stresses are represented on the ordinate axis of Figure 4.

The abscissa of this figure represents various values of compressive or tensile inertial stress which may occur parallel to the first order fault, as it develops. The instantaneous values of the least and greatest principal stresses (σ_1' and σ_3') corresponding to any specific value of inertial stress are represented by curves A and B respectively. The instantaneous failure stress associated with the least principal stress (σ_3') can be obtained from equation (12) and is represented by curve F.

It will be seen that except when inertial stresses are zero (in which case $\sigma_1' = \sigma_1$) the momentary values of the greatest principal stress are everywhere greater than the failure stress.

Because the velocity of the P wave is greater than the rate of propagation of the first order fault, the inertial stresses may give rise, ahead of the developing first order fault, to a zone which contains a host of fractures. Such a weakened zone will permit the first order fault to propagate more readily, but in general, the orientation of the fractures will not be that indicated in Figure 3.

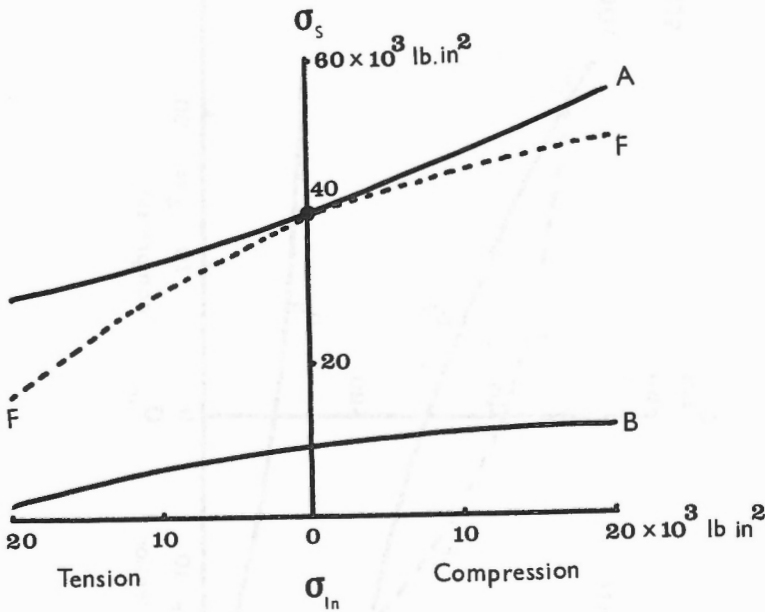


Figure 4. Showing the relationship between inertial stress values and the corresponding momentary values of the greatest and least principal stress (σ_1' and σ_3') in curves A and B. The failure stress corresponding to curve C is given in curve F

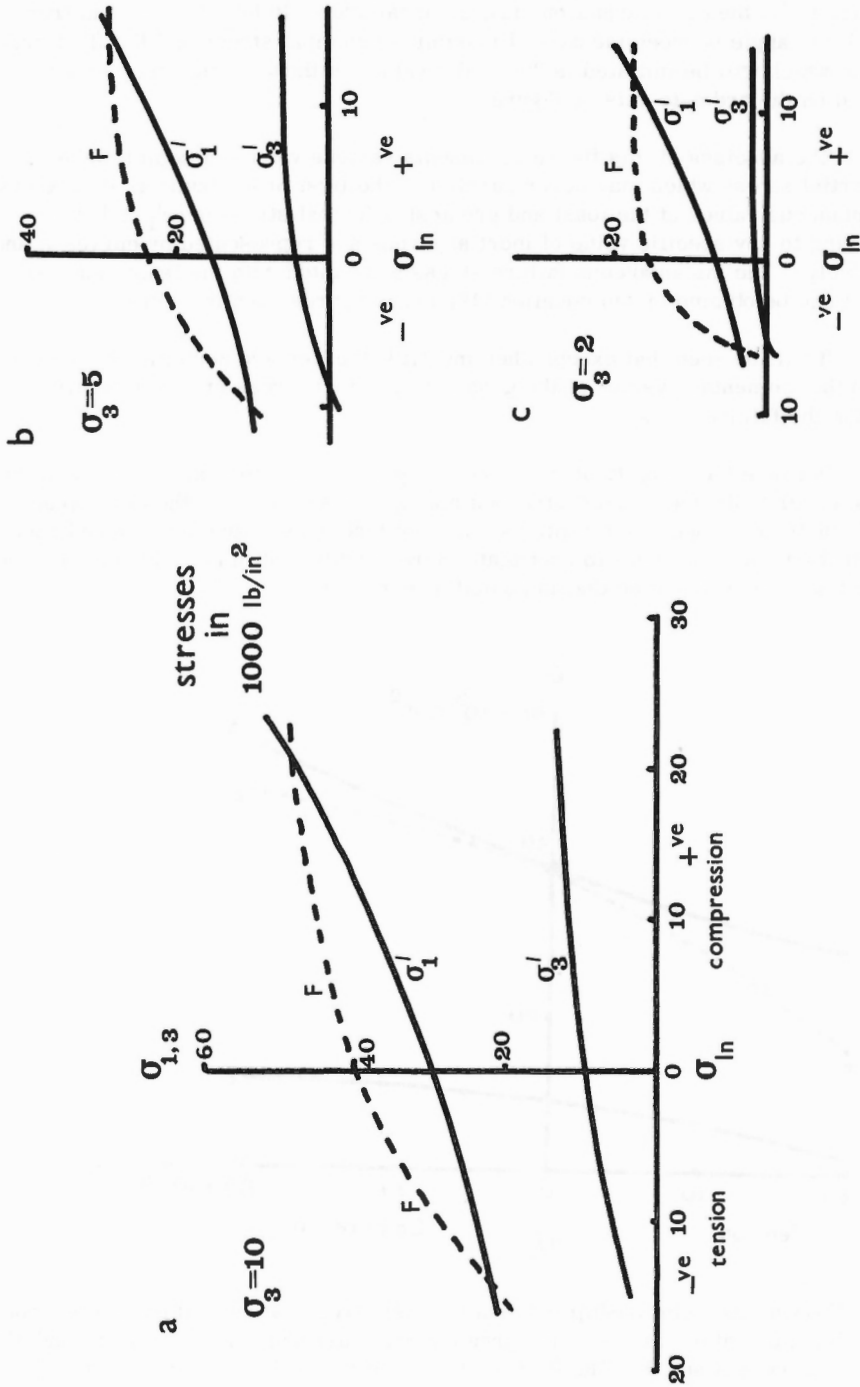


Figure 5. Indicating the relationship between the least and greatest momentary principal stress, with the related failure stress, for various corresponding values of inertial stress, when the least principal static stress has the values of 10,000, 5,000 and 2,000 lb. in². respectively

It may be noted in passing that this shock wave mechanism probably plays an important role in the formation of joint-surface features, i. e. , plumose structures.

RESHEARING ALONG EXISTING FIRST ORDER FAULTS

When considering movement along an existing fracture, the shear stress necessary to initiate such activity is given by equation (2). However, one is no longer limited to the relationship that the maximum principal stress (σ_1 , i. e. , the static stress) must be oriented at an angle θ determined by equation (6). In this instance θ may vary between quite wide limits. However, for ease of presentation of the argument it will first be assumed that $\phi = 30^\circ$ (corresponding to a value of $\phi = 30^\circ$ in equation (6)); the more general case will be considered later.

For the situation under consideration, where C_0 , and hence σ_0 , along the length of the first order fault is zero, the relation necessary to cause fresh movement is given by

$$\sigma_1 = 3. \sigma_3 \quad (13)$$

The initial stress conditions necessary to cause reshearing when σ_3 equals 10,000, 5,000 and 2,000 lb. in². respectively are shown on the ordinate axes of Figure 5 a, b and c. The instantaneous principal stresses (σ_1' and σ_3') corresponding to the appropriate inertial stresses are indicated by the symbols. Because we are interested in the possibility of second order shears, the failure stress condition (Curve F), based on the values of σ_3' , are calculated from equation (12).

It will be seen that for small values of inertial stress σ_1' is less than the failure stress. However, when in Figure 5a the inertial stresses reach a value of -14,500 lb. in². or 22,000 lb. in². , σ_1' equals the failure stress. The corresponding points in Figure 5b and c occur when the inertial stresses attain values of -10,000 and 15,000 lb. in². and -5,250 and 12,000 lb. in². respectively. These points represent possible conditions in which second order fractures may develop. It will be noted that two of the conditions of tensile inertial stress cited above were used as examples earlier in the text and can certainly give rise to second order fractures. The significance of the condition when the inertial stresses are compressive will be considered later.

First order faults may exist and be active throughout many tens or hundreds of millions of years and during this time the stress field may change in orientation and intensities due to agencies other than fault movement.

It has been pointed out that reshearing along a first order fault may take place when $\theta = 45^\circ - \phi/2$ and this condition may be taken to be the general case, which will now be investigated.

If there is to be movement along an existing first order fault plane, then from equations (2) and (5)

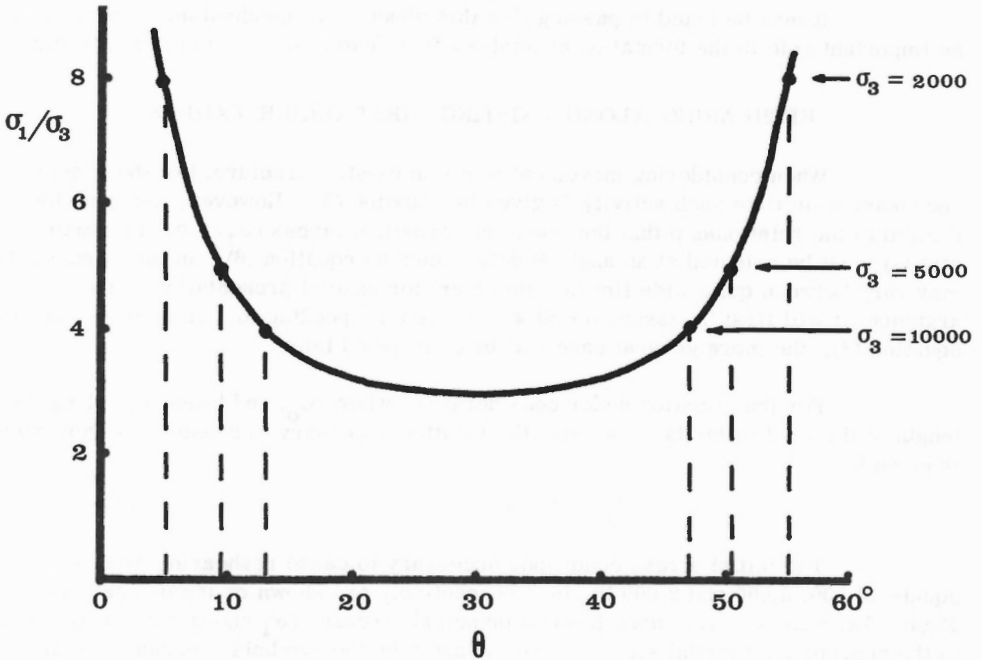


Figure 6. Showing the relationship between the ratios of the principal stresses which exist when slipping occurs on a first order fault and the maximum principal stress makes an angle θ with the first order fault plane. Maximum permissible ratios when σ_3 equals 2,000, 5,000, and 10,000 lb. in². are also shown.

$$\sigma_y \cdot \tan \phi = \frac{(\sigma_1 + \sigma_3)}{2} - \frac{(\sigma_1 - \sigma_3)}{2} \cos 2\theta \quad (14)$$

From equations (7) and (14) it follows that

$$\frac{\sigma_1}{\sigma_3} = \frac{1+d}{1-d} \quad (15)$$

where

$$d = \frac{\sin 2\theta + \cos 2\theta \cdot \tan \phi}{\tan \phi}$$

If, as before, we let $\phi = 30^\circ$, equation 15 can be expressed graphically as a relationship between the ratio of principal stresses (σ_1/σ_3) and θ , see Figure 6. It will be seen that limits are set to the ratio of the principal stresses by the failure conditions (equation (12)) so that when $\sigma_3 = 2,000$ lb. in². $\sigma_1/\sigma_3 = 8.0$ and this ratio is attained only if σ_1 makes an angle of 5° or 55° with the first order fault plane. The corresponding angles when σ_3 equals 5,000 and 10,000 lb. in². are indicated in Figure 6.

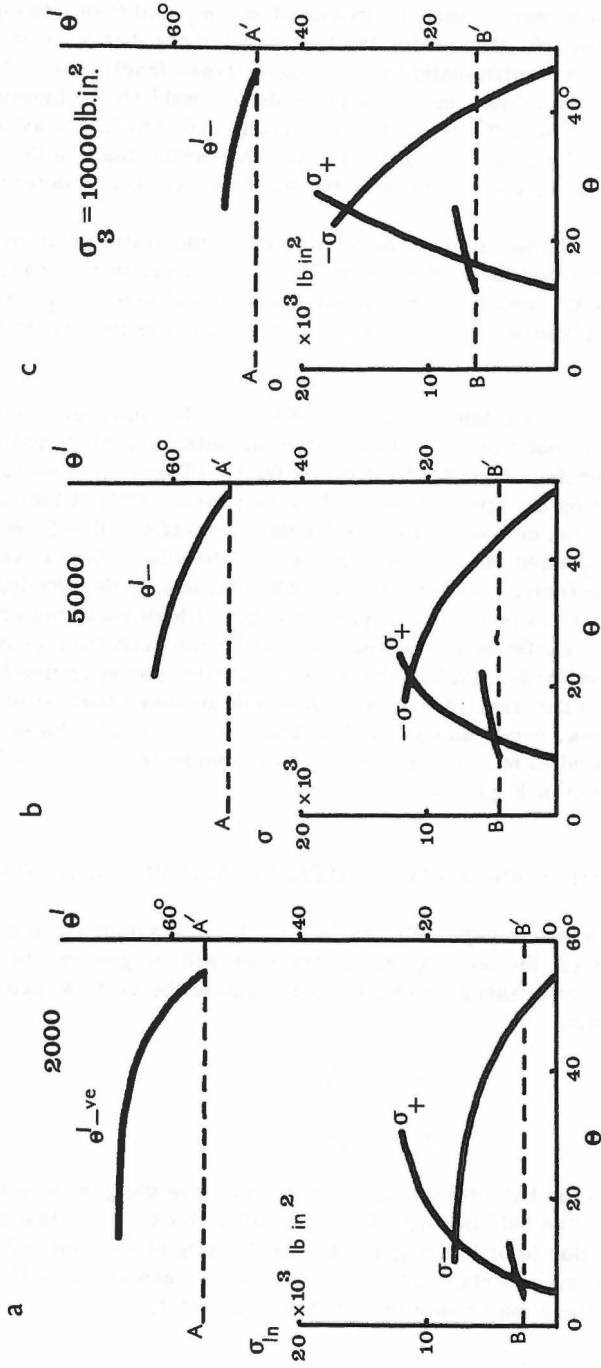


Figure 7. Shows the relationship between the value of the inertial stresses necessary to cause failure for various values of θ . The corresponding value of θ for these data are also shown for values of confining pressure of 2,000, 5,000, and 10,000 lb. in².

Let us now assume that the values of σ_1 , σ_3 and Θ satisfy equation (15), so that movement along the first order fault is possible but that the ratio of the principal stresses is not sufficiently large to cause fresh fracturing. Then, by using the techniques previously described, it is possible to establish the inertial stresses necessary to give a ratio of σ_1'/σ_3' such that second order failure may occur as the result of reshearing along the first order fault. The orientations of the instantaneous principal stresses when these conditions are satisfied can also be determined.

The interrelationship between Θ (the angle the static principal stress σ_1 makes with the first order fault), the inertial stresses necessary to cause second order failure and the angle Θ' , which the instantaneous principal stress σ_1' makes with the first order fault, is given for three values of confining pressure (σ_3) in Figure 7 a, b and c.

In these figures, horizontal lines AA' and BB' represent limiting angles. If the value of Θ' falls between these limits, the instantaneous principal stresses will be dissipated by shearing along the first order fault. (That this is so can be demonstrated by constructing the appropriate Mohr's diagram). Only if the value of Θ' falls outside these limits can new second order fractures develop. It will be seen that this condition occurs only when the inertial stresses are tensile. For the values of σ_3 represented in these figures, the value of Θ' , when failure by the development of new second order fractures is possible, ranges from 45° at high confining pressures to more than 60° at low confining pressures. It may be inferred from equation (6), therefore, that second order, strike-slip shears may develop at angles between 15° and more than 30° to the first order fault. It should be noted that, at low confining pressures, failure may occur as normal 'faulting', in which case, these dip-slip fractures will be parallel to the higher of the two momentary, horizontal principal stresses, as indicated in Figure 3.

INFLUENCE OF PORE-WATER PRESSURE AND UNIAXIAL STRENGTH

Hitherto in this paper, the rocks have been assumed to be dry. In the earth's crust, however, the pore-spaces in the rock will, in general, be filled with a fluid, usually water, at pressure (p) which is related to the vertical geostatic pressure (σ_z) by the expression

$$p = \lambda \cdot \sigma_z \quad (16)$$

where

$$\sigma_z = \rho \cdot g \cdot z. \quad (17)$$

In equation (17) ρ is the bulk density of the wet rock, g is the gravitational constant and z is the depth. The bulk density of rock is often about 2.5, so that the value of λ for water pressure due to ordinary gravitational loading of the fluid will be approximately 0.4. However, in certain circumstances, e. g. when the pore fluid is trapped and unable to migrate, λ may reach the limiting value of 1.0.

The relationship between the total principal stresses ($S_{1, 2, 3}$) and the effective principal stresses ($\sigma_{1, 2, 3}$) are

$$\begin{aligned} S_1 &= \sigma_1 + p \\ S_2 &= \sigma_2 + p \\ S_3 &= \sigma_3 + p \end{aligned} \tag{18}$$

Let us assume that S_2 for all examples and data so far given is equal to 20,000 lb. in². For one group of data $\sigma_3 = 10,000$ lb. in². and $\sigma_1 = 30,000$ lb. in²., therefore, because S_2 is fixed at 20,000 lb. in²., σ_2 must fall in the range 10,000 to 20,000 lb. in². so that p must be in the range 0 to 10,000 lb. in². and hence $\lambda = 0$ to 0.5. For the other groups of data, when σ_3 equals 5,000 and 2,000 lb. in² and $S_2 = 20,000$ lb. in². the range of values for λ are 0.25 to 0.75 and 0.7 to 0.9 respectively. These groups of examples therefore cover most values of λ likely to occur in nature.

It has been shown (Price, 1958) that pore-water pressure has little or no influence upon the angle of friction (ϕ), so that k too is unaffected. However, pore-water causes a reduction in the uniaxial strength which may be as much as 50 per cent if the rock has a porosity of 10 to 20 per cent.

If it is assumed that the rock type under discussion, with a uniaxial dry strength of 10,000 lb. in²., has a strength of 5,000 lb. in². when wet, the relationship between effective principal stresses at failure is given by

$$\sigma_1 = 5,000 + 3. \sigma_3$$

The values of inertial stress necessary to cause second order failure, when $\sigma_0 = 5,000$ lb. in². through a range of confining pressures when the maximum principal static stress makes an angle of 30° with the first order fault, are indicated in Figure 8.

If fault movement is controlled by a massive competent unit, while the units above or below are considerably weaker, second order failure may occur in the relatively incompetent material when the inertial stresses are relatively small. The inertial stresses necessary to cause failure in material with a uniaxial strength of 2,000 lb. in². and value $k = 3.0$ are also indicated in Figure 8. If k is less than 3.0 there will be a corresponding decrease in the magnitude of the inertial stresses necessary to cause second order failure.

If the angle which the maximum principal static stress (σ_1) makes with the first order fault is significantly different from 30°, then from the arguments presented in the previous section, the inertial stresses necessary to bring about second order failure will be further reduced, reaching zero magnitude at the various limiting angles.

It follows from these arguments that the intensity of inertial stress necessary to initiate second order faulting depends upon a number of factors. But in

many instances, especially when the rock is weak, pore-water pressure is high, the effective least principal stress is low and the angle between the axis of greatest principal static stress and the first order fault is between 40° and 50°, the magnitude of the inertial stress needed to cause second order fracture may be quite small: as little, perhaps as a few hundred, or at most a few thousand pounds per square inch.

FREQUENCY AND AMPLITUDE OF VIBRATION

It has been noted that the inertial stress is related to the frequency (f) and the amplitude (u) of vibration by

$$\sigma_{In} = K.f^2.u \quad (3)$$

If it is assumed that the density of the rock is 2.7 and that the displacement, or amplitude of vibration (u) is measured in inches, then the inertial stress is given in pounds per square inch when the constant K has the value 3.8×10^{-3} . This expression is represented graphically in Figure 9 for values of stress up to 3,000 lb. in². and amplitudes of vibration of 0.5, 1.0, 2.0 and 10.0 inches. It will be seen that if the amplitude of the shock wave is about 0.5 inch, the frequency of vibration necessary to

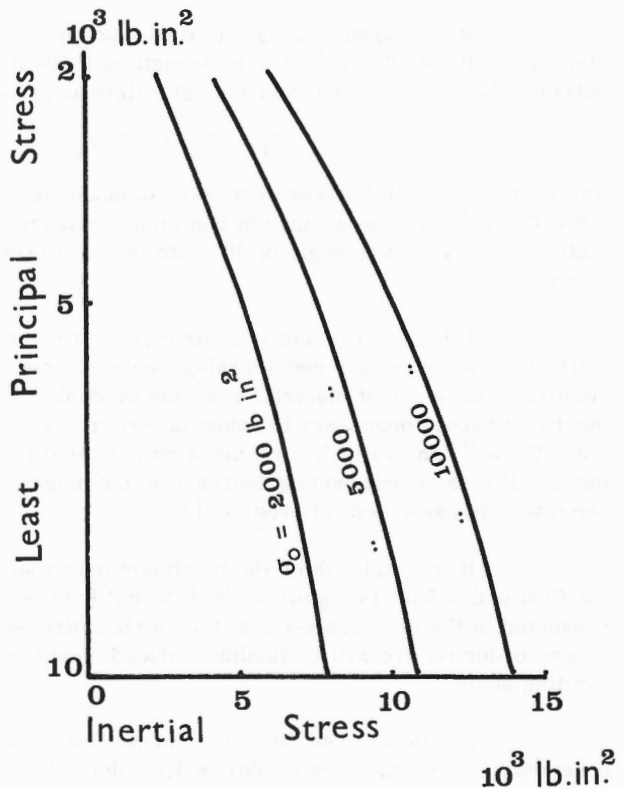


Figure 8.

Showing the relationship between inertial stress necessary to cause failure for specific values of the least principal stress and uniaxial strength (when the maximum principal stress makes an angle of 30° with the first order fault plane).

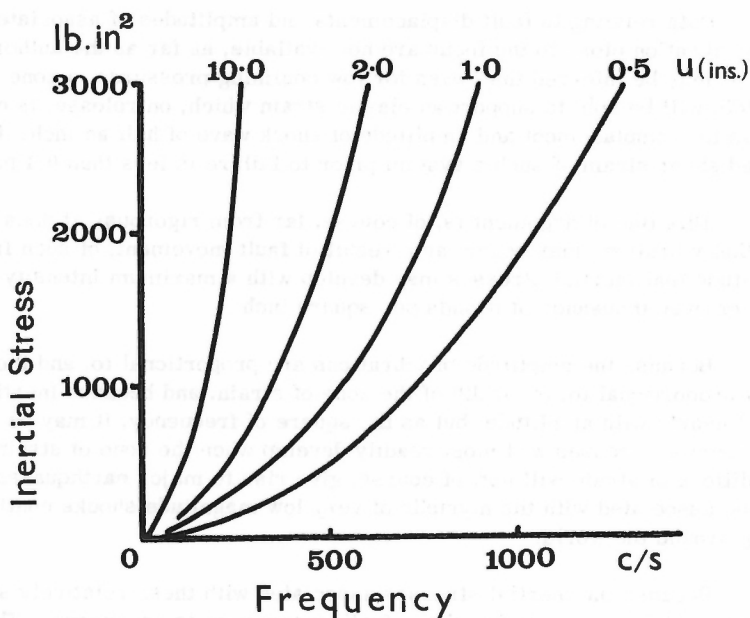


Figure 9. Relationship between frequency (f) and displacement (u) for values of inertial stress up to 3,000 lb. in².

generate an inertial stress of 2,000 lb. in². will be approximately 1,000 cycles per second. Such a frequency is two, or even three orders of magnitude higher than those which usually figure in the seismographic records of major earthquakes. However, these records are often obtained at some distance from the earthquake focus.

The model postulated here relates to wave conditions within a reasonably close proximity to the focus and in this context, Bullen (1953) states "in near earthquakes, waves of periods of less than 0.01 seconds may be significant" (p. 146). Further, Ambraseys (personal communication) has recently shown from theoretical arguments that the frequency of vibration associated with sudden fault movement in solid rock is related in a linear fashion to the width of the zone of strain adjoining a fault plane. He estimates that a transient vibration with a frequency of about 1,000 cycles per second would be initiated if the strain extended in a narrow zone some 35 feet on either side of a fault plane were released by sudden movement along the plane¹.

¹This width of zone is possible if the stresses immediately following failure fall to zero. For more probable conditions when there are residual stresses, the width of the zone will be correspondingly reduced.

Data relating to fault displacements and amplitudes of associated high frequency vibration close to the focus are not available, as far as the author is aware. However, it may be inferred that, even for low confining pressures, a zone some 70 feet in width will be able to support an elastic strain which, on release, is capable of giving rise to a displacement and amplitude of shock wave of half an inch: for the distributed shear strain of such a system prior to failure is less than 0.1 per cent.

This line of argument is, of course, far from rigorous; it does however indicate that vibrations may occur, as a result of fault movement, of such frequency and amplitude that inertial stresses may develop with a maximum intensity of many hundreds or even thousands of pounds per square inch.

Because the amplitude of vibrations are proportional to, and the frequency inversely proportional to, the width of the zone of strain, and because inertial stresses increase linearly with amplitude, but as the square of frequency, it may be inferred that high inertial stresses will most readily develop when the zone of strain is narrow. Such conditions of strain will not, of course, give rise to major earthquakes, but are likely to be associated with the myriads of very low magnitude shocks continually occurring around the world.

Because the inertial stresses associated with these relatively small disturbances act for very brief periods, further comment is necessary. The Navier-Coulomb criterion of failure used in this paper is independent of time. It is known, however, that rock failure is influenced by the duration of application of load. For tests of long duration (i. e. many weeks) the failure strength is significantly below the level of stress the rock will support if the load is applied at the usual test rate of 100 lb. in² per sec. If the failure load is applied in milliseconds the strength is further increased. Data for concrete (Evans, 1958) show that for times to failure between 10 seconds and 0.01 seconds the strength is essentially constant but increases for tests of shorter duration (0.001 sec) by approximately 25 per cent. Assuming this relationship can be applied to rock, then, for the sake of this analysis, whenever strength data are quoted we merely assume that these data refer to the 'milli-second' strengths and that the equivalent standard-test strengths would be some 20 - 30 per cent lower.

DEVELOPMENT OF SECOND ORDER FAULTS

It will be realized that, while the wave train lasts, the states of stress around the first order fault are continually varying. Nevertheless, for a portion of one cycle the variation is not great, so as a first approximation the stress field can be considered to be constant in orientation and intensity for a short time 't' which has a duration of about 10 per cent of one cycle of vibration. The length (L_t) of a second order fracture which may develop during the passage of one P wave will therefore approximate to

$$L_t \approx V_f/10.f$$

where V_f is the velocity of propagation of the fracture. For the stress environment

envisaged V_f may be as high as 10,000 feet/sec. If the frequency of the P wave is 1,000 cycles per second then the length of the second order fracture which may develop during one cycle will be about one foot. Once this fracture has formed it can be extended and propagate with every successive cycle of vibration. Hence, from a sequence of P waves resulting from one increment of movement along a first order fault a small second order fault, a few feet or tens of feet may develop. The presence of such a minor second order fault introduces a degree of anisotropy into the problem, so that repeated movement and propagation of this minor fault can take place more readily during shocks due to further increments of movement on the first order fault: for slip on the second order fault can now occur at values of transient principal stress of smaller magnitude than those necessary to initiate second order failure.

Thus, although the second order structure is initially of very limited extent, it can, through successive cycles of vibration and during successive increments of slip along the first order fault, develop into relatively large-scale structures.

INFLUENCE OF INERTIAL STRESSES DUE TO S WAVES

It is convenient at this point to consider briefly the influence of the inertial stresses due to the S waves. In this simple treatment it will be assumed that the values of the inertial stresses due to the S waves are equal in magnitude to those generated by the P waves. Only two instances will be considered, they are that the inertial stresses due to the P waves and the S waves are either exactly in phase or exactly out of phase.

The initial stress conditions assumed in this example are $\sigma_3 = 10,000$ lb. in². and $\sigma_1 = 30,000$ lb. in². acting at an angle $\theta = 30^\circ$ to the first order fault. The relationship between the instantaneous principal stresses (σ'_1 and σ'_3) and the inertial stresses when the P and S waves are in and out of phase are represented in Figure 10 a and b respectively.

It will be seen in Figure 10 a that when both the inertial stresses are compressive, second order failure is not possible. However, when both the inertial stresses are tensile and attain a value of 5,000 lb. in². second order failure is possible; moreover, it will be noted, this is a lower value than need be reached by the inertial stress due to the P wave alone (see Fig. 5 a). When the stresses are out of phase failure can occur when the inertial stress due to the P wave reaches -14,000 lb. in². (a value which is comparable to that necessary to cause second order failure when only the P wave operates). However, failure conditions are reached when the P wave reaches a value of only 4,000 lb. in². When this condition is attained $\theta' = 20^\circ$, so that these stresses will be dissipated by causing further movement along the first order fault.

In general, therefore, one may conclude that although the S waves may help, they probably add only a little to the development of second order faults.

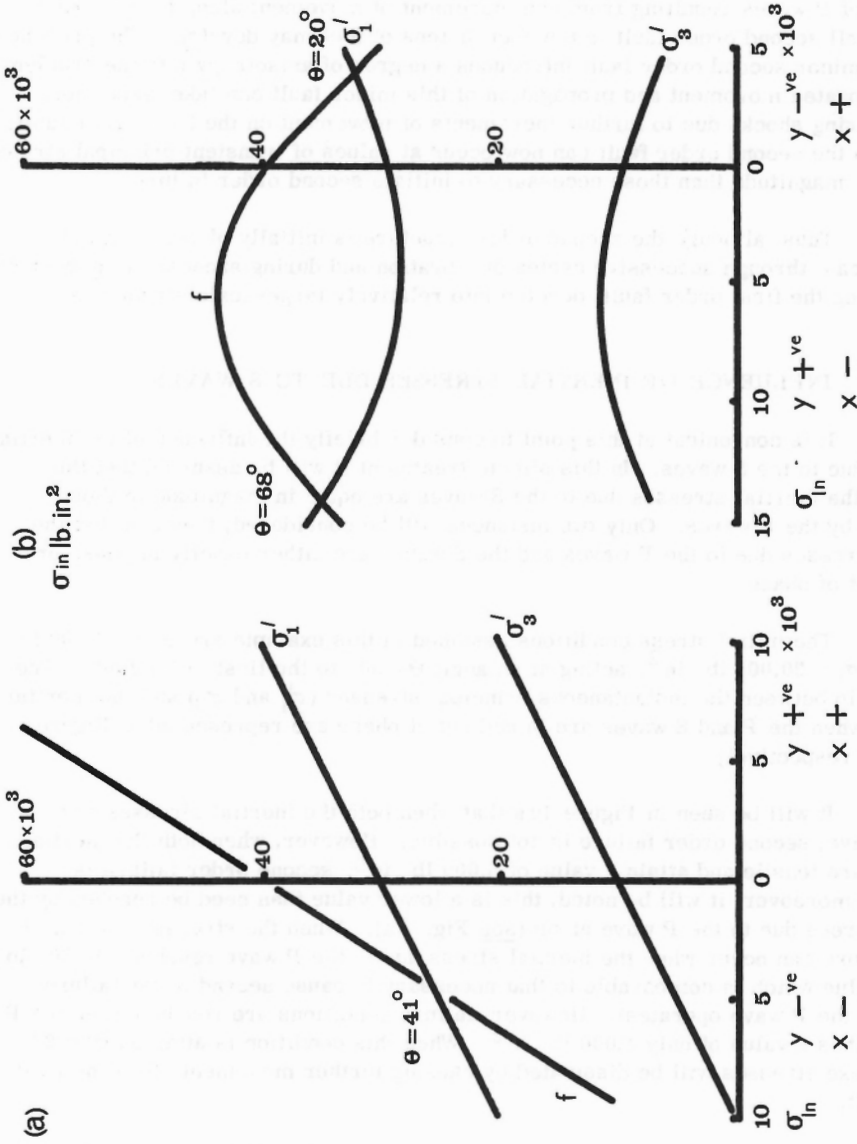


Figure 10. Indicating influence of S on P wave stresses on instantaneous values of greatest and least principal stresses when the associated are equal in magnitude and (a) in phase and (b) 90° out of phase.

ZONE OF SECOND ORDER FAULTING

The direction of propagation of shock waves has hitherto in this paper been assumed to be in a direction parallel to the first order fault. This assumption holds as a close approximation adjacent to the main fault plane itself. However, the area of strain initiating the shock wave may be small compared with the extent of the main fault. The wave-front, in the horizontal plane, resulting from such a relatively small source of disturbance will be approximately circular. Assuming the focus of disturbance (I), in Figure 11 a, is at such a distance (d) from elements Q, Q' etc. that the wave-front acting on any of these elements may be taken as linear, with the direction of vibration of the P wave acting along the radius centred at I, then, at point Q', the component of inertial stress parallel to the main fault will be

$$\sigma_{In_x} = \sigma_{In} \cdot \cos^2 \Psi$$

and

$$\sigma_{In_y} = \sigma_{In} \cdot \sin^2 \Psi \quad (20)$$

If it is assumed that the inertial stresses are just able to cause second order failure at point Q adjacent to the first order fault, the stress intensities at points Q' etc. obtained by introducing equation (20) into the analysis are expressed as percentages of the instantaneous failure stress. These data are plotted against Ψ in Figure 11b where Ψ' etc. are the angles that IQ' etc. make with the first order fault. The relative rapid fall-off in intensity of the instantaneous stresses away from the first order fault, indicated in this figure, can be invoked to explain why second order faults occur in relatively narrow zones on either side of the first order fault.

RECAPITULATION AND CONCLUSIONS

It has not been possible to explain the development of second order, strike-slip faults by using the approach in which only the static stresses before and after faulting are considered. However, increments of fault displacement frequently occur so quickly that the movements generate vibrations of the rock mass. In certain circumstances the frequency and the amplitude of the shock waves and the stresses associated with these vibrations can so alter the static stress field that the orientation and intensities of the principal stresses are momentarily such that small second order fractures may develop. These fractures, it is suggested, propagate and extend with the passing of every shock-wave and during subsequent increments of movement of the first order fault.

Depending upon the initial stresses, particularly the intensity of the vertical principal stress, the second order fractures which develop may be either strike-slip or dip-slip structures.

The intensity of the transient inertial stresses necessary to cause second order fractures are relatively high, but are lowest when the rock is weak, the pore-water pressure is high, the least effective principal stress is low and the angle which

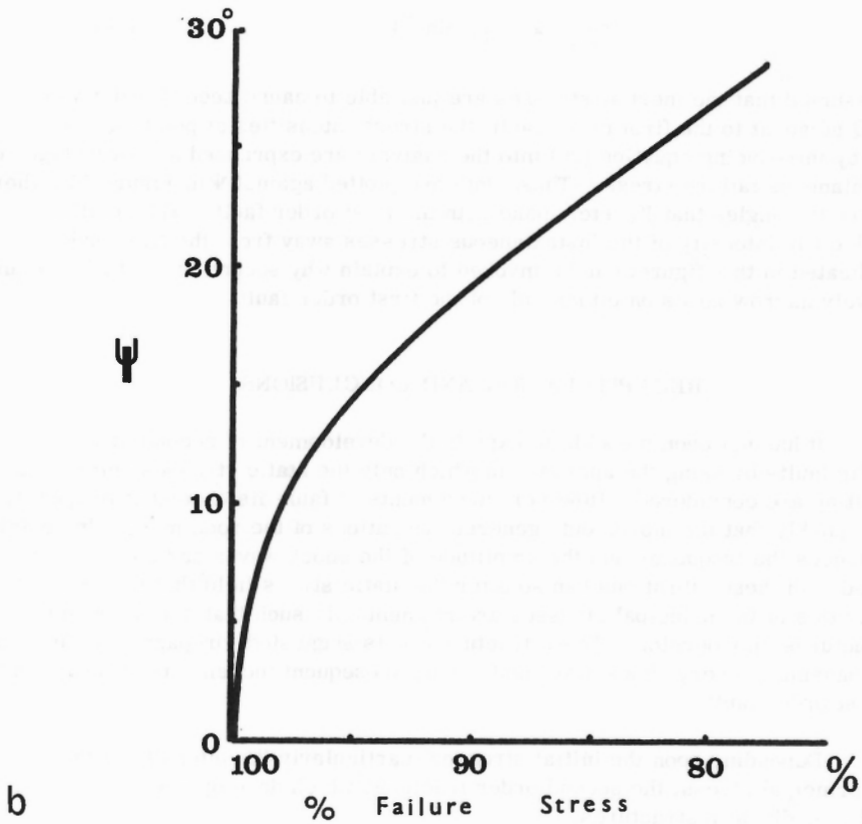
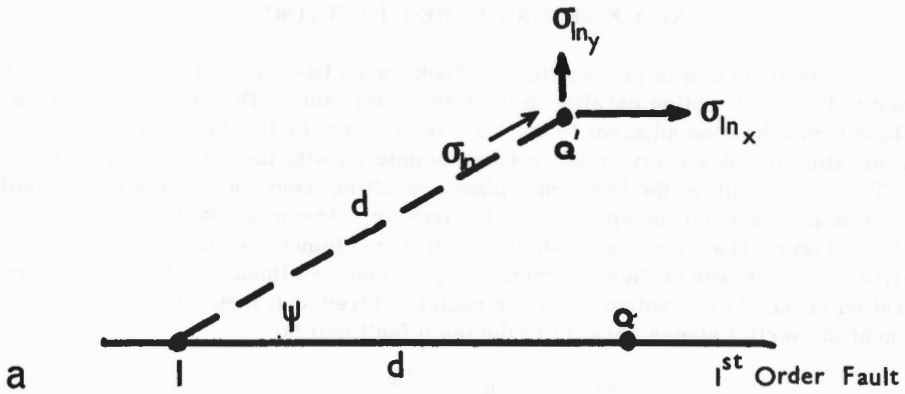


Figure 11a. Schematic representation of inertial stresses for a circular wave front when resolved parallel and perpendicular to the first order fault plane.
b. Relationship between ψ and failure stress for a value of inertial stress just able to cause failure when $\psi = 0$

the axis of greatest principal stress makes with the first order fault is relatively high (40° - 50°). These conditions may appear somewhat special, nevertheless, it may transpire that second order faults only develop when most of these various conditions are satisfied.

ACKNOWLEDGMENTS

The author wishes to express his indebtedness to his colleagues, Prof. J. G. Ramsay and Dr. E. Hoek, for their critical reading of the manuscript and particularly wishes to thank Dr. N. Ambraseys for his many helpful suggestions and generous permission to quote the results of unpublished work.

REFERENCES

- Anderson, E. M.
1951: The dynamics of faulting and dyke formation with applications to Britain; Edinburgh, Oliver and Boyd, 2nd ed.
- Bullen, K. E.
1953: An introduction to the theory of seismology; Cambridge Univ. Press, 2nd ed.
- Chinnery, M. A.
1966: Secondary faulting; Can. J. Earth Sci., vol. 3, No. 2, pp. 163-190.
- Evans, R. H.
1958: The effect of rate of loading on some mechanical properties of concrete; Proceedings Conference on mechanical properties of non-metallic brittle materials, London, Butterworth.
- Jaeger, J. C.
1964: Elasticity, plasticity and flow; London, Methuen.
- McKinstry, H. E.
1953: Shears of the second order; Am. J. Sci., vol. 251, pp. 401-414.
- Price, N. J.
1958: A study of rock properties in conditions of triaxial stress; Proceedings Conference on mechanical properties of non-metallic brittle materials, London, Butterworth.
1966: Fault and joint development in brittle and semi-brittle rock; London, Pergamon.

DISCUSSION

T. B. Anderson pointed out that according to Dr. Price's hypothesis, the orientation of the second order fractures depends not only on the orientation of the stress field, but also on the values of the inertial stresses. These inertial stresses are generated as a series of pulses and in succeeding pulses the stress values are not likely to be exactly the same. If the splay is growing as a series of small increments, orientation of these increments should therefore change slightly and the splay might be obviously curved. He asked the author if he had observed curved second order fractures.

The author mentioned that second order fractures are generally of the order of 3 to 10 feet and seem to be reasonably straight. He suggested that larger fractures might appear as valleys or gullies, but he did not know of any data pertinent to this problem.

K. Barron (written comments)

1. I understand that, in general, a second order fault stems out from only one side of the first order fault in the manner illustrated by Price in Figure 1. Price suggests that the second order fault is created by the action of the stress wave on a flaw ahead of the propagating first order fault, this stress wave being created by and preceding the propagating first order fault. If this is so, why should this second order fault be formed so conveniently that, when the propagating first order fault reaches it, it stems out from only one side of the first order fault rather than, in general, cutting across it?

2. Assuming that the second order fracture is formed as suggested, what happens when the propagating first order fault reaches it? Price suggests that the first order fault proceeds along its path as if the second order fault did not exist. From two points of view, I doubt that this is the case:

(a) The redistribution of the local stresses due to the second order fracture would, in my opinion, be highly likely to affect the direction of propagation of the first order fault, even locally.

(b) The first order fault will propagate in a direction that demands minimum energy loss from the system. When the first order fault hits the second order fracture the energy will be split between the two systems and, depending on the orientation of the second order fault, could result in an extension of both the first and second order faults, or a deviation of the first order fault along the second order fault, or finally the case Price suggests. With the orientation shown in Figure 1, of Price I think that the last case would be the more remote possibility.

3. Whilst not denying the possible mechanisms suggested by Price, I believe that it is not necessary to assume that a high magnitude stress wave is generated by the propagating first order fault and that a flaw exist in its path, in order to postulate mechanisms of second order faulting.

Two possible mechanisms come to mind:

(a) To regard the propagating first order fault as a long thin ellipsoidal crack and examine, in a general manner, the energy balance of the system when a crack of length $2c$ extends by an increment dc .

(i) There is a loss in potential energy of the externally applied forces due to the displacements reduced by crack propagation. If W is the total potential energy of the external forces, the change in W due to a change in crack length is dW/dc .

(ii) There is a gain in the excess strain energy in the material around the crack due to lengthening of the crack. If the initial excess strain is We , the gain in We due to change of length dc is dWe/dc .

(iii) There is a gain in the surface energy of the crack because of the creation of the new surface. If the initial total surface energy is Ws then the change of Ws due to the change of dc in crack length is dWs/dc .

(iv) There is a gain in the kinetic energy of the system due to propagation of the crack. If the total kinetic is initially Wk , this increase due to extension dc is dWk/dc .

Thus, ignoring any expenditure of energy in plastic deformation (i. e. assuming brittle behaviour), since energy balance must be maintained then:

$$\frac{dW}{dc} = \frac{dWe}{dc} + \frac{dWs}{dc} + \frac{dWk}{dc} \quad (1)$$

Now it can be shown (Love, 1906) that

$$\frac{dWe}{dc} = \frac{1}{2} \frac{dW}{dc} \quad (2)$$

and thus (1) becomes:

$$\frac{dWe}{dc} = \frac{dWs}{dc} + \frac{dWk}{dc} \quad (3)$$

For a slowly moving crack $dWk/dc \approx 0$ and $dWe/dc = dWs/dc$ which has been shown to be the same as Griffith's criterion for fracture initiation at a crack (Griffith, 1925).

Now, in a crack which propagates it has been shown (Craggs, 1960) that the force required to maintain a steady rate of extension of the crack decreases as the rate increases and that there is a limiting velocity of propagation of a single crack. Once a crack reaches its terminal velocity the kinetic energy associated with crack extension will also become constant. However, the released energy increases with crack length and thus this additional energy can only be dissipated by the formation of a new crack surface. This results in the well known phenomenon of forking or branching of a crack and the production of additional cracks at an angle to the original.

Could not, therefore, this be a possible explanation of secondary faulting?

(b) Another possible mechanism for secondary faulting is suggested from the work of Hoek (1965) who studied the initiation of fracture from artificially induced closed cracks in glass, loaded under static stress conditions. Figure A is a photograph reproduced from Hoek's work. It appears to me that the generation of the short fractures along the length of the initial closed crack could well be analogous to what might be regarded, on a larger scale, as secondary faulting.

The mechanism suggested by Hoek to explain this phenomenon can be briefly described as follows: Due to irregularities in the crack surface, sections of the crack are forced into intimate contact and develop a high frictional shear resistance when the crack is subjected to compressive stress. Between these sections of high shear resistance one can visualize short open Griffith's cracks. Fracture first initiates at or near the tips of these short open cracks, producing the 'secondary faulting'. As the applied stress level increases, a stage is reached when the frictional shear resistance due to contact between the crack surfaces is overcome. At this stage the initial crack can be regarded as a Griffith's closed crack and eventually fracture initiation will take place at the ends of this closed crack.

I emphasize, that the two mechanisms suggested above do not invalidate Price's argument. I propose them merely to point out that there is insufficient experimental evidence in existence to allow unique solutions to these problems to be established.

References

1. Love, A.F.H. A treatise in the mathematical theory of elasticity; 2nd ed., Cambridge Univ., Press London, 1906.
2. Griffith, A.A. Theory of rupture; Proc. 1st Int. Congress App. Mechanics, J. Waltman Press, Pelft, 1925.
3. Craggs, J.W. On the propagation of a crack in an elastic-brittle material; J. Meek a Phys. of Solids, vol. 8, pp. 66-75, 1960.

4. Hoek, E. Rock fracture under static stress conditions; N.M. E. R. I., C. S. I. R., Pretoria, South Africa, Report MEG 383, October, 1965.

Dr. Price (submitted the following reply) With reference to the first two points made by Mr. Barron, I would like to emphasize that I conclude in my paper that second order faults do not develop when the first order fault is itself propagating, but rather do they result from reshearing of an already existing first order fault. Hence problems of deviation of the first order fault do not arise.

As to the question why second order faults sometimes develop on one side of the first order fault (in any one exposed locality: this may be attributed to the behaviour pattern, noted by Coates (this volume), i. e. only a single stress pulse may occur with one movement of the first order fault. It will be recalled that second order fractures are associated only with the tensile pulse, so that such fractures can only occur in the far fault block (Fig. 1 of my paper) to the left of the source of the shock wave and to the right of the source in the near fault block.

With reference to the energy argument and the Griffith crack mechanism, Mr. Barron's suggestions certainly are feasible especially as regards the development of the 'tensile feather-fractures' so often associated with minor first order shears. However, it would be necessary to explain how such tensile fractures eventually turn into second order shear fractures. Also, I am tempted to enquire in turn of Mr. Barron how he would explain the frequently observed fact that tensile feather-fractures occur only on one side of the first order fault.

D. F. Coates (written comments) Those of us working in rock mechanics heartily congratulate the organizers of this conference as it focuses attention on an area of geology where we would like to have more answers. Specifically, it would be very helpful in analyzing ground control problems to have more information, either conceptionally or empirically, on the probable stress regimes associated with various structural features. For this reason, we are particularly grateful to contributors like Dr. Price who are willing to enter into this difficult border zone. Having tried to make a contribution in this area myself, I have a distinct awareness of the problems that must be faced regarding boundary and deformation conditions that are implied by the various structural actions.

In the case of this paper, I would offer some comments and ask some questions that may be of assistance to those who are doing the real work in advancing this subject. The concept of explaining some commonly observed fracture or joint patterns by the transient, or dynamic, stresses associated with sudden fault action is very ingenious. It is conceivable that some combination of static and transient stresses may explain some of the fracture

phenomena observed. The concept is similar to that which has been suggested as the source of signals emitted by rockbursts and recorded on seismographs. In this latter case, it has been suggested that a relief wave originates at the pillar which has burst and a compressive shock wave is generated at the abutments by the sudden redistribution of stresses.

In the case of faults, I would envisage that the relief of stress implied by faulting could produce a relief wave with a magnitude, or amplitude, no greater than the pre-existing stress, be it compression or shear. Hence, these dynamic stresses need not be assumed completely arbitrarily and their directions should be such as to be radiating from the point or area of release and hence unlikely to be planar. Also, as the initial disturbance would be in the nature of a shock, or have a conventional oscillatory wave, it is improbable that the input would be in the nature of vibrations unless the faulting occurs in a rapid series of slip-stick failures. Signals that are picked up some distance from the fault can be oscillatory due to the change that will occur in a shock wave as a result of radiation from its source and also as a result of reflection and refraction from discontinuities.

The effective stress concept has been mentioned also in this paper and the example presented might be clarified. The principle, as originated in soil mechanics, can be expressed as follows:

$$\begin{aligned}\tau_f &= c + (\sigma - u) \tan^2 (45 + \varphi/2) \\ &= c + \sigma \cdot k\end{aligned}$$

where τ_f = the shear stress on the plane of failure c = the intercept on the Y-axis of the failure envelope plotted on a Mohr diagram, σ = the total normal stress on the plane of failure, u = the pore pressure, φ = the angle of inclination of the failure envelope, σ = the effective normal stress and $k = \tan^2(45 + \varphi/2)$. As such, it is not expected that the pore pressure, u , would have any effect on the angle defining the failure plane, $45^\circ + \varphi/2$; although it is known that some minerals have different coefficients of friction when they are wet and when they are dry. Furthermore, any effect on apparent strength, ignoring such transient conditions associated with relatively high strain rates with respect to permeability, should occur through the presence of pore pressures and should not be related to porosity. It would be helpful to know if the author agrees with these concepts.

The actual examples cited are interpreted as follows:

$$\sigma_1 = Q + k\sigma_3$$

or $(\sigma_1 - u) = Q + k(\sigma_3 - u)$

or
$$\sigma_1 = Q + k\sigma_3 - u(k - 1)$$

Where Q is a constant the maximal compressive strength when $u = 0$.

It is stated that the dry strength of the sample is 10,000 psi and the apparent strength when wet is 5,000 psi; in other words, the total major principal stress at failure is 5,000 psi and the total minor principal stress is 0, e. g.,

$$5,000 = 10,000 + 3 \times 0 - u(3 - 1)$$

hence
$$u = 2,500 \text{ psi}$$

Therefore, if it could be assumed that the pore pressure would remain constant at 2,500 psi under all loading conditions, which would not normally be a good assumption, the following equation could be written

$$\sigma_1 = 5,000 + 3\sigma_3$$

This looks like the same equation given by the author, except that the above equation is in total stresses as opposed to effective stresses. Perhaps the author could clarify or correct my interpretation of his data.

Dr. Price (submitted the following reply) The inertial or pulse stresses assumed in my paper were less than the pre-existing stresses. Also, a recent paper (Idriss and Seed, Report Soil Mech. and Bit. Matls Lab. California, Berkley, April, 1966) indicates that even at some distance from the source, pulse stresses can attain values of about 1,000 lb. in², so that near the source stresses of the magnitude needed to enable the shock mechanism to produce second order fractures will almost certainly be available.

I agree with Coates that if an increment of fault displacement occurs as a single movement and does not involve a stick-slip oscillation, then close to the source, any shock will occur as a single pulse and not as an oscillatory wave. However, a first order fault formed by brittle fracturing may develop from thousands, or even tens of thousands of separate increments of movement. These increments and their attendant shock pulses would provide ample opportunity for a small second order fracture to develop into a fault even if the inertial stresses occurred as a single pulse per movement rather than as an oscillatory wave.

With reference to the pore-water pressure, I have found that the uniaxial strength of saturated rock was less than 50 per cent of its oven-dry strength. The reduction in strength, I suggest, is due more to the reduction of the surface energy of the rock by the adsorbed water than to the mechanical

effect of pore-water pressure. One specific rock type (Darley Dale Sandstone) has a dry strength of a little over 10,000 lb in² and a rock strength of 5,000 lb in² (c.f. the data used in the paper). The estimated pore-water pressure developed in the rock in the wet uniaxial test was of the order 250 lb in². This pressure is less than 10 per cent of the pore-water pressure postulated in the paper, so in view of the other simplifying assumptions in the presented analysis, I felt that little error would be incurred in assuming that all the reduction in strength in uniaxial tests of wet rock could be attributed to a reduction in surface energy rather than to a mechanical effect of the pore-water pressure.

FRACTURE AS A MECHANISM OF FLOW IN NATURALLY
DEFORMED LAYERED ROCKS

D. W. Stearns
Texas A&M University
College Station, Texas

Abstract

Fracture as a mechanism of flow (cataclasis) has long been recognized by experimenters and field geologists alike. Therefore, there is nothing profound to be said about the phenomenon itself. However, the parameters affecting the phenomenon as an active agent in geological deformation have received very little attention. Examination of natural examples of cataclasis and the apparent controls affecting the mechanism suggest that the role of cataclasis has not always been evaluated properly by geologists. In particular, it forces a way of thinking that questions certain ill-defined concepts such as 'competency' and 'bulk behaviour'. It also leads to conclusions concerning the changes in the behaviour characteristics of certain rocks during the deformation. Certain rocks behave as brittle materials early in the deformation and as a result are able to respond in a ductile manner later in the deformation.

Cataclasis can be an active mechanism on all scales from grain to grain up to total sections several thousand feet thick. A given rock type can behave as a brittle member in one part of the structure and a ductile member in another part of the structure. The fracturing involved ranges from well ordered to completely unordered. Some of the parameters that seem to control cataclasis observed in natural studies are: rock type, total strain or strain rate, bedding thickness, degree of contrast in physical properties of adjoining layers, scale, and structural style. The most important control results from various combinations of these parameters.

INTRODUCTION

Fracture as a mechanism of flow (cataclasis) has long been recognized by experimenters and field geologists alike. However, cataclasis is not usually regarded as an active large-scale agent in geologic deformation. More frequently the field geologist restricts the concept of cataclasis to the formation of mylonites or certain metamorphic textures. Handin (Handin and Hager, 1957) observed cataclastic flow as a phenomenon in the experimental deformation of sandstones and states: "Cataclastic flow involves displacements of constituent grains of an aggregate relative to one another, accompanied by mechanical granulation, breaking, or crushing of grains". This definition properly describes the behaviour of small laboratory specimens of sandstone, but it can be extended to describe a natural deformation style common to many rock types by removing any limitation of scale. Once a rock layer loses cohesion along fractures and separates into discrete parts, no matter what their size, it can begin to flow by 'displacements of constituent' parts 'relative to one another accompanied by mechanical granulation, breaking, or crushing'. Therefore, a brittle

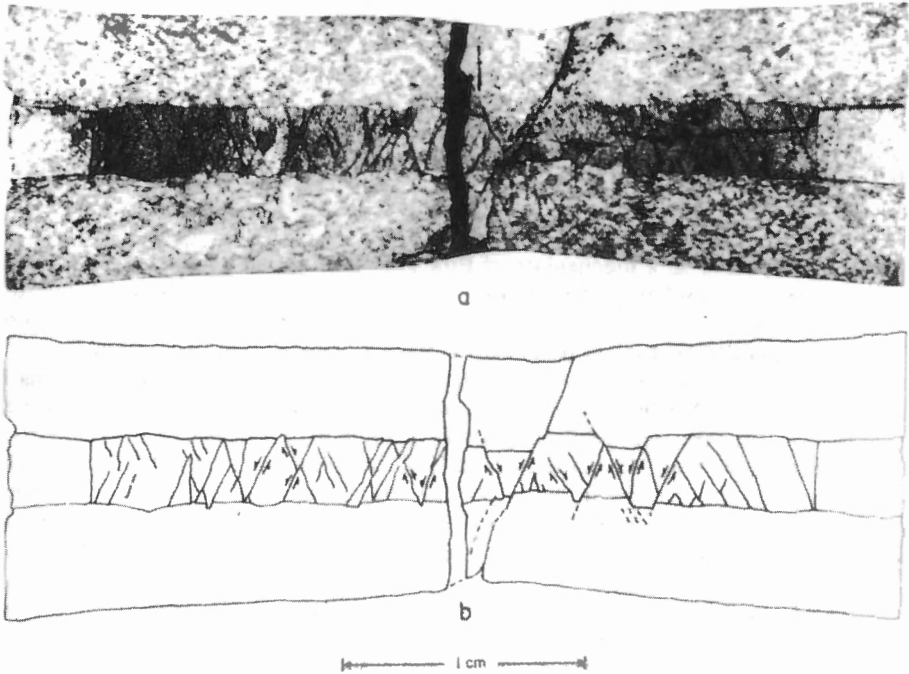


Figure 1. Triaxial extension test, outer core limestone, inner core dolomite (after Griggs and Handin, 1960).

rock unit can flow and behave in a macroscopically ductile manner once it becomes fragmented. Figure 1 illustrates a triaxial extension test on a cylinder made up of an outer core of limestone and an inner core of dolomite. The limestone has been elongated and necked by intragranular flow while the dolomite deformed primarily by slip along shear fractures. The stress-strain curve for this experiment did not indicate a loss of resistance to stress difference even though the dolomite itself fractured. The elongation of the dolomite equals that of the limestone. Therefore, the dolomite behaved as a macroscopically ductile material and was able to flow cataclastically while the limestone was flowing by intragranular mechanisms.

In the not too distant past the geologist assigned mechanical properties to rocks by intuition alone, and frequently this intuition drew heavily upon the response of rocks to his pick. From this experience limestones, for example, were thought to have about the same mechanical properties as dolomites. Today, through the careful work of several experimenters, the characteristics of many rocks under varying conditions of confining pressure, pore pressure, temperature, and even time are appreciated by the geologist. However, this advance in thinking is all too often accompanied by the failure to distinguish between the response of a small, intact, homogeneous laboratory specimen and the bulk behaviour of its natural counterpart.

FIELD OBSERVATIONS

The size of fractures found in naturally deformed rocks spans at least eight orders of magnitude. Fracture over this entire range operates as a mechanism of cataclastic flow. An illustration of the smallest scale with which the author is familiar is found in deformed Mesozoic sandstones near Fruta, Colorado. Nearly flat-lying, thick (\pm 350 ft.) sandstone units are draped over sharp discontinuities in the crystalline basement. The basement faults frequently die out abruptly upwards within the first 100 feet of the overlying clastics so that the upper parts of these units are macroscopically continuous. The folds are characterized by two nearly parallel hinges about one-quarter mile apart. Across the first hinge the dip changes abruptly from 0° to 10° or 12° . Across the second hinge the gently dipping beds roll sharply to a nearly vertical position. In the low-dipping section the beds are thinned about 10 per cent. Here the interval studied is composed of nearly pure quartz sandstones (less than 1.5 per cent calcite cement).

There is no increase in undulose extinction or of quartz deformation lamellae over those observed in the undeformed part of the bed. Therefore, it can be concluded that thinning was not accomplished by intragranular flow. Widely spaced macrofractures are the only observable discontinuities in the beds and there is no increase in these in the low-dipping deformed sections. There is less than 1.5 per cent decrease in pore space between the undeformed sandstone and sandstone in the section thinned 10 per cent, thus ruling out the mechanism of bulk volume change. Petrographic examination reveals no change in either the number of microfractures that transect individual grains or the development of unhealed microfractures (Table 1). The only mechanism seems to be fracturing of grain edges, probably as the result of intergranular rotation. These fractures are too small to be observable in standard petrographic examination, but their presence is demonstrated by a comparison of the sorting curves for the undeformed and deformed sandstones (Fig. 2). The percentage of every size fraction within the limits measured is reduced in the deformed sands. The percentage of silt and the sorting coefficient are both larger in the deformed material, while the average grain size is smaller (Table 1). Thinning must have been accomplished by cataclastic flow, that is, intergranular rotation and grain edge fracture. These small-scale fractures are thus a mechanism of macroscopically uniform flow that extends and thins the beds. As flow continues and thinning becomes more extreme at the second hinge, increases in the microfracturing of the individual grains and the percentages of unhealed fractures are observable (Table 1).

Larger scale macrofractures that serve as mechanisms of cataclastic flow are common in the field. In the author's experience, every large fold that contains dolomites or quartzites deformed under relatively low confining pressures (less than about 25,000 feet of overburden) is an example of large-scale cataclasis. Rocks that are steeply folded and yet show no trace of intragranular flow or recrystallization must have deformed by cataclastic flow. In very steep or overturned folds it is not uncommon to observe quartzites and dolomites that contain no macroscopically continuous rock fragments larger than fist size.

TABLE 1

Comparison of certain parameters for undeformed sandstones. Number in parenthesis refers to number of samples averaged. Superscripts: 1. Computed after method of Borg *et al.* (1960) and Friedman (1963). 2. Samples from section of 10° - 12° uniform dip, 10 per cent thinning. 3. Samples from steep sections, thinning extreme.

	Undeformed		Deformed	
Per cent Silt	15	(7)	30	(9)
Average Grain Size	0.11	(7)	0.08	(9)
Average Sorting Coefficient	1.28	(7)	1.51	(8)
Average Microfracture Number ¹	209	(4)	194	(4) ² 255 (4) ³
Per cent Unhealed Fractures	62	(4)	61	(4) ² 81 (4) ³

Figure 3 illustrates cataclastic flow in which the fractures are visible to the unaided eye. The lower sandstone units are overlain by marls, shales, limestones, and sandy limestones in that order. Each of these units responds as might be predicted. The most ductile unit, shale, contains very few fractures, while the sandstones that were dragged against the fault are shattered. The limestones fall between these two

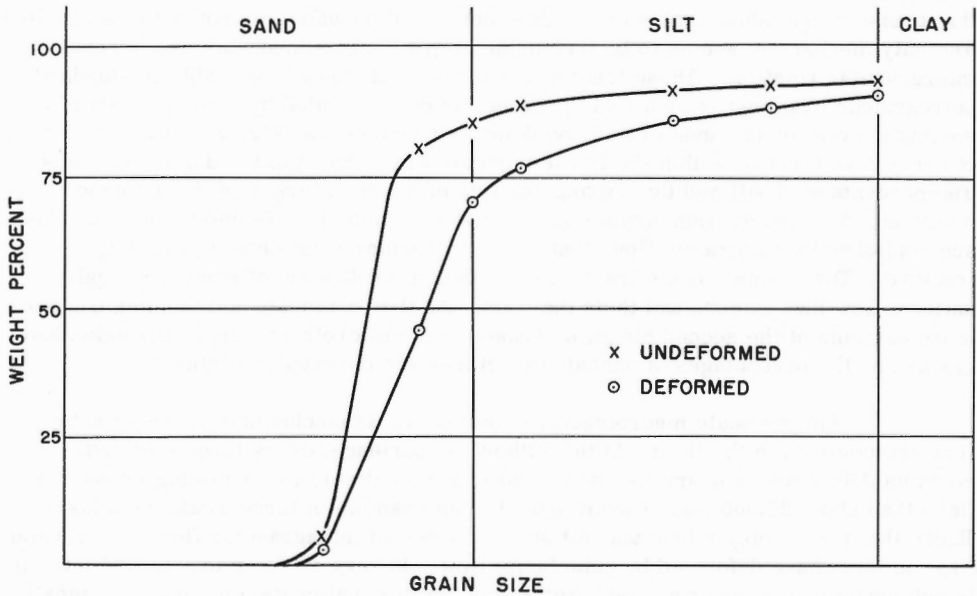


Figure 2. Average sorting curve for 8 undeformed sandstone samples and average sorting curve for 9 deformed sandstone samples.



Figure 3. Photograph of small drag fold into a steep fault showing cataclastic flow.

extremes in the degree of fracturing that can be observed. That the highly fractured sandstones have conformed to the flow of the shales is apparent from the relic bedding that can be followed through the drag folds into the fault zone. This is not a phenomenon of 'shearing off' or 'smearing out' of the sandstone. Rather, the originally flat bedding surfaces follow the same curvature into the fold as do those of the shale and limestone. Again, the active mechanism is fracture that allows the unit to flow cataclastically.

That the rocks fractured during folding is attested to by the fact that shale has flowed into the fractures in the upper limestone layers. The very thin limestone unit near the top of Figure 3 is completely separated so that limestone blocks are suspended in shale.

In the field, ordering of the fracturing varies from nearly random to strong preferred orientations from which the common geometry of two shear fractures and the associated extension fracture is easily determinable. Usually the disorder increases with the number of fractures, probably because of the increased number of stress concentrations that can develop once the rock becomes fragmented. However, in some extremely fractured rock, there is a high degree of order to the fractures. This is particularly true of folded dolomites. One good example of this from Teton anticline in northwest Montana was studied in the summer of 1967. The anticline is

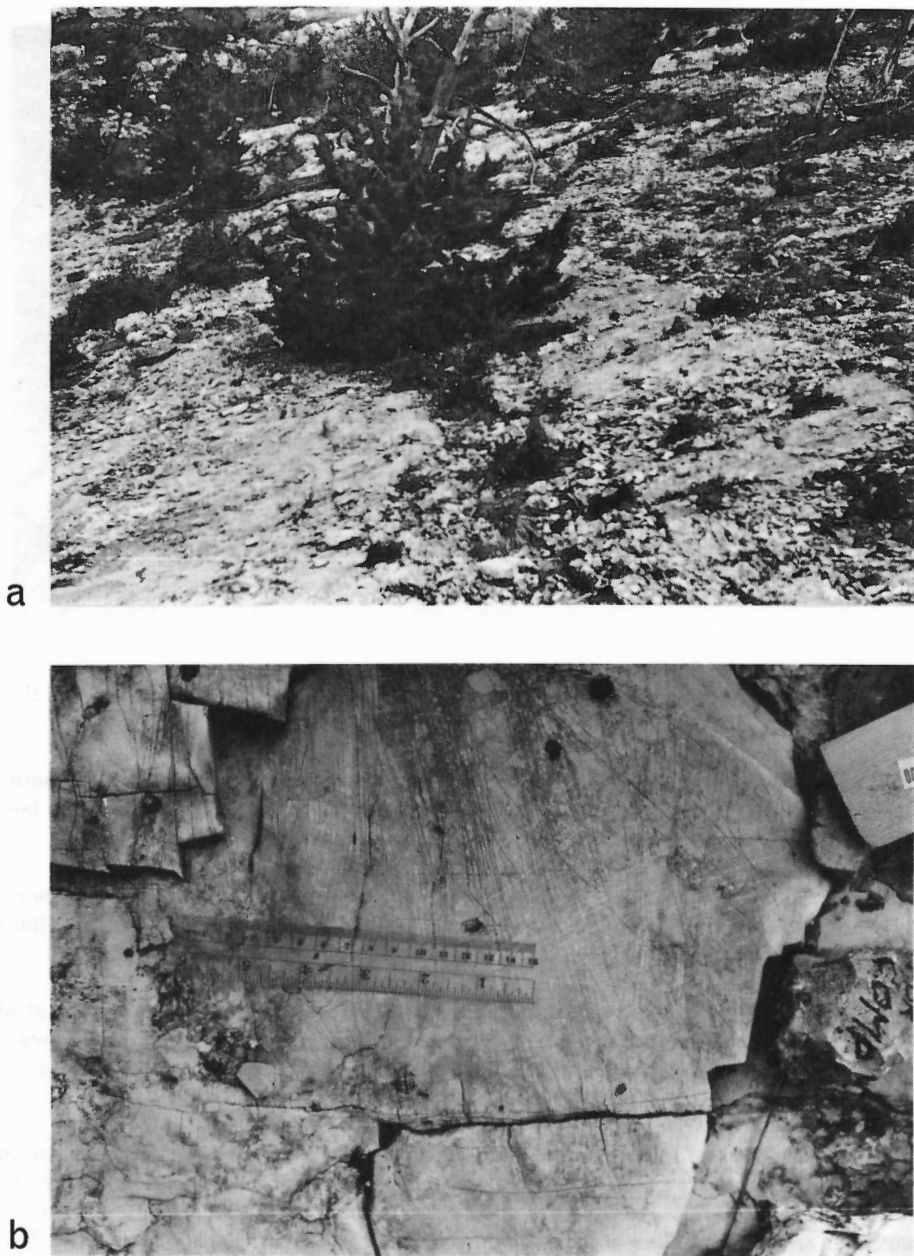


Figure 4. Fracture zones in dolomite. (a) Generalized view of zone showing alignment of vegetation; (b) Close up of fractures looking down on bedding in zone shown in Figure 4a.

asymmetrical; the gentle flank dips 25° - 30° and the steep flank 55° - 65° . The outcrop pattern is such that large exposures of single bedding surfaces are seen on the gentle side. On these slopes are zones of high intensity fracturing that trend parallel to the anticlinal axis. Along these zones the general vegetation, especially small pines, is much denser than on the surrounding nearly barren slope. As a result, the zones of intense fracturing stand out as lineations on the air photographs. Over a slope distance of about 1 mile these lineations are quite regularly spaced about 60 feet apart.¹ Figure 4a is a photograph of one of these zones. The four small pine trees in the upper left all line up along the fracture zone. When the zones that are linear and parallel to the anticlinal axis are studied in detail, they are found to be composed in general of three sets of fractures only one of which is actually parallel to the zone trend. The fracture number (average number of fractures per 100 feet) is as high as 15,000; yet there is good order (Fig. 4b). The orientations of the many fracture groups associated with this entire structure have previously been described (Stearns, 1964, 1968). The orientation of the fractures within these particular zones is illustrated in Figure 5. All the data for the histogram come from the zone shown in Figure 4, but the same pattern is reflected in all the zones.

The average trend of the high frequency peaks in the histogram are plotted in the circular insert in Figure 5.² This pattern is interpreted to be two shear fractures forming an acute (44°) angle bisected by the associated extension fracture, which is parallel to the bedding strike. The orientations of the three principal stresses can be derived from the fracture pattern. The maximum and minimum principal compressive stresses lie in the bedding plane; the maximum is parallel to the dip direction of the bed; and the intermediate is perpendicular to bedding. In other words, the hairline fractures that make up the fracture zones in the dolomite layers down the entire flank of the anticline indicate a stretching of the bed perpendicular to the anticlinal axis.

These dolomite beds are over- and underlain by limestone beds of much lower fracture intensity. The limestone was able to deform by intragranular flow mechanisms (e. g. , mechanical twinning of calcite) while the dolomite kept pace by cataclastic flow. The well-ordered fracturing, then, can be considered to be as much a mechanism of uniform flow as the twinning is in the limestone.

In order for this flow to have occurred during tectonism, it is necessary that fractures be syntectonic. The arguments for the age of fracturing are many and this is not the place to go into these arguments. However, it should be mentioned that, along with other arguments, the fracture pattern described in Figure 5 is found in the same beds where there are fractures indicating σ_1 and σ_3 parallel to bedding

¹This uniform spacing is not as easily observed on the ground because the entire bed is highly fractured, and those zones of highest intensity are not as obvious.

²Most of the fractures are too fine for measurement of dips in every case, but where three-dimensional observation is possible, the fractures are all normal to bedding .

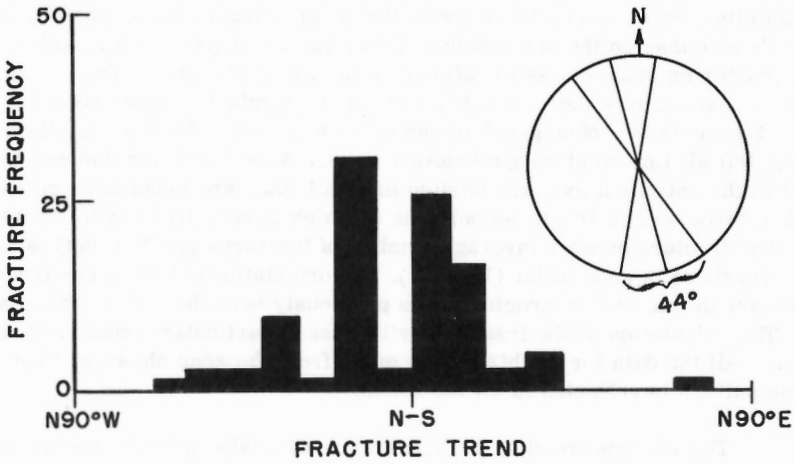


Figure 5. Histograms showing orientation of fractures from the zone photographed in Figure 3. Total number of fractures that intersect two lines 18 inches long; one parallel to the dip and one parallel to strike of the bed. Insert shows the trend of the average of each of the three peaks in the histogram.

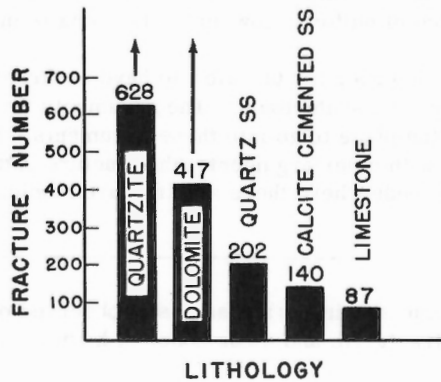


Figure 6. Bar graph showing average number of fractures per 100 feet for different lithologies in a fold.

with σ_1 in the dip direction. In this case it would be difficult to explain the fractures illustrated in Figure 5 as release, because σ_2 remains normal to bedding for both sets. Here, late formation would require a 90° change in σ_1 and σ_3 , but no change in σ_2 .¹ Further, even if fractures were late, the bed has been extended normal to the axial strike by, in this case, late cataclastic flow.

CONDITIONS THAT AFFECT CATACLASTIC FLOW

Certain parameters that affect large-scale cataclastic flow can be delineated from field observations alone. The first of these is rock type. Figure 6 shows the average fracture number for different rock types from a fold, deformed under about 10,000 feet of overburden. If we reasonably assume that the amount of fracturing is an indication of relative ductility, then these rock types fall into the same order from most brittle to most ductile as was measured in laboratory tests (Handin, Hager, Friedman, Feather, 1963, p. 749). All these rock types are found in the same fold and therefore, must accommodate themselves to the same final geometry. Even though a given rock type is capable of deforming easily by intragranular flow, it cannot fold at a faster pace or to a higher degree than the most resistant layer. Therefore, Figure 6 can be used in two ways: (1) the amount of fracturing indicates relative ductility, and (2) the amount of fracturing indicates the dependency of the rock type on flow by a cataclastic mechanism.

Total strain, or perhaps strain rate, are also parameters that affect large-scale cataclastic flow. In the sharp hinge areas of drape folds, for example, there is frequently a marked increase in the fracturing of a particular layer. This is well displayed along the hinge at Rattlesnake Mountain near Cody, Wyoming. In a lateral distance of only a few hundred feet, beds of coarse-grained limestones change in dip from 10° to 90°. Out of the hinge area these beds are capable of intragranular flow and, therefore, have a low density of macrofracturing, but in the hinge area they are shattered, almost as if the fracturing had been explosive. Few continuous pieces of rock are larger than a few inches across (Fig. 7). Bedding is often still discernible and no measurable change in thickness occurs in the hinge area. Therefore, it is concluded that the major deformation of these beds is dilatation through stretching parallel to the dip direction. Whether this extreme cataclastic flow is the result of high total strain or of high strain rate is now unknown.

The geometry of the layering may also influence the mode of deformation. Certainly, field geologists have noted, all other parameters being equal, that thin beds contain more fractures than do thick beds (Harris, Taylor, and Walper, 1960). G. M. Sowers (personal communication, 1968) is currently working on the thesis that fracture spacing is related to elastic instabilities developed within the extended layer. If this theory has merit, then thickness of the layer, as well as contrasts in elastic moduli will have an important effect on the role of cataclastic flow.

¹This change in orientation can be explained if the fracturing is syntectonic as the result of bending (Stearns, 1968).



Figure 7. Hinge area in a drape fold. Layered coarse-grained limestones have been extended in the dip direction by shattering but there is no apparent thinning in the beds.

An excellent sample of the effect of ductility contrast is given by Prucha (1965). He describes small folds he has observed in deformed rock salt interbedded with dolomite. Prucha states: "Upon reaching a radius of curvature critical for a given thickness, the dolomite beds began to fail on extension fractures normal to bedding, and the salt flowed into the dilatant zones thus produced." Because of the extreme contrast in ductility, once cataclastic flow began in the dolomite, the salt could flow into small fractures and cause actual separation of the dolomite layers. This behavior is also characteristic of brittle rocks imbedded in certain ductile shales. The ductile material does not, however, always cause complete separation so that the brittle fragments are 'floating' as in Prucha's example. Frequently the shale penetrates only a short distance into the fractures that originate at the contact and serves to prop the fracture open.

CONCLUSIONS

The relative ductilities of the common sedimentary rocks as determined in laboratory tests correlate with the relative intensity of fracturing found in these same rock types in the field, thereby establishing the validity of this order in naturally

deformed rocks. However, one should not assign the adjective 'competent' to certain naturally deformed rocks solely on the basis of the stress-strain relationships of the intact laboratory specimen. In folded rocks one must consider the 'bulk' behavior of not only the single layer or unit but also the entire sequence. Indeed, a strong, brittle rock may have a stress-strain curve that is nearly linear to rupture, and in the laboratory may not flow at all. However, this same rock type when confined within a layered sequence may be able to flow easily after it has been ruptured.

In applying the concept of 'competence', one should keep the following facts in mind: (1) A rock that is strong and brittle by laboratory standards may be a competent member of a layered sequence early in the folding process. As such, it carries a disproportionate share of the load and reaches the critical load for fracture before much folding can take place. Once it becomes fragmented, it can flow cataclastically and it may no longer control the folding of the layered sequence. (2) As folding continues, the layer that is flowing cataclastically may become 'locked' and must again fail before folding can continue. In other words, an imaginary stress-strain curve for the entire sequence would show 'work hardening'. In this case, no rock unit serves as a competent member throughout the folding, but is intermittently competent and incompetent. (3) The foregoing may apply if folds are thought of as bending phenomena. However, if folding is due to buckling as proposed by Biot (1961), then the wave length is established early, and most of the folding involves only rigid body rotations. In this case, not only the physical properties of the competent member but also the nature of the layering and the properties of the surrounding media determine which is the controlling member. If the theory of Sowers that fracture spacing is also an instability phenomena can be established, then we would have a further criterion to add to Biot's for determining competency or lack thereof.

In summary, it is necessary to consider the bulk behavior of layered rocks in order to establish competency. It is insufficient to depend upon the stress-strain relationships as determined in the laboratory without taking into account the possibility of cataclastic flow. The parameters that from field observations seem to influence cataclastic flow are: rock type, total strain or strain rate, bedding thickness, and contrast in ductility with adjoining layers. All of these in addition to the folding history must be considered before a given layer can be designated as 'the competent layer' throughout the development of the fold.

ACKNOWLEDGMENTS

I wish to acknowledge the many helpful discussions with my colleagues, M. Friedman, J. W. Handin, J. M. Logan, and G. M. Sowers. Appreciation is also extended for the capable help in the field from D. Barber and R. C. Wilson.

REFERENCES

Biot, M. A.

- 1961: Theory of folding of stratified viscoelastic media and its duplications in tectonics and orogenesis; Bull. Geol. Soc. Am., vol. 72, pp. 1595-1620.

Borg, I., Friedman, M., Handin, J., and Higgs, D.

- 1960: Experimental deformation of St. Peter Sand: A study of cataclastic flow; in Rock deformation, D. Griggs and J. Handin, editors, Geol. Soc. Am., Mem. 79, pp. 133-192.

Friedman, M.

- 1963: Petrofabric analysis of experimentally deformed calcite-cemented sandstones; J. Geol., vol. 71, No. 1, p. 18.

Griggs, D., and Handin, J. W.

- 1960: Observations on fracture and a hypothesis of earthquakes; in Rock deformation, Geol. Soc. Am., Mem. 79, pp. 347-364.

Handin, J. W., and Hager, R. V.

- 1957: Experimental deformation of sedimentary rocks under confining pressure; Test at room temperature on dry samples; Bull. Am. Assoc. Petrol. Geologists, vol. 41, No. 1.

Handin, J. W., Hager, R. V., Friedman, M., and Feather, J. N.

- 1963: Experimental deformation of sedimentary rocks under confining pressure: Pore pressure tests; Bull. Am. Assoc. Petrol. Geologists, vol. 47, No. 5.

Harris, S. F., Taylor, G. L., and Walper, J. J.

- 1960: Relation of deformational fractures in sedimentary rocks to regional and local structure; Bull. Am. Assoc. Petrol. Geologists, vol. 44, pp. 1853-1873.

Prucha, J. J.

- 1965: Deformation of silurian salt in Cayuga Rock Salt Company Mine, Myers, New York; Trans. Am. Geophys. Union, vol. 46, No. 1, (Abstract).

Stearns, D. W.

- 1964: Macrofracture patterns on Teton anticline, Northwest Montana; Trans. Am. Geophys. Union, vol. 45, pp. 107-108 (Abstract).

- 1968: Certain aspects of fracture in naturally deformed rocks; in NSF Advanced Science Seminar in Rock Mechanics, R. E. Riecker, editor, Special Report, Air Force Cambridge Research Laboratories, Bedford, Mass.

DISCUSSION

H.A.K. Charlesworth wondered if the author would agree that the term 'flow' should be restricted to homogeneous deformation, and if he would comment on the use of the term 'flow' as defined by deformation including a loss of cohesion.

The author replied that the concept of flow can be gained from an imaginary stress-strain curve in which there was some indication of ductility. However, we can not tell from the stress-strain curve what the mechanism of flow is, and whether the strain is homogeneous or not. Referring to Figure 1 of his paper¹, he pointed out that from the stress-strain curve one could not have told that the mechanism of deformation was not intergranular flow in the dolomite. The strain is not homogeneous within the dolomite, nor is it homogeneous within the limestone, although we do not hesitate to talk of intergranular flow in the latter case. When working in the field, the author uses flow as a way of describing materials that have macroscopic ductility, whether the strain was homogeneous or not. He thought that a discussion on the loss of cohesion during deformation would need too long an explanation to have its place here. He referred to previously published observations of J.J. Prucha (see also below) on fragments of dolomite layers in salt. His own observations in interlayered sandstones and shales showed that the loss of cohesion of the sandstones had taken place during deformation, because the shales had flowed into the fractures. Bedding planes of both rock types were parallel and no one objected to the terms flow for the deformation of the shale, although it probably was due to the same phenomenon on the microscopic scale as that of the sandstone. One must consider scale and if loss of cohesion is on a smaller scale than the body one is considering, it can be a mechanism of flow, i. e. cataclastic flow.

M. Stauffer commented on the sorting curves presented by the author (Fig. 2). He suggested that because the size of some grains decreased during deformation, it might be possible to trace deformation paths. Commenting on Stearn's Figure 2 he observed that the largest grains and the smallest grains would appear not to deform, but that the medium-grained fraction would. He asked if the author had an explanation for this, and if grain shape or possibly sampling procedure might be responsible.

The author tentatively suggested that the small grains were possibly too small to deform further. As to the large grains, he thought that it might be more difficult to develop stress concentrations required to break them up because of their size. He suggested in addition that rotation of smaller grains might start more easily because of their size than for larger ones. He considered that grain shape had probably a great influence on the deformation,

¹ This figure was not used in the oral presentation (Edit.).

but he could not find, from his petrographic examinations, any particular orientation of the grains. He doubted that sampling played any role in the shape of the curves and suggested that before using sorting curves for environmental determinations, stratigraphers should make sure that their samples did not come from deformed rocks.

P. S. Simony asked the author how he measured the intensity of fracturing and if he corrected his results for fractures oblique to the direction of measurement.

The author said that there was of course no way to represent the three-dimensional aspect of fracturing intensity. His measurements were in a plane normal to the fractures. In practice, he would lay out a measuring tape in one, two or three convenient directions and would then measure the number of fractures that intersected the tape. In addition the azimuth, the plunge and the linear distance of the tape were measured. Each measurement could then be computed as a number of fractures along a line normal to each particular fracture set.

P. S. Simony also asked if flow by cataclastic mechanism could produce the same kind of geometry that we normally associate with flow, and if, for instance, quartzite could form folds suggesting incompetent behaviour.

The author said cataclasis is a flow mechanism. Further he knew of folds in the Rocky Mountains where quartzite beds actually thicken over the hinge. He did not think, however, that thinning or thickening should be the decisive argument concerning the competence of a bed. Taking the example of a dolomite bed in salt, he would imagine that early in the load build-up, there had been a continuous layer of dolomite, carrying a much larger proportion of the load than was the salt and therefore was more competent. However, after separation of the dolomite the salt was carrying the greater load and was, therefore, more competent. The author did not think that there would ever be as much flow in deformed sedimentary terrain as in a metamorphic terrain, or that quartzites could ever become as ductile as shales. The type of flow he was talking about was simply a local macroscopic flow sufficient to allow folding to continue. This folding would in most cases, but not all, be of the parallel type.

J. J. Prucha mentioned an interesting road cut south of Catskill (New York) showing an anticline of interbedded shale and chert. The chert beds range in thickness up to 1 foot and have been folded by cataclasis, but the shale has flowed into the dilatant zones. Once a critical rate of curvature was reached, the chert beds could no longer fold by the fracturing mechanism, and thrusting took place. The net result was that in the outcrop as a whole, there was substantial thickening of the total chert-shale unit over the

hinge of the anticline, but there was no thickening of individual beds of chert. This mechanically very heterogeneous sequence thus gives a beautiful example of cataclastic flow, on a scale entirely different from that discussed by Stearns.

D. U. Wise described the case of a drape fold of the Paleozoic section across the Beartooth fault, about 20 miles north of the Rattlesnake Mountain anticline, Wyoming. There is about 1,500 feet of vertical displacement in the basement 'eaten' by 800 feet or 1,000 feet of Cambrian shale and about 2,000 feet of Paleozoic, draped across the fault without apparent break. By contrast, 1 mile from this, a fault with a 50-foot displacement in the basement, breaks its way through the entire Paleozoic section. In this second case, one can argue that breaking occurred after mountain uplift with the Paleozoic carbonates behaving in a brittle fashion under little confining pressure. In the first case there only seems to be minor displacement after range uplift with the drape of sediments taking place under deeper burial. Thus, Wise agreed with Prucha that the difference between the two faults might be attributed to a change in stress conditions.

W. C. Brisbin (written comments) Recent work by the Department of Geology, University of Manitoba, in the Precambrian shield near the Manitoba-Ontario Boundary has revealed a deformational mechanism similar to that described by D. W. Stearns.

The work in this area

(1) Supports the contention that brittle fracture can be an important mechanism leading to flow in naturally deformed rocks, resulting in the phenomenon referred to as cataclastic flow.

(2) Indicates that cataclastic flow can occur over a large range in scale.

(3) Indicates that rock types exercise some control over the development of this type of deformation.

Pebble Deformation in the San Antonio Formation

The San Antonio Formation is a feldspathic quartzite in which there is abundant microscopic evidence that the clastic constituents of the formation have been displaced relatively to one another, resulting in mechanical granulation, breaking and crushing of the grains. The rock has lost cohesion along these fractures and has undergone a cataclastic flow resulting in the development of a definite curvilinear foliation. Layering has been deformed passively by this process, as have pebbles within the conglomerate layers of the formation.

The deformation of three predominant pebble types has been studied in some detail by K. Bell at the University of Manitoba. The pebbles are from a single structural domain on the limb of a fold and metamorphic conditions at the time of deformation have been identified as being in the lower greenschist facies. All pebbles are ellipsoidal in shape and their long, intermediate and short dimensional axes show good alignment. The ellipsoidal shape of all pebble types has been interpreted as the result of deformation. Thin section examination of the clasts reveals that their strain behaviour has been identical to that of the quartzite matrix in which they are set, i. e. by cataclastic flow. However, the degree to which the pebbles have deformed by cataclastic flow is variable and is related to rock type. Measurements of the orthogonal dimensional ratios of several hundred pebbles reveals the following relationship between rock type and dimension ratios:

	<u>Long Dimension</u>	<u>Intermediate Dimension</u>	<u>Short Dimension</u>
Volcanic pebbles	6.3	4.5	1.0
Quartz pebbles	2.3	1.5	1.0
Granitic pebbles	2.0	1.5	1.0

The field and laboratory studies indicate that all pebble types have responded initially to stress by brittle fragmentation. After fragmentation, additional strain has been macroscopically ductile as a result of cataclastic flow. Amounts of pebble strain were governed by the relative 'ductilities' of the fragmented pebbles.

The Winnetka Lake Stock

The Winnetka Lake Stock is a quartz monzonite pluton approximately 4 miles long and 1 mile wide, which has been emplaced in the Falcon Lake-Kenora greenstone belt. Structural analysis of the metamorphosed sedimentary and volcanic rocks adjacent to the stock has revealed evidence of at least two periods of deformation, the last of which was by the mechanism of passive slip. The stock was emplaced prior to this deformational event, for it shows definite evidence of strain, consistent with the geometry and strain behaviour of the deformation in the surrounding host rocks. Metamorphic conditions at the time of deformation have been tentatively identified as being in the greenschist facies.

Studies by O. Vagt at the University of Manitoba have indicated that the initial strain response of the stock to the deformation was brittle. Micro-fractures developed and served as surfaces on which small displacements occurred. Displacements were accompanied by mechanical granulation, crushing and breaking of grains, resulting in the development of a cataclastic flow foliation which has an orientation parallel to that of the passive slip surfaces on which movements took place in the host rocks. At the western

end of the stock the transition from passive slip in the host rocks to cataclastic flow in the quartz monzonite can be observed across the contact between the stock and the host rocks. The contact at this location is oriented at right-angles to the tectonic foliation in both bodies. The change in character of the tectonic foliation across this contact reveals the role played by the relative ductility of the two rock types during the beginning stages of deformation.

The direction and amounts of movement on the cataclastic flow surfaces within the stock are difficult to ascertain; however, studies of inclusions within the stock indicate that these bodies have been deformed and aligned by cataclastic flow. Preliminary analysis indicates that both the orientation and the orthogonal dimensional ratios of these inclusions are consistent throughout the stock.

J. J. Prucha (written comments) In dealing with the concept of competence in folded beds, the sequence of events in the folding history may be of great importance, as Stearns has suggested. This is well illustrated in the Firtree Point anticline in central New York State, about 5 miles north of Ithaca, where interbedded dolomite and rock salt beds of Late Silurian age (Syracuse Formation) have been deformed together in compressional folding.

The extensive workings of the Cayuga Rock Salt Company mine reveal that in the initial stages of folding the interbeds of dolomite behaved in a very competent manner, with development of sinusoidal folds having characteristic wave lengths and amplitudes determined by the effective thickness of the individual beds. At this stage of the folding the salt behaved in a passive manner and adjusted itself to the changing geometries of the buckling dolomite layers. When individual dolomite layers reached a critical radius of curvature, the flexural slip mechanism was supplanted by extension fracturing normal to bedding, which destroyed the structural integrity of the beds, and flowage of the salt became the dominant mode of deformation. There was, thus, a reversal in the relative active and passive roles of dolomite and salt as a function of the stage of folding.

Ultimately the entire package of interbedded rock salt and dolomite was sufficiently stiffened so that the sequence of beds began to deform as an integral structural unit, with development of larger folds having new wave-length and amplitude characteristics. It is clear, therefore, that the concept of competence must be related to a particular stage in the entire deformation episode.

The example just cited is in no way inconsistent with laboratory experiments on the mechanical properties of either dolomite or rock salt, but as Stearns has pointed out, one can't simply write a direct equation between experimentally determined mechanical properties and the role of the respective rocks in a tectonic situation. The example is not, of course, one of purely cataclastic flow; rather, it is an example of the essential part that cataclasis played in the early stage of a deformation episode in which, overall, the dominant deformation mechanism was intracrystalline gliding.

BRITTLE FRACTURE IN DIRECT SHEAR AND THE DEVELOPMENT OF
SECOND ORDER FAULTS AND TENSION GASHES

E. Z. Lajtai

Department of Geology, The University of New Brunswick,
Fredericton, New Brunswick

Abstract

The possible origin of second order shear fractures and tension gashes associated with first order or primary faults is examined from the static viewpoint. A static mechanism is developed which is based on the assumption that normal stresses acting on planes perpendicular to displacement are fully or partially relieved. Depending on the actual state of stress after faulting and the strength of rock against tensile or shear stresses, failure will be either by tension (tension gash) or shear (second order shear fractures).

NOMENCLATURE

σ	psi	normal stress
σ_a	psi	normal stress in direct shear
σ_b	psi	transverse normal stress in modified direct shear
σ_f	psi	normal stress on plane of fault at point of first order failure
σ_c	psi	uniaxial compressive strength
$\sigma_I, \sigma_{II}, \sigma_{III}$	psi	first order principal stresses
$\sigma_1, \sigma_2, \sigma_3$	psi	second order principal stresses
τ	psi	shear stress
τ_a	psi	shear stress in direct shear at point of second order failure
τ_f	psi	shear stress in fault plane at point of first order failure
τ_k	psi	maximum frictional resistance in plane of fault (McKinstry's condition).
ϕ_i	degree	angle of internal friction
ϕ_p	degree	angle of planar friction
ϕ_u	degree	angle of friction at ultimate strength (angle of internal friction for granulated material)

μ	---	coefficient of friction, $\mu = \tan \phi$
θ	degree	angle between plane θ and the fault plane
θ_1	degree	orientation of maximum principal plane
θ_3	degree	orientation of minimum principal plane and tension fracture
α_I, α_{II}	degree	orientation of conjugate first order shear fractures
α_1, α_2	degree	orientation of conjugate second order shear fractures
T_s	psi	tensile strength (negative number)
S_o	psi	fundamental shear strength
S_d	psi	pure shear strength
S	psi	total shear strength (shear strength envelope)
S_i	psi	internal friction
S_p	psi	planar (joint) friction
S_u	psi	ultimate shear strength (crushed material in failure zone)

INTRODUCTION

A number of authors (Anderson, 1951; McKinstry, 1953; Moody and Hill, 1956; Chinnery, 1966) have investigated the possible origin of second order faults by considering the change in static stress condition following faulting. Price (1968), concluding that an analysis based on the static viewpoint cannot account for secondary faults forming at points other than the ends of the fault, used a dynamic approach. The main objection to the static analysis is that stress concentrations occur only at the ends of the fault plane; they do not reach sufficient intensity at any other point to overcome the strength of rock located on either side of the primary failure plane. Consideration is not given, however, to the possibility that faulting may result in relief of normal stresses acting on planes perpendicular to direction of displacement along the fault, and that failure in secondary directions could take place as a consequence of diminishing confinement and not as a result of stress concentrations. The acceptance of this proposition allows the formulation of a failure mechanism which can account for the origin of not only secondary faults but also tension gashes. The failure mechanism is similar to that occurring in a direct shear test and it is essentially the same as that implied in McKinstry's approach.

The postulated change from a primary to a secondary state of stress is shown on Figure 1. The first diagram illustrates how the second order state of stress at a point on one side of the fault (Element B) is derived from a uniaxial first order stress condition. Circle 1 represents the state of stress just before first order shear failure occurs at α_I and α_{II} , as shown in

the corresponding Element A at the left of the diagram. According to McKinstry the normal stress σ_f is fully transmitted across the fault plane, but the shear stress τ_f decreases to the level of frictional resistance, $\tau_k = \alpha_f \tan \varphi_u$. The second order state of stress on the small element B taken from one side of the fault plane, and shown enlarged below, is represented by Circle 2. Obviously the stress circle is not large enough to reach the shear envelopes and consequently no second order shear fracture could develop. Failure may occur, however, in tension if $|\sigma_3| \geq |T_s|$, as shown on Figure 1a, in which case the tension fracture would be at θ_3 coinciding with the direction of σ_1 (Element B, Figure 1a).

If the primary stress condition is a more general one (Circle 1, Figure 1b) conditions for secondary faulting become more favourable. Circle 2 represents again the secondary stress condition according to McKinstry. Circle 2 cuts both the shear strength ($S = S_0 + \sigma \tan \varphi_1$) and the tensile strength ($\sigma = T_s$) envelopes. It is obvious that the state of stress is not compatible with the strength of rock and hence equilibrium does not prevail. The condition for the development of one, or a conjugate set of second order faults (α_1, α_2) is represented by Circle 3 which just touches the shear strength envelopes. The corresponding shear planes and their relation to the fault plane and the all-compressive first order stress field ($\sigma_I, \sigma_{II} = \sigma_{III}$) are shown on Element C.

It is possible, however, to impose a state of stress for which the shear stress could be maintained at the level of frictional resistance. Such a condition is represented by Circle 4. This is, however, no longer a direct shear loading condition. The significant difference is the appearance of normal stress (σ_b) on planes normal to the direction of displacement along the fault plane (Element D). This transverse normal stress (σ_b) would, of course, be still much smaller than the normal stress which existed in this direction prior to faulting. The condition ($\sigma_b > 0$), then, would represent a case of only partial relief of normal stress acting parallel to the direction of the displacement along the fault plane. The minimum principal stress (σ_3) would tend to become compressive with increasing value of σ_b and the possibility of tensile failure would be eliminated.

Figures 1a and 1b represent two of many possible combinations of parameters controlling failure in a second order stress field. Failure in general occurs when stresses become greater than the strength of rock. Unfortunately these two basic parameters are very difficult to define. There is an infinite number of stress fields for which first order failure in rock is possible. In accordance with the arguments expounded so far, however, only the normal stress (α_f) acting on the plane of the fault remains unchanged after faulting. Hence, the first order stress field is of consequence only in defining the orientation of the fault plane and the magnitude of σ_a (normal stress in direct shear loading) which is assumed to be equal to α_f . It is further assumed that the intermediate principal stress remains unchanged during the whole process of primary and secondary faulting. These assumptions appear to be reasonable. An additional assumption introduced in McKinstry's analysis that the shear stress in the fault plane is fixed at the level of frictional resistance is not, in the author's opinion, justified. It follows from the previous arguments that shear stress in the fault plane is dependent on the strength of rock (tensile and shear strength envelopes) and the other second order stress parameters namely σ_a and σ_b (for $\sigma_b > 0$). The actual value of the shear stress must, therefore, be a dependent variable. It may be less than

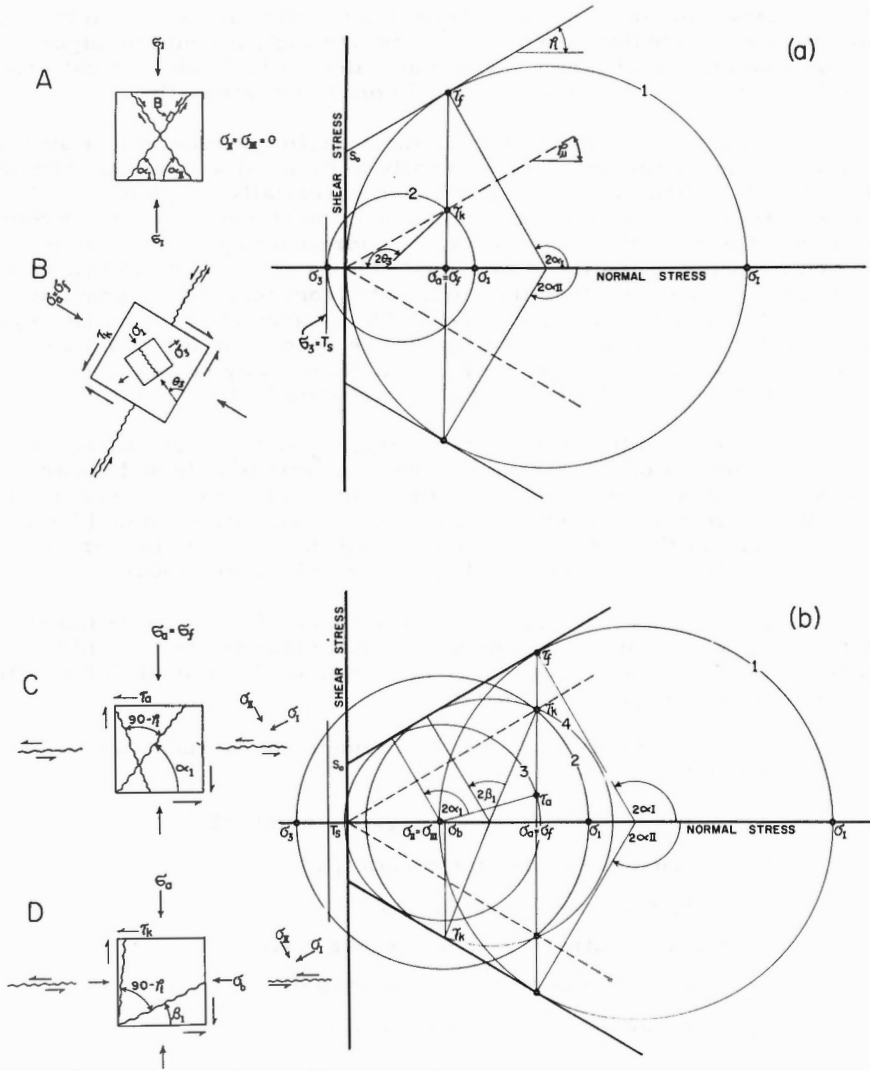


Figure 1. The development of the second order stress field following first order faulting.

- (a) uniaxial first order state of stress
 - A - element corresponding to Circle 1
 - B - element corresponding to Circle 2
- (b) general first order state of stress
 - C - element corresponding to Circle 3
 - D - element corresponding to Circle 4

τ_k if secondary fracturing occurs before frictional resistance can be fully mobilized (i. e. immediately after primary faulting); it could be higher than τ_k if, for example, reshearing takes place along a fault where first order failure had not resulted in a total loss of cohesive strength.

There is the implication in most earlier works on this subject that second order structures are generally associated with strike-slip faults. Anderson's classification of faults is based essentially on geometrical considerations in reference to a vertical-horizontal coordinate system. From the dynamic point of view the only acceptable coordinate system is the one which is defined in terms of the three principal stresses. The actual source of these stresses - i. e. whether they originate from tectonic or gravitational forces - and their orientation with regard to an unrelated coordinate system are completely immaterial in defining failure conditions for both first and second order fracture. Hence, there is no reason why second order structures should show a preference toward strike-slip faults.

In addition to stress parameters, σ_a and σ_b , conditions for second order failure depend on the strength of rock against tensile and shear stresses. For this analysis the Coulomb-Navier criterion for shear strength and the maximum principal stress theory for tensile strength will be used. The comparison of the two fracture modes will be based on the simplest case of the modified Griffith criterion (McClintock and Walsh, 1962).

In order to simplify the analysis it will further be assumed that the strength of rocks on either side of the fault plane is not altered by primary faulting. The whole procedure, however, could be modified readily for a more complex strength relationship.

In the following analyses the influence of all these factors will be examined, namely:

T_s = tensile strength (psi, negative number)

S_0 = fundamental shear strength (psi)

μ = friction coefficient, $\mu = \tan \phi_1$

σ_a = normal stress in direct shear (psi)

τ_a = shear stress in direct shear (psi)

σ_b = transverse normal stress (psi)

An analysis which incorporates all the above factors should leave very little unknown.

As a first step, conditions defining the origin of tension gashes and secondary shear fractures will be examined for direct shear loading ($\sigma_b = 0$). Finally, by introducing σ_b the analysis will be extended to include a general state of stress.

All curves shown on figures have been graphically derived, although a rigorous mathematical analysis of the whole problem is nearing completion and will be included in a later publication.

THE DERIVATION OF THE DIRECT SHEAR PARABOLA AND DIRECT SHEAR CURVE

Figure 2 shows the development of two types of relationship between τ_a and σ_a (shear loading), dependent upon the application of the maximum principal stress theory for failure in tension or the Coulomb-Navier criterion for shear failure. The modified Griffith criterion (McClintock and Walsh, 1962) offers a convenient and reasonably accurate connection between the two ($S_0 = 2|T_s|$). Both curves have been developed by assigning values to σ_a and defining τ_a by the construction of corresponding Mohr's circles, the radii of which are selected in such a way that the circles are tangential to either the $\sigma_a = T_s$ line for tensile failure (direct shear parabola), or to the shear strength envelope for failure in shear (direct shear curve). The orientation of fracture planes with respect to the fault plane is given by θ_3 and α_1 for tension and shear fractures respectively. The conjugate shear fracture α_2 makes $(90^\circ - \alpha_1)$ with α_1 .

Mathematical analysis of the same conditions has defined the direct shear parabola in the form of

$$\tau_a = [T_s(T_s - \sigma_a)]^{1/2} \tag{1}$$

and the direct shear curve in the form of

$$\tau_a = \frac{1}{2} \left[\frac{(2S_0 + \mu \sigma_a)^2}{1 + \mu^2} - \sigma_a^2 \right]^{1/2} \tag{2}$$

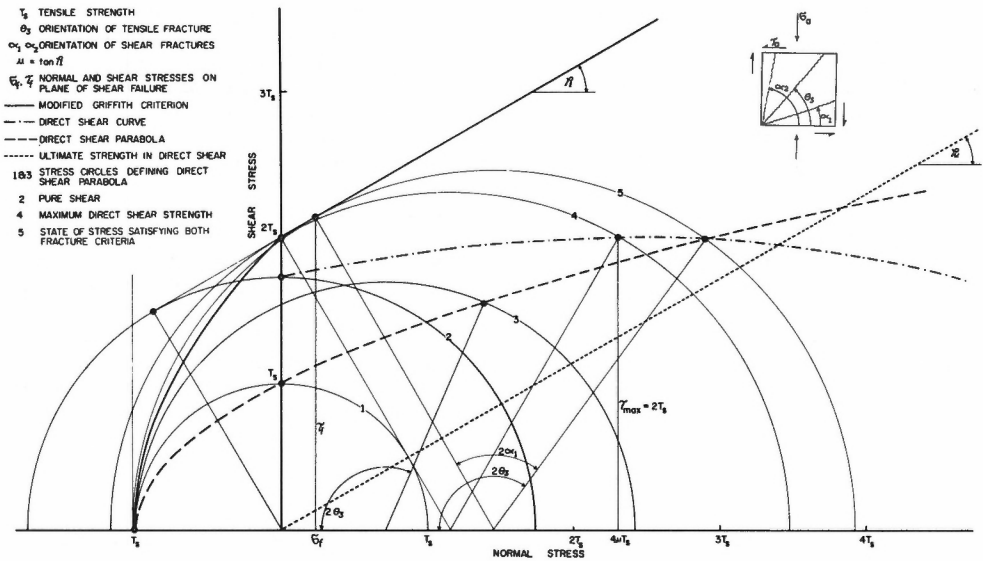


Figure 2. Derivation of direct shear parabola and direct shear curve from the modified Griffith criterion of brittle failure.

The orientation of the fracture planes is given by

$$\tan 2\theta_3 = - \frac{2\tau_a}{\sigma_a} \quad (3)$$

for the direct shear parabola (tension gash) and by

$$\tan 2\alpha_1 = \frac{2\mu\tau_a + \sigma_a}{2\tau_a - \mu\sigma_a} \quad (4)$$

for secondary shear fractures.

The Direct Shear Parabola

The direct shear parabola represents those values of τ_a and σ_a for which the minimum principal stress (σ_3) reaches the value of the tensile strength of the material and hence a tension gash forms at θ_3 . The critical shear stress in the plane of the fault (τ_a) according to (1) depends on σ_a and T_s . The influence of tensile strength can be seen on Figure 3 where a number of parabolas are plotted for different magnitudes of tensile strength, ranging from 10 to 1,000 psi. The $\tau_a = 0$ and $\sigma_a = 0$ intercepts are T_s and $-T_s$ respectively (Fig. 2). For increasing positive values of σ_a , τ_a also increases but at a relatively slow rate. Consequently at some value of σ_a the parabola is intersected by the ultimate strength or friction line (Fig. 3). The latter represents the pure frictional resistance along a completely granulated shear zone ($\tau_a = \sigma_a \tan \varphi_u$). Although the slope of this line is not necessarily the same as the angle of internal friction the difference should be small. For values of σ_a to the right of the point of intersection, maximum shear strength is determined by the friction line. It is possible that the parabola will still define conditions for the formation of tension gashes. As shear stress increases to its maximum value (as defined by the friction line) the tension fractures, however, are generally destroyed and a zone of completely granulated rock forms in the area affected by direct shear loading (i. e. the immediate neighbourhood of the primary fault plane). Accordingly the preservation of tension gashes at such values of σ_a would be unusual.

The direct shear parabola is independent of the friction coefficient but its point of intersection with the friction line is not. Consequently the range of σ_a values for which the formation and preservation of tension gashes is at an optimum will depend on the slope of the ultimate strength line. From Figure 3 it appears that the secant between $\sigma_a = 0$ and the intersection point offers a simple approximation for the parabola. The slope of the secant depends on φ_u alone (Fig. 4). Figure 5 demonstrates that the range of σ_a for which the formation of tension gashes is favourable increases with decreasing values of friction coefficient as the point of intersection between the direct shear parabola and the ultimate strength line shifts toward higher values of normal stress.

The orientation of the resulting tension gash, as determined by (3), will rotate from a $\theta_3 = 0$ position at $\sigma_a = T_s$ to $\theta_3 = 90^\circ$ at an infinitely high value of normal stress (Fig. 6).

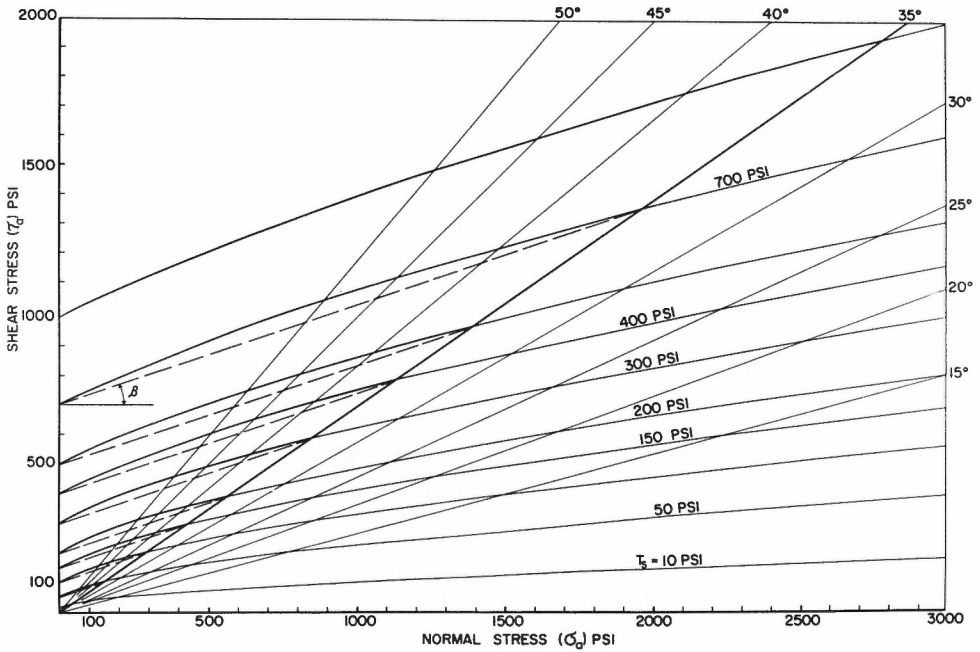


Figure 3. Direct shear parabola for various values of tensile strength.

The Direct Shear Curve

The direct shear curve represents the criterion of failure in shear for direct shear loading. The critical shear stress in the plane of fault according to (2) depends on σ_a , S_0 and μ . It is not a direct function of T_s , although according to the original and the modified Griffith theories $S_0 = 2|T_s|$. Hence by selecting the latter theory the conditions of failure in tension and shear can be readily compared.

In contrast to the direct shear parabola, where τ_a increases with increasing σ_a infinitely, the direct shear curve reaches a maximum then decreases and becomes zero (Fig. 7).

$$\text{at } \sigma_a = 0, \tau_a = S_d = S_0 \left(\frac{1}{1+\mu} 2 \right)^{1/2}$$

$$\sigma_a^{\text{max}} = 2\mu S_0, \tau_a = S_0$$

$$\sigma_a = \sigma_c, \tau_a = 0$$

where σ_c is the uniaxial compressive strength of the material (this is true only if failure in uniaxial compression occurs by shear fracturing).

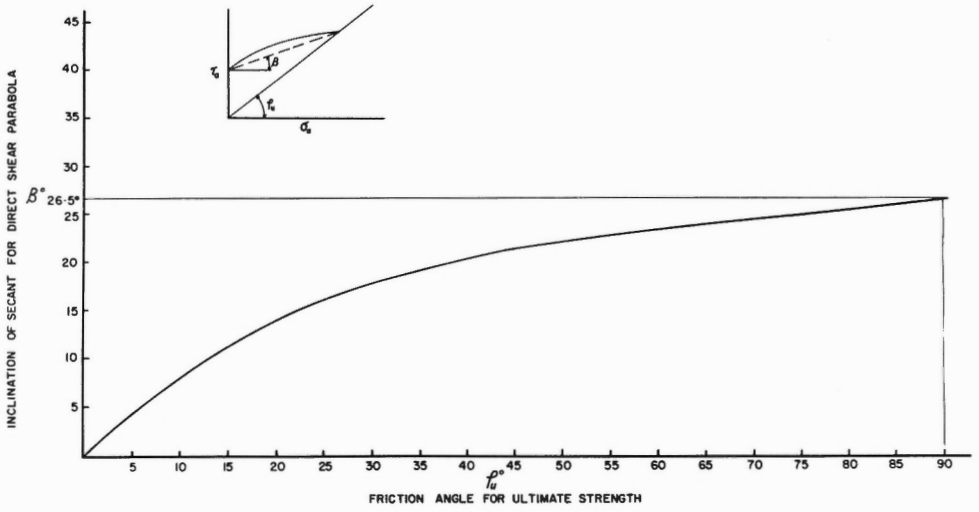


Figure 4. Orientation of secant to direct shear parabola as a function of the angle of friction at ultimate strength.

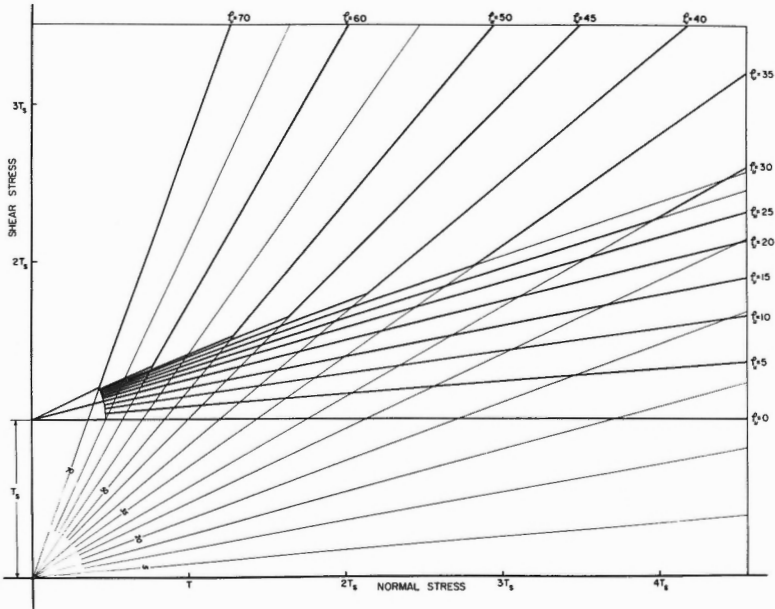


Figure 5. Simplified limit curves consisting of secant and line of ultimate strength as a function of the angle of internal friction.

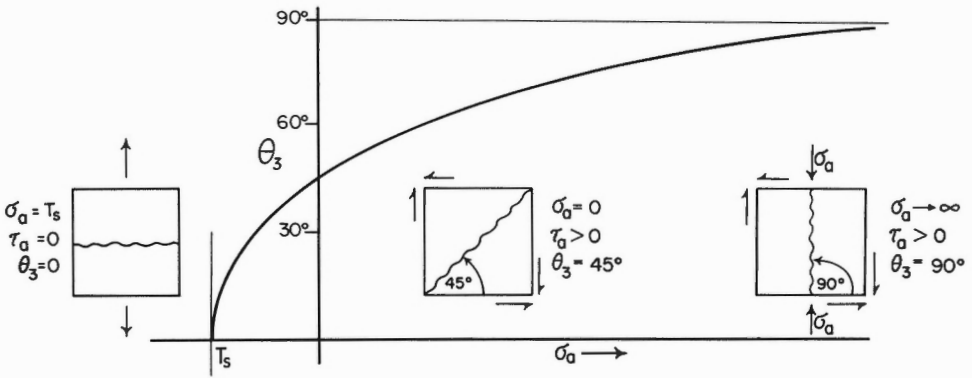


Figure 6. Orientation of tension gashes as a function of normal stress.

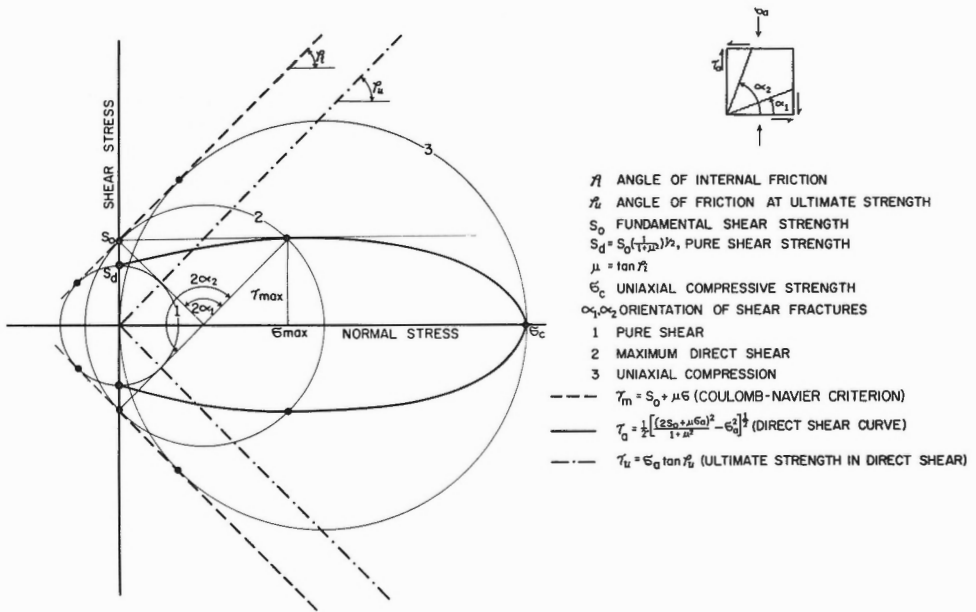


Figure 7. Derivation of the direct shear curve from the Coulomb-Navier criterion of brittle failure in shear.

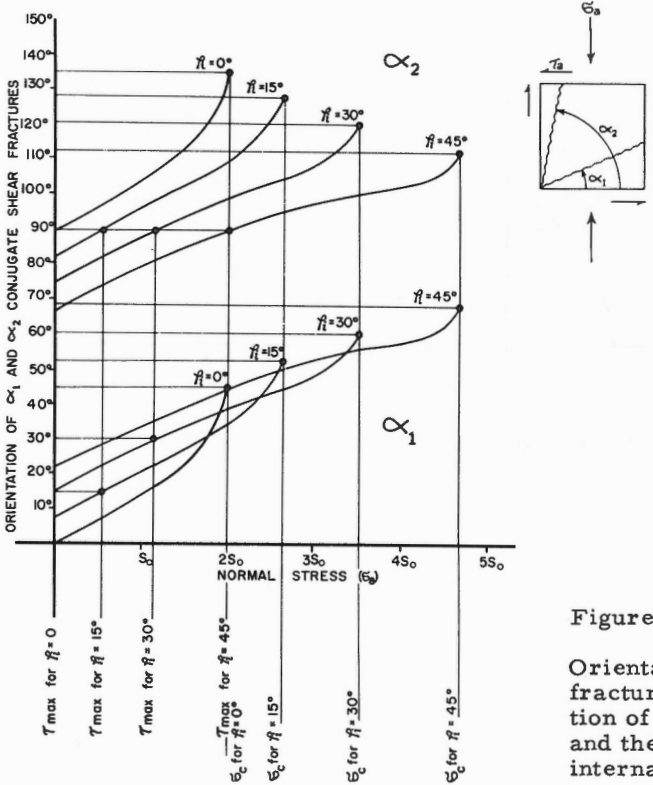


Figure 8.
Orientation of shear fractures as a function of normal stress and the angle of internal friction.

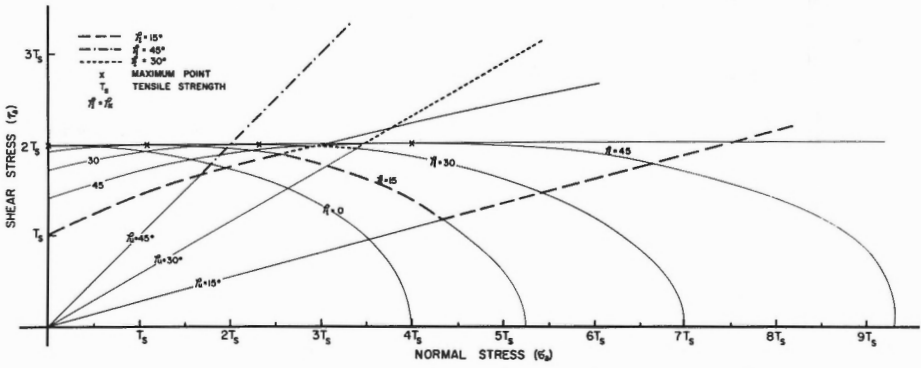


Figure 9. Composite limit curves for direct shear.

Because of its shape, the direct shear curve will intersect both the direct shear parabola and the line of ultimate strength.

The direction of conjugate shear fractures, α_1 and α_2 , as given by (4) varies with σ_a and μ as shown on Figure 8.

On Figure 9 all possible failure criteria in direct shear are plotted for $\varphi_i = \varphi_u = 0, 15, 30, \text{ and } 45$ degrees and in terms of the modified Griffith criterion where $S_o = 2|T_s|$.

For low values of σ_a (including negative σ_a) failure should occur in tension as the direct shear parabola runs below the direct shear curve for any value of φ_i . At higher σ_a as the direct shear curve starts decreasing, failure in shear becomes possible, provided φ_i is about 30° or less. For higher values of the angle of internal friction the ultimate strength criterion becomes applicable before shear failure is possible.

THE INFLUENCE OF TRANSVERSE NORMAL STRESS

The assumption of direct shear loading in the development of secondary faults and tension gashes is fundamental to all considerations expounded so far. In the writer's judgment it is a reasonable one and probably valid for a number of situations. It is still tempting to investigate, however, how conditions for the two modes of fracture would be affected by the introduction of normal stress on planes perpendicular to the direction of displacement along the primary fault plane. With the inclusion of a transverse normal stress (σ_b) the state of stress becomes a general one.

Figure 10 shows how the direct shear parabola changes as σ_b is increased from zero to σ_a . The general equation defining conditions for tensile failure becomes

$$\tau_a = \left[(T_s - \sigma_a)(T_s - \sigma_b) \right]^{1/2} \quad (5)$$

which will reduce to $|1|$ if $\sigma_b = 0$. For $\sigma_b = \sigma_a$, (5) reduces to two straight lines sloping at 45° and intersecting the $\sigma_a = 0$ axis at $\pm T_s$. Figure 10c shows that the 'apparent shear resistance' will be higher for increasing σ_b , and that the influence of σ_b is more pronounced at high σ_a . The transverse normal stress will, in addition, tend to decrease the angle tension gashes make with the fault plane. This decrease becomes sharper as σ_a increases (Fig. 10d).

A similarly significant change is noticeable in the direct shear curves as σ_b increases from zero to σ_a (Fig. 11a).

The conditions for failure in shear under the influence of an additional normal stress (σ_b) is defined by (6)

$$\tau_a = \frac{1}{2} \left\{ \frac{[2S_o + \mu(\sigma_a + \sigma_b)]^2}{1 + \mu^2} - (\sigma_a - \sigma_b)^2 \right\}^{1/2} \quad (6)$$

which will reduce to (2) if $\sigma_b = 0$. For $\sigma_b = \sigma_a$ (6) again reduces to two straight lines:

$$\tau_a = \pm \left\{ \frac{S_0}{(1+\mu^2)^{1/2}} + \frac{\mu}{(1+\mu^2)^{1/2}} \sigma_a \right\} \quad (7)$$

It follows from (6) that above a certain value of $K = \sigma_b/\sigma_a$ the modified direct shear curve will not reduce to zero at any positive value of σ_a . The limiting value of K above which no closure is possible (K_c) is defined by (8)

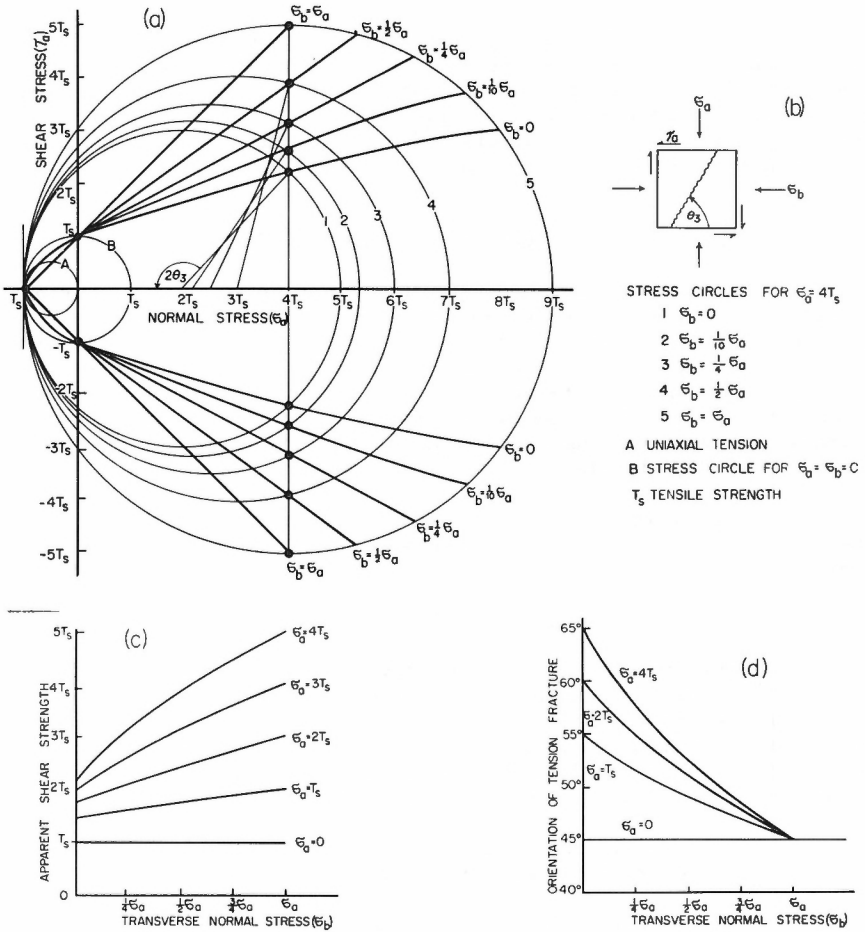


Figure 10. The influence of transverse normal stress on brittle tensile failure in modified direct shear
 (a) modified direct shear parabolas for various ratios of σ_b/σ_a
 (b) state of stress at point of tensile failure
 (c) influence of σ_b on 'apparent shear strength'
 (d) influence of σ_b on orientation of tension gash.

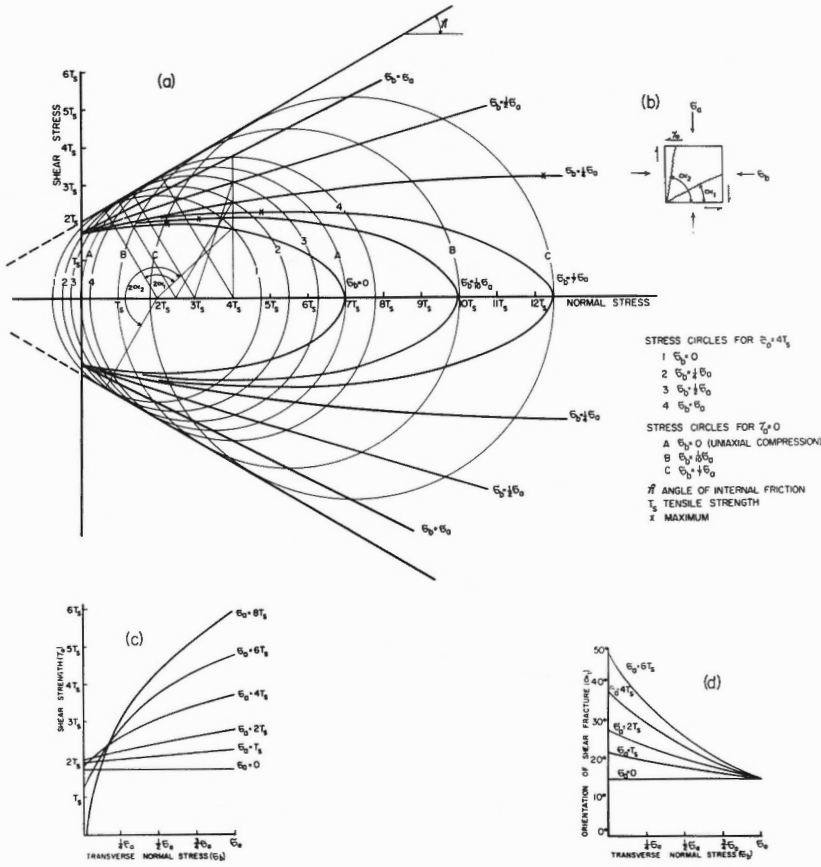


Figure 11. The influence of transverse normal stress on brittle shear failure in modified direct shear for $\phi_i = 30^\circ$
 (a) modified direct shear curves for various ratios of σ_b/σ_a
 (b) state of stress at point of shear failure
 (c) influence of σ_b on shear strength
 (d) influence of σ_b on orientation of shear fractures.

$$K_C = \frac{(1+\mu^2)^{1/2} - \mu}{(1+\mu^2)^{1/2} + \mu} \quad (8)$$

For $\phi_i = 30^\circ$, for example, $K \approx 1/3$. For any value of K below K_C there will be a maximum point at

$$\sigma_a^{\max} = \frac{2S_0\mu(1+K)}{(1+\mu^2)(1-K)^2 - \mu^2(1+K)^2} \quad (9)$$

and

$$\tau_a^{\max} = \frac{S_o}{\left\{ 1 + \mu^2 \left[1 - \left(\frac{1+K}{1-K} \right)^2 \right] \right\}^{1/2}}$$

It is apparent from Figures 11a and 11c that shear resistance will be higher for increasing σ_b and again the increase will be more pronounced at higher values of σ_a . The angle will decrease with increasing σ_b , and again as K approaches 1 the decrease will become sharper.

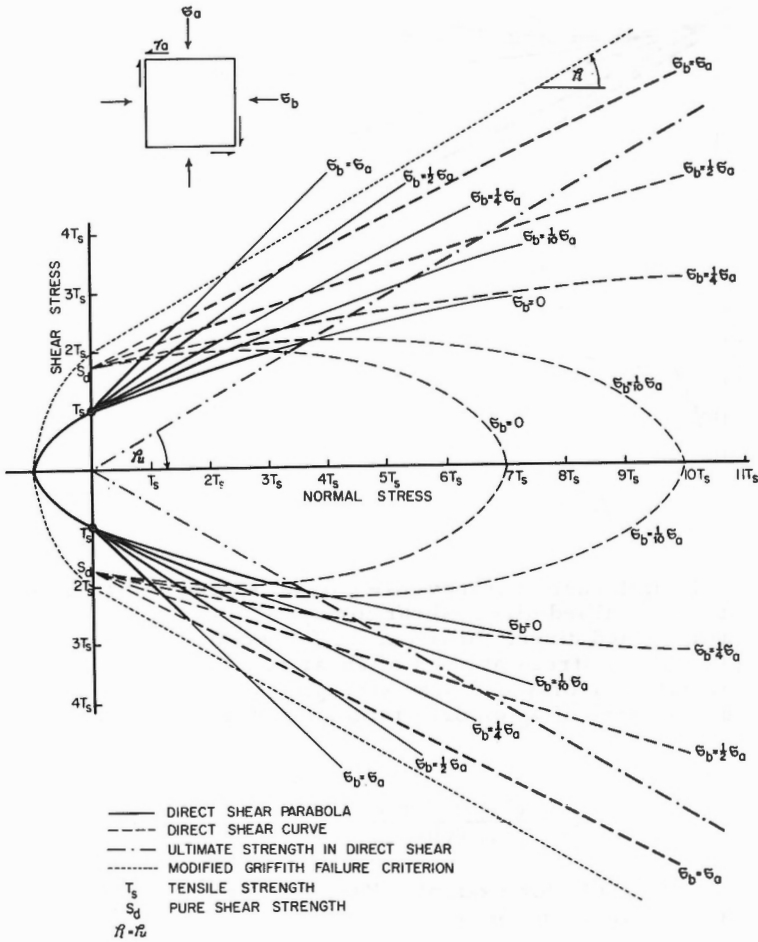


Figure 12. Composite limit curves for modified direct shear and $\phi_1 = 30^\circ$.

Figure 12 superimposes the modified direct shear parabolas and curves so that composite limit curves can be constructed in the manner of Figure 9. Again $2|T_s|$ is substituted for S_0 . If the $\sigma_b = 0$ and the $\sigma_b > 0$ limits are compared it is readily noticed that the range of σ_a for which tension failure is possible becomes more restricted to negative and small positive values. In contrast, increasing σ_b will extend the range of σ_a for which failure in shear becomes possible.

SUMMARY AND CONCLUSIONS

Brittle fracture of rock due to a static state of stress following primary faulting is possible if the normal stress acting parallel to the displacement along the fault plane is completely or partly relieved. The new state of stress will be one of direct shear ($\sigma_b = 0$) or modified direct shear ($\sigma_b > 0$). Depending on the actual state of stress after faulting and the strength of rock against tensile or shear stresses, failure will be either by tension or shear fracturing.

Conditions for failure in tension and the orientation of the resulting tension gash are described by the direct shear parabola which takes the form:

$$\tau_a = [T_s(T_s - \sigma_a)]^{1/2}$$

if normal stress acting parallel to displacement is completely relieved ($\sigma_b = 0$) and

$$\tau_a = [(T_s - \sigma_a)(T_s - \sigma_b)]^{1/2}$$

if same is greater than zero ($\sigma_b > 0$).

Conditions for failure in shear and the orientation of the resulting second order fault plane according to the Coulomb-Navier criterion are described by

$$\tau_a = \frac{1}{2} \left[\frac{[2S_0 + \mu \sigma_a]^2}{1 + \mu^2} - \sigma_a^2 \right]^{1/2} \quad \text{for } \sigma_b = 0$$

and

$$\tau_a = \frac{1}{2} \left\{ \frac{[2S_0 + \mu(\sigma_a + \sigma_b)]^2}{1 + \mu^2} - (\sigma_a - \sigma_b)^2 \right\}^{1/2} \quad \text{for } \sigma_b > 0$$

For large values of σ_a the maximum shear stress (τ_a) that can be applied in direct shear or modified direct shear loading, is defined by ultimate strength (internal friction in the crushed material) conditions.

$$\tau_a = \sigma_a \tan \phi_u$$

The resulting structure is a shear zone composed of completely granulated material.

Tension gashes form when σ_a is negative or relatively small, shear zones when σ_a is very large. For intermediate values of σ_a second order shear failure may occur, depending on the magnitude of the transverse normal stress (if larger than zero) and the angle of internal friction. As the transverse normal stress is increased, conditions for the development of shear fractures become more favourable. A high angle of internal friction favours the development of tension gashes at low σ_a and that of shear zones (granulated material) at high σ_a .

ACKNOWLEDGMENTS

The author wishes to express his appreciation to the National Research Council of Canada and the Mines Branch of the Department of Energy, Mines and Resources of Canada for sponsoring rock mechanics research at the University of New Brunswick. Special thanks are due to colleagues in the Geology Department, especially to R. L. Brown for suggesting the study, and to A. C. Fleming and J. M. Dawson for assistance in the technical aspects of the research.

REFERENCES

- Anderson, E. M.
1951: The dynamics of faulting and dyke formation with applications to Britain; Edinburgh, Oliver and Boyd, 2nd ed.
- Chinnery, M. A.
1966: Secondary faulting; Can. J. Earth Sci., vol. 3, No. 2, pp. 163-190.
- McClintock, F. A. and Walsh, J.
1962: Friction on Griffith cracks in rocks under pressure. Proc. Fourth U.S. Nat. Cong. Applied Mechanics, Berkeley, California.
- McKinstry, H. E.
1953: Shears of the second order; Am. J. Sci., vol. 251, pp. 401-414.
- Moody, J. D. and Hill, M. J.
1956: Wrench - fault tectonics; Bull. Geol. Soc. Am., vol. 67, pp. 1207-1246.
- Price, N. J.
1968: A Dynamic mechanism for the development of second order faults and related structures; see this report.

DISCUSSION

W. F. Brace and F. A. Donath took part in the discussion on Dr. Lajtai's paper, but because of technical difficulties most of the discussion was not recorded.

THE MECHANICAL EFFECTS OF PORE PRESSURE
ON FRACTURING OF ROCKS

W.F. Brace
Department of Geology and Geophysics,
Massachusetts Institute of Technology,
Cambridge, Massachusetts

Abstract

The law of effective stress has been observed elsewhere to hold for porous sedimentary rocks of low clay content, for some porous crystalline rocks, and for concrete. We conducted experiments to see if this conclusion also holds for crystalline rocks of low porosity (.001 to .03) such as granite and dunite. Triaxial experiments were performed at strain rates which ranged from about 10^{-3} to 10^{-8} per sec., using water, acetone and silicone oil.

The tests revealed that the law of effective stress holds for these rocks only when the loading rate is less than some critical value. This critical value depends on permeability of the rock, viscosity of the pore fluid and sample geometry. In our experiments with Westerly granite it was about 10^{-7} per sec., for example, with water as the fluid. The form and orientation of fractures was in no way dependent on the presence of fluids, or on strain rate.

In experiments at loading rates greater than the critical value, the rock under pore pressure is stronger than it is under zero pore pressure. This effect can be explained by the dilatancy hardening of Frank (1965). For very ductile rocks such as marble this effect is enhanced by a marked reduction in permeability which can be traced to a 'sealing off' of the pore structure, due apparently to plastic flow of the calcite grains.

INTRODUCTION

It is now well established that the fracture of rock is controlled by the effective stress. That is, the stress at which fracture occurs is determined not by confining pressure alone, but by the effective confining pressure (Fig. 1). The effective confining pressure, $\bar{\sigma}_1$, is the difference between confining pressure, σ_1 , and the pressure of pore fluids, P .

This dependence of strength on effective stress, first noted by Terzaghi (1943) for soils, has been widely observed for porous sedimentary rocks (Robinson, 1959; Handin et al., 1963), concrete (Newman, 1956) and even dense crystalline rocks like granite (Brace and Martin, in press). An example for sandstone is given in Figure 2. However, behavior is not universally in accordance with this principle. Heard (1963) noted that the brittle-ductile transition of Solenhofen limestone was virtually independent of pore pressure. And according to Handin et al. (1963) the deformation of a crystalline marble and a dolomite also failed to show the usual dependence on

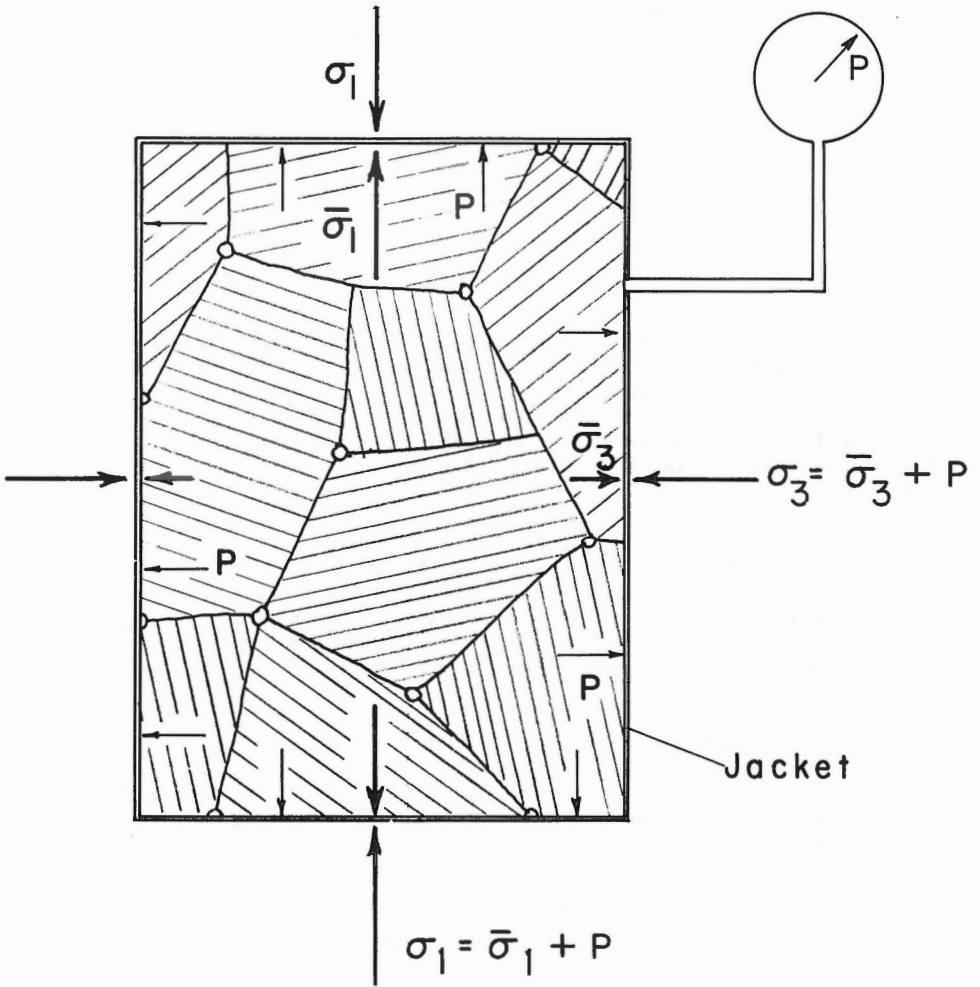


Figure 1. Schematic diagram of rock under total stresses, σ_1 and σ_3 and pore pressure, P . Total stresses are shown as being applied through an impervious jacket. In a triaxial compression test, σ_1 is usually called the confining pressure.

effective rather than total stress. This was believed to be due to the low porosity of these three rocks. Low porosity implies low permeability and, in rocks of low permeability, fluid may not completely permeate the pore space. This is necessary in order that the pore pressure be transmitted throughout the rock. In rocks of low permeability such as granite or marble, pore pressure changes can only occur slowly. The rate at which the rock is deformed, therefore, becomes an additional factor. Granite or marble

might fracture according to the principle of effective stress at slow rates, but show marked disagreement at rapid rates of loading. We recently studied this effect (Brace and Martin, in press) in order to see how rapid a loading rate would be required to bring about disagreement. Our results are summarized below, together with a brief discussion of the general applicability of the principle of effective stress to rocks of low porosity under geologic and engineering conditions.

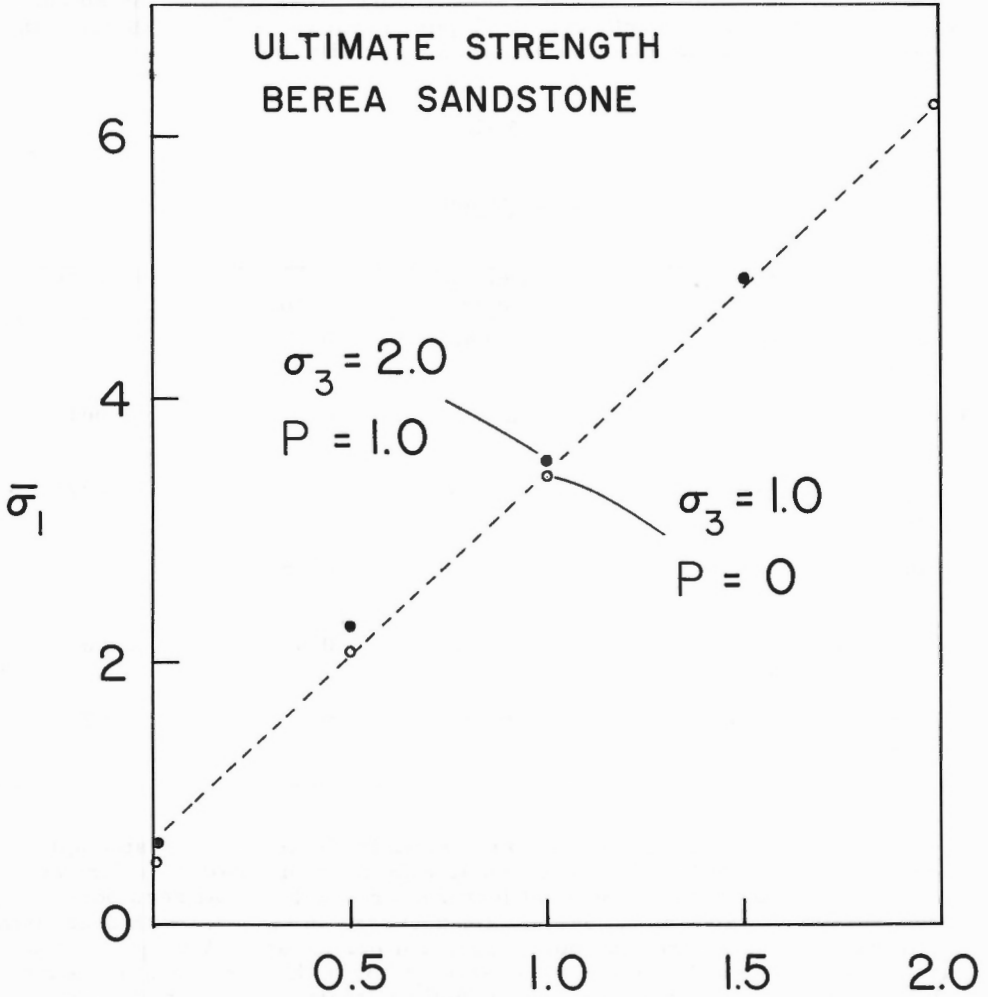


Figure 2. Effective stresses at fracture of sandstone. After Handin et al. (1963).

OBSERVATIONS

The general procedure was as follows. We selected a group of fine-grained crystalline rocks of low porosity (Table 1). For each rock, samples were stressed to fracture at different strain rates, while holding confining pressure and pore pressure constant. The experiments were then repeated at zero pore pressure, at the same effective confining pressure. Specifically, we compared strength at zero pore pressure and 1.56 kb confining pressure with strength at 1.56 kb pore pressure and 3.12 kb confining pressure. As fluids we used water, acetone or silicone oil.

TABLE 1

Rock properties

Rock	Density g/cm ³	d mm	Porosity
Granite, Westerly Rhode Island	2.646	0.75	0.007
Blair Dolomite, West Virginia	2.847	0.075	0.001
Gabbro, San Marcos California	2.819	2.0	0.002
Diabase, Columbia South Carolina	2.979	0.75	0
Dunite, Spruce Pine North Carolina	3.262	0.5	0.001
Sandstone (Pottsville) Spring City, Tenn.	2.620	0.2	0.026

The results for granite are shown in Figure 3. The strength, shown as a stress difference, is given as a function of strain rate for two fluids, water and acetone. Several features are evident. At zero pore pressure, there was a small systematic decrease in strength with decreasing strain rate; this amounted to about 3 per cent per decade. With pore pressure there was a marked increase in strength over the zero pore pressure value; this increase became greater at higher strain rates. There was no systematic difference between the results for water and acetone. Strengths with and without pore pressure agreed at a strain rate around 10^{-7} per sec. Apparently, the effective stress law held at this strain rate, but broke down at more rapid strain rates. That is, the rock became stronger when strained rapidly.

We obtained a similar result for four other rocks (Fig. 4). All of these rocks became appreciably stronger when strained more rapidly than about 10^{-7} to 10^{-8} per sec. The increase in strength amounted to as much as 50 per cent.

We obtained an interesting result with two very different fluids (Fig. 5). For the sandstone, a relatively permeable rock, there was no anomalous strengthening at any strain rate when the pore fluid was water. However, with silicone oil, strengths with pore pressure again were greater than those without pore pressure at strain rates faster than around 10^{-7} per sec.

We can generalize these results in a way which emphasizes the important features (Fig. 6). The full line shows the behavior for zero pore pressure; we see the typical slight decrease in strength with decreasing strain rate. The dotted line suggests a typical result for any one fluid under pore pressure. At slow strain rates, both lines coincide. Here, the effective stress law apparently holds. Beyond some critical strain rate, strengths with pore pressure exceed those without pore pressure. The difference between the two increases with increasing strain rate up to a point at which the difference remains constant.

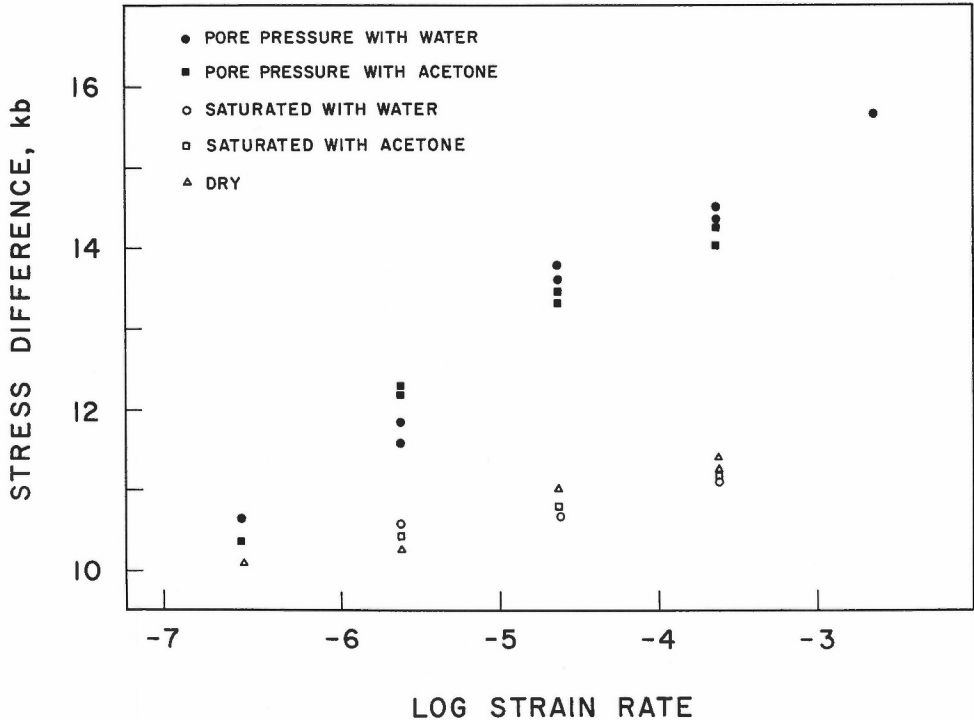


Figure 3. Strength of Westerly granite as a function of strain rate (Brace and Martin, in press).

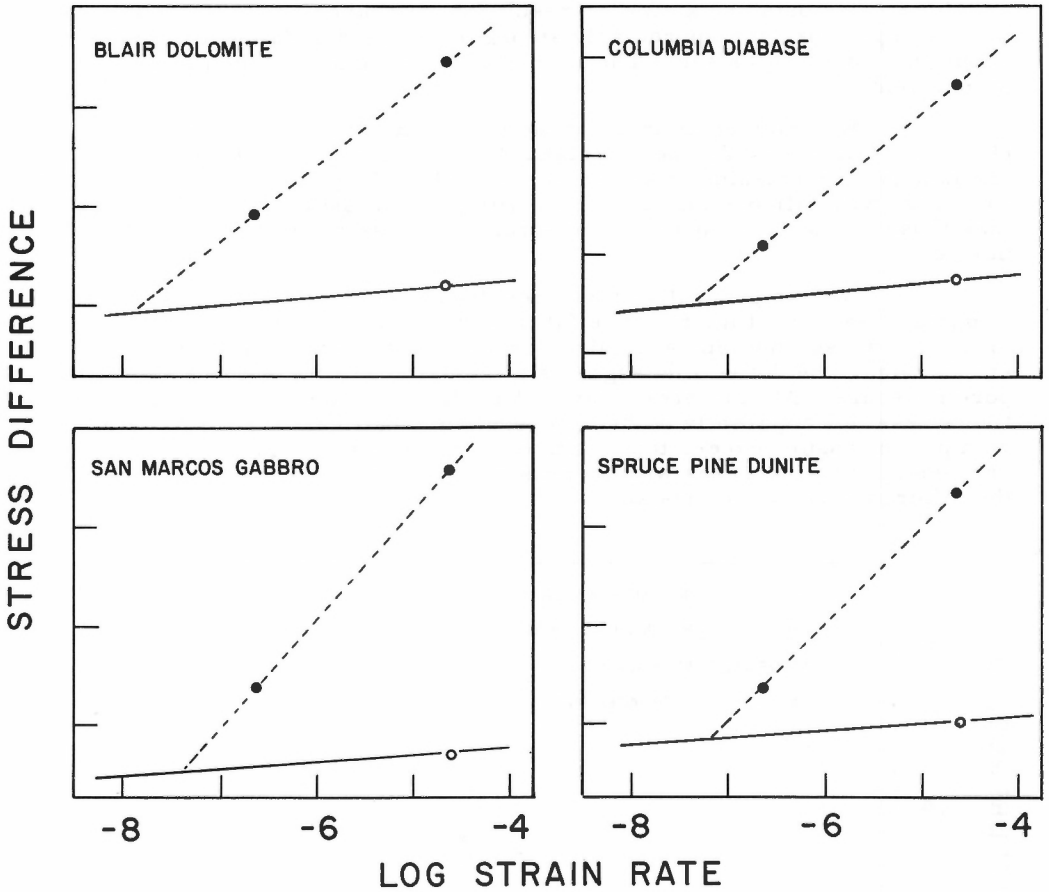


Figure 4. Strength of four rocks as a function of strain rate (Brace and Martin, in press).

These marked variations in strength suggested that there also might be marked differences in the fracture patterns in our samples. We examined our material with some care to explore this possibility.

Typically, a sample was cut by a single major fault, along which a small shear displacement had occurred. The inclination of this fault to the direction of maximum compression was $30^\circ + 3^\circ$; there was no apparent difference in angle between samples fractured with pore pressure and those fractured dry or saturated. Although there was typically a single through-going fault, many small fractures were common. These were parallel or conjugate to the main fault, and the length ranged up to half that of the main fault. Although the density of these small fractures varied somewhat from sample to sample, there was no obvious correlation of fracture density with either strain rate or with pore pressure. The major fault typically intersected one of the end surfaces of the sample near a corner; there was no

obvious preference for that corner near the fluid reservoir, except for a few of the runs at high strain rate with pore pressure. There, as one might anticipate, the end nearest the source of fluid seemed to be the end from which the main fracture emanated. To sum up, there seemed to be little in the pattern of fracturing which might correlate with either strain rate or the presence of a fluid under pressure. Of course, we observed surface features only (through the transparent jacket); more thorough study of fractures within the sample might still reveal significant differences in density, spacing or distribution of the many subsidiary fractures.

DISCUSSION

To what can we attribute the anomalous strengthening shown above? One clue was given by the pore pressure changes observed as stress was raised. Although, as stated above, pore pressure was maintained constant during an experiment, pore pressure tended to change. If allowed to change, it decreased in a characteristic way. In a typical result for granite (Fig. 7), pore pressure first increased slightly, and then at about half the fracture stress, began to drop. At fracture, pressure had dropped several

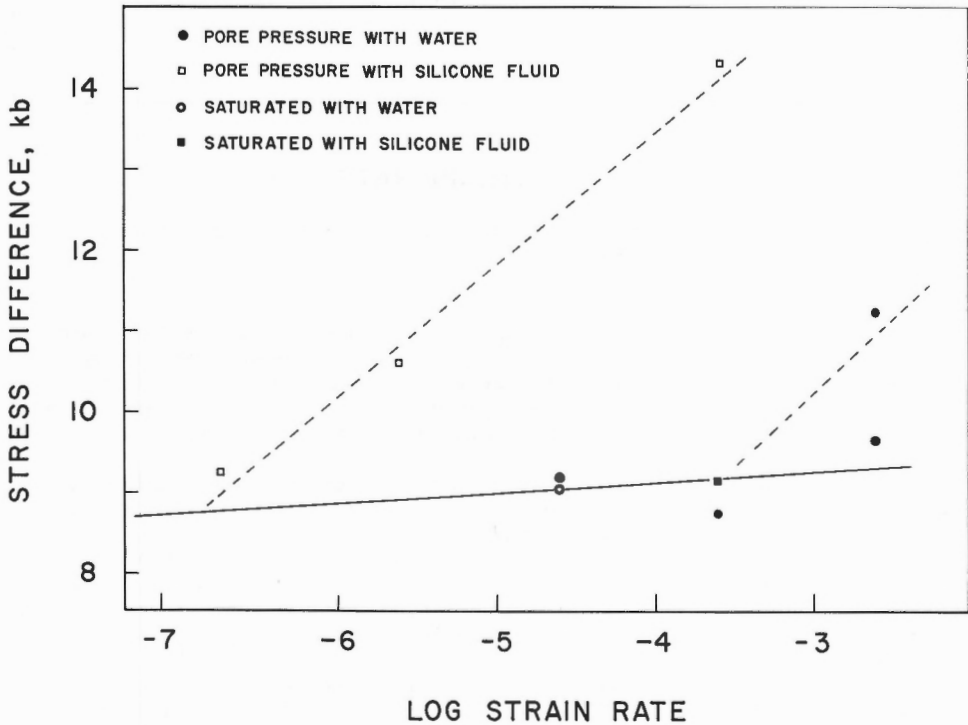


Figure 5. Strength of sandstone as a function of strain rate for two different fluids (Brace and Martin, in press).

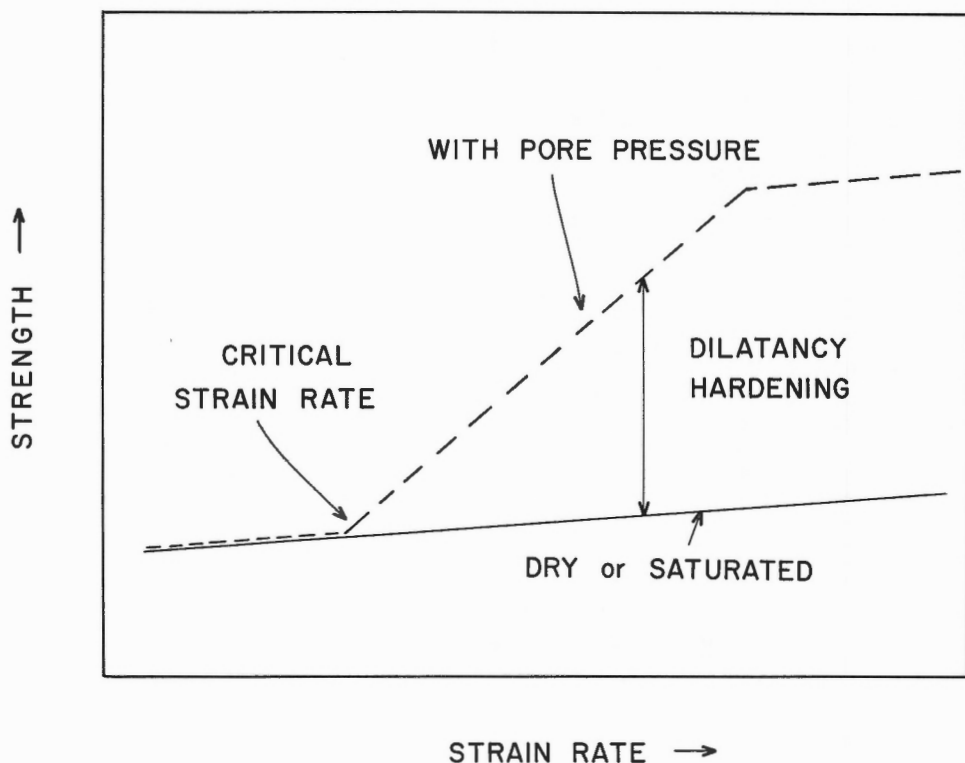


Figure 6. Generalized dependence of strength on strain rate for a given rock and pore fluid.

hundred bars, or by about 30 per cent. As indicated in Figure 1 the pore fluids form a closed system, so that a decrease in pressure (at constant temperature) could only mean that pore volume had increased. This increase in porosity or dilatancy is an almost universal feature of rocks, even under high confining pressure (Brace, Walsh and Frangos, in press).

We can now readily account for the anomalous strengthening observed in our experiments. Under stress, the rocks became dilatant; this tended to cause pore pressure to drop. At very slow strain rates, or in rocks of high permeability, pore pressure within the rock could be constantly restored by external adjustments. However, in tests done rapidly, pore pressure changes within the rock lagged behind those in the external part of the system, so that pore pressure within the rock dropped. For this case, effective confining pressure on the rock was actually greater than the value shown by the external pressure gages. Because the strength of rocks increases with effective confining pressure, rocks strained rapidly were stronger. As this effect is due to dilatancy, it is called, following Frank (1965), dilatancy hardening.

Why was the dilatancy hardening dependent on the strain rate and on the type of fluid, when the amount of dilatancy was almost certainly the same irrespective of fluid and strain rate? Here, permeability of rock and viscosity of fluid must be considered. Drop in pore pressure due to dilatancy will be quickly restored if the rock is highly permeable or if the fluid is of low viscosity. Dilatancy hardening should disappear for any rock-fluid combination if we strain the rock slowly enough. The critical strain rate at which dilatancy hardening disappears is the strain rate at which the effective stress law holds.

A point of some general significance is that the critical strain rate is not a 'rock property'. It depends on fluid viscosity as the results for sandstone saturated with water and silicone oil indicate. It also depends on specimen geometry and size and on the way in which pore fluids have access to the rock. The greater the distance which fluid has to move in a particular mass of rock under stress then the lower the critical strain rate. It can be shown by an approximate analysis (Brace and Martin, in press) that the pore pressure is restored by an amount which is proportional to rock permeability, but inversely proportional to fluid viscosity and to the square of distance from a 'reservoir' of fluid at constant pressure.

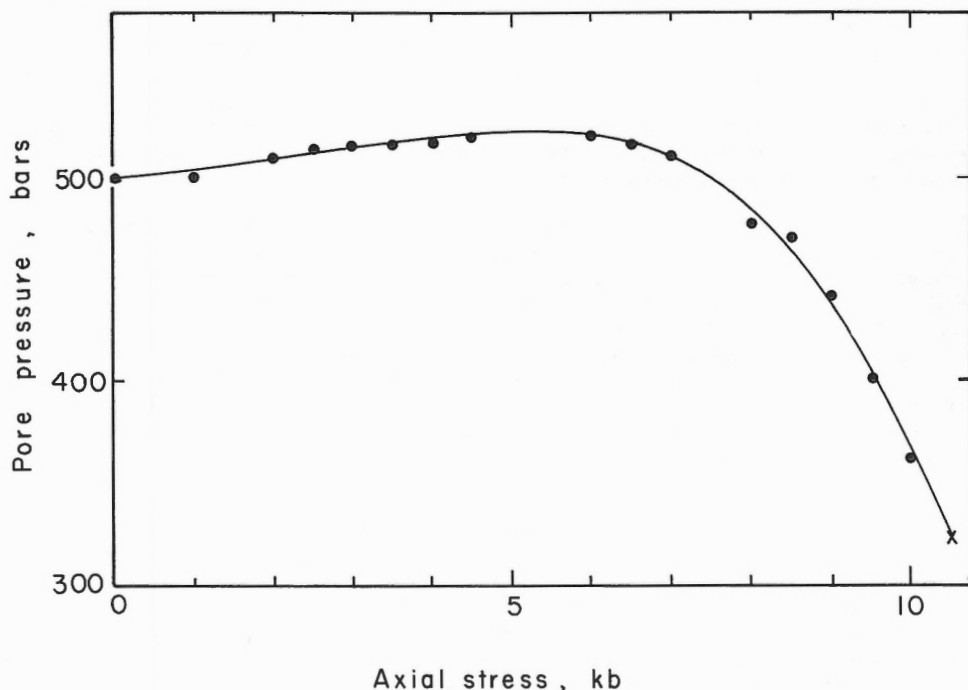


Figure 7. Change of pore pressure with axial stress, σ_3 , for Westerly granite at a confining pressure of 1.58 kb. Fracture occurred at the point marked X. After Brace and Orange (in press).

CONCLUSIONS

To what extent are the results presented here general for rocks, and to what extent are they applicable to geology or to engineering practice? The behavior suggested in Figure 6 probably holds in a general way for all rocks; there must, however, be a wide variation in the critical strain rate. And, the critical strain rate itself will depend, as we have seen, on both the dimensions of a rock mass and its permeability. For most crystalline rocks permeability is small but measurable. Both by direct observation (Brace, Walsh and Frangos, in press) and by inference from electrical properties, permeability of typical crystalline rocks will range from 1 to 10 nanodarcies (1 nanodarcy equals 10^{-9} darcy) at pressures up to 5 kb. For samples the size of those used here (length of several cm) critical strain rates will be around 10^{-7} to 10^{-8} per sec.

Under certain conditions, permeability may be a great deal lower than the above values. Brace and Orange (in press) observed that calcite marble became virtually impermeable as a result of deformation at a few hundred bars confining pressure. This may have caused the anomalous behavior of Solenhofen limestone and dolomite reported by Heard (1963) and Handin et al. (1963). These materials are apparently capable of true plastic flow to a limited degree; at least there is ample evidence that the minerals calcite and dolomite undergo twin- and translation-gliding. Perhaps this is responsible for cutting off the minute passageways which permit fluid flow. One might expect, based on this, that decrease in permeability, with an accompanied lowering of the critical rate for dilatancy hardening, would occur for any rock when conditions were reached which enhance mineral plasticity. Unfortunately, our understanding of these conditions for typical silicate rocks is still very incomplete. It is probably safe to say that they are not reached until fairly deep in the earth's crust.

To return to the question of the generality of these results, we conclude that, in view of the slow strain rates considered typical of tectonic processes, silicate rocks will show no anomalous strength due to dilatancy. With water as the fluid, even for rock masses cut by joints spaced on the order of metres, critical strain rates will probably not be slower than 10^{-10} per sec. Geologic strain rates are usually considered to be 10^{-14} per sec., or less. Under these conditions, the law of effective stress will hold. We conclude, therefore, that this law is of even greater generality than previously realized, in that it applies to crystalline silicate rocks as long as loading rates are kept below certain critical values.

In certain engineering applications, departures from the law of effective stress due to dilatancy hardening may have to be considered. Two situations illustrate the possibilities. One is encountered in water-saturated rock surrounding buried nuclear explosions. There, a strengthening will probably accompany the high strain rates imposed on the rock. This strengthening could be calculated from a knowledge of such factors as porosity of the rock and its dilatancy. As shown in Figure 6 this strengthening has a definite limit; it gives the 'shelf' shown at the high rates, which expresses the obvious feature that pore pressure cannot decrease below zero.

Another situation of interest occurs when rock is loaded suddenly as in blasting, or as a result of a landslide. If it becomes dilatant then the

rock might show anomalous strength, and could thus be loaded momentarily in excess of its normal strength. With time, however, this anomalous strengthening would disappear as the normal pressure is restored. Sudden failure might ensue as strength returns to normal. This delayed failure might account for some of the activity observed in deep mines some time after blasting.

ACKNOWLEDGEMENTS

This work was supported by the National Science Foundation as Grant GA-613 and by Advanced Research Projects Agency under Contract DADA01-67-c-0090.

REFERENCES

- Brace, W. F., Paulding, B. W., Jr. and Scholz, C. H.
1966: Dilatancy in the fracture of crystalline rocks; J. Geophys. Res., vol. 71, pp. 3939-3954.
- Brace, W. F. and Martin, R. J., III.
in press: A test of the law of effective stress for crystalline rocks of low porosity; Internat. J. Rock Mechanics Mining Sci.
- Brace, W. F. and Orange, A. S.
in press: Electrical resistivity changes in saturated rocks during fracture and frictional sliding; J. Geophys. Res.
- Brace, W. F., Walsh, J. B. and Frangos, W. T.
in press: Permeability of granite under high pressure; J. Geophys. Res.
- Frank, F. C.
1965: On dilatancy in relation to seismic sources; Rev. Geophysics, vol. 3, pp. 484-503.
- Handin, J., Hager, R. V., Jr., Friedman, M., and Feather, J. N.
1963: Experimental deformation of sedimentary rocks under confining pressure: Pore pressure tests; Bull. Am. Assoc. Petrol. Geol., vol. 47, pp. 717-755.
- Heard, H. C.
1963: Effect of large changes in strain rate in the experimental deformation of Yule marble; J. Geol., vol. 71, pp. 162-195.
- Newman, K.
1956: Properties of concrete; in Structural Concrete, vol. 2, pp. 2-34.
- Robinson, L. H., Jr.
1959: The effect of pore and confining pressure on the failure process in sedimentary rock; Colo. School Mines Quart., vol. 54, No. 3, pp. 177-199.
- Terzaghi, C.
1943: Theoretical soil mechanics; New York, John Wiley and Sons.

DISCUSSION

W.M. Schwerdtner asked the author if he had tried to use oil to fill the pores of the rocks in his experiments, and whether he (Schwerdtner) was correct in assuming that dilatancy would affect the rock earlier if the rate of deformation was slow, than it would if that rate was fast.

The author said that he had attempted to get a fluid less viscous than water, to study the toe of the curve showing presence of anomalous strength, and that oil, of course, would not have been the right fluid in this case. He had noticed some difference in the onset of dilatancy with different strain rates, but his measurements were not accurate enough regarding this problem.

D.F. Coates (written comments) This is a very helpful paper in that it supplies empirical data for rocks regarding concepts that have been inherited from soil mechanics and assumed to be valid for rocks. Some speculations are raised in the paper for which information exists in either soils or borderline materials like clay-shales. For example, the comment that no differences occurred in the fracture angle between samples fractured with pore pressure and those fractured dry is consistent with the theoretical concepts of effective stresses and with empirical data in clays. Secondly, the observation of apparent increase in strength arising from dilatancy has been known for many years in soil mechanics, as the negative pore pressures often developed during uniaxial compressive testing in clays give rise to abnormal apparent strengths. Thirdly, the interaction of pore water dissipation, or flow over time, in a relatively impermeable material and the resultant change in effective stresses leading to failure some considerable time after the original causal action, has been documented for cases of slope and foundation failures in clays.

For those who may plan on conducting similar work, it would be of value if the author could provide some information on dispersion of test results assuming that the data represented in the various graphs are mean values. Furthermore, in the light of the description that confining pressures and pore pressures were held constant during the tests, it would be interesting to have some discussion on the degree of certainty that the pore pressures within the body of the sample were known, and were actually constant, having in mind that with relatively impermeable materials, transient conditions can take a long time to dissipate.

SOME OBSERVATIONS ON THE AGE OF JOINTING
IN MACROSCOPICALLY FOLDED ROCKS

H.A.K. Charlesworth
Geology Department, University of Alberta, Edmonton

Abstract

The dispersion of joints within associated joint sets, and the extent to which the sets are veined may enable their relative ages to be determined. The relative ages of joint sets in macroscopically folded sandstones belonging to the Cretaceous Cardium Formation in the Bow River area of the Rocky Mountain Foothills are consistent with the possibility that the two stress fields responsible for jointing were modified residuals of the orogenic stress field.

INTRODUCTION

Joints in sedimentary rock may be defined as regularly spaced, planar fractures, oblique to bedding, across which no appreciable movement has occurred. They differ from faults for example in their regular spacing, in their association with plumose structure, and in the absence of appreciable displacement. Sedimentary rock in macroscopic folds is generally divisible into domains within which both bedding and jointing are penetrative.

From the standpoint of age joints in macroscopically folded rocks may be preorogenic, synorogenic or postorogenic. Price (1959, pp. 157-161) has argued that joints are postorogenic and are related to the remnants of the orogenic stress field modified by horizontal extension related to isostatic uplift and by erosional reduction in gravitational load. To this one might add the effect of cooling as erosion brings rocks once deeply buried and therefore hot, closer to the topographic surface.

The purpose of this paper is to see whether or not this hypothesis concerning the origin of joints is applicable to jointing in the macroscopically folded Cretaceous Cardium sandstones in the Bow River area of the Rocky Mountain Foothills (Muecke and Charlesworth, 1966). These sandstones, which are about 100 feet thick, and are underlain and overlain by shales of the order of 1,000 feet thick, have been gently buckle-folded about northerly trending axes. Most of the joints fall into four types of sets, all of which are approximately normal to bedding (Fig. 1). Type 1 is extensional and subparallel to the associated fold axis B. Types 3 and 4, found only in western domains, form conjugate shear sets whose acute bisectrices are approximately normal to type 1, and whose dihedral angles tend to decrease eastwards. Type 2 is subnormal to type 1; each type 2 set tends to have an elongate maximum and therefore to represent two merging shear sets of small dihedral angle. The slickensides on joints of types 2-4 are approximately parallel to bedding whereas those on type 1 joints are nearly normal to bedding.

Because of the regularity in orientation of slickensides within a joint set, and because in the case of types 2 to 4 they are approximately normal to the line of intersection of conjugate shear sets, slickensides are assumed to date from the period of initial fracturing. Thus the joint sets appear to form two age groups. Group A (types 2-4) originated when the maximum principal stress or compression (σ_1) was approximately parallel to bedding and normal to B and when the minimum principal stress (σ_3) was approximately parallel to B, whereas group B (type 1) developed when σ_1 was approximately normal to bedding and when σ_3 was approximately parallel to bedding and normal to B. The possibility of using dispersion and veining to determine the relative ages of the two groups will now be discussed.

DISPERSION

The usefulness of dispersion in establishing the relative ages of associated sets depends on the validity of the following argument. Until the formation of the older of two joint sets the principal stress trajectories should have maintained a fairly constant orientation throughout the unfractured rock. Thus the joints that formed in response to this stress system should be grouped with low dispersion about the mean joint plane. The fractured nature of the rock should have caused the stress field associated with the younger joints to be less regularly oriented than before, with the result that the dispersion of these joints about their mean plane should be greater than the older.

The dispersion of a joint set can be determined only if the orientations of a number of constituent joints are known. This sample of the joint set should ideally be random, but in practice this is rarely possible because, for example, of subjective selection on the part of the field geologist, outcrop distribution, and the relationship between outcrop shape and joint orientation. Two methods of evaluating dispersion will now be described.

If joints in a joint set have a spherical-normal or Fisher distribution, the joint poles have axial symmetry about the mean pole and conform to the probability density function

$$P(\phi) = \text{const } e^{K \cos \phi} \quad (1)$$

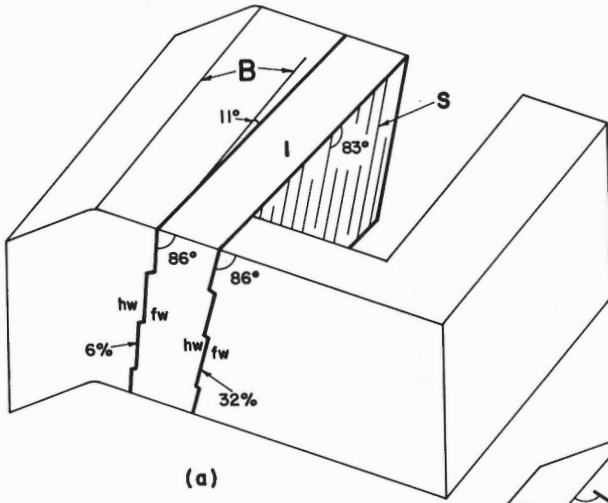
where ϕ is the angular distance from the mean pole (Fisher, 1953). K , the three-dimensional analogue of the inverse of variance, is a measure of the dispersion of the joints about the vector mean; the higher its value, the lower the dispersion. As long as K is greater than 3, a good approximation of the best estimate \hat{K} of K is given by

$$\hat{K} = \frac{N-1}{N-R} \quad (2)$$

where N is the number of measurements, where

$$R^2 = \left(\sum_{i=1}^N l_i \right)^2 + \left(\sum_{i=1}^N m_i \right)^2 + \left(\sum_{i=1}^N n_i \right)^2 \quad (3)$$

and where (l_i, m_i, n_i) ($i=1, 2, \dots, N$) are the direction cosines of individual joint poles. As N increases, \hat{K} approaches the true value of K .



B - fold axis
hw - hanging wall
fw - footwall
X - acute bisectrix
s - slickensides

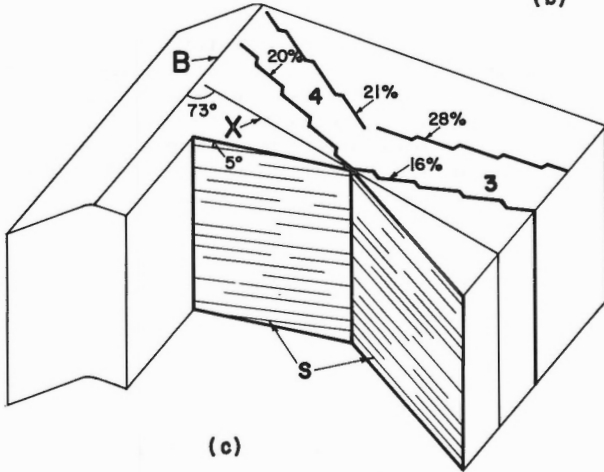
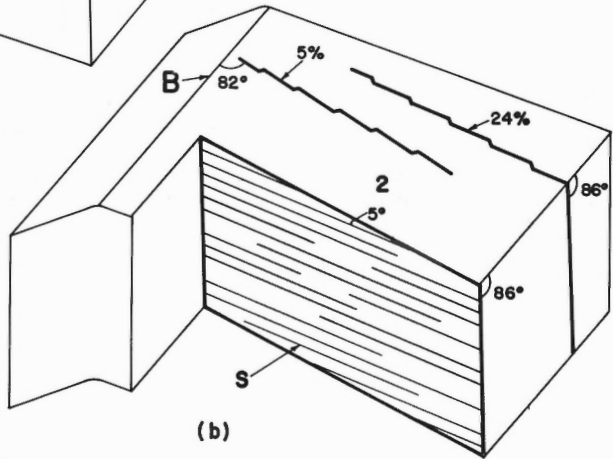


Figure 1.

Diagrammatic block diagrams of the east limbs of anticlines showing some geometric features of joint sets belonging to type 1 (a), type 2 (b), and types 3 and 4 (c).

(Muecke and Charlesworth, 1966).

If joints in a set have distribution such that, the joint poles have axial symmetry about the mean pole and conform to the probability density function

$$P_2(\phi) = \text{const } e^{k \cos^2 \phi} \quad (4)$$

k is the parameter of dispersion analagous to K in (1); its value also increases with decreasing dispersion. The dispersion of such a joint set may be estimated using the symmetrical matrix

$$M = \begin{matrix} \sum l_i^2 & \sum l_i m_i & \sum l_i n_i \\ \sum m_i l_i & \sum m_i^2 & \sum m_i n_i \\ \sum n_i l_i & \sum n_i m_i & \sum n_i^2 \end{matrix} \quad (5)$$

The three eigenvalues of this matrix are always positive and add up to N, and the three eigenvectors associated with these eigenvalues are always perpendicular to each other (Watson, 1966). The eigenvalues are related to the sum of the moments of inertia of particles of unit mass placed at the termini of unit vectors representing the joint poles. The moment of inertia I of this set of N particles about an axis of direction d is, in matrix notation,

$$I = N - d'Md, \quad (6)$$

$$= N - \sum_{i=1}^3 \sum_{j=1}^3 d_i d_j M_{ij} \quad (7)$$

where d_1, d_2 and d_3 are the direction cosines of the direction d. The axis that is associated with the least moment of inertia is that which maximizes $d'Md$. The largest value of $d'Md$, λ_1 , is the greatest eigenvalue of M. The direction d, the eigenvector associated with λ_1 , parallels the pole to the mean joint plane. The magnitude of λ_1/N is a measure of the dispersion of the joint poles about the mean, such that the smaller this parameter the greater the dispersion. k is related to this parameter by

$$\frac{\int_0^1 t^2 e^{kt^2} dt}{\int_0^1 e^{kt^2} dt} = \frac{\lambda_1}{N} \quad (8)$$

where $t = \cos \phi$ (Watson, 1966).

Most joint sets probably do not conform precisely to either of the distributions discussed above, so K and k may be used only to estimate dispersion.

Both K and k , as defined in equations 1 and 4, for the four types of joint set in the various domains are given in Table 1. Group A is represented in domains 1-9 by types 3 and 4, and in domains 10-20 by type 2. Group B is everywhere represented by type 1. In domains 1-9 the average values for K and k of group B sets are 35 and 20, whereas those of group A sets are 56 and 32. Thus, applying the criterion of dispersion, group A joints would appear to be the older. In domains 10-20 the average values for K and k of group B joint sets (36 and 19) are similar to those in domains 1-9, but those of group A (34 and 18) are considerably lower than the corresponding values in domains 1-9. This could be taken to indicate that the group A joints in domains 10-20 are the younger. However, the relatively high dispersion of group A joint sets in domains 10-20 is probably related to the fact that each of these sets represents two merging shear sets.

VEINING

Joints are commonly associated with veins, and the percentage of veined joints in one set is usually different from that in another set. All things being equal (e.g. the sets being compared are both extensional), the older set should have the greater percentage of veins, for in its case there has been more time for precipitation to occur.

The percentages of veined joints belonging to the four types of joint sets in the various domains are shown in Table 1. Twenty per cent of the joints in the extensional type 2 sets are infilled with vein material as opposed to only 5 per cent in type 1 extensional sets. From this the type 2, and thus the group A, joints would appear to be the older. Only 3 per cent of the group A joints in sets belonging to types 3 and 4 have veins. The smallness of this percentage stems not from their being younger than group B joints, but from the fact that the majority of joints belonging to types 3 and 4 are shear fractures that formed at considerable angles to σ_1 , and so should not have been associated with much normal displacement.

POSTOROGENIC STRESS HISTORY

By applying the criteria involving dispersion and veining, group A joints would appear to be the older and group B the younger. Let us now use Price's theory to predict the nature and history of jointing in the Bow River area. During the course of this discussion the three principal stresses, which at all times after orogenesis should have been approximately east-west, north-south and vertical, will be referred to as σ_e , σ_n and σ_v .

The stress field immediately after orogenesis (Fig. 2) was such that $\sigma_e = \sigma_1$, $\sigma_n = \sigma_2$ and $\sigma_v = \sigma_3$. Postorogenic decrease in the values of σ_e and σ_n should have altered the nature of the stress field such that $\sigma_e = \sigma_1$, σ_n (tensile) = σ_3 and $\sigma_v = \sigma_2$. Eventually jointing associated with east-west contraction and north-south extension should have occurred (Fig. 2).

Immediately after jointing, the stress field should have been such that $\sigma_e = \sigma_2$, $\sigma_n = \sigma_3 \approx 0$ and $\sigma_v = \sigma_1$ (Fig. 2). Further horizontal extension could have been taken up in the north-south direction by opening of pre-existing joints, so the value of σ_n should have remained approximately zero.

Table 1.

Dispersion, in terms of K and k, and the occurrence v (in per cent) of veins for the four types of joint set in Cardium sandstones along the Bow River. The numbering of the domains increases eastwards.

Domain	Type of joint-set											
	1			2			3			4		
	K	k	v	K	k	v	K	k	v	K	k	v
1	36	19	1	71	36	26	89	45	1	14	21	11
2	26	14	4	-	-	-	61	31	2	122	58	3
3	27	13	0	-	-	-	26	14	0	8	50	13
4	17	28	0	-	-	-	12	19	0	67	16	0
5	47	24	0	-	-	-	31	17	0	66	34	0
6	46	24	0	-	-	-	54	30	0	122	47	0
7	48	21	0	-	-	-	57	30	0	73	37	1
8	33	18	1	-	-	-	55	28	0	53	27	1
9	35	22	3	-	-	-	52	27	11	74	38	13
10	18	11	0	28	16	5	-	-	-	-	-	-
11	44	22	0	28	16	6	-	-	-	-	-	-
12	61	32	0	91	46	21	-	-	-	-	-	-
13	22	12	7	27	15	35	-	-	-	-	-	-
14	42	22	27	22	12	41	-	-	-	-	-	-
15	26	15	6	18	10	24	-	-	-	-	-	-
16	45	23	8	15	9	29	-	-	-	-	-	-
17	30	16	15	15	9	29	-	-	-	-	-	-
18	24	14	12	17	9	17	-	-	-	-	-	-
19	72	37	0	99	51	2	-	-	-	-	-	-
20	9	6	9	17	10	11	-	-	-	-	-	-

Such extension could not have occurred in the east-west direction, so the value of σ_e would have reduced to the point where σ_e (tensile) = σ_3 , $\sigma_n = \sigma_2 \approx 0$ and $\sigma_v = \sigma_1$. Eventually jointing associated with vertical contraction and east-west extension and symmetrically disposed with respect to the older joints should have developed (Fig. 2).

Asymmetrical steps on slickensided joints (Fig. 1) suggest that the majority of secondary joints experienced 'normal fault' displacement. This type of displacement could have originated as follows. From the end of orogenesis until the period of formation of group B joints the principal stress-axes appear to have been approximately orthogonal to bedding in the gently folded competent sandstones. After and to a certain extent during jointing, σ_v should have approached the vertical more closely than before, with the result that continued horizontal extension should have led to further opening of group A joints and to 'normal fault' displacements along group B joints.

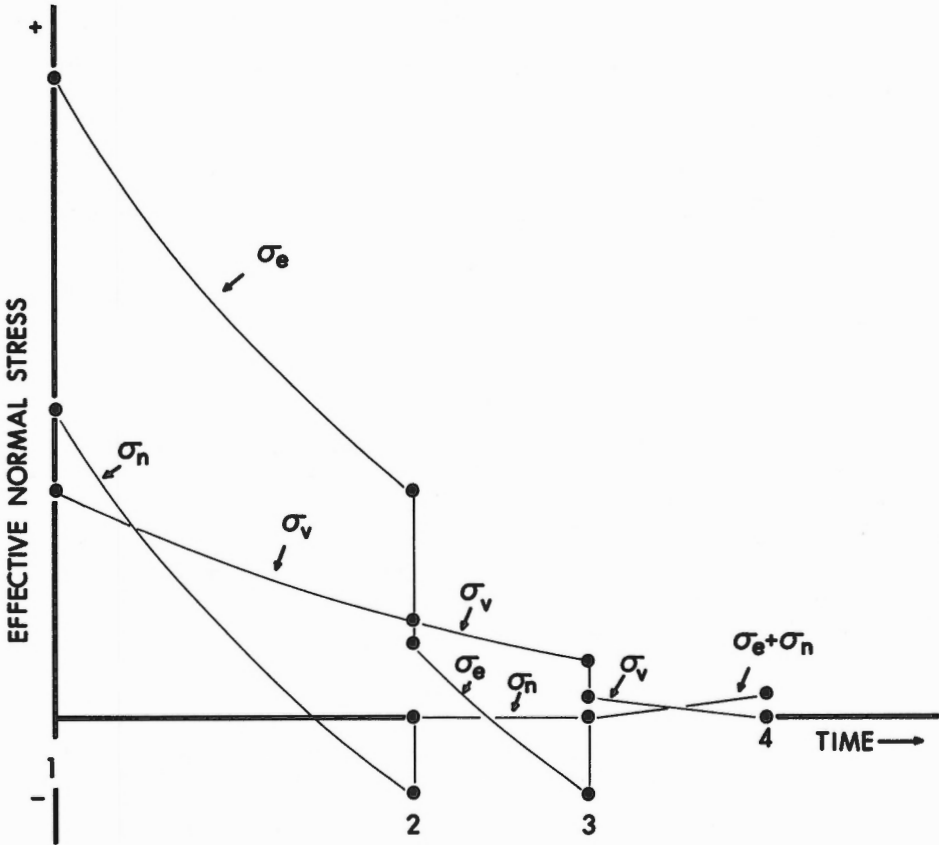


Figure 2. Variation in σ_e , σ_n and σ_v between the end of orogenesis (1) and the period of unroofing of the jointed rock (4). 2 - formation of group A joints. 3 - formation of group B joints.

At the end of jointing according to the theory discussed above, the essentially vertical principal stress was compressive, and the two essentially horizontal principal stresses were approximately zero. However, in many regions the principal horizontal stresses close to the surface have been observed to be compressive and even in some cases to be greater than the vertical (see e.g. Imrie, 1967, pp. 28-41). How can these observations be reconciled with Price's theory? The answer to this question probably lies in the fact that the values of the principal stresses referred to in the preceding paragraphs are the effective principal stresses (i. e. the total principal stresses less the pore pressures). Thus the total horizontal principal stresses immediately after jointing would have been compressive and equal to the pore pressure. During the period between jointing (when the rocks were still at considerable depths) and exposure through erosion of the jointed rocks at the surface, the pore pressure decreased to zero (the stress measurements referred to above were made above the water table). Thus if the value of the total horizontal principal stresses remained constant throughout this period, the effective horizontal principal stresses close to the surface should be compressive and equal to the pore pressure at the time of jointing. During the period between jointing and exposure the value of the vertical principal stress decreased to zero, so that at the surface the horizontal principal stresses should exceed the vertical by an amount approximately equal to the pore pressure at the time of jointing. The situation described above is complicated by the fact that during the period between jointing and exposure at the surface, the value of the total horizontal principal stresses continued to fall because of horizontal extension, erosional reduction in gravitational load, and cooling. Thus the existence at the surface of horizontal principal stresses in excess of the vertical can be accounted for on the basis of the above theory only if the amount by which the total horizontal principal stresses were reduced during unroofing of the jointed rock was less than the pore pressure at the time of jointing.

DISCUSSION

Thus both the nature and history of jointing in the macroscopically folded sandstones of the Bow River area, predicted by Price's theory, agree with the observed geometry, and with the history established using the criteria of dispersion and veining. Let us look at the possibility that the jointing and folding were contemporaneous. The fact that the joints are not displaced by bedding plane slip would appear to disprove this possibility. However, Norris (1967, p. 313) has pointed out that very little slip on a mesoscopic scale is required to produce striae, so the usefulness of this criterion for establishing the relative age of folding and jointing is doubtful.

The dihedral angle of group A conjugate shear sets decreases from about 70° in the west of the Bow River area to essentially zero in the east. This means that the angle θ that a joint made with σ_1 at the time of fracturing decreased eastwards. Brace (1964) found that, although the angle θ remains relatively constant for experimentally produced fractures when the differential stress is large, when it is small and σ_3 is tensile, θ decreases with the value of σ_3 and that there is a continuous transition from shear fractures to extension fractures. Thus if joints may be compared to these experimental fractures, they formed at a time when the differential stress was small. This conclusion, which is supported by the small displacements across joints and their close spacing (Price, 1966, p. 142), suggests that

jointing is postorogenic because the differential stress throughout folding must have been large except where the 'beam effect' was present (see e.g. Stearns, 1964; Norris, 1967). This effect, characteristic of buckle folds with small radii of curvature and relatively widely spaced surfaces of bedding plane slip, was probably unimportant in macroscopic folds such as those under discussion where the radii of curvature are more than three orders of magnitude larger than the spacing of surfaces of bedding plane slip. Thus jointing is unlikely to be synorogenic.

Another possibility concerning the origin of jointing should be mentioned. The folds in the Cardium sandstones of the Bow River area are cut by a number of thrust faults, so clearly the differential stress in the sandstones during folding approached the failure stress. Under these conditions microscopic cracks are likely to form in the sandstone (see e.g. Brace et al., 1966, pp. 3942-3949). These cracks may grow into mesoscopic joints with the postorogenic reduction in confining pressure. Thus the orientation of group A joints may reflect that of the stress field at the onset of folding, although they may not have existed as mesoscopic fractures until long after folding had ceased. The variation in dihedral angle associated with these joints may in this case reflect the easterly decrease in confining pressure to which the Cardium sandstones were subjected during orogenesis.

CONCLUSIONS

Most of the jointing in the macroscopically folded Cardium sandstones of the Bow River area originated at two distinct periods after folding had ceased, and developed in response to a modified residual of the orogenic stress field. Another possibility is that the joints, although postorogenic, are related to microscopic cracks that propagated during orogenesis.

ACKNOWLEDGMENTS

The author wishes to thank Mr. D.M. Cruden of Imperial College, London, and Dr. J.R. McGregor of the University of Alberta, for their constructive criticism, help and advice during the preparation of this article. He would also like to acknowledge the receipt of grants in aid of research awarded by the National Research Council of Canada and the Geological Survey of Canada.

REFERENCES

- Brace, W.F.
1964: Brittle fracture of rocks; in State of stress of the earth's crust, Judd, W.R., editor, Elsevier, New York, pp. 111-174.
- Brace, W.F., Paulding, B.W. Jr., and Scholz, C.
1966: Dilatancy in the fracture of crystalline rocks; J. Geophys. Res., vol. 71, pp. 3939-3953.
- Fisher, R.A.
1953: Dispersion on a sphere; Proc. Roy. Soc. (London), Ser. A. vol. 217, pp. 295-305.
- Imrie, A.S.
1967: Analysis of the underground powerhouse arch at the Portage Mountain dam; Univ. Alberta, Edmonton, unpubl. M.Sc. thesis.
- Muecke, G.K., and Charlesworth, H.A.K.
1966: Jointing in folded Cardium sandstones along the Bow River, Alberta; Can. J. Earth Sci., vol. 3, pp. 579-596.
- Norris, D.K.
1967: Structural analysis of the Queensway folds, Ottawa, Canada; Can. J. Earth Sci., vol. 4, pp. 299-321.
- Price, N.J.
1959: Mechanics of jointing in rocks; Geol. Mag., vol. 96, pp. 149-167.
1966: Fault and joint development in brittle and semi-brittle rock, Oxford, Pergamon.
- Stearns, D.W.
1964: Macrofracture patterns on Teton anticline, northwestern Montana, Trans. Am. Geophys. Union, vol. 45, pp. 107-108.
- Watson, G.S.
1966: The statistics of orientation data, J. Geol., vol. 74, pp. 786-797.

DISCUSSION

W.M. Schwerdtner asked on what method the values of absolute stress quoted in the presentation were based, and suggested that depending on the method, values might in fact indicate effective stress and not absolute stress.

W.F. Brace suggested that this was such a complex subject that it might be better not to get involved in it at this point.

D. T. Secor remarked that on stereographic plots showed by the author, maxima seemed to be much better developed in the north and west than in the south and east. This, he suggested, would reflect tilting of the joints, or non-verticality of the principal stress at the time of jointing.

R. A. Price observed that if joints represented residual stresses during faulting and stresses existing during uplift and unroofing, as suggested by the author, one should notice some difference in the orientation of joints in shallow dipping and steeply dipping beds.

The author expressed his regrets that he had only been able to measure joints in shallow dipping strata and said he would expect to find a difference in steeply dipping strata, but he did not really have an answer to this question.

A. Brown asked for more details concerning joint sets J₃ and J₄.

The author explained that his extensional type 1 and type 2 sets displayed only one maximum on the stereographic projection, although some of them showed plumose structures and others displayed slickensides. He expected that slickensides would appear where the joint pattern formed at a slight angle to the local orientation of σ_3 .

STRUCTURAL ANALYSIS OF FEATURES ON
NATURAL AND ARTIFICIAL FAULTS

D. K. Norris
Institute of Sedimentary and Petroleum Geology
Geological Survey of Canada, Calgary, Alberta

and

K. Barron
Mining Research Centre
Ottawa, Ontario

Abstract

Many beds in the coal measures of the eastern Cordillera have been detached from one another because of buckling and of differential translation on thrust surfaces. Striae, steps and polish on bedding faults were compared with similar features produced in the laboratory to evaluate their usefulness in kinematic analysis.

Pitches of striae on the same bed at various localities in Upper Marsh seam in the eastern Cordillera approximate a circular normal distribution with a preferred direction of slip essentially perpendicular to the regional strike. This distribution includes a very large number of discrete directions of slip representing some phase of the kinematic activity on bedding. Statistical tests provide reasonable assurance that samples of pitch of striae from one and more slip surfaces are from the same movement picture.

Steps on bedding and on extension faults are of two basic types: those of mineralized gouge plastered on the slip surface (accretion) and those cut into the solid rock (fracture). Both types may be linear or arcuate in projection on the slip surface; they commonly trend about at right angles to the preferred direction of slip and they may be modified or erased by later movement. Accretion steps adjacent to Upper Marsh seam are usually localized at irregularities in surface configuration. In any specimen or locality they characteristically occur on the same flank of depressions. Microscopically they consist of a complex lamination of quartz and carbonate with carbonaceous gouge. Layers of gouge feathered out in the quartz and carbonate, sigmoidal tension gashes, tension fissures filled with mineralization, and fragments of steps plucked from the risers indicate that these steps commonly face in the preferred direction of slip of the opposed wall. The steps are, therefore, plastered in the lee of irregularities in the rock surface. The fine structure, however, suggests modification of some steps of slip in a reversed direction consistent with observations of some faults which have themselves been cut and displaced in the coal seam. Fracture steps may originate in at least three ways in and adjacent to Upper Marsh seam: by inheritance from the initial fracture configuration of the slip surface, by plucking of platy fragments, and by faulting of the slip surface.

Polish on and within beds is widespread adjacent to Upper Marsh seam. It may be due to relatively large shear displacement over considerable area on individual beds or to microscopic shear on a multitude of slip surfaces of limited area within beds.

Steps and striae were created in the laboratory on prepared and induced slip surfaces in cylindrical specimens of soapstone, mudstone and siltstone loaded axially under confining pressures up to 9,000 psi. The steps were similar to the two basic types observed in the field. Both were oriented more or less perpendicular to the direction of the striae. Risers on accretion steps were observed to face in opposing directions depending largely on whether the fragments of compressed gouge stuck to one side or other of the specimen when the slip surfaces were separated for viewing. The directions in which the risers faced, therefore, were not consistent with the known sense of slip. Prominent fracture steps were observed to be due to faulting of the principal slip surface on the conjugate shear set. They consequently opposed motion on the principal surface.

Both field and laboratory data, therefore, indicate that accretion steps are formed as slip surfaces are parted, and depending on which wall retains the gouge, the steps will face in the one direction or other. Because the gouge is more readily bonded to the lee flank of irregularities, however, it commonly sticks there so that risers face preferentially in the direction of motion of the opposed block. Fracture steps on the other hand can face in either direction and therefore cannot be used indiscriminately as a definitive criterion for sense of slip. Where their nature and origin are understood, however, both kinds of steps may be used with meaningful samples of pitch measurements to establish directions of slip and therefore to document at least part of the kinematic history of faulting and folding in orogenesis.

INTRODUCTION

With increasing knowledge of the structural geometry of orogenic belts there is a proportionate demand for reliable criteria for assessing the direction and magnitude of relative displacement on detachment surfaces, whether parallel or at an angle to bedding. Only when reliable and meaningful data are available, can an accurate analysis be made of the kinematics and perhaps also of the dynamics of orogeny.

The acquisition of meaningful samples of data is more often than not fraught with difficulties because of limited, accessible outcrop in structural positions critical to the analysis. It may be difficult, moreover, to sample adequately the fabric of a given surface in a specific structural position. Fortunately in the eastern Cordillera of Canada some of these sampling difficulties are overcome through the existence of underground mines, locally extending a few miles along strike and as much as a mile down dip, in one and the same bed. Exposures are fresh and extensive; they reveal in minute detail some of the Laramide deformational history as it may have been recorded in the coal measures of the eastern Cordillera.

The coal measures there are intimately involved in the thrusting and folding and unquestionably play a fundamental role in the style of the deformation. Thrust faults, both major and minor, are commonly localized in the coal seams; bedding thrusts at these and other preferred horizons (Norris, 1961, p. 184) lead to the fault habit first outlined by McConnell (1887, p. 33D) who not only documented that thrusts parallel the layering along strike and down dip, but also recognized the fundamental similarity between the structure of the southern Rocky Mountains and that in the southern Appalachians (*idem*, p. 32D).

Of the number of fabric elements which have been used in qualitative evaluations of the kinematics and dynamics of orogenesis (see, for example Roder, 1960; Lindstrom, 1962; Price, 1967), slickensides¹ and steps on slip surfaces are of prime importance in an objective analysis. The pitch of striae defines the orientation of the kinematic axis. Steps commonly face in one direction or other in a given structural position, and according to most textbooks the sense of relative motion along the slip surface may be determined from them. According to Billings (*op. cit.*, p. 149) for example, "These rough surfaces can be used . . . in much the same way that roches moutonnées indicate the direction in which glacial ice was moving". The steep faces or risers of the steps would, therefore, face in the direction of relative motion of the opposed block.

The first to challenge the textbook description of sense of slip was, to the writers' knowledge, Dzulynski (1953, p. 332) who provided field evidence to support the thesis that the risers more commonly face the oncoming, opposed block. His argument was supported, moreover, by Paterson (1958, p. 469) who, from laboratory studies of faulting in Wombeyan marble, demonstrated the unequivocal existence of steps with their risers facing in the manner described by Dzulynski. He concluded (*idem*, p. 474) that "the sense of shearing should not be inferred from the appearance of a slickensided surface only, but should be confirmed by mapping". Additional field evidence was supplied by Tjia (1964) and laboratory evidence by Riecker (1965) to support the views of Dzulynski and Paterson. However, in a discussion of Riecker's and Tjia's papers, Rod (1966, p. 1163) writes "it seems that steplike breaks of very different origin have been lumped together" and points out that steplike breaks on well preserved, slickensided faults in Northern Australia appear to be secondary faults "the majority of which belong to a shear system having a sense of movement opposite to the one along the master fault". He emphasized that the rule of thumb (or finger) for roughness and consequently for sense of slip is still valid because "it never applied to the steps caused by secondary faulting". Like Paterson, he states "only mapping can give certainty". In a detailed account of directional indicators on faults Tjia (1967, p. 394) confirmed Rod's suggestion that the large step on the fault, cited to strengthen Paterson's arguments, was in fact a secondary fault. He maintained (*idem*, p. 396), however, his earlier stand "that the smoothness criterion for detecting fault displacements should be discarded".

¹"Slickensides are polished and striated surfaces . . . along the fault plane".
Billings, 1954, p. 149.

It would seem from the preceding discussion that incontrovertible evidence on the kinematic significance of steps must come, ideally, from a situation where there has been one and only one direction of motion, and where the magnitude of displacement can be measured from the rupture and offset of features known to have been in existence prior to displacement. In reality, however, it may be difficult if not impossible to ascertain the true nature of the movement picture. In the coal mines of the eastern Cordillera, for example, striae on faults vary widely in pitch (Norris, 1966a, p. 194) and the direction of motion on bedding has been up- as well as down-dip (Norris, 1966b, p. 115). It is therefore impossible to identify steps on bedding with one particular direction of slip and hence impossible to relate the orientation of risers to a specific sense of motion. Under these circumstances, it was found necessary to examine critically the micro-structure of the steps in search of criteria useful in determining sense of slip.

UPPER MARSH SEAM

Geological Setting

The coal measures of the southeastern Canadian Cordillera are Jurassic and (?) Lower Cretaceous in age. They make up the Kootenay Formation, a succession of non-marine shale, siltstone, sandstone, and conglomerate. The formation rests with gradational contact on the marine, Jurassic Fernie Group and is overlain disconformably by Lower Cretaceous Cadomin Formation in Cascade Coal Area (Fig. 1). The outcrop thickness of the Kootenay ranges from 230 feet a few miles south of Crowsnest Pass (Norris, 1959, p. 233) to 3,070 feet near Canmore (Norris, 1957, p. 5).

Upper Marsh seam lies 1,600 feet stratigraphically above the base of the Kootenay Formation. It ranges in thickness from 3 to 12 feet in the area mined, averaging about 9 feet. The coal is low volatile bituminous in rank. Although commonly sheared, it is locally bright and blocky, in spite of considerable Laramide kinematic activity in and adjacent to the coal.

The structural position of Upper Marsh seam is the gently dipping east flank of the asymmetrical to overturned Mount Allan syncline (Plate 1), which extends throughout the length of the Cascade Coal Area. The measures are bounded on the west by Mount Rundle thrust (Norris, 1957, p. 6) and are underlain conformably by the Jurassic Fernie Group of the Lac des Arcs thrust plate.

The Cascade Coal Area lies in a series of overlapping plates (see Fig. 1). The major thrust faults with their associated splays and folds impart a north to north-west trending structural grain to the east-central Cordillera. Vertical to west-dipping axial surfaces characterize the folds and in conjunction with the thrust faults impart a strong asymmetry to the deformation. Wrench faults, occurring singly or in swarms, commonly trend subperpendicularly to the structural grain, are vertical to steeply dipping and locally have large displacement. The bulk shortening arising from the thrusting and folding does not appear to vary appreciably within the region so that an increase or decrease in horizontal displacement on any one thrust is apparently compensated by corresponding changes in displacement on faults lying en echelon to it (Norris, 1966a, p. 193),

Structural Fabric

The principal mesoscopic elements contributing to the structural fabric in and adjacent to Upper Marsh seam are bedding, slickensides and steps, joints and cleats, and extension and contraction faults. Bedding is abundantly polished, commonly striated and locally stepped as a consequence of kinematic activity during the Laramide orogeny. Successive beds have been detached from one another as a consequence of interbed slip (Plate 2) caused by differential translation on thrust surfaces and by

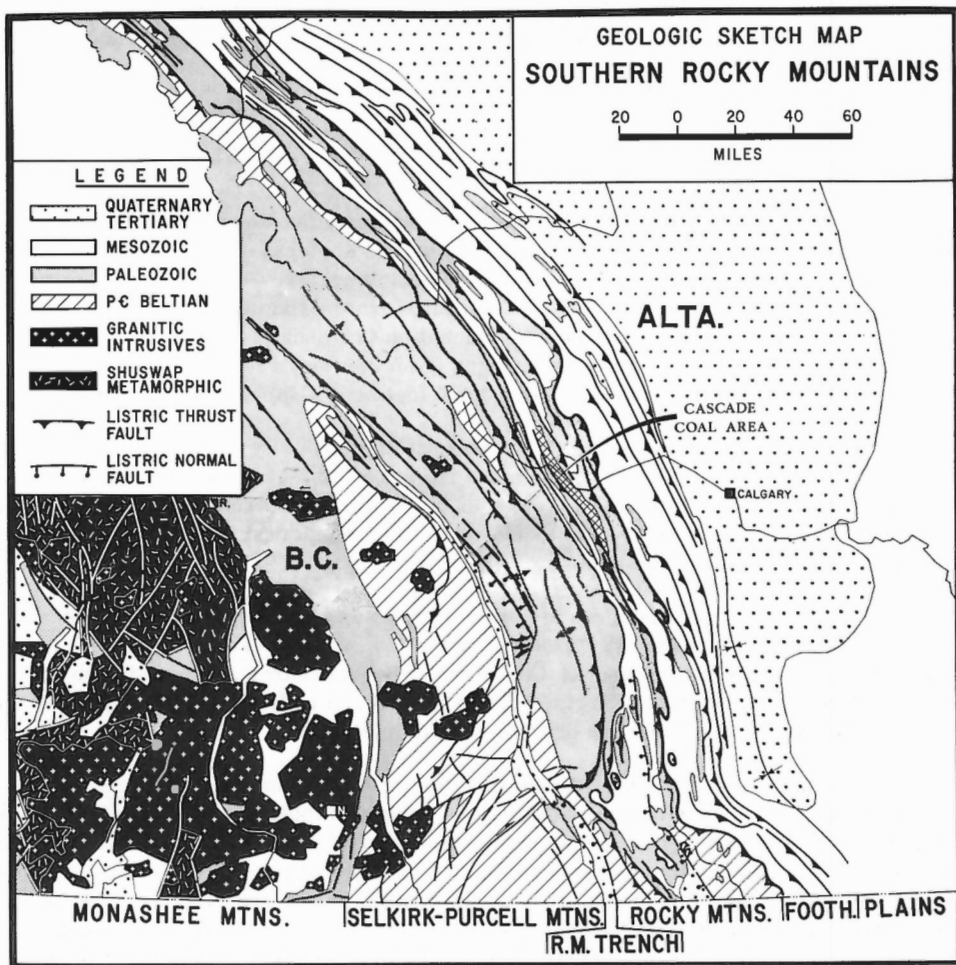


Figure 1. Geologic map of the southeastern Cordillera of Canada. Cascade Coal Area contains band of Mesozoic rocks beneath Mt. Rundle thrust in the vicinity of Canmore, Alberta. (After Bailey *et al.*, 1966)



Plate 1. Mount Allan syncline of the Cascade Coal Area beneath Mt. Rundle thrust. View looking southeast.



Plate 2.

Slickensides on bedding approximately one foot stratigraphically above Upper Marsh seam, Canmore, Alberta. Striae pitch of 86° from North arrow. Accretion steps face down-dip. Arrow is one foot long.

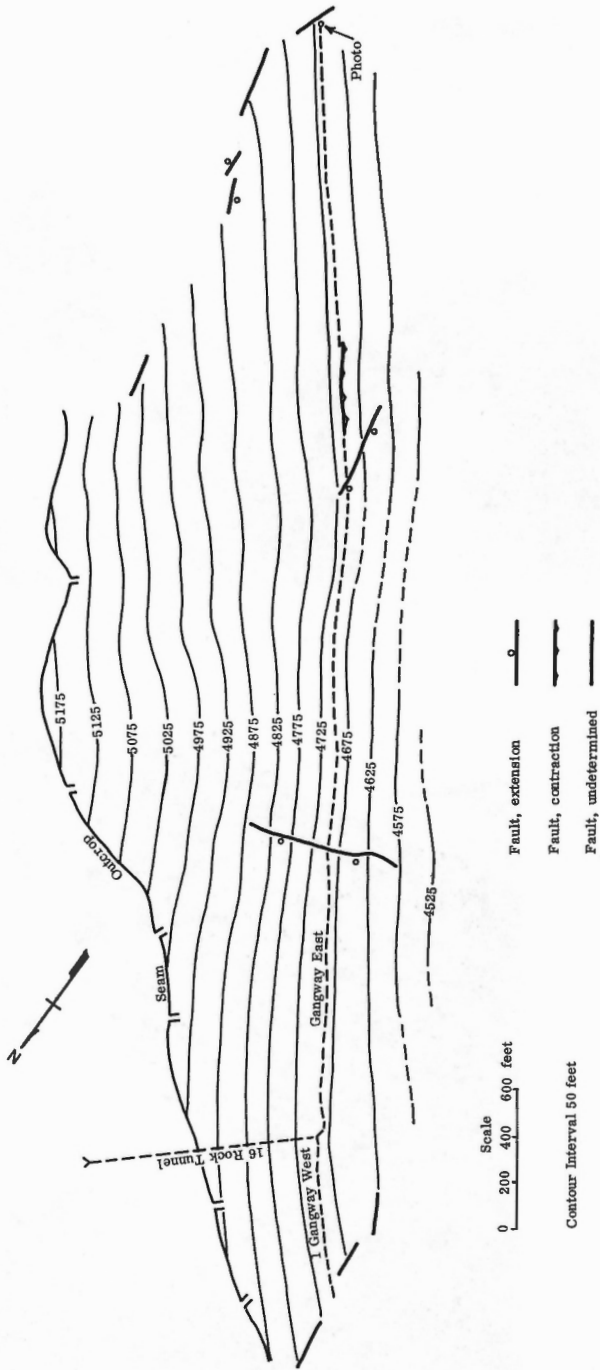


Figure 2. Structure contour map of roof of Upper Marsh seam, Canmore, Alberta.

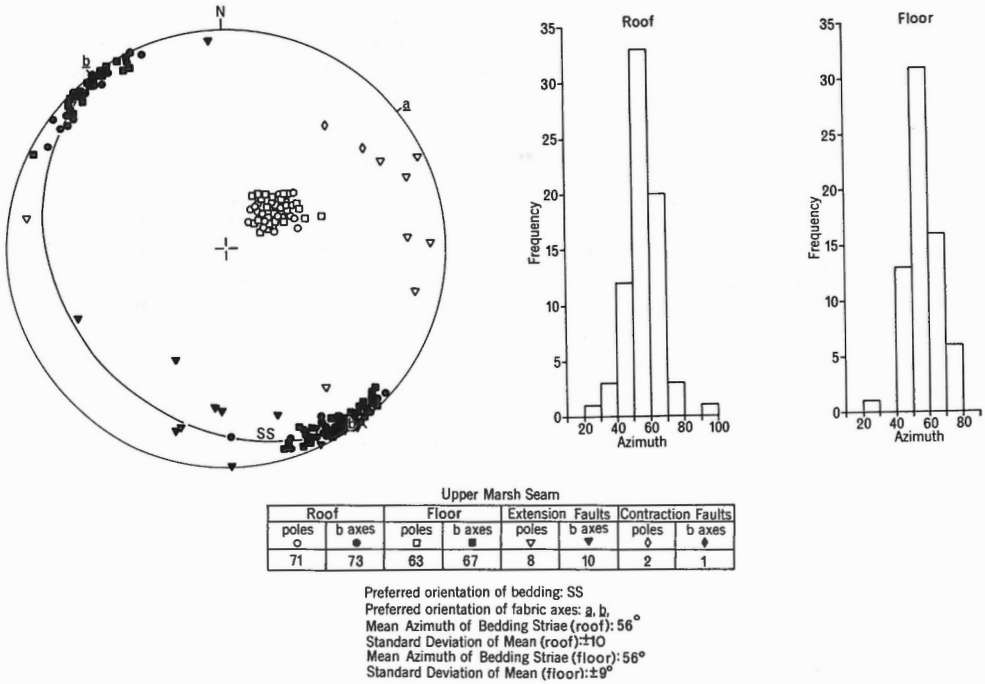


Figure 3. Structural fabric adjacent to Upper Marsh seam. Schmidt equal area projection from the lower hemisphere.

buckling. Joints pervade the rock mass. They are commonly perpendicular and sub-perpendicular to bedding and their spacing ranges from less than an inch to a few feet. Cleats and a tectonic joint system are preserved in the coal in those areas where the seam is not highly sheared.

The bedding throughout the accessible parts of Upper Marsh seam is quite planar, with the strike averaging 323° and the dip 23° to the southwest (see Fig. 2). The fabric and kinematic axes are readily defined. In contrast to other seams examined in mines of the Cascade Coal Area, Upper Marsh seam is cut by relatively few faults. Five extension faults were studied in the accessible workings, with strikes ranging from north to east and characteristically with steep west to north dips (see Fig. 3). The one contraction fault, like those in other seams in the eastern Cordillera, parallels the region structural grain and dips southwest in the manner of the major thrusts.

The axes of slip (b) for slickenside striae on roof and floor range through an angle of 62° and demonstrate wide variation in orientation of kinematic axes adjacent to the coal. Because of these variations, a meaningful kinematic analysis cannot be made until the following questions are answered: (1) Are these kinematic axes stochastically independent? (2) What is the nature of the frequency distribution

of these axes for a given slip surface? (3) Are samples of axes from two or more surfaces from the same movement picture? and (4) Is the distribution of axes characteristic of and unique to the eastern Cordillera? Answers to these questions are found in the analysis of striae on faults.

STRIAE ON NATURAL FAULTS

Observations of pitch of slickenside striae on roof and floor of Upper Marsh seam were reduced to a common reference surface by rotation of striae into the horizontal about the local strike of the bedding. Insofar as the plunge of Mount Allan syncline is less than about 5 degrees in the area of study, no correction for plunge was made in the rotation. As demonstrated by Ramsay (1961, p. 89, Fig. 5) for plunges less than 5 degrees and dips of surface elements less than 40°, the angular error resulting from neglect of plunge is about 2 degrees.

A number of statistical tests were then performed (see Appendix) to demonstrate the usefulness of pitch measurements in kinematic analysis. The mutual

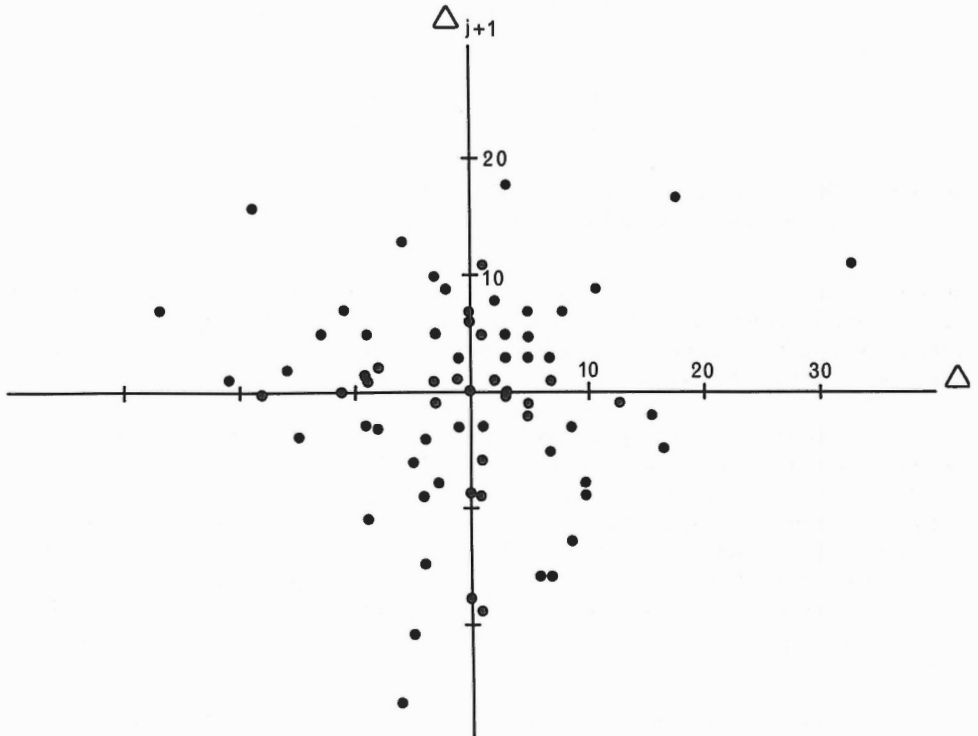


Figure 4. Scatter diagram of Δ_j against $\Delta_j + 1$ to demonstrate lack of mutual dependence of adjacent pitch measurements on roof of Upper Marsh seam, Canmore, Alberta.

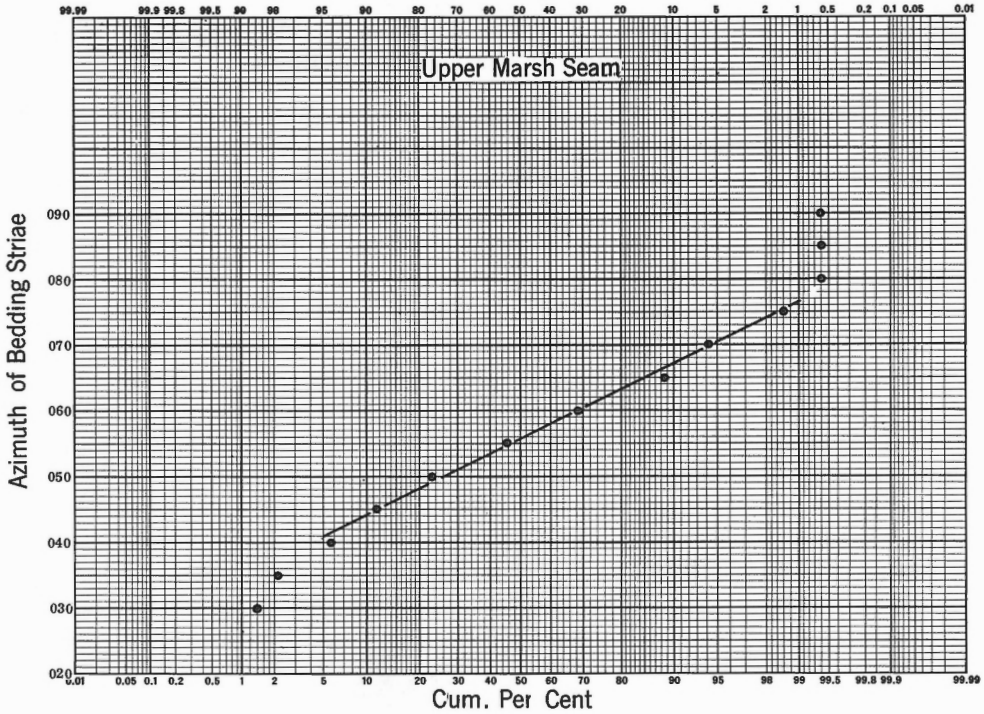


Figure 5. Distribution of azimuths of striae on bedding adjacent to Upper Marsh seam, Canmore, Alberta.

independence of adjacent measurements of the a kinematic direction on a given bed was tested (Fig. 4) because it is impossible to conduct meaningful significance tests on measurements unless stochastic independence is fulfilled. The arithmetic means and standard deviations were calculated for the a kinematic directions for roof and floor of Upper Marsh seam and statistical tests performed to demonstrate reasonable assurance that roof and floor samples of pitch measurements are from the same normally distributed population of striae (Fig. 5). A sample of intersecting sets of striae on roof and floor were then shown to confirm the assumption that interbed slip adjacent to Upper Marsh seam may be represented by a single movement picture (Fig. 6). It includes a very large number of discrete, temporally distinct, randomly used axes of slip with a circular normal distribution representing at least in part the latest kinematic activity of the surfaces.

Of fundamental importance, moreover, is the fact that the mean orientation of the (ac) deformation plane (056°) is subparallel to the mean counterdip direction (053°) and is therefore in near coincidence with the presumed direction of relative transport of thrust plates in this part of the Cordillera.

The circular normal distribution of pitches of striae with a preferred direction of slip perpendicular to the regional strike defines the basic structure of the kinematic pattern for bedding slip in the east-central Cordillera.

In the preceding discussion care has been taken to imply nothing regarding direction of slip because a given set of striae simply define the (time-dependent) a kinematic axis. The problem now at hand is, therefore, to find definitive criteria which may be used to establish direction of slip. It may be argued that if a fault cuts

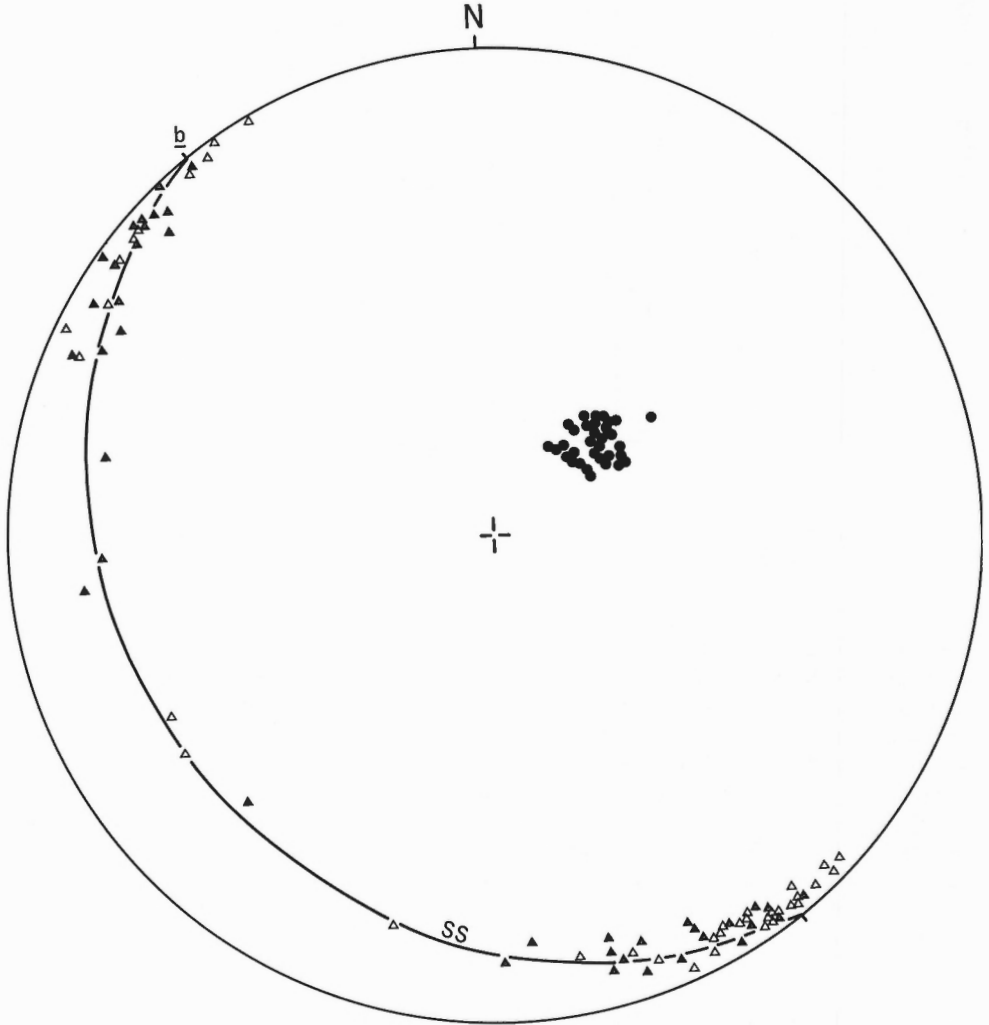


Figure 6. Axes of slip (b) for relatively younger (▲) and older (△) striae on roof and floor of Upper Marsh seam. Schmidt equal area projection from the lower hemisphere.

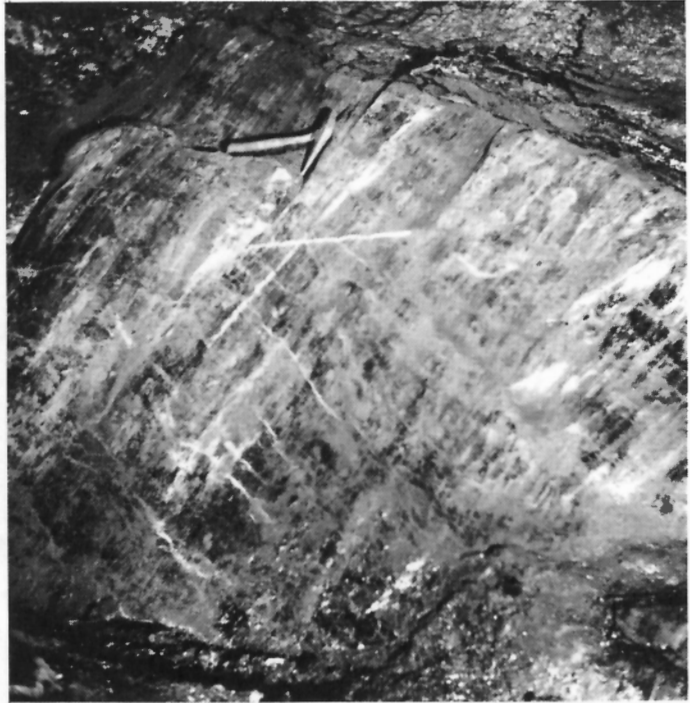


Plate 3.

Extension fault at face of Number 1 Gangway East, Upper Marsh seam. Fault in roof and floor are in line with one another. Hammer rests on step in solid rock.

from the roof rock, through the coal into the floor, but has in turn been faulted because of bedding slip in or adjacent to the seam, it may be possible to attach a sense of motion to associated bedding striae.

That Upper Marsh seam is cut by relatively few faults is unfortunate for determining sense of slip on bedding but is ideal for studying the spectrum of kinematic axes because of the minimum effect faults might have in impeding or altering the course of interbed slip. Only the fault at the face of Number 1 Gangway East (Plate 3) was recognized in both roof and floor. It was not offset in the coal seam and may, therefore, have developed upon cessation of interbed slip. Experience with faults in other seams (see Plate 4) on the northeast flank of Mount Allan syncline, however, documents the fact that there has been up-dip as well as down-dip slip of roof over coal, that the classical model of flexural-slip may in reality be too simple, and that the sense of offset in the seam determined by these faults and from steps on bedding may bear no kinematic relation to a particular set of striae preserved on roof and floor. The net slip on bedding faults may, therefore, be indeterminate.

STEPS ON NATURAL FAULTS

Because bedding striae define only the orientation of the a kinematic axis for interbed slip, and offset faults indicate both up- and down-slip motion on bedding, an analysis was made of steps as a criterion for sense of slip. It is apparent,

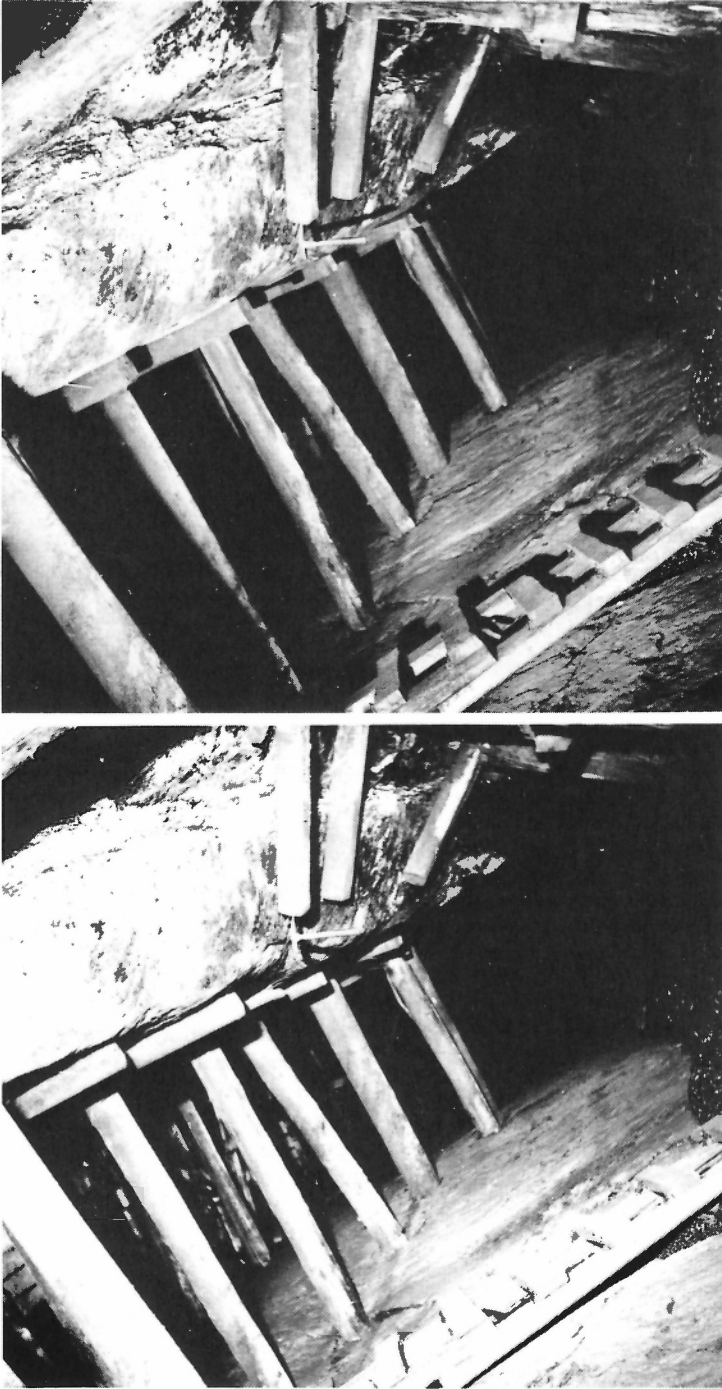


Plate 4. Extension fault in roof of Stewart seam, Canmore, Number 1 Gangway West. Net slip in direction of dominant striae is 4.0 feet at hammer. Note that fault is not present in floor in projection from roof. Stereoscopic pair.

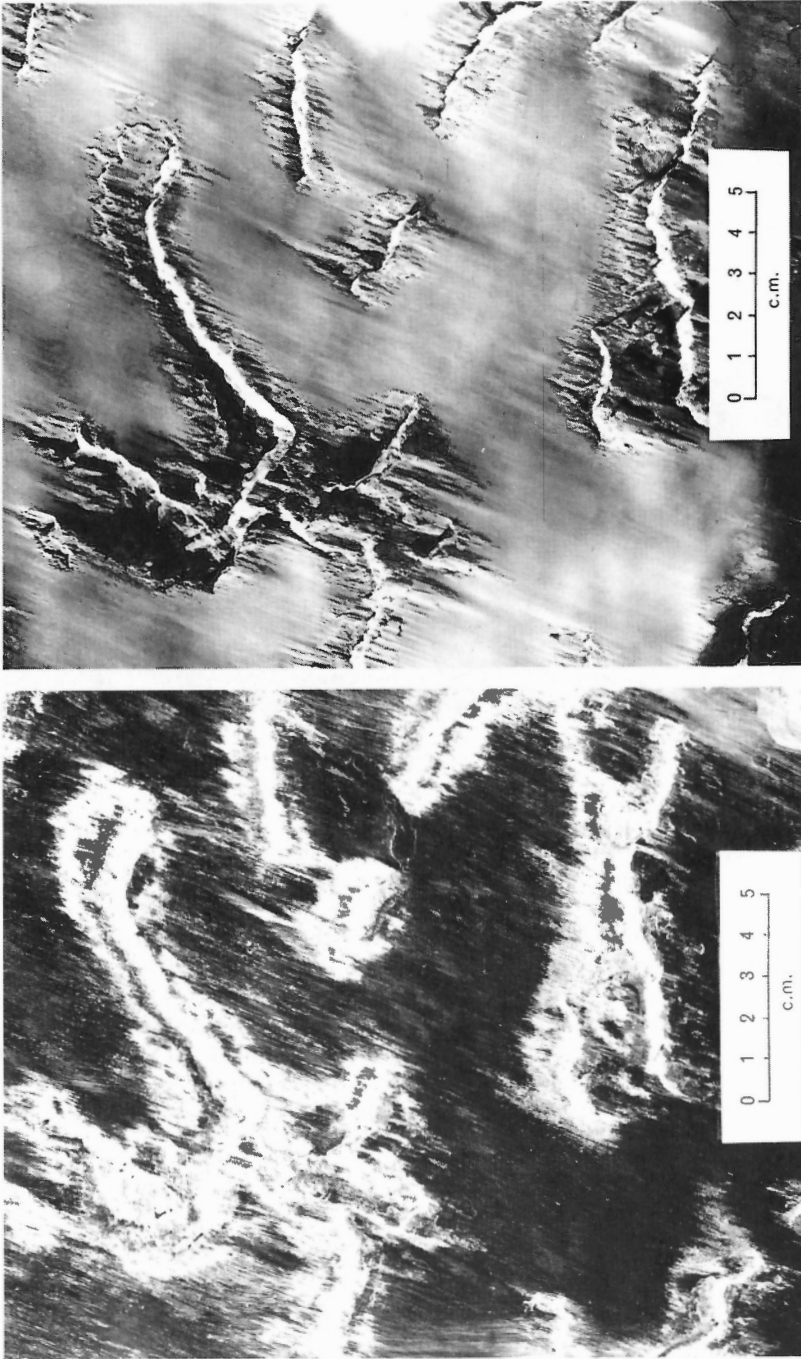


Plate 5. Details of steps and striae in roof of Upper Marsh seam shown in Plate 2.

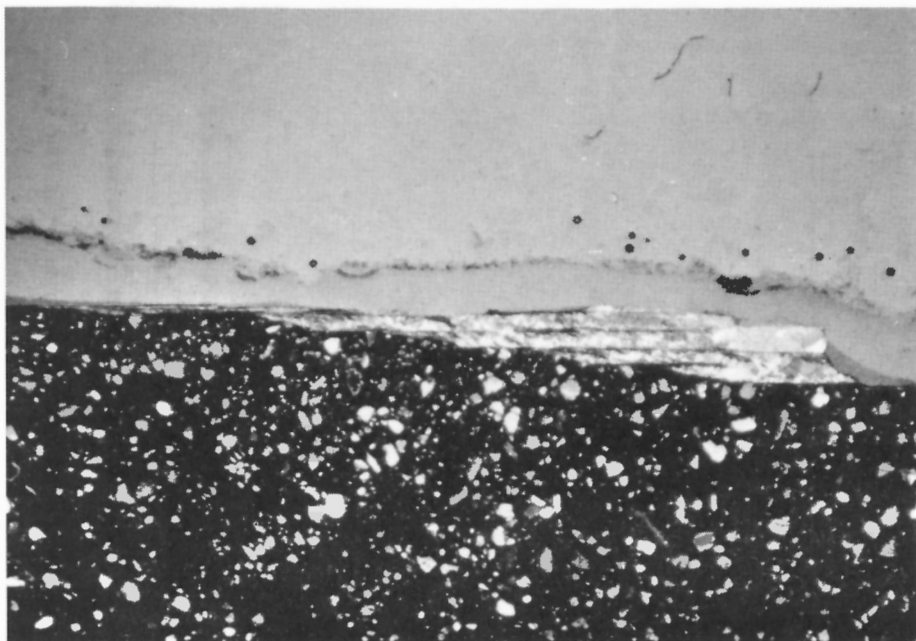


Plate 6. Thin section of step on sedimentary rock from southwestern Alberta. Note laminae and cross laminae of gouge in carbonate and quartz.

moreover, that steps, as products of slip, may provide further documentation of the complexities of the movement picture during orogenesis.

The steps on bedding and on faults cutting the bedding appear to be of two basic types: those of mineralized gouge plastered on the surface, herein termed accretion steps¹, and those cut into the solid rock, herein termed fracture steps (Fig. 7). If the steps are oriented to oppose shear, they will be said to be incongruous, otherwise they will be congruous. They may be linear or arcuate in projection on the slip surface (see Plate 5), are commonly in swarms, trend more or less at right angles to the preferred direction of slip, and may be rounded off, worn down or erased by later movement.

Accretion Steps

Accretion steps composed of ground up coal at the contacts between coal and rock were observed to have their risers facing up- or down-dip, depending upon

¹Term suggested to the writers by N. C. Ollerenshaw, Geological Survey of Canada.

whether or not the coal stuck to the rock. They were, therefore, of no value in determining sense of slip. Steps of mineralized gouge up to one-eighth inch high were observed on slip surfaces in the mudstone or siltstone above and below the coal. Those steps on the tops of slip surfaces characteristically faced up-dip, and those on the bottoms, down-dip.

In this section it is apparent from the bedrock profile that accretion steps are plastered on the slip surface (Plate 6). They are, moreover, commonly localized on the sides of irregularities in surface configuration. Their microscopic structure is a complex lamination of quartz, carbonate and carbonaceous gouge suggesting a succession of temporally distinct periods of slip and mineralization. The thin laminae of gouge are often truncated against risers and treads. Variable extinction of quartz in the gouge suggests that some of the crystals have been strained. Evidence of stretching in the mineralized gouge is seen in sigmoidal tension gashes and tension cracks infilled with quartz and carbonate (Plate 7). Some tension cracks, inclined towards the risers, are traceable into the rock mass and indicate that the stretching was not confined to the gouge. Cross-laminae dip away from the risers and towards them, suggesting that the gouge was introduced to the steps because of both forward and reversed senses of motion. The feathering out of this gouge, the sigmoidal tension gashes, the tension fractures in the steps and the plucking from the risers support the hypothesis that accretion steps are generally congruous. They are, therefore, commonly plastered in the lee of irregularities in the rock surface although the micro-structure of some of the laminae suggest instances of slip in a reversed sense.

No voids or cavities are apparent between adjoining walls of bedding slip surfaces in the coal measures. Patches of mineralized gouge fill the spaces caused by mismatch in slip surface configuration. It is apparent, therefore, that accretion steps must be formed as the walls are parted, and depending upon which wall the gouge sticks to, the risers may face in the one direction or other.

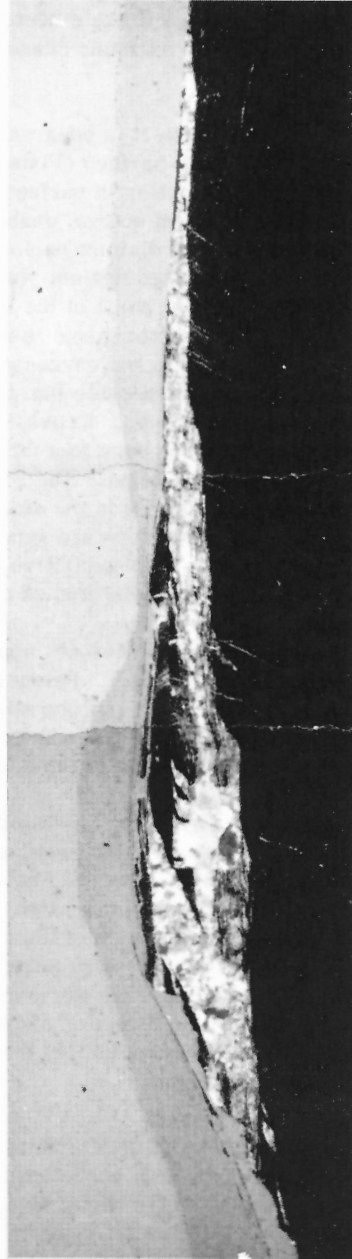
In the lee of irregularities there is opportunity for mineral matter to bond itself to the fresh surface of the rock, whereas on the forward side there is active shear, and gouge may be introduced between the mineral matter and the adjoining slip surface. The one extremity of a patch sticks more readily to the one wall where it is protected from shearing motion of the adjoining surface, and the other extremity to the opposite wall, as the surfaces are parted (see Fig. 8). The probability is, therefore, that accretion steps oriented in the manner described in most textbooks are formed, their risers facing in the direction of relative motion of the adjoining wall. The slopes of the risers are, moreover, simply the fracture angles of the gouge and have no direct relation to slip on the fault.

The sense of slip determined from the orientation of the risers as well as from the micro-structure of accretion steps is generally consistent with the flexural slip model for growth of the Mount Allan syncline and with the differential eastward motion of progressively higher beds in the Lac des Arcs thrust plate.



a

0,0 0,1 0,2 0,3 inches



b

Plate 7. Thin sections of steps on bedding in roof of Upper Marsh seam. Note sigmoidal tension gashes in step in Plate 7a and family of mineralized tension cracks in roof rock in 7b.


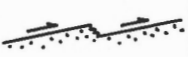
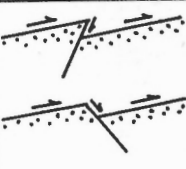
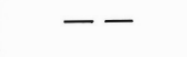


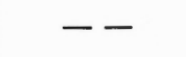
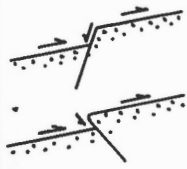
Steps	ACCRETION	FRACTURE		
		Pluck	Synthetic	Antithetic
Congruous				
Incongruous				

Figure 7. Kinds of steps on slip surfaces (schematic).

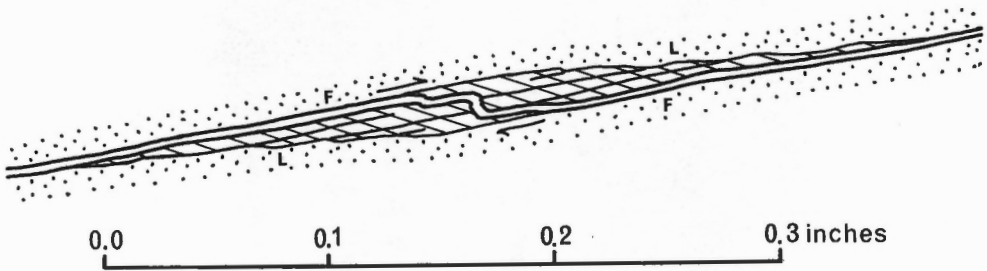


Figure 8. Schematic cross-section of patch of mineralized gouge showing disposition of lee (L) and forward (F) flanks of irregularities for a given sense of slip. Surfaces are slightly separated to suggest manner in which gouge preferably sticks to the one surface or other.

Fracture Steps

Fracture steps on bedding and on faults cutting across Upper Marsh seam appear to have originated in at least three ways: some are simply irregularities in surface configuration due to original fracture geometry; others are due to plucking of plates from the slip surface. Still others are due to faults intersecting the slip surface. All may be modified by abrasion during slip, by plucking of rock from the risers and by plastering with gouge. On bedding the height of fracture steps due to fracture configuration or plucking is commonly from one- to two-tenths of an inch although on faults at an angle to bedding, it may be up to several inches (Plate 3). Those (fault) steps with synthetic displacement (Hoepfner, 1955, Fig. 7) are necessarily congruous and those with antithetic displacement, incongruous (Fig. 7). All types of fracture

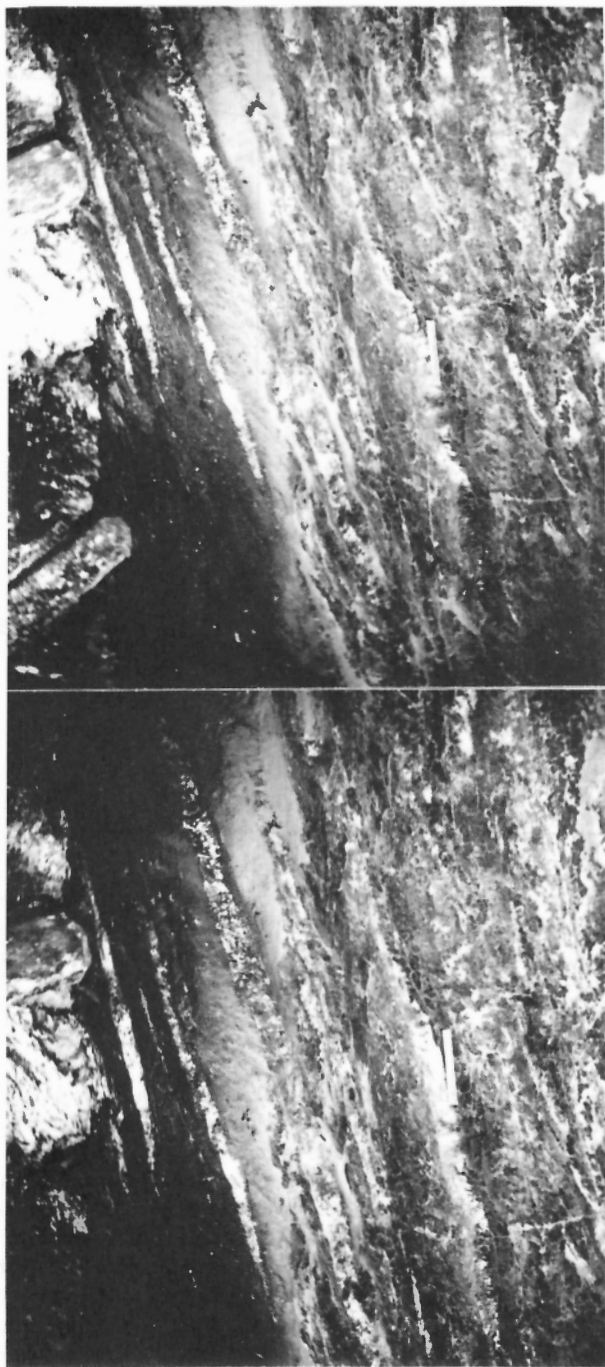


Plate 8. Family of extension faults in floor of Stewart seam, Canmore, Alberta. Note variation in separation along individual faults. Maximum displacement is about three inches. Stereoscopic pair. Scale is 6 inches long.

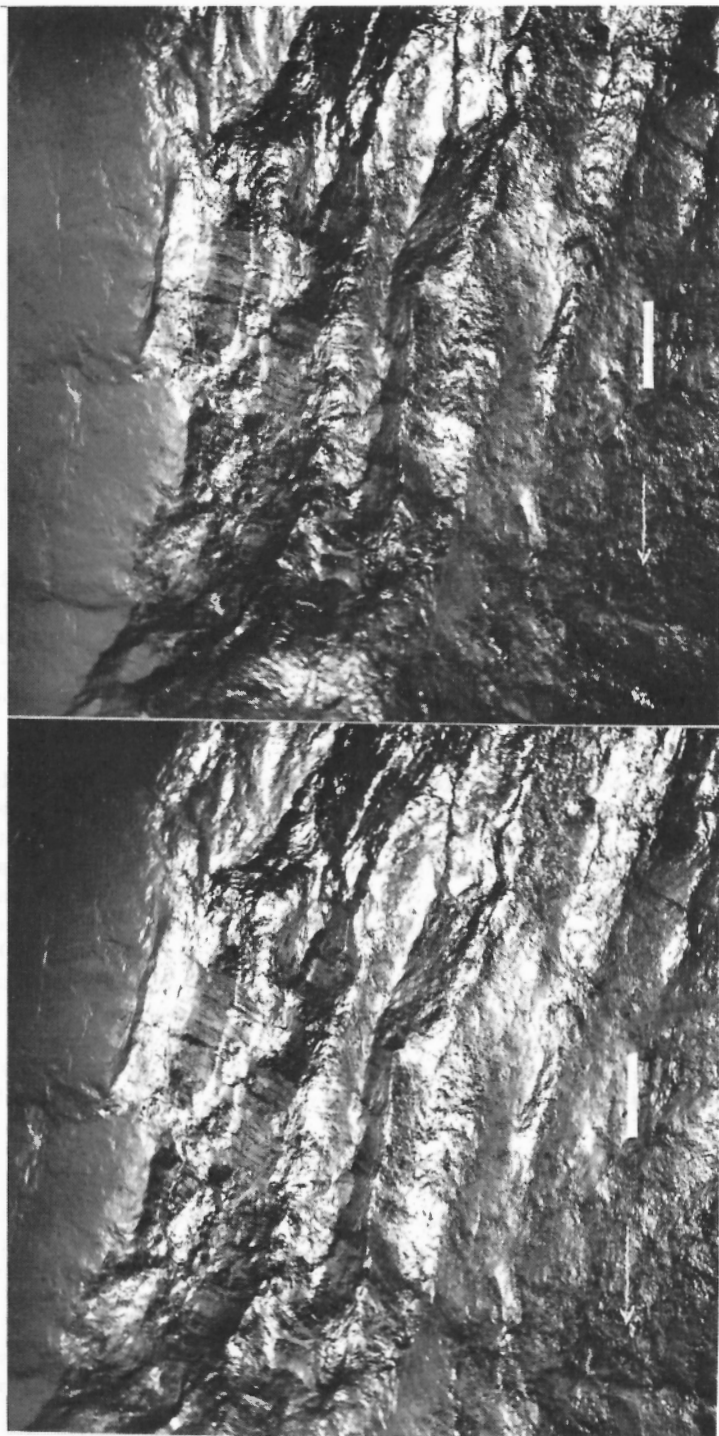


Plate 9. Family of extension faults in floor of Stewart seam, Canmore, Alberta. Maximum stratigraphic separation on faults ranges from 1 to 12 inches. The unfaulted floor of the seam is the flat area at top of photos and beneath the ruler at the bottom. Stereoscopic pair. Scale is 6 inches long.

steps of appreciable size in the immediate roof or floor of the coal seams have caused total destruction of the depositional and structural fabric of the coal as they plowed their way.

Synthetic and antithetic fracture steps commonly occur in swarms, generally trending parallel or at an acute angle to the strike of the coal measures. They range in net slip from the microscopic scale to several feet. If widely spaced, they appear as in Plate 8, and if closely spaced, as in Plate 9. The aggregate or net slip in the latter changes only gradually over the length of the swarm, although displacement on individual elements may change moderately rapidly along their length. This variation in displacement for the aggregate and for individual faults mocks in a general way the thrust and normal fault habit of the east-central Cordillera.

POLISHED BEDDING

Throughout the coal mines of the eastern Cordillera polish is abundant on bedding and on surfaces parallel to bedding. It is the product of shear brought about by differential motion in the layered succession by thrusting and by flexural slip.

In Upper Marsh mine there was opportunity to examine these polished surfaces and to gain some insight into the mechanical response of the measures when they were faulted and folded. Slickensided surfaces were observed at many stratigraphic levels in the first few feet of roof and floor; they were spaced at intervals ranging from one-quarter inch to one foot within mudstone or siltstone beds and paralleled textural lamination.

While attempting to withdraw a specimen from the roof of Upper Marsh seam, which ostensibly contained the lateral extension of the slip surface shown in Plate 2, the authors discovered that the surface ended virtually at the limit of the exposed area. The significance of this lies in the conclusion that within beds slip surfaces may be of limited area. They overlap one another in space and perhaps also in time of origin. Highly stepped and slickensided though they may be, the amount of movement on them can be microscopic. Movement on contacts between beds, however, could undoubtedly be many orders of magnitude larger because of the greater areal extent of beds. This is seen for example in coal seams which are detached at their contacts over areas measured in square miles. There, parts of faults may be displaced from one another by several tens of feet. Accommodation of the measures to shear parallel to the layering took place within as well as at contacts between beds.

STEPS AND STRIAE ON ARTIFICIAL FAULTS

Steps and striae were produced in the laboratory on prepared and induced slip surfaces in cylindrical specimens of soapstone, mudstone and siltstone loaded axially under confining pressures up to 9,000 psi. For the prepared specimens, diagonal cuts were made at angles of approximately 25 and 30 degrees to their longitudinal axis. The surfaces of these cuts were then lapped to ensure even contact. The specimens were placed in a triaxial bomb and confining pressure was raised to 1,500 psi. The axial load was then increased while maintaining the confining pressure

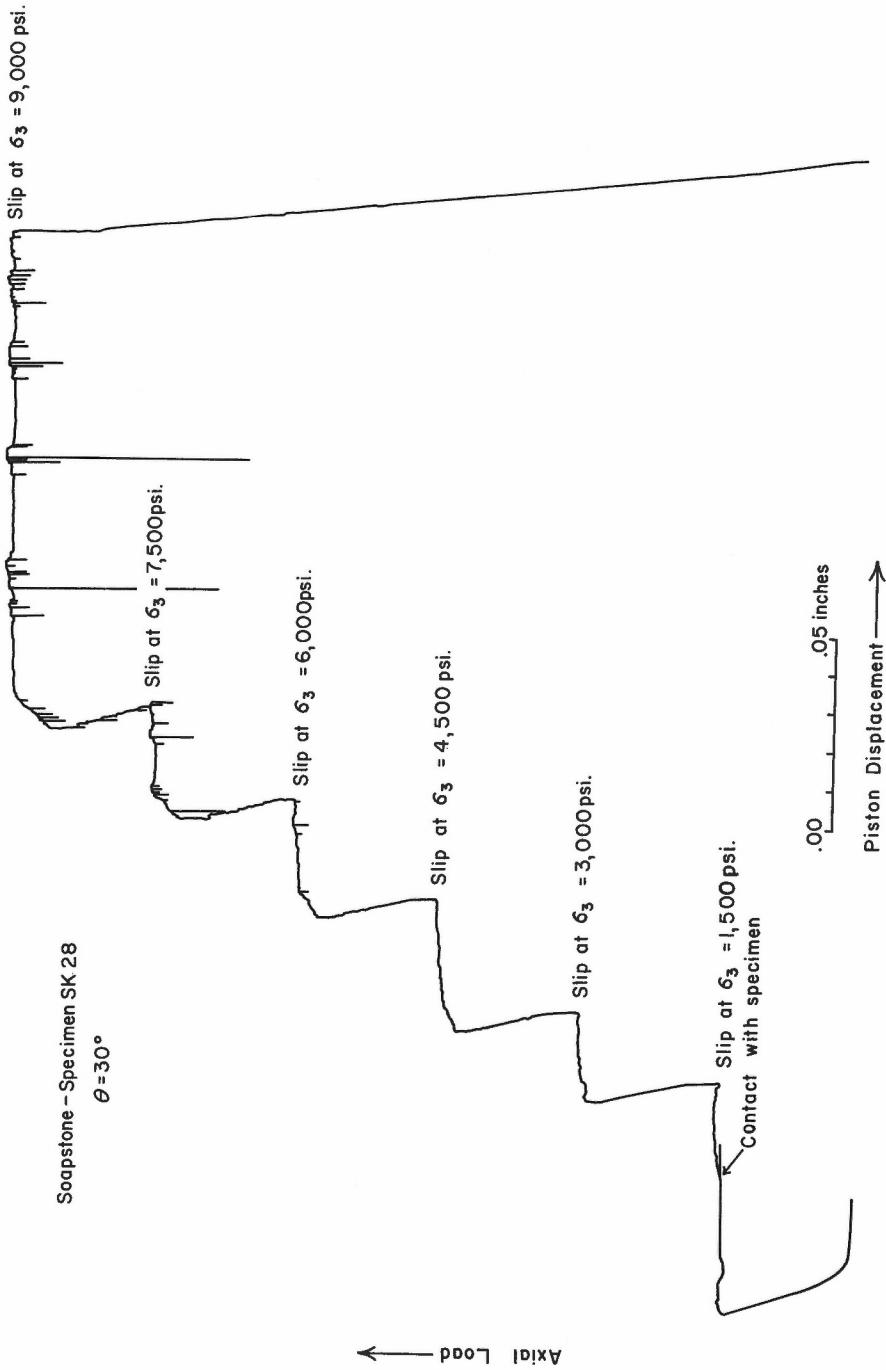


Figure 9. Typical XY recording of a slip test on a cut specimen.

at 1,500 psi by bleeding oil from the bomb, until slip occurred. The axial load was recorded on the one axis of an XY recorder and the displacement of the loading piston on the other. Slip was clearly indicated when there was steady piston displacement without increase of axial load. The confining pressure was then increased to 3,000, 4,500, 6,000, 7,500 and 9,000 psi in steps and the axial load increased at each step until slip occurred. On occasion abrupt deflections in axial load occur at higher confining pressures and are accompanied by an audible snapping sound which results from the alternating stick-slip of the juxtaposed surfaces, the typical behavior of moving unlubricated surfaces under load (Bowden and Tabor, 1964, p. 78). The specimens were then unloaded by carefully releasing both the axial and confining pressures so that little or no further displacement of the slip surfaces occurred. Figure 9 shows a typical XY recording obtained in such an experiment.

In order to conduct similar tests on uncut specimens it was first necessary to produce slip surfaces. This was done by loading solid, cylindrical specimens in the triaxial bomb until failure occurred. All these failures were produced at the confining pressure of 9,000 psi. After specimen failure, the axial and confining pressures were dropped to zero and slip tests, identical to those described for the prepared specimens, were carried out over the same range of steps and confining pressures from 1,500 to 9,000 psi. On removal from the triaxial bomb, the halves of these and prepared specimens were separated and visually inspected.

In most cases the specimens failed on only one plane. However, in some instances specimens had wedge type failures, because of slip on conjugate shear sets. In other cases, two non-intersecting failure surfaces occurred, the surfaces making approximately the same angle to the specimen axis, although not necessarily parallel or subparallel to one another.

Striae and steps were most easily produced on lapped and fracture slip surfaces on soapstone, to some extent on mudstone and with least success on siltstone. The striae were characteristically in the plane containing the long axis of the specimen. The steps were similar to the two basic types observed in the field and both types were oriented approximately perpendicular to the direction of the striae. Risers on accretion steps were observed to face in opposing directions (as did those of steps comprised of ground up coal on the roof or floor of Upper Marsh seam) depending largely on whether the fragments of compressed gouge stuck to one side or other of the specimen when the slip surfaces were separated for viewing. Among the 36 specimens studied, however, one had the appearance of that displayed by Paterson (1958, Plate 2) from the Wombeyan marble. The steps produced in these laboratory tests, therefore, were not consistently congruous. Prominent fracture steps were observed to be due to deformation of the principal slip surface by displacement on the conjugate shear set. They were antithetic and therefore incongruous.

The lapped surfaces on one specimen of soapstone were found to have triangular patches of gouge on them which suggested a mechanism of generation of rock flour and of formation of accretion steps (Plate 10). The patches of gouge were observed to be plastered in indentations, to be in the shape of isosceles triangles up to one-half inch high in the plane of slip, and to have small-scale steps at their base.

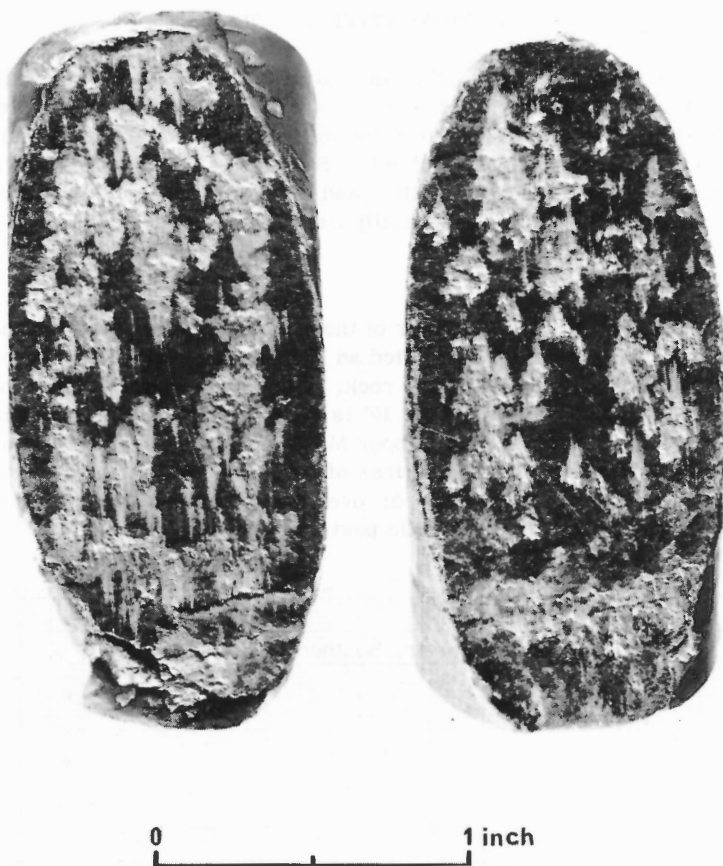


Plate 10. Triangular patches of gouge on lapped slip surface on soapstone.

It would appear that gouging begins at numerous points on the lapped surface, and is self-reinforcing so that the more rock flour present, the wider and deeper the indentation. This concept is supported by the fact that the height of the triangular patches of gouge is commonly greater than the magnitude of slip. Under the confining pressures of the triaxial bomb, the accumulated gouge is presumed to press against the forward end of the indentations, causing them to shear off as a series of imbricate scales, which are ground up to produce more gouge. The result is a family of triangular indentations on each slip surface, filled or overflowing with ground rock, with their apices pointing in the direction of motion of the block of which they are a part.

Depending on whether the compressed gouge stuck to the one or other surface, indentations and steps were formed and the risers faced in either direction. The orientations of the risers, therefore, could not be used to determine sense of slip but the direction in which the apices of the triangles were pointed, could. The apices on adjoining surfaces face in opposite directions and point in the direction of slip of the surface on which they lie.

COMPARATIVE STUDIES

In order to evaluate further the nature of the relationship of the distribution of azimuths of a kinematic axes and of the orientation of steps to tectonic environment, comparative studies were carried out in the fold belt of the northern Appalachians and on the craton of the St. Lawrence Lowlands. Samples of striae and steps from tectonic environments dominated by thrust faulting and by folding were compared with those from a simple fold in an area of essentially flat-lying rocks.

Southern Anthracite Field

A detailed study of the floor of the Mammoth seam in the Southern Anthracite Field of Pennsylvania revealed an abundance of striae which was due to displacement of the coal relative to the rock. The plot of the cumulative per cent of kinematic axes against azimuth (Fig. 10) is approximately circular normal and very similar in appearance to that for the Upper Marsh seam. It seems reasonable to assume that the distribution of orientations of a kinematic axes must represent a significant part of the movement picture; overprinting here as elsewhere was not effective in totally erasing the kinematic past.

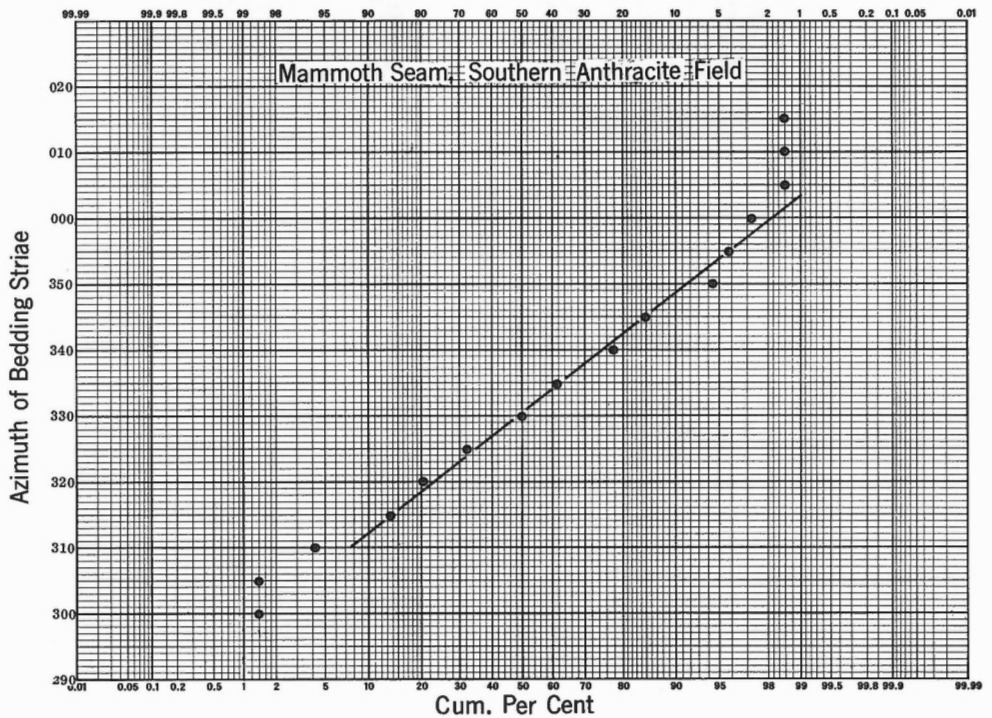


Figure 10. Distribution of azimuths of striae on bedding in the Mammoth seam, Tamaqua, Pennsylvania.

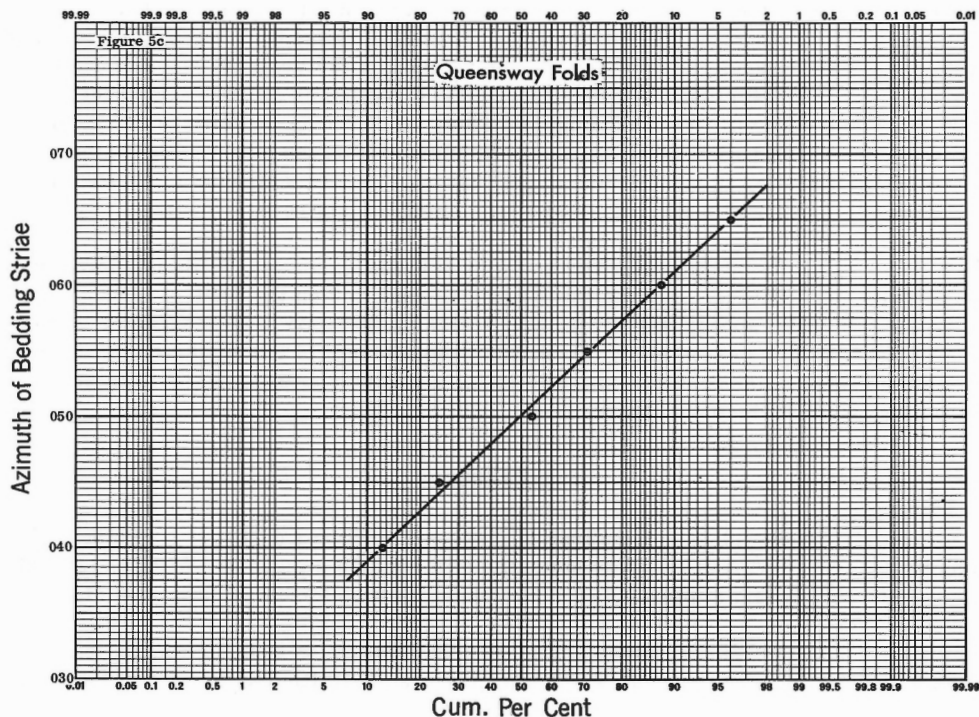


Figure 11. Distribution of azimuths of striae on bedding in the Queensway folds, Ottawa, Ontario.

The fact that the distributions of kinematic axes are similar for a thrust and fold belt suggests that the movement picture for interbed slip is the same for both belts. The picture is one of slip in a variety of directions with a preferred motion perpendicular or subperpendicular to the strike of the fault or to the fold axis. No observations of steps were made adjacent to Mammoth seam and no faults could be used to document magnitude and sense of slip because only the foot-wall remained for study. It was, therefore, impossible to say whether there was slip both up- and down-dip at a point in the northern Appalachian fold belt similar to that documented in the east-central Cordillera.

St. Lawrence Lowlands

In the Queensway folds of the St. Lawrence Lowlands (Norris, 1967), it was possible to measure the magnitude and sense of slip in various structural positions. Veins, oriented approximately in the bc fabric plane, were used in conjunction with steps on slickensided bedding. That some of the veins were offset on bedding and others were not would suggest that some veins may have developed after folding. Others in the syncline and on one flank of the anticline indicated sliding of higher strata over lower ones away from the axial surfaces, in conformity with the classical model

of flexural-slip folding. Of the twelve accretion steps observed, nine were congruous with the sense of slip established by means of the mineralized fractures (Norris, *idem*, Fig. 12). The preponderance of data therefore support the textbook descriptions (e. g. Billings, 1954, p. 149) that the risers face in the direction of relative slip of the opposed block. The presence of accretion steps which do not conform to the textbook descriptions would suggest that some may be plastered on the slip surface in the manner simulated by Riecker (1965, p. 746) during shear experiments on powdered olivine pellets, or that some may be due to minor slip in a reversed sense.

The distribution of a kinematic axes in the Queensway folds is approximately circular normal (Fig. 11) as in the Mammoth seam and on the flank of Mount Allan syncline. It would appear, therefore, that such a distribution is not characteristic of the thrust belt of the east-central Cordillera, the fold belt of the northern Appalachians or of the craton of the St. Lawrence Lowlands, but rather is fundamental to interbed slip in a variety of tectonic environments.

CONCLUSIONS

Meaningful interpretations of movement pictures of thrust plates and folds can be derived only from adequate sampling of the fabric elements. With too few data a kinematic or dynamic interpretation may be more a statement of faith than of fact.

(1) Slickenside striae define only the orientation of the a kinematic axis and unless markers are present which have been faulted little can be said of the sense of slip.

(2) Both mesoscopic and microscopic observations in the field and laboratory confirm that steps plastered on the slip surface are formed and preserved as a consequence of shear such that the risers commonly face in the direction of slip of the opposed block. These observations support the textbook descriptions and the observations of Rod (*op. cit.*) but modify the conclusions of Dzulynski (1953), Tjia (1964, 1967) and Paterson (1958).

It would appear, however, that a major problem is the inferring of sense of slip on faults from gross tectonic relations.

(3) Where the sense of slip is known, as in the Queensway folds, the majority of (accretion) steps face in the direction of motion of the opposed block (i. e. they are congruous) and they may therefore be used with caution to infer the sense of slip in other more complex tectonic environments.

(4) In the eastern Cordillera, where both up- and down-dip slip is documented on a given bed, the majority of (accretion) steps conform to the dominant pattern established in the Queensway folds; those that do not conform may have developed as a consequence of reversed motion or because the gouge stuck to the opposing surface and the need to appeal to the arguments of Dzulynski and others is avoided. It is difficult to conceive how steps of either of the two basic types can be preserved in their sharp and undeformed state if they are oriented to oppose slip.

(5) Risers which are known to face in opposing directions or which do not conform to textbook descriptions suggest complexities in the movement picture. Steps need not necessarily be congruent with sense of slip inferred from the regional structure although those that are congruent should predominate. When their nature and origin are recognized, steps may be used with meaningful samples of measurements of pitch of striae to establish at least part of the kinematic history of faulting and folding in orogenesis.

ACKNOWLEDGMENTS

The writers wish to thank F. P. Agterberg and N. C. Ollerenshaw of the Geological Survey of Canada for helpful discussions and for critically reviewing the manuscript. They are also indebted to S. Carbone for preparing the thin sections of steps on slip surfaces and to S. Cook and J. Sullivan for preparing the test specimens for laboratory studies of structural features on slip surfaces.

APPENDIX

Statistical Analysis of Pitch Measurements

The mutual independence of adjacent measurements of the a kinematic direction on a given bed was first tested. Unless stochastic independence is fulfilled it is impossible to conduct meaningful significance tests on measurements (Agterberg and Briggs, 1963, p. 397).

Observations on roof of Upper Marsh seam were used. The arithmetic mean of the a kinematic directions and the deviations from the mean $\Delta_j (= x_j - \bar{x})$ were determined. The deviations are, of course, both positive and negative and their algebraic sum must equal zero. According to Agterberg and Briggs (idem) in cases of dependence, a certain value will be preceded and followed by values of the same size. If Δ_j is taken as the abscissa and adjacent value Δ_{j+1} is taken as the corresponding ordinate, all values would scatter around the line $\Delta_j = \Delta_{j+1}$, having a slope of 45 degrees. It is evident from Figure 4, a scatter diagram for these roof data, that there is no such concentration about this line. Because the scatter is shotgun it may be safely assumed that successive measurements are stochastically independent and that a basic condition for further statistical testing is met.

Insofar as statistical theory is based on the so-called normal distribution, the tests applied to the data necessarily imply certain assumptions about the distribution of the a kinematic directions. Theoretically the orientation of directional features is circular normal because it is a modification of the case in which the data have a cyclical distribution (Agterberg and Briggs, op. cit., p. 398). There appears, moreover, to be no significant difference between the circular normal and normal distributions when the standard deviation is 30 degrees or less because the distribution functions give similar values of the dependent variable for small values of the exponent (Agterberg and Briggs, idem).

The arithmetic means and standard deviations of the a kinematic directions for roof and floor of Upper Marsh seam were calculated on the assumption that the samples may be approximated by normal distributions. The results are tabulated in Figure 3. Although the means are the same, the problem remains whether the standard deviations are sufficiently similar to justify the belief that the samples from the roof and floor are from the same population of striae. The ratio of variances, denoted by F, equals $100/78 = 1.28$. If this value is not significantly greater than one, it may be assumed with some degree of assurance that the variances are for the same population of striae. For the roof, there were 73 observations, and therefore 72 degrees of freedom; and for the floor, 67 observations, and 66 degrees of freedom. From tables (Hoel, 1966, p. 339) it is found that at the 95 per cent level of confidence, the corresponding F value is 1.76. Since $F = 1.28$ for this problem is appreciably less than the critical value from the tables, the data are in agreement with the hypothesis that the samples of orientation of a kinematic axes from roof and floor are from the same population of striae.

Because of the possibility that two or more populations could be mixed whose means and standard deviations were close to one another the combined data were plotted on arithmetic probability paper (Fig. 5). A normally distributed sample will plot as a straight line whose slope is determined by the standard deviation of the sample. If the sample were in fact a mixture of two or more distributions which are themselves normally distributed, the plot will give rise to a curve which is the resultant of two or more straight lines (Harding, 1949, p. 142). If one ignores the extremities of the plot where the data are few, it is apparent that the curve is sublinear and that the sample approximates a circular normal distribution.

Although intersecting striae on bedding are common adjacent to Upper Marsh seam, the determination of the relative ages of two or more sets is often difficult. A most careful search of roof and floor revealed 39 sets whose relative ages could be established with reasonable confidence (see Fig. 6). It is apparent from the distribution of (b) axes of slip that the relatively older or younger axes are not confined to one or other part of the fabric diagram but are intermingled along the trace of mean bedding in the projection.

To test the possibility that these sets could have arisen from more than one movement picture they were divided into two groups, that containing the relatively younger striae and that containing the relatively older. Their mean orientations and standard deviations were calculated and F and t tests performed. Designating the mean orientation of the kinematic a axis for the relatively older striae as \bar{a}_o , for the younger as \bar{a}_y and their respective variances by σ_o^2 and σ_y^2 , the following values were obtained:

$$\begin{array}{ll} \bar{a}_o = 61^\circ & \sigma_o^2 = 653 \text{ sq. deg.} \\ \bar{a}_y = 62^\circ & \sigma_y^2 = 558 \text{ sq. deg.} \end{array}$$

Now $F_{\text{obs.}} = 653/558 = 1.17$ and according to Hoel (ibid)

$F_{\text{tab.}} = 1.72$ at the 95 per cent level of confidence for 38 degrees of freedom in the numerator and denominator of the ratio of the variances. Thus $F_{\text{obs.}}$ is appreciably less than $F_{\text{tab.}}$ and we may, with reasonable assurance accept the hypothesis that the variances of the samples of older and younger striae are sufficiently alike to warrant the assumption that they are independent estimates of the same population variance.

To test the hypothesis that the arithmetic means \bar{a}_o and \bar{a}_y are independent estimates of the same population mean, we calculate Student t (see Moroney, 1951, p. 228, for example), where $t_{\text{obs.}} = \frac{\bar{a}_o - \bar{a}_y}{\sigma_o} \sqrt{n-1}$ and $n = \text{no. of observations of } a_o$.

$$\text{Thus } t'_{\text{obs.}} = \frac{1 \times 6.16}{25.6} = 0.241$$

Now $t_{\text{tab.}} = 2.02$ at the 95 per cent level of confidence, for 38 degrees of freedom (Hoel, *op cit.*, p. 330). Thus $t_{\text{obs.}}$ is appreciably less than the tabulated value and the difference in means is probably not significant.

REFERENCES

- Agterberg, F. P., and Briggs, G.
1963: Statistical analysis of ripple marks in Atokan and Desmoinesian rocks in the Arkoma basin of east-central Oklahoma; J. Sediment. Petrol., vol. 33, pp. 393-410.
- Bally, A. W., Gordy, P. L., and Stewart, G. A.
1966: Structure, seismic data and orogenic evolution of southern Canadian Rocky Mountains; Bull. Can. Petrol. Geol., vol. 14, pp. 337-381.
- Billings, M. P.
1954: Structural geology; New York, Prentice-Hall, 2nd ed.
- Bowden, F. P., and Tabor, D.
1964: The friction and lubrication of solids, Part 2; London, Oxford University Press.
- Dzulynski, St.
1953: Tektonika pd. czesci Wyzyny Krakowskiej; Acta. Geol. Polon., vol. 3, pp. 325-439.
- Harding, J. P.
1949: The use of probability paper for the graphical analysis of polymodal frequency distributions; J. Marine Biol. Assoc. U.K., vol. 28, pp. 141-153.
- Hoel, P. G.
1966: Elementary statistics; New York, John Wiley and Sons, 2nd ed.

Hoepfener, R.

1955: Tektonik im Schiefergebirge; Geol. Rundschau, vol. 44, pp. 26-55.

Lindstrom, M.

1962: A structural study of the southern end of the French Jura; Geol. Mag., vol. 99, pp. 193-207.

McConnell, R. G.

1887: Report on the geological structure of a portion of the Rocky Mountains; Geol. Nat. Hist. Surv., Canada, Pt. D, Ann. Rept., 1886, pp. 5D-41D.

Moroney, M. J.

1951: Facts from figures; Harmondsworth, England, Penguin Books Ltd.

Norris, D. K.

1957: Canmore, Alberta; Geol. Surv. Can., Paper 57-4.

1959: Type section of the Kootenay Formation, Grassy Mountain, Alberta; J. Alta. Soc. Petrol. Geol., vol. 7, pp. 223-233.

1961: An interstratal peel on Maverick Hill, Alberta; J. Alta. Soc. Petrol. Geol., vol. 9, pp. 177-191.

1966a: The mesoscopic fabric of rock masses about some Canadian coal mines; Proc. First Congress, International Society of Rock Mechanics, vol. 1, pp. 191-198.

1966b: Interbed slip in some Cordilleran coal mines; in Report of Activities, May to October, 1965, Geol. Surv. Can., Paper 66-1, pp. 114-115.

1967: Structural analysis of the Queensway folds, Ottawa, Canada; Can. J. Earth Sci., vol. 4, pp. 299-321.

Paterson, M. S.

1958: Experimental deformation and faulting in Wombeyan marble; Bull. Geol. Soc. Am., vol. 69, pp. 465-476.

Price, R. A.

1967: The tectonic significance of mesoscopic subfabrics in the southern Rocky Mountains of Alberta and British Columbia; Can. J. Earth Sci., vol. 4, pp. 39-70.

Ramsay, J. G.

1961: The effects of folding upon the orientation of sedimentation structures; J. Geol., vol. 69, pp. 84-100.

Riecker, R. E.

- 1965: Fault plane features: an alternative explanation; J. Sediment. Petrol., vol. 35, pp. 746-748.

Rod, E.

- 1966: A discussion of the paper: 'Fault plane features: an alternate explanation'; J. Sediment. Petrol., vol. 36, pp. 1163-1165.

Roder, D.

- 1960: Der tektonische Stil der Rocky Mountains in Alberta, Canada; Geol. Rundschau, vol. 50, pp. 577-594.

Tjia, H. D.

- 1964: Slickensides and fault movements; Bull. Geol. Soc. Am., vol. 75, pp. 683-686.
- 1967: Sense of fault displacements; Geol. Mijnbouw, 46e Jaargang, pp. 392-396.
-

DISCUSSION

W. F. Brace asked D. K. Norris if he had attempted to section some accretion steps generated in the laboratory and what the section might show.

D. K. Norris said he had not, because of technical difficulties with the impregnation of the ground-up material.

R. A. Price asked D. K. Norris if the apparent 'cross-bedding' laminae of some accretion steps might represent small accretion increments built up in the horizon of the step.

The author said that he considered the gouge of accretion steps to be built up as well as eroded through successive instances of slip, dilation and mineralization. Some cross-laminae are, therefore, actually truncated by the slip surface. What he was looking for and found in accretion steps was some record of the slip history of the surface.

J. B. Currie (written comments)

Legend for Figures

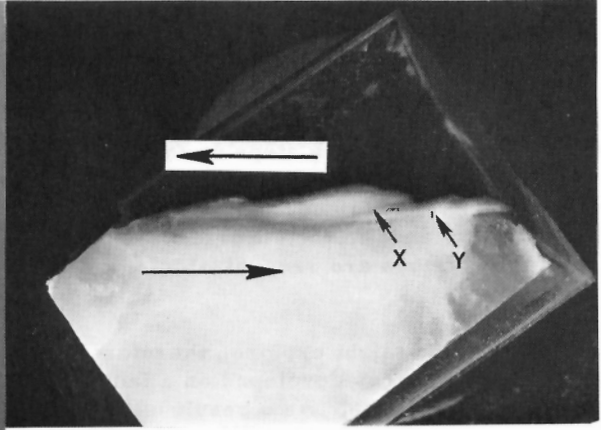
- Figure (1a) Steps on a fracture surface in alabaster. Cylindrical sample; diameter 1 inch. Arrow indicates motion of the upper block. Confining pressure 69 bars.
- (1b) Cross section of one fault block; sample diameter 1 inch. Steps on profile of the fracture surface face the motion of the opposing block. Arrows X and Y point to fractures along which cohesion is retained.
- (1c) Thin section of one step on a fracture profile (X25). The gentle 'riser' of the step is indicated by the arrow at Z.
- (1d) Thin section showing cross fractures that comprise part of the deformation within steps on a fracture surface in alabaster (X25).

Figure 2 on page 171

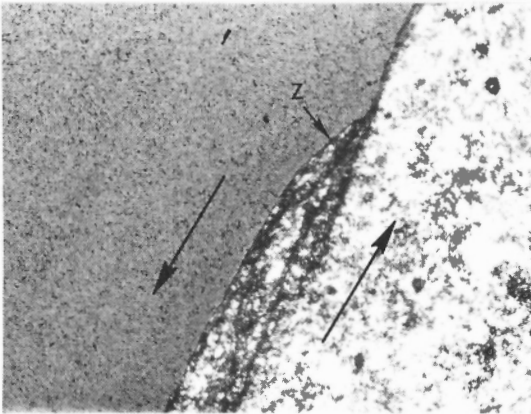
- (2a) Steps on fracture surfaces in a sandstone cylinder, 0.6 inches in diameter. Confining pressure 321 bars.
- (2b) Thin section of one step on the sandstone fracture surface illustrated in (2a), (X25).
- (2c) Steps on fracture surfaces in a limestone cylinder, 0.6 inches in diameter. Confining pressure 1,046 bars.
- (2d) Thin section of one step on the limestone fracture surface illustrated in (2c); (X100). A major fracture can be traced from K downward to its terminus. A minor stepped fracture zone is evident at L.



a



b



c



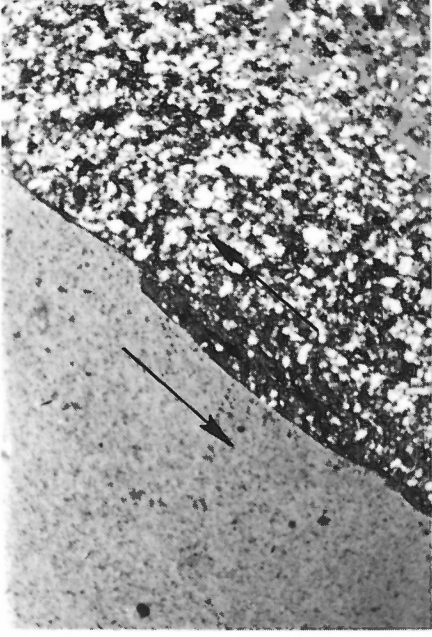
d

The field and experimental evidence cited by Norris and Barron draws attention forcefully to the value of studying features on fault surfaces. They have shown how these features, in the case of Upper March coal seam, serve to document the kinematic pattern. Tjia (1967) records more than six distinct types of geometric features that occur on fault surfaces. One of these features, namely steps on fault surfaces, has not always served satisfactorily as an unequivocal indicator of displacement sense. In partial explanation, Rod (1966) suggests that 'steplike breaks' can develop in more than one way and, in fact, Norris and Barron conclude from their study that at least two types are recognizable, i. e. 'accretion' steps and 'fracture' steps.

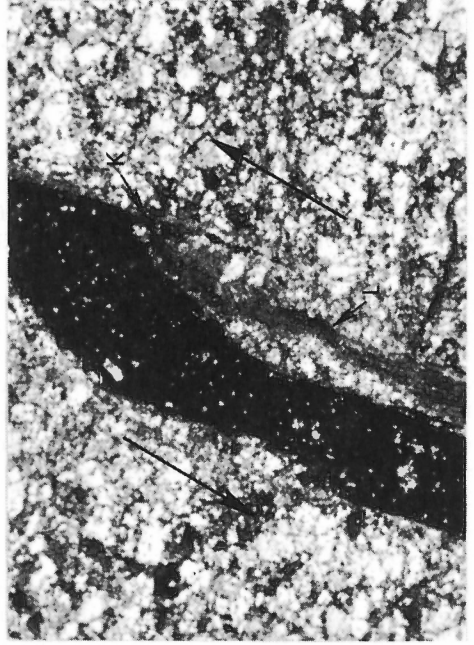
One might explore, therefore, the possibility that the character and type of features developed on a fault surface may depend on the conditions of deformation. As a result of this dependency the facing and nature of steps on fracture surfaces may reflect not only the sense of displacement on faults but also the conditions under which rupture and movement took place. Paterson (1958) noted that steps on fault surfaces produced in cylinders of Wombeyan marble faced the motion of the opposing block. Similar relations have been consistently encountered in a series of experiments in which fine-grained alabaster was deformed over a range of confining pressures.

Figure 1a shows the fracture surface that accompanied rupture under a confining pressure of 69 bars. Steps on the surface trend approximately normal to the direction of fault movement and their 'risers' face against the movement undergone by the opposite fault block (indicated by arrow). Figure 1b provides a sectional view of the fault surface. The steps face against the motion of the opposing block. Two arrows (X and Y) point to fractures that are part of the main rupture zone but along which cohesion has been retained. In Figure 1c is shown the thin-section view of a step on the fracture surface. Traces of several fractures almost parallel to the main rupture are evident and one can note also a general parallelism among the less obvious cross-fractures that trend subparallel to the 'riser' segment of the step (at Z). A closer view of these minor cross-fractures is afforded by Figure 1d taken from an experiment in which cohesion along the main fracture was retained. The cross fractures evidently permit continuity of slip between one major fracture (at the top right of the figure) and another (at the lower left of the figure).

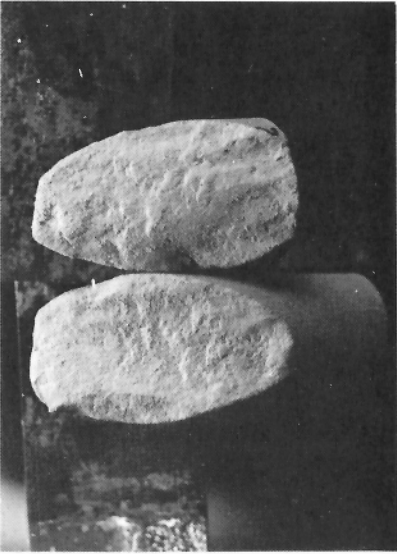
In a series of experiments covering a range of confining pressures, one notes that development of steps on fracture surfaces in alabaster is most obvious within an interval of confining pressures between about 20 and 200 bars. Below this interval rupture causes an irregular fracture surface along which some granulation of material is evident. Above confining pressures of some 200 bars, failure takes place within a deformation zone, of variable width, along which cohesion is retained even in advanced stages of strain.



b



d



a



c

Deformation of a fine-grained sandstone having a micaceous matrix has also shown the development of steps on fracture surfaces. Figure 2a highlights steps on both pieces of a fractured cylinder. The direction of fault displacement, parallel to the sample axis, is made visible by vague slickensides. A thin-section of one step on the fracture profile (Fig. 2b) illustrates its shape and the degree to which material in the step is deformed. Deformation of fine-grained limestone, at relatively low confining pressure (Fig. 2c), further illustrates the development of steps on fracture surfaces. Besides the several obvious steps visible on the fault surface, close inspection shows a very large number of small steps across the entire area of the fracture. For microscopic examination the two pieces of the specimen were cemented together and thin-sectioned. Figure 2d depicts a close sectional view of one step on the fracture. From the point K one can trace a major fracture downward toward its terminus. At L, a minor 'stepped' fracture zone is evident. Prominent development of steps on fractures in the sandstone and limestone samples employed in these experiments appears to occur over a definite interval of confining pressures. For the sandstone, this occurred between 300 and 500 bars, a somewhat higher range than that encountered in the alabaster experiments.

The foregoing evidence suggests that development of stepped fracture surfaces in experiments is governed by the conditions under which samples are deformed. For this series of tests their occurrence was controlled by the confining pressure at which experiments were conducted. This does not imply that temperature, pore pressure and strain rate are not also significant variables. The results do suggest however that at least one type of structural feature commonly found on fault surfaces may reflect something of the conditions of deformation, in addition to revealing the sense of fault displacement. The occurrence of other fault-surface features, such as pluck marks or drags, may also be conditioned by deformational parameters. If this is so, they may acquire greater value in structural interpretation.

References

1. Paterson, M.S. Experimental deformation and faulting in Wombeyan marble; Geol. Soc. Am., vol. 69, pp. 465-476, 1958.
2. Rod, E. A discussion of the paper 'Fault plane features: an alternate explanation'; J. Sed. Pet., vol. 36, pp. 1163-1165, 1966.
3. Tjia, H.D. Sense of fault displacements; Geol. en Mijnbouw, 46 Jaargang, pp. 393-396, 1967.

Authors' reply to J.B. Currie (written comments) The authors would like to thank Dr. Currie for his contribution; he has raised some interesting points. The steps shown by Dr. Currie would appear to be 'fracture steps' as defined by us in the paper, i. e. they are irregularities of the

fracture surface. As such, when the surface is first formed, we believe that these steps could face in either direction. However, if movement occurs on this surface it would seem likely that those facing against the motion of the opposite surface would gradually get destroyed. It would seem likely therefore that the specimens shown in Dr. Currie's photographs have been subject to little or no relative movement between the surfaces. Had there been significant displacement between these surfaces there should be evidence of gouge (and possibly accretion steps), which is not apparent on the photographs. Unmodified fracture steps, therefore, rather than indicating the sense of motion between surfaces, might perhaps be considered to indicate a lack of relative motion between the surfaces.

The evidence presented by Dr. Currie that the occurrence of stepped fracture surfaces is dependent in some way on the confining pressure is significant. However, rather than attributing this to be the 'degree of deformation' of the specimen, we think that this is related to the fracture mechanism occurring in the specimen. A plausible qualitative explanation might be as follows:

At low confining pressures the rock behaves in a brittle manner and fracture initiates in the rock from single 'Griffith's cracks'. Now if the confining pressure is sufficiently low, conditions can be defined in which this fracture initiation propagates immediately to 'ultimate failure' of the specimen, the crack propagating at, presumably, terminal velocity. This would result in crack forking, granulation etc. on the surface. Above this level of confining pressure the material would still behave in a brittle manner, fracture initiating at critically oriented Griffith's cracks. However, the confinement is now sufficiently high to prevent this initiation propagating immediately to failure. Instead fracture will initiate at successively less critically oriented cracks and critically oriented cracks will grow in a stable manner, until at some stage this array of microcracks coalesces to form the fracture surface. In this region the fracture surface has been formed in a more or less controlled manner, consequently granulation of the surface because of unstable fracture propagation will be minimal; it might be expected that pronounced fracture steps would be apparent (which could face in either direction).

At very high confining pressures the material would behave in a completely ductile manner and a shear failure of the specimen would be anticipated on which there would be no fracture steps. There will, of course, be some transition zone between completely brittle and completely ductile behaviour of the rock, in this region a gradual fading out of fracture steps would be anticipated as confining pressure increases.

If the above tentative explanation is true then it would be of interest to examine the development of potential fracture surfaces in the brittle region prior to ultimate failure, and to see if in fact potential fracture steps are indicated and if there is a preferred direction of the steps. This could be

done by stopping a test before ultimate failure but after the onset of fracture initiation, and then examining thin sections of the specimen. Now fracture initiation in the specimen can be recorded in an experiment by observing the onset of microseismic activity. In consequence it would be possible to test a series of specimens at gradually increasing stress levels above onset of fracture initiation and before failure.

Hoek (1965) did stop one experiment before failure and examined the microcracks in it. His photograph (Fig. 24, p.) shows that steps in the crack path can face in opposite directions.

Reference

1. Hoek, E. Rock fracture under static stress conditions; National Mechanical Engineering Research Institute, C.S.I.R., Pretoria, South Africa, Report MEG 383, October 1965, 1965.

W.C. Brisbin asked J.B. Currie about the effect of confining pressure on fractures developing during the long translation of one side past the other in his experiments.

J.B. Currie answered that much of the slope is due to curving of the fracture steps, as a result of the movement of one side past the other.

REGIONAL AND SUB-CONTINENTAL SIZED FRACTURE SYSTEMS
DETECTABLE BY TOPOGRAPHIC SHADOW TECHNIQUES

Donald U. Wise
Franklin and Marshall College
Lancaster, Pennsylvania

Abstract

Topographic linear analysis for underlying fracture control is a subtle mixture of science, art, and self-delusion. Radar imagery of real topography or photos of side illuminated raised plastic relief maps enhance many elements of linear topography, particularly those valleys with strikes at acute angles to the light source so that illumination grazes one of the walls. Dozens to hundreds of topographic linears appear on all relief maps examined with scales from 1:62,500 to 1:1,000,000. They are commonly arranged in six to eight strike sets with individual linears persisting for a hundred miles or more, the sets themselves continuing for many hundreds of miles. The shadow enhancement permits rapid mapping of the linears over vast areas; the requirement of the same linear appearing under a variety of lighting directions provides some control on operator generated pseudo-linears.

Complex fracture networks occur with constant orientation over vast areas of North America, Europe, and Iceland, some elements of the networks being correlatable with known fault or fracture systems. The systems extend without change to the edges of continents; they extend unchanged across portions of the Mediterranean; they are strongly developed on the youthful crust of Iceland; they are independent of local curvatures and geometry of the mountain systems in which they occur; they continue unchanged from the Appalachian region into the youthful Coastal Plain. The relations suggest tectonic heredity of older systems being propagated upward through youthful covering sediments and/or near modern stress trajectories of constant orientation over extremely large areas. The areal magnitude of the system, complexity of sets, and independence of regional structure, suggest that many traditional methods of regional fracture analysis may be too small in areal coverage, too limited in statistical ability to separate sets of small dihedral angle, naive in failing to consider tectonic heredity and misguided in trying to do stress-strain analysis of the pattern in terms of local tectonic features.

INTRODUCTION

Despite excellent theoretical and laboratory studies of the behavior of brittle materials, explanation of origins of fracture systems observable in outcrop is among the least satisfactory aspects of structural geology. Thesis of this paper is that fracture systems in nature are more complex in number of sets, in hereditary links with a geologic past, and in vast areal extent, than ordinarily considered in assumptions and techniques used to analyze those patterns.

TECTONIC HEREDITY AND JOINTING BY EXTENSION

A common but questionable assumption of fracture analysis is that time of fracturing is the same as time of application of tectonic stresses. Difficulties with this assumption were pointed out by Chapman (1958) working with joints which break and hence are younger than post-glacial sheeting in coastal Maine. These youthful joints are associated with areal extension and downhill creep of the post-glacial sheets. They tend to form two joint sets at any location, both sets vertical but one parallel with the topographic contour and the other perpendicular to it. Despite this link of jointing to topography, the fractures themselves are restricted to a number of orientations remaining constant across the region. Chapman concludes that regional tectonic stresses left a number of directions of preferential weakness in the rocks in the form of planes of fluid inclusions. Subsequent directions of extension controlled by topography permitted only a few of the potential fracture directions to develop into visible joints.

Similar mechanisms operate on a larger time scale in basement rocks of Montana-Wyoming, where the name tectonic heredity was coined for the phenomenon (Wise, 1964). In that region eight recurring fracture directions appeared in basement over an area of at least 50,000 square miles during at least seven periods of extension fracturing ranging over 2.6 billion years. The earliest indications of these eight directions appear in orientations of pegmatite and quartz veinlets and of basic dike swarms dating from the closing phases of regional metamorphism. At least four more systems of Precambrian basaltic dikes show the same orientation pattern (Table 1). The same eight directions were reactivated by a pervasive system of microjoints with spacing of a few millimeters developed during sideward expansion of rising Laramide block mountains. However, the microjoint pattern at most locations involves strong development of only two perpendicular sets of the eight potential sets. The final event was the development of common joints, many of which break post-glacial sheeting and commonly show two strong sets roughly perpendicular to each other. Spencer (1959), on the basis of 25,000 joint measurements in the Beartooth Mountains, found the same eight recurring directions (Table 1).

Tectonic heredity implies that a pattern of numerous potential fracture directions can be set into basement soon after crustal solidification. These directions seem particularly susceptible to reactivation by successive extensional environments. Consequently, elements of the complex system can appear in sets of Precambrian dikes of one orientation, Laramide microjoints of other orientations, and Pleistocene or recent common joints of still other orientations, all within the same outcrop but nevertheless linked by tectonic heredity to the same eight potential fracture directions and to stresses of an early Precambrian world.

The seemingly 'reasonable' approach of measuring jointing directions in basement of the Rockies and trying to relate these patterns to Laramide stress patterns would be unlikely to yield any interpretable results.

Table 1

Comparison of orientation of Middle Rocky Mountain microjoint sets with those of common joint sets and dikes of the Beartooth Mountains, Montana and Wyoming (Wise, 1964)

Microjoint maxima from composite plots of stations throughout Middle Rocky Mountains	Most prevalent common joints in basement of Central Beartooth Mountains ^{1*}	Precambrian dikes in Beartooth Mountains ^{2**}
N 70 W	N 60-70 W	N 60-80 W
N 45 W	N 45 W	N 30-45 W
N 10 W	N 15-20 W	N 20 W
N 10 E	N 0-10 E	N 0-10 E
N 25 E	N 15-25 E	
N 45 E	N 45 E	N 30-45 E
N 65 E	N 60 E	N 60 E
N 85 E	N 85-90 E	N 90 E

1* From Spencer (1959, p. 494) summary

2** From Spencer (1959, p. 499) as grouped by Wise

COMPLEXITY AND NUMBER OF FRACTURE SETS

The fact that only a few fracture sets are strongly developed in most outcrops lends the appearance of disarming simplicity to the problem of fracture analysis. Unfortunately most regional studies show a total of five to nine fracture directions with a possible 'magic number' of eight directions. Consequently joint sets might differ in strike by only 20-25 degrees resulting in real difficulties in separating the sets by contouring plots of a few hundred joint orientations.

The familiar problem of double maxima in contoured joint plots may reflect the above difficulty. One explanation of double maxima is that of Muehlberger (1961) involving very brittle conjugate shearing. Another is that of Wise (1964) utilizing tectonic heredity and extension opening of two sets of possible joints differing by only 20-25 degrees. Once the extensile stresses have been released by jointing along those two sets, the remaining extensile stresses are most likely to form another joint set, possibly involving a double maximum, at right angles to the first.

In view of the complications of: tectonic heredity, development of only a few member sets of the system, some scatter of data, effects of topography, human bias, and double maxima, it should not be surprising that joint plots from adjacent outcrops are rarely identical and only rarely can be correlated with any degree of certainty.

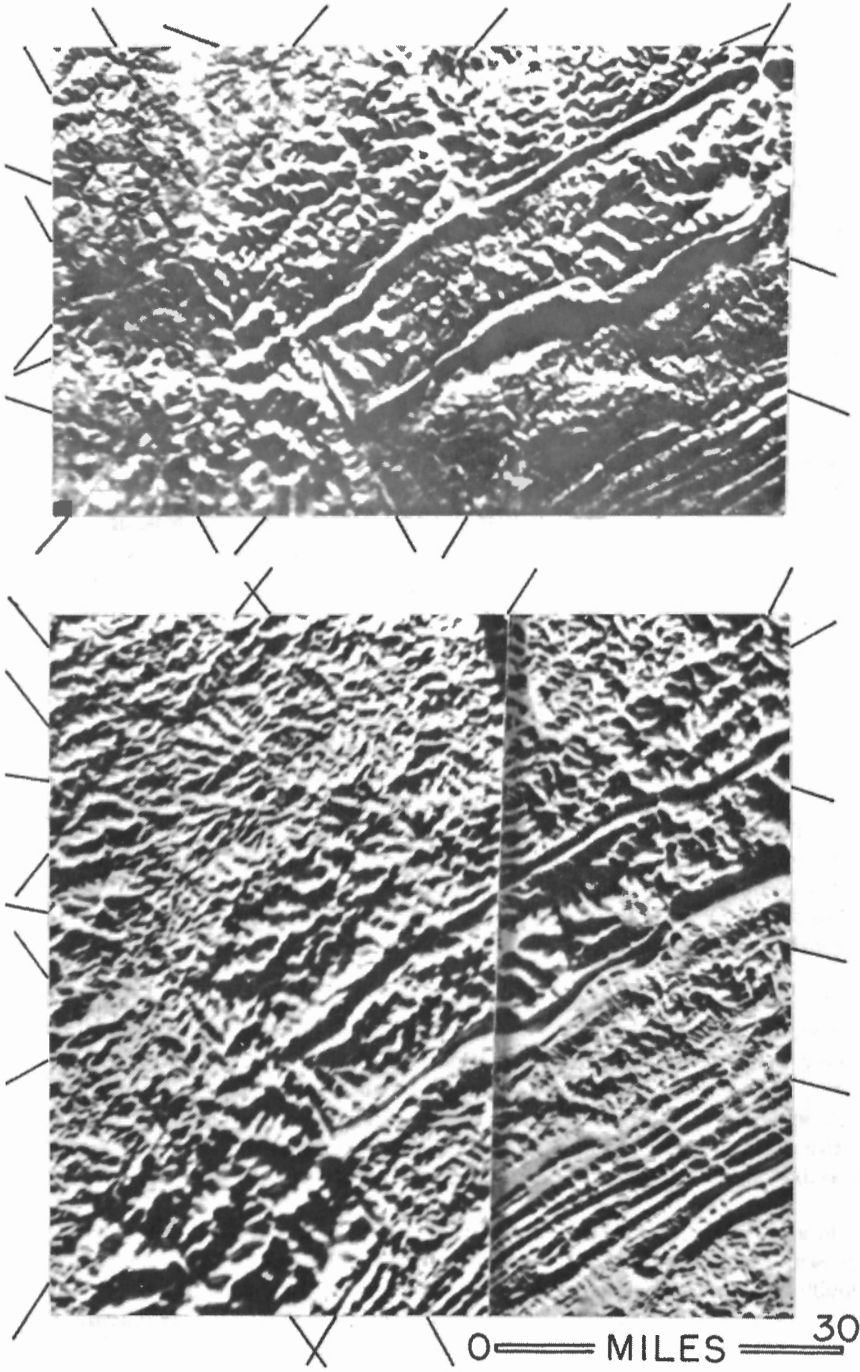


Figure 1. Contrast of linears on true radar image (right) and photograph of a raised plastic relief map (left). The area is the Pine Mountain or Cumberland thrust of Tennessee and Kentucky. Note that east-west scale of the radar image is not the same as that of the map, reflecting a mis-match in ratio of film advance to aircraft flight speed. The result is some angular distortion of the radar image.

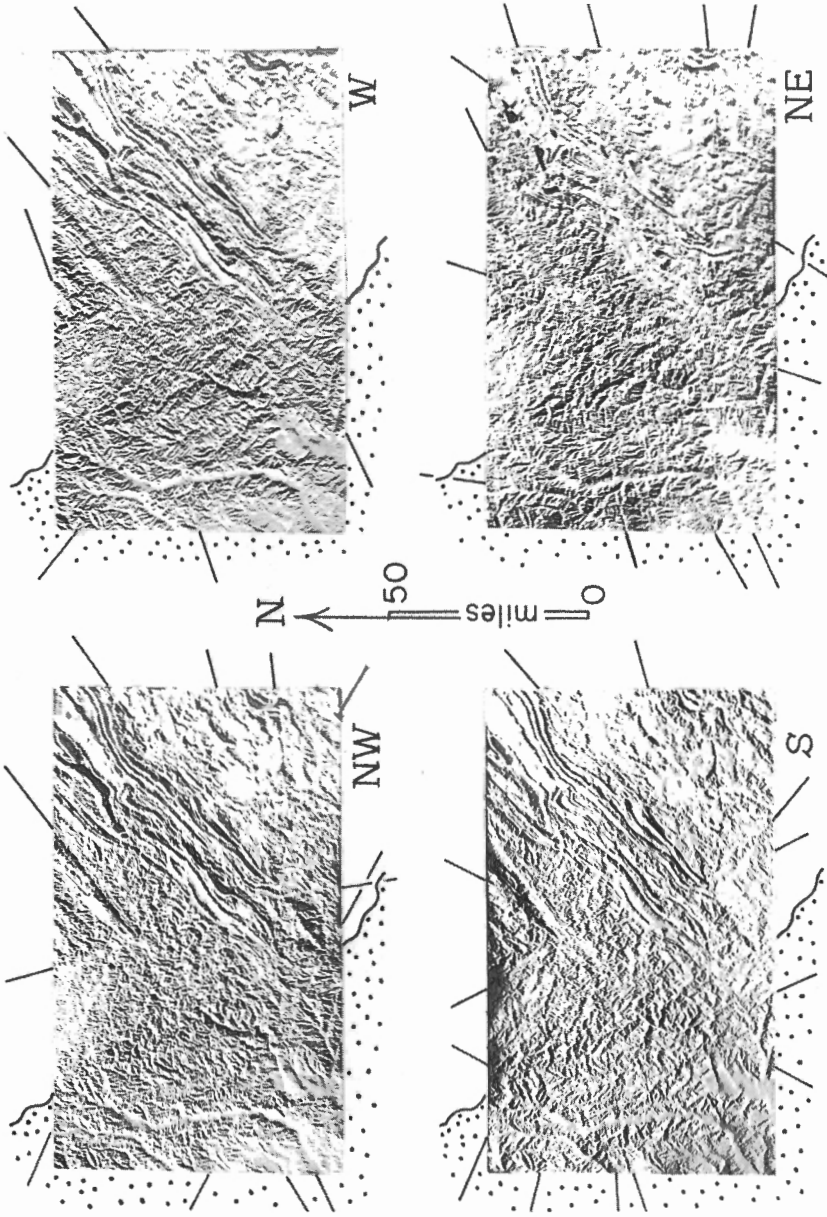


Figure 2. Contrast of systems of topographic linear features enhanced by differing lighting directions. The map is the Birmingham, Alabama, 1 degree by 2 degree sheet. Illumination direction is indicated at lower right of each photo. Coastal plain cover occupies the southwestern third of the area as indicated by the stipples but the linear patterns transgress the boundary with no apparent change.

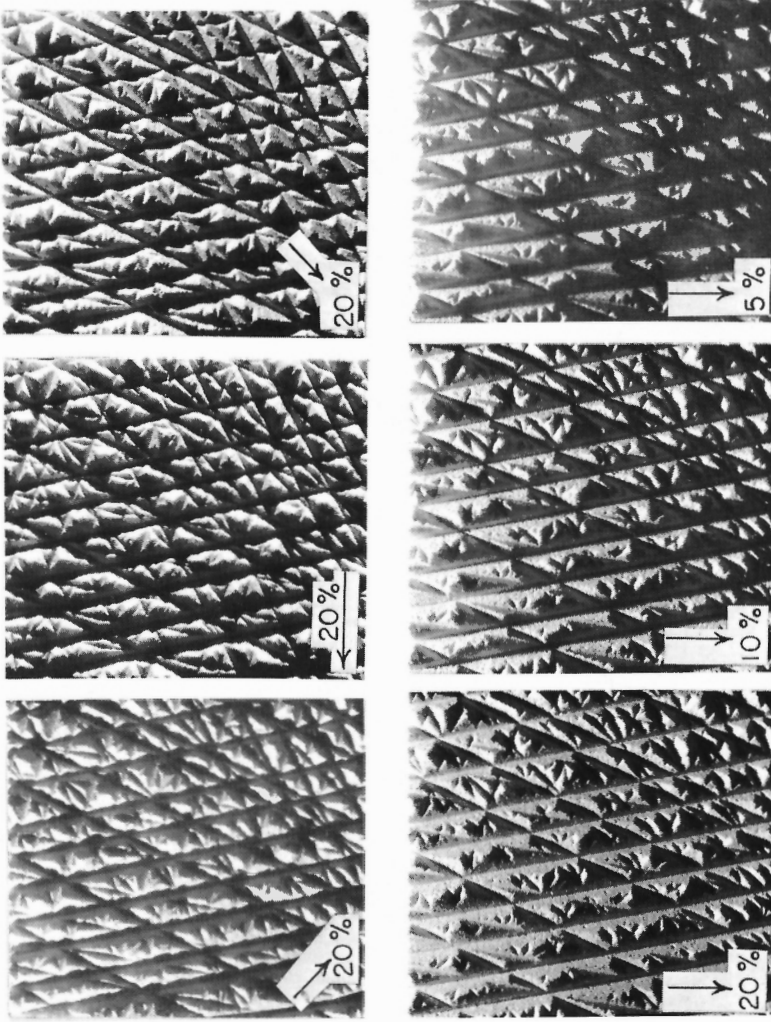


Figure 3. Effect of illumination direction and inclination on visibility of linear patterns. Light direction and inclination is indicated at lower left of each photo. The model is a 1 foot square of polystyrene cut with eight directions of linear patterns having 45 degree valley slopes and strikes identical to those of the Beartooth area, Table 1. Number and depth of cuts were determined by random number tables. Top row shows same light inclination but differing azimuth. Bottom row shows same azimuth (North) but differing inclination of light.

As a substitute for laborious collection of field data, a number of more rapid techniques are commonly applied using the principle that topographic linears may represent the etching of weakness directions of bedrock associated with fracture systems. The method may be more rapid but involves many of the same pitfalls: separations of numerous linear sets of small dihedral angle and recognition of the possibility of tectonic heredity.

LOW ANGLE ILLUMINATION AND TOPOGRAPHIC LINEARS

Recent development of side-looking airborne radar, involving imprinting the radar return on a film strip advancing proportionally to aircraft speed, has revealed previously undetected topographic linears of considerable areal extent (Dellwig, et al., 1966). In an effort to understand image enhancement of topographic linears by low angle illumination, the author began experimenting with photography of raised plastic relief maps lighted from one side. If light source for the plastic maps is in a direction comparable to the airborne radar, the resulting images can be remarkably similar (Fig. 1). The plastic map image is without the angular distortions likely to be produced by radar film advance at a rate non-proportional to aircraft speed. The similarity of results suggests that it is not a particular property of radar wavelengths which reveals the linears but rather the low angle shadowing coupled with reduction of detail over large regions. Figure 1 (right) is the only true radar image in this paper; all others are taken from raised plastic relief maps.

Topographic linears appearing on any particular image vary markedly with direction of illumination (Fig. 2). The most strongly enhanced topographic linears are ordinarily at acute angles of azimuth to the illumination source. With any one illumination direction, only about half of the total numbers of linears in the topography appear clearly.

As an experiment in selective enhancement of linears by shadowing, a one-foot square sheet of polystyrene was marked by eight directions of circular-saw cuts with 'valley slopes' all at 45 degrees. The strikes of the eight sets of linears are the same as in Table 1 but the depth and number of cuts was determined by tables of random numbers. Six different illuminations of this artificial topography are illustrated in Figure 3, the top row showing variable azimuth of light but constant angle of incidence and the bottom row illustrating the reverse.

From these experiments it appears that the linears which will be most strongly enhanced by side illumination will be those having one valley wall completely shadowed, the other wall completely illuminated. This condition obtains when the illumination is in grazing incidence with one wall of the valley, a condition necessitating, an acute angle between azimuth of valley and azimuth of light source as illustrated in Figure 4. From that figure, the basic relationship:

$$\sin \alpha = \frac{BC}{AC} = \frac{DC/\tan \alpha}{DC/\tan \beta} = \frac{\tan \beta}{\tan \alpha}$$

determines the linear favored by optimum enhancement. The relationship is plotted in Figure 5. For instance, valleys with average slopes of 30 degrees illuminated by a light source with a 10 degree slope would appear under many orientations but would appear most prominently when oriented at 18 degrees from the azimuth of the light source. When using raised plastic relief maps, the customary vertical exaggeration must be included in the angle of valley slope.

Because of dependence of shadow linear enhancement on azimuth of light source, a minimum of four directions of illumination is advisable, although the author has experimented with up to eighteen directions of illumination (10 degree increments through 180 degrees).

QUALITATIVE RELATIONSHIPS

To date more than 250 raised plastic relief maps at scales ranging from 1:1,000,000 to 1:62,500 have been photographed at many azimuths of low angle illumination. Most have been integrated into regional mosaics. All relief maps

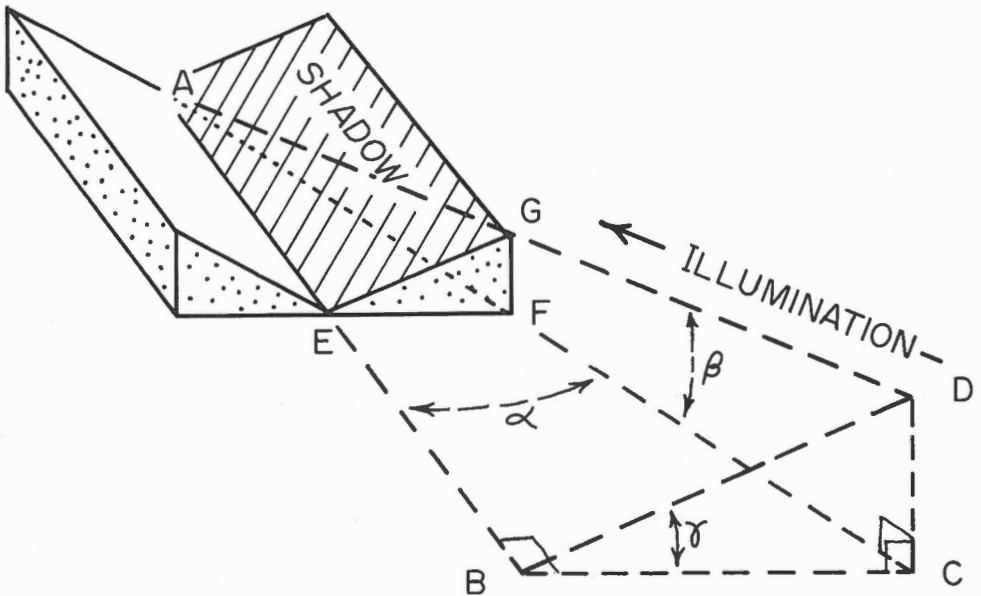


Figure 4. Geometric conditions for oblique illumination producing maximum shadow enhancement of a linear valley by grazing contact with one valley wall and full illumination of the other wall. The condition necessitates an acute angle (α) between azimuth of linear and azimuth of illumination source.

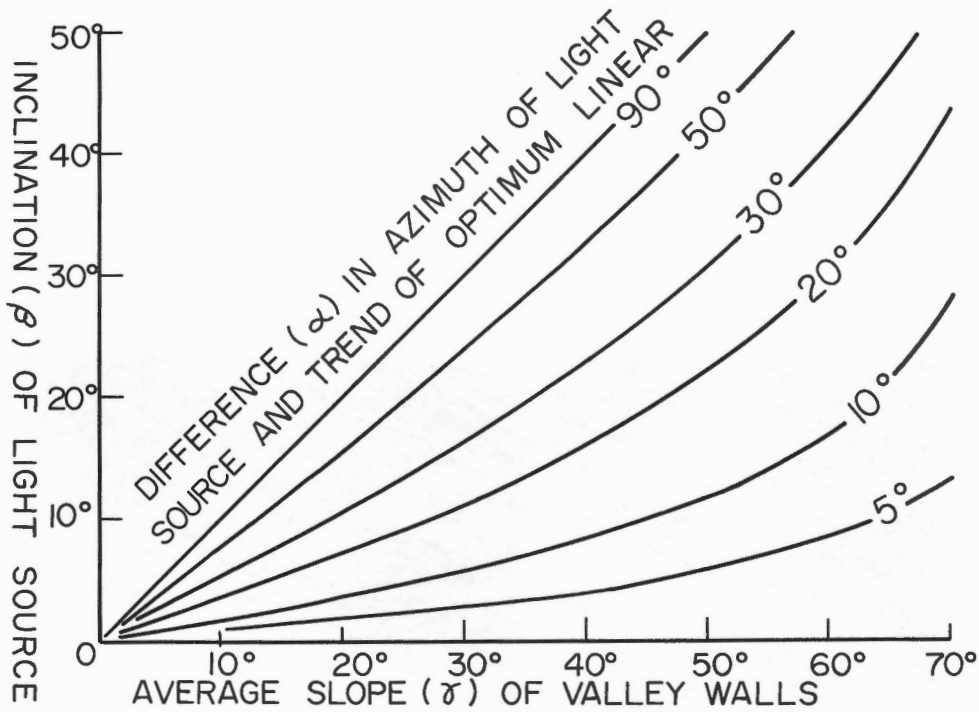


Figure 5. Conditions for maximum enhancement of a topographic linear by shadow techniques. Other lines will appear in the shadowed image but the one enjoying maximum shadow enhancement by grazing illumination is indicated on the plot. The definitions of angles and relationships are derived from Figure 4. If raised plastic relief maps are used, the vertical exaggeration must be included for average valley slope.

examined, regardless of scale or youth of geology, show strongly developed systems of topographic linears.

Figures 6-10 are designed to illustrate some of the qualitative characteristics of shadow linears:

- (1) Linears are ubiquitous, commonly closely spaced and continue with constant trends for a distance of 10 - 100 miles.
- (2) The linears are independent of the scale of the maps.
- (3) In any one area there are a sizeable number of sets comprising the total system of linears.

- (4) The same linear and same sets of linears can be traced into adjacent maps.
- (5) The linear pattern does not change in passing into an area of coastal plain cover, in approaching the edge of the continent, or in passing into a curving part of a mountain system.
- (6) Many of the linears can be correlated with known geologic fractures.

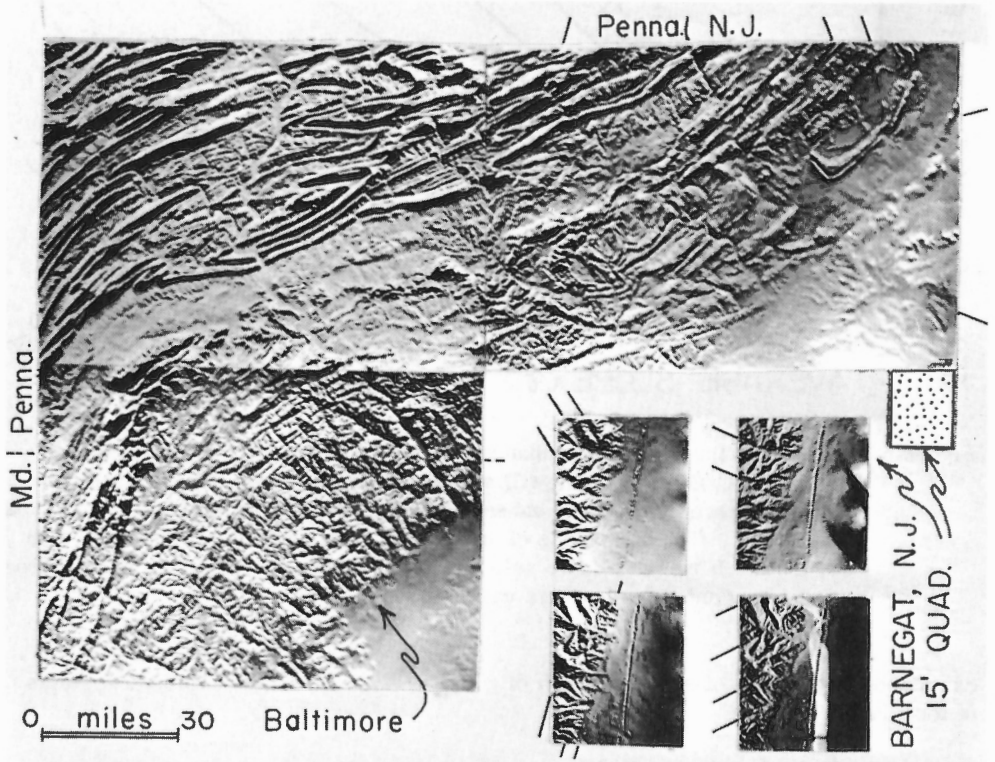


Figure 6. Similar orientations of shadow linears on maps of differing scales. The area is the New Jersey, Pennsylvania, and Maryland Arc of the Appalachians composed of three 1 degree by 2 degree quadrangles at 1:250,000 scale. The Barnegat, New Jersey, 15-minute quadrangle at 1:62,500 is illustrated with four lighting conditions showing the barrier beach and the topography having maximum relief of 150 feet. Location of the Barnegat quadrangle is indicated by the stippled square. Note that the same linears carry over a much larger area and are relatively independent of Appalachian curvature and of Coastal Plain cover.

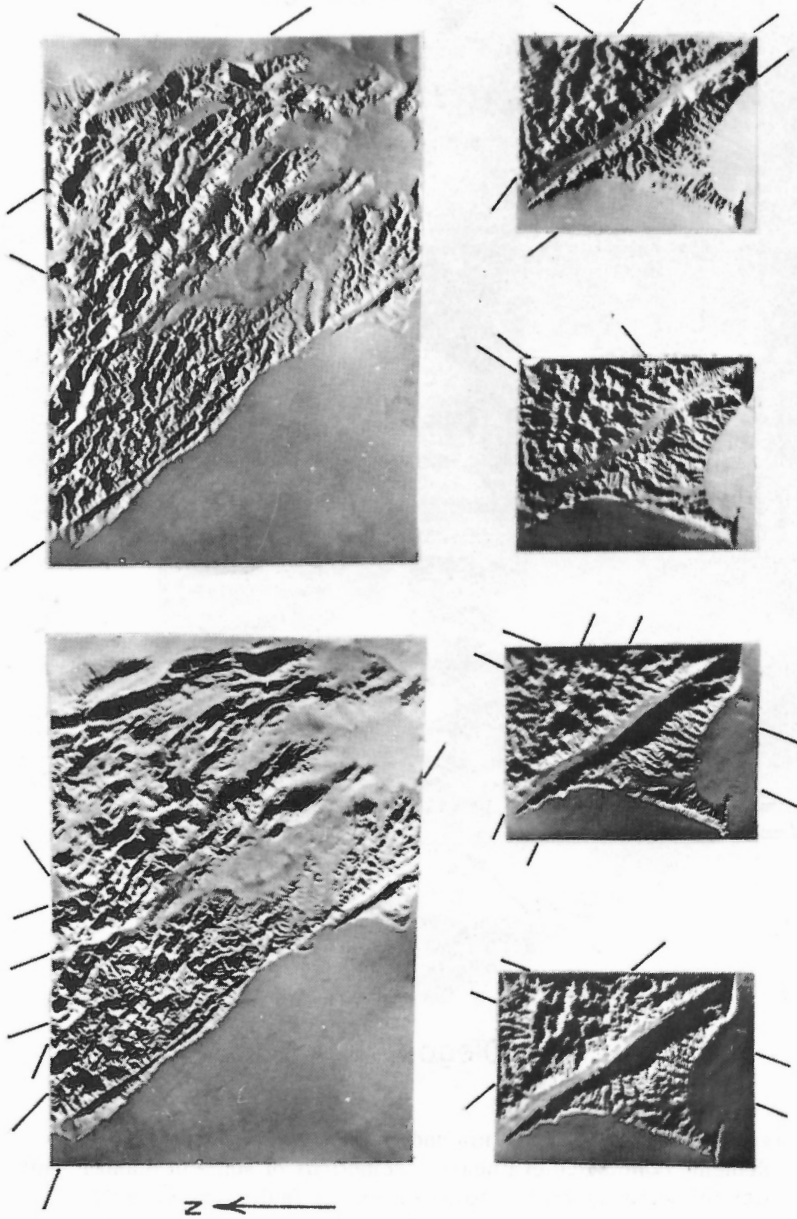


Figure 7. Point Reyes Quadrangle, California, and the San Andreas Fault. The lower illustrations are four different illuminations of the 15 minute quadrangle; the upper illustrations are two lightings of the 1:250,000 1 degree by 2 degree quadrangle in which the smaller quadrangle appears. Note that many of the same linears appear at both scales.

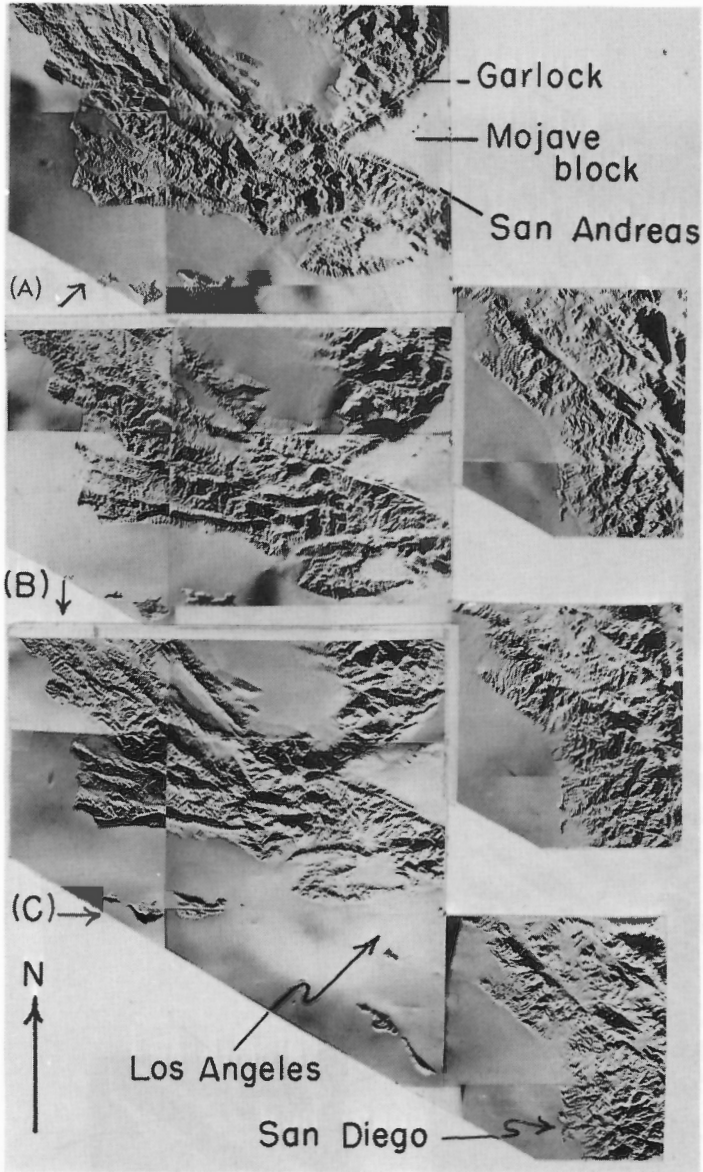


Figure 8. Fault region of Southern California under three different illuminations. Note: changing dominance of linears, projections of some of master faults, parallelism of some linear sets to these master faults, and general constancy of orientation of linear sets between adjacent fault blocks.

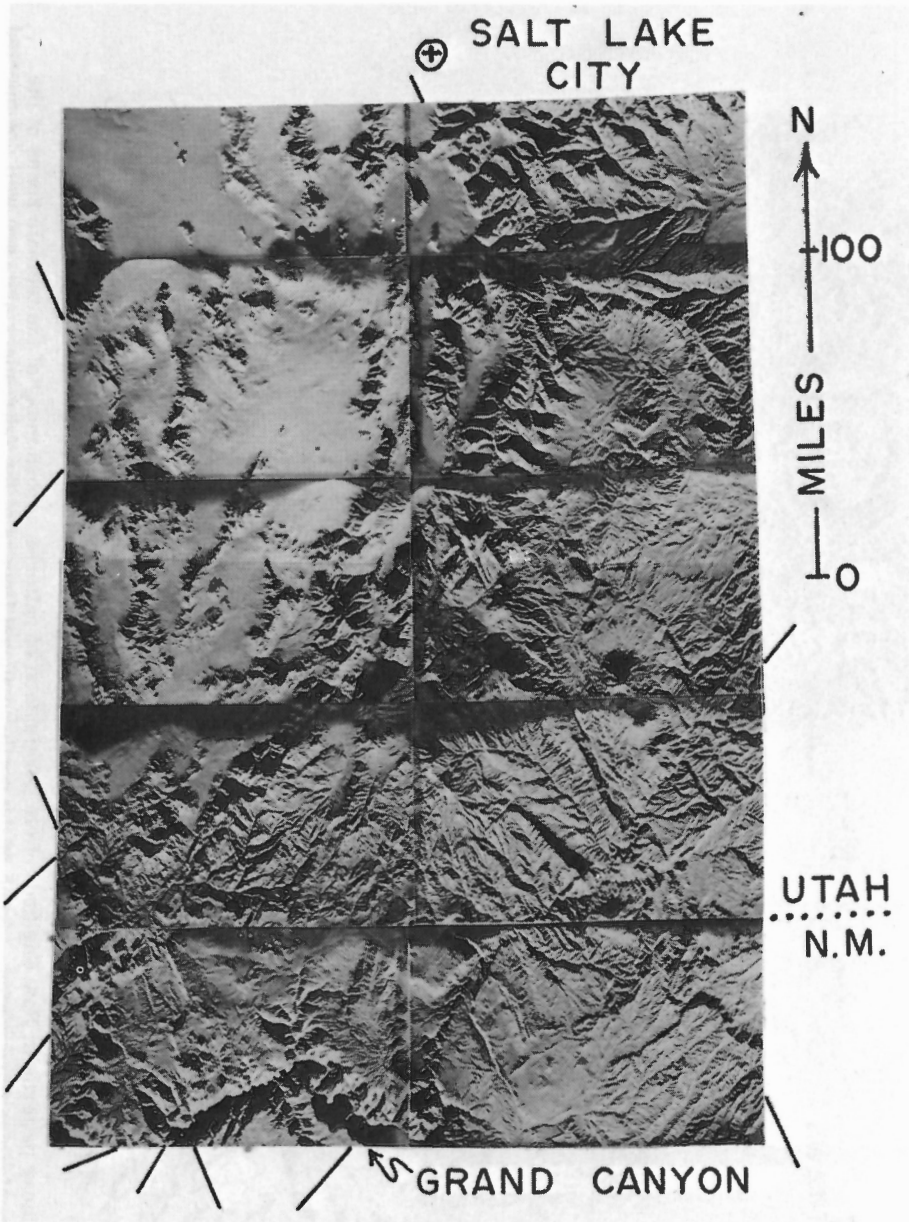


Figure 9. Linears in the Grand Canyon, Colorado Plateau, Great Basin country. North-northeast and north-northwest linears persist over the region passing across the boundary between the two provinces. Many linears in the Grand Canyon area correspond to small faults on existing geologic maps.

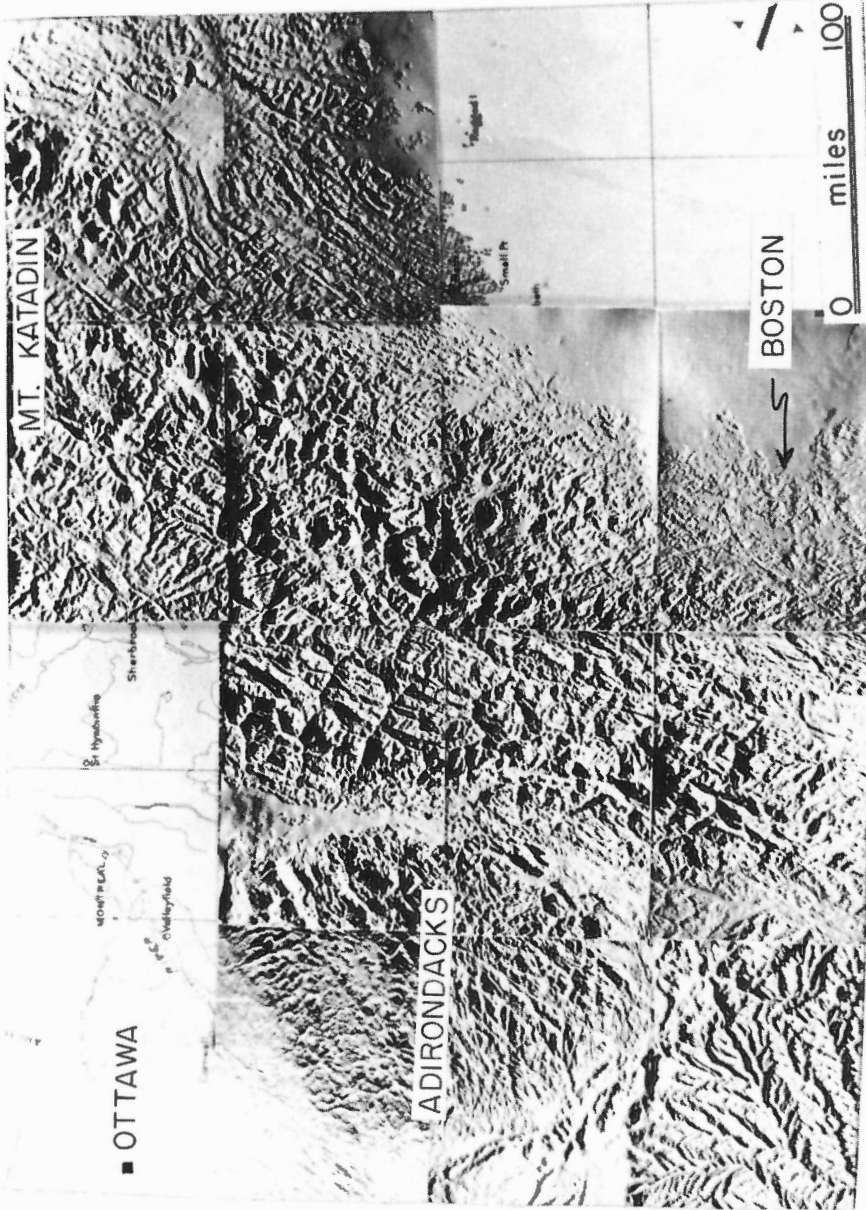


Figure 10. Linear patterns in New England. Note persistence of patterns across many of the tectonic zones of the Appalachian core region. Some of the north-northeast linear features of the Adirondack area are well documented faults.

SEMI-QUANTITATIVE ANALYSIS OF SHADOW LINEARS

Quantitative analysis of the shifting patterns of shadow linears is a major problem. Some sets of major steep slopes can cast arrays of very short shadows which appear as a fine grain moving continuously with azimuth of lighting. In addition, the psychologic factor of operator enthusiasm for drawing linears can result in a line between any two prominent points on the image.

In an attempt to minimize some of the difficulties, a semi-quantitative technique was devised for the shadow linears. Figure 11 (top) is a low angle illumination image of the Black Hills of South Dakota region with each quadrangle representing an area of 1 degree by 2 degrees, at a scale of 1:250,000. Figure 11 (bottom) is a tracing of all major linears greater than 20 miles length visible in the upper image. Similar tracings were done for three other lighting conditions of the same plastic relief maps. For each of the four quadrangles on each of the four tracings, a wind rose plot of sets of linears was prepared (Fig. 12, top). Rotation of a sheet of ruled paper beneath the tracing permits visual averaging of orientations of sets and judgments of whether the set is weak, intermediate, or strong.

For each quadrangle, linear directions which appear with medium or strong development in three of the four lighting directions with azimuth differences of only 5 degrees are indicated as valid fracture sets on the bottom of Figure 12. Sets appearing under two of the four lighting conditions may be real; the remainder probably have sizeable illusionary aspects.

The Black Hills plot (Fig. 12) illustrates the independence of the shadow linears from the local structure of the uplift. Instead, the pattern is characteristic of the surrounding Great Plains. A typical study of the linears of the Black Hills attempting to relate the linears to stresses which created the uplift would seem ill-advised.

Similar techniques of analysis were applied to Southern Europe (Figs. 13 and 14) using 1:1,000,000 scale relief maps. Very prominent linear systems carry through the region, including excellent east-northeast sets across the Alps and the Riviera. Progressive changes in azimuth of some sets across the region suggest that these features could represent clues to stress trajectories curving across continental or larger sized areas.

It is significant that these linear patterns extend without apparent change across a curving youthful mountain system, project across some of the semi-oceanic crust of the Mediterranean and cause alignments of some of the islands of Greece. The imagery from Asia Minor (Fig. 15) suggests continuation of many of the same trends farther east.

In an attempt to avoid some of the difficulties of unknown crustal movements in an area of ancient crust, the shadow linears of Iceland were examined (Fig. 16). The area is supposedly one of extension and creation of new crust along the mid-Atlantic Rise. The Iceland Graben appears but is no more strongly developed

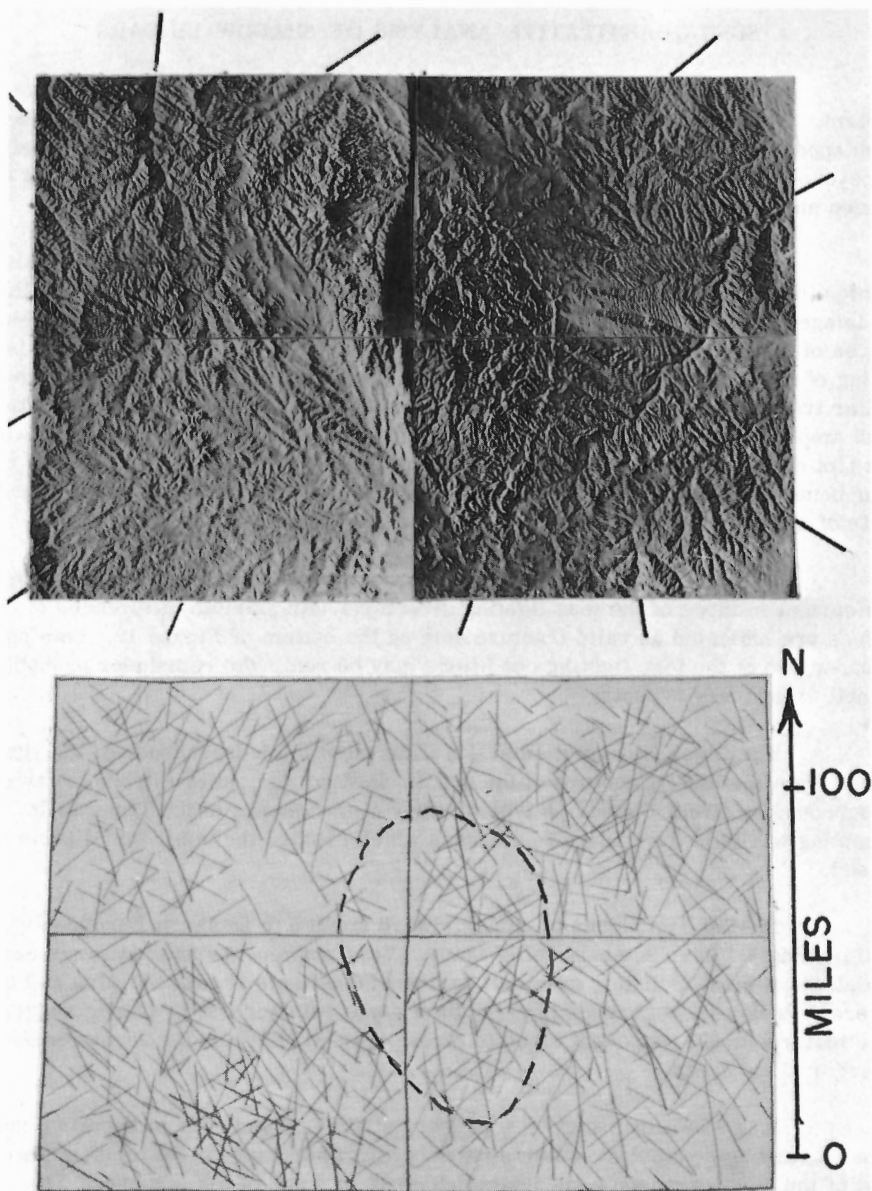


Figure 11. Linears of the Black Hills, South Dakota. Note that many of the linears carry into or through the mountains from the surrounding Great Plains. Lower portion is a tracing from the original negatives of the more prominent linears visible in this lighting.

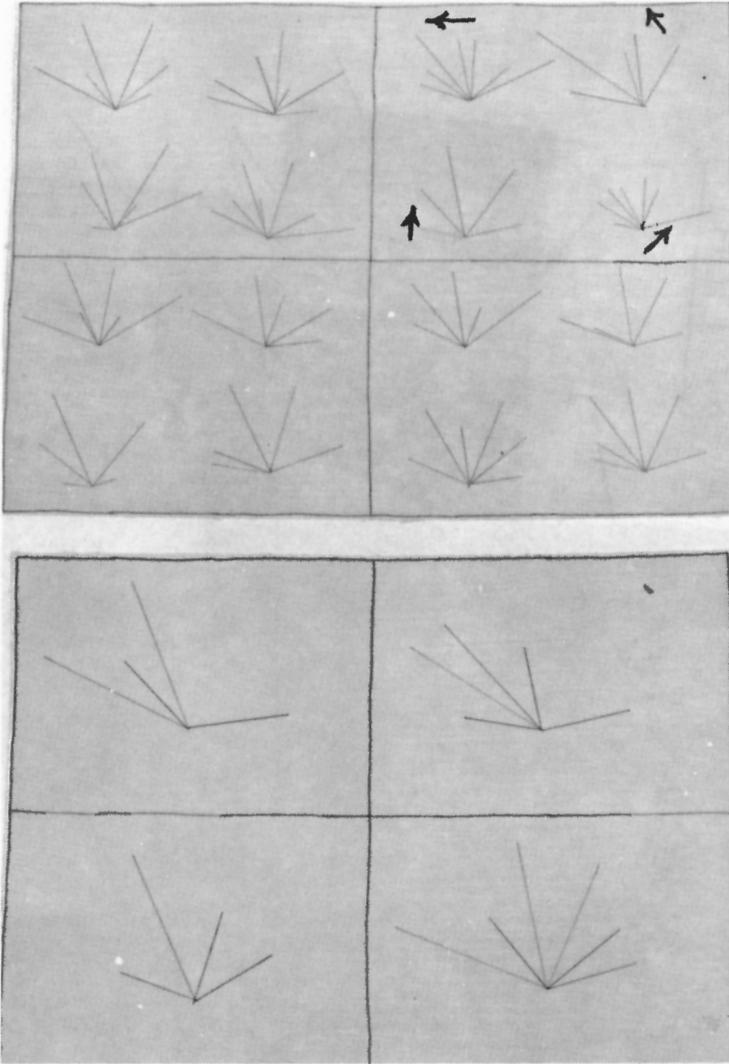


Figure 12. Analysis of linears of the Black Hills. Data from each quadrangle from Figure 11 and three other sets of images of different lighting are represented by the wind roses of the upper diagram. Lighting directions are indicated by the small arrows; strength of a linear set is indicated by length of lines on the wind rose. Lower diagram is a composite of linear sets appearing in each quadrangle within 5 degrees of strike with intermediate or strong representation in two-thirds or three-quarters of the lighting orientations. These are interpreted as real fracture directions existing in the topography.

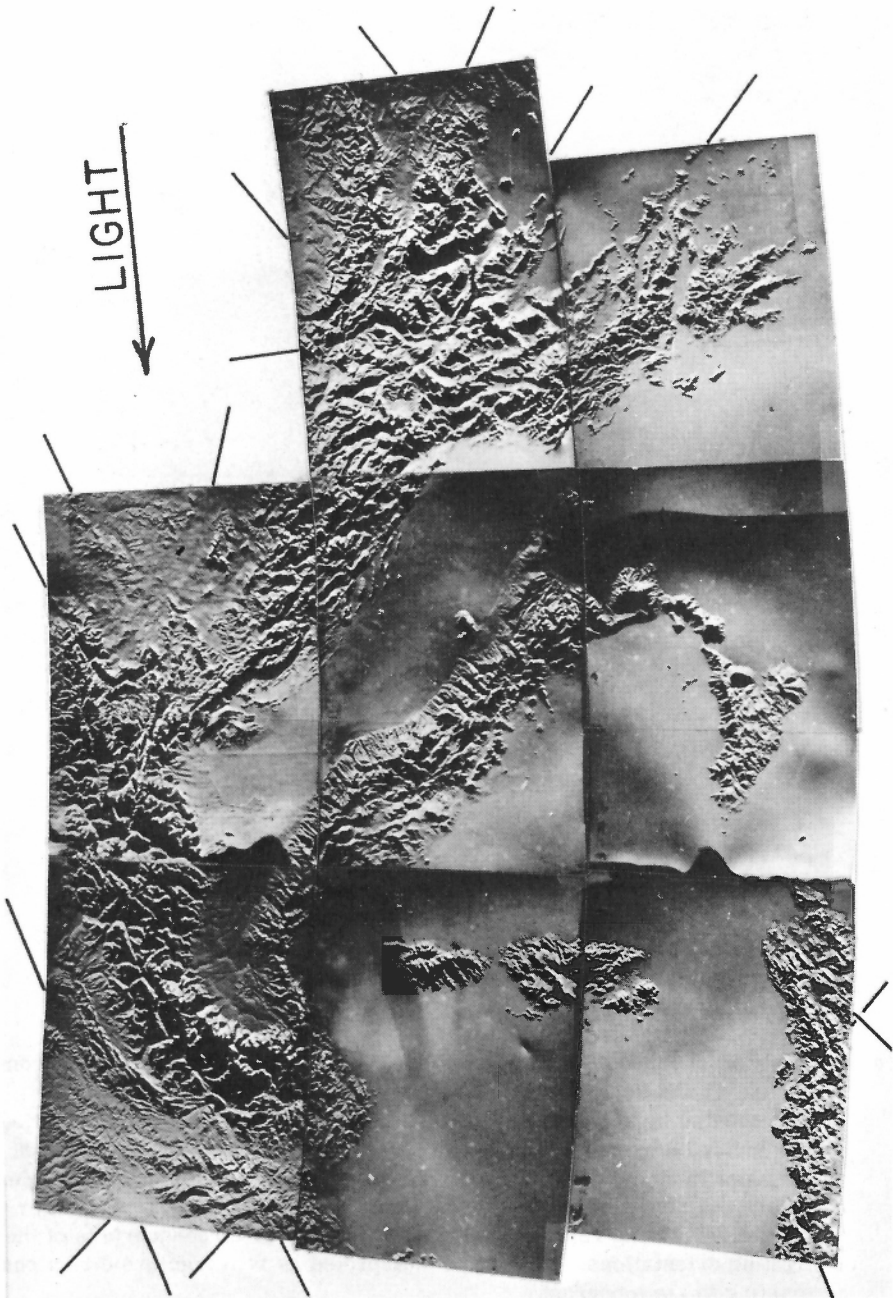


Figure 13. Shadow linears in the topography of Southern Europe as lighted from the east.

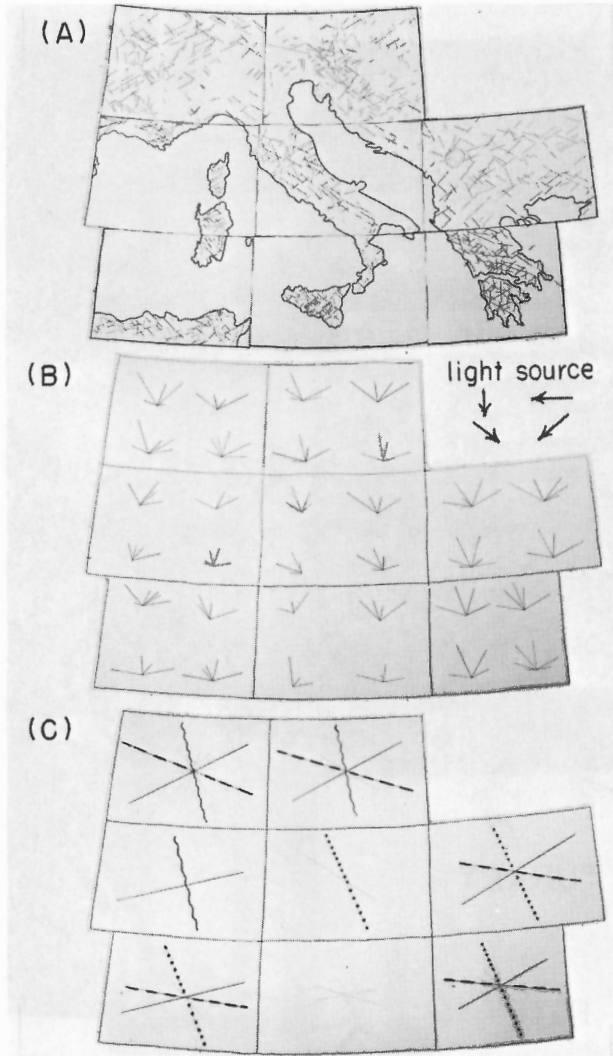


Figure 14. Fracture patterns of Southern Europe treated as in Figure 11 and 12. (A) Linears visible in previous figure (lighting from the east). Note circular depression in Yugoslavia. (B) Wind roses of major fracture directions for each quadrangle as lighted from four directions. (C) Master fracture patterns of each quadrangle as indicated by intermediate or strong fracture sets within 5° of strike appearing in two or three of the four lighting directions. Weakly developed directions are indicated by lighter lines.

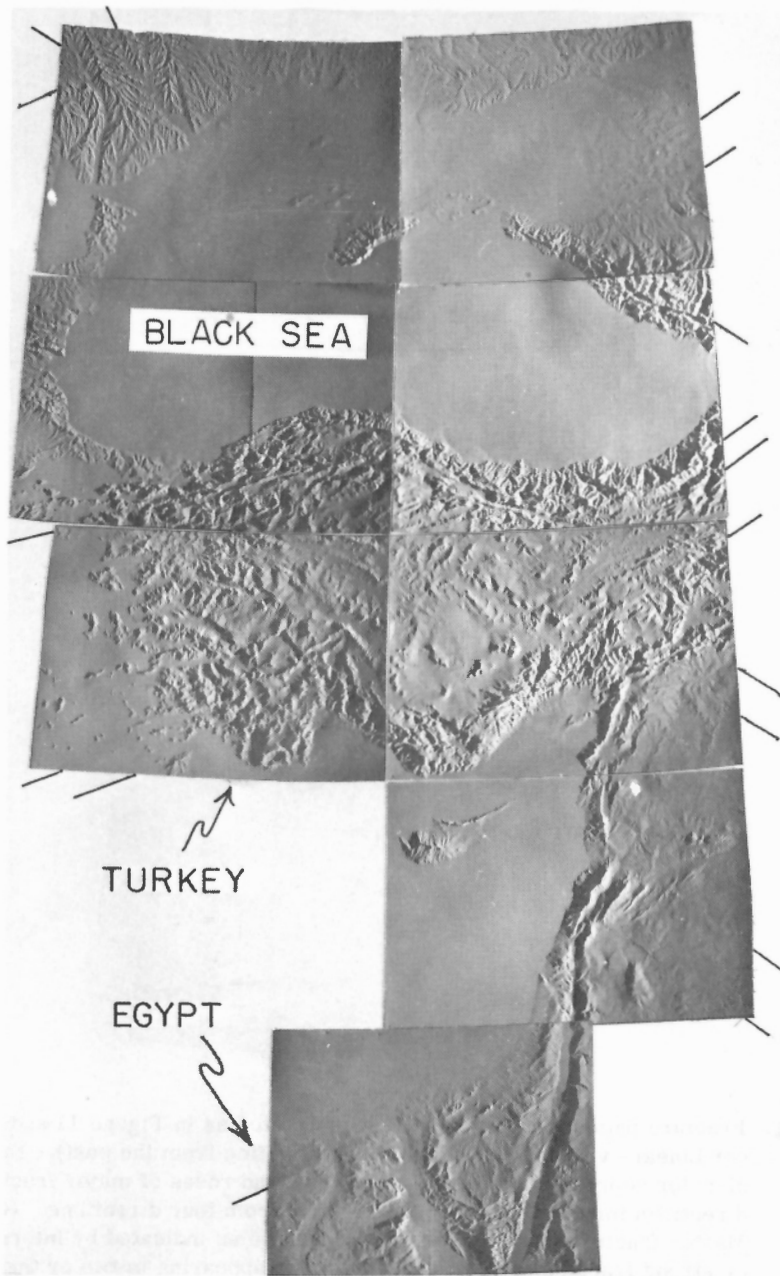


Figure 15. Linear elements in the eastern Mediterranean - Black Sea region. Lighting from the east.

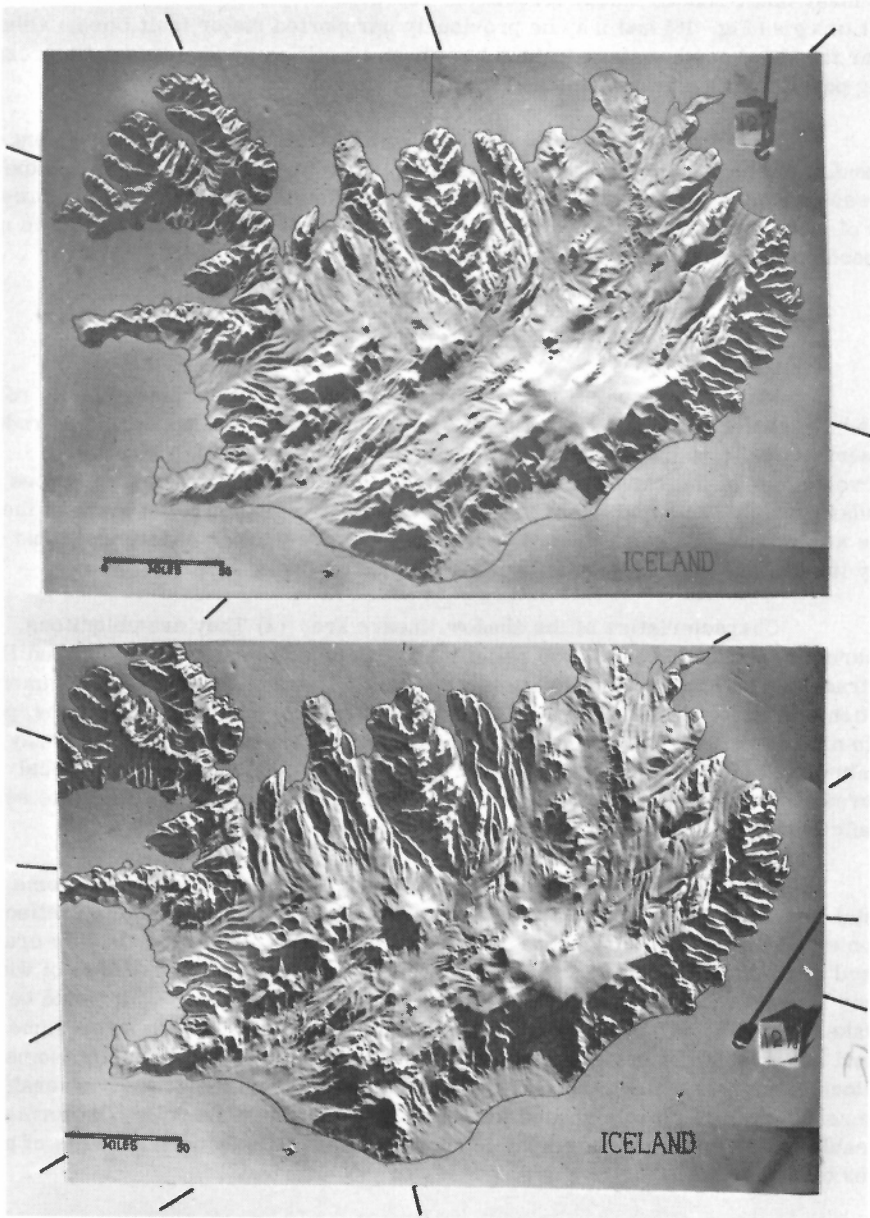


Figure 16. Oblique illumination and shadow linears of Iceland. Note that complex fracture patterns persist with little change across the island and with little apparent change or symmetrical relationship across the central graben.

than many other shadow linear directions. Several very prominent linears appear in most images (Fig. 16) and may be previously unreported major fault lines. Other linear trends of northwestern Iceland have been identified by Sigurdsson (in press) as being parallel with dike swarms and fracture patterns.

Even in the supposedly simple, youthful tectonic stress environment of Iceland, the topographic linears seem as complex as in most other areas. Either the stresses generating them over the oceanic rise are quite complex or they represent part of some far more extensive crustal system of stress trajectories which is merely exposed on the crest of the Rise.

CONCLUSIONS

Many topographic linears enhanced by shadowing of raised plastic relief maps have geologic reality because: (1) They duplicate linears appearing on radar imagery of real topography and, hence, are not artifacts of map production. (2) Projections of individual linears and orientations of linear sets carry across map boundaries. (3) The same linears appear on several scales of relief maps of the same areas. (4) The same linears appear under many lighting conditions. And (5) many linears are matchable with known geologic fractures.

Characteristics of the shadow linears are: (1) They are ubiquitous, appearing in abundance on all 250 relief maps examined to date. (2) Individual linears are traceable for distances of ten to two hundred miles and spacings are commonly a fraction of a mile. (3) A large number of sets of linears exists on most maps, possibly six to nine directions, but only some of the directions appear strongly under any single illumination. (4) Fractures are of vast regional extent and independent of local features, curvatures of mountain systems, edges of continent, transitions into semi-oceanic Mediterranean crust, or coastal plain cover.

Origin of the topographic shadow linears is an open question. Some in the coastal plain of eastern United States and in areas of glacial moraine may reflect tectonic heredity and upward propagation from basement. Others in the new crust of Iceland or in the active Alpine and Mediterranean area may reflect results of wide-spread stress systems of the present or comparatively recent past. It would be a mistake to consider all of the fractures of a single origin or a single age: some in Iceland are dike swarms, some in California and Oregon are recent faults, some in the Rockies involve tectonic heredity. In tracing linears on the ground, several appear to be zones of more closely spaced jointing. Two linears at La Jolla, California, are traceable for 10 miles in topography to appear in sea cliffs as normal faults of a few inches displacement.

In short, any set of systematic inhomogeneities persisting for a number of miles in bedrock could produce a set of topographic linears. The total picture could represent some combination of the older hereditary trends and the modern stress systems. Possibilities of the causal stresses, both recent and ancient, include deep seated viscous movements of the earth, changes in speed of earth rotation, and daily tidal working, shifting blocks of the earth's crust.

Shadow linear analyses may have considerable utility in a number of fields: The degree of structural control of topography seems far greater than expected by even experienced workers, suggesting that the familiar method of stream pattern analysis by random walk techniques may have its limitations. The difficulties of detecting all the linears with one direction of illumination should generate some caution in radar-linear interpretation. For certain types of prospecting one may find the linears a rapid and cheap exploration tool: ground water probably finds the fractures long before they are etched and continues to follow the fractures after etching; the Bingham copper pit occurs on the intersection of a major topographic linear with the edge of the Great Basin. In lunar geology most of the photo interpretation is done on low angle illumination Orbiter imagery. As under that low angle, light can come only from the east or west on the moon, the possibilities exist for serious bias in lunar fracture analysis. The patterned "tree bark" structure appearing on very low angle illuminated lunar slopes is quite likely to be related to selective shadow enhancement.

From a structural geology viewpoint the shadow linears suggest that much of our fracture analysis may be too restricted geographically and have relatively little relation to local structures and stress patterns. Tectonic heredity may contribute additional complication. Ultimately, it may be possible to map some of the master sets of the linears on continental or even global scales, a project in which the author is now engaged. At present, the shadow linears may provide some of the clues for reduction of the existing gulf between experimental theoretical studies of brittle fracture and the applications to natural fracture systems.

ACKNOWLEDGEMENTS

This work was supported entirely by a faculty research grant of Franklin and Marshall College. Greg McKelvey and Peter Thompson performed much of the photographic work.

REFERENCES

- Chapman, C. A.
1958: Control of jointing by topography; J. Geol., vol. 66, pp. 552-558.
- Dellwig, L. F., Kirk, J. N., and Walters, R. L.
1966: The potential of low-resolution radar imagery in regional geologic studies; J. Geophys. Res., vol. 71, pp. 4995-4998
- Muehlberger, W. R.
1964: Conjugate joint sets of small dihedral angle; J. Geol., vol. 67, pp. 211-219.
- Sigurdsson, H.
1967: Dykes, fractures and folds in the basalt plateau of western Iceland; in Iceland and the mid-ocean ridges, Sveinbjorn Bjorussun, editor.

Spencer, E. W.

- 1959: Fracture patterns in the Beartooth Mountains, Montana and Wyoming; Bull. Geol. Soc. Am., vol. 70, pp. 467-508.

Wise, D. U.

- 1964: Microjointing in basement, Middle Rocky Mountains of Montana and Wyoming; Bull. Geol. Soc. Am., vol: 75, pp. 287-306.
- 1967: Previously unreported fracture systems over vast areas of Appalachians, United States Cordillera and Europe (Abstract); Trans. Am. Geophys. Union, vol. 48, No. 1, p. 214.

DISCUSSION

G. R. Stevens drew the audience's attention to laser light photography which could be used to reconstruct a three dimensional picture from a two dimensional photograph. He suggested that this might be useful to select different linears apparent in photographs.

The author said he had looked into this but that the costs of such techniques were extremely high.

C. Dahlstrom pointed to the work done by T. Blanchet some five or ten years ago. Except for the fact that the sets of linears are real, it did not seem that Blanchet had been able to do very much with them. C. Dahlstrom also mentioned having had different people study air photographs to see if all operators would see the same linears. It seemed that 50 per cent of linears could be seen by anybody, but only one operator out of four or five would see the least obvious 10 per cent.

W. F. Brace asked if such linears formed great circle sets around the globe, and if there appeared to be some consistency across the United States.

The author said that he had not had access to raised plastic relief-maps of sufficiently large areas to answer the first part of the question. As to the second part, he could see constant patterns over areas half the size of the Colorado Plateau for instance, but he did not know if he could believe extrapolations over larger areas because there were only 20 degrees to 25 degrees in strike between sets.

L. E. Weiss asked if the author had tried to analyze random patterns and what he had found in them.

The author said he had attempted to throw handfuls of nails, photograph them and analyze them, and that some preferred directions were apparent as functions of light reflections off the rounded edges of certain orientations of the 'random' pattern. He had also set relief-maps on turntables, illuminated them at a very low angle and rotated them slowly. Under these conditions, given sets of linears would appear or disappear suddenly, within a few degrees of each other. This seemed to suggest that the distribution of these topographic linears was not random.

G. R. Stevens indicated that similar linears appeared also on planar rock surfaces when low-angle illumination was used, and that directions of linears were consistent over entire outcrops. Such linears occur in conjugate pairs.

THE GEOMETRY OF A NATURAL ORTHORHOMBIC SYSTEM OF KINK BANDS

T. B. Anderson
Department of Geology, The Queen's University of Belfast
Belfast, N. Ireland

Abstract

A system of kink bands, their development promoted by the presence of a mechanically effective regional cleavage, forms part of the Caledonian deformation in the slates and thinly bedded siltstones of the Ards Peninsula, Northern Ireland. The relationship of these kink bands to their structural environment, their general morphology and their characteristic grouping into recurrent patterns are described. Nearly all of the 526 individual bands examined dip steeply and displace the sub-vertical foliation horizontally. The sense of displacement may be either dextral or sinistral and bands of opposite sense intersect to demonstrate both contemporary and non-contemporary relationships. Pairs of conjugate and contemporary kink bands possess almost perfect orthorhombic symmetry.

The analysis of linear and angular measurements from each kink band leads to conclusions about kink band geometry which have important implications. Typically the kink band makes a smaller angle with the unrotated foliation outside the band than with the rotated folia within, confirming that the kink bands formed by slip confined to the intra-kink plane foliation. Both dextral and sinistral kink bands have strongly preferred orientations, at 018° , 84° SW and at 137° , 88° SW respectively, enclosing an obtuse angle (119°) about the direction of maximum shortening. This angle is bisected by the modal cleavage plane (077° , 86° N) and so the system as a whole also demonstrates orthorhombic symmetry and may be interpreted as a result of compression acting in, or close to, the strike of the cleavage.

The hypotheses which attempt to explain the angular relationship demonstrated by conjugate sets of kink bands are briefly compared and a definition of a kink band, consonant with that current in metallurgy and crystallography but expressed in the terminology of rock deformation, is suggested.

DEFINITION

In a deformed crystal a kink band is defined as "a thin plate of sheared material, transverse to a slip direction, bounded by opposite 'tilt walls' of dislocations" (Frank and Stroh, 1952, p. 811). Examples are common in the deformation of crystals of silver chloride, carbonates and various metals.

Voll (1960) extended the use of the term to describe structures in foliated rocks. In natural and experimental deformation of rocks with a well developed, mechanically effective, planar foliation, structures occur which are so similar to

kink bands in crystals that the use of the same term seems completely justified. In keeping with the sense of the crystallographic definition, a kink band in a foliated rock may be defined as a thin band or plate, transverse to the foliation, bounded by the parallel or subparallel axial surfaces of a pair of angular folds of opposite sense. The axial surfaces of the angular folds are termed kink planes (Hills, 1963, p. 239).

This paper offers a description of a system of natural kink bands, which are part of the Caledonian deformation in the slates and thinly bedded siltstones of the southern part of the Ards Peninsula, County Down, Northern Ireland. It is based on the examination and measurement of 526 individual kink bands, spread over some 18 miles of coastal outcrop between the villages of Cloughy and Kircubbin.

ENVIRONMENT

The Ards Peninsula trends north-south across part of the belt of Lower Palaeozoic sediments which composes the Southern Uplands of Scotland and then continues west-southwestwards into and across Ireland. In the southern part of the Peninsula the rocks are thinly bedded siltstones and shales of Silurian age. Massive siltstone members also occur but these show no kink bands.

The rocks suffered polyphase deformation and igneous intrusion in the Caledonian Orogeny. The first phase took the form of intense folding; the numerous folds are upright and isoclinal or very tight. Parallel to the axial plane of folding is a typically well developed slaty cleavage, of constant attitude (Figs. 1a and 1b). The vertical, isoclinally folded, sedimentary foliation reinforces the slaty cleavage in establishing a very pronounced regional anisotropy. This intense layering is the most essential element in the structural environment which later promotes the development of kink bands. The second phase of deformation is expressed in small monoclinial folds and associated strain-slip or crenulation cleavage. Deformation of this second phase is of local rather than regional significance and is restricted to a small fraction of the total outcrop. Contemporaneous with the later part of the first folding movements

Figure 1. Stereograms showing contoured distributions of poles to cleavage and kink planes. All diagrams are based on Lambert 'Equal-area' projections of the lower hemisphere.

- (a) Unrotated regional cleavage at 403 dextral kink bands. Contoured 0.25 - 10 - 20 - 30 - 40 per cent. Maximum 077° , 86° N
- (b) Unrotated regional cleavage at 110 sinistral kink bands. Contoured 1 - 10 - 20 - 30 - 40 per cent. Maximum 076° , 87° N
- (c) Rotated cleavage within 403 dextral kink bands. Contoured 0.25 - 5 - 10 - 15 - 20 per cent. Maximum 114 vertical
- (d) Rotated cleavage within 110 sinistral kink bands. Contoured 1 - 10 - 20 - 30 per cent. Maximum 040° , 84° NW
- (e) Kink planes - 403 dextral kink bands. Contoured 0.25 - 5 - 10 - 15 - 20 - 25 per cent. Maximum 018° , 84° W
- (f) Kink planes - 110 sinistral kink bands. Contoured 1 - 10 - 20 - 30 - 40 per cent. Maximum 137° , 88° SW

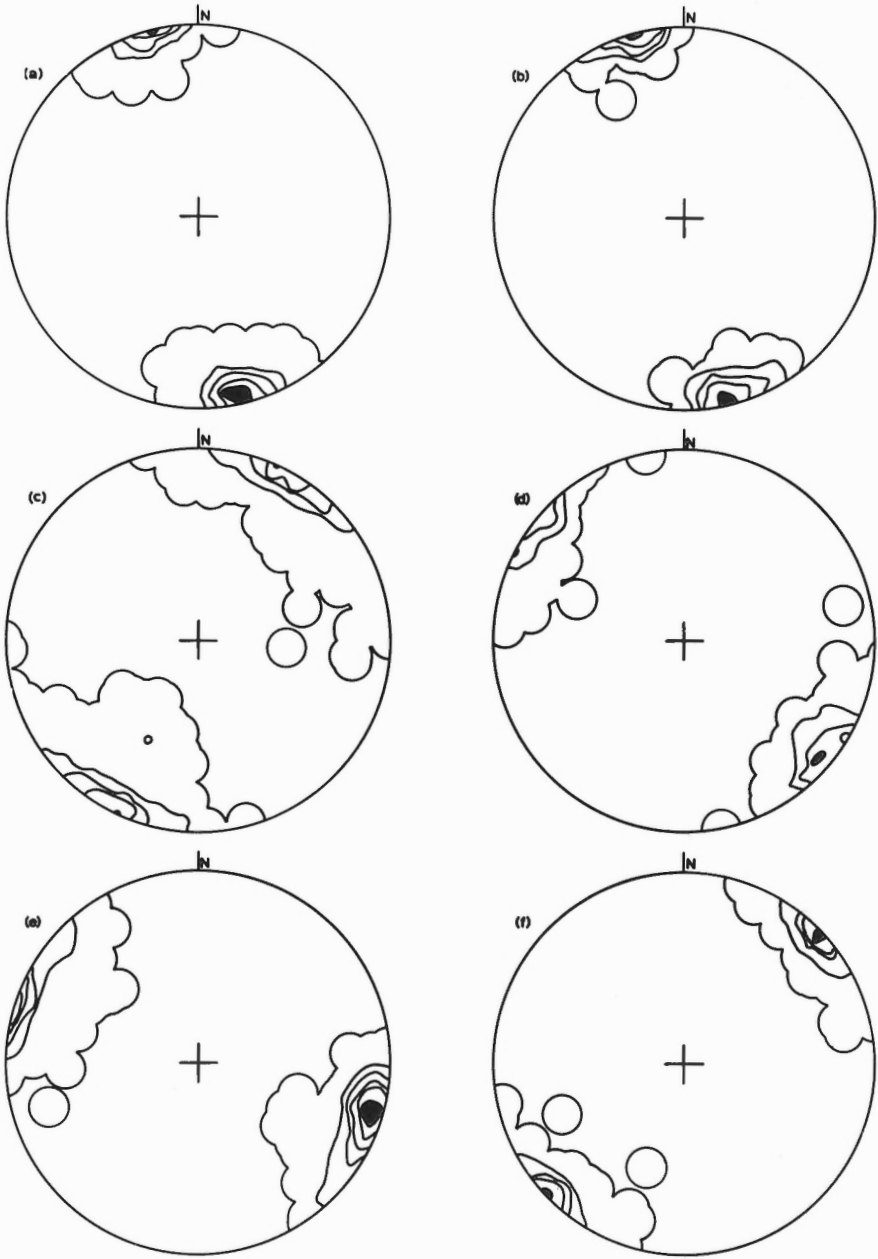


Figure 1 (a-f)

and probably also with the second folding a series of lamprophyre dykes was intruded. These commonly show a weak tectonic foliation roughly parallel to that in the sediments.

The kink bands constitute the third deformation phase and, as seems to be almost invariably true for areas of polyphase deformation, are the last folds to develop.

Later deformation was by faulting, wrench movements predominating. Contemporaneously a second series of lamprophyre dykes, petrologically and structurally distinct from the older series (Reynolds, 1931), were intruded. Dykes of both older and younger series tend to strike parallel to bedding and cleavage.

The kink bands deform both first and second cleavages and may be seen, at a few localities, to displace, and even to cause brecciation in, the older series of lamprophyres. There is nowhere evidence that kinking occurred earlier than any of these structures or intrusions. Conversely the kink bands are invariably truncated or displaced by the later wrench faults and by the younger dykes. There are several hundreds of the latter but none has been observed to suffer kinking. These observations are true of all the kink bands, whether they effect dextral, sinistral, normal or oblique displacements. All demonstrate the same age relationship to the other tectonic structures and to the intrusions.

GENERAL MORPHOLOGY

Some impression of the morphology and scale of the Ards kink bands may be obtained from the accompanying illustrations (Plates 1 - 3, Figs. 2 and 3). In each example the dominant foliation is twice kinked so that within a clearly defined transverse band it has an attitude significantly different from that outside the band. The curvature of the foliation, in most cases slaty cleavage, is concentrated close to the kink planes and varies only from sharply angular (Plate 1A) to slightly rounded (Plate 1B). The slightly rounded kink bands, with narrow zones of curvature, tend to occur in thin-bedded siltstones where active slip planes are more widely spaced than in the slates. The kink planes are commonly, though certainly not invariably, marked by a pair of parallel joints (Plate 1A). In nearly every case individual cleavage or bedding folia are continuous across the band, outlining an open Z shape. Shearing on one or both kink planes, with a consistent sense of displacement, was a feature present in only 35 of the 526 kink bands examined and clearly post-dated the kinking. Therefore in all but a very few examples the relative displacement of foliation across the kink band is effected by folding alone.

The kink planes, and hence the band they contain, typically make an angle of about 60° with the foliation outside the band and a rather greater angle with the rotated foliation within the band, though there is a considerable scatter about both the modal values (Figs. 4 and 5). As the foliation is continuous across the band it follows (Anderson, 1964) that individual foliation planes are more widely separated within the band than without. This is commonly apparent in the field, before measurement, in that weathering etches the more open foliation more deeply; between the kink planes the presence and orientation of the penetrative foliation are more obvious (Plate 3A).



Plate 1A. Dextral kink band showing parallel kink planes marked by joints. (Knockinelder)



Plate 1B. Large kink band with slightly rounded kink folds. No discontinuity at the kink planes. (Ballyferris)



Plate 2A. Small kink band showing lenticular cross section. (Ballyferris)



Plate 2B. Small sinistral kink band of lenticular cross section with segregation veins of quartz separating the dilated folia between the kink planes. Scalariform effect is completed by thin, discontinuous veins along the kink planes. (Port Kelly)



Plate 3A. Sinistral kink band cut by two later dextral kink bands. Note deeply etched cleavage within the kink bands. (Knockinelder)

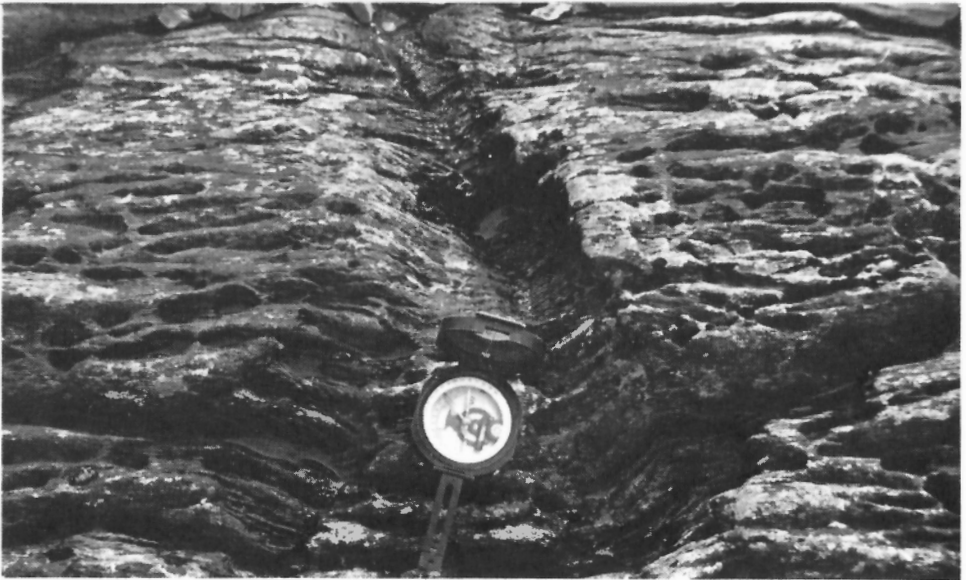


Plate 3B. Conjugate and contemporary dextral and sinistral kink bands meeting in a small chevron fold. Clinometer aligned N-S. (Knockinelder)

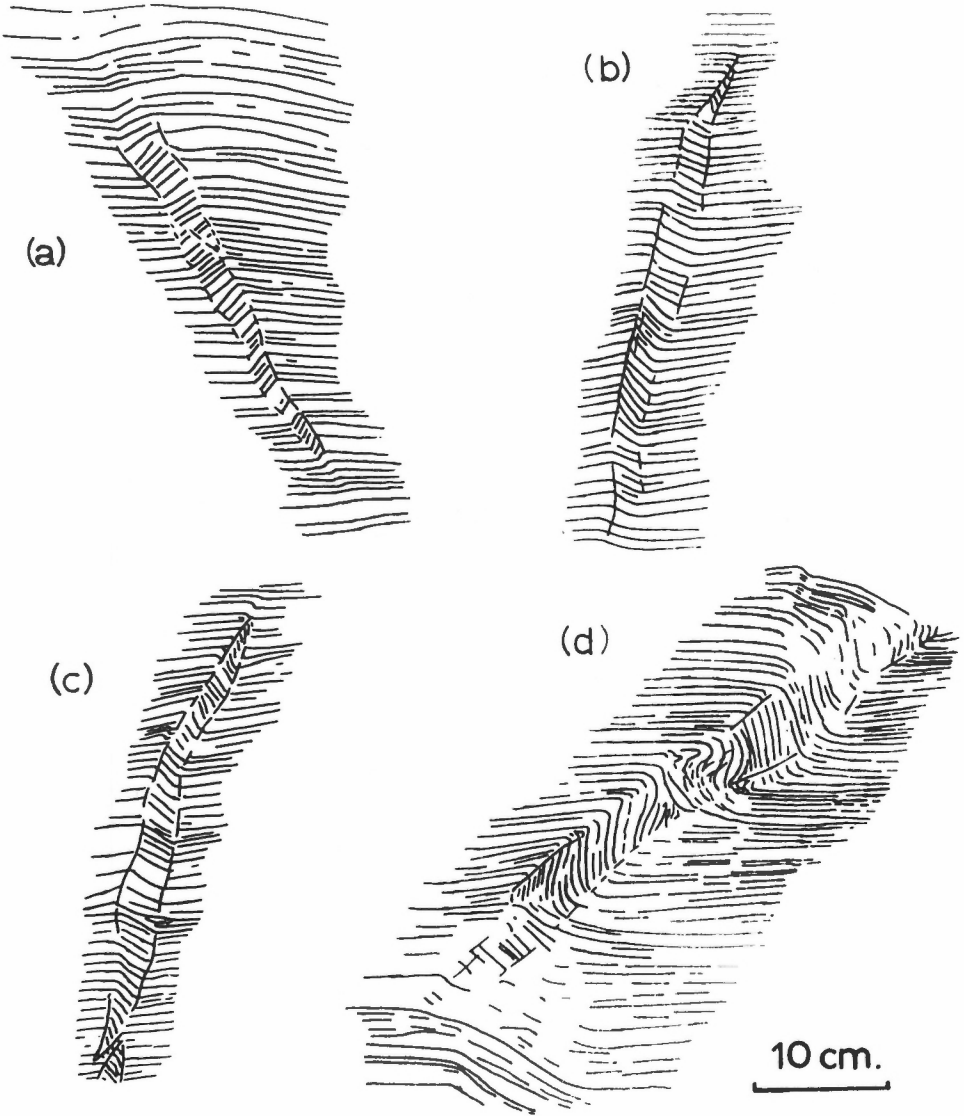


Figure 2. Line drawings of kink bands, all based on photographs: (a) Sinistral kink band lensing out in both directions (Templecowey). (b) Dextral kink band lensing out in both directions. Note decrease in α and β angles towards upper extremity and decrease in β at the place where there is shearing on the kink plane and the folia are not continuous (Templecowey). (c) Dextral kink band showing decrease in α and β angles toward the extremities and also where the band thickness decreases (Kearney). (d) Kink plane shearing and plastic folding associated with a dextral kink band in siltstones. (Port Kelly)

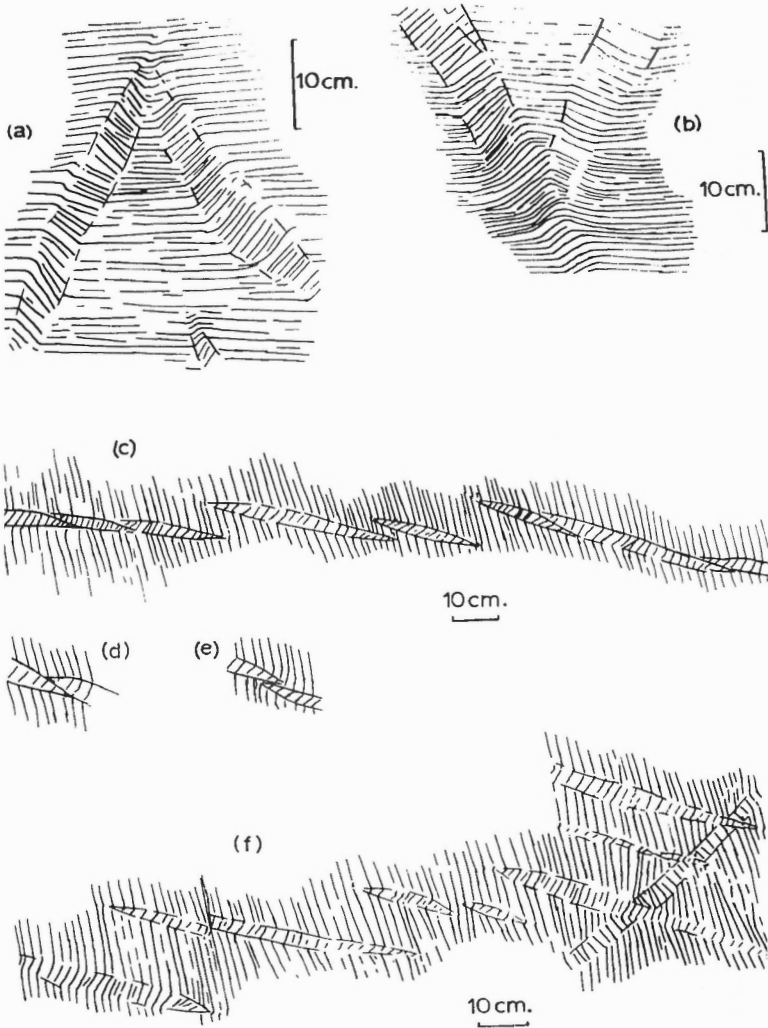


Figure 3. Kink band grouping. Drawings based on photographs. (a) A conjugate set of contemporary dextral and sinistral kink bands meeting in a chevron fold. (Knockinelder). (b) Conjugate set of contemporary dextral and sinistral kink bands meeting in a small chevron fold. The sinistral band only persists beyond the intersection (Knockinelder). (c) 'Train' of dextral kink bands (Kearney). (d) Typical overlap relationship between consecutive dextral kink bands in train. (e) Overlap relationship appears never to be as illustrated here but as in (d). (f) En echelon dextral kink bands and intersection between these and older sinistral kink band. (Knockinelder).

In a few examples this geometry is emphasized by small segregation veins of quartz separating the more widely spaced internal foliation and terminating at the kink planes to give a scalariform appearance (Plate 2B, also cf. Ramsay, 1967, Fig. 7-119).

Few individual kink bands extend for more than a few metres. While a very few pass into faults along their length the majority terminate in all directions through the eventual convergence of the kink planes, which therefore enclose a flat lens of disorientated material (Plates 2A and 2B, Figs. 2 and 3). Close to the wedged extremities of the band there is commonly a gradual but marked increase in the amount of rotation suffered by the foliation within the band; the angle (β) between the kink planes and the rotated foliation actually decreases (Figs. 2b and 2c). A similar relationship may be observed in those kink bands which show changes in thickness, thinning being invariably associated with increased rotation (Fig. 2c). The increased rotation is accompanied by very local shearing and irregularity of shape. Close to the extremities there is also commonly a slight change in the orientation of the band as a whole, so that it tends to make a smaller angle with the regional foliation (Fig 2c).

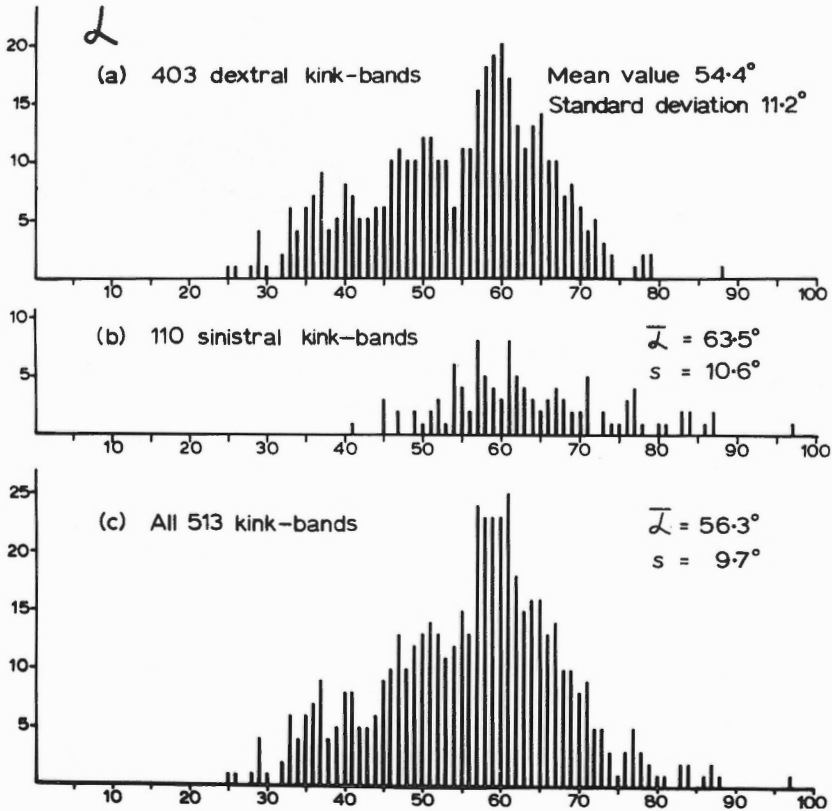


Figure 4. Frequency histograms of α angles in (a) 403 dextral kink bands; (b) 110 sinistral kink bands; (c) all 513 kink bands

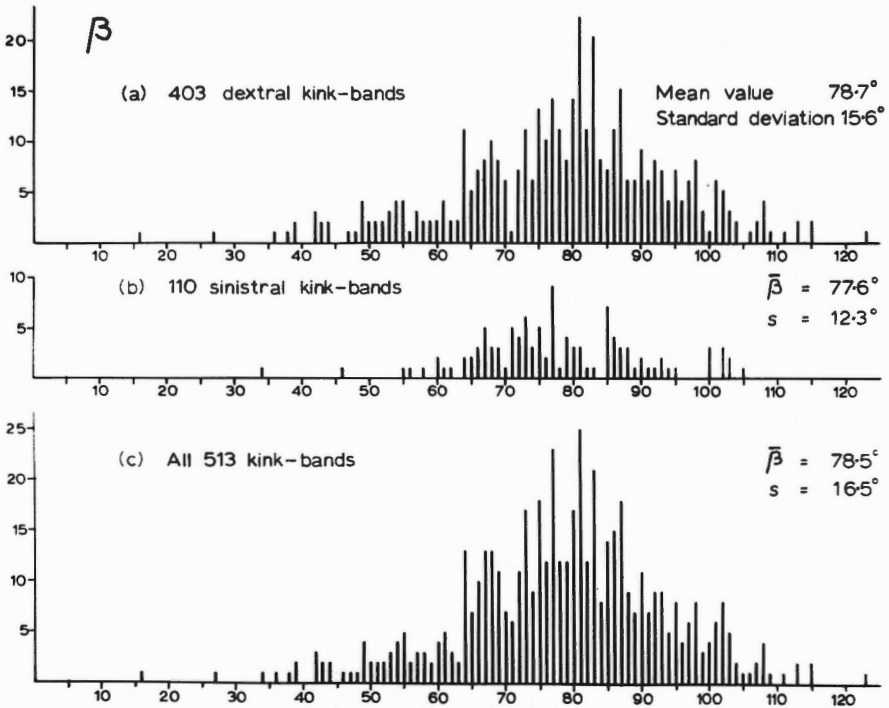


Figure 5. Frequency histograms of β angles in (a) 403 dextral kink bands; (b) 110 sinistral kink bands; (c) all 513 kink bands

The relative displacement across a kink band may be described by considering the latter as if it were a small fault. Nearly all the Ards kink bands are vertical or steeply inclined and so effect an apparent horizontal, strike-slip, displacement in the steeply inclined foliation. The sense of the offset, by analogy with small wrench faults, may be either dextral or sinistral. Thirteen of the 526 kink bands examined were gently inclined, with oblique or normal displacements of the foliation. These were measured but the results are omitted from the later quantitative analyses on the grounds that there are too few for any meaningful treatment or conclusions. Apart from orientation and direction of movement the oblique and normal bands do not appear to differ from the more numerous wrenches.

It is possible to imagine individual kink bands migrating or rotating bodily. If this occurred then some indication, in the form of distortion or brecciation, should be present in the rock immediately outside the kink planes. No such evidence has been found in the Ards examples and therefore it is concluded that while individual kink bands may have extended and thickened, their position and orientation did not otherwise vary during formation and growth.

DISTRIBUTION, GROUPING AND INTERSECTION

The distribution of kink bands throughout the 18 miles of coastal outcrop is extremely uneven. The majority are at seven well separated localities, the remainder occurring as isolated individuals or in small groups. The presence of massive, uncleaved sandstone or siltstone beds seems to have completely inhibited the development of kink bands for at least ten metres on either side. Similarly kink bands do not crop out in the vicinity of thicker dykes of the older series although they do appear close to, and are even intersected by, thick younger series lamprophyres. There are numerous wrench faults but no obvious spatial relationship between faulting and kinking.

The outcrops where kink bands are specially numerous are of shales and shaly siltstones showing well developed slaty cleavage but other outcrops of apparently identical lithology, with similarly well developed cleavage, are completely devoid of kink bands.

At outcrops where bands are numerous all or nearly all tend to show the same sense of displacement. Thus of 157 kink bands in one outcrop at Kearney village 151 were of dextral type. In the coastal strip between Portaferry and Ballyhenry Island 46 kink bands include 37 of sinistral and only 9 of dextral offset. It was thought at first that the local prevalence of dextral or sinistral bands might have been determined by some slight variation in the original orientation of the cleavage. Stereographic analysis shows that this can hardly have been the case. The modal orientation of cleavage in the vicinity of dextral bands is not significantly different from the orientation at sinistral bands (Figs. 1a and 1b). Yet the presence of numbers of both dextral and sinistral kink bands in the same outcrop is uncommon and consequently the critical dextral/sinistral intersections are not numerous.

About ten intersections are well exposed immediately east of Knockinelder beach (Plates 3A and 3B, Figs. 3a and 3b). Plate 3A shows a weak sinistral band cut by two narrow, well developed, dextral kink bands. At both intersections it appears that the sinistral band is the earlier, deformed by the later dextrals. However this is not invariably the relationship displayed at other similar intersections; in some cases the sinistral kink band appears to be the earlier, at others the dextral. In the same outcrop at Knockinelder two intersections, one illustrated on Plate 3B, demonstrate contemporaneous development of dextral and sinistral kink bands. A small chevron fold is formed at the point where the two bands meet and only one band persists beyond the point of intersection (cf. Fig. 3b). A few further intersections, scattered throughout the area of study, demonstrate both contemporary and non-contemporary relationships. It must be concluded that while the kink bands are not all exactly contemporaneous there exist some pairs of dextral and sinistral kink bands which are both complementary and contemporaneous.

Where dextral and sinistral bands occur together their orientation is such that they intersect in, or within a few degrees of, the foliation. The pairs of contemporary bands demonstrate almost perfect orthorhombic symmetry. Modal kink planes for the whole area also intersect in the modal cleavage plane (Fig. 6). It therefore seems clear that the movement direction and displacement lie in a plane perpendicular

to both kink bands and foliation, though Ramsay (1962) has pointed out that this need not be true of all conjugate fold systems.

In the gregarious clustering of kink bands of the same sense of displacement there are recurrent arrangements. For example there is a tendency for bands to form lines or trains along their strike as illustrated in Figure 3c. In such trains individual bands make an angle of less than 15° , and commonly less than 5° , with the train as a whole. As each individual band wedges out it is replaced by the slightly overlapping lens of the next and commonly the overlapping portions are in contact (Fig. 3c). If the kink bands are of dextral sense of displacement consecutive individuals are offset sinistrally along the train: the arrangement is as in Figure 3d, never as in Figure 3e.

The kink bands may also be arranged in en echelon zones of the type illustrated by Ramsay (1962, Text - Fig. 8, cf. Fig. 3f in this paper). Comparing these with the 'trains' just described there is a much greater separation of individual bands and a greater angle between bands and the zone itself. Most of the zones observed make a greater angle with the foliation than do the individual kink bands they contain, as in Ramsay's example and in Figure 3f. The converse relationship, illustrated by Dewey (1965, Figs. 26E and Fig. 28) is rare and imperfectly developed in the Ards Peninsula.

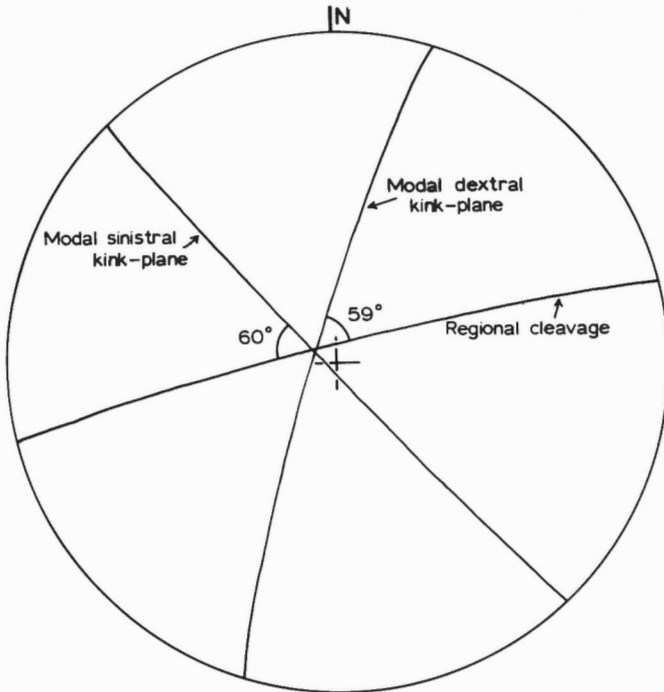


Figure 6.

Diagram illustrating orthorhombic symmetry of the system. Stereogram shows cyclographic projections of modal dextral kink plane, modal sinistral kink plane and modal orientation of unrotated cleavage (cf. Fig. 1).

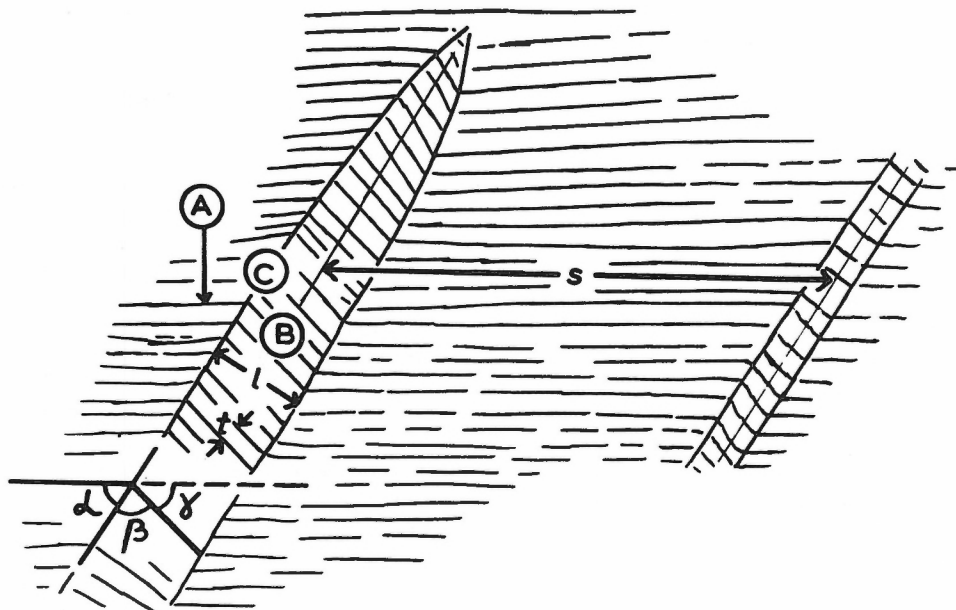


Figure 7. Right cross-section of dextral kink bands on flat-topped outcrop illustrating angles and distances measured for analysis

GEOMETRY

In order to establish a more exact knowledge of the geometry of individual kink bands and of the system as a whole the following observations and measurements were made on each band examined:

- (1) Overall sense of displacement of the foliation across the band.
- (2) Orientation of the unrotated foliation immediately outside the band (at A on Fig. 7).
- (3) Orientation of the rotated foliation within the band where the latter is thickest (at B on Fig. 7). In most kink bands the maximum thickness is maintained for some distance along the length, as in many of the illustrations.
- (4) Orientation of the kink planes, again measured where the band is thickest (at C on Fig. 7). Here the kink planes tend to be parallel and of constant orientation.
- (5) Maximum separation of the kink planes, i. e., maximum thickness of the band (1 on Fig. 7).
- (6) Maximum separation of the foliation planes (t on Fig. 7).

Where possible the distance between kink bands along the strike of the foliation was also measured.

In kink bands where orientations (2), (3) or (4) varied it was necessary to take the mean of several measurements.

Four hundred and three kink bands display a dextral sense of displacement, 110 are sinistral. The predominance of dextrals is a common feature in systems of steeply dipping kink bands in the British Isles. Knill (1961) has described a system composed entirely of dextral kink bands in the Dalradian rocks of Argyllshire and dextral displacements again predominate in the well developed kink bands of the Armorican fold-belt in southwest Ireland (personal observation). The author is not aware of any system where sinistral displacements are the more numerous.

The orientation of the unrotated foliation is remarkably constant around a modal value of 077° , 86° N (Figs. 1a and 1b) and shows no significant difference between dextral and sinistral bands. The rotated foliation has a less strongly preferred orientation (Figs. 1c and 1d) and in the dextral bands the poles lie on a partial girdle about a vertical axis of rotation. Obviously there is considerable variation in the amount of rotation.

Figures 1e and 1f show the orientation of kink planes. In each case there is a single strong maximum and these are symmetrically arrayed about the foliation, clearly demonstrating the overall orthorhombic symmetry of the system (Fig. 6).

The angle between the kink plane and the foliation outside the band (α on Fig. 7) was determined for each band and frequency distributions are presented in Figure 4. For both dextral and sinistral kink bands the modal values are around 60° . However the distribution for dextrals shows a negative skew and that for sinistrals a positive skew so that the mean α value for dextrals (54°) is considerably less than that for sinistrals (63°). There is no obvious reason for this departure from symmetry.

Similar histograms for β (Fig. 7), the angle between kink plane and cleavage within the band, show significantly higher modal values and also a much broader distribution, reflected in the higher values for the standard deviation (Fig. 5).

If the kink bands develop solely by slip on the foliation planes and slip is confined to the rock between the kink planes then β should not be smaller than α in individual bands (cf. Zandvliet, 1960). A plot of α against β (Fig. 8) shows that this condition is satisfied in 451 of the 513 examples. In the remaining 62 a combination of deformation mechanisms is necessary. Examination of these 62 bands indicates that, as well as shear movements on the kink planes, slip on the foliation outside the band and local, non-uniform, plastic flow can occur (Fig. 2d), though it is emphasized that in the Ards examples such modifications are comparatively rare.

The maximum thickness of individual kink bands (1) varies from 0.5 cm. to 50 cm. The mean value for the 513 dextral and sinistral bands is 5.09 cm.

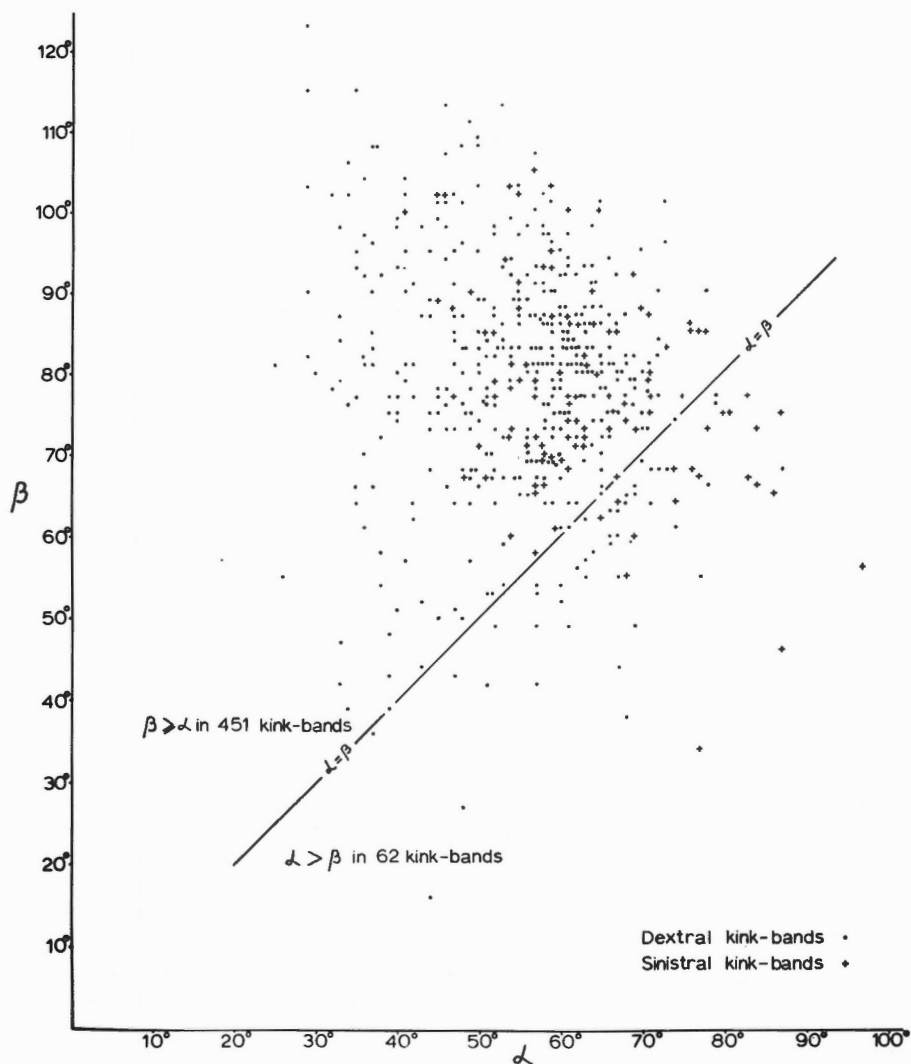


Figure 8. Plot of β against α for each of 513 wrench-type kink bands

Measurement of the separation of foliation planes (t) is difficult and somewhat subjective. In many of the kink bands active slip planes are less than 1 mm apart and field estimates of separation are necessarily approximate. However there appears to be a rough correlation between the thickness of the kink band and that of the thickest discrete layer kinked. Only 15 of the kink bands fold discrete layers which are 10 mm or more thick. The mean width of these 15 bands is 15.4 cm., three times the mean for all bands. The two widest bands observed in the whole area are in siltstones where uncleaved beds 1 cm. thick behave as mechanically distinct layers.

The t/l ratio (cf. Ramsay, 1967, p. 441 et seq.) is generally between 0.1 and 0.01. It is not possible to be more precise because of the difficulty in determining t .

Each kink band effects a shortening in the direction of the regional foliation. The amount is given by the formula $l(1 - \cos \gamma) \operatorname{cosec} \beta$ where l is the thickness of the band, measured perpendicular to the kink planes, and γ is the angle through which the foliation was rotated. The formula assumes that movement was in the plane perpendicular to foliation and kink plane, in which case $\gamma = 180^\circ - \alpha - \beta$, as in Figure 7.

The arithmetic mean of shortening parallel to the regional foliation for all kink bands is 2.57 cm. Quantitatively the strain represented by kinking is very small. Even if the shortening effected by all 513 kink bands is totalled the result is only 13.19 metres, and this is in fact spread over almost 30 km. of wide coastal exposure. At the localities where kink bands are numerous the separation between bands (s on Fig. 7), again measured parallel to the regional foliation, averages 1.07 metres. The separation between successive bands is not uniform; nor is it obviously related to the thickness of the bands concerned or to the amount of shortening effected by them. Thus even at localities where bands are numerous the strain is very non-uniformly distributed. A maximum value is obtained in an outcrop at Kearney, where 27 kink bands occur in a total distance of 7.62 metres, measured parallel to the cleavage. The total shortening caused by rotation in the 27 bands is 23.8 cm., a strain of 3.12 per cent.

COMPARISON WITH OTHER RESULTS

The only other orthorhombic system of kink bands yet described in detail was that produced experimentally by Paterson and Weiss (1966). By compressing jacketed cylinders of phyllite in the direction of the foliation these authors obtained well developed kink bands. The geometry of individual kink bands and of the system is very similar to that described above. In particular a comparison between Figures 4 and 5 of the present paper and Figure 6 of Paterson and Weiss reveals that for the angle between kink plane and the unrotated foliation (α of Anderson (1964) and the present paper, ϕ of Paterson and Weiss) modal values coincide almost exactly. The β maxima (ϕ_k of Paterson and Weiss) and β values generally are 10 to 15 degrees higher in the histograms for the natural kink bands. Under ideal conditions rotation of the foliation might be expected to continue, with progressive decrease in β , until β and α angles were equal. Ideal conditions are probably more nearly achieved in the laboratory than in natural deformation and to this the higher β angles in the kink bands of the Ards Peninsula are tentatively attributed. The histograms also show a wider scatter of values about the modes for both α and β in the natural bands. Again this probably reflects the more homogeneous lithology and more uniform conditions obtaining in the laboratory work. The experimental workers were also fortunate in that well developed intersections between kink bands of opposite displacement were numerous.

CONCLUSIONS AND DISCUSSION

The kink bands formed by slip on the foliation in the zone between the kink planes (Anderson, 1964, Fig. 6). The sense of slip is opposite to the sense of displacement effected by the kink band as a whole. Dextral kink bands may thus be considered as a small pile of sinistral shear planes. While shearing proceeds the foliation in the band is rotated but the attitude of the kink planes does not change. Therefore, as individual folia remain continuous across the kink band, there must be a progressive dilation within the band until the rotating folia are perpendicular to the kink planes and then a progressive contraction until the internal foliation makes the same angle with the kink plane as does the unrotated foliation outside the band. At the point where this symmetrical relationship is achieved ($\alpha = \beta$) the structure becomes locked and movement must cease unless the mechanics of the deformation change. Such a change is apparently uncommon and instead the generation of a further kink band or bands is more likely.

The dextral and sinistral kink bands of the Ards Peninsula, while not all precisely contemporaneous, are part of a single system, the products of one stress field. Pairs of conjugate, contemporary, dextral and sinistral kink bands, and the system as a whole, demonstrate orthorhombic symmetry in which the regional foliation coincides with one of the orthogonal symmetry planes. The sense of displacement of the bands is such that they include an obtuse angle, of about 120° , about the direction of the maximum principal pressure, which, by symmetry, must lie in, or very close to, the regional foliation. Therefore kink bands, planar structures with shear characteristics, may typically form at angles of more than 45° to the maximum compression. The only alternative to this conclusion appears to be the unsatisfactory assumption that all the kink bands are 'second order' to some other shear structure which is either not developed or not exposed.

Two minor deviations from the overall symmetry pattern remain without a convincing explanation: dextral kink bands outnumber sinistral by almost four to one and the histograms of α angles for dextral and sinistral kink bands demonstrate skews which are, respectively, negative and positive. It is possible that in some parts of the area the compression causing kinking did not act exactly parallel to the foliation. If, locally, σ_1 tended to act in a direction slightly clockwise of the foliation, more nearly east to west, this might explain the higher α values shown by some sinistral kink bands and the low α values of some dextrals. However this orientation of σ_1 would also promote the preferential development of sinistral kink bands (cf. the experimental results obtained by Paterson and Weiss (1966, p. 351) in compressing phyllite specimens at 10 degrees and at 25 degrees to the foliation) and clearly this did not occur.

A preliminary description of angular relationships in the kink bands of the Ards Peninsula (Anderson, 1964) has been severely criticized (Marshall, 1964; Dewey, 1965) on the unusual grounds that the observations do not conform, or appear to conform, with orthodox teaching. Dewey (1965, p. 487) observed: "Anderson (1964) has described orthorhombic conjugate kink-band sets where the dihedral angle is apparently $> 90^\circ$. If this alleged relationship is correct the startling corollary must

be invoked of a negative value for the angle of internal friction (ϕ). This is contrary to all the experimental evidence (for a review see Hubbert, 1951) and values computed from conjugate sets elsewhere (lowest ϕ value discovered by computation was 5°). Implicit in this criticism is the now clearly invalid assumption that kink bands are the exact equivalents of shear planes in terms of angular relationship, that they make the same angle as faults with the causal compression. Indeed the experimental evidence referred to is concerned only with faulting. The same assumption often appears where descriptions of kink bands include inferences on the orientation of the stress system responsible for kinking (e. g. Knill, 1961; Dewey, 1966). That it commonly seems necessary to interpret kink bands as second order structures (Marshall, 1964; Dewey, 1965 and 1966) is a direct consequence.

The concept of conjugate kink bands making an obtuse angle about the direction of compression, heresy in 1964, now seems to find more general acceptance. The detailed experimental work of Paterson and Weiss (1966) has established the geometrical relationship to causal stresses in a remarkably unambiguous fashion. Ramsay (1967, pp. 452-3) states that: "It seems unlikely that the axial surfaces (of conjugate folds and kink bands) originate as a primary shear system as suggested by Johnson (1956), Ramsay (1962), and Ramsay and Sturt (1963). The shearing hypotheses put forward by these authors have never satisfactorily accounted for the generally observed geometrical fact that it is the obtuse angle of the conjugate axial surface which faces the maximum shortening in the rock material".

This relationship may now be established but no generally accepted explanation has emerged. Paterson and Weiss (1966, pp. 367-8) refer to the work of Taylor (1934) on the propagation of faults and write that they "would expect an analogous calculation" to show that, in an ideal foliated body compressed parallel to the foliation, kink bands would be "inclined at 60 degrees to the direction of compression as opposed to 45 degrees in Taylor's problem". Their argument derives support from symmetry considerations and also from theoretical models of kink band intersections but the concept of an "analogous calculation" remains disappointingly vague.

It is the author's view that Taylor's (1934) argument is relevant to kink bands as well as to faults. Therefore kink bands in an ideal foliated body might also propagate at 45 degrees to the direction of compression. However just as friction decreases the angle between real faults and the direction of maximum pressure (Anderson, 1942) so it must increase the angle between kink bands and compression. This is because shearing takes place, not on the kink planes, but on the intra-kink band foliation. The orientation of the latter changes during shearing but it is always at a high angle to the kink band and its mean position is approximately perpendicular to the band. The effect of friction on the angular relationship of conjugate pairs of kink bands is therefore exactly opposite to that in faulting. The increase over the theoretical 45 degrees will be approximately the same as the decrease in the case of faulting so that kink bands in rocks compressed parallel to the foliation make an angle of about $\frac{90 + \phi}{2}$ degrees with the major compressive stress. It must be admitted that

2

the hypothesis is not precise, both in that it involves an approximation and in that ϕ is a purely empirical quantity.

Ramsay (1967, pp. 449 et seq.) has offered a mathematical treatment of strain in conjugate kink bands. He concluded that the kink folds become locked in a position such that their axial planes make an angle of between 50 and 60 degrees with the direction of maximum shortening. The mathematical model chosen (Ramsay, 1967, Fig. 7 - 121) involves assumptions which may not be valid. For example it is assumed that in each of the kink folds the axial surface bisects the angle between the fold limbs. If this were to be true throughout folding the axial surfaces (i. e. , the kink planes) and the kink band itself must rotate through the rock. There is no evidence that this occurs. Also the selection of 50° and 60° as the limiting values, based on the graphs in Figure 7 - 122, appears somewhat arbitrary; any values between 40° and 70° might have been chosen. The approach does not necessarily conflict with either of the hypotheses outlined above.

Finally, the kink bands in the Ards Peninsula cause only a very small shortening in the direction of the regional foliation. This seems likely to be generally true of natural kink band systems. To effect shortening of more than a few per cent kink bands must be very well developed and very closely spaced.

REFERENCES

Anderson, E. M.

1942: The Dynamics of Faulting; Edinburgh, Oliver and Boyd Ltd.

Anderson, T. B.

1964: Kink bands and related geological structures; Nature, vol. 202, pp. 272-274.

Dewey, J. F.

1965: Nature and origin of kink bands; Tectonophysics, vol. 1, No. 6, pp. 459-494.

1966: Kink bands in Lower Carboniferous slates of Rush, Co. Dublin; Geol. Mag., vol. 103, pp. 138-142.

Frank, F. C., and Stroh, A. N.

1952: On the theory of kinking; Proc. Phys. Soc. (London), Ser. B, vol. 65, pp. 811-821.

Hills, E. S.

1963: Elements of structural geology; London, Methuen and Co., Ltd.

Hubbert, M. K.

1951: Mechanical basis for certain familiar geological structures; Bull. Geol. Soc. Am., vol. 62, pp. 355-372.

Johnson, M. R. W.

1956: Conjugate fold systems in the Moine Thrust Zone in the Lochcarron and Coulin Forest areas of Wester Ross; Geol. Mag., vol. 93, pp. 345-350.

- Knill, J. L.
1961: Joint-drags in Mid-Argyllshire; Proc. Geol. Assoc., (Engl.), vol. 72, pp. 13-19.
- Marshall, B.
1964: Kink bands and related geological structures; Nature, vol. 204, pp. 772-773.
- Paterson, M. S., and Weiss, L. E.
1966: Experimental deformation and folding in phyllite; Bull. Geol. Soc. Am., vol. 77, pp. 343-374.
- Ramsay, D. M., and Sturt, B. A.
1963: A study of fold styles, their association and symmetry relationships, from Soroy, north Norway; Norsk Geol. Tidsskr., Bind 43, pp. 411-430.
- Ramsay, J. G.
1962: The geometry of conjugate fold systems; Geol. Mag., vol. 99, pp. 516-526.
1967: Folding and fracturing of rocks; New York, McGraw-Hill Book Co.
- Reynolds, D. L.
1931: The dykes of the Ards Peninsula, County Down; Geol. Mag., vol. 68, pp. 97-111, 145-165.
- Taylor, G. I.
1934: Faults in a material which yields to shear stress while retaining its volume elasticity; Proc. Roy. Soc., (London), Ser. A, vol. 145, pp. 1-18.
- Voll, G.
1960: New work on petrofabrics; Liverpool Manchester Geol. J., vol. 2, pp. 503-567.
- Zandvliet, J.
1960: The geology of the upper Salat and Pallaresa Valleys, central Pyrenees; Leidse Geol. Mededel., deel 25, pp. 1-127.

DISCUSSION

Because of time limitations, T. B. Anderson's and P. Clifford's papers were discussed together. See discussion following P. Clifford's paper.

D. K. Norris (written comments) In view of the use of kink bands in evaluating the orientation of the principal tectonic stress axes in geological

materials possessing a strong, planar anisotropy, it is important to define the preferred orientation of kink sets or systems with respect to this anisotropy. Under laboratory conditions, the orientation of the stress axes with respect to specimen geometry and anisotropy is known with some assurance. In the natural geological environment, however, this orientation must be inferred.

Whether laboratory specimens or field examples are being studied, adequate measurements are necessary to draw meaningful conclusions about preferred orientation of kink sets, either singly or as conjugate arrays. The very large sample of measurements of orientation of kink band boundaries with respect to foliation provided by Anderson (this report) appeared to be ideal for such an orientation analysis.

Anderson (this report, Fig. 6) included measurements on 526 kink bands in slates and thinly bedded siltstones of the Ards Peninsula, Northern Ireland. According to him, where the bands are numerous, they nearly all have the same sense of displacement, either dextral or sinistral. Dextral kink bands predominate, however, approximately in the ratio of 4 to 1 in the total area sampled. It is interesting, moreover, that the modal kink planes for the whole area intersect in the modal cleavage plane and the obtuse angle between the dextral and sinistral sets is bisected by the modal cleavage plane.

In his frequency distribution of the angle (α) between kink band boundary and foliation outside the band, Anderson points out that both dextral and sinistral bands have modal values around 60 degrees, coinciding almost exactly with experimental values derived by Paterson and Weiss on phyllite. He indicates, moreover, that the distribution for dextral bands shows a negative skew, and that for the sinistrals, a positive skew. As a possible explanation, he suggests that in some parts of the area the compression causing kinking did not act parallel to the foliation, although he concludes that his total sample of kink bands is part of a single system and the product of one stress field.

If it may be assumed that the frequency distribution of the angle between the kink band boundary and the foliation outside the band should be normally distributed, then the skewness of each distribution may be due to the presence of more than one set of bands, and possibly the product of more than one stress system.

Following the method outlined by Harding (1949), the writer replotted the data from Anderson's Figure 6 on arithmetic probability paper (see Figs. 1 and 2). On this paper, a normal distribution will plot as a straight line, the position of which determines the mean, and its slope, the standard deviation. As pointed out by Harding, a polymodal sample comprised of populations which are themselves normally distributed, will give a curve which is the resultant of two or more straight lines.

It is evident from Figures 1 and 2 that the distributions of these (α) angles are non-linear, and if one may ignore the extremities of the plots where the data are few, one can interpret both samples as being bimodal. Corresponding straight lines representing the two normal populations contributing to the samples for both dextral and sinistral kink bands have been drawn. The relevant conclusions are summarized in the following table:

Sample	Mean	Per cent of sample
Dextral kink bands	$58^{\circ} \pm 7^{\circ}$ (Set I)	75
	$39^{\circ} \pm 6^{\circ}$ (Set II)	25
Sinistral kink bands	$59^{\circ} \pm 7^{\circ}$ (Set I)	80
	$78^{\circ} \pm 7^{\circ}$ (Set II)	20

Each sample is apparently comprised of two sets, the one dominating the other by factors of 3 or 4 to 1. It is immediately apparent, moreover, that the sets may be grouped into two conjugate systems of dextral and sinistral kink bands, both major and minor systems possessing the same angular relations ($58^{\circ} + 59^{\circ} = 39^{\circ} + 78^{\circ}$). That is, they both include an obtuse angle of 117 degrees which contains the foliation.

The dominant system is symmetrically disposed with respect to the modal 'plane' of the foliation and the dilemma of the difference in mean α values from the total samples (54 degrees for dextrals and 63 degrees for sinistrals, according to Anderson) is resolved. The obtuse bisectrix for the minor system, on the other hand, is approximately 19 degrees clockwise out of the 'plane' of the foliation.

As pointed out by Anderson, experimental studies indicate that a clockwise rotation of the maximum principal compressive stress out of the foliation would promote the preferential development of sinistral kink bands. This is obviously not the situation because the 4 to 1 ratio of dextrals over sinistrals prevails for both dominant and minor systems.

The resolution of each of the samples of α values for dextral and sinistral bands into two sets, therefore, provides only a partial answer. The dominant system of kink bands is symmetrical with respect to the foliation and may be explained in terms of the maximum principal stress in the foliation; for the minor system, on the other hand, the clockwise shift in the obtuse bisectrix and possibly also in the corresponding maximum principal stress axis is in the opposite sense to that required to favour nucleation and growth of dextral kink bands.

The facts remain, therefore, that the dominant sets, representing 75 to 80 per cent of the total sample of α values are symmetrically arranged about the foliation but that they are not equally numerous. Perhaps this one-sided development is as much a characteristic of kink band systems as is the

predominance of thrust faults and axial surfaces of folds with a preferred direction of dip in orogenic belts, as seen for example in the eastern Cordillera of Canada.

From another standpoint, it may be, however, that there is more than one preferred value for the angle containing the foliation between conjugate kink sets in the Ards Peninsula. Suppose, for example that Set I of the dextral bands in the above table is grouped with Set II of the sinistrals. The obtuse angle between them is, therefore, $58^\circ + 78^\circ = 136^\circ$. And for the remaining two sets, the angle is $39^\circ + 59^\circ = 98^\circ$.

Neither of these newly formed groups of sets is bisected by the foliation, of course, but their respective angles containing the foliation are similar to those found by some workers. The 136° -angle, for example, coincides almost exactly with that ($2 \times 68^\circ 4' \approx 137^\circ$) derived by Donath (this report) from experimental deformation of Martinsburg slate. The 98° -angle, moreover agrees reasonably well with Clifford's data (this report) for kink bands in the layered sedimentary and volcanic rocks of the Superior Province of the Canadian Shield. Although Clifford does not recognize a preferred value for the inclination (his ϕ) of kink band boundaries with respect to unrotated foliation his data plot in a remarkably linear fashion on arithmetic probability paper, indicating a normal distribution. Accordingly the mean and standard deviation for the inclination of kink band boundaries are $46^\circ \pm 13^\circ$ in his area of study. In view of the large standard deviation (almost twice that for similar data from Anderson), the angle containing the foliation ($92^\circ \pm 26^\circ$) is in reasonable agreement with the value obtained for the minor system derived from Anderson's samples.

It would seem that a basic question, as yet unanswered, is the role of planar anisotropy on the orientation of the principal stress axes at kink band nucleation. Structural studies in coal mines indicate that the lithologic layering plays a fundamental role in the local reorientation of stresses under conditions for faulting. It would appear quite unreasonable, therefore, to accept that stress axes may be located in a strongly foliated medium purely on the basis of a geometrical argument, with total disregard for the effects of anisotropy. Until the orientation of the local stress axes at kink nucleation can be defined, it may not be possible to interpret the preferential nucleation of one kink set over another as well as the wide variation in orientation of kink sets with respect to foliation.

Reference

1. Harding, J.P. The use of probability paper for the graphical analysis of polymodal frequency distributions; J. Marine Biol. Assoc. U.K., vol. 28, pp. 141-153, 1949.

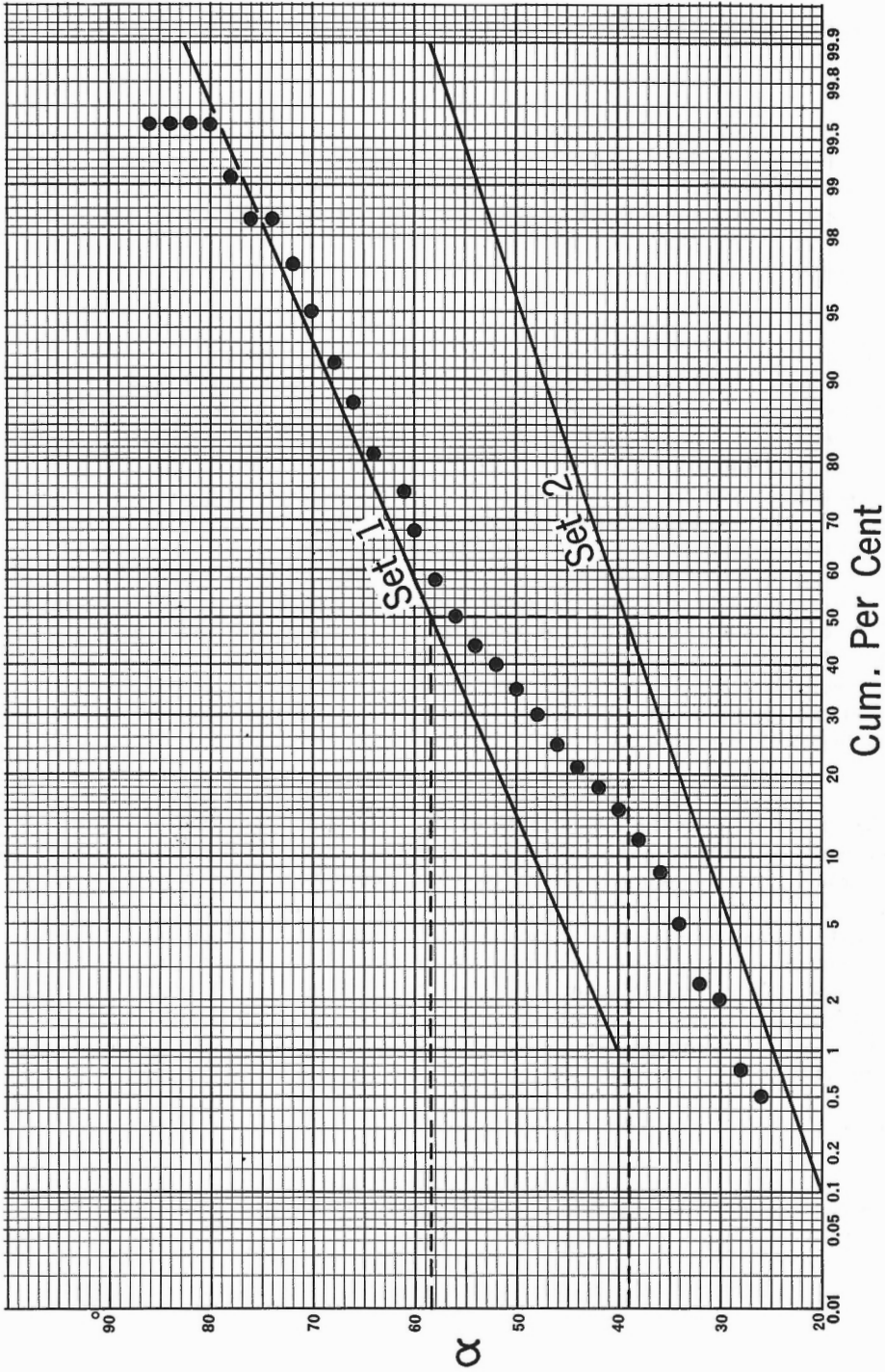


Figure 1. Distribution of angle (α) between kink band boundary and unrotated foliation, for 403 dextral kink bands, Ards Peninsula, Northern Ireland.

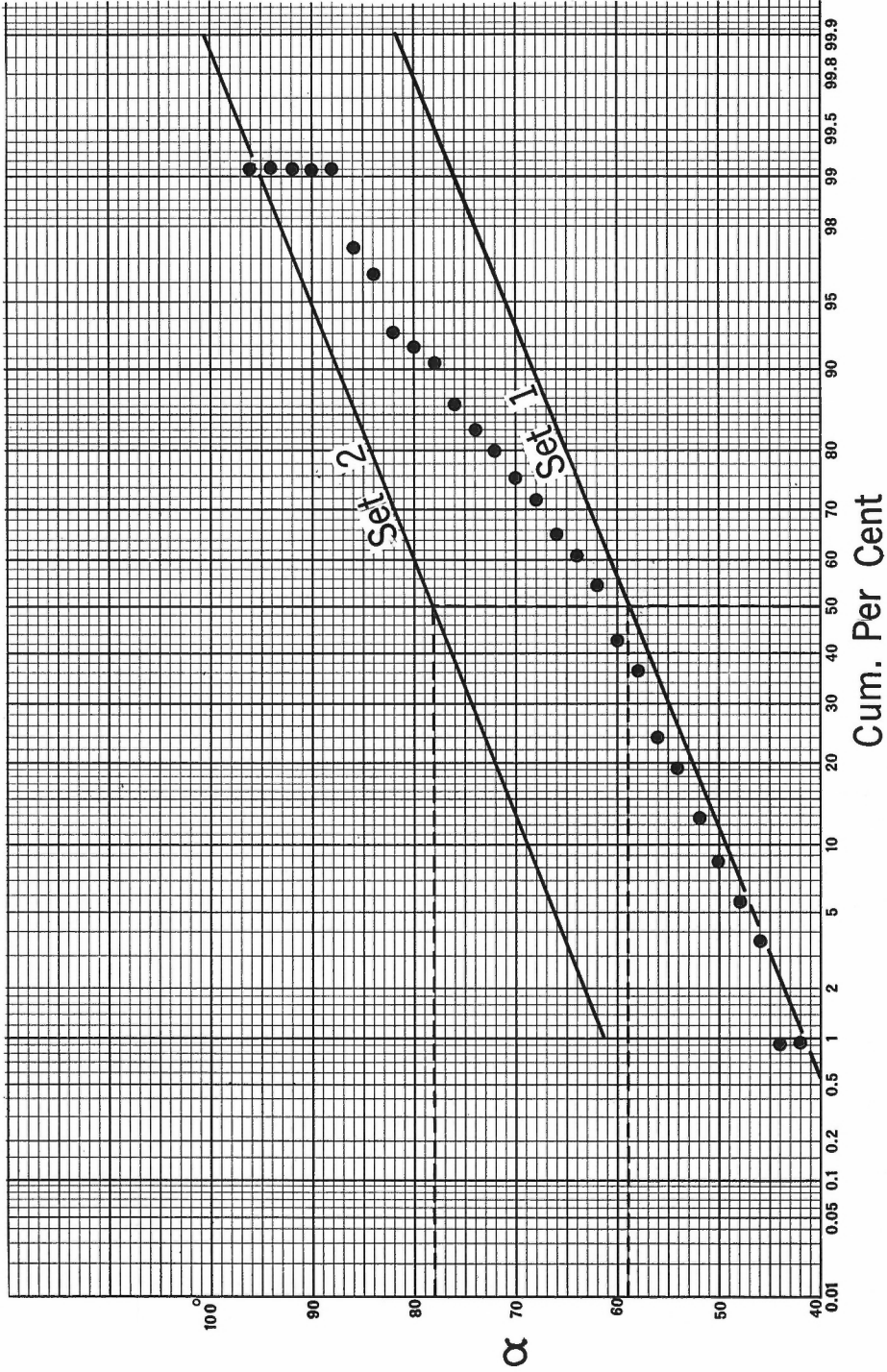


Figure 2. Distribution of angle (α) between kink band boundary and unrotated foliation, for 110 sinistral kink bands, Ards Peninsula, Northern Ireland.

H. E. Rondeel (written comments) Kink bands show either a sinistral or a dextral offset of the foliation across the kink layer. If the axis of maximum compression, σ_1 , is contained in the foliation and one of the other principal axes is perpendicular to this planar anisotropy, there is no reason why the development of one set should be favoured over the other. If, however, σ_1 , makes an angle with the foliation and one of the other axes lies in this plane, kinks in which the foliation rotates away from σ_1 , are commonly generated during the first stages of progressive deformation in the experiments of Weiss (1968).

Anderson (1968) shows a strong preference of dextral over sinistral kink layers to exist in the area studied on the Ards Peninsula, whereas the geometry of the two sets is different. The writer considers these data to indicate deformation with the direction of maximum compression at an angle to the initial direction of the foliation, as all kinks are thought to be products of a single stress field.

If the axis of maximum compression is situated anti-clockwise from the foliation, the angle made being α , experimental evidence is that in the first stage of progressive deformation a single set of dextral kink bands is developed. The kink angles are over X° . F_X is approximately equal to 60. If α is large, sinistral kink layers will not form. The next stage in progressive deformation shows the foliation outside the dextral kink layers to rotate towards σ_1 , thus decreasing the angle α . During this rotation, the dextral kinks widen and new kink bands with the same sense of displacement can be generated. Their kink angle is smaller than that of the kinks formed earlier, though still over X° . As α attains low values, sinistral kink layers with kink angles under X° appear. As α equals zero, kink layers with opposite senses of displacement can be formed at the same time and the kink angles will correspond to X° . In this stage the dextral kinks still predominate.

While α decreases, the kink angles of the dextral kink bands which are being formed thus decrease and the same angles of the sinistral bands increase. Moreover, the angle ϕ (Fig. 1) of earlier formed bands might become modified in such a way that it decreases for dextral and increases for sinistral kinks, if the foliation outside the kink bands rotates in one sense, i. e. towards the maximum compression direction. A rotation like that pointed out here is considered (Weiss, 1968) to result from an attempt to maintain end alignment in test specimen. The most favourable condition is that the foliation directly outside dextral kinks rotates in the direction indicated, whereas that at sinistral kink bands rotates in the opposite sense, causing ϕ to be smaller than ϕ_k since in experiments ϕ_k is seen to change hardly, if at all. It implies, however, that the attitude of the foliation in the 'undeformed' domain at sinistral and dextral kink boundaries should differ significantly, which in Anderson's example is not so. Whichever the case might be, this kind of rotation implies that a frequency distribution diagram of ϕ for dextral kinks should exhibit a negative skew and for sinistral kinks a skew in the opposite sense, which is exactly what Anderson observes.

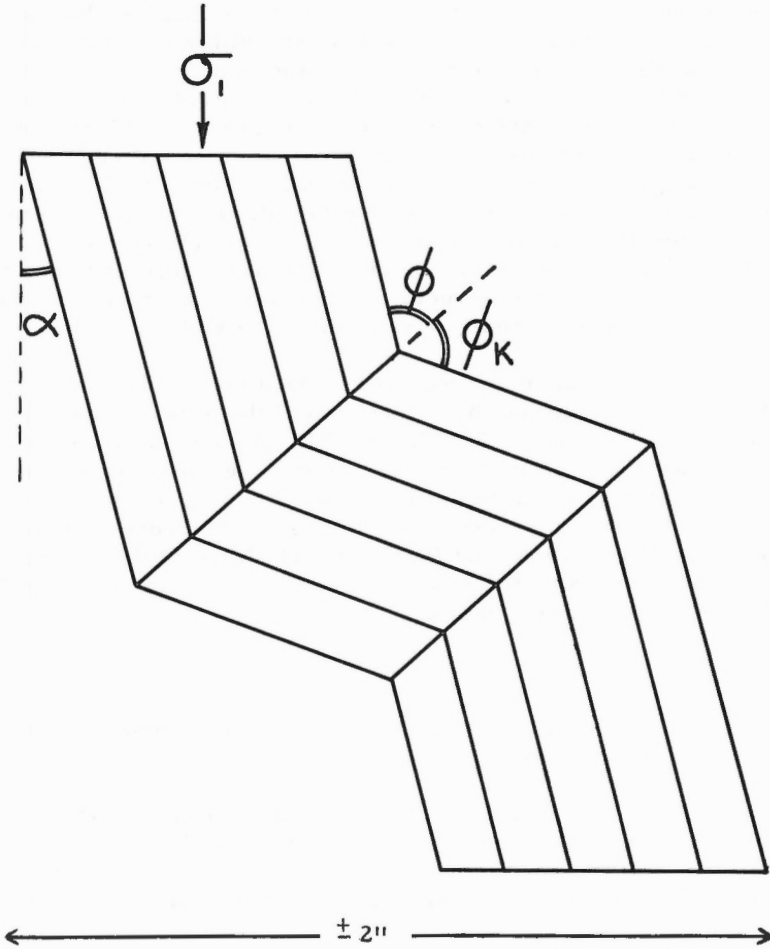


Figure 1. Illustration of the angles referred to in the text.

Moreover, the mean value for ϕ of dextral kinks should be higher than that for sinistral kink layers, again in agreement with Anderson's observations.

As the sinistral kinks form in a relatively late stage of progressive deformation, the variation in ϕ and ϕ_k for these structures should be smaller than that for dextral kink bands. Anderson indeed shows the standard deviation for these angles to reflect this effect, and the range in ϕ and ϕ_k is, moreover, significantly smaller for sinistral than for dextral kink bands.

If rotation of the foliation in the 'undeformed' domains proceeds in the sense dictated by the dextral kink bands, then $\phi < \phi_k$ for dextral and $\phi > \phi_k$

for sinistral kinks. In Anderson's Figure 8, $1/5$ of all kink bands with $\phi < \phi_k$ are sinistral and roughly $1/3$ of all kink layers with $\phi > \phi_k$ show this direction of offset, thus illustrating a preference for the sinistral kinks to be in the field $\phi > \phi_k$. Of course, rotation of the foliation outside kink bands, in case σ_1 is not contained in the foliation, will not occur in every deformation. It seems to depend entirely on the conditions of confinement and constraint. However, Anderson's data are very much in agreement with such an event. It would mean that in the Ards Peninsula the foliation outside domains which might be considered to have been influenced by this phenomenon, should show a mean strike clockwise from the mean strike of the foliation near to the kink bands, at least if this planar structure had a fairly constant orientation at the onset of the deformational phase during which the kink bands were formed.

In conclusion, many features of Anderson's observations can well be accounted for if assuming the orientation of the axis of maximum compression to have been between ENE-WSW and NE-SW, i. e. anti-clockwise from the initial position of the foliation. Of course, the stress trajectories did not have to have been plane, but the angle α was generally in an anti-clockwise direction from the general trend of the foliation. Moreover, it seems that the experiments of Weiss (1968) and Paterson and Weiss (1966) might - at least in some cases - form a better basis for the interpretation of natural deformation by kinking than hitherto realized.

References

1. Anderson, T.B. The geometry of a natural orthorhombic system of kink-bands; this conference, 1968.
 2. Paterson, M.S. and Weiss, L.E. Experimental deformation and folding in phyllite; Geol. Soc. Am., Bull. 77, pp. 343-374, 1966.
 3. Weiss, L.E. Flexural-slip folding of foliated model materials; this conference, 1968.
- P.S. The writer is much indebted to the Organization for Pure Scientific Research (Z. W. O.) for a grant enabling him to attend the Tectonics Research Conference in Ottawa.

KINK BAND DEVELOPMENT IN THE LAKE
ST. JOSEPH AREA, NORTHWESTERN ONTARIO

P. M. Clifford
Department of Geology, McMaster University,
Hamilton, Ontario

Abstract

Measurements from a suite of naturally-occurring kink folds permit the definition of the orientation of the stress field responsible for these folds. Analysis of angular relationships of these folds reveals that the kinked lamination has, in some folds, been rotated to a position more than 60° removed from σ_1 . There is also carbonate filling within the kinked lamination in some folds.

The over-rotation and the carbonate filling both suggest that simple gliding is not the main mode of development of these folds. Over-rotation is prohibited if simple gliding only prevails. In addition, the carbonate filling implies dilation at some stage in the folding process. It appears that the initial folding took place by a simple rotation of laminae about the fold axis. This involved, first, a positive and increasing dilation, followed by a positive but decreasing dilation. As dilation passed through zero, gliding occurred except where the kinked lamination was already at too high an angle to σ_1 . At this stage any further shortening could only be either by lateral migration of kink zone boundaries or by the inauguration of new kinks elsewhere.

This hypothesis implies that the basic geometry of the kink fold is produced by dilation-rotation and gliding, and that lateral migration of kink zone boundaries affects dimensions of the kinked zone.

INTRODUCTION

In the past few years, kink folds have been produced in controlled rock deformation experiments (Borg and Handin, 1966; Donath, 1964, 1968; Paterson and Weiss, 1966). The extensive study by Paterson and Weiss provides a justification for Ramsay's (1962) use of kink folds to determine the orientation of principal axes of stress. In addition, these workers, and others, have offered specific mechanisms for the development of such folds. The present paper analyzes data for some natural kink folds, and assesses them in the light of the data derived from experiments.

The area in which kink folds have been observed by the writer is centred at Lake St. Joseph, some 300 kilometres north-northwest of Port Arthur, Ontario. It is the site of one of the numerous belts of volcanic and sedimentary rocks (the 'Keewatin' belts) characteristic of much of the Superior Province of the Canadian Shield. In the layered rocks of the belt, deformation has produced two sets of large folds affecting the area as a whole. As one consequence of the deformation, the southern portion of the area contains a strip of rock some 35 kilometres long and up to 1.5

kilometres wide within which all material is well laminated. The lamination may be of beds or of cleavage laminae. For the strip as a whole, the mean attitude of the lamination is roughly 090/90, but local departures from this mean value are common.

Within this strip a suite of kink folds has been developed. Distribution of these folds is somewhat erratic, but they are most common in the central portion of the belt. These kink folds are here described separately from the overall structural development of the area (Clifford, in press), because they are easily distinguished from other suites of folds, and because they have clearer implications as to stress fields than other structures. However, it must be emphasized that the prime purpose of the field work which provided the data used here was a general survey of the area; the amount of reliable information for kink folds is rather small.

GENERAL KINK FOLD GEOMETRY

Kink zones in rocks "... consist ideally of parallel-sided domains with sharp boundaries at which the foliation is bent through a large angle; they are separated by undeformed domains" (Paterson and Weiss, 1966). Subsequent experimental work (Donath, 1968; Weiss, 1968) suggests that there are no undeformed domains. With this possible emendation in mind, we may define a kink fold as two undeformed (?) domains separated by a kink zone. The great majority of kink folds in the Lake St. Joseph area conform closely to this definition, though the domain boundaries are not always parallel, and the sharpness of the bend in the foliation varies from fold to fold.

The kink folds occur in one of two ways. Either they appear as singular kink folds, having one sense of external rotation and having a generally monoclinic symmetry, or they appear in double arrays having opposed senses of external rotation in adjacent folds, the symmetry of which may be orthorhombic or lower. Such fold arrays have been termed 'conjugate' (Johnson, 1956; Ramsay, 1962). They are developed systematically only in rocks where laminae are two millimetres or less in thickness. This means that the principal deformed surface is usually a cleavage, but there are kink folds affecting bedding only.

Widths of kink zones, measured in the lamination, vary from a few millimetres up to about ten centimetres. There is an ill-defined tendency for kink band widths to be smaller in the western portion of the area than elsewhere. On other grounds, the western portion of the area is thought to have been a high-pressure zone, so that there is a very tentative inverse correlation between kink band width and confining pressure, corresponding to the experimental data (Donath, 1964). Also, if a local set of beds contains a unit, say, 5 centimetres thick interlayered with otherwise finely laminated material, the kink bands developed there are much wider than in the thinly laminated material alone, and the lamination has a gradual rather than abrupt change in attitude across the zone boundary.

ORIENTATION OF THE RESPONSIBLE STRESS FIELD

Kink folds in conjugate array were used by Johnson (1956) to infer the axis of maximum compressive stress. Subsequently, Ramsay (1962) formalized the use of such arrays. His method, adopted here, involves plotting the kink zone boundaries¹ (KZB). The intersections of these boundaries coincide with orientation of the intermediate principal stress axis σ_2 , and their two bisectrices to the maximum and minimum principal stress axes, σ_1 and σ_3 respectively. Ramsay selected the correct bisectrix for σ_1 on the basis of the symmetry of the conjugate array. This commonly resulted in σ_1 lying in the obtuse bisectrix. This is in accord with experimental data. Experimentally produced kink zones have boundaries at angles of 40° to 80° to the undeformed lamination where conjugate arrays were produced by compression (σ_1) parallel to the lamination. Only 4 of 475 measurements were below 45° and the mean value was about 60° (Paterson and Weiss, 1966).

In the Lake St. Joseph area, ten conjugate arrays have been seen, for which adequate measurements have been made. Symmetry is monoclinic for seven samples, orthorhombic for the other three. Figure 2 shows the orientation of principal stress axes determined for these arrays by Ramsay's method. Paterson and Weiss (1966, pp. 350-352) point out that conjugacy is confined largely to those samples where σ_1 lay parallel or close to the lamination, so that σ_1 may immediately be located within or close to the mean undeformed lamination for these folds. The tight clustering is a measure of the directional constancy of the stress field for these folds, observed over an east-west distance of 12 kilometres. The mean orientations of principal stress axes are:

σ_1	085/00
σ_2	vertical
σ_3	355/00

The data do not warrant refined figures.

In their experiments, Paterson and Weiss observed that specimens of phyllite deformed when σ_1 did not lie in the lamination, commonly did not have conjugate arrays of kink folds, but rather singular kink folds having a single sense of external rotation. Folds of this kind are common at Lake St. Joseph. It seems reasonable to plot poles to KZB for such folds as if the entire suite of singular folds were actually conjugate. This has been done for 49 KZB in Figure 3. The mean orientations of principal stress axes inferable from this plot are:

σ_1	085/10
σ_2	275/80
σ_3	355/00

¹ In his paper, Ramsay referred to 'axial planes'. He also regarded these as equivalent to conjugate shears, a view recently abandoned (Ramsay, 1967).

It is here assumed that the kink folds all belong to one phase of deformation. All are later than other types of folds in the area; they show a common style and common attitudes of planar and linear elements; the majority are affected by later brittle fractures. It seems reasonable to infer that a common stress field was responsible for the generation of these folds. Examples of these kink folds are shown in Figure 1.

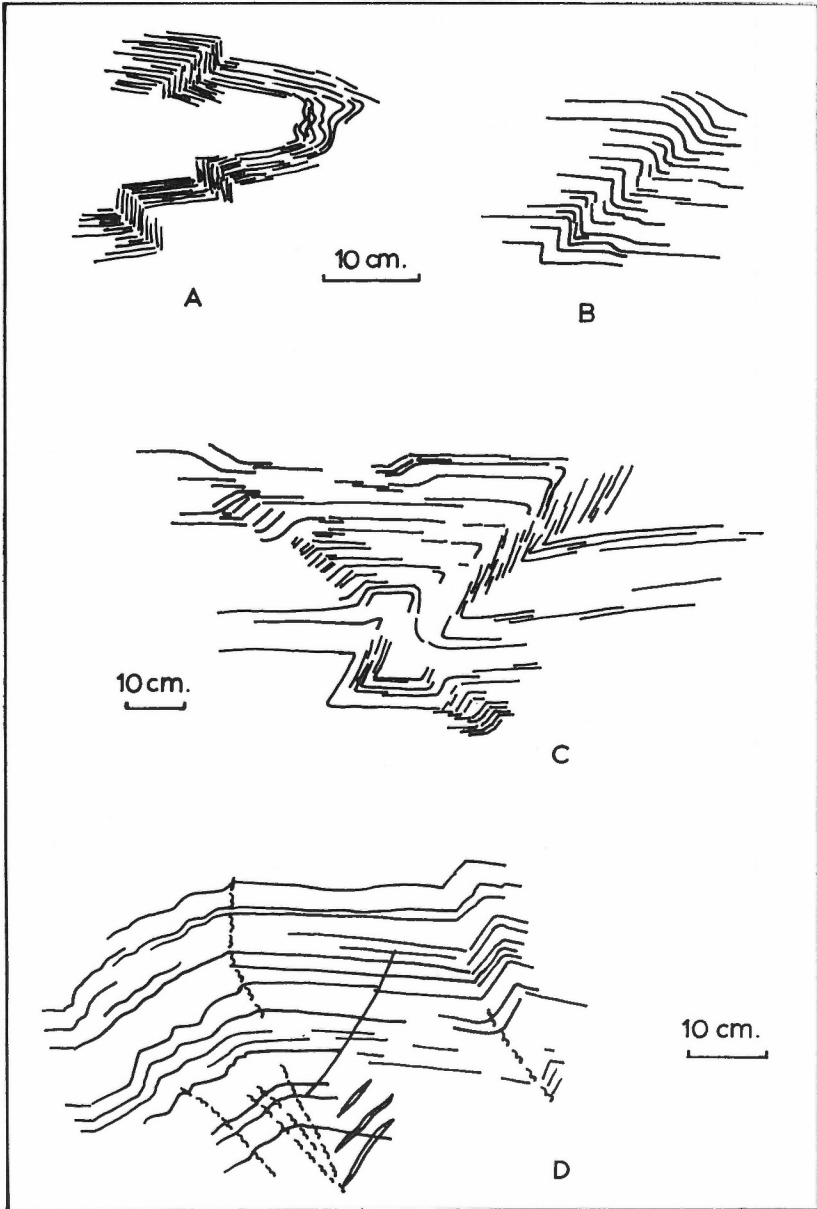


Figure 1. Profiles of kink folds in the Lake St. Joseph area.

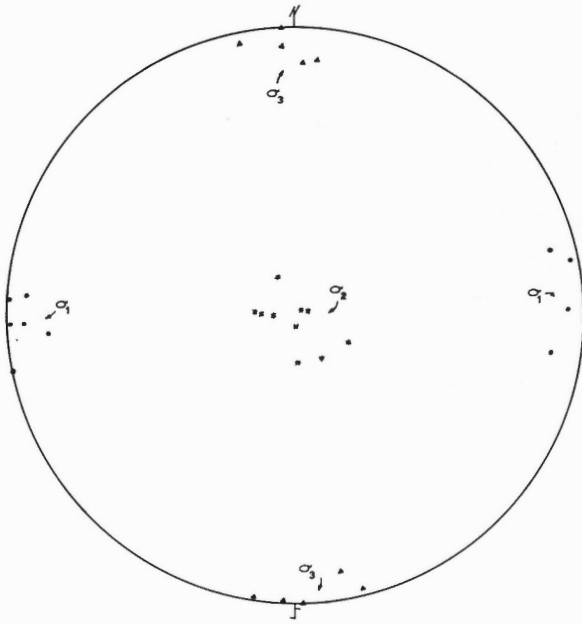


Figure 2.

Calculated orientations of stress field for 10 conjugate arrays of kink folds.

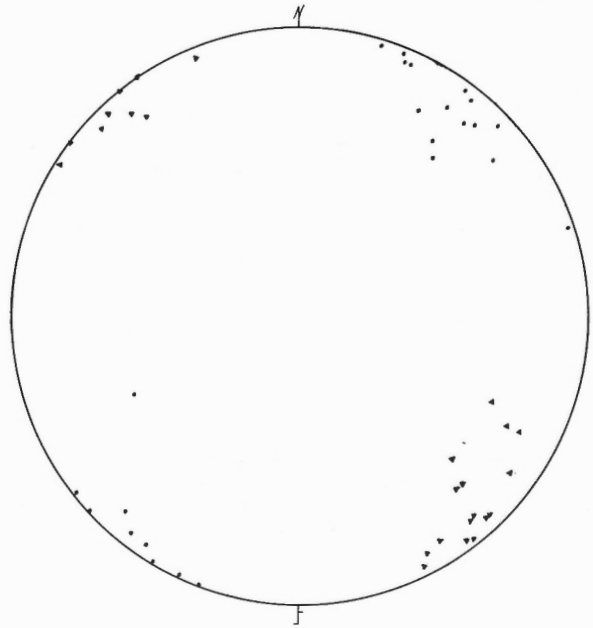


Figure 3.

Poles to KZB of 49 singular kink folds.

Δ dextrally-rotated kink bands.

\circ sinistrally-rotated kink bands.

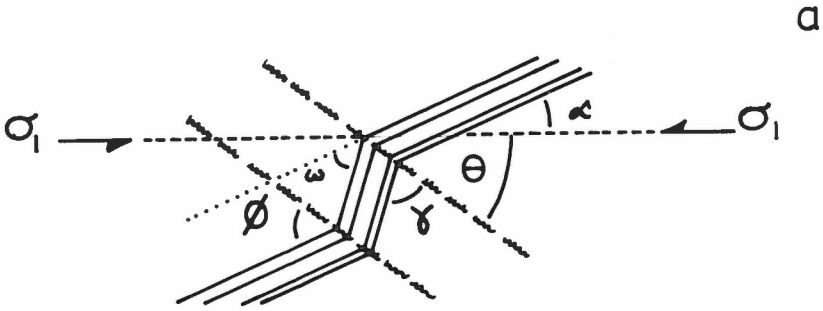


Figure 4. Angles measured for use in Figures 5-8.

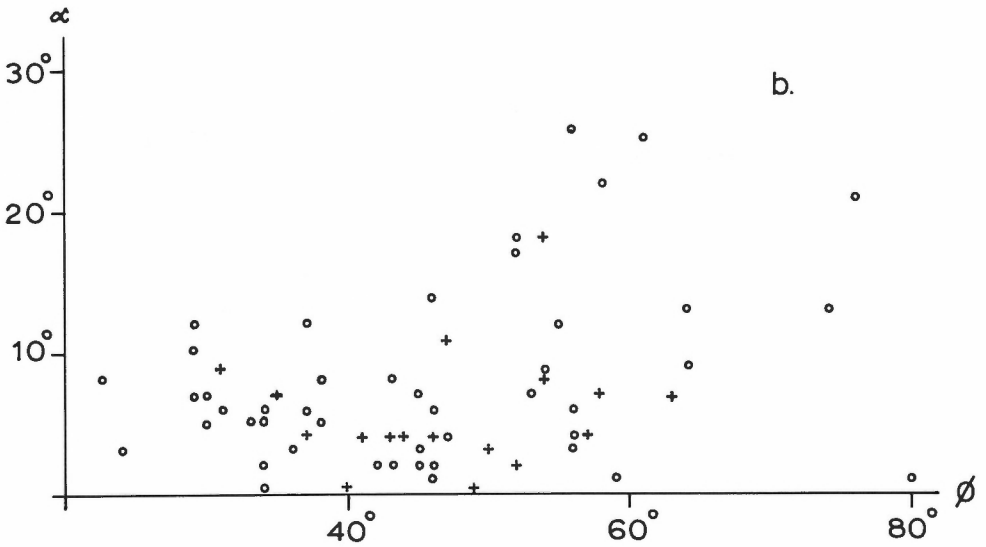


Figure 5. α v. ϕ for 17 conjugate (+) and 46 singular (o) kink folds.

The conformity with orientations inferred from the conjugate arrays is striking, and suggests that truly conjugate arrays of kink bands are not vital to the determination of stress field orientation, provided that singular kink folds of both rotational senses occur.

RELATIONSHIP OF GEOMETRY AND STRESS ORIENTATION

Knowing the orientation of σ_1 , we may examine various angular relationships of the natural folds. The angles of interest are defined in Figure 4. From this figure, $\theta + \alpha = \emptyset$ which is true for all the natural folds within $\pm 3^\circ$. The angles have been calculated from field measurements for 63 kink folds, including 17 from conjugate arrays. Not all examples could be used in every case, so that not all diagrams have 63 points.

- (a) α v. \emptyset : values of α and \emptyset from 63 kink folds are plotted in Figure 5. They show that (i) no obvious difference exists between conjugate (+) and singular (o) kink folds, though the scatter of points for conjugate folds is somewhat less than for the singular folds;
- (ii) the angle \emptyset ranges from 22° to 80° ;
- (iii) α , the inclination of undeformed lamination to σ_1 , does not exceed 28° . 75% of all folds have $\alpha < 10^\circ$;
- (iv) there seems to be no preferred value for \emptyset .

The range in \emptyset exceeds the range reported from the experiments by nearly 20° but the range in α accords well with experimental values. Kink zones were developed when specimen foliation was inclined at 25° to σ_1 , but not at any higher inclination. The lack of a preferred value of \emptyset contrasts with the 60° average for \emptyset seen in the experiments. This may be due to the small number of observations made on the natural folds, or it may be significant.

(b) α v. γ : values of α and γ for 39 kink folds are given in Figure 6. These show that:

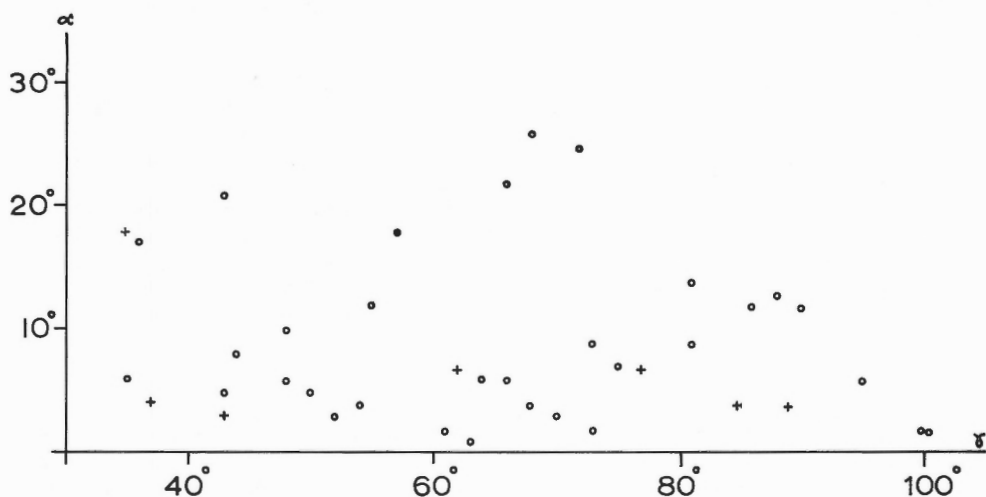


Figure 6. α v. γ for 7 conjugate (+) and 32 singular (o) kink folds.

- (i) no obvious distinction can be made between conjugate (+) and singular (o) folds;
- (ii) the angle γ varies from 34° to 100° ;
- (iii) there is no preferred value for γ .

The angle γ is equivalent to θ_K of Paterson and Weiss. The range of γ is greater than the experimental values by about 20° , and it has no preferred value.

(c) γ v. θ : values of γ and θ for 40 samples are shown in Figure 7. They show a wide scatter, with no preferred value for either angle (see (a) and (b) above) and no clear correlation between them.

This last point is quite important. For experimental folds, bilateral symmetry is apparently common i.e. $\theta \approx \gamma$ (using the angles as defined here). This is quite obviously not the case for these natural kink folds. In addition, 20% of the natural samples have $\theta > \gamma$. This is opposed to the experimental observation that $\theta < \gamma$ always (Paterson and Weiss, 1966, p. 352). The experimental data are not plotted in this fashion, so that it is impossible to tell how great are the departures from bilateral symmetry, or how consistently $\theta < \gamma$.

MECHANISMS OF KINK FOLDING

Several mechanisms have been proposed for the development of kink folds. Johnson (1956) and Ramsay (1962) postulated that the kink zone boundaries represent a primary shear system with the laminae in the kink zone undergoing gliding as the kink develops. Paterson and Weiss (1966) suggest that, once developed, kink zones grow by lateral migration of KZB; they offer no suggestion as to the initial phase of development. A possible mechanism for this early development stage is by rotation of laminae of constant length between KZB of fixed orientation to a position of mechanical stability.

There are several discussions of kink folds, in which the authors reject the notion that KZB are equivalent to conjugate shear planes (see Anderson, 1964; Paterson and Weiss, 1966; Ramsay, 1967). All these writers note that conjugate shear planes are formed by σ_1 acting in their acute bisectrix, whereas conjugate kink folds commonly have σ_1 in the obtuse bisectrix of the KZB. Taken individually the Lake St. Joseph folds show both possibilities. However, any failure by shear in these rocks appears to be younger than the initiation of kink folding, exploiting KZB largely because they were already zones of weakness. A conjugate shear hypothesis is accordingly rejected for the Lake St. Joseph folds, as it has been for other occurrences.

The idea of gliding on laminae, however, is not so simply rejected. Donath (1964) writes of laminae undergoing gliding between fixed KZB. The crucial factor in this mechanism is the balance between resolved shear stress on the laminae and the frictional resistance to gliding. Where the shear stress falls below the frictional resistance, motion on the laminae should cease; any further shortening can be accomplished only by developing further kink folds or by faulting at the KZB. Experiment (Donath, 1961) and theory (Jaeger, 1960) show that high inclinations of the lamination in the kink

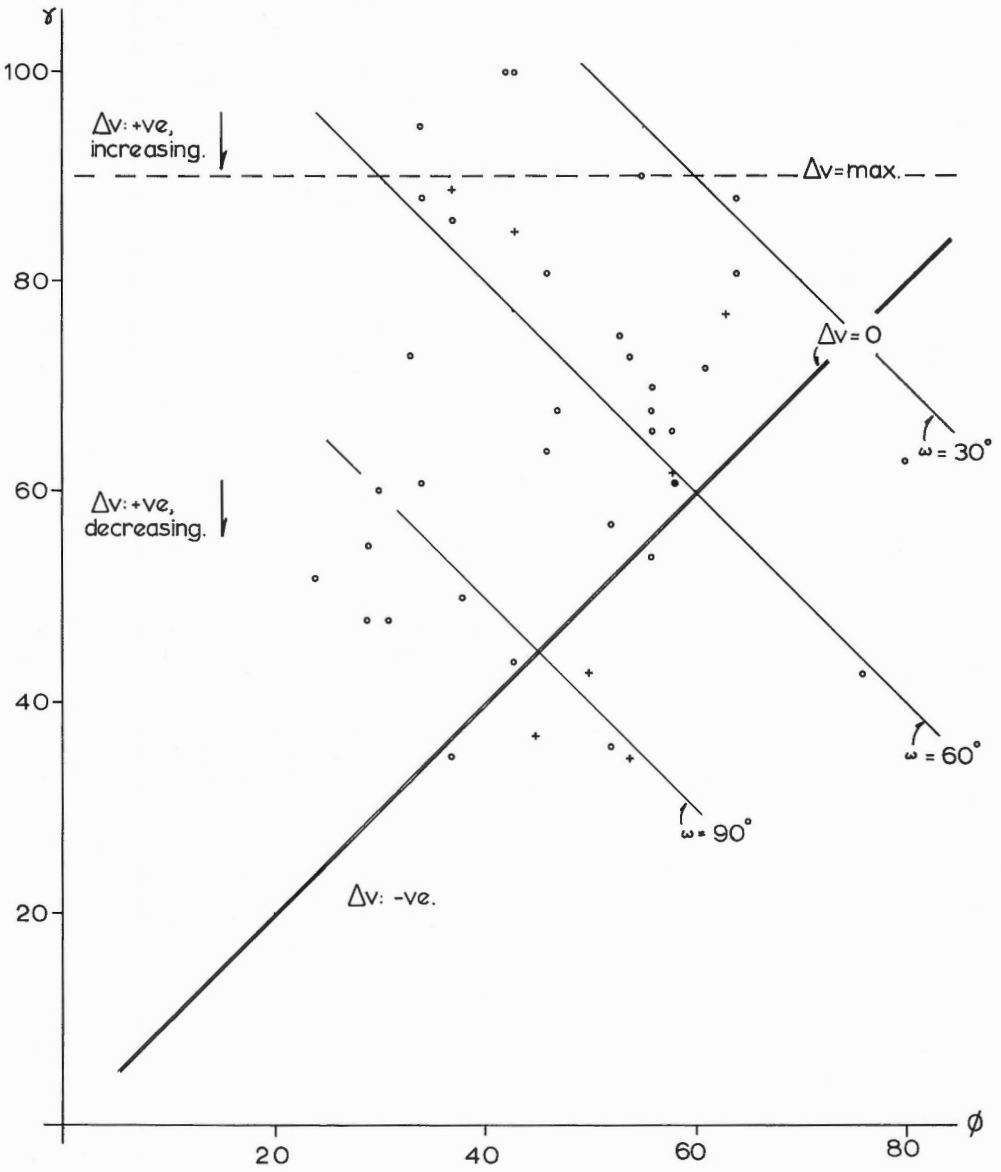


Figure 7. γ v. ϕ for 7 conjugate (+) and 33 singular (o) kink folds. The solid circle represents the experimental mean values for these angles (see Paterson and Weiss, 1966, p. 352.). v is dilation (see Fig. 8).

zone prohibit gliding. The experiments give an upper limit of about 60° for the inclination of lamination to σ_1 . A gliding mechanism for kink band development, therefore, will be effective only up to $(\gamma + \theta) \geq 120^\circ$. Expressed another way, $\omega \leq 60^\circ$. Fifty per cent of the natural folds (Fig. 7) have $\omega > 60^\circ$, and the gliding hypothesis therefore, must be regarded as of secondary importance if it applies at all.

An hypothesis of rotation plus dilation avoids this angular limitation. If we assume that two KZB are formed, having fixed orientation, and that shortening occurs by progressive rotation of laminae between KZB in a hinge-like manner, then the amount of rotation which may occur is conditioned by the angle $(\theta + \alpha)$. A hinge-like rotation involves separation of laminae - dilation - in the kink zone, rising from zero at $\gamma = 180 - (\theta + \alpha)$ to a maximum at $\gamma = 90^\circ$. The dilation decreases to zero at $\gamma = (\theta + \alpha)$ and to negative values thereafter (Fig. 8). For $\gamma > 0$, laminae are not in contact, no frictional resistance to gliding exists, and folds can form with $(\theta + \alpha) < 60^\circ$ and $\gamma < 60^\circ$.

Certain of the natural folds do have these properties. The tightest of the folds has $\gamma = 35^\circ$ and $\theta [\approx (\theta + \alpha)] = 38^\circ$. Twenty-five per cent of the total (Fig. 7) have $\alpha + \theta + \gamma \leq 90^\circ$. Four folds have carbonate layers between laminae in the kink band, in rocks where carbonate is virtually unknown. The writer regards these facts as strong support for the rotation-dilation mechanism.

The simple hypothesis, however, fails to explain the wide scatter of points in Figure 7, particularly those points representing folds having an apparent $\Delta v < 0$.

Full rotation i. e. from $\Delta v = 0$ at $\gamma = 180 - \theta$ through a maximum and back to $\Delta v = 0$ at $\gamma = \theta$ is clearly not the case for the majority of the Lake St. Joseph folds. Three possible explanations occur to the writer, for the situation where $\gamma > \theta$.

(i) At a position for which $\gamma > \theta$ rupture may occur at the KZB. The dilation in the zone will fall to zero instantaneously, and laminae will come into full contact. Further rotational motion can only be by gliding, and this is permissible only if $(\gamma + \theta) > 120^\circ$ at the instant of failure. This would allow the development of a fold with a low ω value and $\gamma > \theta$.

(ii) Any filling of the dilatant zone by crushed material due to cataclasis, as reported by Donath (1968), would maintain a frictional contact between laminae and would impose the same angular restriction as the glide mechanism proper.

(iii) Infilling of the dilatant zones by quartz or carbonate material, as reported above, would tend to jam the rotational mechanism if the filling occurred in the angular range $90 > \gamma > \theta$. Filling when $\gamma > 90$ would still permit rotation without gliding over the range $2(\gamma - 90)$ from the position of filling.

For folds where $\gamma < \theta$, a negative dilation is implied. If a true negative dilation does occur, then some modification to the mineralogy may be anticipated. No such effect has been seen even where the apparent dilation is -40 per cent. Alternatively, it seems likely that at $\gamma = \theta$ rotation - plus - dilation ceases, and a steady 'thinning' of laminae occurs, permitting gliding.

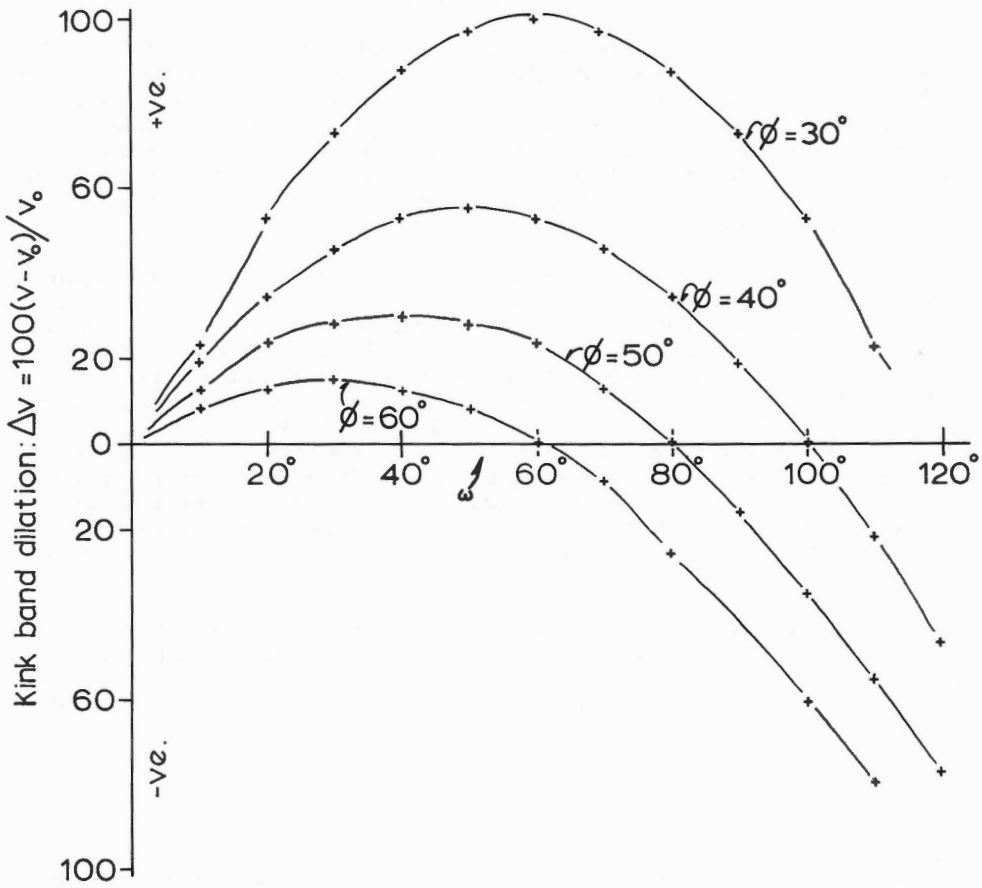


Figure 8. Kink band dilation (%) as a function of ω and ϕ , assuming simple rotation and plane strain.

This naturally will lead to aberrant kink band width measurements. It is suggested that measurements of kink band width be made only on those folds where $\gamma \geq \phi$.

One further point which arises from Figure 7 is that statistically the orientation of the KZB remains constant throughout fold development. The scatter of points has a generally vertical distribution, parallel to the γ axis. Comparable diagrams are given by Anderson (1968) for other field examples and by Donath (1968) for experimentally - produced folds.

CONCLUSIONS

Data from a suite of natural kink folds in the Lake St. Joseph area lead to the rejection of a simple gliding mechanism for the production of those kink folds, pointing instead to a rotation - dilation mechanism. The bulk of these natural folds did not undergo the fullest possible rotation before collapse of the kink zone boundary took place, leading to an effective jamming of the rotation either instantaneously, or before frictional resistance to gliding overcame shear stress acting on the lamination. No explanation is available for folds which have suffered over-rotation.

The mechanism outlined by Paterson and Weiss (1966) applies strictly to the continued growth of kink zones from some initial geometry. The writer suggests that the mechanism outlined here produces the initial geometry, and that subsequently the kink zone boundaries may migrate laterally. One might anticipate that with increasing confining pressure the initial width of the kink band will decrease, to minimize the absolute dilation. Such a relationship has been recorded by Donath (1964). Under such circumstances, lateral migration of kink zone boundaries would be the only way of accomplishing significant shortening by kink folds at high confining pressures, and such shortening would be gradual. By contrast, the rotation - dilation mechanism operating at low confining pressures would give a large semi-instantaneous shortening initially followed by a period of much slower shortening.

Finally, the data from the natural folds lend support to the notion that the "kinking will begin at a local imperfection in the material . . ." (Paterson and Weiss, 1966, p. 367). Values of $(\theta + \alpha)$ vary quite arbitrarily over a wide range and attest the influence of local flaws having random distribution and orientation.

REFERENCES

- Anderson, T.B.
1964: Kink bands and related geological structures; Nature, vol. 202, pp. 272-274.
- 1968: The geometry of a natural orthorhombic system of kink bands; see this report,
- Borg, I. and Handin, J.
1966: Experimental deformation of crystalline rocks; Tectonophysics, vol. 3, pp. 249-367.
- Clifford, P.M.
(in press): The Geology of the West Lake St. Joseph area, District of Kenora, Northwest Ontario; Ont. Dept. Mines, rept.
- Donath, F.A.
1961: Experimental study of shear failure in anisotropic rocks; Bull. Geol. Soc. Am., vol. 72, pp. 985-990.

- Donath, F.A. (cont'd.)
1964: Strength variation and deformational behaviour in anisotropic rock; in State of stress in the earth's crust, W.R. Judd, editor, pp. 281-298, Am. Elsevier, New York.
- 1968: Experimental study of kink band development in Martinsburg Slate; see this report,
- Jaeger, J.C.
1960: Shear failure of anisotropic rocks; Geol. Mag., vol. 97, pp. 65-72.
- Johnson, M.R.W.
1956: Conjugate fold systems in the Moine Thrust Zone in the Lochcarron and Coulin Forest areas of Wester Ross; Geol. Mag., vol. 93, pp. 345-350.
- Paterson, M. and Weiss, L.E.
1966: Experimental deformation and folding in phyllite; Bull. Geol. Soc. Am., vol. 77, pp. 343-374.
- Ramsay, J.G.
1962: The geometry of conjugate fold systems; Geol. Mag., vol. 99, pp. 516-526.
- 1967: Folding and fracturing of rocks; New York, McGraw-Hill.
- Weiss, L.E.
1968: Flexural slip folding of foliated model materials; see this report,

DISCUSSION

H. R. Wynne-Edwards wondered if either Dr. Anderson or Dr. Clifford would like to comment on the orientation of kink bands with respect to folds and other major structures in the same area. In cases he could remember, inter-section of the kink-zone boundary with the foliation was at a high angle to a prominent mineral lineation, and subparallel to axes of major folds.

T. B. Anderson replied that in his example, hinges of the first folds are almost perpendicular to the kink bands which plunge very steeply in the plane of foliation. Folds of the second generation do not appear to exercise any control on the position of the kink bands. No mineral lineations are associated with the kink bands themselves. There is a weak 'stretching direction' or 'a' lineation associated with the first folding, and crenulation associated with the second folding, both at various angles to the kink bands and not obviously related to them in position or in time.

P. Clifford said that in northern Ontario there did not seem to be any constant relationship between folds and kink bands. Formation of the axial plane of the first folds was a primary feature on which was superposed a second deformation ('bath tub tectonics') due to emplacement of diapiric granites. This second deformation had created a stretching lineation plunging very steeply in the cleavage plane. Lineations of kink folds were everywhere steep (80° or more), and with no consistent relationship to any earlier folds.

G. R. Stevens asked Dr. Anderson if his sets of kink bands were really orthorhombic as far as strains and stresses were concerned.

T. B. Anderson replied that individual kink bands have monoclinic symmetry, but that the system formed by combination of two kink bands of opposite sense of displacement and the foliation, has orthorhombic symmetry. In that dextral kink bands are more abundant than sinistral the system as a whole is not completely symmetrical but the angular symmetry is preserved.

L. E. Weiss commented on Dr. Anderson's paper and particularly on the fact that total strain appears to be very small. This fact would make such kink bands extremely useful. There had been a great deal of discussion in the past about relating stresses to folds, but for large strains, the state of strain is not a function of stress. The strain indicated by the author (3 metres in 18 kilometres) was of the order of magnitude of an elastic strain which should give excellent results for stress analyses. Similar relationships had been proven by work on calcite twinning lamellae, where small strains on few thin lamellae would give much better concentration in the pattern of compression-tension points than would thick lamellae representing larger strain. He indicated his belief that study of kink bands is important.

PROFILE VARIATION IN A KINK SET

W. K. Fyson
Department of Geology, University of Ottawa
Ottawa, Canada

Abstract

Steep kink bands cross vertical foliation in slates and siltstones near Lunenburg, Nova Scotia. The profiles of 70 bands exposed on a 25 by 600 foot horizontal surface exhibit variations that warrant explanation by any general theory of kink origin.

The rotated kink limbs are 0.25 to 47 inches in length, and the bands are 1 to 25 feet apart. The narrowest kink bands lie within wide bands near the bounding surfaces, particularly where these diverge and the kinks die out. Bands curve up to 15° and boundaries are 65° to 90° to the external foliation. The parts of bands at high angles to the external foliation tend to be the widest. No kinks meet or cross each other.

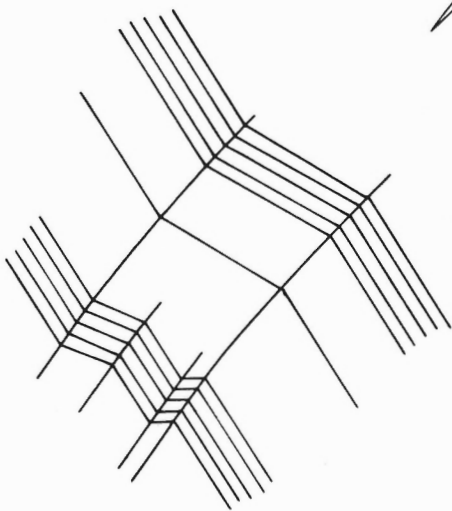
The angular deviation or rotation of the kinked foliation ranges from 15° to over 45°, and for individuals of variable width is greater the shorter the kinked limb. Toward silty layers, band widening and curving to the normal to the foliation is accompanied by decreased rotation and many bands become diffuse. Nevertheless, the longer, less rotated limbs increase both the offset and shortening across the kinks.

A preliminary suggestion is that the kinks initially propagated as narrow bands that like refracted joints tended to curve normal to competent layers. Where normal, further strain was accomplished by widening, but where oblique to the foliation, there was continued internal rotation and the bands remained comparatively narrow.

INTRODUCTION

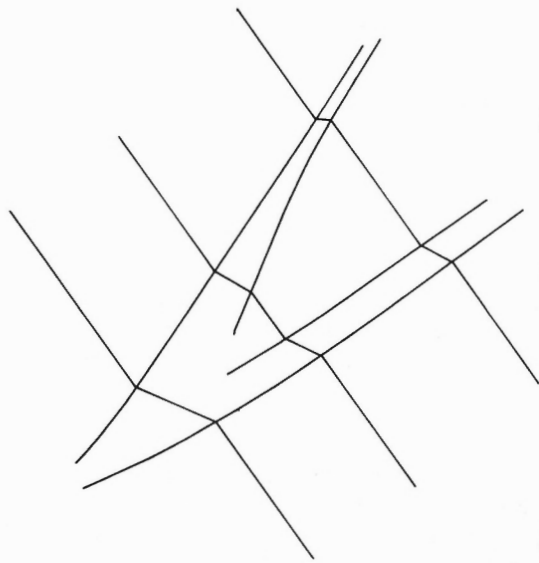
Steep sinistral kink bands affect Lower Palaeozoic slates in a large area of Nova Scotia. On a regional scale the bands strike constantly northwest, and they may have formed in response to compression aligned approximately east-west (Fyson, 1966). Though generally rectilinear in plan view, in detail many bands curve and vary in width, and the internal foliation is not constant in orientation. It is hoped that a study of these variations will be pertinent to problems of kink genesis, such as the controlling factors for what determines the direction of kink boundaries and the amount of internal rotation.

The following is a preliminary description of angular and linear variations in profile as exhibited by 70 northwest striking kink bands exposed on a 25 by 600 foot portion of a beach platform on the south side of Kings Bay, near Lunenburg, Nova Scotia.



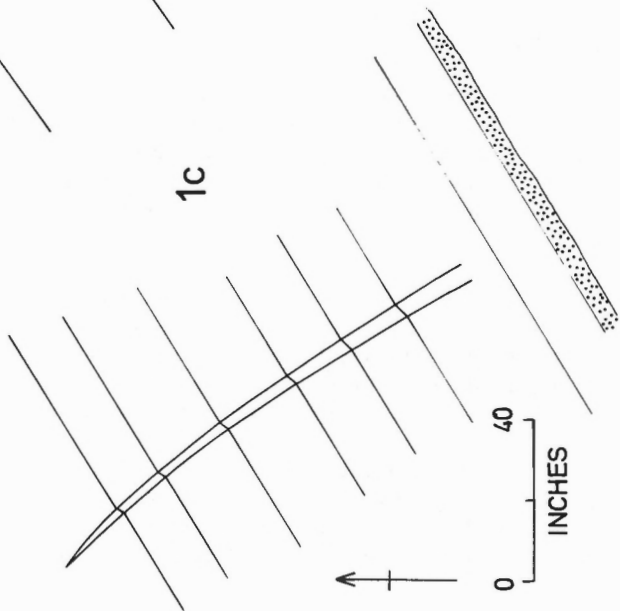
0 10
INCHES

1a



0 20
INCHES

1c



0 40
INCHES

1b

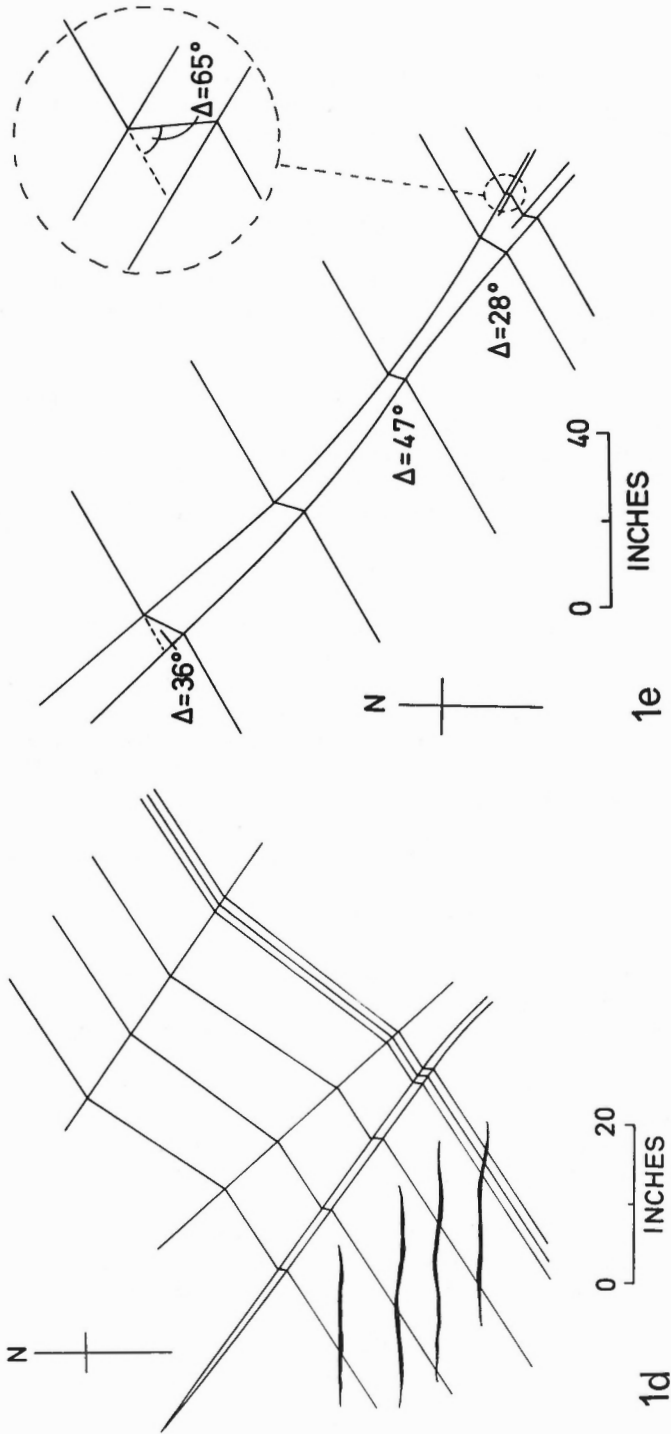


Figure 1. Sketches of kink band profiles based on field measurements

Slates and thinly laminated siltstones are crossed by subvertical cleavage foliation that varies no more than 5° in strike (055° to 060°) outside the kinked zones. The cleavage is parallel to the axial surfaces of earlier, low-plunging, upright folds, and the kink bands affecting both the cleavage and the bedding surfaces cross the limbs and hinge areas of small parasitic folds on the northern limb of a larger, earlier anticline.

GENERAL MORPHOLOGY

All the kink bands are sinistral, and most are reverse kinks (Dewey, 1965) that result in a component of shortening parallel to the external foliation. No bands cross each other; there are none in conjugate relation.

The kinked limbs within the bands are 0.25 to 47 inches in length, and excluding those of narrow bands lying within wider, the arithmetic mean length is close to 1 foot. Spacing between bands is 9 to 300 inches with a mean of about 8 feet. Some bands, including those only 2 to 3 inches wide, extend over 25 feet across the foliation, others for only a few feet. Compared with much smaller structures formed experimentally that have apical angles of about 120° (Paterson and Weiss, 1966), the kink folds are more open with apical angles most commonly 150° to 160° .

The bounding surfaces are irregular in orientation on a small scale, but the bands exhibit general patterns illustrated from field measurements (Fig. 1). Some bands terminate by a shortening of the kinked limb and a merging of the boundaries to form a lens shape. However, many die out not by a convergence, but by a divergence of the bounding surfaces and a decrease in the limb deviation so that the kink fold opens (Fig. 1b). As shown in the figure, this widening and diffusion of the kink bands is particularly noticeable as the bands are followed toward silty layers. Many of the silty beds, which are up to one foot thick, lack a well defined cleavage foliation, but they are crossed by a few bands, apparently utilizing the laminae as the necessary slip planes. Bands across the silts are less angular than across the slates, the curved hinge areas are wider, and those with small limb deviations pass into open undulations.

Within several of the wider kink bands there are narrow internal kinks (limb length 0.25 to 2.5 inches for the 8 measured) that lie along the bounding surfaces, particularly where these diverge and the wide band dies out (Fig. 1c, 1e). In effect, the band splits into two subsidiary diverging bands. Other bands pass into two or more subsidiary kinks with little divergence (Fig. 1a), and some bands are replaced by a single narrow band along one of the bounding surfaces, the other surface terminating by an opening of the fold. Some independent bands not within or adjacent to larger structures, are as narrow (2 inches and less) as the internal bands.

In a few examples, one kink boundary is straight, and the other consists of a set of en echelon surfaces, each well defined for a few inches by angular changes in foliation, then diffusing to be replaced step-wise by another surface.

In addition to a widening toward the silty layers, bands gently curve so that the boundaries tend to become normal to the external foliation (Fig. 1b). In

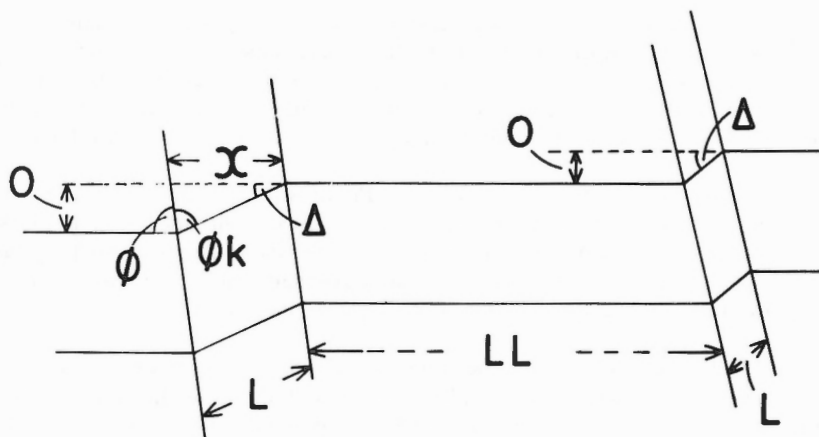


Figure 2. Measured and calculated parameters of kink bands.
 ϕ, ϕ_k angles between kink boundary and external and internal foliation.
 Δ angular deviation of internal foliation.
 L length of kink limb.
 LL spacing between kink bands along external foliation.
 O offset ($L \sin \Delta$).
 Shortening across kink band parallel to $LL = L (1 - \cos \Delta)$.

contrast, where the bands terminate by lensing out, some curve in the opposite sense to make a smaller angle to the foliation (cf Anderson, 1968, Fig. 3).

Impersistent fractures follow the bounding surfaces of many kinks, and in one example there is a small strike-slip fault with undetermined offset. In four localities sets of east-west fractures obliquely cross the foliation near a kink band (Fig. 1d). Possibly these are joints normal to a tensional direction, and they may have been initiated in response to the general east-west compression assumed to have led to the kinking.

ANGULAR AND LINEAR RELATIONS

The main parameters to be considered are shown in Figure 2. It is important to note that the angular deviation Δ of the kinked foliation is independent of the angle ϕ between the bounding surface and the external foliation. With boundaries that are not parallel, the deviation in one part of a band may be constant, whereas from one side to the other ϕ varies as much as 20° . It is apparent that if ϕ_k is less than ϕ , the kinked limb would be thinned. This assumes that the external foliation is undeformed. Small variations in orientation of the external foliation do occur, and as demonstrated by Weiss (1968), it is probable that during kinking there was some rotation; but the amount relative to that of the internal foliation would be small.

Figure 2 also illustrates the general relations observed in the field that the shorter kinked limbs L of the narrower bands, or parts of bands, deviate at higher

angles than the longer limbs of wider bands. The bounding surface angle ϕ tends to be smaller for the narrower bands with higher deviations, which therefore are more oblique to the foliation. In individuals this relationship is expressed by curvature of the bands. No obvious correlation between the spacing of bands LL and the other parameters has yet been found, and this factor will not be considered further.

Graphical relations are shown in Figures 3, 4, 5, and 6. In a majority of measurements (65 of 94) ϕ is greater than ϕ_k (Fig. 3) in contrast to kinks measured elsewhere (Anderson, 1968). The modal value for $\phi - \phi_k$ is about 10° but ϕ_k varies from 50° less than ϕ to 25° greater (the graph averages measurements each side of bands and the largest negative values of $\phi - \phi_k$ are not shown).

The deviation Δ varies between 13° and 67° , but a majority of kink limbs deviate between 20° and 30° (apical angles 150° to 160°). Although the kink folds are thus very open structures, for most kinks ϕ_k is dominantly less than ϕ , therefore the rotated limb must have been thinned.

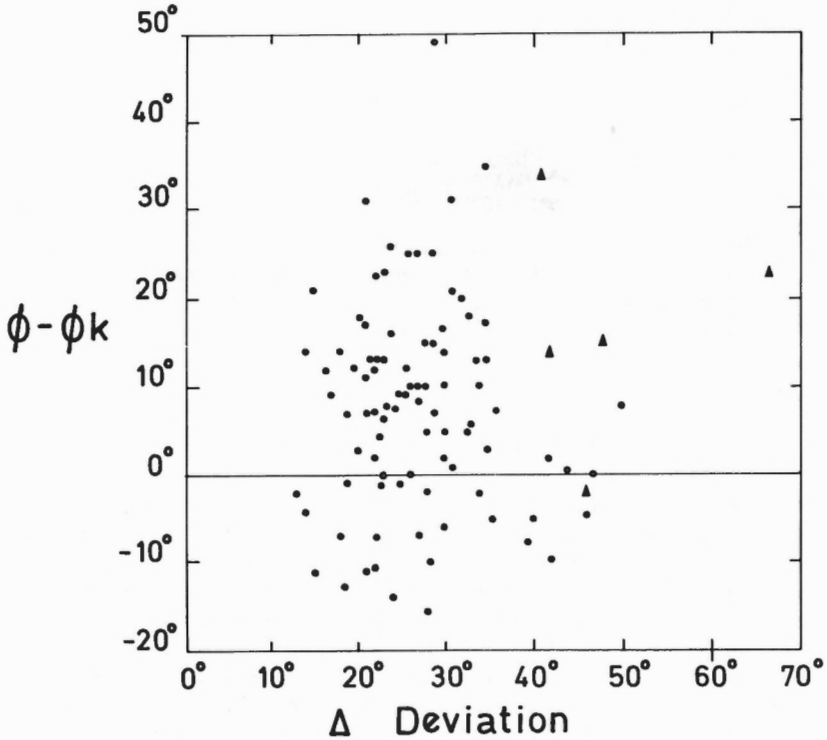


Figure 3. Angular deviation Δ of kinked foliation compared with $\phi - \phi_k$; 94 measurements. Triangles are from internal bands

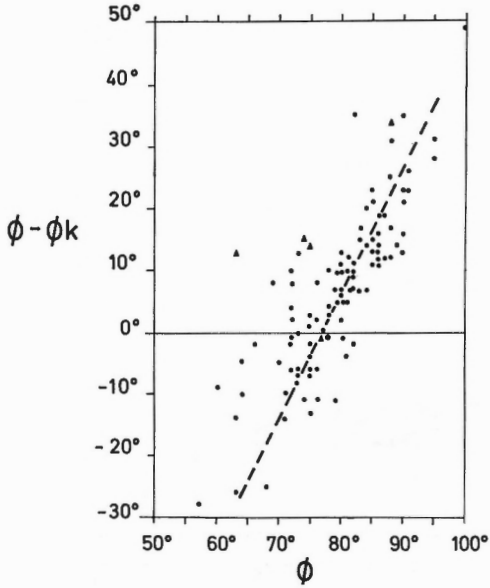


Figure 4.

Angle ϕ of kink boundary compared with $\phi - \phi_k$; 100 measurements. Triangles are from internal bands

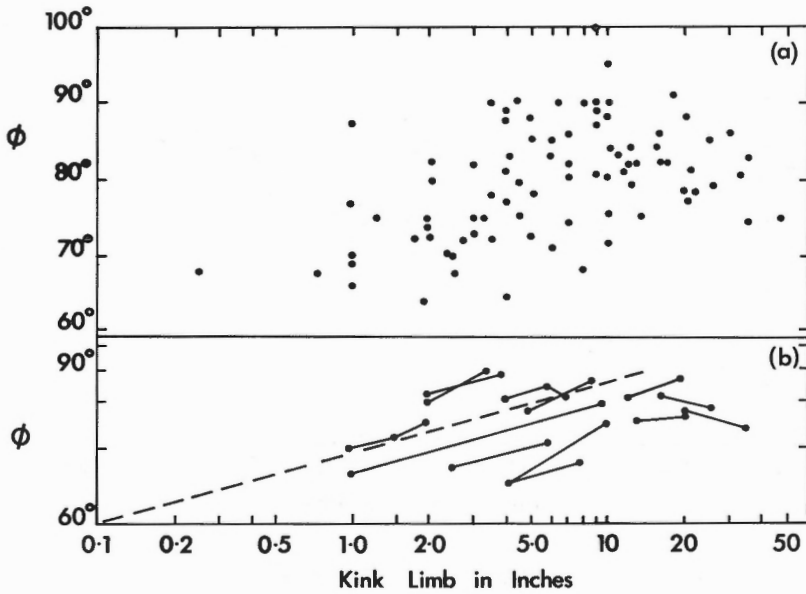


Figure 5. Kink limb length L compared with angle ϕ .
a. 85 measurements; L logarithmic scale.
b. Longitudinal variations measured from 2 to 3 parts of 12 bands; L and ϕ logarithmic scales

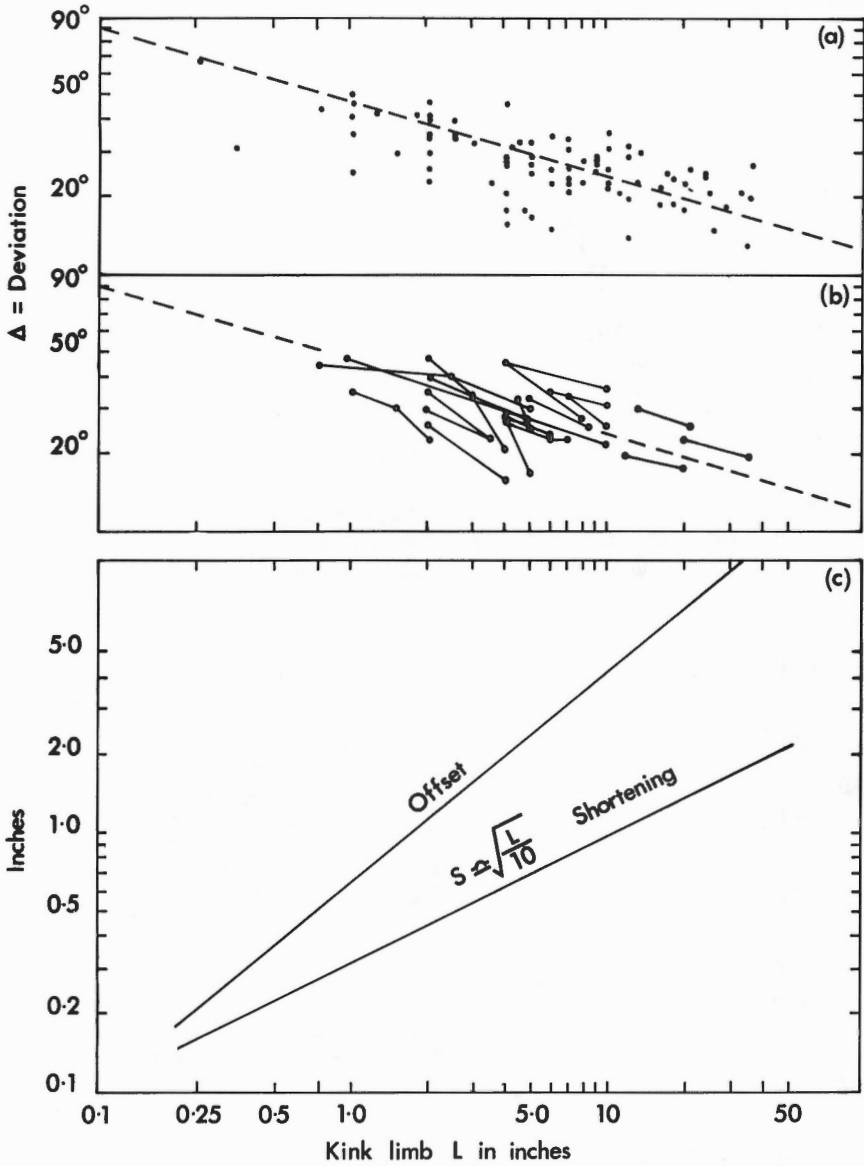


Figure 6. Kink limb length L compared with angular deviation Δ ; logarithmic scales.
a. 94 measurements.
b. Longitudinal variations in 2 to 3 parts of 20 bands.
c. Offset and shortening trends calculated from average trend of a and b.

The graph (Fig. 3) exhibits no obvious general relationship between Δ and $\phi - \phi_k$. For some individuals $\phi - \phi_k$ decreases with increased Δ , but for others there is an increase. Foliation in the narrow bands within wider tends to deviate the most but $\phi - \phi$ for these kinks is not appreciably different from that of independent bands.

Between $\phi - \phi_k$ and the limb length L, as with the comparison with Δ , there is a variable relationship for individuals and for the group of kinks as a whole (graph not illustrated).

The variation of $\phi - \phi_k$ is more readily correlated with ϕ (Fig. 4). The bands with high ϕ tend to have the lowest relative ϕ_k ($\phi - \phi_k$ is greatest). Evidently the rotated limbs of these bands at high angles to the external foliation are thinned the most. An average trend line passes through $\phi - \phi_k = 0$ at about $\phi = 77^\circ$. At this angle the kinked limb is unchanged in thickness. For the more oblique kinks with $\phi = 60 - 70^\circ$, ϕ_k is larger than ϕ and the limbs are dilated. The average trend line shown is such that $\phi = 77 + \frac{1}{2}(\phi - \phi_k)$. By substitution [$\Delta = 180 - (\phi + \phi_k)$]. Δ is constant at 26° along the trend line. This angle is in agreement with the dominant clustering of Δ between 20° and 30° in Figure 3. (No marked modal peak for Δ is apparent in a frequency graph not shown).

A significant conclusion from Figure 4, which is supported by observations on individual bands, is that although the kinked limb may remain at a constant deviation from the unkinked foliation, the bounding surface angle ϕ can vary considerably and thus change the ϕ to ϕ_k relations. The curvature of the bands is thus not a function of the deviation, such as expected if the boundaries migrated and rotated with increased deviation so that they tended to bisect the apical angles. This relationship is also apparent from a comparison of ϕ with the deviation Δ (not illustrated). Apart from a few bands, ϕ does not decrease at one half the rate of Δ increase as would occur if dependent.

The angle ϕ is not clearly related to the limb length L when all kink bands are considered (Fig. 5a). For example ϕ is 90° for L varying between 3.5 and 20 inches. However, of the 12 bands measured with appreciable variations in both L and ϕ , 10 exhibit an increase of ϕ and L, and the relative rate of change expressed logarithmically is remarkably constant (Fig. 5b). As shown, it is possible to extrapolate to small values of L with ϕ at about 60° , but there are too few control points to significantly establish an average position for the trend line.

An inverse relationship between the deviation Δ and the limb length L is apparent in Fig. 6. This tendency is true for the group as a whole (Fig. 6a) and for individuals (Fig. 6b). The straight trend line plotted on the logarithmic graph, is very close to a line satisfying the equation $\text{Cos } \Delta = 1 - \frac{1}{\sqrt{10 L}}$. (The trend line is a maximum of 2° from the equation).

At first sight, the decrease in deviation with increasing limb length might be associated with a decrease in strain as the bands widen and die out. But by converting Δ and L into terms of shortening along the external foliation and offset it is apparent that there is actually a strain increase with increasing L (Fig. 6c).

Calculations for the shortening trend are as follows:

$$\begin{aligned} \text{Shortening } S \text{ parallel to LL (Fig. 2)} &= L - x \\ &= L(1 - \cos \Delta) \end{aligned} \quad (1)$$

$$\text{From the graph (Fig. 6) } \cos \Delta \approx \frac{1 - 1}{\sqrt{10L}} \quad (2)$$

$$\text{Therefore from (1) and (2) } S \approx \sqrt{\frac{L}{10}} \quad (3)$$

If Δ remained constant, then S would be a direct function of L and increase at a greater rate than indicated by equation 3.

An interesting feature suggested by extrapolating the trends in Fig. 6 is that for very small values of L ($L = 0.1$ inches) the deviation would approach 90° with shortening and offset both equal to L . Obviously many more measurements of narrow kink bands are necessary, and the trends need testing by much more data.

DISCUSSION

The observed kink bands differ in geometry from small kinks in finely foliated, homogeneous material, the development of which is described by Paterson and Weiss (1966) and Weiss (1968). In particular the curvature and widening with a decrease in deviation but increased shortening differs from the ideal models which widen with either a fixed or increased deviation. The inhomogeneity of the rock is obviously a contributing factor, but the exact mechanism of development is not clear.

One tentative growth model, which adapts that of Paterson and Weiss and assumes flexural slip, suggests that the kinks propagate from a nucleus as initially very narrow bands, behaving very much as joints in response to rock inhomogeneities and local variations in the stress field. Thus the bands oblique to the foliation in slates refract toward the more competent silty layers, and like joints, tend to cross these at right angles.

The initial very narrow band would thus be curved (Fig. 7a), but the kinked limb would have a small deviation that was constant. The relationship between ϕ and $\phi - \phi_k$ would be similar to that suggested by Figure 4. Shortening and offset across the narrow band with a constant limb length would be constant. However, toward the competent layers where ϕ approached 90° and exceeded ϕ_k , there would be compression across the rotated foliation, whereas where the band was oblique and ϕ was less than ϕ_k , there would be dilation.

With further external compression the band would respond in different ways in the regions of compression and dilation across the internal foliation. Where there was compression, slip and hence rotation was hindered and the band accomplished shortening and offset by outward migration of the boundaries, but little increase in deviation. In contrast, in the dilated region strain was accomplished mainly by rotation and the band remained narrow (Fig. 7b).

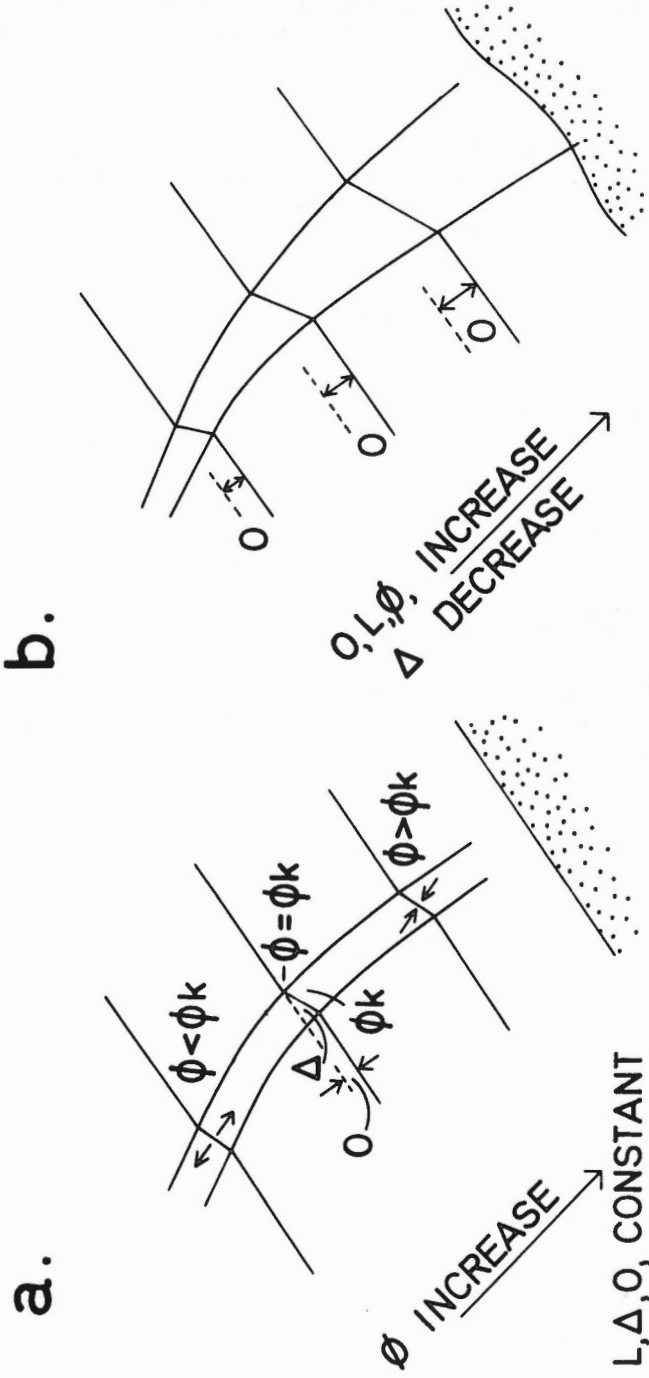


Figure 7. Growth model for kink band development.

- a. Initial very narrow kink band, curvature exaggerated; small arrows indicate internal compression and dilation.
- b. Subsequent band after lateral migration of boundaries where $\phi > \phi_k$ and internal rotation where $\phi < \phi_k$

Finally, secondary narrow bands would develop along the bounding surfaces, that is along the kink fold hinges, where, regardless of ϕ and ϕ_k relations, there would be local dilation. Possibly late strike-slip movements, as indicated by the single fault, increased the internal rotation of some kink bands.

The mechanism does not account for the increased shortening and offset for the wider, less rotated parts of bands. Possibly local reorientation of the compressive stress more closely parallel to the competent layers resulted in a larger component effective for layer shortening.

REFERENCES

Anderson, T. B.

1968: The geometry of a natural orthorhombic system of kink bands; see this report, pp.

Dewey, J. F.

1965: Nature and origin of kink bands; Tectonophysics, vol. 1, pp. 459-494.

Fyson, W. K.

1966: Structures in the Lower Paleozoic Meguma Group, Nova Scotia; Bull. Geol. Soc. Am., vol. 77, pp. 931-944.

Paterson, M. S., and Weiss, L. E.

1966: Experimental deformation and folding in phyllite; Bull. Geol. Soc. Am., vol. 77, pp. 343-374.

Weiss, L. E.

1968: Flexural-slip folding of foliated model materials; see this report, pp.

DISCUSSION

See General Session.

EXPERIMENTAL STUDY OF KINK-BAND DEVELOPMENT
IN MARTINSBURG SLATE

F. A. Donath
Department of Geology, University of Illinois
Urbana, Illinois

Abstract

Compression at low angles to well-developed planar anisotropy may cause slip on the anisotropy and instability that results in the formation of a kink band. Kink bands formed in slate at relatively low confining pressures (e. g. , between 800 and 2,000 bars) are a brittle phenomenon, and represent externally rotated foliation segments of constant length that are bounded by kink planes of fixed position. Initially straight and parallel kink planes remain straight and parallel during continued compression, but tend to approach one another because of rotation of the foliation segments between them. This rotation is caused by slip on the cleavage within the kink band and continues until the orientation is such that slip is no longer possible. Further deformation causes faulting parallel to the kink band boundaries, produces new kink bands, or results in the thinning (stretching) of foliation segments within the original kink band.

Although the angle defined by the kink plane and the cleavage within the kink band may vary widely (91 to 52 degrees), the angle between the kink plane and the cleavage outside the kink band remains reasonably constant (mean value, 68.4 degrees). The inclination of the kink planes appears to be independent of confining pressure, total strain, and strain history; the mean value determined from this study is 47.5 degrees to the direction of maximum compression.

In some instances two narrow kink bands form sufficiently close to one another that, following complete rotation of the foliation segments within them, further deformation causes the foliation segments between these initial kink bands to rotate to the same "limiting" inclination, thus forming a compound kink (or deformation) band. These events in the strain history of the specimen are reflected in the stress-strain curves.

INTRODUCTION

General Remarks

Recent experimental work indicates that the modes of deformation in strongly anisotropic rock are related to the inclination of anisotropy to the direction of maximum compression (σ_1), as well as to the environmental conditions at the time of deformation (see Donath, 1961; 1964a; 1968). Specimens of slate cored at 15 degrees to the cleavage almost invariably develop kink bands at the higher confining pressures (1,000 bars and above) when deformed several per cent beyond the yield point. Less frequently, kink bands form in the 30-degree orientation of slate, but

then only at high pressures (e. g. , 2,000 bars) in slate specimens that have high cohesion.

The observation that kink bands commonly develop in the 15-degree orientation of slate led to a more detailed study of the deformational behavior of this orientation, in general, and of the characteristic features of experimentally produced kink bands, in particular. The results of that study indicate that the formation of kink bands in slate is not caused solely by simple gliding on cleavage, but reflects the operation of several mechanisms - namely, gliding on cleavage accompanied by cataclasis, definition of kink planes along planes of high shear stress, and rotation of the foliation segments between the kink planes, with slip, cataclasis, and dilatation all occurring within the kink band. The evidence on which these conclusions are based is discussed fully in another paper (Donath, 1968). The study presented here is an extension of the earlier work, and deals with certain more complex relationships encountered in the experimentally produced kink bands.

Test Apparatus and Procedure

Specimen material and preparation

All specimens used for the present study were of the 15-degree orientation. These were obtained from a single block of Martinsburg slate (Ordovician; Bangor, Pennsylvania) which is a dark gray, massive slate with a well developed slaty cleavage. A preferred crystallographic orientation of platy minerals (muscovite and chlorite) and shape orientation of quartz grains exists in the slate. The platy minerals define the slaty cleavage. The quartz grains tend to lie parallel to one another in this foliation, and are scattered uniformly throughout the rock, with a few rare local concentrations of coarser quartz grains in lenses.

Test specimens were taken from the bulk material with a one-half inch diameter coring tool. The cores thus obtained were cut to lengths slightly greater than one inch, placed in the collet of a tool and cutter grinder, and the ends ground flat to form perfect right cylinders one-half inch in diameter by one inch in length. The dimensions of the finished cylinders were measured with a micrometer and recorded.

Test apparatus

The test apparatus used in the study is shown in Figure 1. The press consists of two construction steel U-channels held together by cylindrical tie rods. A 50-ton ram is mounted in a hole centered in the upper channel between each pair of tie rods; a load cell for force measurement is attached to each ram. During a test the load cell is mechanically linked to the piston of the pressure vessel by a cylindrical piece of hardened steel placed between them.

The test specimen is placed between mild steel spacers and inserted in a jacket made of annealed copper tubing; a hardened steel piston and anvil are then inserted in opposite ends of the jacket to form the piston-specimen assembly. The assembly is protected from the confining pressure medium by o-rings mounted near

the ends of the piston and anvil, respectively, which seal against the inside of the jacket. Because the copper is thin (0.008") and annealed, no strength correction is required for the minute axial load sustained by the jacket. The piston-specimen assembly is inserted in the pressure vessel, pressure seals and end plugs are emplaced, and the pressure vessel is positioned in the press.

The change in length of the specimen is calculated from the displacement of the piston into the vessel, which, in turn, is determined from the movement of the ram piston relative to the vessel body. The displacement is measured with a linear variable differential transformer. The measured displacement consists of the elastic distortion of the apparatus as well as shortening of the specimen. The apparatus distortion was determined for different confining pressures and axial loads, and was subtracted in the data reduction procedure.

A hydraulic pump was used to actuate the ram and produce axial load; confining pressure was also produced with a hydraulic pump. Kerosene was used as the confining pressure medium, and the confining pressure was held constant throughout a test. All tests were compression tests run at room temperature and at a strain rate of about 0.36×10^{-3} per second.

Data reduction

The electrical outputs of the displacement gauge and the load cell were fed into separate channels of an x-y recorder to provide a continuous record of load versus displacement. Because the raw data thus obtained had to be corrected for changes in cross-sectional area of the specimen and elastic distortion of the apparatus to give true axial stress and specimen strain, points had to be picked from the load-displacement record for data reduction. These points were picked sufficiently closely that the straight line segments connecting them adequately represented the basic curve.

Equations for the reduction of data have been written into a program for the IBM 7094 computer. The output from this program gives the specimen length, per cent strain, differential stress, and axial stress for each of the picked points. It also provides a continuous plot of differential stress versus strain for the test. The differential stress is equal to the axial stress minus the confining pressure; the strain is given as the per cent shortening relative to the original length of the specimen.

Method of specimen study

Test specimens were photographed in their copper jackets after a test to provide a visual record of the mode of deformation for any specimen damaged during jacket removal or subsequent handling. Next, the copper jacket was carefully cut through along its entire length on opposite sides and the upper half cautiously removed. The deformed specimen was then photographed unjacketed.

Angular relationships and kink-band widths generally were measured on 10 to 1 enlargements of the specimens, although thin sections were made of several specimens to permit detailed study. Measurement of foliation-segment lengths within

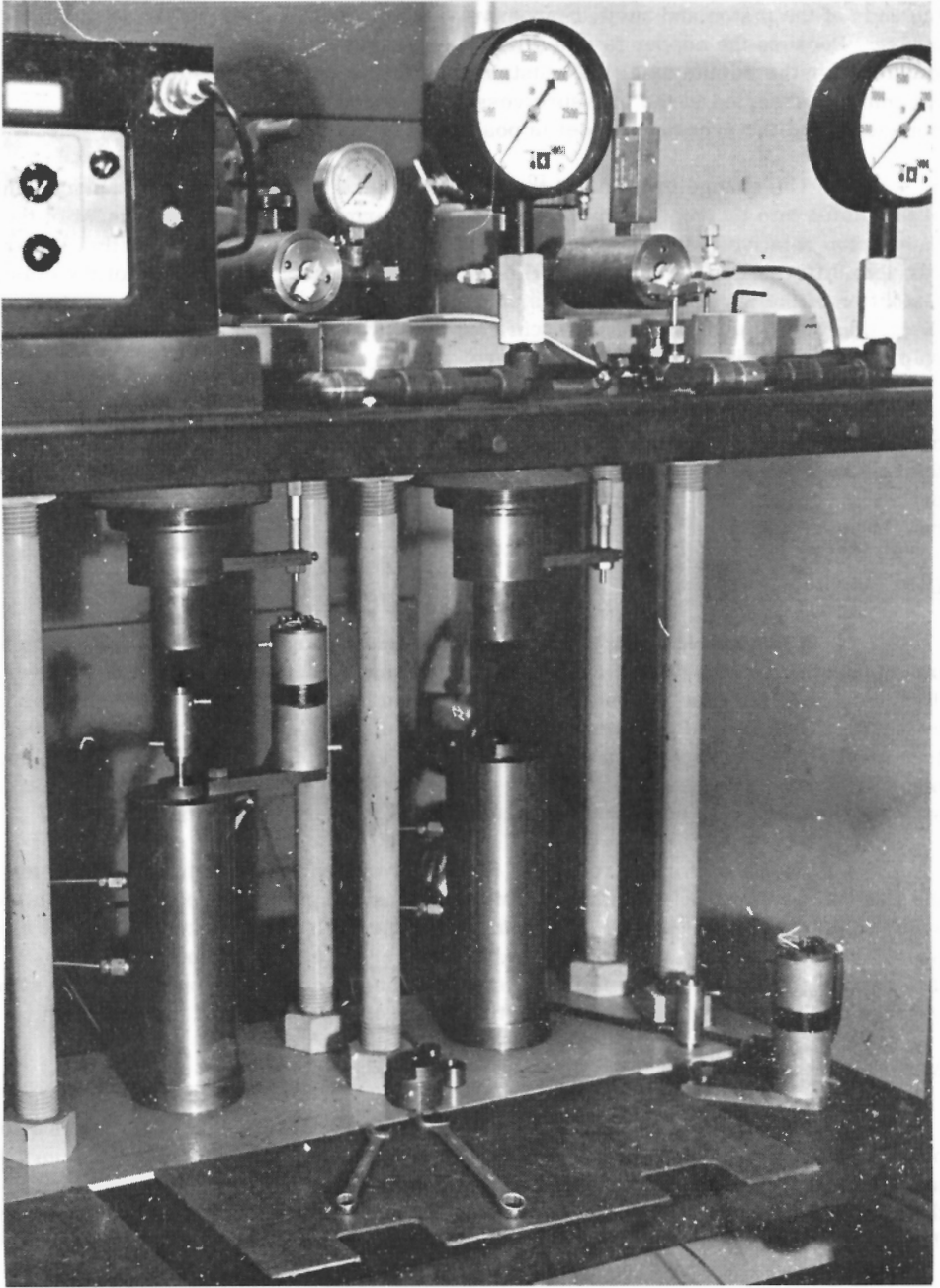


Figure 1. Test apparatus. Vessel at left, in place, ready for testing

the kink bands could readily be made to 0.1 mm, and angular measurements could be reproduced within a couple of degrees for all but very poorly defined features.

Strength Relationships

The block of slate used in this study is characterized by a high yield strength relative to blocks used in previous work. Although the material of each of the blocks is macroscopically homogeneous and mineralogically identical, cohesion along the cleavage differs from one block to the next and affects both the strength and the mode of deformation.

Because the effects of confining pressure and anisotropy orientation on the strength and mode of deformation in slate have been summarized elsewhere and the results of this study are consistent with previous conclusions, these effects will not be treated in detail in this paper. Instead, the discussion will deal primarily with certain more complex relationships observed in this study of experimentally produced kink bands in Martinsburg slate.

Twenty-seven tests were run in this test series. One was not valid because the copper jacket leaked and the effective confining pressure (total pressure minus pore pressure) was therefore much lower than the nominal confining pressure. Tests were run at confining pressures between 1,000 and 2,000 bars, at 200-bar intervals.

The yield stress is plotted as a function of confining pressure in Figure 2 for the block of slate used in this study. In principle, the yield stress is that differential stress which, if exceeded, will result in permanent deformation. Most of the stress-strain curves obtained for the 15-degree orientation of slate show a steep, linear initial slope followed by an abrupt loss of resistance to differential stress (see, e.g., Fig. 12). The stress drop occurs at the point at which gliding on the cleavage is initiated, designated the faulting point. Thus, the faulting point and the yield point coincide for most tests. However, the faulting point does not always coincide with the yield point, as permanent deformation may take place before faulting actually occurs. For purposes of this study the faulting point (or point at which slip is initiated) is taken to be the yield point, as this is a well-defined and easily picked event.

For most tests the yield stress, as here defined, also represents the ultimate strength of the rock, i.e., the maximum differential stress that can be sustained under the conditions of deformation. In several instances the differential stress sustained by the specimen subsequent to faulting was equal to or exceeded the yield stress (see Figs. 12 and 18). As seen in Figure 2, the ultimate strength for this block of slate increases linearly with confining pressure from 1,000 to 2,000 bars, but the yield stress (stress at the faulting point) tends to fall off this linear trend at the higher pressures.

The stress-strain curves presented have not been "smoothed", and consist of the straight-line segments connecting stress-strain values derived from all maxima, minima, inflection points, and other significant events on the original load-displacement records. The curves adequately represent the true stress-strain relationships.

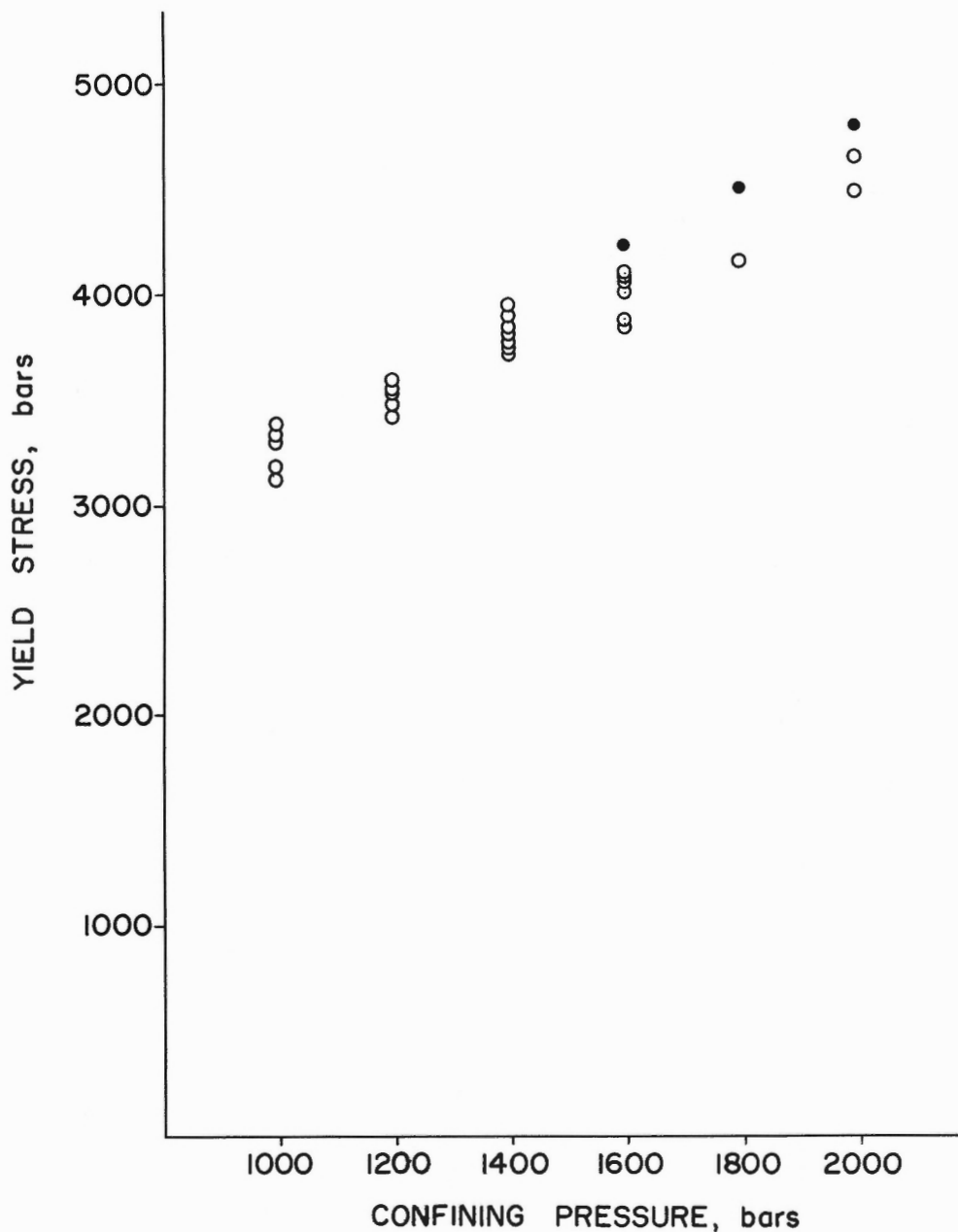


Figure 2. Yield stress versus confining pressure for 15-degree specimens of Martinsburg slate used in this study. Open circles are for tests in which ultimate strength and yield stress were identical; solid circles indicate ultimate strength beyond the yield point

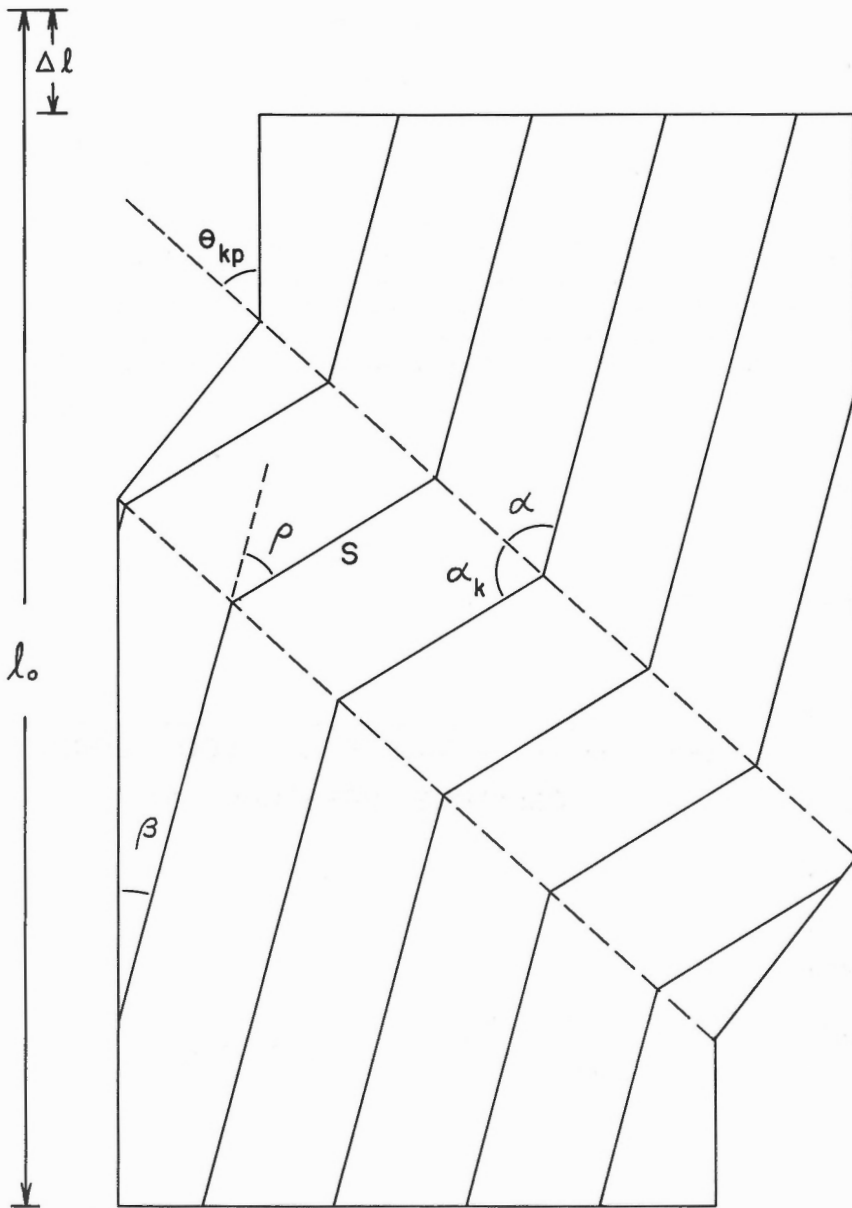


Figure 3. Geometry of ideal kink band in strongly anisotropic material

KINK BAND CHARACTERISTICS

Inclination of Kink Planes

Figure 3 shows the ideal geometry of a kink band. An initial right circular cylinder of material characterized by well-developed planar anisotropy and of original length l_0 has been shortened by an amount Δl . This shortening has produced two kink planes inclined at an angle θ_{kp} to the direction of maximum compression. The attitude of the anisotropy across these kink planes changes abruptly, and the area between them constitutes a kink band. The anisotropy within the kink band, initially oriented at an angle β to the direction of maximum compression, now is inclined at an angle $(\beta + \rho)$. The anisotropy outside the kink band makes an angle α with the kink plane; within the kink band the anisotropy and the kink plane define an angle α_k . Because of the possible

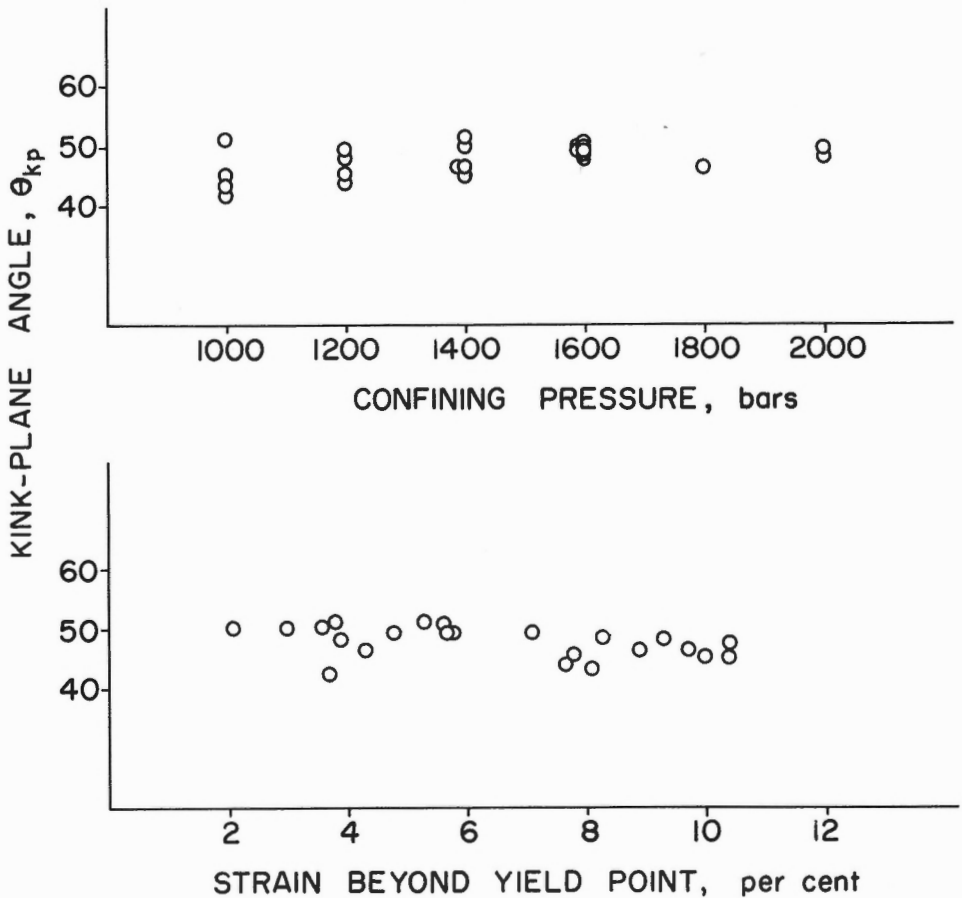


Figure 4. Kink-plane inclination to direction of maximum compression versus confining pressure and strain beyond the yield point

variation in the angle α_k , a more characteristic dimension of the kink band than its perpendicular width is the length of the foliation segment between the two kink planes, here designated S.

The inclination of all kink bands formed in this test series is plotted in Figure 4 as a function of confining pressure and strain beyond the yield point, respectively. Because the measured values of the two kink planes bounding each observed kink band were nearly always within two or three degrees of one another, the average of the two planes for each specimen is plotted in Figure 4.

The kink bands are all inclined between 42 and 51 degrees to the direction of maximum compression, with a mean inclination of 47.5 degrees – virtually identical to the mean inclination of 47.4 degrees determined from previous work (Donath, 1968). There appears to be more deviation from the mean inclination at the lower pressures, but the inclination of kink planes to the direction of maximum compression appears to be quite independent of confining pressure. Similarly, no systematic variation in the kink-plane inclination is observed as a function of strain beyond the yield point. The observed lack of effect of either confining pressure or total strain on the inclination of the kink planes in this study confirms earlier observations.

Rotation of Foliation Segments

The inclination of the foliation segments within the kink bands increases with increasing deformation. Figure 5(a) shows three specimens that were deformed at 1,200 bars confining pressure to strains beyond the yield point of 5.5, 6.3, and 8.2 per cent, left to right, with corresponding inclinations of the foliation segments of 42, 47, and 55 degrees, respectively. The numerous light gray parallel lines of powdery material (gouge) on the surfaces of the specimens reflect the cataclasis that has occurred along discrete cleavage surfaces by gliding on the cleavage. The gouge is particularly well developed within the kink bands themselves – indicating that the number of active slip surfaces within the kink bands is appreciably greater than outside the bands – and along the kink-band boundaries, notably along the upper ends of the upper kink planes and along the lower ends of the lower kink planes bounding the kink bands.

Figure 5(b) shows a thin section (right) and photomicrograph enlargement (left) of a kink band developed in a specimen deformed at 800 bars confining pressure to 9.5 per cent strain beyond the yield point. Since the inclination of the cleavage, initially 15 degrees, is now 21 degrees outside the kink band, an external rotation of 6 degrees occurred during the initial slip on the cleavage. Within the kink band the foliation-segment inclination is 39 degrees, indicating that an external rotation of the foliation segments of 18 degrees occurred as a result of the kinking process.

Even in the earliest stages of the development of "brittle" kink bands in slate, evidence is present of cataclasis along the kink boundaries and of local loss of continuity across the kink planes. This is clearly seen at the upper end of the upper kink plane in the thin section shown in Figure 5(b), and can be observed at numerous other places along the kink plane (note arrow in photomicrograph).

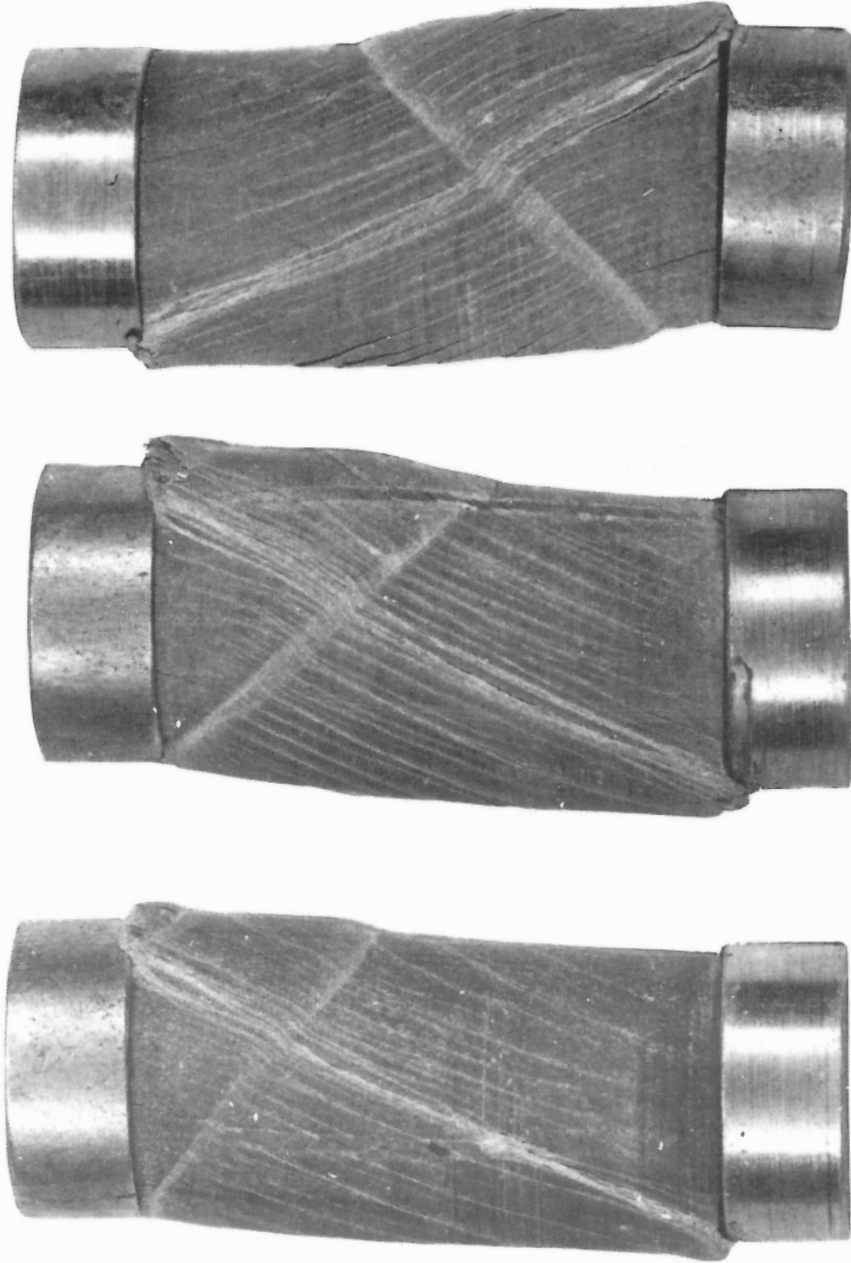


Figure 5 (a). Three 15-degree specimens deformed at 1,200 bars confining pressure to strains beyond the yield point of 5.5, 6.3, and 8.2 per cent, respectively. Corresponding foliation-segment inclinations are 42, 47, and 55 degrees

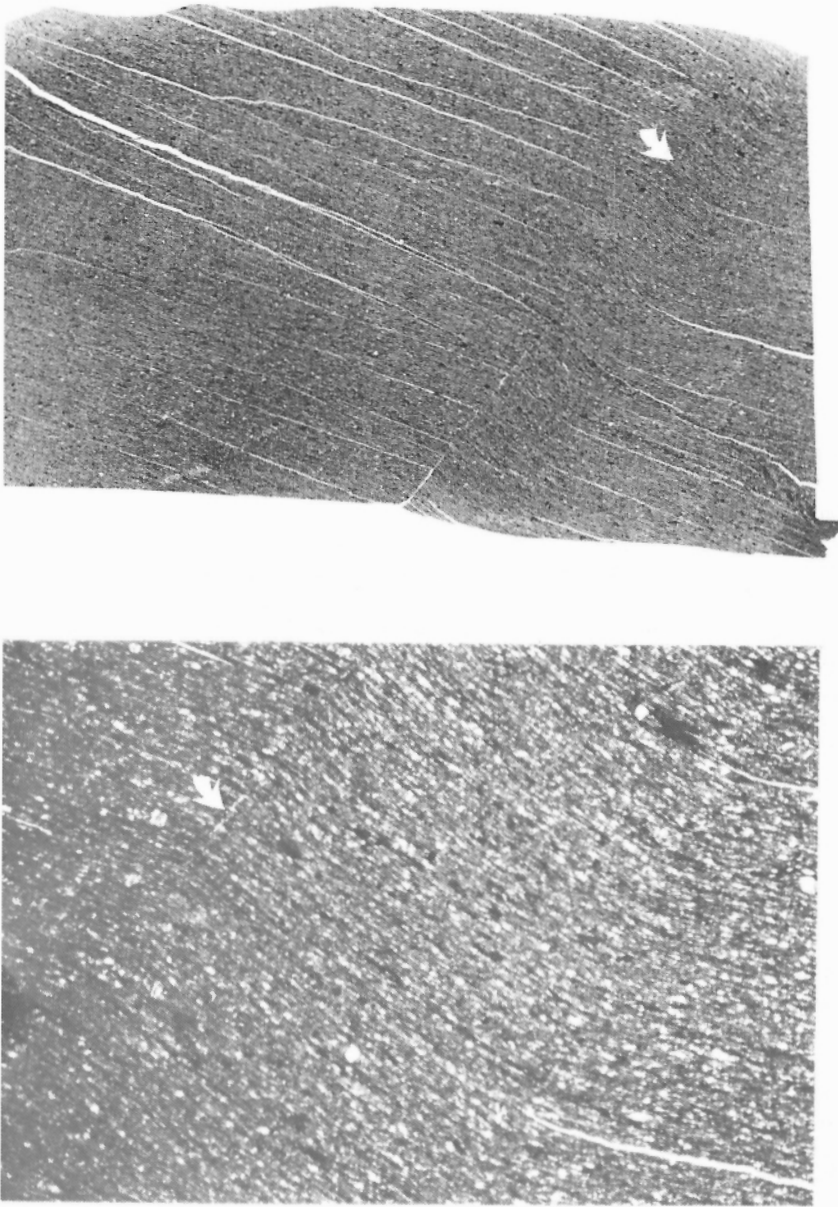


Figure 5 (b). Thin section (right) and photomicrograph (left) of specimen deformed 9.5 per cent strain beyond the yield point at 800 bars confining pressure. Foliation-segment inclination is 39 degrees. Arrows indicate corresponding points

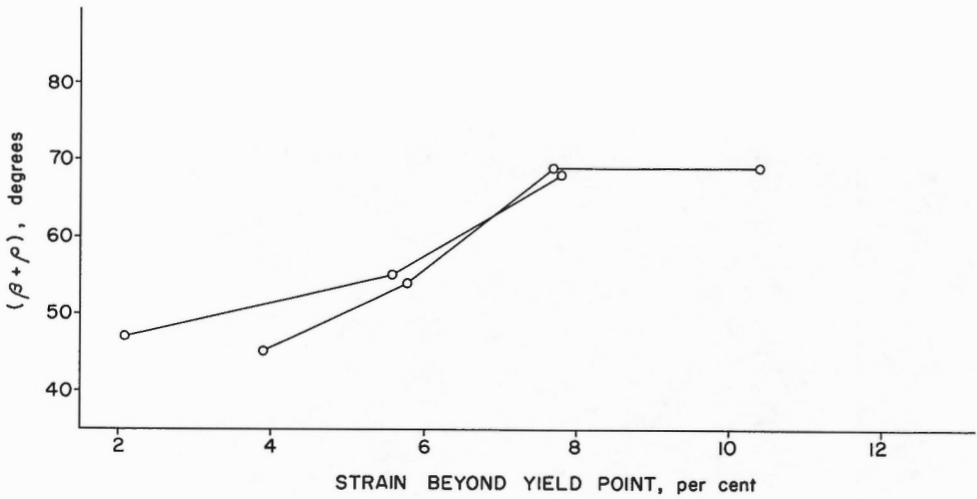


Figure 6. Inclination of kink-band foliation segments as function of increasing strain beyond the yield point. Four tests at 1,200 bars and three at 1,400 bars confining pressure

The data presented in Figure 6 are for four specimens deformed to increasingly higher strains at 1,200 bars confining pressure and for three specimens deformed to increasingly higher strains at 1,400 bars. As seen in this figure, the inclination of the foliation segments to the direction of maximum compression clearly increases as the strain beyond the yield point increases, for strains beyond the yield point of up to 8 per cent. The specimen deformed more than 8 per cent beyond the yield point shows no additional increase in the inclination of the foliation segments within the kink band.

If foliation segments within different kink bands show different inclinations, then one can expect the angle α_k defined by the kink plane and the foliation segment to differ from the angle α defined by the kink plane and the anisotropy outside the kink band, unless, of course, the kink-plane angle, θ_{kp} , varies correspondingly. However, we have noted that the angle θ_{kp} does not vary systematically with either confining pressure or total strain; it therefore should not affect the angles α_k and α . The relationship between α_k and α for the seven specimens referred to above is indicated in Figure 7. To simplify the diagram for purposes of illustration, the averages of the two values of α_k and α for each kink band were plotted. The points representing each confining pressure series, 1,200 bars and 1,400 bars, are connected by arrows showing the changes associated with increasing strain beyond the yield point. For both pressure series the angle α maintains a fairly constant value, but the angle α_k decreases systematically until it is equal to α .

The relationship between the angles α_k and α for all kink bands in this test series, in which accurate measurements could be made, is indicated in Figure 8 for both the upper and lower kink planes of each kink band. Although the angle between

the kink plane and the cleavage outside the kink band, α , remains reasonably constant (mean value of 68.4), the angle between the kink plane and the foliation segments within the kink band, α_k , varies systematically from 91 to 52 degrees. The points that lie above the 45-degree line designating equal angles represent relationships in those specimens that show relatively small inclinations of the foliation segments, and those below the line represent relationships for foliation segments that have been rotated to large inclinations to the direction of maximum compression.

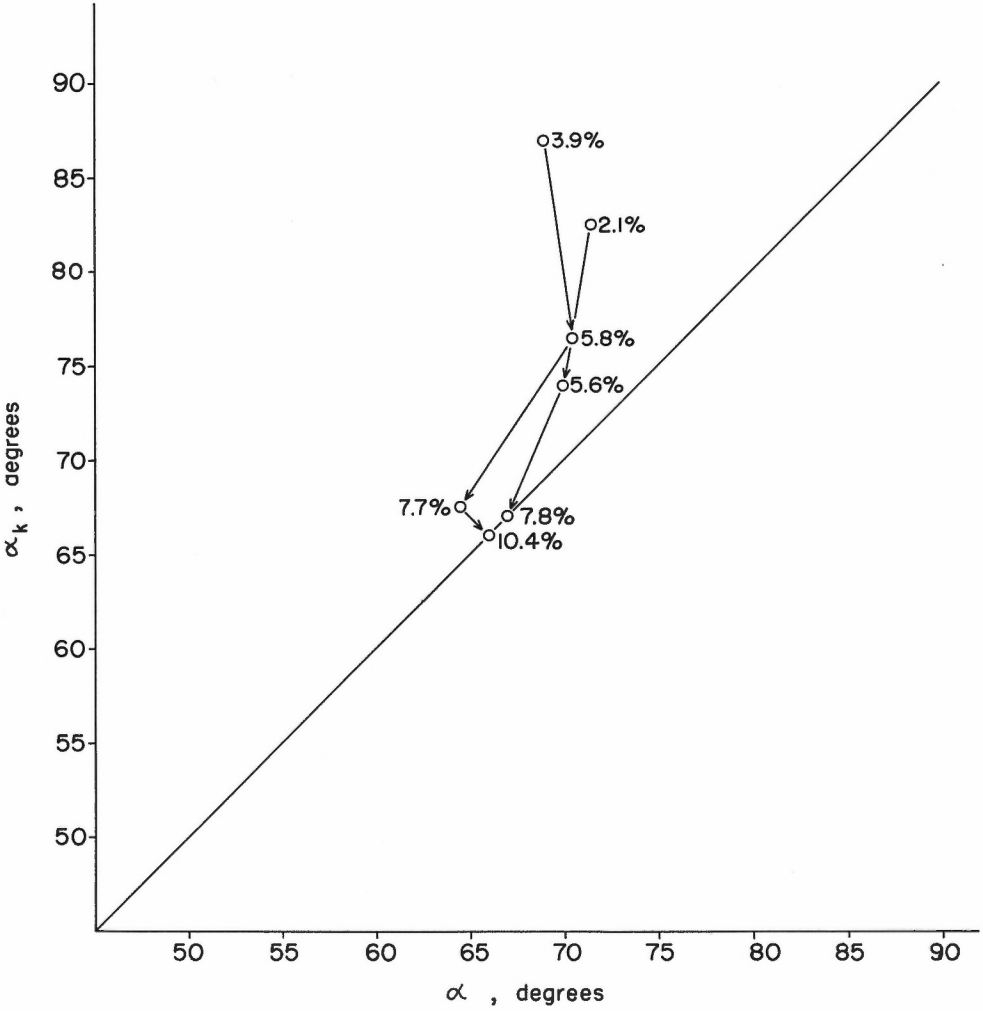


Figure 7. Angle between kink plane and cleavage within kink band versus angle between kink plane and cleavage outside kink band for progressive strain. Four tests at 1,200 bars and three at 1,400 bars confining pressure

If gliding on the cleavage were the sole mechanism of kink band formation in the Martinsburg slate, then this would require that the angle defined by the cleavage within and outside the kink band be divided symmetrically by the kink plane, i. e., α_k would have to equal α . For, if these angles were not equal, then the foliation thickness, measured between any two discrete cleavage planes outside the kink band, could not equal the corresponding thickness measured inside the kink band (refer to Fig. 3). When α_k is greater than α , the foliation thickness within the kink band must also be greater, implying that cataclasis, separation along the anisotropy, or some other mechanism has contributed to the deformation, in addition to simple gliding, to cause the dilatation. The greatest discrepancy in the foliation thickness before α_k equals α obviously occurs when the foliation segments within the kink band are perpendicular to the kink plane. For this condition, α_k equals 90 degrees and the angle of rotation of the cleavage within the kink band from its orientation outside the kink band, the angle ρ in Figure 3, is equal to $(90^\circ - \alpha)$.

The strain perpendicular to the foliation within the kink band can be expressed as:

$$\epsilon_f = (\sin \alpha_k / \sin \alpha) - 1. \quad (1)$$

Thus, the maximum strains represented by the relationships in Figure 8 are dilatation of 8.6 per cent ($\alpha = 67^\circ$, $\alpha_k = 91^\circ$) at one extreme, and a thinning of 13.1 per cent ($\alpha = 65^\circ$, $\alpha_k = 52^\circ$) at the other.

Figures 5, 7, and 8 show that the angle α_k does not always equal α in the kink bands developed in this test series of experimentally deformed Martinsburg slate. Therefore, simple gliding on the cleavage, by itself, cannot explain the development of these kink bands. The conclusion just drawn from results of this study are in complete accord with conclusions drawn previously (Donath, 1964b; 1968) - namely, that the development of kink bands in experimentally deformed slate reflects the operation of several mechanisms. These are gliding on cleavage accompanied by cataclasis, definition of kink planes along planes of high shear stress, and rotation of the foliation segments between the kink planes with slip, cataclasis, and dilatation all occurring within the kink band.

By the rotational mechanism outlined above and discussed in detail elsewhere, a systematic relationship should exist between the angle of rotation and the amount of strain beyond the point at which the kink band is initiated. Such a relationship is indicated by the test sequences represented in Figure 6. Previous work has shown that the kink band is initiated in the strain interval of steepest negative slope on the stress-strain curve (i. e., greatest stress drop in one per cent strain) immediately beyond the yield point. The kink bands previously studied had developed within less than 2 per cent strain beyond the yield point.

Figure 9 shows the inclination of the foliation segments to the direction of maximum compression ($\beta + \rho$), as a function of strain beyond the yield point for the specimens in this test series. The data indicate a general increase in rotation with increasing strain beyond the yield point, but there is no obvious systematic relationship. This is perhaps not too surprising since the rotation that occurs is related to

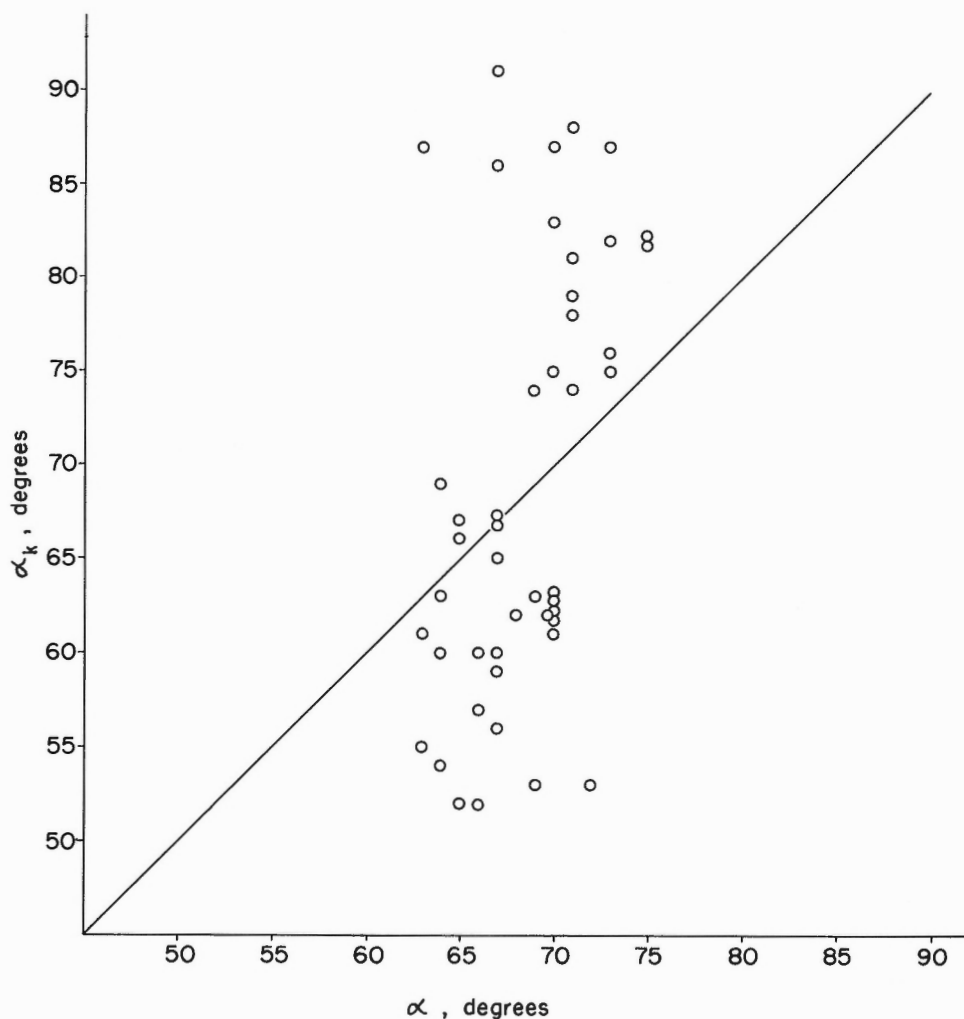


Figure 8. Angle between kink plane and cleavage within kink band versus angle between kink plane and cleavage outside kink band

the length of the foliation segment, S , as well as to the strain. The relationship can be expressed as follows:

$$\cos (\beta + \rho) = \cos \beta - \epsilon \epsilon_0 / S. \quad (2)$$

where ϵ is the longitudinal strain of the specimen produced by the kinking mechanism. Nevertheless, the curves for equation (2) do not fit the data of Figure 9 very well, as they had in previous work, thus suggesting that the strain owing to the rotational mechanism of kink band formation cannot be closely correlated with the strain beyond the yield point.

Kink-Band Width

Variation of the angle α_K makes the length of the foliation segment between the kink planes, S , a more characteristic dimension of the kink band than its perpendicular width, and this parameter is therefore used to represent kink-band "width".

Although previous work had suggested a possible dependence of foliation-segment length on confining pressure, no such relationship is indicated by the data of Figure 10. Whereas the earlier work had indicated no obvious relationship between the foliation-segment length and strain beyond yield point, the results of the present study suggest that there might be one (Fig. 11). Other apparent disagreements with previous conclusions were also encountered. For example, the longitudinal strain attributable to the rotational mechanism of kinking can be calculated from the relation:

$$\epsilon = S/\iota_o [\cos \beta - \cos (\beta + \rho)] \tag{3}$$

When solutions for equation (3) had been obtained for certain specimens on the basis of measurements of S , ι_o , β , and ρ in individual specimens of this test series, it was found that in some instances the value of strain thus obtained actually exceeded the total strain for the test. In earlier work the calculated strains showed excellent agreement with known strains from the stress-strain curves (Donath, 1968). The discrepancies cannot be explained by errors in measurement of foliation-segment length or the angles β and ρ ; thus, something is obviously quite different from the earlier test series for certain of these tests. The differences are clearly reflected in both the nature of the kink bands and in the corresponding stress-strain curves.

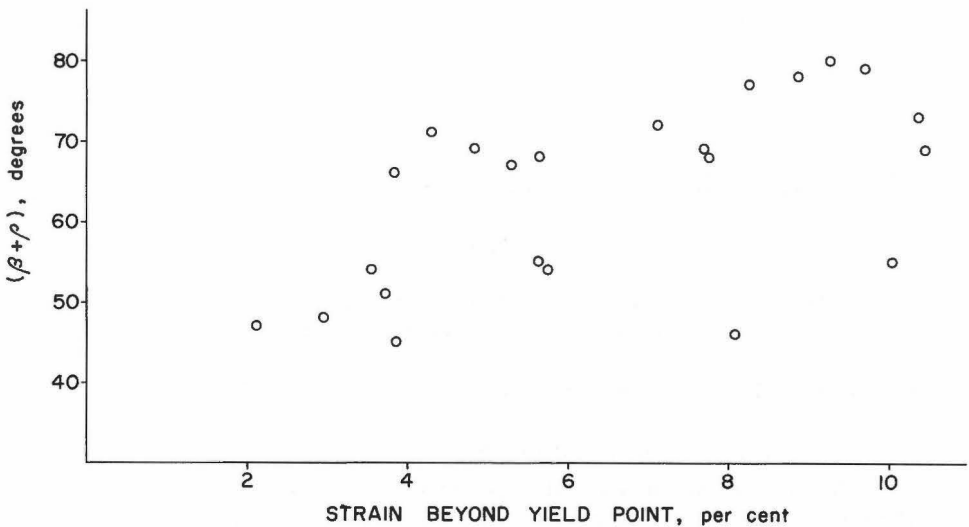


Figure 9. Inclination of kink-band foliation segments as a function of increasing strain beyond the yield point

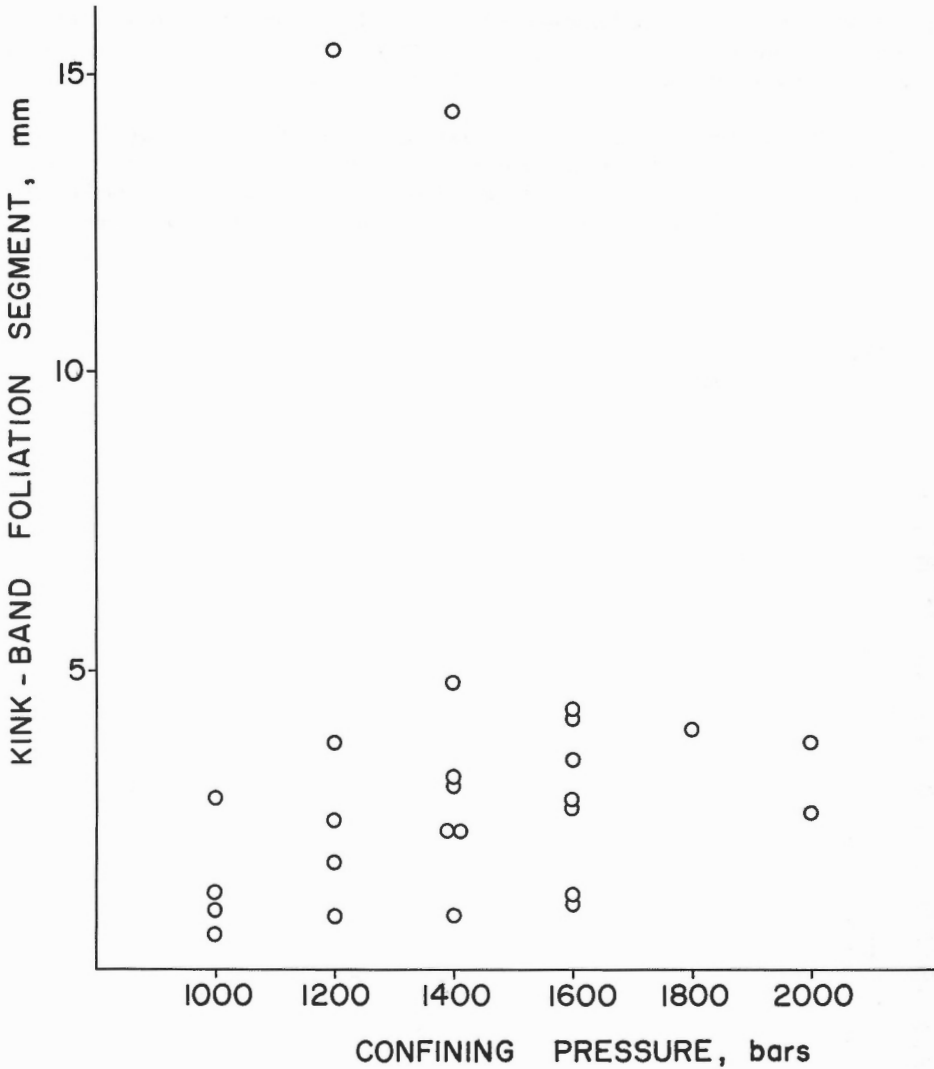


Figure 10. Foliation-segment length versus confining pressure

The stress-strain curves shown in Figure 12 are like those obtained in previous tests on the 15-degree orientation of Martinsburg slate. Following the initial, abrupt drop in differential stress that occurs with slip along the cleavage, there is increasing resistance to further deformation reflected by an increase in differential stress. This resistance has been caused by the formation of kink planes and the rotation of foliation segments between them, thereby "locking" the cleavage and preventing slip from occurring across the kink planes. Continued deformation

causes further rotation of the foliation segments, with slip occurring between them. The greater differential stress is required to attain the critical resolved shear stress necessary to cause slip on the cleavage within the kink band.

Three of the specimens corresponding to the curves in Figure 12 are shown in the upper half of Figure 13; the fourth is the 1,000-bar specimen at the far right of the lower half of Figure 13. These specimens, like their corresponding stress-strain curves, show the characteristic features of kink bands previously observed.

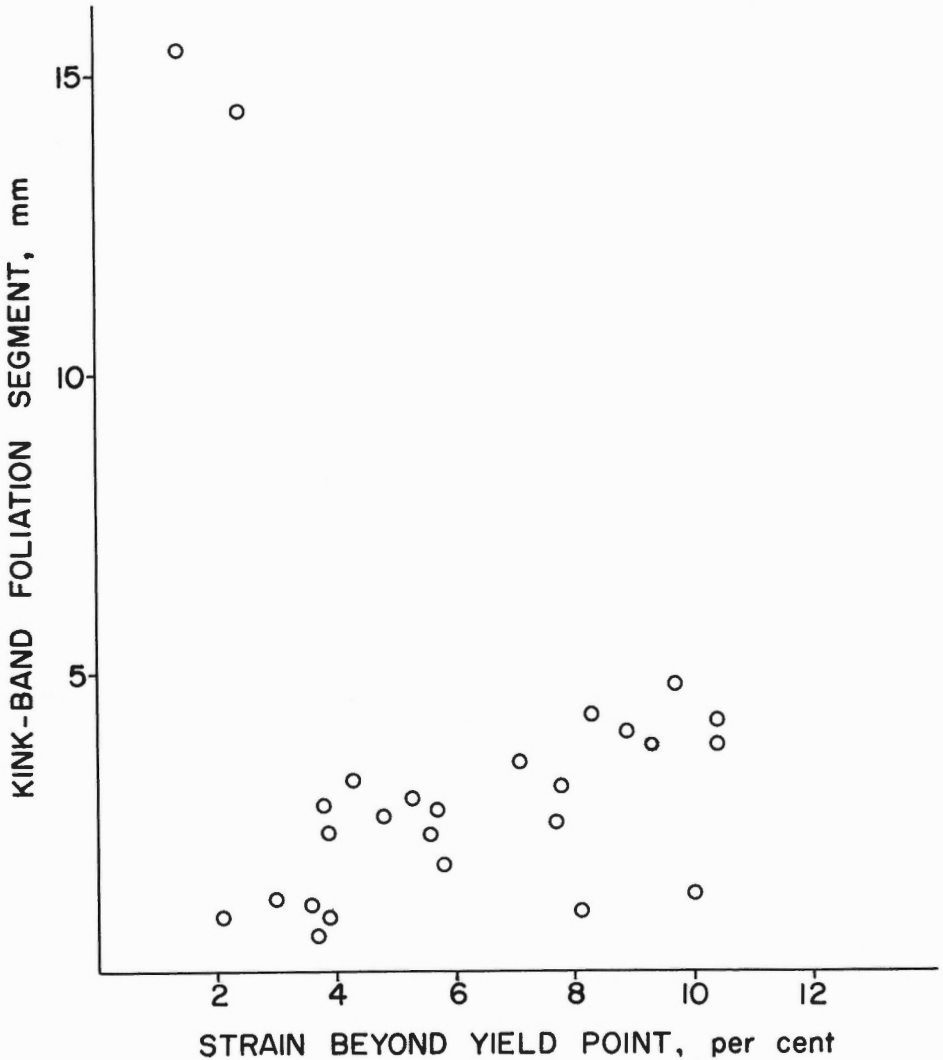


Figure 11. Foliation-segment length versus strain beyond the yield point

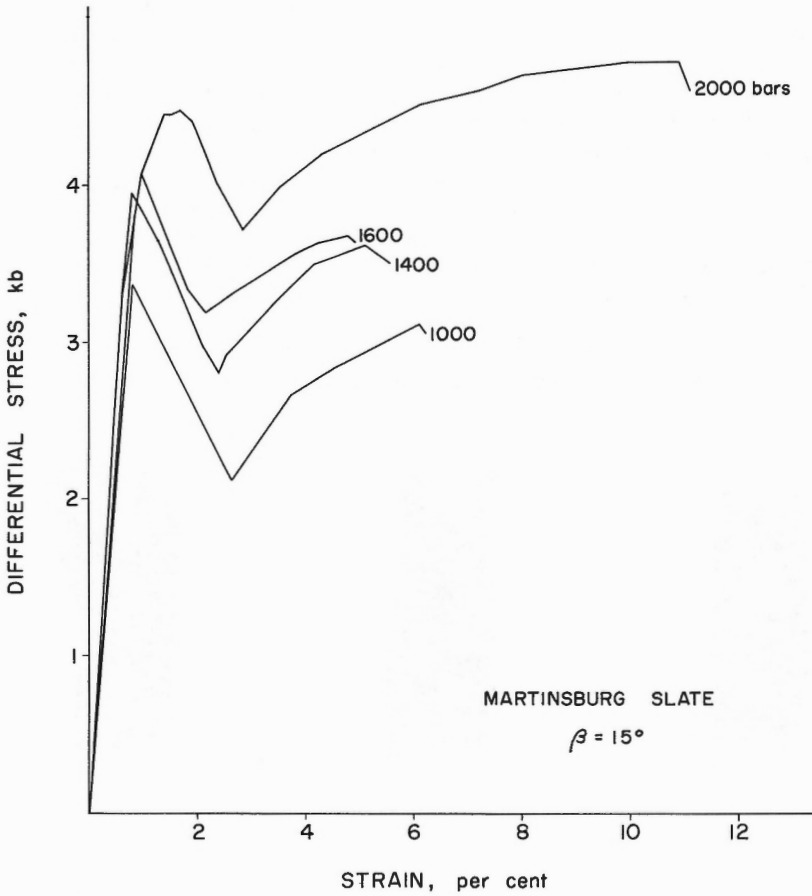


Figure 12. Stress-strain curves for several ideal "brittle" kink bands formed at different confining pressures

The three specimens shown in the lower half of Figure 13 were all deformed in this test series at 1,000 bars confining pressure. The stress-strain curves for these specimens are given in Figure 14. The curves are clearly very different. The specimen at the left (AN 10-17) and in the middle (AN 10-15) of Figure 13 (lower half) were deformed to total strains of 8.9 and 11.3 per cent, respectively (8.1 and 10.0 per cent beyond the yield point), as compared with 6.1 per cent (5.3 per cent beyond the yield point) for specimen AN 10-19 at the far right. The foliation-segment inclination within the kink band is 46 degrees for specimen AN 10-17 and 55 degrees for specimen AN 10-15, as compared with 67 degrees for specimen AN 10-19. The foliation-segment lengths are also narrower, 1.0 and 1.3 mm, respectively, as compared with 2.9 mm.

Previous work indicated that kink bands were initiated during slip on the cleavage when the strain rates were relatively high (0.3 per cent per second or greater) and sustained over a strain interval not less than 0.7 per cent. The strain interval of highest sustained strain rate is the steepest negative slope of the stress-strain curve beyond the yield point. If the earlier results can be applied here, then the kink bands in specimens AN 10-17 and AN 10-15 were initiated at strains far beyond the yield point, and they were subjected to very little additional strain following their formation. This conclusion is, in fact, supported by the small (and incomplete) rotation of the foliation segments, and by the evidence in these two specimens of a greater amount of slip on cleavage throughout the specimen as reflected by the large number of cleavage surfaces having gouge along them.

The preceding comments would suggest that the strain attributable to the rotational mechanism of kink band formation might be more closely correlated with the

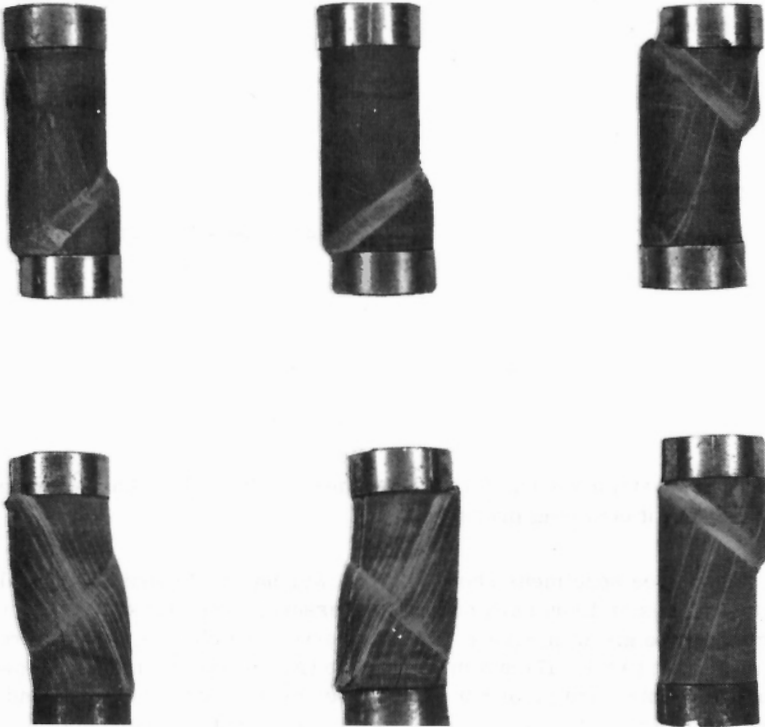


Figure 13. (Upper) Kink bands formed at 1,400, 1,600 and 2,000 bars (left to right) (Lower) Kink bands formed at 1,000 bars confining pressure. Foliation-segment inclinations are (left to right) 46, 55, and 67 degrees at strains beyond the yield point of 8.1, 10.0, and 5.3 per cent

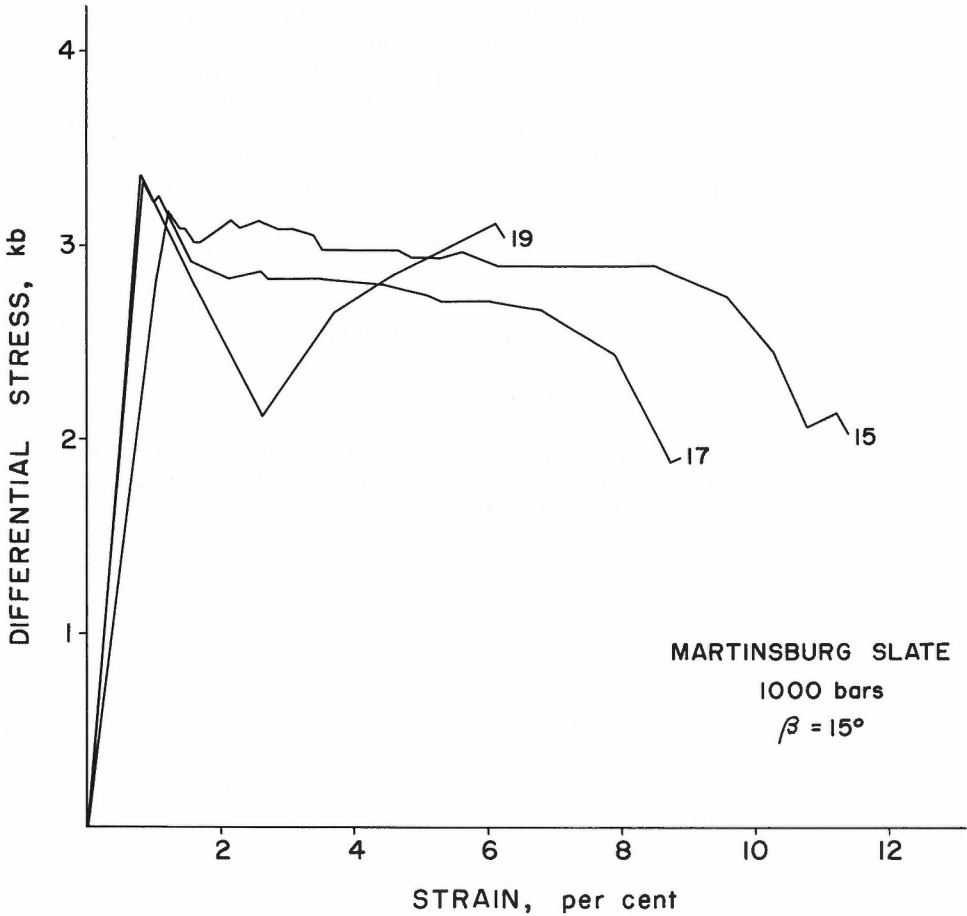


Figure 14. Stress-strain curves for specimens shown in lower half of Figure 13

strain beyond the minimum point of the stress-strain curve, i. e. , the point at the foot of the longest negative slope of the curve. If this were so, then the rotation of the foliation segments within the kink band should also correlate with the strain beyond this point.

Figure 15 is a plot of the foliation-segment inclination, $(\beta + \rho)$, versus strain beyond the minimum point. The curves representing equation (3) for foliation-segment lengths of 1, 2, and 3 mm and a cleavage inclination of 19 degrees immediately preceding initiation of the kink are also shown in Figure 15. (The value of β equal to 19 degrees assumes that 4 degrees of external rotation occurred as a result of the initial slip on cleavage prior to kinking). The observed data are separated into three groups according to foliation-segment lengths, and appear to be in good general agreement with the theoretical curves. If a kink band having foliation segments 1 mm long

were initiated precisely at the minimum point and developed entirely by the rotational mechanism, then the data point for that particular kink band would fall on the 1 mm curve for its respective strain and foliation-segment inclination. The distance the point lies away from the curve, parallel to the abscissa of the graph, is a measure of the strain that has taken place between the point of initiation of the kink band and the minimum point of the stress-strain curve. Because all but two of the points lie to the left of their corresponding theoretical curves, it means that the kink bands were initiated before the minimum point was reached. The two exceptions are very narrow kink bands with low foliation-segment inclinations; the possibility of error in measurement is greatest in this type.

KINK BAND DEVELOPMENT

Ideal "Brittle" Kink Bands

Although the development of ideal "brittle" kink bands has been discussed at length elsewhere (Donath, 1968) and referred to in parts of preceding sections, it might be well to summarize briefly here the sequence of development and supporting

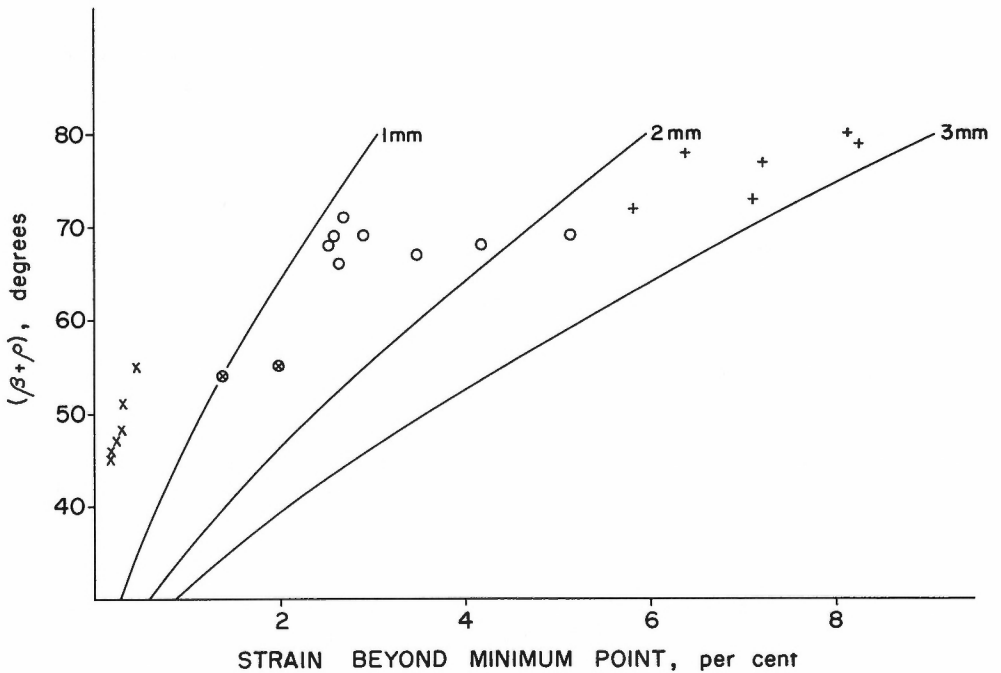


Figure 15. Inclination of kink-band foliation segments as a function of increasing strain beyond the minimum point. Symbols indicate foliation-segment lengths: x = 0.6 - 1.3 mm, o = 2.5 - 3.2 mm, + = 3.5 - 4.8 mm

lines of evidence. The term "brittle" is here applied to those kink bands which develop in strongly anisotropic rock, such as slate, that undergo faulting or slip on the anisotropy with release of stored elastic strain energy before 2 per cent strain is reached. For the specimens of Martinsburg slate used in this test series, faulting or slip invariably occurred before 2 per cent strain, indicating the rock to be very brittle.

The initial deformation in the 15-degree orientation of slate is always gliding along the cleavage. The slip is accompanied by loss of resistance to differential stress, and may be restricted to several closely spaced surfaces or distributed uniformly on numerous surfaces throughout the specimen. This initial deformation normally causes a 3 to 5 degree external rotation of the cleavage and the formation of gouge along the cleavage planes, owing to cataclasis.

Comparison of the calculated strain attributable to kinking (using measured kink-band characteristics and assuming the rotational mechanism) with actual stress-strain relationships for ideal brittle kink bands indicates that the kink bands develop in the strain interval represented by the steepest negative slope of the stress-strain curve. For deformation of a block of slate having lower strength and cohesion than that used in the present study, it was found that if a kink band were to form, the strain rate during slip on the cleavage generally had to exceed 0.3 per cent per second and had to be sustained over a strain interval not less than 0.7 per cent. For strain rates during slip less than 0.3 per cent per second sustained over strain intervals less than 0.4 per cent, the deformation was invariably characterized entirely by slip on the cleavage. The critical factor appears to be the amount of displacement that occurs during the gliding process. A kink band occasionally developed at slow strain rates if these rates were sustained over a sufficiently large strain interval. Unfortunately, the possible significance of strain rate was not recognized at the time the present study was undertaken, and the data were recorded on an x-y recorder rather than on a strip-chart recorder; thus, time was not a recorded variable.

Rapid simultaneous displacement along numerous cleavage planes over a finite strain interval apparently causes the instability that results in the initiation of a kink plane. The mean inclination of 47.5 degrees of kink planes to the direction of maximum compression suggests that they develop along or close to planes of maximum shear stress, which would be oriented at 45 degrees in isotropic material. However, the principal stress directions within the 15-degree orientation of the slate specimens are rotated, owing to the presence of the anisotropy and to slip along it, and the inclination of the kink planes to the direction of maximum compression at the moment of their inception is therefore less than 45 degrees. Failure resulting in the formation of the kink planes may occur along those surfaces that have the most favorable ratio of shear to normal stress, thus showing the effects of internal friction, as for the development of shear fractures in isotropic materials. The kink planes thus formed remain fixed in position (as well as in orientation) during continued deformation because of the cataclasis that occurs along them (see Fig. 5).

Rotation of the foliation segments between kink planes, once these planes have formed, is the typical response to further deformation. When the rotation progresses far enough it "locks" the cleavage, and slip across the kink planes is no

longer possible. Instead, slip occurs only on the cleavage within the kink band, and further deformation is effected by rotation of the foliation segments between the kink-band boundaries. Because of the rotation and increasing inclination of the foliation segments to the direction of maximum compression, increasingly larger loads are required to attain the critical resolved shear stress necessary for slip on the cleavage - hence, the rise in differential stress required to produce additional longitudinal strain. Rotation of the foliation segments continues until they reach a limiting orientation, beyond which slip on them is no longer possible because the resistance to gliding is greater than the resolved shear stress on the foliation segments. If the differential stress increases so as to cause further deformation, another kink band is initiated or faulting occurs along the kink-band boundaries, as evidenced by gouge at the boundaries and the loss of resistance to differential stress. The activation of a new mechanism, such as faulting or the development of secondary slip surfaces, can cause additional rotation of the foliation segments within the original kink band. The "limiting orientation" of foliation segments in the simple kink band, resulting from the rotational mechanism alone, appears to be between 60 and 65 degrees to the direction of maximum compression, in excellent agreement with previous data on the effects of planar anisotropy (Donath, 1961; 1964a).

Compound "Brittle" Kink Bands

The upper half of Figure 16 shows four specimens that were deformed at a confining pressure of 1,200 bars to strains beyond the yield point of 3.9, 5.8, 7.7, and 10.4 per cent, respectively. The corresponding foliation-segment inclinations measured for these specimens are 45, 54, 69, and 69 degrees; these values are plotted against strain beyond the yield point in Figure 6. The stress-strain curves are given in Figure 17.

The stress-strain curves of Figure 17 are quite different from those for the ideal "brittle" kink bands (Fig. 12). The strain interval between the yield point and the minimum point is quite large and characterized by numerous irregularities. Sustained steep negative slopes do not occur before about 4 per cent strain, suggesting that kink planes were not initiated until then and that about 3 per cent strain was produced by slip on the cleavage, a possibility that is strongly supported by the evidence of movement (gouge) along numerous cleavage surfaces throughout the specimens.

As with the stress-strain curves, the appearance of the specimens in this test sequence is quite unlike that of the more ideal "brittle" kink bands shown in Figure 13. The presence of gouge along numerous cleavage planes has been mentioned, but there is also considerable variation in the character of the individual kink bands. In specimen AN 10-11 (far left) the kink band is at a very early stage of development and appears to be quite narrow; the second specimen (AN 10-13), deformed 5.8 per cent beyond the yield point, shows complex relationships at the upper end; specimen AN 10-14 looks quite simple, but cataclasis appears to have been more active in narrow zones adjacent to the kink-band boundaries than within the central part of the kink band; and, the fourth specimen (AN 10-10), deformed 10.4 per cent beyond the yield point, shows zonation reflecting differing degrees of cataclasis within the kink band.

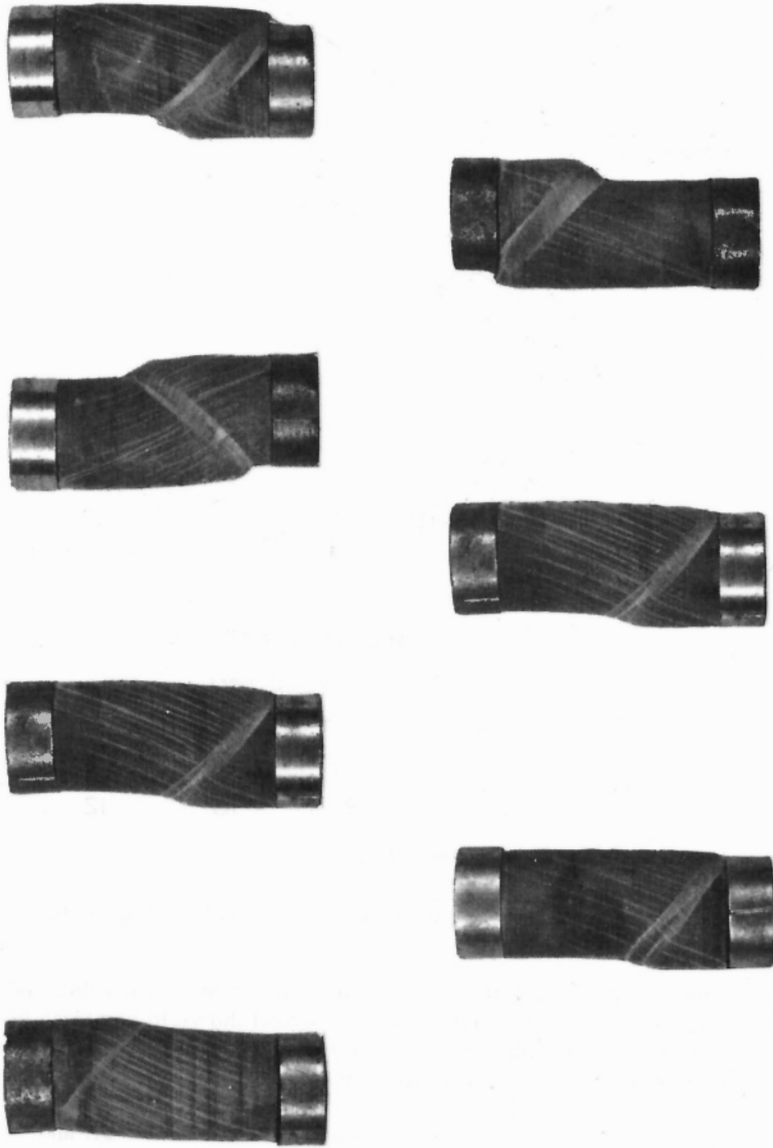


Figure 16. (Upper) Kink bands developed at 1,200 bars confining pressure at strains beyond the yield stress of 3.9, 5.8, 7.7, and 10.4 per cent (left to right) with corresponding foliation-segment inclinations of 45, 54, 69, and 69 degrees. (Lower) Kink bands developed at confining pressures of 1,400, 1,200, and 1,800 bars (left to right) and strains beyond the yield point of 3.9, 5.8, and 8.9 per cent

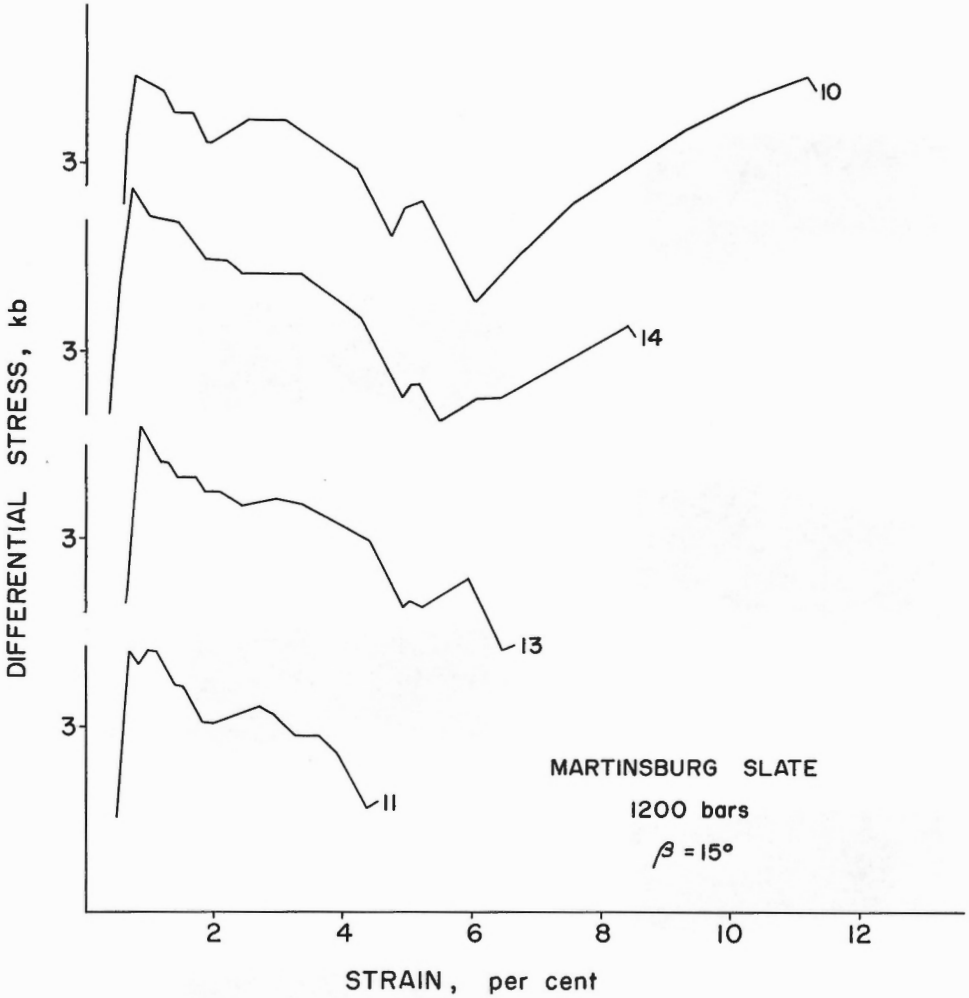


Figure 17. Stress-strain curves for specimens shown in upper half of Figure 16.

In view of these differences, it is interesting that a systematic relationship between the foliation-segment inclination and the strain beyond the yield point can be observed (Fig. 6). Apparently, the kink bands were initiated at about the same strain beyond the yield point, thus preserving the relationship.

The "irregularities" in the kink bands of specimens AN 10-13, 14, and 10, mentioned above, are matched by irregularities in the respective stress-strain curves. The curves are quite similar from the yield point down to the bottom of the long moderate-to-steep negative slope. Beyond this, the curves for specimens 13 and 10, and to a lesser degree, 14, begin to rise again before falling off along another steep

negative slope. This event on the stress-strain curve appears to be related to the development of another kink band. Specimens 14 and 10 were subjected to sufficient additional strain that the relationships are masked, but an earlier stage of development is seen in specimen 13.

Specimen AN 10-13 is shown again in the lower half (center) of Figure 16 along with specimens deformed at 1,400 bars (left) and 1,800 bars (right). The corresponding stress-strain curves are given in Figure 18. Note the similarity in the curves for the specimens at 1,400 bars and 1,800 bars up to the terminal point of the former; the 1,800-bar specimen has undergone 5.7 per cent more strain. Close

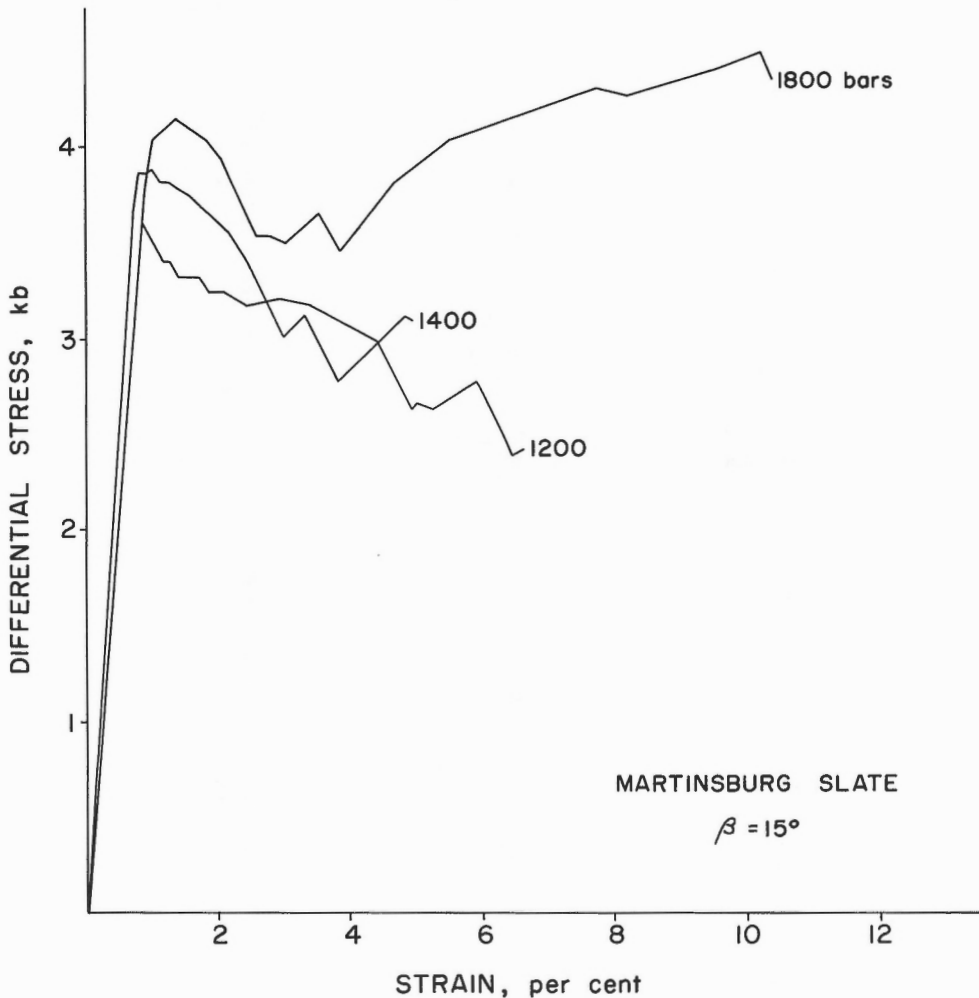


Figure 18. Stress-strain curves for specimens shown in lower half of Figure 16

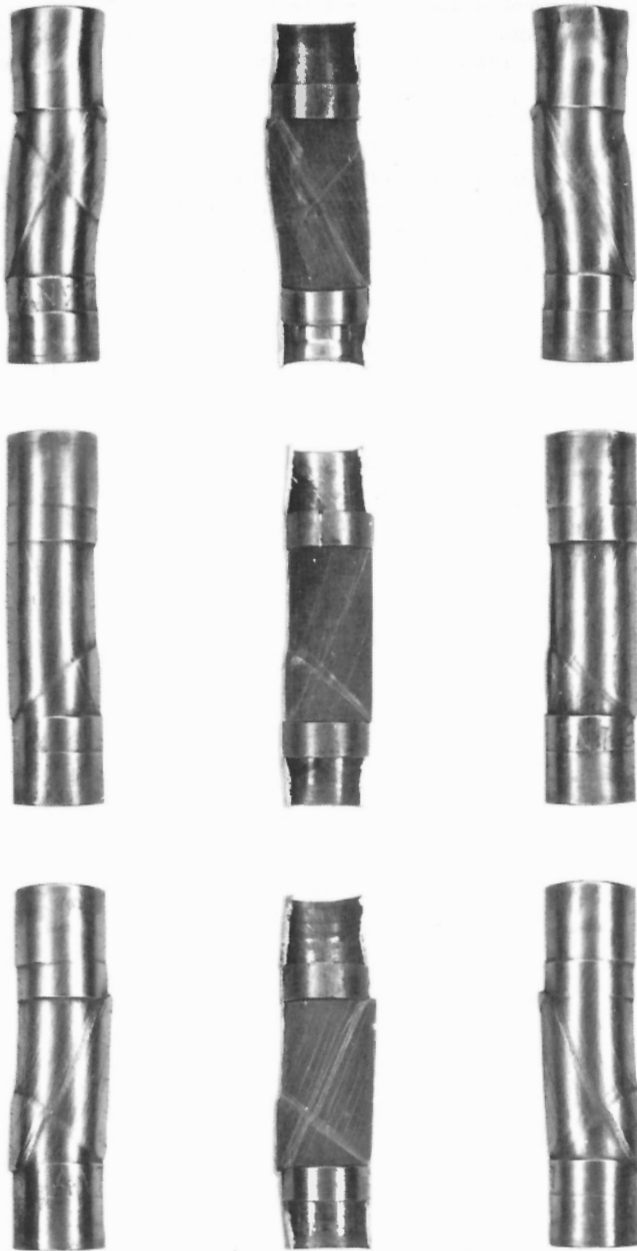


Figure 19. Kink bands developed in three specimens of slate deformed at 1,600 (top), 1,800 (middle), and 1,400 (bottom) bars confining pressure, respectively, at strains beyond the yield point of 6.5, 1.1, and 7.6 per cent

examination of the 1,800-bar specimen reveals that the kink band in it actually consists of two kink bands that have merged. Evidence of this is seen in the differing degrees of cataclasis within the band, and in the break in the "profile" of the kink band along the right side of the specimen. The kink band in this specimen appears to represent a later stage of development of the compound kink band seen in the 1,400-bar specimen. Specimen AN 10-13 has a more complex stress-strain curve and shows more complex relationships within the kink band; yet, it appears to approximate an intermediate stage of development between the other two.

In some instances, aspects of the strain history of the deformed specimen are better preserved in the copper jackets than in the relationships observed within the specimens themselves. Figure 19 shows three specimens, jacketed and unjacketed, that were deformed at confining pressures of 1,400, 1,600, and 1,800 bars. The unjacketed 1,600-bar specimen (top) shows two very narrow, almost incipient, kink bands that are only slightly separated. These are clearly reflected in the copper jacket, as seen at the right. On the back side of the jacketed specimen (left) the kinks are seen to merge. Two narrow and closely spaced kink bands are present also in the 1,800-bar specimen (center). The kink bands in this specimen are better developed, slightly wider, and are beginning to merge by involving the foliation segments between them. The kinks were initially separate and distinct, as shown by the jacketed specimen at the right. Again, in the 1,400-bar specimen (bottom) there is evidence of two initial narrow kink bands, shown clearly in the copper jacket at the right. In the unjacketed specimen the initial kink bands are seen to have almost totally involved the foliation segments between them to produce a single deformation band.

Figures 20 (a) and 20 (b) show jacketed and unjacketed views, a thin section, and a photomicrograph of a portion of the thin section for a specimen in which two initial kink bands are at an intermediate stage of merging. That two kink bands were initially present is clearly shown by the deformation in the copper jacket and the relationships observed in the thin section. Although the deformation had progressed to the point where the relationships at the surface of the specimen appear to be simple, the rotation of foliation segments between the initial kink bands was not complete. The thin section reveals the more complex relationships.

The different amounts of rotation that have occurred in different parts of the deformation band can be seen in the photomicrograph. The orientation of the cleavage outside the deformation band is seen in the upper left and lower right corners. The foliation segments within the lower kink band (just below the arrow) appear to have rotated to their "limiting" orientation, as have the foliation segments in the somewhat broader upper kink band. The foliation segments between the two kink bands have rotated approximately 10 degrees from the attitude of the cleavage outside the deformation band.

The specimen shown in Figures 20 (a) and 20 (b) also shows interesting end effects. Significant displacement was concentrated along several closely spaced cleavage surfaces prior to the development of the kink band, as shown by the relative offset at the upper left and lower right corners of the specimen. The restrictions to further displacement along these surfaces provided by the jacketing conditions at the

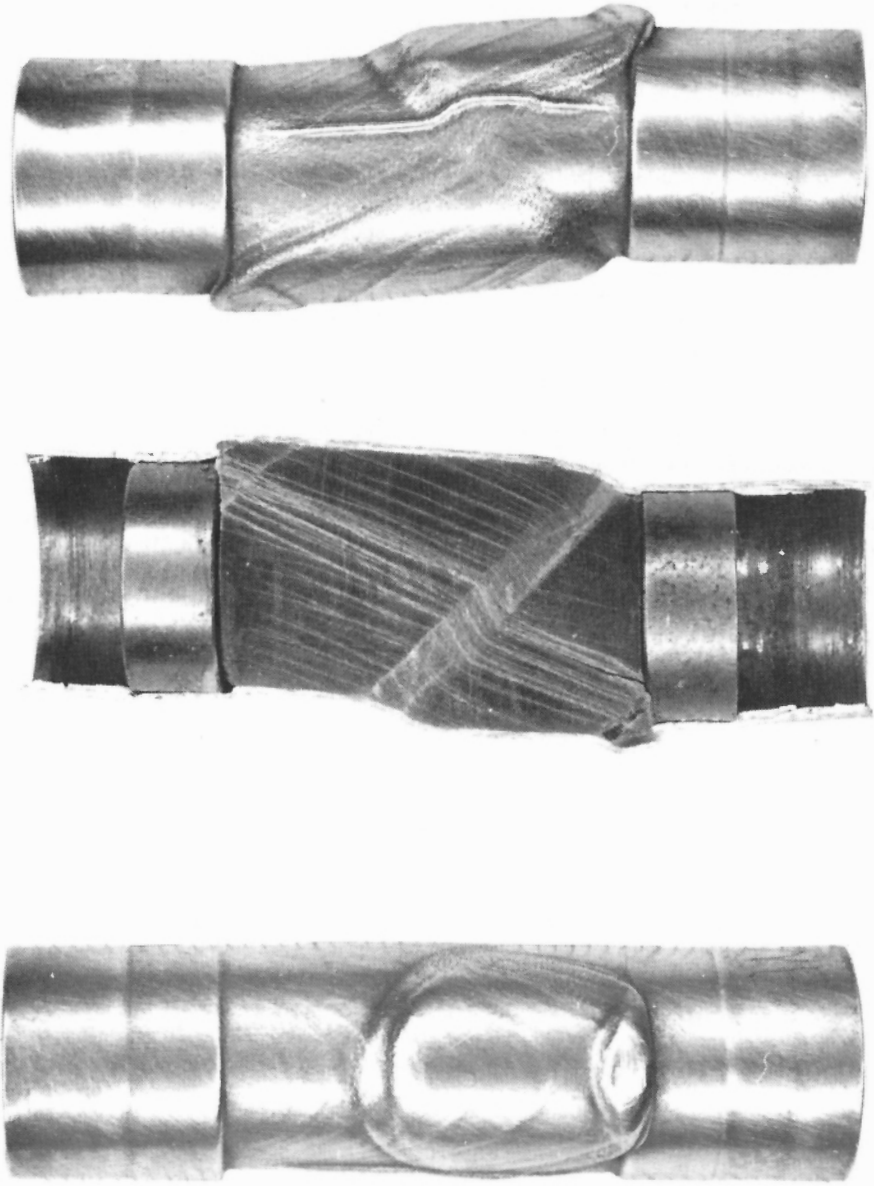


Figure 20 (a). Three views of specimen deformed at 1,200 bars confining pressure to strain beyond the yield point of 12.3 per cent

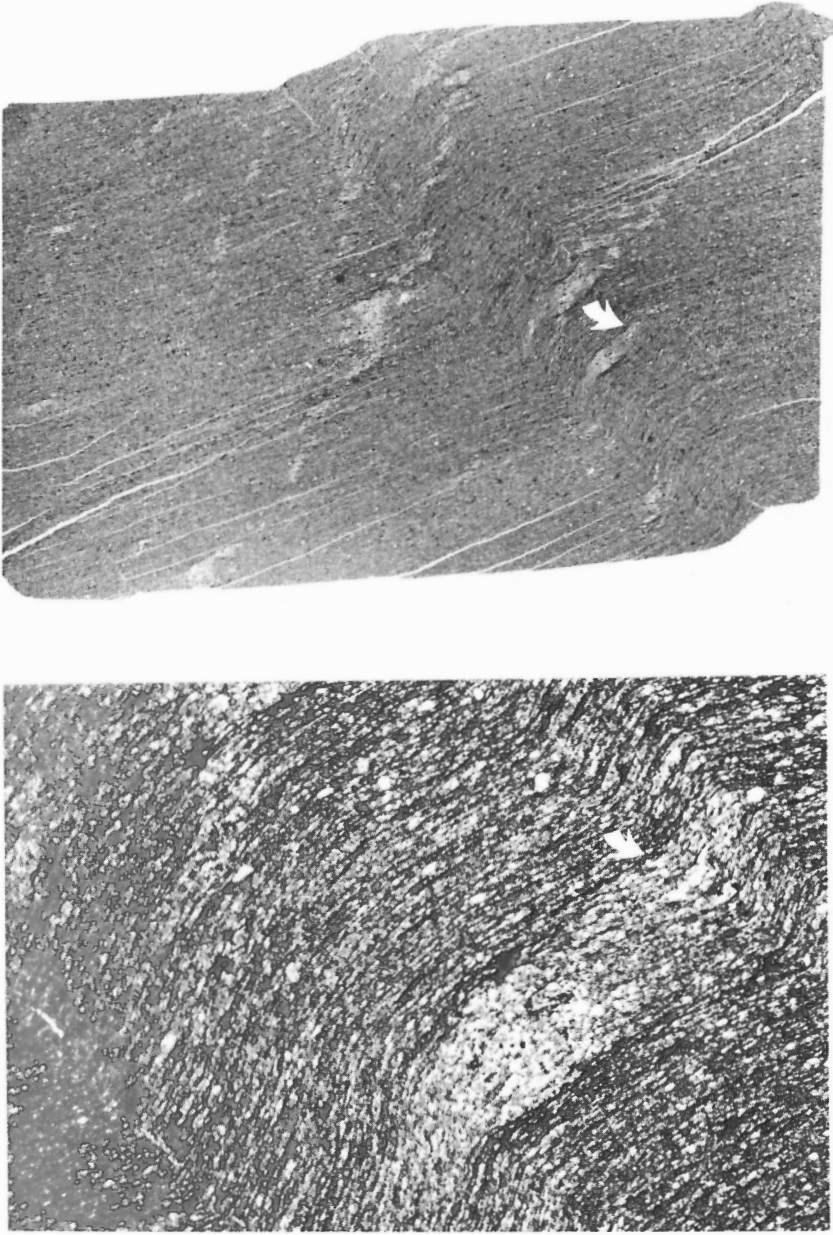


Figure 20 (b). Thin section (right) and photomicrograph (left) of specimen shown in Figure 20 (a). See text

ends of the specimen resulted in the formation of a couple of minor kink bands at the lower corner and a minor kink band at the upper corner. The large compound kink band through the center of the specimen developed subsequent to the localized gliding on cleavage.

Although the majority of kink bands illustrated in this paper intersect the ends of the specimens, the end conditions apparently were not the controlling factors in the development of the kink bands. Approximately 25 per cent of the kink bands in this study formed away from the ends of the specimens; of the remainder, half intersected the piston end and half intersected the anvil end.

CONCLUSIONS

The results of this study are consistent with earlier work and indicate that the formation of kink bands in brittle anisotropic rock such as slate reflects several mechanisms in addition to simple gliding on cleavage. The explanation advanced by Paterson and Weiss (1964; 1966) to explain the development of kink bands in experimentally deformed Nelligen phyllite, which assumes that gliding on the cleavage is the sole mechanism of kink band formation, requires that (1) bilateral symmetry across the kink planes be maintained throughout the deformation, and (2) that the kink planes migrate laterally into undeformed material with continuing deformation, thus maintaining a fixed orientation but not a fixed position in space. Neither of these conditions is satisfied by the kink bands developed experimentally in Martinsburg slate.

For low inclinations of the cleavage to the direction of maximum compression, slip on the cleavage at a relatively rapid rate (0.3 per cent per second) over a sufficiently large strain interval (greater than 0.7 per cent) causes instability that results in the formation of kink planes. The kink planes form along planes of high shear stress and are positions of localized cataclasis; once formed, they remain fixed in both position and orientation. Further deformation causes the foliation segments between the kink planes to rotate until the resistance to slip exceeds the resolved shear stress on the foliation segments. The greater amount of gouge within the kink band indicates that a much larger number of cleavage surfaces within the kink band were active at this stage of the deformation, than during the initial slip prior to the kink band inception. If deformation continues beyond the point at which the foliation segments attain their limiting orientation, faulting, secondary slip surfaces, or another kink band forms, or stretching and thinning of the foliation segments within the original kink band occurs.

In some specimens of slate two narrow kink bands form a small distance apart and, following rotation of the foliation segments within them to some limiting orientation, the foliation segments between the initial kink bands are externally rotated to the same inclination. The initial kink bands may be so narrow that the foliation segments rotate almost instantaneously to the limiting orientation. Thus, they define, in effect, kink-band boundaries for the foliation segments between them. The amount of strain required to rotate a segment fully is a function of its original inclination and its length. For a given foliation segment length it takes an increasingly greater

increment of strain to produce each additional increment of rotation; short foliation segments require much less strain than longer segments to rotate completely to their limiting orientation.

Because of the rotation of foliation segments within the kink band, the angle defined by the kink plane and the cleavage within the kink band, α_k , does not always equal the corresponding angle outside the kink band, α . In this study the mean value of α was 68.4 degrees, but α_k varied from 91 to 52 degrees. Dilation within the kink band occurs for angles of α_k greater than α , and thinning of the foliation segments permits α_k to be less than α in those specimens subjected to large total strains.

The complex history of certain compound kink bands developed in the slate specimens used in this study is generally reflected in the stress-strain curves and in the copper jackets. However, without careful examination a compound kink band may appear to be relatively simple from its external appearance, and any measurements made on it would likely be misleading. The variation in spacing of the initial kink bands in a compound kink band is largely responsible for the observed variation of kink-band widths, but an additional factor is the thinning (stretching) of foliation segments caused by further deformation after the foliation segments have reached their "limiting" orientation. The inclination of the foliation segments may be increased beyond this orientation by faulting parallel to the kink-band boundaries, development of secondary slip surfaces within the kink band, or by flow of the foliation segments themselves.

Of interest experimentally and of greatest possible significance to applications in dynamic structural geology is the observation that the inclination of the kink planes remains fairly constant regardless of the confining pressure, total strain, or complexities of development of the kink bands. The mean inclination of the kink planes to the direction of maximum principal stress is 47.5 degrees.

ACKNOWLEDGMENTS

The experimental work was carried out in the Rock Deformation Laboratory at Columbia University with the assistance of L. S. Fruth and P. M. Clifford, whose help is gratefully acknowledged. Thanks are due also to the National Science Foundation (Research Grant NSF-G24349) for financial assistance, to Dr. Fruth for his assistance with microscopic measurements and data reduction, and to Mrs. Marie Rev for preparation of the thin sections.

REFERENCES

Donath, F. A.

- 1961: Experimental study of shear failure in anisotropic rocks; Bull. Geol. Soc. Am., vol. 72, pp. 985-990.
- 1964a: Strength variation and deformational behavior in anisotropic rocks; in State of Stress in the Earth's Crust, Judd, W. R., editor, Elsevier, New York, pp. 281-297.
- 1964b: Kink-banding as a mechanism of faulting in anisotropic rock (Abstract); Trans. Am. Geophys. Union, vol. 45, pp. 103-104.
- 1968: The development of kink bands in brittle anisotropic rock; Geol. Soc. Am., in volume in honor of A. Poldervaart.

Paterson, M. S., and Weiss, L. E.

- 1964: Experimental folding in phyllite (Abstract); Trans. Am. Geophys. Union, vol. 45, p. 104.
- 1966: Experimental deformation and folding in phyllite; Bull. Geol. Soc. Am., vol. 77, pp. 343-374.

DISCUSSION

A good part of the general discussion of Friday afternoon was occupied by a discussion centred on Dr. Donath's paper. Other contributions presented during the afternoon and referring to kink bands are grouped together under General Session.

G. R. Stevens asked Dr. Donath if he found any constancy in the strike of the kink bands, and if he did, he wondered if this could be due to a pre-existing anisotropy or possibly to the experimental set-up.

The author said that the kink axis was always parallel to the strike of the anisotropy (cleavage), and normal to the direction of slip on it. There was no relationship to any lineation that might have existed in the cleavage prior to the experiment.

E. Z. Lajtai wondered about the stress-strain diagrams related to the formation of kink bands and presented by the author. He understood that in the author's opinion, the first of the two peaks that developed (Donath's paper, Fig. 12) indicated failure conditions in the plane of weakness whereas the second one represented conditions of formation of the kink band itself.

He would have liked to know what type of Mohr's strength envelope would result from plotting values representing these two peaks in a Mohr's diagram. He also asked the author if the second peak could not form as a result of plastic in isotropic materials as well.

The author answered the second part of the question first by saying that anisotropy was an essential condition to formation of the kinks. Slip always occurred on the anisotropy before the kink bands formed. By calculating the amount of strain that could be attributed to the rotation mechanism, one could fix the point at which the kink was initiated within certain limits. All measurements related to strain were very consistent with the author's own interpretation, and indicated that the kink bands were initiated between the first peak and the minimum of the stress-strain curve. The rise in differential stress beyond the minimum point is a function of several factors. It requires more energy to get dilatation, to induce localized cataclasis and overcome resistance to slip on numerous additional cleavage surfaces, and to produce the larger resolved shear stress required by the rotation of cleavage segments within the kink band. Each time another mechanism became operative (for example slip or faulting) a correlative drop would appear on the stress-strain curve.

E. Z. Lajtai realizing that he was probably simplifying the problem considerably suggested that the two peaks indicated on the stress-strain curves indicate the presence of two independent failure mechanisms. The first one could represent failure on the plane of weakness and the second one, plastic deformation for the kink band. The author could show numerous examples, he said, in which the amount of rotation of foliation segments within the kink band varied as a function of the amount of strain proceeding beyond the yield point (first peak). The amount of slip as expressed by cataclasis on some of the cleavage planes was also related to the distance between peaks on the curve. On other curves, formation of successive peaks could be shown to coincide with appearance of new kink bands. The author did not have any doubt that the first peak represented slip on the anisotropy and each of the following ones the formation of a kink band.

E. Z. Lajtai thought that deformation bands similar to kink bands might possibly develop in isotropic material with plastic deformation, at very high confining pressure. In some illustrations of the author, the angle between kink bands and maximum compression appeared to be very close to 45 degrees, which is the angle predicted by the maximum shear strength theory.

The author agreed that this appeared to be the case, but pointed out that the principal stresses within the specimen were being rotated because of the presence of pre-existing anisotropy and because of slip occurring on it. Although the mean angle of $47 \frac{1}{2}$ degrees was very close to the plane of

maximum shear stress for isotropic material, because of rotation of the principal stresses within the anisotropic specimen the direction of maximum compression was actually forming a much smaller angle with the kink planes. The kink planes probably formed at an angle providing the most favourable ratio of shear stress to normal stress on the plane.

L. E. Weiss remarked that some illustrations presented by the author demonstrated quite well the point he was making; they also showed that as kink bands were rotating, they were becoming wider.

The author, however, commented that although it was difficult to see the exact boundary of the kink bands in the illustration referred to by Dr. Weiss, he did not think there was an appreciable widening of the bands.

L. E. Weiss wanted to know if the author had also carried out experiments with larger strains.

The author said that in the first series of experiments he had tried to obtain 'ideal' kink bands and had therefore stopped after rotation was completed. In later tests at higher strains (up to about 16%), he had noticed a large amount of slip on the anisotropy, but only a fraction of the strain was involved in the kinking process itself.

L. E. Weiss pointed out further that slip on the anisotropy was only possible in asymmetric situations, with compression oblique to the cleavage. This fact indicated that in such a situation there had to be some sympathetic slip in the background at the time of formation of the kink bands.

The author agreed and added he should have mentioned that, before kinking begins, external rotation of the cleavage by 3 to 5 degrees also takes place. This rotation was greater in specimens where kinking was appearing late than in those where kinking was early. Kinks would only develop when the strain rate during the initial slip on anisotropy was high enough. The kink planes possibly represent planes of shear failure that form when there is sufficient release of stored elastic strain energy. Subsequent deformation also includes rotation but restricted to the foliation segments between kink planes. The author also recalled a point he had made a few years previously. If pressure dependence observed at times was real (and he was almost certain of this), then, at high confining pressures with constraint, kinks would become much narrower. Rotation of such narrow kinks would be almost instantaneous, because of the shortness of the segment involved, but these kink bands would likely be so ductile that they would not fracture. The body could deform like the cards in Dr. Weiss' experiments or like an ideal foliated body. In a few examples the author had observed curved kink planes; obviously, the segments involved in the kink bands varied in length. For a

given amount of strain and a given length of foliation segment, the amount of rotation would thus vary. This was a case quite similar to that described by Dr. Fyson. Dr. Donath presented an example of just such a case. He also remarked that it would be wrong to speak there of undeformed domains outside the kink bands because there had been slip on the anisotropy and rotation of the cleavage before kinking.

To comments of D. U. Wise and G. R. Stevens concerning the possible development of slip in the kink band in line with the foliation outside the kink band, the author said he doubted if that were the case. In his experience, and except for one isolated case, he had never seen deformation cutting across a kink band. Faults might develop parallel to kink boundaries, other kink bands might form, or secondary slip surfaces within or adjacent to the kink bands might develop, but no cross-cutting features would appear.

W. K. Fyson said that such fractures apparently younger than the kink bands were visible in some examples he had described.

D. M. Carmichael remarked that the one obvious difference between the natural kink bands and the paper cards of Dr. Weiss on one hand and the experimentally deformed samples of Dr. Donath on the other hand was in the presence of fractures along the kink boundaries in the latter's samples. He wondered if such fractures might not have formed during unloading, and have been absent throughout the time the kink bands were forming.

The author accepted the possibility of such a mechanism but pointed out that the position of the kink planes was fixed and that evidence of cataclasis along the kink planes was apparent as soon as the slightest rotation had taken place.

F. B. Anderson commented on the presence of fracturing along the kink planes and on similarity between experimental features and natural occurrences, illustrating his discussion with a number of colour slides. He then went on to discuss the angle of roughly 60 degrees between kink bands and foliation and repeated a tentative suggestion he had first made in 1964, that in the symmetrical orthorhombic situations considered, the kink bands form at an angle of $45^\circ + \phi/2$ to compression in the foliation plane. The frictional coefficients of the cards used by Dr. Weiss are 0.5 and 0.6 (i. e. $\tan \phi = 9.5$ or 0.6). For the first value, $45^\circ + \phi/2 = 58.3^\circ$ for the second value, $45^\circ + \phi/2 = 60.5^\circ$, which are in good agreement with the actual value of 60 degrees.

F. A. Donath said that experimental asymmetrical kink bands form at somewhat lower angles to the direction of maximum compression and that

F. A. Donath said that experimental asymmetrical kink bands form at somewhat lower angles to the direction of maximum compression and that in some natural situations it might be expected that rotation of principal stress axes would also exist.

L. E. Weiss observed that such a rotation did not occur in the deformation of the cards. He had checked this specific point.

J. Handin did not think that we could yet resolve the general relations between kink bands and principal stress directions in the field. If both types (symmetrical and asymmetrical) qualify geometrically as 'kink bands', then they may reflect different modes of deformation (ductile and brittle). That is to say, the influence of friction may be important for brittle, but not ductile deformations. Relations to the principal stresses could then be expected to be different, so that in the field one would have to determine which type he was dealing with. What independent evidence did Dr. Anderson have that the direction of maximum compression bisected the obtuse rather than the acute angle between 'conjugate' kink bands? More importantly, what would the criteria be where only one set was visible? Did anyone know of examples of single kink bands that were demonstrably inclined at 30 degrees rather than 60 degrees to the direction of maximum compression?

T. B. Anderson said that in the Ards Peninsula the arrangement of dextral and sinistral kink bands is such that compression must have bisected the obtuse angle. In cases where kink bands of only one sense of displacement are visible there seems to be no obvious way to determine the orientation of σ_1 .

M. R. Stauffer suggested that in the latter case, although conjugate sets do not occur together, 'right-handed' and 'left-handed' sets existing in the same general area would presumably correspond to conjugate sets elsewhere, and all would belong together.

T. B. Anderson pointed out that in the case he had studied, axes of the kink folds are vertical and they displace the vertical foliation horizontally. Therefore no possibility of such confusion exists.

OTHER CONTRIBUTIONS

Important contributions were offered by a number of geologists who described their own observations or gave their own thoughts of kink bands in general. These contributions and the discussions they led to are grouped under General Session.

FLEXURAL-SLIP FOLDING OF FOLIATED MODEL MATERIALS

L. E. Weiss
Department of Geology and Geophysics
University of California, Berkeley

Abstract

Small decks of thin, strong paper cards are used as a model of a strongly foliated or laminated rock such as slate, shale or phyllite. The decks are shortened 55 to 37 per cent parallel or oblique to the cards in an orthogonal hydraulic press designed to simulate deformation under constrained conditions in the earth's crust.

Fold structures developed in the cards are found to depend mainly upon lateral load. All structures observed can be explained in terms of 'conjugate kinking', a type of flexural slip folding involving planar slip between and within the cards. Typically, a progressively deformed specimen develops several generations of kink and conjugate kink folds, each subsequent generation having smaller amplitude than the last.

In some specimens this sequence is interrupted by the development of a late major conjugate fold by selective lateral growth of kink layers. Early kink folds become internally rotated within these large kink layers and the resulting major fold has minor 'parasitic' folds on its limbs.

In none of the experiments are folds in the cards seen to develop entirely by gradual appression of initially 'open' folds. The first folds observed to form are always kink or conjugate kink folds with apical angles close to 120° which remain constant throughout much of a progressive deformation. Chevron folds with apical angles close to 60° and axial surfaces subperpendicular to the compression axis form at kink intersections and these too preserve much the same apical angle until most or all undeformed domains in the specimen have been invaded by kinks. Further deformation of a completely folded specimen generally results in progressive decrease in the apical angles of all folds simultaneously.

INTRODUCTION

In a recent paper (Paterson and Weiss, 1966) experimental folding of a fine grained platy phyllite at high confining pressure and lateral constraint was described and a model of flexural slip folding of an 'ideal foliated body' by conjugate kinking outlined. The present study continues this investigation with a series of experiments involving folding of 'foliated' model materials (decks of thin paper cards) in an orthogonally acting hydraulic press. In this apparatus one surface of a test specimen is exposed and the formation and evolution of folds and related structures can be directly observed and recorded with still and ciné photography at all stages of an experiment.

The material chosen for the experiments resembles in its behavior the phyllite used in the high pressure experiments cited above. This resemblance is geometrical rather than mechanical and in the following discussion emphasis is placed on similarities in form and evolution between structures formed in the card decks and in the phyllite rather than on mechanical parallels. The main usefulness of the results of the experiments appears to lie in the light they shed on the possible sequence of development and modification of flexural slip folds of the kink and chevron type formed in strongly anisotropic thinly laminated media under certain simple dynamic conditions.

The following discussion centers around a series of photographic plates and idealized figures. Most of the plates contain selected photographic frames in a sequence taken during progressive deformation of a specimen and show clearly the evolution of fold structures. For this reason no detailed description of each plate is given; instead, important features of some of the plates are described and illustrated where necessary with idealized sketches expressing a possible interpretation of the structure present. Other interpretations of these structures may suggest themselves to a reader who studies the plates.

ACKNOWLEDGMENTS

The experiments were carried out at the Department of Geology and Geophysics of the University of California, Berkeley. Support at various stages of the work given by the National Science Foundation (grant GA 420) and the Miller Institute for Basic Research in Science of the University of California is gratefully acknowledged. Thanks are due also to Dr. M. S. Paterson of the Department of Geophysics, Australian National University, Canberra for discussions and suggestions and to Professor D. T. Griggs of the Institute of Geophysics and Planetary Physics, University of California, Los Angeles, for stimulating me to begin this study.

EXPERIMENTAL PROCEDURE

Apparatus

The orthogonal hydraulic press is shown schematically in Figure 1. A strong steel frame 15 ins. square and 4 ins. thick (black in Fig. 1) supports two 20 ton hydraulic rams R_1 and R_2 which act along mutually perpendicular lines. To the rams are fixed heavy steel blocks (B_1 and B_2) which transmit the two loads to the test specimen S . These blocks slide on teflon pads against the ground tool steel inner lining of the frame (oblique shading) with very low friction at all loads.

The vertical ram R_1 applies the deforming load and is fed through an electric pump P_1 the flow from which is variably controlled by a needle valve V_1 . When V_1 is fully closed all the output of the pump reaches the ram: progressive opening of V_1 gradually reduces the rate of increase of pressure in R_1 and allows any rate of loading to be selected. The pressure in this pumping system is shown on a gauge G_1 calibrated to read as a load.

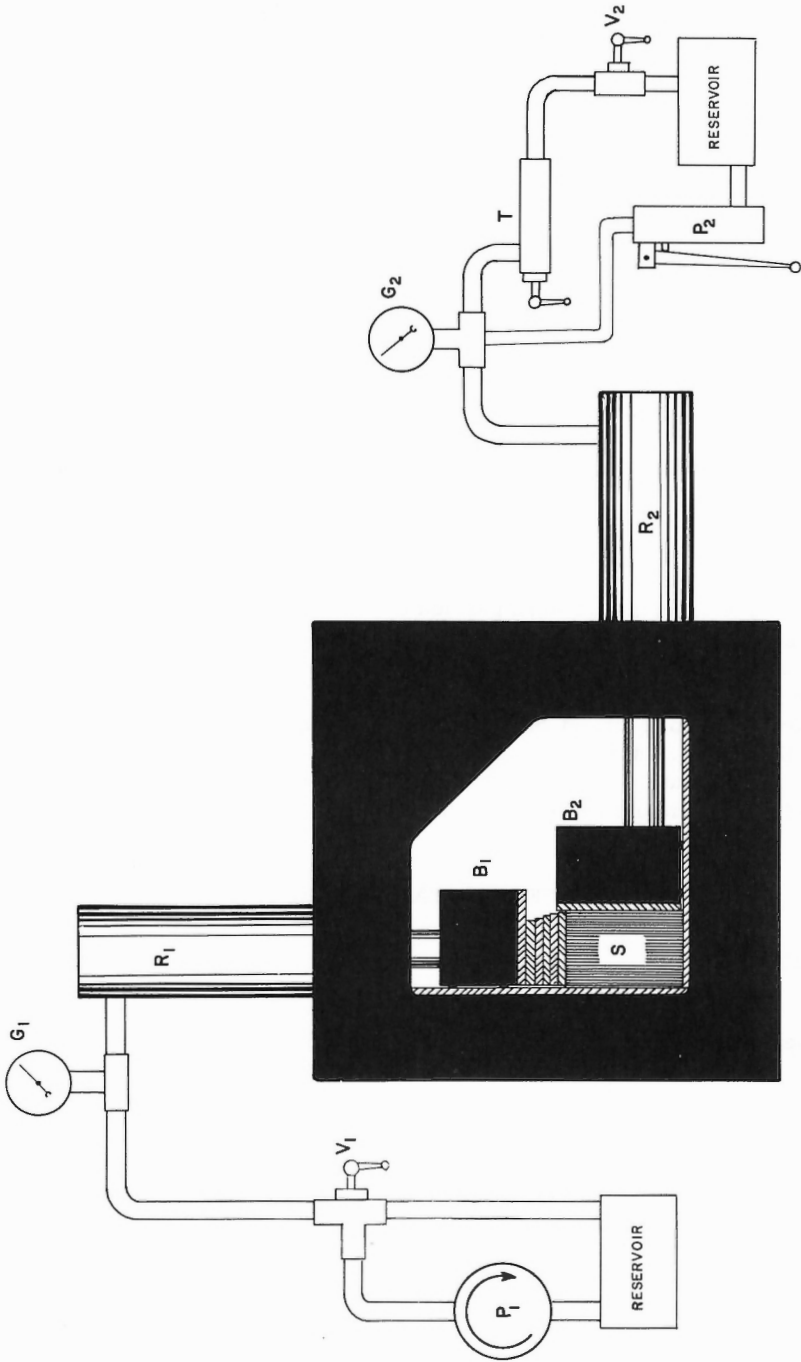


Figure 1. Orthogonal hydraulic press (described in text).

The horizontal ram R_2 applies a lateral or constraining load to the specimen and is fed through a hand pump P_2 by way of a variable pressure release valve T. This valve permits the pressure in R_2 to be set and maintained at a constant selected value throughout an experiment, independently of increase in the deforming load, and it can be by-passed if desired by closing the shut-off needle valve V_2 . The pressure on this system is shown on gauge G_2 calibrated to read as a load.

A still or movie camera mounted in front of the press records the appearance and dimensions of the front surface of a test specimen either at selected intervals or continuously throughout an experiment. At the time of each still photograph the loads on the two gauges are recorded and from these readings and the dimensions of the specimen as determined from photographs the approximate stresses across the loaded surfaces (assuming these to be homogeneous) can be determined. From enlarged still photographs or from movies the structural evolution of specimens can be studied and development of structures related to approximate states of strain and loading.

In a typical experiment the following procedure is adopted. The test specimen, always a rectangular parallelepiped in form, is placed in the apparatus with its front surface flush with the frame. By means of hand pump P_2 the lateral load is applied to some predetermined value by adjusting the pressure release valve T for the required reading on gauge G_2 . As a result of this loading the specimen acquires a definite lateral dimension. A hard steel block is selected (from a set cut at 2 mm increments) of width less than but most nearly equal to this lateral dimension and is placed on top of the specimen. The deforming load is then applied gradually through a small stack of similar but smaller blocks (oblique shading in Fig. 1) by operation of the electric pump P_1 and the variable flow valve V_1 . By this means the load from the deforming ram is distributed fairly evenly over the upper surface of the specimen which is in contact with hardened steel plates over four of its six surfaces.

The deforming ram is then advanced at a chosen rate and the lateral loading ram moves slowly outward keeping the constant load selected by valve T. As this ram moves outward the lateral dimension of the upper surface of the test specimen gradually increases and the deforming ram must be periodically retracted so that a slightly larger hard steel block can be inserted on top of the test specimen to keep the deforming load distributed as nearly as possible over the whole of the upper surface of the test specimen. In practice this procedure leads to a discontinuous pattern of stress across the upper surface with time and to markedly heterogeneous stress distributions in the upper right hand corner of the specimens where unsupported areas of variable size are periodically present throughout one experiment.

The experiment is continued in this fashion until the required amount of vertical shortening of the specimen is achieved or until the 18,000 kg capacity of the deforming ram is reached.

In some experiments the pressure release valve in the lateral loading system was by-passed by closing valve V_2 so that the lateral load increases as the deforming ram is advanced. This second procedure yielded results similar to those

obtained by the first except that uncertainty as to the horizontal stress was in general increased. In all experiments described below the first procedure was adopted.

The design of the apparatus is such as to simulate as closely as possible the conditions of constrained deformation in thick metal jackets used in the high pressure experiments on phyllite (Paterson and Weiss, 1966, pp. 359-362). The shape-change in the specimens was proscribed at all stages of deformation and end-alignment was preserved, even where decks were shortened oblique to the plane of the cards.

Materials

After trial of many different media (most of which behaved very similarly to the cards used) a single, uniform and easily obtainable material was chosen for the whole series of experiments. This material folded and otherwise deformed in a manner geometrically similar to Nelligen phyllite at 5 kb confining pressure (Paterson and Weiss, 1966) and consisted of small decks of 1.5 in. by 3.5 in. white cards.¹ The cards are .185 mm thick and a test specimen generally contained either 300 or 150 cards. Tensile strength of the material in the plane of the cards is about 700 bars and at small loads the coefficient of static friction between cards is about 0.6 and of sliding friction about 0.5.

Internally the cards are planar mats of flattened slippery fibers and are strongly anisotropic mechanically. Under high loads normal to the cards they are markedly compressible, primarily because of their high initial porosity, and only a relatively small part of this effect is reversible in unloading. The remaining distortion is permanent and appears to be a result of compaction between the fibers. Under very high normal loads (above 5,000 kg.) the decks undergo slight isotropic elongation in the plane of the cards without any sign of rupture. Most experiments were performed within a range of lateral loading for which such elongations were zero or imperceptible.

In addition to the above types of behavior the cards show also some creep (time dependent deformation) for loadings at moderate stress for long periods. To reduce the effects of creep most experiments were performed as rapidly as possible, the average duration of an experiment being about ten minutes.

To emphasize the individual cards for photographic purposes and to provide a scale for the plates, one side of each deck was stained black and alternate cards were reversed so that each of the two unsupported faces of a deck showed cards alternately with black and white edges. In the photographic plates therefore the fine black and white stripes correspond to individual cards each .185 mm thick (in some plates fine irregular striations inclined at about 45° to the undeformed cards are marks left by the paper guillotine).

¹ These cards are available in boxes of approximately 300 cards each from Visual Education Association, Inc., 321 Hopeland Street, Dayton 8, Ohio. They are marketed as student 'flash cards' under the trade name 'Vis-Ed'.

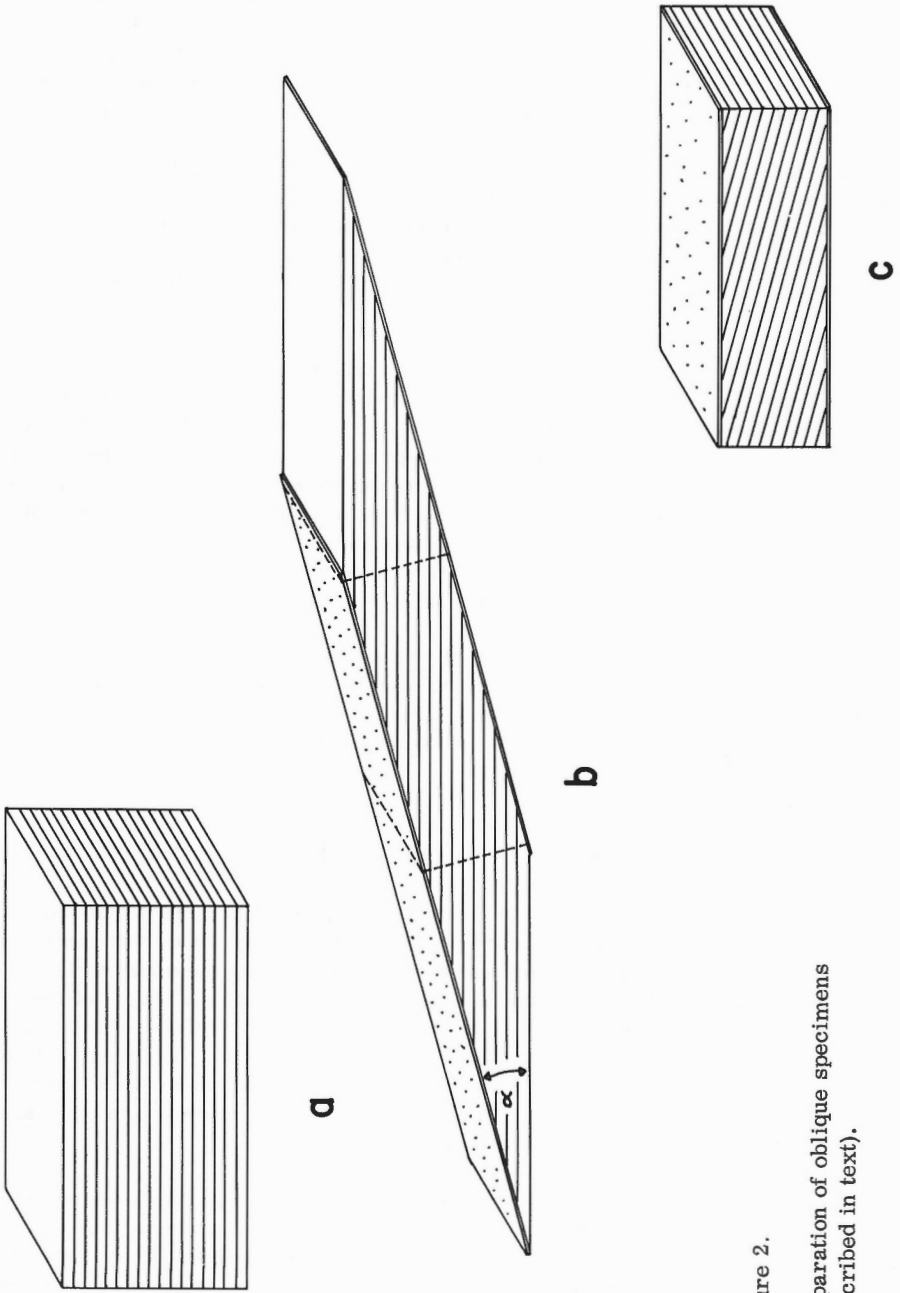


Figure 2.
Preparation of oblique specimens
(described in text).

Most experiments involved compression of decks in the plane of the cards parallel to their longest dimension ('parallel specimens'). In some experiments compression was oblique to the cards, the specimens for which ('oblique specimens') are prepared as outlined in Figure 2. A card deck (Fig. 2a) is uniformly sheared by sliding in the cards until the angle α between the plane of the cards and the longest edge of the specimen is the desired angle between the plane of the cards and the compression direction (the line of action of the deforming ram). Adhesive drafting tape of the correct width (stippled in Fig. 2b) is stuck firmly along the sheared face of the deck and the wedge shaped ends of the deck are cut off along the broken lines with a paper guillotine. Pieces of thin plastic adhesive tape around the ends of the deck then hold the specimen in the form of a rectangular parallelepiped (Fig. 2c) for insertion into the press. The dimensions of the oblique decks so obtained are variable and depend upon the choice of α .

In some trial experiments layers of various thickness of a variety of materials were placed between test specimens and the lateral faces of the press. The effect of these layers was in general only to modify the scale of folding in the specimens. Some of the material, such as 0.5 in. thick neoprene rubber sheet, could be indented by the folding cards so that larger scale folds were developed at higher loads. But other effects such as local extension of the rubber layers at high loads with consequent local stress concentrations in the test specimens made these experiments less reproducible in their properties and results described below were all based on experiments in which the cards were directly in contact with the steel platens.

In other experiments an attempt was made to study the behavior of thicker but ductile mechanically isotropic layers enclosed in the card decks in order to simulate the presence of more 'competent' layers. For this purpose one or more annealed copper sheets 1 mm thick were introduced into the card decks which were then deformed in the manner outlined above.

MECHANICAL PROPERTIES

The design of the apparatus prohibits the preparation of adequate stress-strain curves for deformation of the card decks. The only quantities that can be measured with any degree of accuracy are the stresses across the upper and right lateral faces of the specimens (σ_1 and σ_2 respectively) at various stages of the shortening and these measurements involve the neglect of frictional effects and assumption of homogeneous stress distribution across the faces. The front and rear faces of the specimens are unsupported and the stress across these (σ_3) is assumed to be zero. Stress in the specimens can be viewed two dimensionally and expressed in terms of a differentially longitudinal stress $\sigma = \sigma_1 - \sigma_2$.

The curves in Figures 3 and 4 show σ (in kgs/cm²) plotted against per cent shortening of the specimen in the direction of compression. Because of the periodically discontinuous path of loading in the course of one experiment these curves are only a crude indication of the stress-strain properties of the card decks and only their main features are of interest. During one experiment both σ_1 and σ_2 vary in a manner

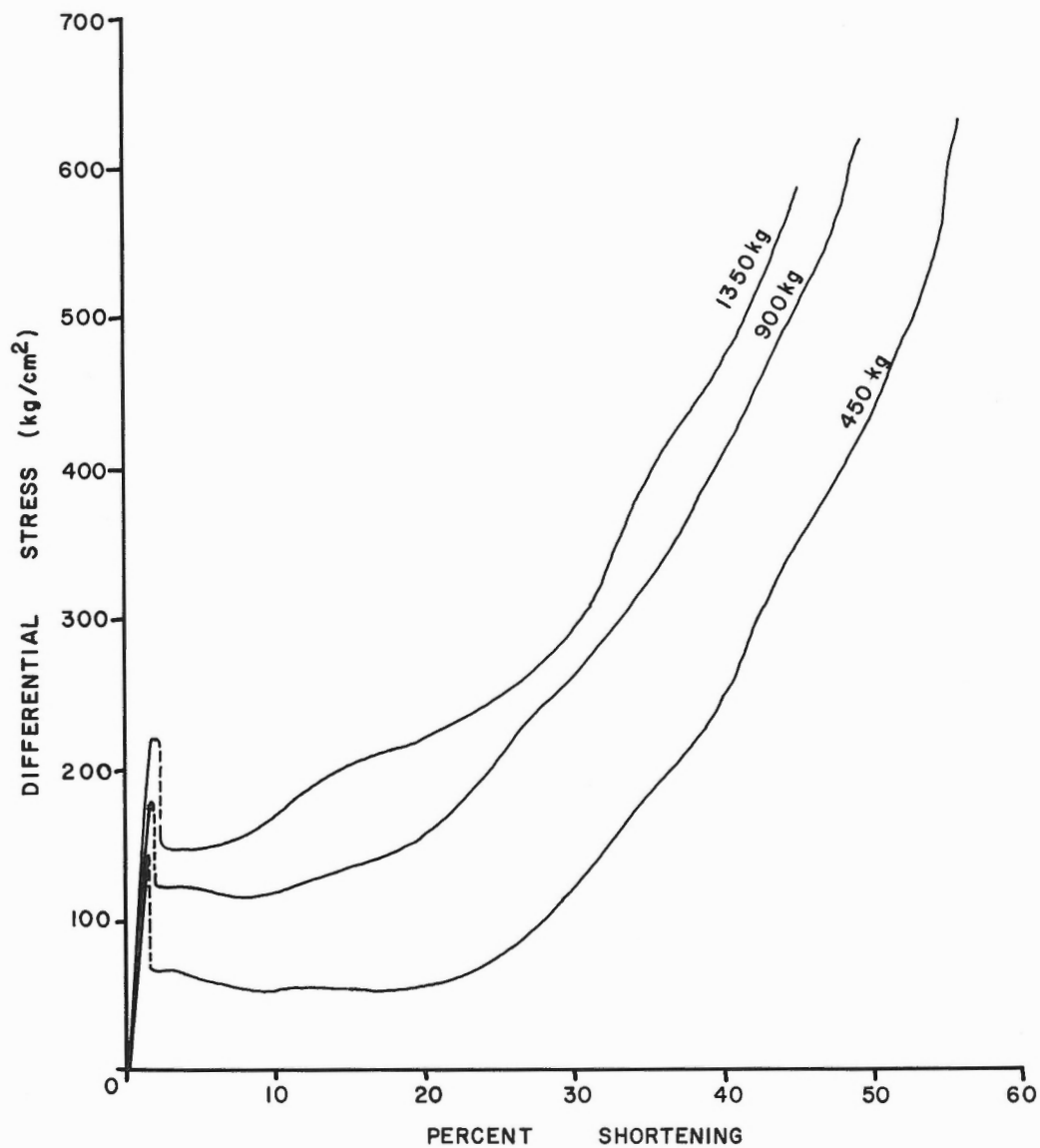


Figure 3. Differential stress-shortening curves for parallel specimens of group 1 at constant lateral loads, indicated on each curve.

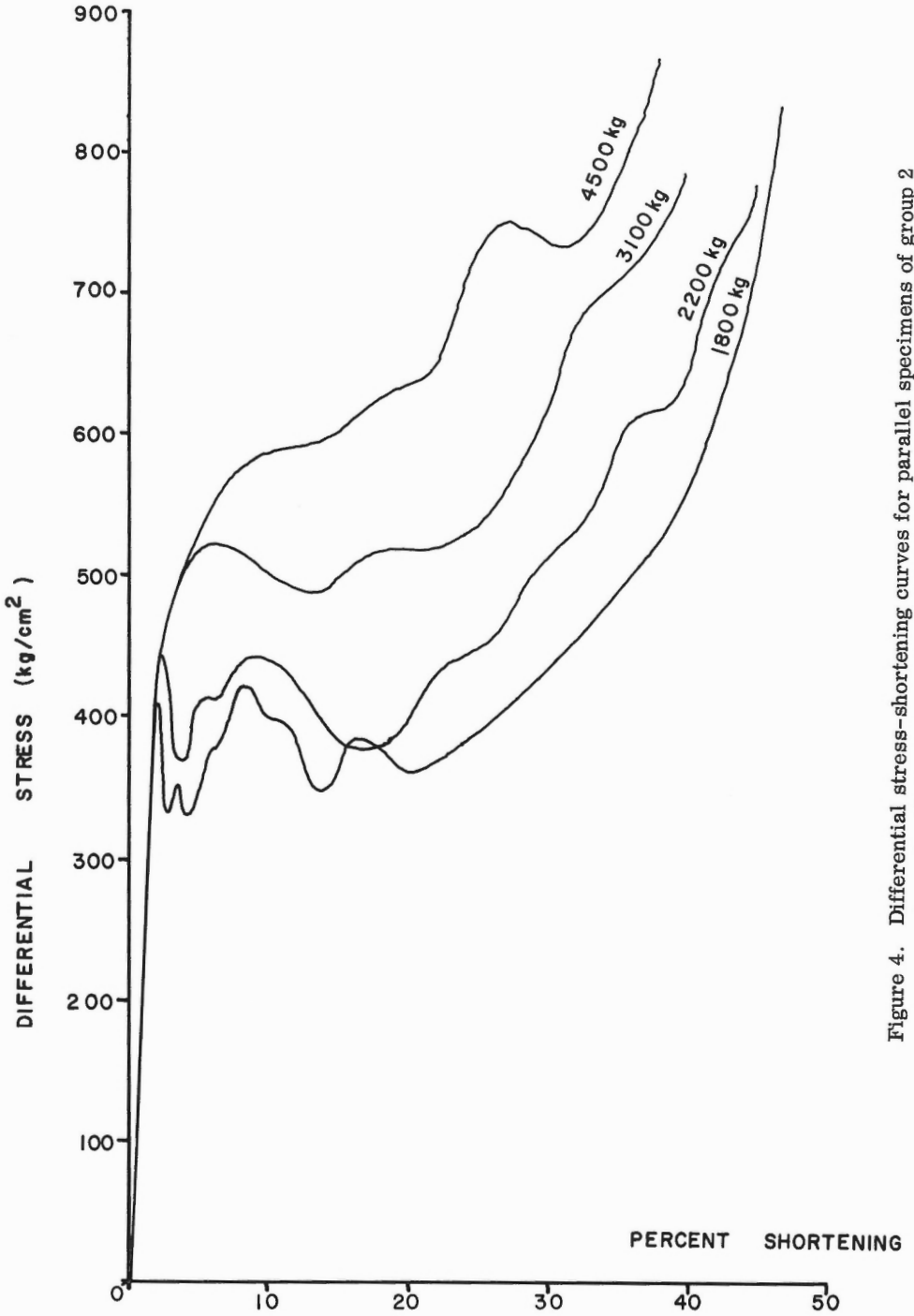


Figure 4. Differential stress-shortening curves for parallel specimens of group 2 at constant lateral loads, indicated on each curve.

controlled by the maintenance of a constant pressure in the lateral loading ram by the pressure release valve T. As shortening of a specimen proceeds, σ_2 rises as a result of the reduction of the area of contact between the specimen and the lateral loading platen. Measurement of the height of the specimen from photographs permits a value of σ_2 to be obtained at a given stage of deformation; but this value increases along with σ_1 so that the 'hydrostatic' component of the plane stress $\sigma^1 = \frac{\sigma_1 + \sigma_2}{2}$

generally increases progressively with specimen shortening. Thus, extension of the specimen perpendicular to the plane of loading increases with increasing load and can reach up to 4 per cent for the most heavily loaded specimens (lateral load 4,500 kg, deforming load 18,000 kg, $\sigma^1 = 650 \text{ kg/cm}^2$). But for the range of loading used in most experiments ($\sigma^1 < 500 \text{ kg/cm}^2$) the per cent elongation in this direction is less than 0.5 for short-term loading.

The curves in Figures 3 and 4 do not therefore correspond to the constant 'confining pressure' curves usually used to present the stress-strain relationships of deformed rocks. For each curve only the lateral load is constant and its value is shown on each curve. But the peculiar dynamic situation employed may resemble some natural situations in which an increasing horizontal load acts on a geologic body loaded vertically by a fixed overlying weight.

The straight, steep, first-parts of the curves in Figures 3 and 4 correspond to an initial period of elastic deformation, although some of the recorded shortening results from compaction of fibers and is permanent. For present purposes a yield point is reached as the first folds are nucleated. On most of the curves this is a sharp peak beyond which the curve falls rapidly. The differential longitudinal stress for nucleation of folds increases as the lateral load is increased.

On the basis of their behavior during fold nucleation the parallel specimens can be divided into two groups: group 1 contains specimens loaded laterally up to 1,500 kg and group 2 contains specimens loaded laterally at 1,500 kg or above. Curves for specimens of the two groups are shown respectively in Figures 3 and 4. The lateral loading used is shown on each curve.

Curves for specimens in group 1 show a sharp yield point followed by an almost instantaneous stress drop (indicated by the broken line segments of curves in Figure 3). This sudden yield is accompanied by extremely rapid nucleation and propagation of kink layers and the emission of a loud noise as a result of the sudden release of elastic strain energy in the specimen and in the distorted frame of the apparatus. Folding generally ceases once the stress drop has occurred and the deforming load must be reapplied before the folds continue to spread at approximately constant stress (the level segments of the curves in Figure 3). This behavior reflects in part the properties of the apparatus. The use of hydraulic rams to apply the loads makes the apparatus 'hard', in the engineering sense, and the load transmitted by the rams at any one time depends greatly on the state of strain of a specimen. In an apparatus in which the load could be maintained uniformly whatever the strain path followed by the specimen (a 'soft' apparatus) the behavior would be different; no pause in the propagation of the first folds would be expected and the stress drop associated with nucleation of the first folds would be less marked.

The remaining ascending parts of the curves in Figure 3 correspond to the gradual spread of folding through the whole specimen as described below. As a specimen becomes completely folded (that is, virtually all undeformed domains of the specimen vanish) its strength increases markedly and the curve rises steeply, as can be seen in Figure 3.

Curves for specimens of group 2 show a gradual disappearance of the stress drop accompanying initial fold nucleation as lateral load is increased (Fig. 4). In addition, the stress drop where it does occur in specimens in the lower part of the loading range is not sudden and is unaccompanied by emission of noise. Above lateral loads of 4,000 kg there is no detectable initial stress drop, only a smooth change in the slope of the curve as folds gradually appear locally and spread slowly throughout the specimen. After initial fold nucleation the curves for all specimens of group 2 are somewhat irregular but become increasingly steep and smooth as load increases. The irregular parts of the curves correspond to periods of fold development in different parts of the specimens. In all specimens of group 1 and group 2 differential longitudinal stress for fold nucleation rises with increasing load.

In Figures 3 and 4 only the per cent shortening of the specimens in the direction of compression is specified. Because of the design of the apparatus the overall strain of a specimen is ideally constrained to follow a path of progressive pure strain in which principal strain axes for the overall strain remain fixed in orientation and parallel to the orthogonal edges of the specimen at all stages. If volume dilatation and extension of the specimen in the unconfined direction are ignored the strain path is a progressive finite pure shear.

Internally, deformation is heterogeneous and the local strains vary widely as indicated by the folded configuration adopted by the initially planar cards. Where deformation is restricted to slip on cards or laminar shear on the platy fibers within the cards the specimen becomes divided into shear domains (planar limbs of folds) in which strain approaches very closely to a finite simple shear. The boundaries between these shear domains are axial surfaces of folds.

The differential stress-shortening curves for oblique specimens are not included because the very low stress for nucleation of first kink layers was difficult to measure. No marked stress drops were observed at nucleation of the first folds and the curves were in general smoother. Parallel specimens containing annealed copper layers behaved similarly to other parallel specimens except that for a given lateral loading higher differential stress was required for fold nucleation and that stress drops, where they occurred at nucleation of the first folds, were less pronounced.

PATTERNS OF FOLDING

General

The results of selected experiments are presented in the photographic plates as follows:

Plate 1: Patterns of first fold nucleation in parallel specimens at various lateral loads.

Plates 2 to 5: Progressive deformation of parallel specimens of group 1.

Plates 6 to 8: Progressive deformation of parallel specimens of group 2.

Plates 9 to 12: Progressive deformation of oblique specimens at various lateral loads.

Plates 13 to 16: Progressive deformation at various lateral loads of specimens containing annealed copper layers.

Plates 17 to 19: Details of deformed specimens.

The plates are fully described in their captions.

In the following discussion only certain features of some of the plates are considered and illustrated with idealized sketches. These features seem to have some geological implications with respect to the flexural slip folding of strongly laminated or foliated rocks and bear upon the behavior of phyllite experimentally deformed at high pressure (Paterson and Weiss, 1966). In the discussion it is not always possible to refer to the plates in their numbered sequence. In particular, plates 18 and 19 illustrating details of structure in a variety of specimens will be referred to periodically throughout the discussion.

In each specimen distinction can be made between the first appearance of folds ('first fold nucleation') and the spread of folding throughout the whole specimen during progressive deformation. In most specimens this spread involves both propagation of existing kink boundaries (axial surfaces of folds) and nucleation of new kinks.

All observed folding resembles closely the model of kinking and conjugate kinking proposed for the 'ideal foliated body' by Paterson and Weiss (1966, pp. 368-371) and the discussion will be in terms of this model, the salient geometrical features of which are now briefly reviewed.

Ideal Flexural-Slip Folding by Conjugate Kinking

In both parallel and oblique specimens initial folding is by 'kinking', that is, localization of strain in generally narrow layers inclined obliquely to the plane of the cards (henceforth referred to as 'foliation') in which the main mode of deformation is laminar slip on the foliation. The geometric features of ideal kinking have been discussed by Paterson and Weiss (1966, pp. 364-365). The angles ϕ and ϕ_k respectively between the foliation without and within the kink and the kink boundary are ideally equal and the finite shear strain within a kink is given by $2 \cot \phi$ or by $2 \tan \psi/2$ where ψ is the angle of external rotation of the foliation in the kink layer (Fig. 5a). In phyllite (Paterson and Weiss, 1966, pp. 352-355) observed values of ϕ , ϕ_k and ψ are all close to 60° in parallel specimens and 'conjugate kinking' is the main mode of

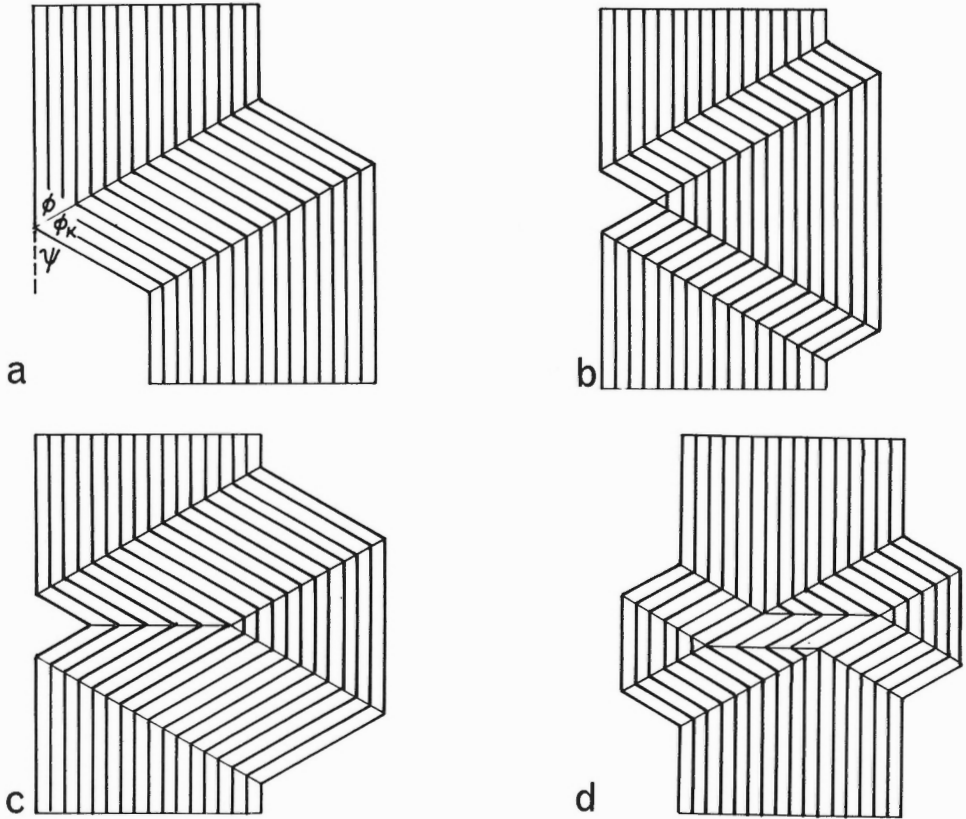


Figure 5. Types of kink boundary:

- a. simple kink with primary boundaries.
- b. conjugate kinks with primary boundaries.
- c. conjugate kinks meeting in a secondary boundary (horizontal).
- d. kink intersection with primary and secondary boundaries.

deformation. Two sets of parallel kink layers appear symmetrically inclined to the compression direction (and the foliation) which is always the obtuse bisectrix of the kink boundaries. Possible relationships between two such conjugate kinks as they meet can be seen in Figures 5b, c, and d for ideal kinks where $\phi = \phi_k = 60^\circ$. In the simplest situation kinks meet only at the edge of a specimen (Fig. 5b) and do not cross one another. In another situation (Fig. 5c) two kinks of opposite senses can come into contact along a boundary that is the acute bisectrix of the kink boundaries. This second type of kink boundary differs from the first in separating two deformed domains instead of a deformed from an undeformed domain and will be termed here a 'secondary' kink boundary in contradistinction to the simpler kind (Fig. 5a) here termed 'primary'. In the most general situation (Fig. 5d) kinks of opposite sense can intersect and cross one another if the kink angles ϕ and ϕ_k are close to 60° . In the example the displaced kink is termed right-handed and the undisplaced kink left-handed.

An intersection in which a right-handed kink is displaced is also termed a right-handed intersection. Left-handed intersections can also occur (Paterson and Weiss, 1966, pp. 355-357) and in both types of intersection the foliation acquires the configuration of a conjugate fold and a central domain of kink intersection appears in which two equal shear strains are superposed. Note that the secondary kink boundary separating this domain from the left-handed kink domains is in the same orientation as the boundary in Figure 5d, but that the geometrically symmetric fold so defined, unlike that in Figure 5c is not symmetric in its strain properties.

In Figure 6 the geometry of deformation in a kink intersection is illustrated. Domain ABCD is simply kinked in Figure 6b with shear angle $\omega_k = 49^\circ 6'$ for $\phi = 60^\circ$. A conjugate kink shears ABCD as shown in Figure 6c to give a shear angle $\omega_1 = 66^\circ 30'$ for $\phi = 60^\circ$. The orientation of the principal strain axes X and Z for this two dimensional view are as shown for the two strains.

In oblique specimens only one set of initial kink layers appears and these are always inclined to the compression axis in a sense approximately conjugate to the foliation. These kinks differ from the first formed kinks in parallel specimens in that the material on both sides of the kink boundary appears to be deformed. The foliation between the kink layers always rotates from its initial angle of inclination α to a smaller angle of inclination α' (Fig. 7). The subsequent folding history of oblique specimens is discussed below.

In the ideal model of progressive conjugate kinking proposed to account for the behavior of Nelligen phyllite (Paterson and Weiss, 1966, pp. 368-371) two phases in the spread of a kink layer were recognized as follows:

1. Longitudinal propagation of lenticular kink nucleus, generally at high velocity (Fig. 8a, b, c).
2. Lateral propagation (boundary migration) by which a longitudinally propagated kink grows in width, generally at low velocity (Fig. 8d).

Both types of behavior are observed at all stages in the present experiments. However, because of the constraints an outside shape imposed at all stages in deformation by the design of the apparatus, only limited amounts of deformation can be achieved by longitudinal and lateral propagation of an initial set of kinks. Much more important in progressive deformation is nucleation and limited propagation of successive generations of kinks, generally in undeformed domains. These new generations of kinks have geometric properties similar to those of the initial sets, but they are generally on a scale that becomes smaller and smaller for each successive generation, probably because of the increasing value of σ^1 during the course of an experiment. One exception to this sequence, namely the development of a single large conjugate fold late in the course of many of the experiments, is another result of the design of the apparatus and will be discussed below.

In the experiments, therefore, the final chevron folded form of a card deck is the result of a process in which new and smaller scale folds are continuously forming

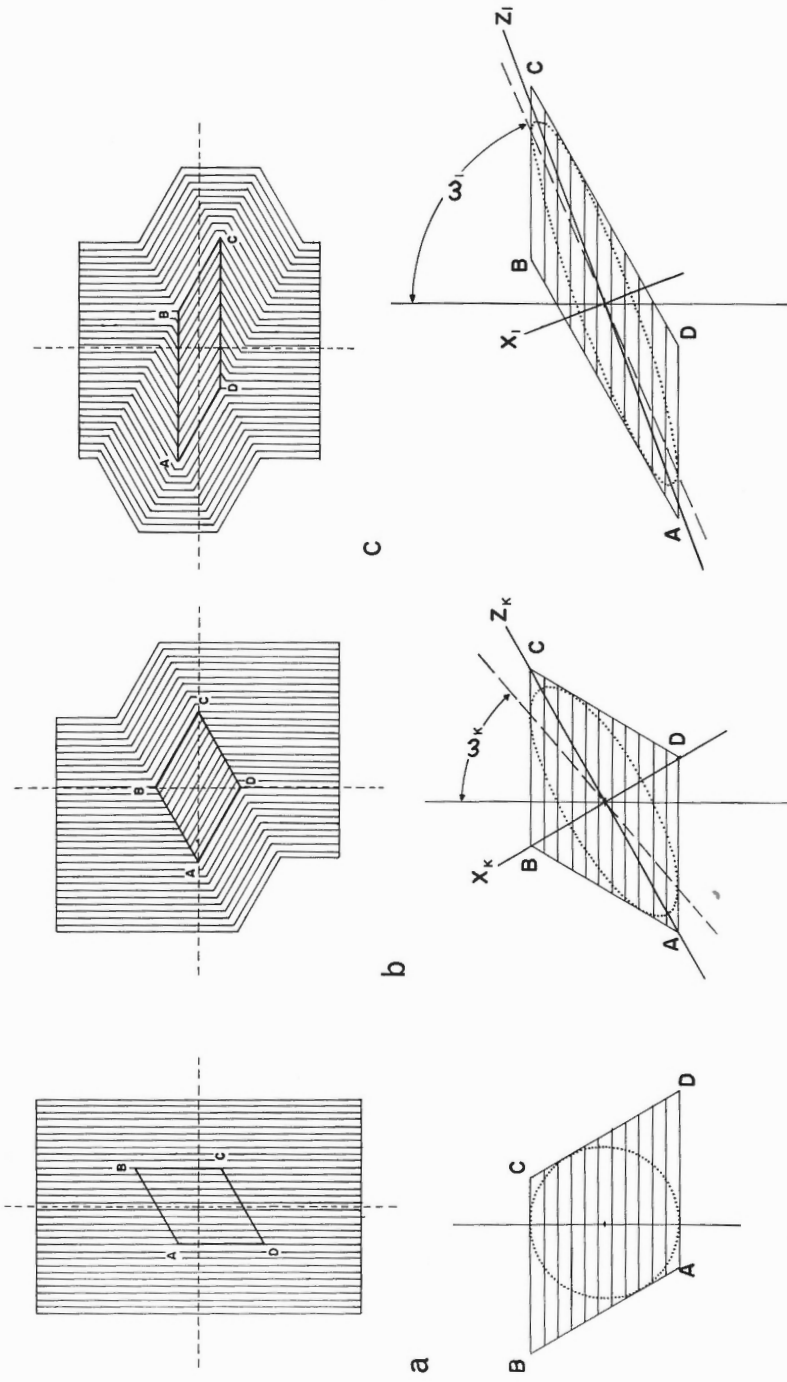


Figure 6. Finite shearing strains in b, a kink and, c, a conjugate kink intersection; shearing distortion of element ABCD. X and Z are the corresponding principal strain directions.

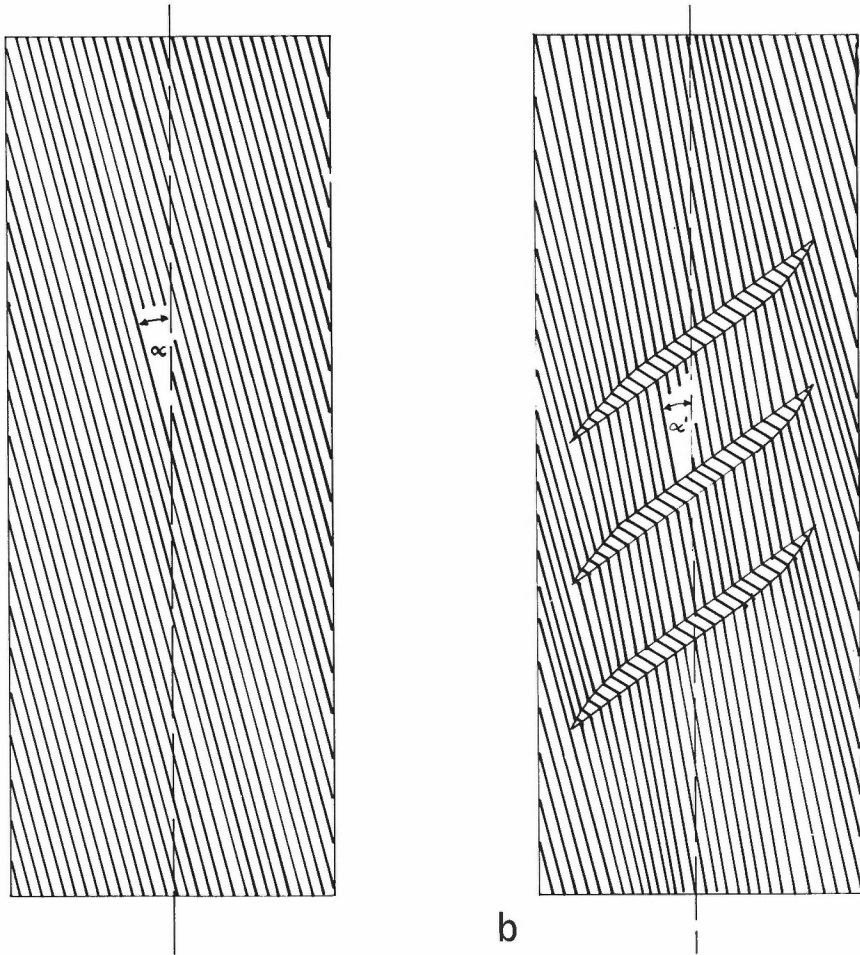


Figure 7. Initial kinks in oblique specimen compressed at α to foliation:
After nucleation $\alpha' < \alpha$

in the undeformed material. The specimens contain, therefore, chevron folds of many different sizes, the smaller folds being generally, but not always, younger than the large folds. When all undeformed material has disappeared from parallel specimens the resulting chevron folds have axial planes that are secondary kink boundaries oriented subperpendicular to the compression axis. This picture contrasts with, and is a more realistic model of folding in a laminated body, than the uniform pattern of chevron folding initially proposed by Paterson and Weiss (1966, p. 369, Fig. 18). Although geometrically possible, their simple pattern of evolution is not reproduced exactly in the present experiments.

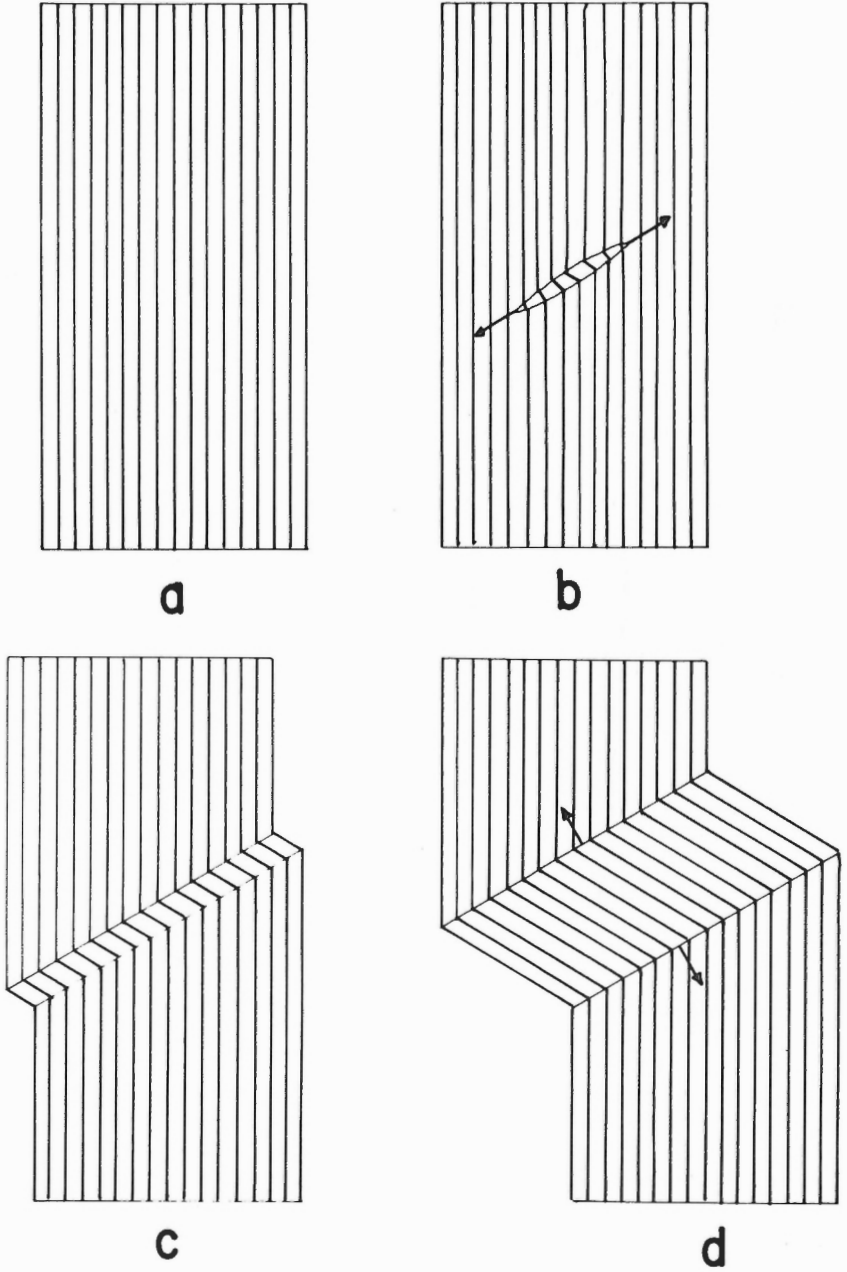


Figure 8. Growth of an ideal kink:
b. Longitudinal propagation of kink nucleus.
d. Lateral propagation of kink boundary.

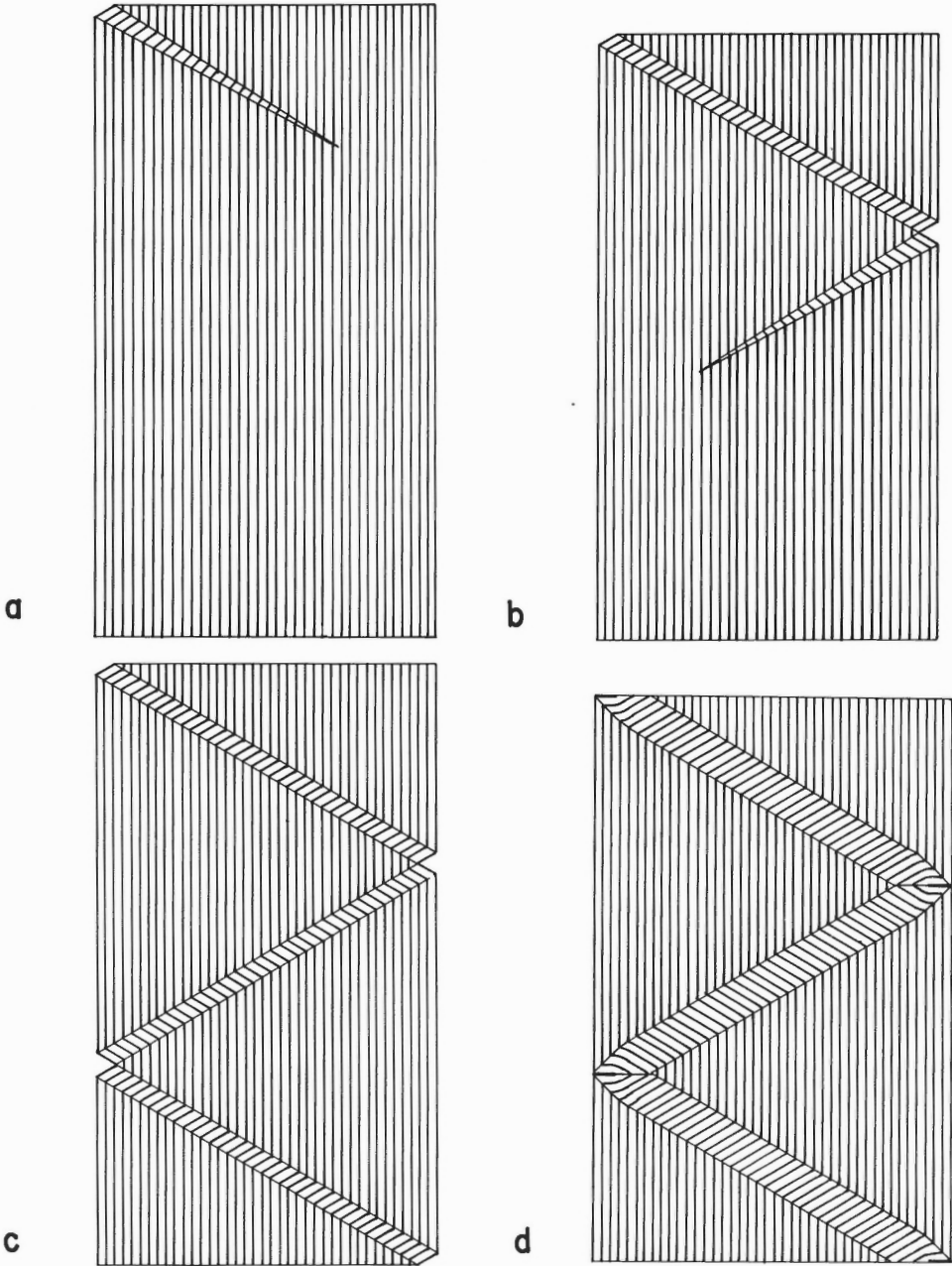


Figure 9. Initial kink pattern in parallel specimens of group 1 compressed between rigid platens: a to c completion of initial zig-zag kink pattern by longitudinal propagation. d. Lateral growth of kink layers associated with appression of marginal folds and appearance of secondary kink boundaries.

Fold Nucleation

Fold nucleation, that is the appearance of primary and secondary kink boundaries, continues throughout progressive deformation of specimens. Of particular importance to the subsequent structural history of specimens are the patterns of nucleation of the first folds to appear which are now described.

Lateral loads used ranged from 225 kg to 4,500 kg. Through this range the differential stress $\sigma = (\sigma_1 - \sigma_2)$ required for first fold nucleation in parallel specimens ranged from less than 80 kg/cm² to 400 kg/cm².

The grouping of the parallel specimens on the basis of the form of the differential stress-shortening curves given above is reflected also in the pattern of the first nucleated folds. In specimens of group 1 the initial pattern of kinking consists of a single kink layer which is seen to nucleate in one corner of the specimen (Fig. 9a) and propagate generally at high velocity along a zig-zag path down the specimen undergoing 'reflection' from the lateral steel platens. This layer may propagate through the whole length of the specimen at the nucleation stress; but generally it pauses before propagation is complete (Fig. 9b) and the deforming load must be reapplied before propagation resumes and the pattern is completed (Fig. 9c). This behavior is again in part a reflection of the 'hard' nature of the apparatus.

Specimens of group 1 at the stage just after nucleation of the first kinks are shown in Plates 1 A, B, C, D and E in order of increasing lateral load. The zig-zag pattern of initial kinking is present in all specimens but detailed features of the kinks change progressively as the magnitude of the lateral load increases. At lower loads (up to 800 kg) the kink layers are broad and the kink folds have markedly curved hinges (Plates 1 A and B). At higher lateral loads the initial kink layers are narrower and the hinges of kink folds sharper (Plates 1 C, D and E). In Figure 10 a the widths in millimeters of initial kinks in group 1 specimens are plotted against lateral load in kilograms (dots). The points lie approximately in a linear group (indicated by line W₁) suggesting a linear narrowing of initial kinks with increasing load.

Study of Plates 1 A to E reveals also that the angles ϕ and ϕ_k decrease with increasing load. These angles differ from one another by from 1 to 5 degrees in either sense and the angle $\phi_{av} = \frac{\phi + \phi_k}{2}$ is plotted in Figure 10 b against lateral load (dots). This angle changes from near 75° for specimens loaded laterally at 225 kg to slightly less than 60° for specimens laterally loaded at 1,350 kg. Again, the grouping of points is essentially linear as indicated by line A₁ in Figure 10 b.

In specimens of group 2 (lateral loading exceeding 1,500 kgs) the simple zig-zag pattern of initial kinking does not appear. Instead, narrow kinks, some of which are lenticular, appear simultaneously in different parts of the specimen. These kink layers are thinnest, most numerous and most uniformly distributed in specimens with the highest lateral loading used (4,550 kg). The change in this initial pattern with increasing lateral load can be seen in the sequence Plate 1 F to 1 J.

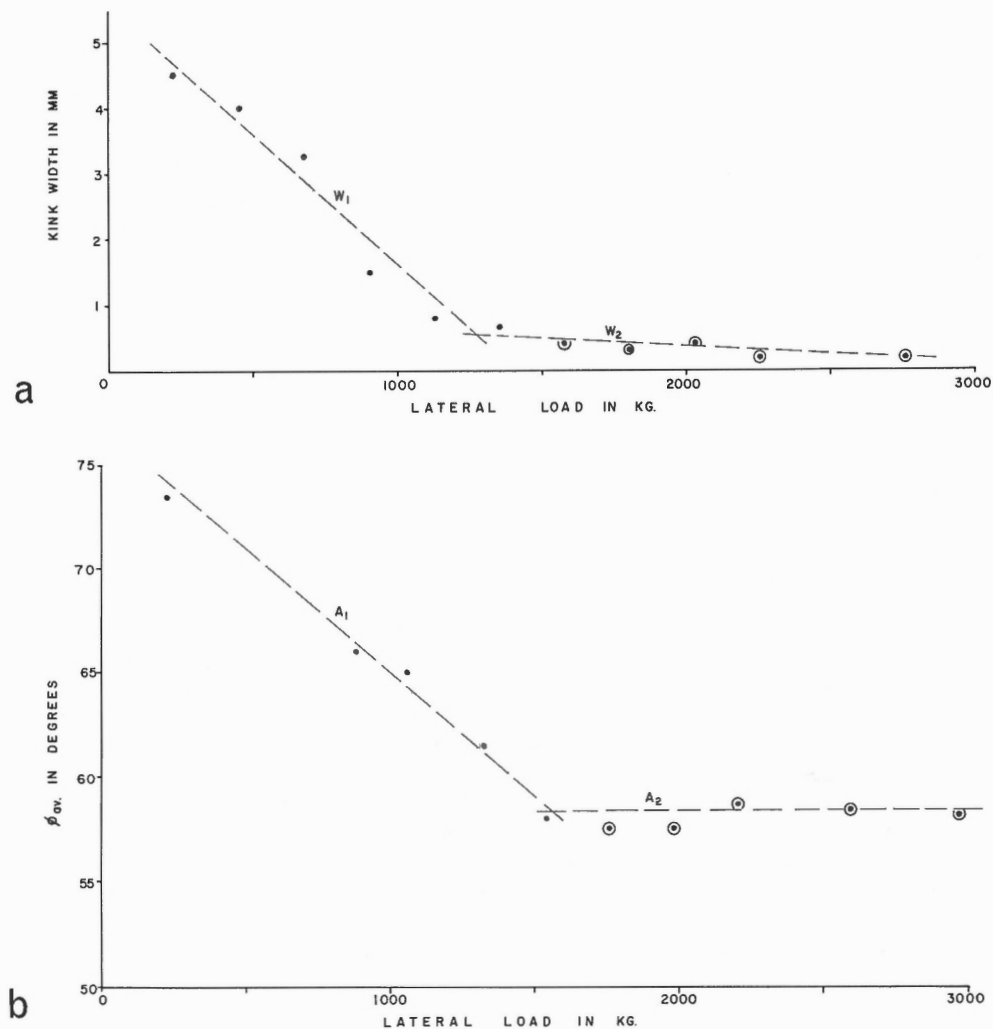


Figure 10. Properties of first-formed kinks.

- a. Width of kinks versus lateral load at nucleation.
- b. ϕ_{av} versus lateral load at nucleation. Dots, specimens of group 1; dots in circles specimens of group 2.

The thicknesses of these initial kinks plotted against lateral load are given by the dots within circles in Figure 10 a. They form another generally linear group (indicated by line W_2) with a slope gentler than the slope of the first group. Likewise, the same symbol for ϕ_{av} in group 2 specimens plotted against lateral load in Figure 10 b suggests the presence of an almost horizontal linear grouping around line A_2 corresponding to $\phi_{av} = 58^\circ$. Lines W and A in Figure 10 are intended only to indicate the general directions of elongation of the point groupings.

The distributions in Figures 10 a and b each appear to have two branches of different slope which meet close to the same value of lateral loading (1,500 kg) chosen on the basis of mechanical behavior as the dividing line between specimens of groups 1 and 2. This value of lateral loading seems to correspond to genuine differences in the mode of deformation of the cards. It seems likely that below this value of lateral loading the dominant mode of deformation is by frictional sliding on the card surfaces with relatively little distributed shear within the cards. The kinks are thick in relationship to the cards and easily propagate through the whole width of the specimen to give a sudden yield. In specimens laterally loaded above 1,500 kg frictional forces across the card surfaces increase and sliding on these surfaces is no longer favored over distributed shear within the cards. At these loads, therefore, slip in kinking is dominantly between the platy fibers of the cards and the kinks are sharper and narrower as a result of the closer spacing of the kink surfaces. Many of the kinks nucleated in specimens at very high lateral loads are in fact thinner than the cards (Plate 1 J) and microscopic study of these specimens confirms that the cards are internally kinked on a very small scale, particularly in places where the cards are apparently thickened in the hinges of larger folds (Plate 18 A). These kinks do not propagate rapidly across the whole specimen and no sudden release of strain energy in the apparatus is caused by their gradual growth.

Because nucleation of conjugate kink layers occurs simultaneously in various parts of specimens of group 2 and because kink angles ϕ and ϕ_R are close to 60° , conjugate kink intersections appear as part of the initial kink pattern as a result of an earlier kink being crossed and sheared by a later kink in conjugate relationship as illustrated schematically in Figure 11. However, not all kink intersections are formed in this way. Some are nucleated apparently by conjugate kinking at a point and kinks propagate outwards in four directions as shown in Figure 12. There appears to be no distinguishing geometric difference between intersections of the two types except that there is no reason why ϕ and ϕ_R should be close to 60° for intersections of the second kind. For example, in Figure 12 d is shown an intersection $\phi = \phi_R = 80^\circ$. Such an intersection is possible within the restrictions of the ideal kink model provided that it nucleates as shown in Figure 12 e as a result of local buckling of a foliated body rather than by propagation of one kink layer across another.

In oblique specimens only one set of kinks appears, always in a sense conjugate to the inclination of the foliation to the compression axis, as described above. These kinks are elliptical in shape and do not in general reach the platens. They tend to become thinner and less symmetric with increasing lateral load. The parallel specimens with copper layers will be discussed below.

Progressive Folding of Parallel Specimens

The structural evolution of a progressively deformed specimen depends largely upon the pattern of initial kinking and thus upon the lateral load. Most specimens were progressively shortened as far as the apparatus would permit. Shortenings achieved ranged from 55 per cent in specimens laterally loaded at 225 kg to about 37 per cent for specimens laterally loaded at 4,550 kg. In each instance the 18,000 kg capacity of the deforming ram was reached at the stated per cent shortening.

The figures for large shortenings can be related only roughly to an actual state of strain of the specimens because of volume dilatation and extension of the specimens perpendicular to the plane of the rams at the high loads involved. These effects are ignored in the following discussion and emphasis is placed on the structural evolution of the specimens as expressed by development of fold patterns during progressive shortening.

In parallel specimens of group 1 (Plates 2 to 5) the first 'phase' of folding is completion of zig-zag initial kink pattern by longitudinal propagation as shown schematically in Figures 9a to c. For the ideal kink model the kink boundaries are

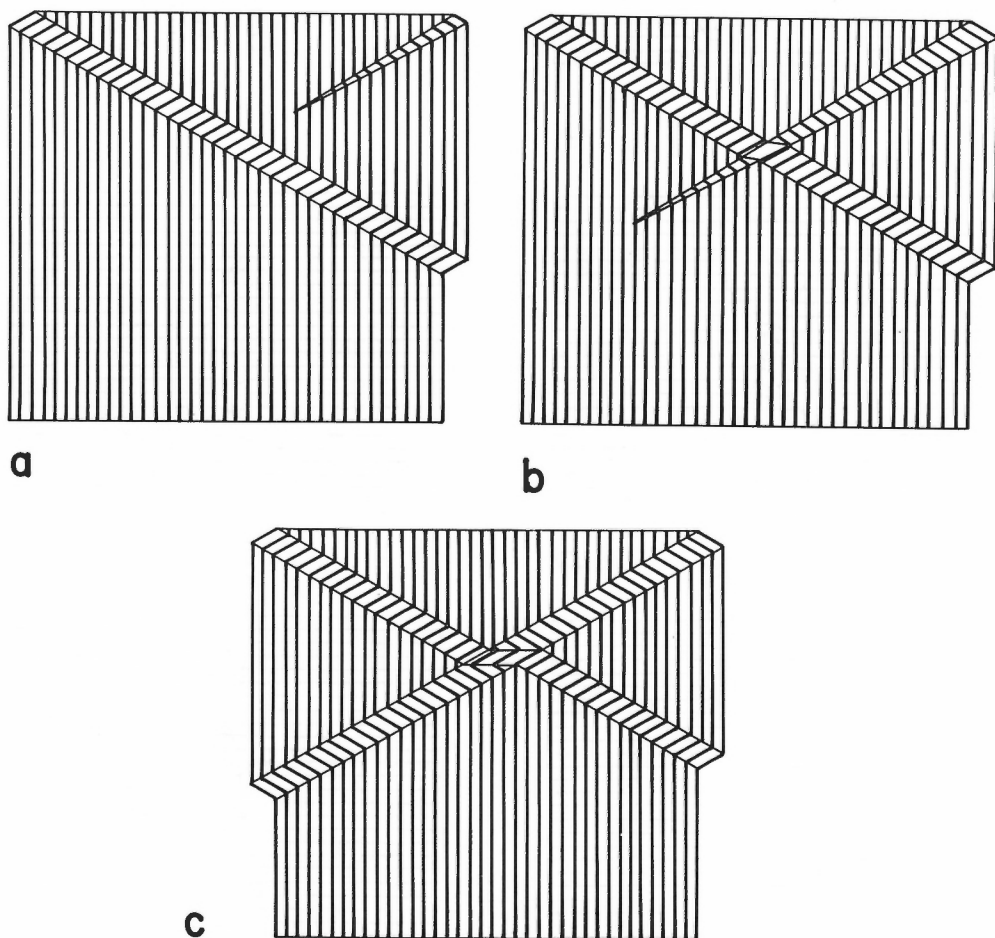
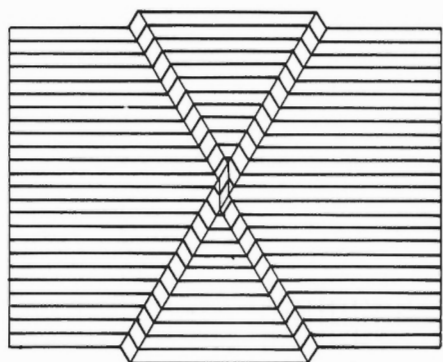
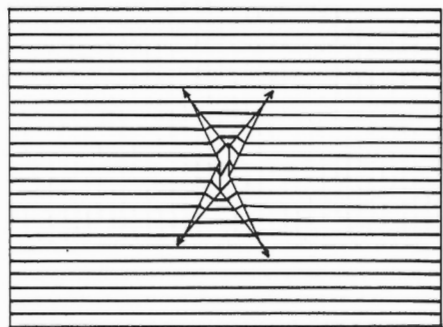


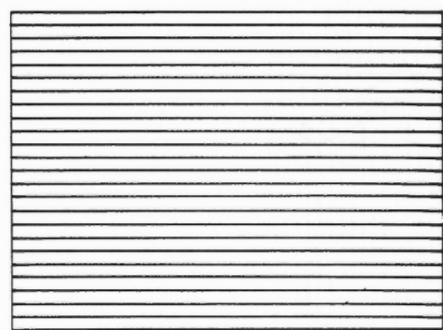
Figure 11. Right-handed kink intersection with $\phi = \phi_k = 60^\circ$ formed by propagation of a later left-handed kink across an earlier right-handed kink.



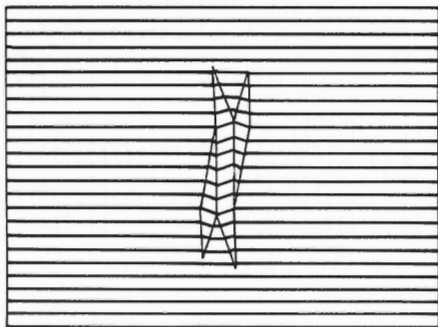
c



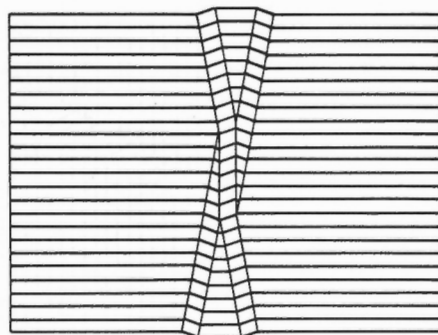
b



a



e



d

Figure 12.

Left-handed kink intersections nucleated at a point by outward propagation of four kink layers: a to c, for intersection where $\phi_k = 60^\circ$ d, e, for intersection where $\phi_k = 80^\circ$

'locked' at this stage and no lateral propagation of boundaries is possible. In the experiments some widening of the initial kink layers does in fact occur in association with the closing of the open spaces in the hinges of the folds at the platens as shown diagrammatically in Figure 9d. This appression of the marginal folds is achieved by local curvature of the folded cards and fits very closely the geometry of ideal kinking. Widening of the first kinks results in the formation of secondary kink boundaries at the hinges of the marginal folds which are propagated into the specimen a distance determined by the increase in thickness of the initial kink layers. At lateral loads below 1,000 kg (Plates 2 and 3) the secondary kink boundaries may extend more than half way across the specimen.

Further deformation of these specimens increases the length of the secondary boundaries and reduces the apical angles of the chevron folds which have the secondary boundaries as axial surfaces with the result that the center part of the specimen becomes chevron folded in a symmetric way (Plates 2 and 3, D, E and F, and Plate 18 B). Coupled with this appression of the chevron folds, which apparently involves equal amounts of slip on the cards forming opposing fold limbs, is nucleation of a new phase of small conjugate kinks in the wedge-shaped undeformed domains at the specimen edges. These kinks are generally too thin to propagate across the kinks of the first phase, but they have ϕ_{av} close to 60° and they intersect one another (Plate 18 C). Further deformation can cause the appearance of sets of elliptical kinks in approximately conjugate orientation to the oblique foliation in the limbs of the chevron folds towards the center of the specimens (Plate 18 D), coupled with general appression of all folds and nucleation of still smaller kinks within any surviving undeformed domains.

Structural evolution of group 1 specimens laterally loaded between 1,000 and 1,500 kg (Plates 4 and 5) is similar, but the first phase kinks are narrower and very large undeformed domains survive. The kinks nucleated in these domains by further deformation tend to be similar in width to the first phase kinks and are locally propagated across them to give kink intersections (Plates 4 C and 5 C). Ideally, a network of conjugate kinks develops as illustrated schematically in Figure 13. The kinks are not always of the same width and in places two kinks of the same sense may coalesce to form a wider kink. The intersections formed are left and right handed in about equal proportions, but they do not have the very regular pattern of distribution used as a first model by Paterson and Weiss (1966, p. 369, Fig. 18b).

Further deformation of such specimens (and of all parallel specimens at higher lateral loads) results in a characteristic pattern of large scale heterogeneous deformation controlled by the design of the apparatus. Unsupported areas of the specimens of appreciable size are present at the upper right hand corner during most of an experiment, and at lateral loads exceeding 1,000 kg specimens become unstable. Contributing to this effect are high frictional forces on the ends of the specimen and the asymmetry of the lateral load arising from the fact that the lateral loading piston moves outward to the right with respect to the three other loading surfaces. The result of these irregularities in loading is the development at a relatively late stage of a thick pair of conjugate kinks forming a 'major' conjugate fold. These kinks grow in width by lateral propagation of their boundaries as deformation proceeds. Such

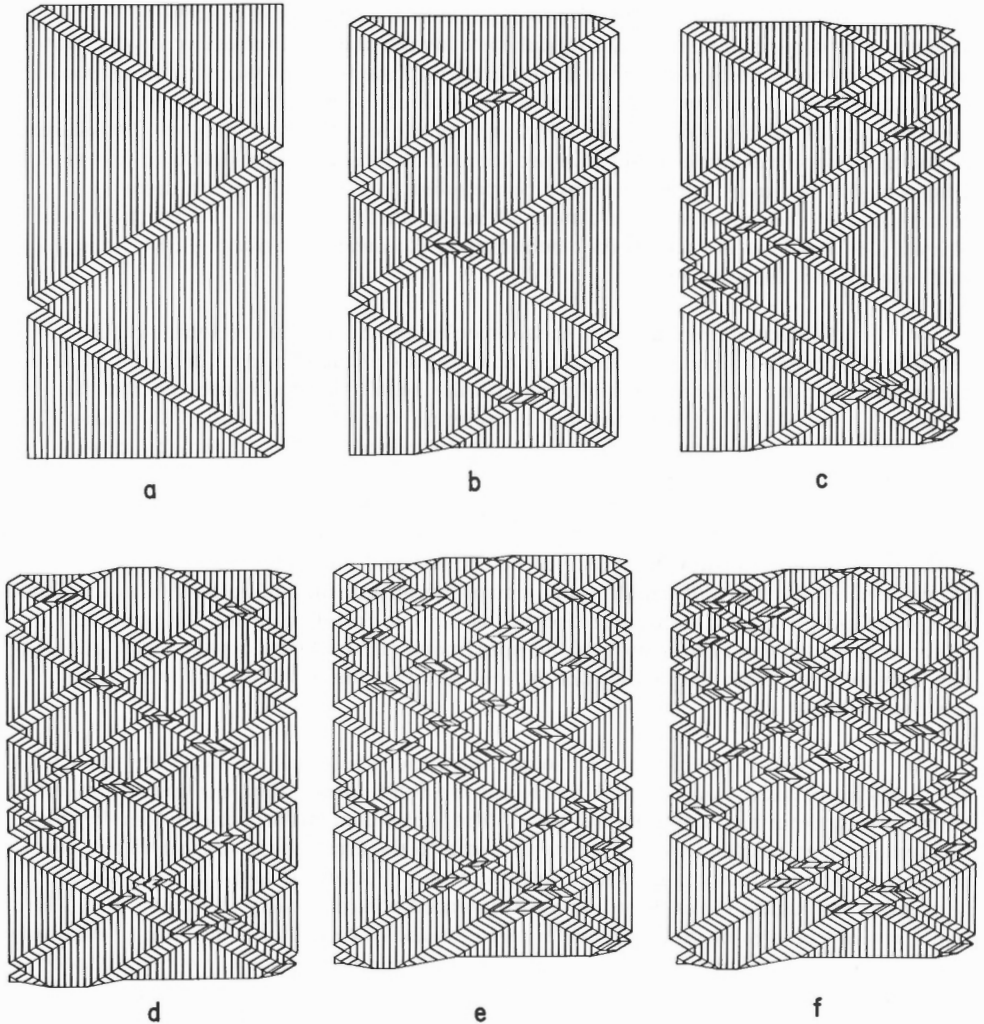


Figure 13. Growth of kink network (for $\phi = \phi_k = 60^\circ$) by repeated nucleation and propagation of kink layers of similar width.

behavior is illustrated diagrammatically in Figure 14 for a specimen already containing an ideal network of conjugate kinks. The two major conjugate kinks that outline the late fold (Fig. 14 c) form by widening and coalescence of kink sets of opposite sense in the two halves of the specimen. The boundaries of these major kinks laterally migrate through a background pattern of 'minor' conjugate kinks and contain intersections of both senses. For the ideal kink network the resulting structures within the major kinks depend upon the sense of the intersections and kink layers engulfed by the growing major kinks. In Figure 15 the two possible distinct situations are illustrated for

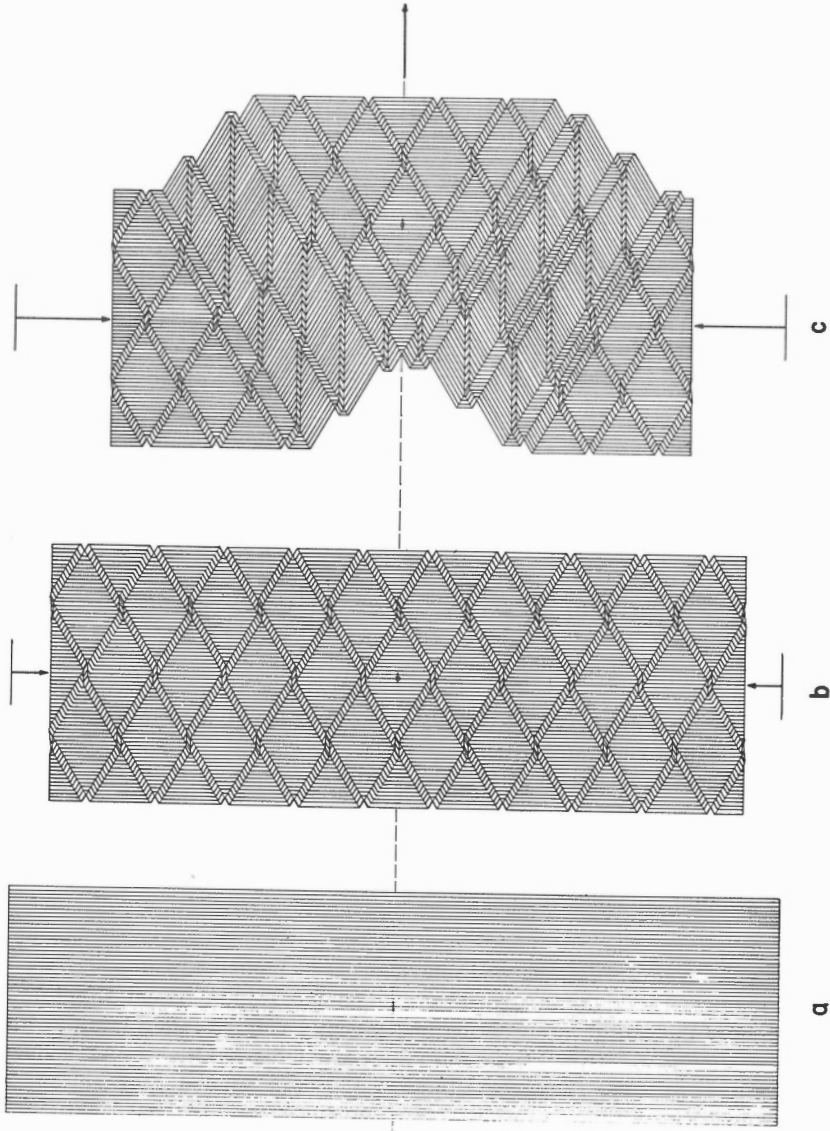


Figure 14. Growth of major conjugate kink fold in material with ideal network of minor early conjugate kinks. Early kink layers in b become internally rotated to form parasitic folds on the limbs of the major conjugate fold in C.

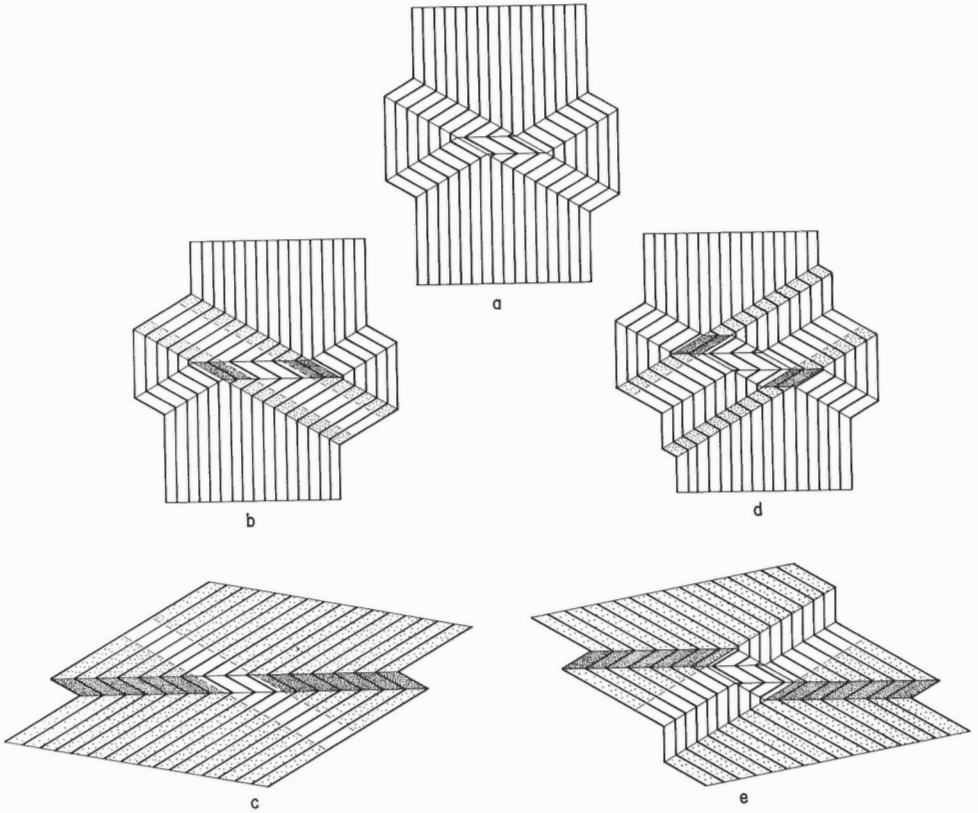


Figure 15. Internal rotation of early kink layers of the type illustrated in Figure 14 c.
a. Left-handed kink intersection.
b and c. Growth of left-handed kink by lateral propagation.
d and e. Growth of right-handed kink by lateral propagation; note survival of undeformed domains and primary kink boundaries.
Light stipple; domains of simple kinking.
Heavy stipple; domains of intersection.

the ideal kink model. An initial left-handed intersection in Figure 15 a is progressively engulfed in Figures 15 b and c by growth of a right-handed kink (light stipple). The left-handed kink of the initial intersection is internally rotated into a laminar kink intersection (heavy stipple) separated from the major right-handed kink by secondary kink boundaries (Fig. 15 c). The converse situation of a right-handed intersection progressively engulfed by a left-handed major kink is illustrated for ideal kinking in Figures 15 d and e. In this situation two types of minor fold appear within the major kink, as follows:

1. Some parts of the initial right-handed kinks are internally rotated (heavy stipple) and give rise to chevron folds with secondary kink boundaries as axial surfaces, as in the last example.
2. Undeformed domains survive at the intersection; and monoclinical folds with primary kink boundaries as axial surfaces are preserved. The axial surfaces of these folds are oblique to minor folds of type 1.

Both limbs of the major conjugate fold, therefore, contain small 'parasitic' folds of each type representing the internally rotated remnants of the initial pattern of their conjugate kinks. Most of these small folds have axial surfaces subperpendicular to the compression axis and parallel to the bisecting plane of the major conjugate fold. Such a pattern is a common feature of natural folds in thinly layered rocks.

One feature of the pattern of kinematic importance is that small folds of type 1, although symmetric across their axial surfaces, are not symmetric in their strain properties. One limb is a result of simple kinking and has a shearing strain given by $2 \cot \phi$. The other shorter limb is a domain of intersection and has shearing strain $4 \cot \phi$. Similarly one limb of the monoclinical folds of type 2 (also symmetric across their axial surfaces) is a domain of simple kinking and the other is undeformed.

Development of late major kink folds of the kind just described can be seen in Plates 4 and 5 D, E and F. Close-up photographs of the development of parasitic folds on one limb of a late major kink fold are shown in the sequence in Plate 17. In this sequence the major kink develops by the growth and coalescence of a set of left-handed kinks (the black dot represents the same point in each photograph).

Parallel specimens of group 2 (Plates 6 to 8) show a similar pattern of structural evolution after initial kinking, but apparent differences are introduced by the absence of the initial phase of zig-zag kinking and by the small scale of the subsequent kinking. Above lateral loadings of 2,000 kg some even of the first formed kinks are thinner than the cards and involve internal slip and kinking. At the highest lateral load used (4,500 kg) a uniform network of kinks develops composed entirely of kinks of this kind (Plate 8). The development of a late major kink fold is observed also in specimens of group 2, generally of smaller amplitude than at lower lateral loads. At lower lateral loads (Plates 6 and 7) a typical pattern of parasitic folding appears on the limbs. At higher lateral loads (Plate 8) the fold is a gentle warp in foliation already tightly folded by internal kinking on the cards. Details from such specimens are illustrated in Plates 19 A, B and C. The very small folds in Plate 19 A are typical of all specimens at the highest deforming load (18,000 kg). In specimens of group 1 they appear as a last phase of folding in any undeformed domains left between the earlier generations of kinks. For example, in Figure 16 a is shown an undeformed domain at the edge of a specimen bounded by a pair of conjugate kinks. In Figure 16 b the domain is invaded by smaller conjugate kinks of a later generation. The undeformed domains still surviving are invaded by still smaller sets of conjugate kinks with increasing deforming load (Fig. 16 c) and so on until the whole undeformed domain in Figure 16 a is folded. The change in shape of the domain is accommodated by slip in the initial pair of conjugate kinks. The pattern of repeated conjugate kinking

on smaller and smaller scales leads to a structure such as that illustrated in Fig. 16 d. The original pair of conjugate kinks are the limbs of an appressed fold with a wedge-shaped hinge region folded on a smaller scale. Such structures can be seen in Plates 4 F and 5 F.

A similar process in specimens with an early network of conjugate kinks as in Figure 17 a (the same as Fig. 13 f) leads to the pattern in Figure 17 b. In a

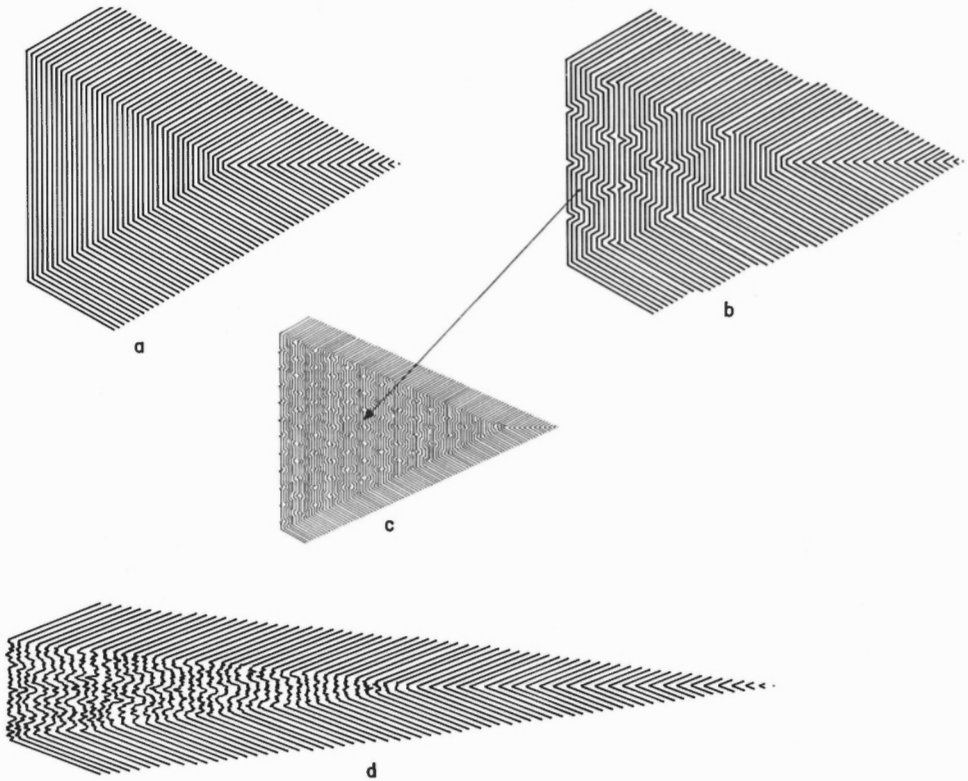
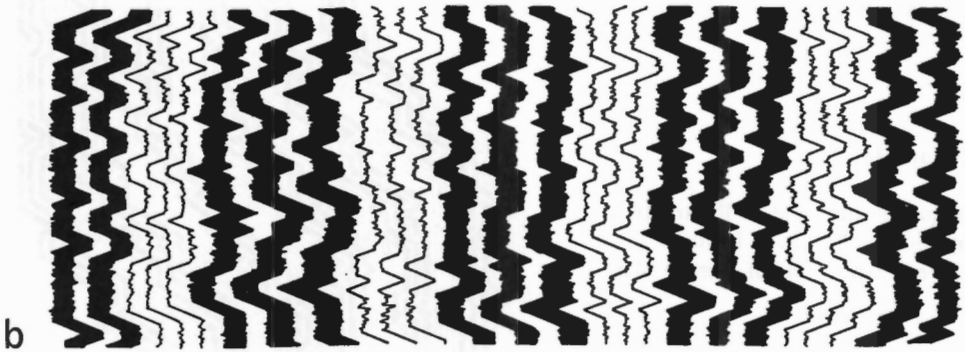
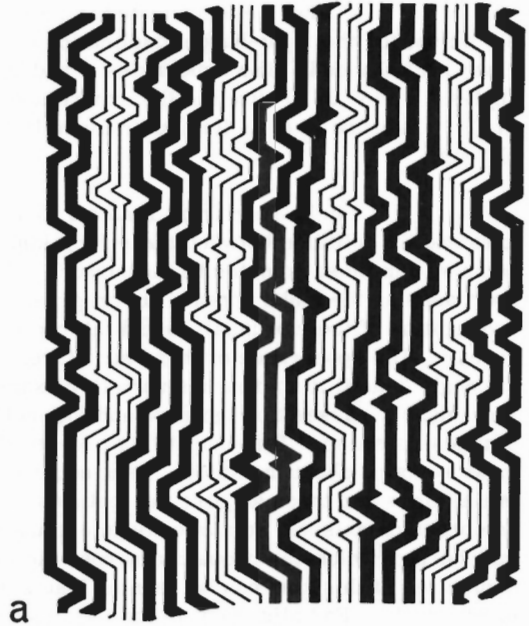


Figure 16. Progressive deformation by nucleation of successive generations of conjugate kinks.

- a. First generation conjugate kink fold with primary kink boundaries and undeformed domain.
- b. Nucleation of second generation of smaller kinks in undeformed domains.
- c. Nucleation of third generation of smaller kinks in undeformed domain of b.
- d. Final appearance of a; undeformed domain contains tight chevron folds of different sizes and limbs of earliest conjugate kink fold are appressed to give a smaller interlimb angle.

Figure 17.

Sequence outlined in Figure 16 applied to the network of conjugate kinks in Figure 13 f.



specimen with a late major kink fold as in Figure 18 a (the same as the lower kink in Figure 14 c) progressive small scale kink folding leads to the configuration in Fig. 18 b. An internally rotated older thick kink in a background of later small scale kink folding is shown in Plate 19 B, and a late kink front migrating laterally over a background of earlier small scale conjugate kink folds in Plate 19 C.

Progressive Folding in Oblique Specimens

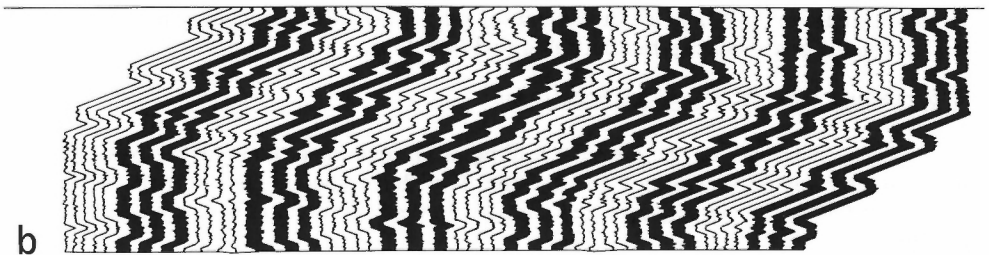
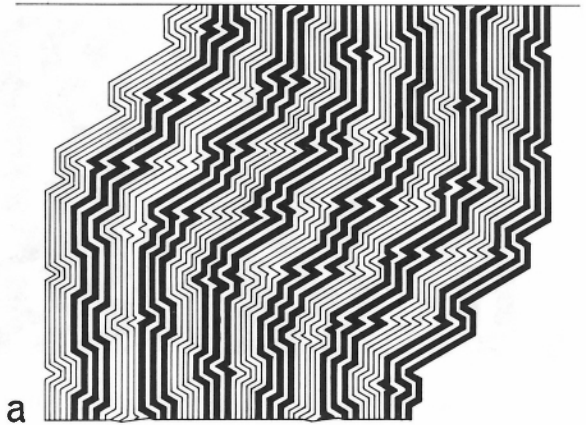
Examples of progressive folding of oblique specimens at various lateral loads are presented in Plates 9 to 12. The first three specimens (laterally loaded between 1,000 and 2,000 kg) are very similar in their structural evolution and are considered first.

The first kinks nucleated in these specimens comprise a parallel lenticular set which, for the right-handed inclination of the cards used in the experiments, is always left-handed. The kink angles ϕ and ϕ_k are variable, but for initial inclination angles $\alpha = 15^\circ$ to 20° used in the experiments ϕ_{av} for the first formed kinks is 60° to 65° . Because of their lenticular form these kinks generally do not reach the lateral platens.

It can be seen from Plates 9 to 11 that the angle between the compression axes and the foliation between these first kinks changes from its initial value and that some slip in these domains has occurred. The angle α in these domains always decreases as the kinks appear. In progressive deformation the kinks widen by lateral propagation of their boundaries and later kinks, subparallel to the first kinks, may appear. The appearance of these structures is associated with further reduction in the angle α until it approaches zero (for example, in Plate 11C, center). In some specimens α passes through zero and the inclination of the foliation in these domains changes its sense. Throughout this process the orientation of the foliation within the kinks remains about the same. As α acquires a low value in the domains between the initial kinks and these acquire the features of a parallel specimen with respect to the compression axis and sets of conjugate kinks are generally nucleated the thicker members of which can propagate across the initial kinks to form kink intersections. Structures of this kind can be seen in Plates 9 to 11 and are schematically illustrated in Figure 19. End alignment in the specimen is maintained in this way.

Figure 18.

Sequence outlined in Figure 16 applied to the lower limb of the conjugate fold of Figure 14c.



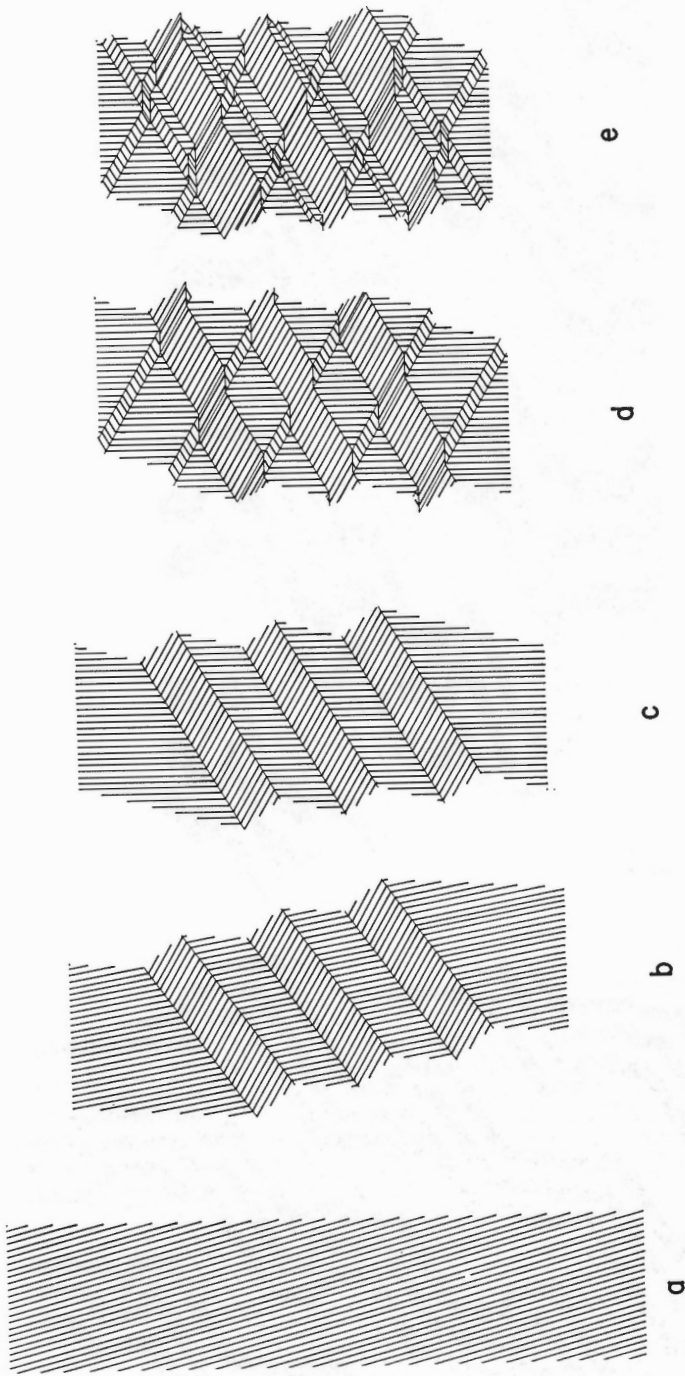
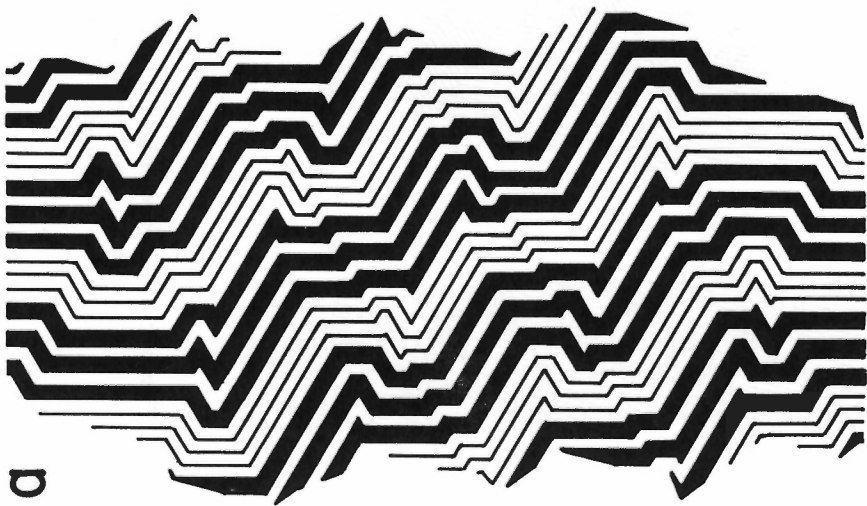


Figure 19. Sequence of kinking in oblique specimens:
a to c. growth of first kinks
d to e. nucleation of conjugate kink networks in domains separating first kinks.



a



b

Figure 20. Sequence outlined in Figure 16 applied to network of kinks in Figure 19 e.

Subsequent history of the oblique specimens resembles closely that of the parallel specimens. The conjugate kinks nucleated in the domains between the thick initial kinks become smaller and smaller as the deformation increases and the initial kinks are deformed by internal slip. The resulting pattern is indicated schematically in Figure 20 (Fig. 20 a is the same as Fig. 19 e). Folds appear with one set of plane limbs corresponding to internally rotated initial kinks and the other set of limbs tightly folded in a much smaller scale. An example of such a structure developed in one of the oblique specimens at the end of deformation is shown in Plate 19 D.

Deformation of an oblique specimen loaded laterally at 4,500 kg is shown in Plate 12. The development of folds is similar to that just described, but the first kinks are mostly thinner than the cards and the scale of the final folds is correspondingly reduced. A close up photograph of a section of Plate 12 is shown in Plate 19 E: the same pattern of folding as sketched in Figure 20 b is seen to be present on a very small scale.

Progressive Folding of Specimens Containing Copper Layers

Annealed copper sheets 1 mm thick were introduced into some of the parallel specimens to simulate more 'competent' isotropic layers. The behavior of these layers was found to depend on lateral load as illustrated in Plates 13 to 16.

At low lateral loads corresponding to specimens of group 1 (for example, the specimen in Plate 13 loaded laterally at 900 kg) the presence of a copper layer does not seem to affect the appearance of the first zig-zag pattern of kinks. At this stage (Plates 13 C and D) the layer acquires the form of a 'box-fold'. Further deformation forms chevron folds of the same kind in the cards and copper layer.

At loads corresponding to the lower range of group 2 specimens (for example, Plate 14, loaded laterally at 2,200 kg) the initial kink pattern in the cards is much the same as in specimens without isotropic layers (compare, for example, Plates 7 C and 14 C), but the layer begins, after a small amount of shortening, to buckle in a periodic way not entirely governed by kinking in the cards. At still higher lateral loads (3,600 and 4,500 kg, respectively in Plates 15, upper and lower) control of kinking in the cards on fold nucleation in the copper layers is even less pronounced and the initial folds in the copper layer seem to represent instability of the layer rather than instability of the cards. The cards, however, still deform by much the same kink mechanism as that described above for high lateral loads, but deformation is markedly heterogeneous and the cards tend to accommodate to the sinusoidal buckles in the copper layers. At these lateral loads the copper layers become ptygmatically folded by large amounts of shortening.

Finally, in Plate 16 is shown the progressive deformation of a specimen containing four copper layers. Lateral loading was 2,200 kg and folds in the layers are seen to evolve from box or conjugate folds in the early frames to typically concentric or ptygmatic folds in the later frames. Kinking in the matrix seems to play the dominant role in fixing the position and amplitude of folds in the layers of this lateral loading. In this sequence too, early kink folds can be seen internally rotated to form 'parasitic' folds on the limbs of the larger folds, folds of both kinds having axial surfaces of approximately the same orientation.

POSSIBLE GEOLOGIC IMPLICATIONS

How far the behavior of card decks in the experiments corresponds to the behavior of foliated and layered rocks undergoing flexural slip folding in response to tectonic forces in the earth's crust is at present a matter for conjecture. Some possible geologic implications of the experiments are now briefly reviewed.

The experiments suggest that all nucleation of flexural slip folds in constrained foliated bodies under pressure is by kinking and conjugate kinking. First formed folds are generally kink folds with axial surfaces inclined obliquely to the direction of greatest principal stress at the time of nucleation. In symmetric situations (corresponding to 'parallel specimens' in the experiments) kink angles (ϕ and ϕ_k) close to 60° permit the appearance of kink intersections by propagation of one kink across another. But conjugate intersections can appear for any kink angle if they are of the kind which nucleates at a point and propagates outwards as four kink layers. In either instance, secondary boundaries appear as axial surfaces of chevron folds perpendicular to the axis of greatest shortening.

The amplitudes of kink folds at the time of nucleation appears to depend upon two factors, as follows:

1. The smaller the spacing of the 'slip surfaces' in a foliated body, the smaller the amplitude of the folds. Thus, folds nucleated in a phyllite with a strong pervasive foliation are likely to be of smaller amplitude in a given dynamic situation than folds in a series of laminated rocks such as bedded cherts with shaly partings.

2. At higher confining pressures (in the experiments given by $\sigma^1 = \frac{\sigma_1 + \sigma_2}{2}$

at the time of nucleation) in the same foliated body smaller folds are nucleated. Experiments suggest also that, if layers are internally anisotropic, increased confining pressure can cause shearing strain (slip) to be more uniformly distributed through the body by forcing more foliation surfaces into active roles as slip surfaces. This phenomenon also appears to contribute to a decrease in amplitude of initial folds.

Flexural slip folds of the kink type seem to nucleate with a characteristic interlimb angle. In most of the experiments this angle is between 110° and 130° and it is approximately bisected by the axial surface of the fold (kink boundary). There is no evidence that such folds form by a gradual closing of the limbs towards this angle. In fact, for primary kink boundaries, any change in this interlimb angle is impossible for a fixed orientation of the kink boundary without substantial departures from finite simple shear in the deformed domain. In asymmetric situations (corresponding to oblique specimens) some appression of initial kink folds is possible by simultaneous simple shear in both limbs, and folds with much smaller interlimb angles (60° or less) are likely to have secondary kink boundaries as axial surfaces and be associated with kink intersections. Folds of this kind can have their interlimb angles appressed below the nucleation value by progressive deformation.

Most flexural slip folds of the symmetric chevron type (with axial surfaces approximately bisecting the interlimb angle) must therefore be asymmetric in their strain properties. Except for very special cases the finite simple shear on one limb will be different from the finite simple shear on the other. The two extreme cases arising in symmetric situations are first, folds with primary kink boundaries as axial surfaces in which only one limb is deformed, and second, folds associated with conjugate kink intersections with secondary kink boundaries as axial surfaces in which the shearing strain in one limb is twice that in the other. In between lie the folds developed in asymmetric situations in which both limbs are deformed but by different amounts.

Progressive deformation of a foliated body following a path corresponding to an increasing finite pure strain leads to complete folding dominantly by kink phenomena of two kinds, as follows:

1. Limited lateral propagation of kink boundaries can extend the length of the limbs of early formed kink folds so that at successive stages in the development of the fold its axial surface may not occupy the same material plane of the deformed body. Such widening of kinks is inhibited by the presence of kink intersections which have a 'locking' effect on primary kink boundaries.
2. Most progressive folding takes place by nucleation of successive generations of kink and conjugate kink folds in undeformed domains of a foliated body. In general, each successive generation is on a smaller scale and requires increasing differential stress for nucleation. A pattern of folds of various amplitudes results. Some folds, particularly in asymmetric situations have one set of planar limbs with much smaller chevron folds on their other limbs or in their hinge regions. Progressive nucleation of smaller scale folds in undeformed domains is generally associated with appression of the interlimb angles of already formed chevron folds with secondary kink boundaries as axial surfaces.

The experiments suggest a possible origin for some minor 'parasitic' or 'drag folds' found on the limbs of some major flexural slip folds. If the large fold developed as a conjugate kink fold in a foliated body containing a network of small scale conjugate kink layers, kink layers of one sense can become internally rotated by the major kink of the other sense so that secondary kink boundaries appear on the limbs of the major fold parallel to its axial surface. These boundaries are axial surfaces of small folds with one long and one short limb. The distribution of shearing strain in these minor folds is again asymmetric with twice as much shear in the short as in the long limbs.

An important question posed by the experiments is, how widespread in nature are kink folds and related flexural slip folds of the kind produced? They are common enough in well foliated rocks and few geologists working in metamorphic rocks have not reported them, although there is a tendency to report them as 'brittle' or superficial phenomena associated with near surface deformation. The experiments suggest, however, that the development of thin sharply angular kink layers of the kind most commonly noticed by geologists is favored by increasing pressure and constraint

rather than the reverse, and that these structures should be viewed more as the first evidence of a phase of progressive folding that would lead (if it went to completion) to the appearance of tightly appressed chevron folds of the kind acknowledged by most geologists to have formed at depth in the crust and in no sense to be an expression of brittle behavior.

There are in addition, factors that seem to limit the recognition of kink and conjugate kink folds in nature. The most important of these is scale of development. Such folds are easily observed and recognized in platy rocks if they are developed on a small scale and can be studied directly. Larger (macroscopic) folds of this kind are less easily recognized unless the hinge regions are properly exposed and the narrowness of the zone of curvature can be clearly seen. Also, some of the later stages in the proposed folding process may appear in the field as regions of planar foliation (rotated early kinks) followed by zones of tight small scale chevron folding. This situation can be envisaged by picturing Plate 19 or Figure 20b as cross-sections of large bodies of foliated rock.

Another factor of the same kind is the difficulty of recognizing such folds in coarsely or massively layered rocks such as thick sedimentary sequences. The 'slip surfaces' in such sequences might be shaly partings between massive isotropic layers of limestone, sandstone or quartzite and can be spaced hundreds of feet apart. 'Kink' or 'conjugate kink folds' forming in such sequences may have amplitudes of many hundreds or thousands of feet and have hinge regions that are only sharp 'kink surfaces' with respect to the dimensions of the whole fold, and in many such sequences the great thickness of the sliding layers prohibits these surfaces from being sharply defined on any scale. But the common occurrence of 'box-folds' (large scale conjugate folds) in such sequences in the early stages of folding is becoming increasingly obvious to geologists, and folds with long straight limbs and narrow hinge regions are more typical of weakly folded bedded sequences than gentle concentric or sinusoidal warps commonly pictured.

Belousov (1965, p. 3) for example writes:

"Field observations have shown that in many cases the usually accepted notions about the shapes and associations of folds, appearing in the standard books on structural geology, are by no means exact. The inevitable generalizations necessitated by the scale of the presentation often led to distortions in the sizes of the folds of the various orders when they were shown in cross sections. The shapes of the folds were also thus distorted. Particularly distorted were those folds the shapes of which could not be interpreted as having resulted from horizontal compression of the Earth's crust. Thus, for instance, box folds were often overlooked by geologists, either purposely or, most probably, unconsciously. We could cite numerous examples where such folds are shown to be much more rounded in cross-section than they actually are. Such inexactitudes and schematic representations inevitably hampered the correct understanding of these folds. Our prime aim should be the comprehension of the correct shape and size of the folds, while attempting to avoid any distortions due to schematic representation".

In the proposed scheme of development of flexural slip folds the phase in which conjugate or box folds are present is an early one. Prolonged deformation gradually involves all undeformed domains in folding, and the conjugate and kink folds with primary kink boundaries as axial surfaces become progressively replaced by chevron types with much smaller interlimb angles. On a larger scale, isotropic layers acquire rounded 'concentric' hinge forms and thin mechanically weaker layers tend to thicken in the spaces between the hinges of adjacent layers commonly by chevron folding on a much smaller scale.

Considerations of this kind suggest that many large folds in massive layered sedimentary sequences formed as a result of bedding plane slip may evolve through box-like conjugate forms with many planar segments to more rounded forms at later stages. Such a sequence for widely separated layers is depicted in Plate 16. Experiments on card decks with many closely spaced layers of copper yield similar results. In particular, a horizontally compressed sedimentary sequence separated from stronger basement rocks by a planar décollement (such as has been proposed for the sediments of the Jura mountains) may behave similarly to the group 1 specimens described above. Initial folding may involve development of a zig-zag pattern of primary kinks between the basement and the upper surface of the sediments as they slide on the décollement surface. Some published sections through the Jura folds are suggestive of such a pattern with many of the primary kink boundaries subsequently replaced by thrust faults.

Clearly, many folds in sedimentary and metamorphic rocks are not simple flexural slip folds in which the main mechanism of deformation is slip on the folded surface coupled with flexure of individual layers. Some folds have pronounced secondary foliations developed parallel to their axial planes; others contain deformed dimensional markers such as pebbles, fossils, oolites and other structures strain analysis of which indicates the presence of strain components, such as flattening in the axial plane or extensions in specific directions such as along the fold axis, not compatible with flexural slip alone. But many of these folds may have been nucleated initially by flexural slip, and later in the history of development been modified as the folded surface acquired a passive role in the deformation during a period of more homogeneous strain, generally under metamorphic conditions. Such a sequence could be modeled in the experiments at very high lateral loads where axial extension of the specimens perpendicular to the loading plane (not possible by flexural slip) led to a general appression of the chevron folds nucleated at lower loads by conjugate kinking.

Similarly, the present discussion does not apply directly to the commonly considered situation of an isotropic layer or set of layers with one set of material properties enclosed in a matrix with another, except in so far as this situation is represented by the behavior of an annealed copper layer embedded in a card deck. Experiments on such specimens suggest that in some dynamic situations (lower ranges of confining pressure in the experiments) nucleation of folds in the isotropic layer is controlled dominantly by kinking in the matrix as suggested elsewhere for the folding behavior of thin quartz veins in phyllite (Paterson and Weiss, 1968). In other dynamic situations (higher ranges of confining pressure in the experiments) folding of the layer seems to be a buckling phenomenon controlled in part by the shape and thickness of

the layer. The matrix seems to accommodate to the form of the buckled layer by very small scale kink folding (contrast, for example, the behavior of the layers in Plates 13 and 15).

A few experiments not described above involved deformation of card decks in which the plane of the cards was inclined obliquely to the loading plane. This dynamic situation represents the most general one to be found in nature. Conjugate kink folds are formed, but the line of intersection of the kink layers does not lie in the plane of the cards. Such conjugate kink folds are commonly observed in natural rocks (see for example, Ramsay, 1962). Further deformation of such structures could be expected to yield folds of a generally conical form (for example, Wilson, 1967).

Finally, an important question not yet completely answered by the experiments is the reason for the observed values of kink angles ϕ and ϕ_k . Although these two angles tend to be equal both in experiments and in nature, there is a small but definite difference between them, generally with ϕ_k slightly larger than ϕ . This difference is not intuitively surprising because kink folds are not kinematically symmetric across their axial surfaces, only one limb being deformed, and is probably connected with the introduction of small scale discontinuities and irregularities in the deformed limb which is not a mirror image of the undeformed limb. More important and less easily explained are the particular values of kink angle observed. In symmetric situations in both phyllite and card decks these angles are close to 60° (generally a little less). Observations on natural symmetric conjugate kink folds in rocks yield similar values (for example, Anderson, 1964, p. 274). For asymmetric situations the angles seem to be larger.

The solution to this problem would seem to lie in the nature of the kink nucleus. The manner of kink propagation observed in the experiments suggests that the kink angle is decided at the time of nucleation when the direction of longitudinal kink propagation (approximately the bisectrix of the angle between the undeformed and kinked foliation) is also fixed. Some progress has been made in understanding angles typical of symmetric situations by considering the work densities required to form kinks of specific orientations; but this study is in an early stage and cannot be reported here.

REFERENCES

- Anderson, T. B.
1964: Kink-bands and related geological structures; Nature, vol. 202, No. 4929, pp. 272-274.
- Belousov, V. V.
1965: Folded deformations in the earth's crust; Academy of Sciences, U. S. S. R., a collection of papers edited by V. V. Belousov and A. A. Sorskii, translated from Russian by Israel Program for Scientific Translation, Jerusalem, pp. 1-367.

Paterson, M. S. , and Weiss, L. E.

1966: Experimental deformation and folding in phyllite; Bull. Geol. Soc. Am. ,
vol. 77, pp. 343-374.

in press: Folding and boudinage of quartz-rich layers in experimentally deformed
phyllite; Bull. Geol. Soc. Am.

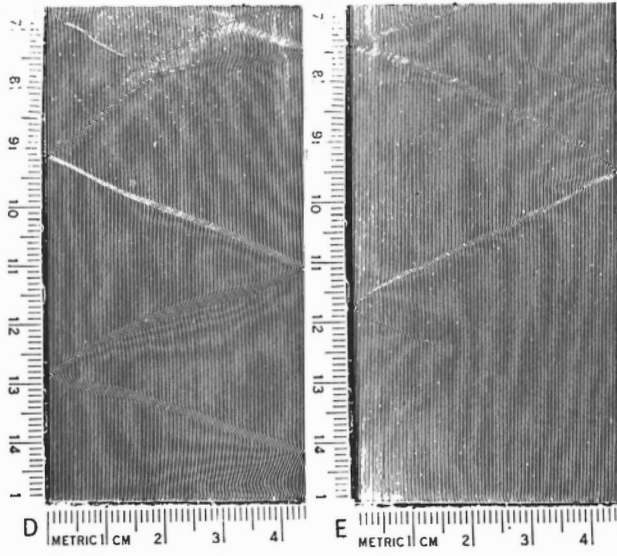
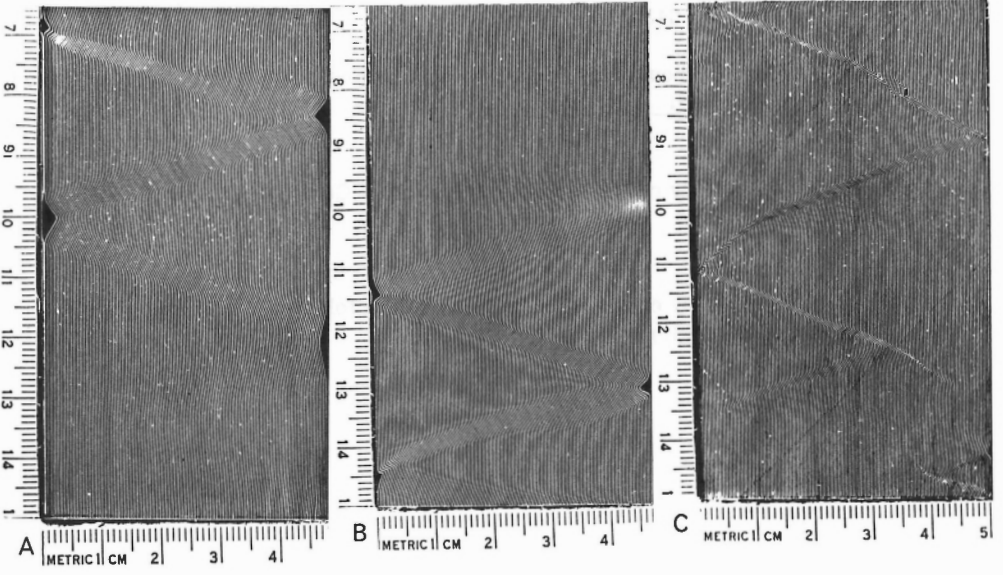
Ramsay, J. G.

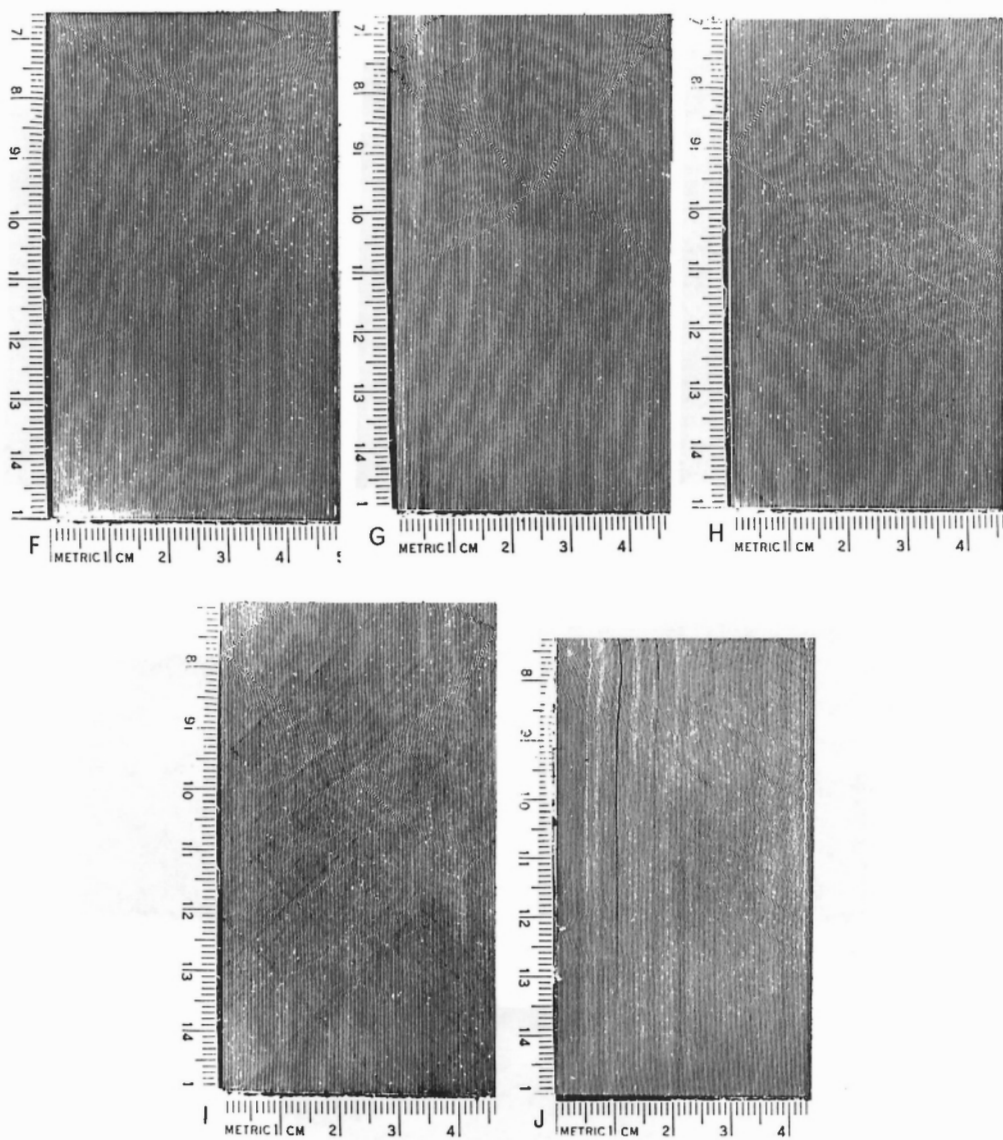
1962: The geometry of conjugate fold systems; Geol. Mag. , vol. 99,
pp. 516-529.

Wilson, G.

1967: The geometry of cylindrical and conical folds; Proc. Geologists'
Assoc. , (Engl.), vol. 78, pp. 179-210.

Plate 1





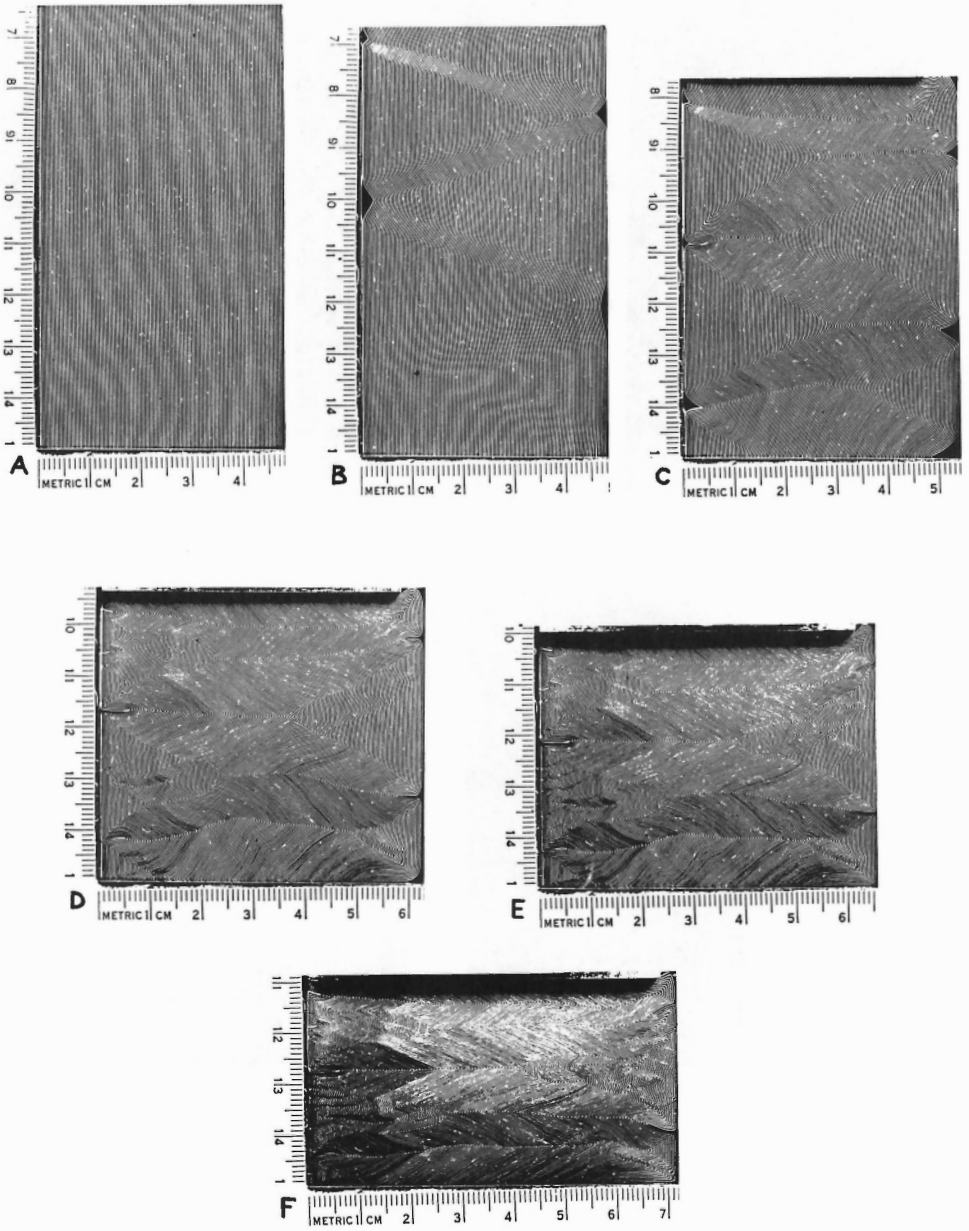
Patterns of fold nucleation in parallel specimens at different lateral loads.

A to E, group 1 specimens; lateral loads as follows (kg):

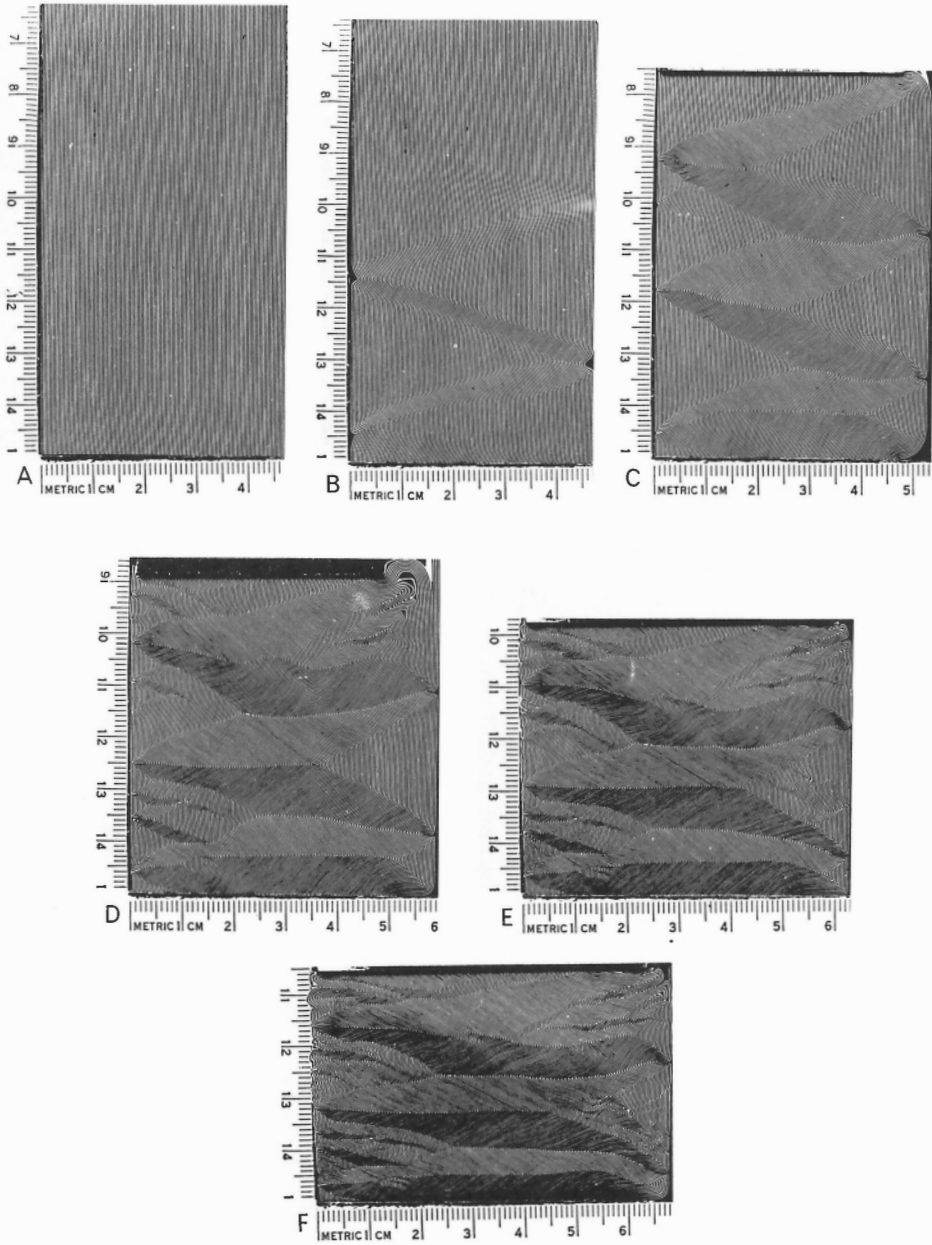
A. 225; B. 675; C. 900; D. 1,125; E. 1,350.

F to J, group 2 specimens; lateral loads as follows (kg):

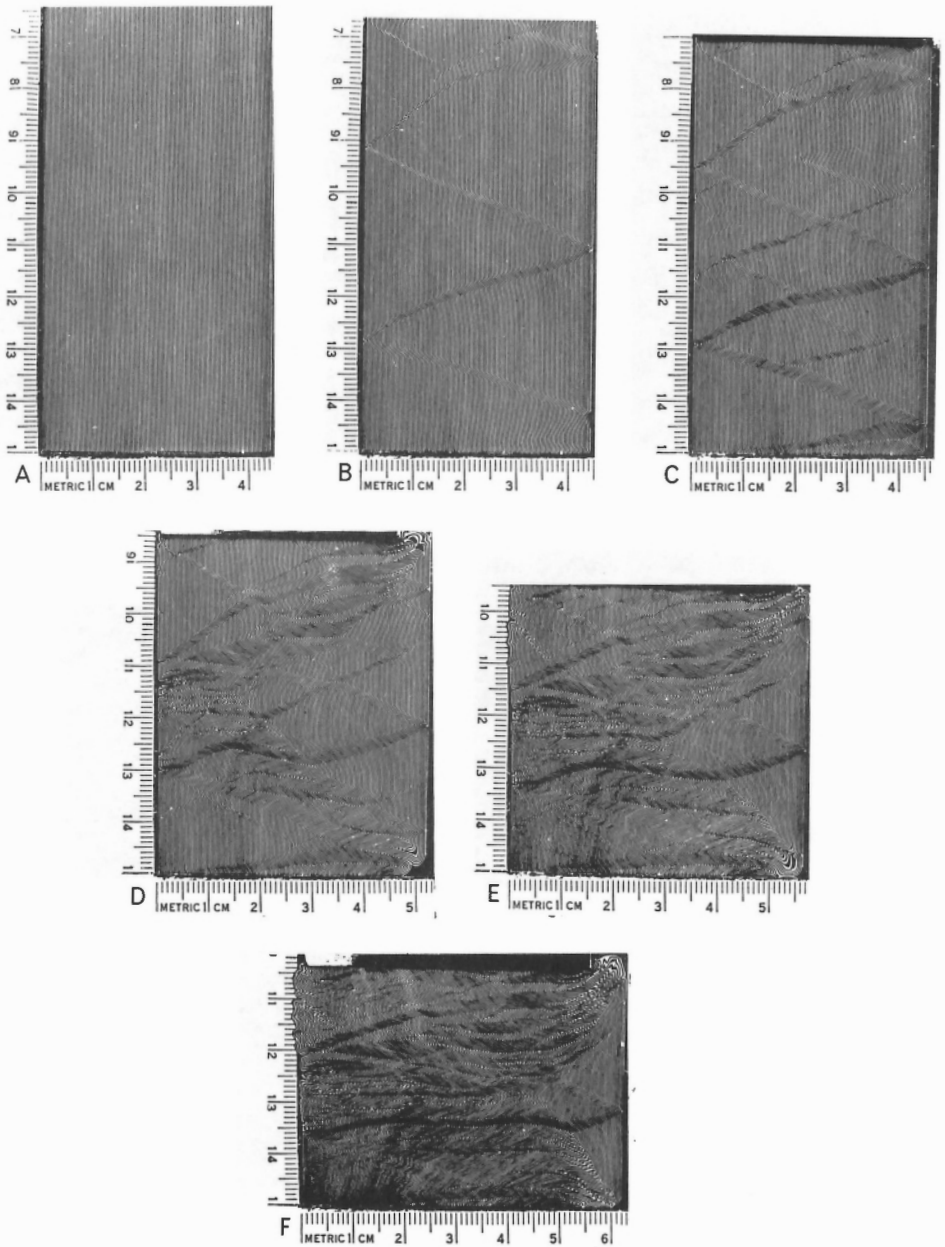
F. 1,600; G. 1,800; H. 2,050; I. 2,275; J. 4,550.



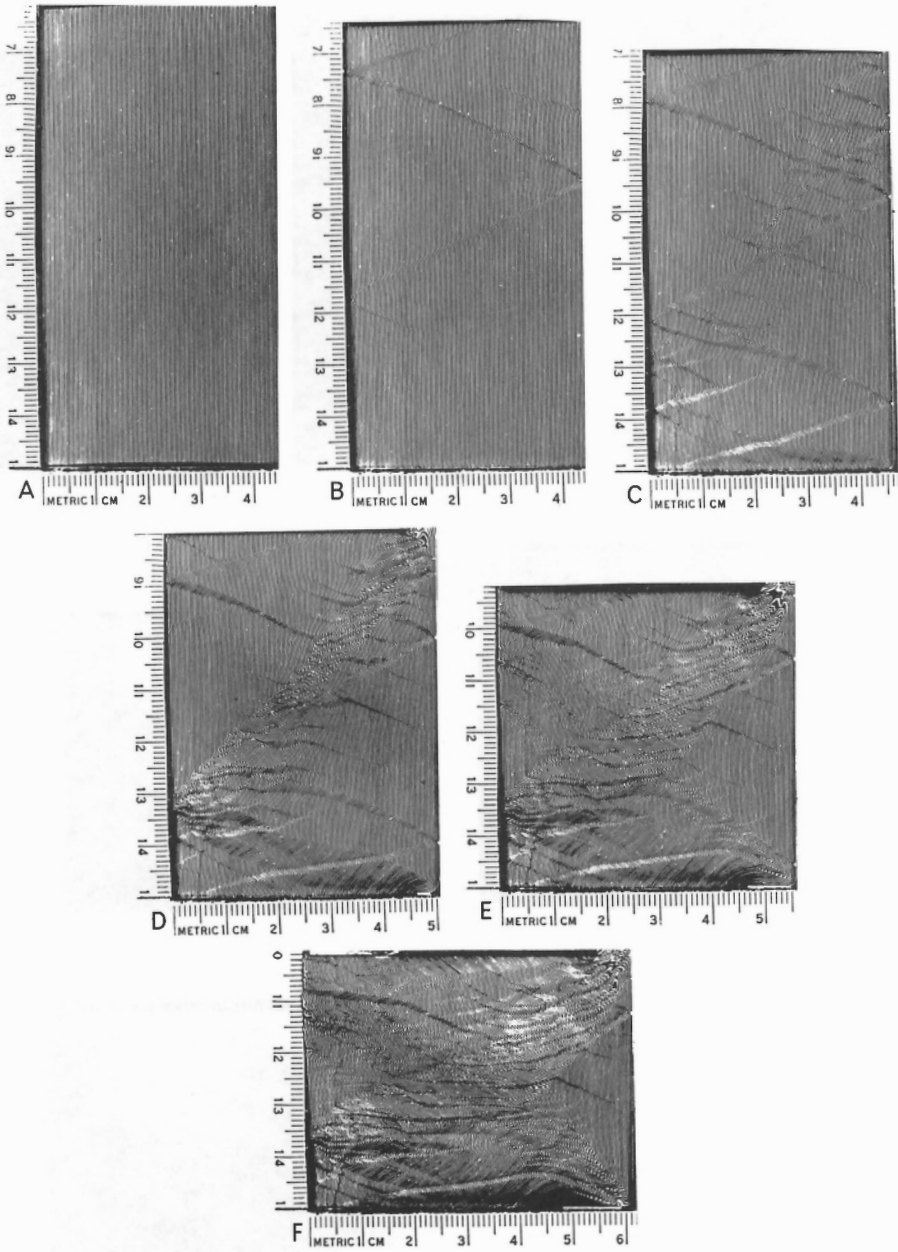
Progressive folding of parallel specimen laterally loaded at 225 kg.



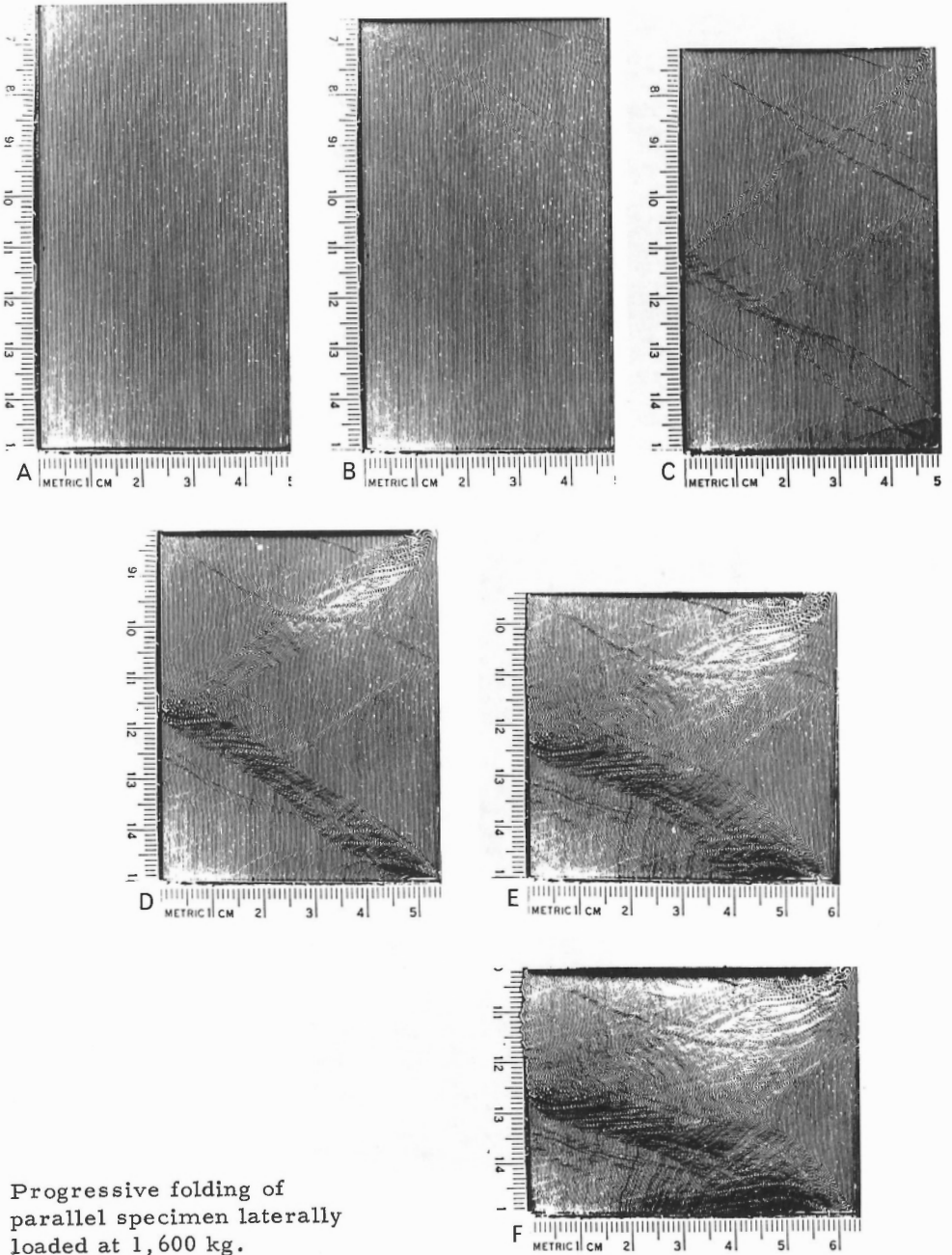
Progressive folding of parallel specimen laterally loaded at 675 kg.



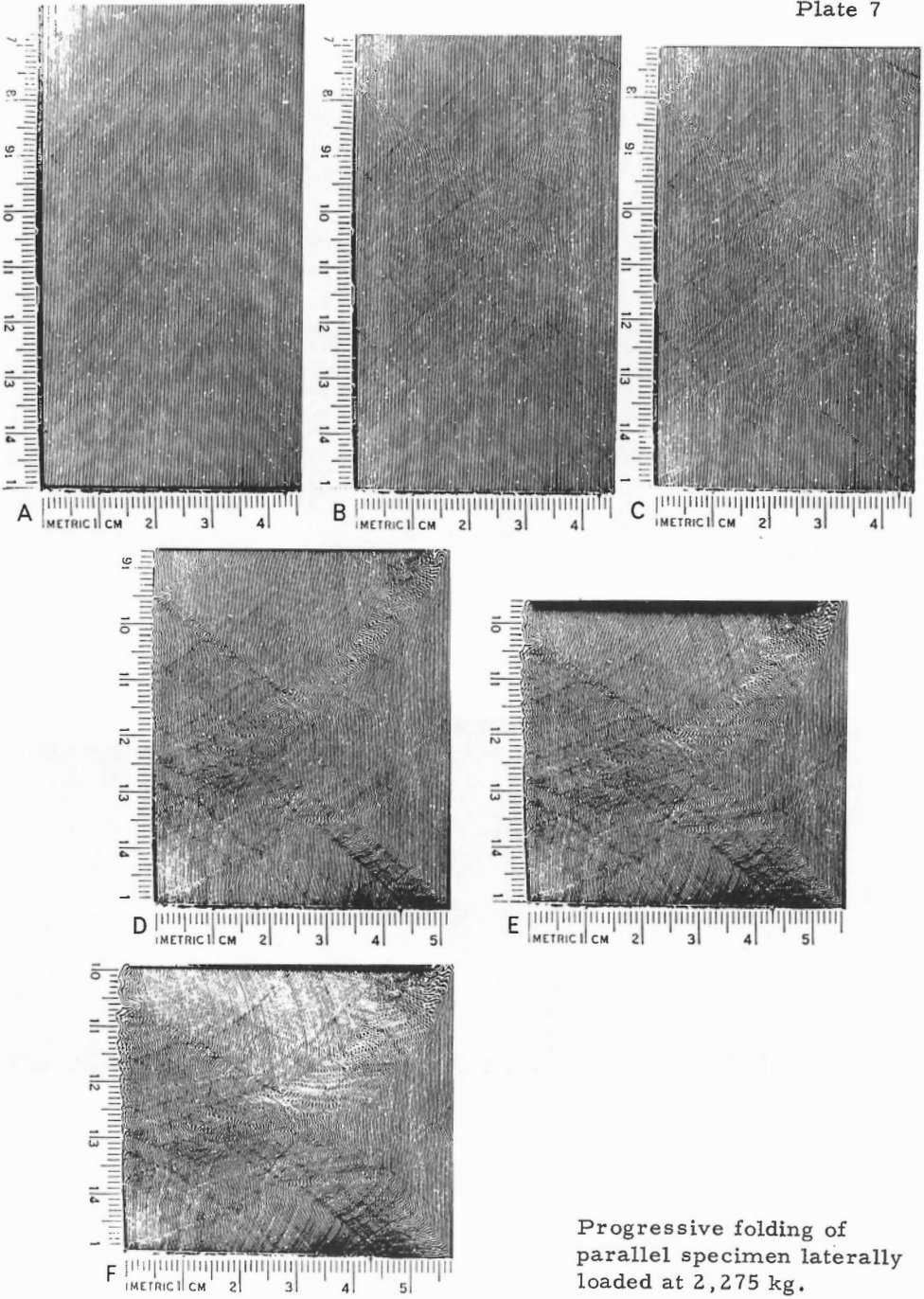
Progressive folding of parallel specimen laterally loaded at 1,125 kg.



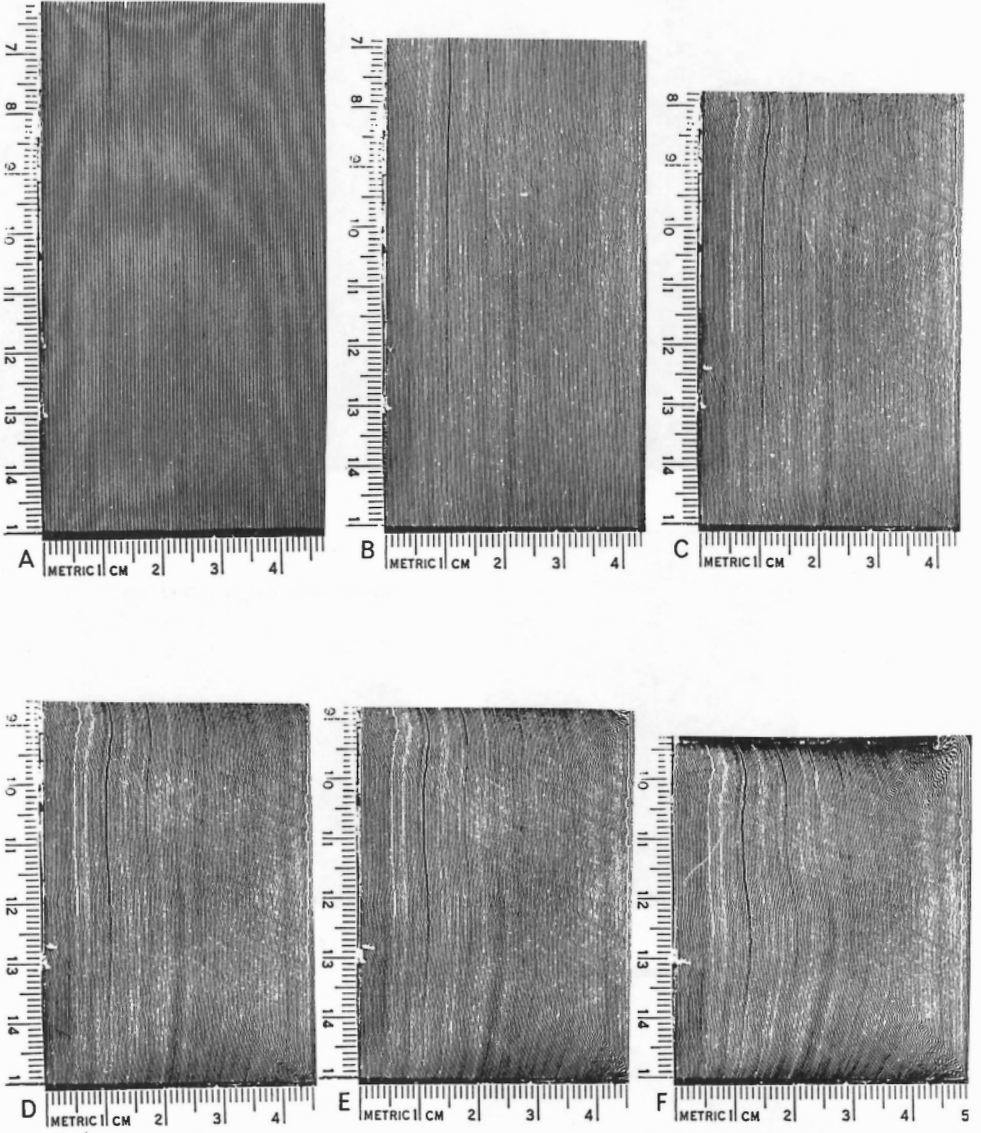
Progressive folding of parallel specimen, laterally loaded at 1,350 kg.



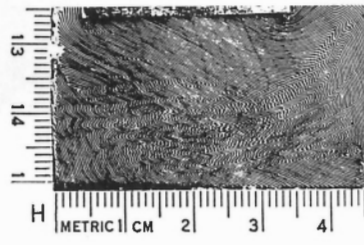
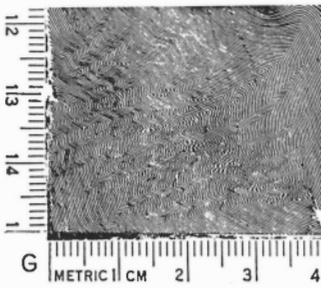
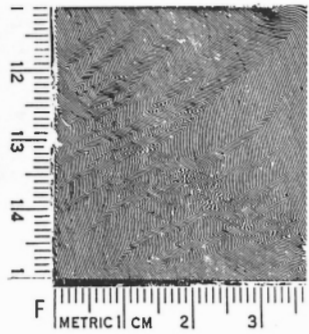
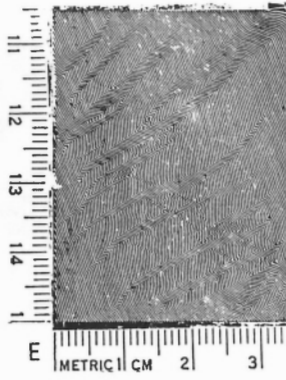
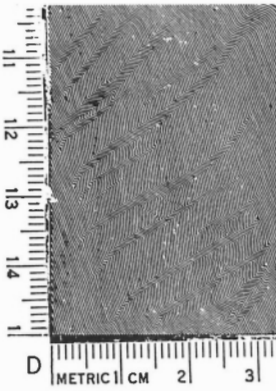
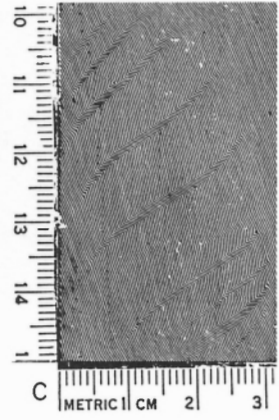
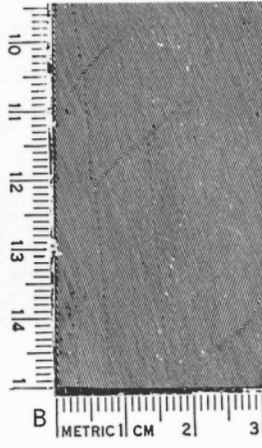
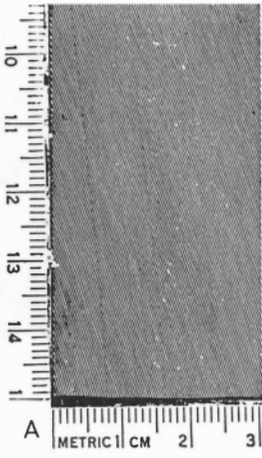
Progressive folding of parallel specimen laterally loaded at 1,600 kg.



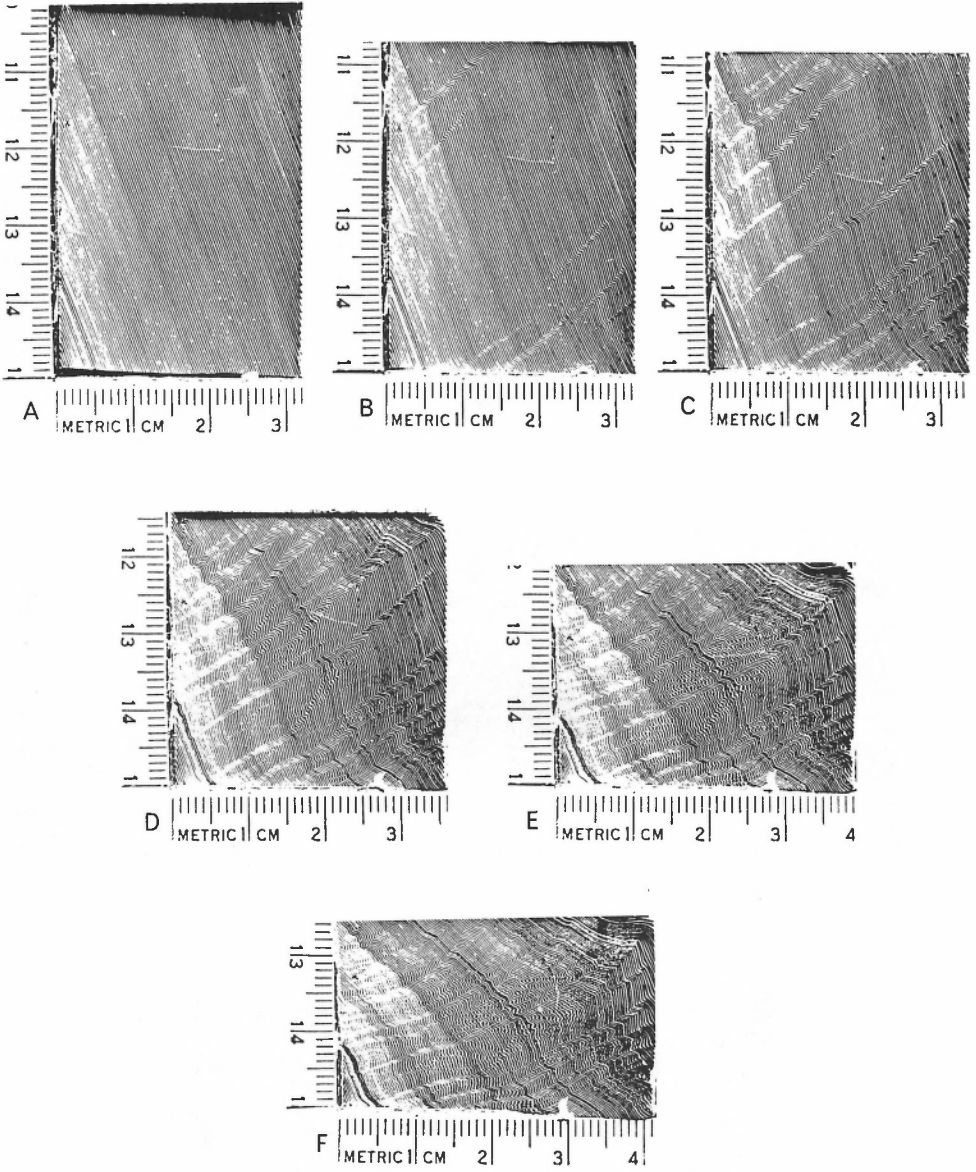
Progressive folding of parallel specimen laterally loaded at 2,275 kg.



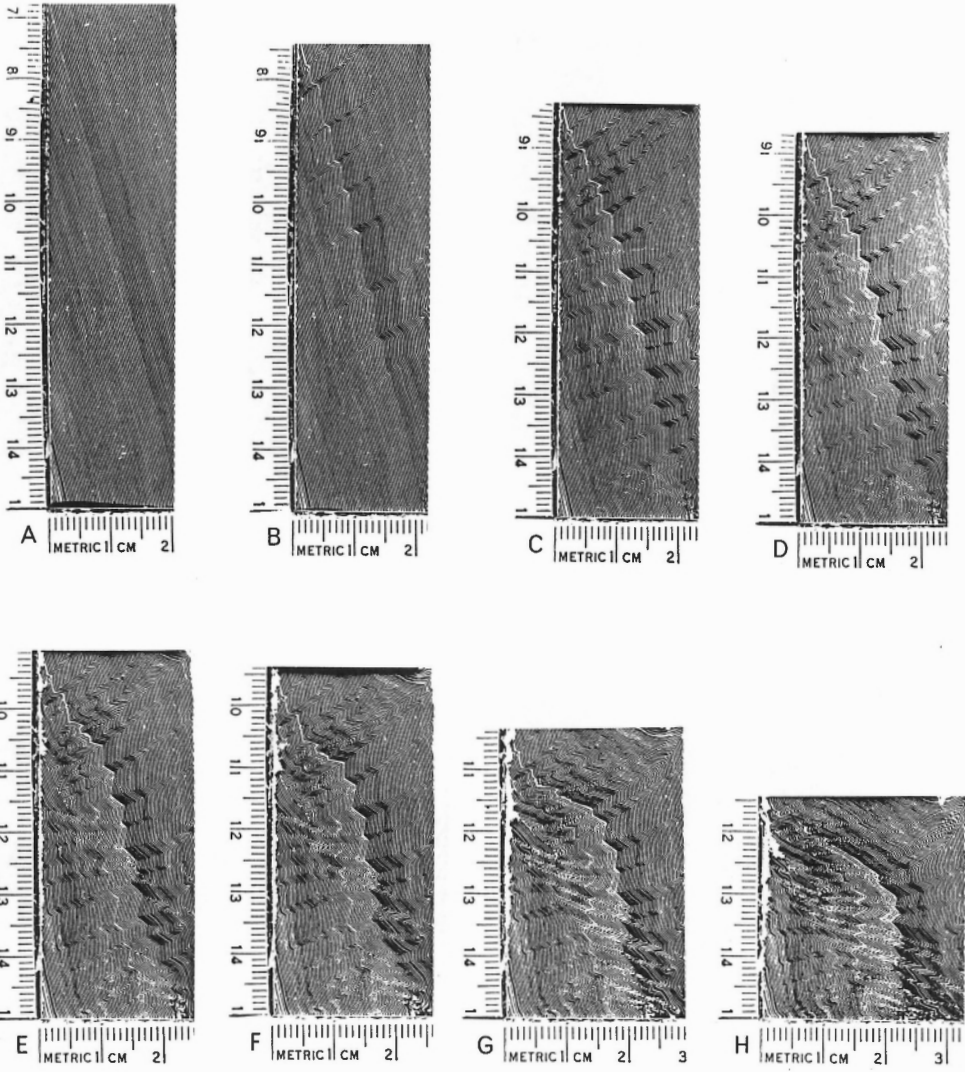
Progressive folding of parallel specimen laterally loaded at 4,550 kg.



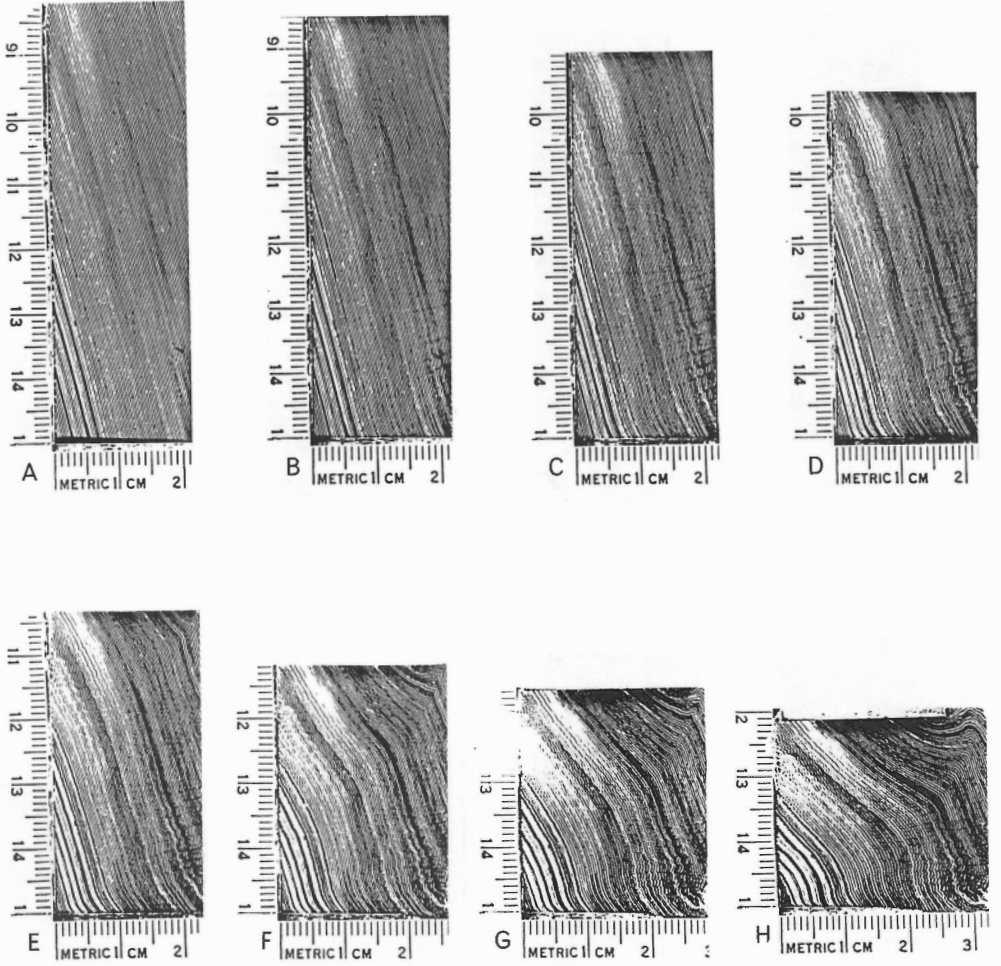
Progressive folding of oblique specimen ($\alpha = 20^\circ$) laterally loaded at 1,125 kg.



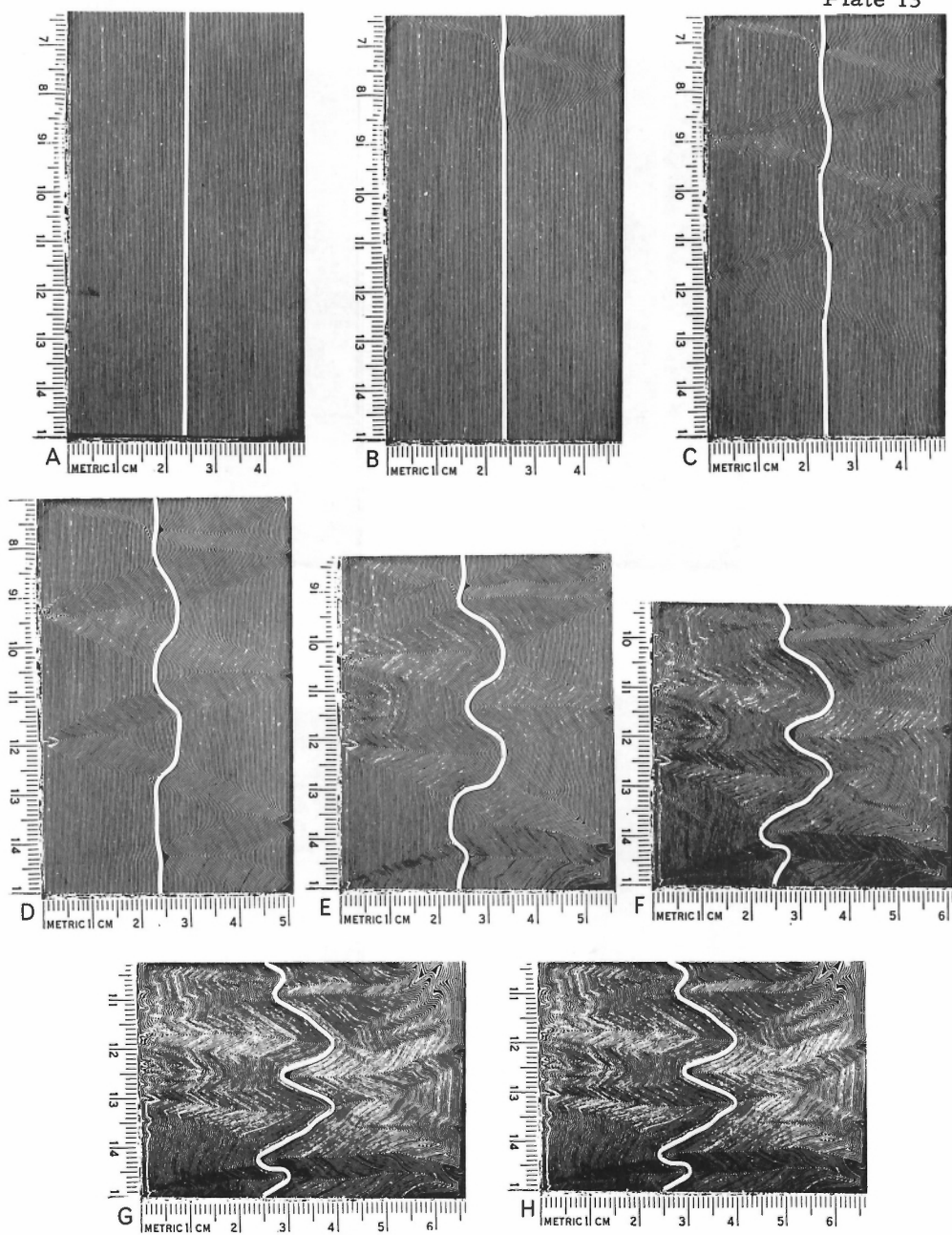
Progressive folding of oblique specimen ($\alpha = 20^\circ$) laterally loaded at 1,350 kg.



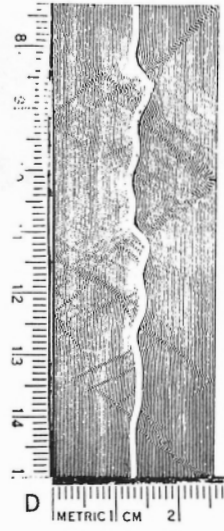
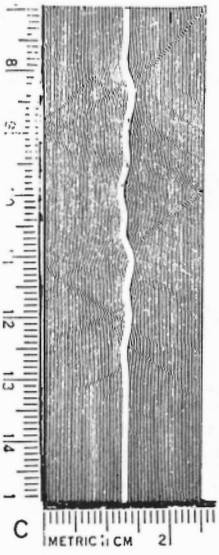
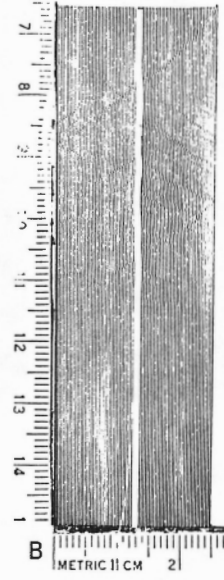
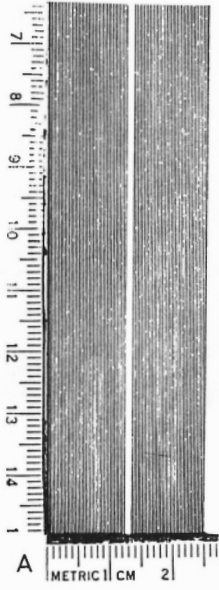
Progressive folding of oblique specimen ($\alpha = 14^\circ$) laterally loaded at 1,800 kg.

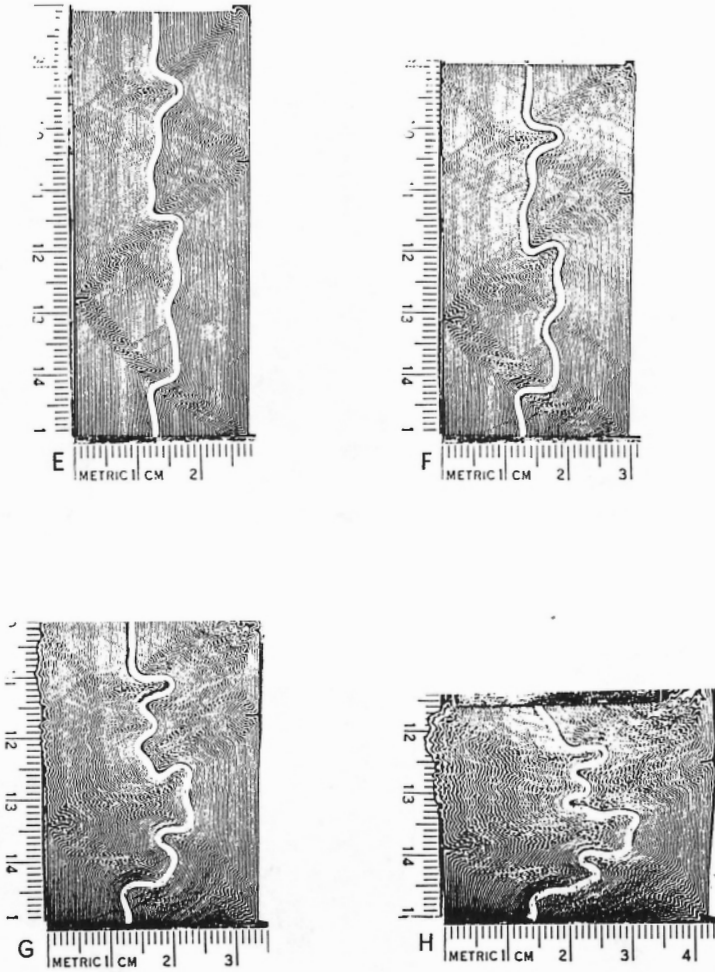


Progressive folding of oblique specimen ($\alpha = 15^\circ$) laterally loaded at 4,550 kg.

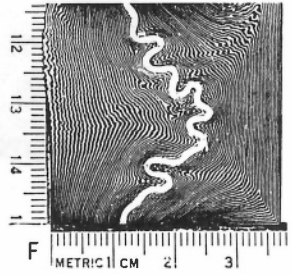
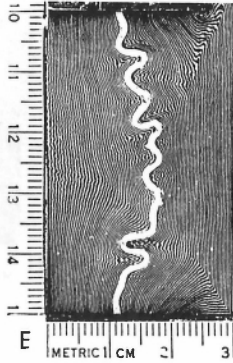
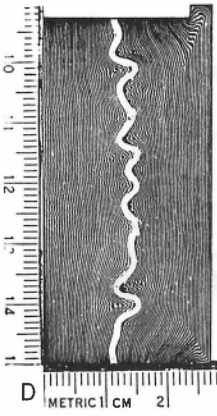
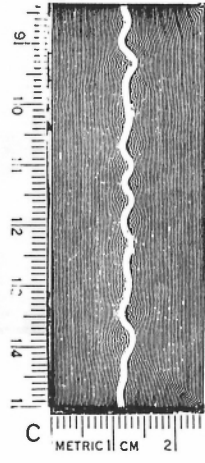
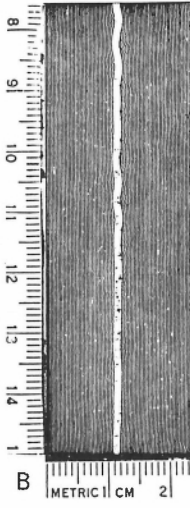
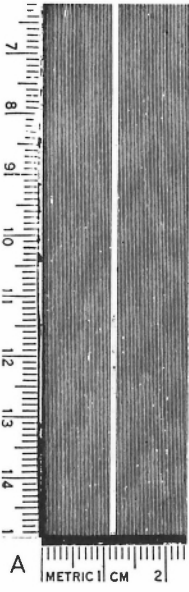


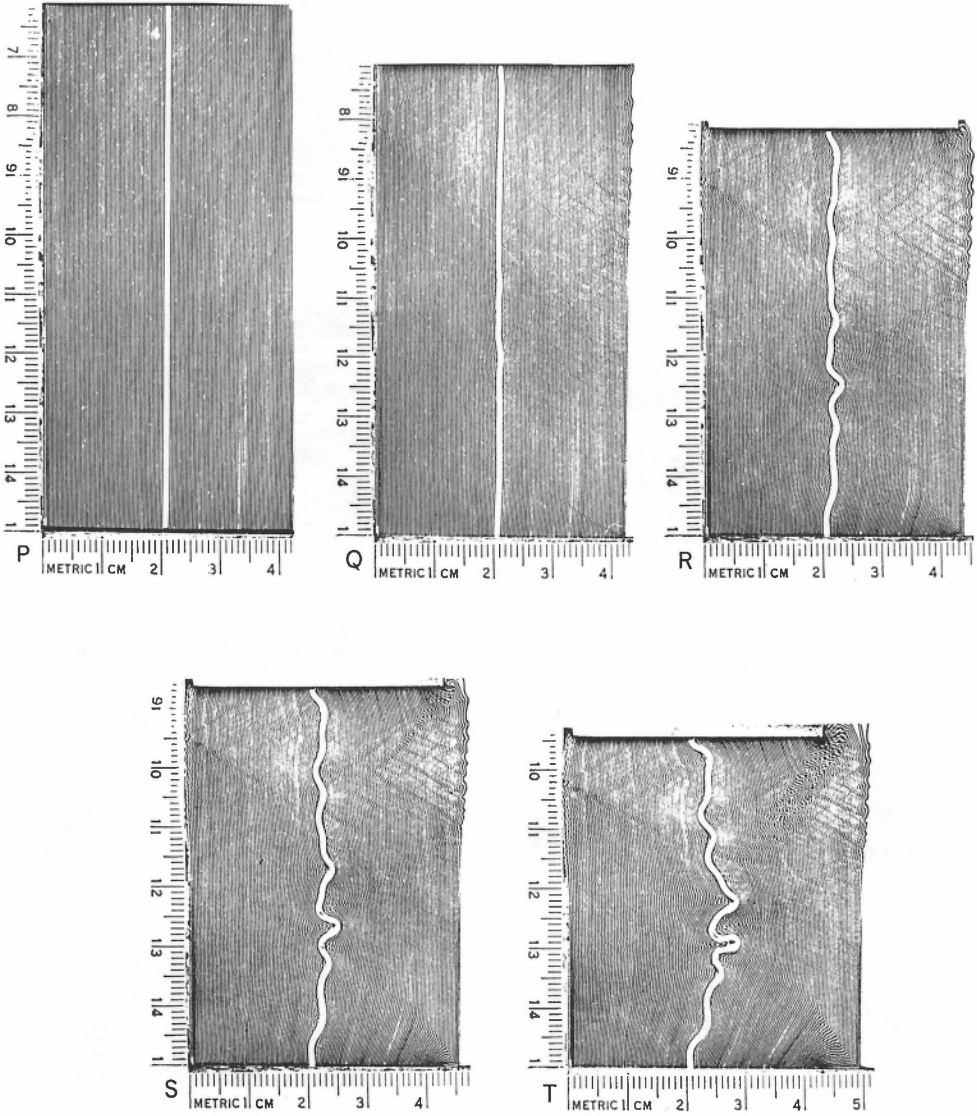
Progressive folding of parallel specimen containing annealed copper layer laterally loaded at 900 kg.



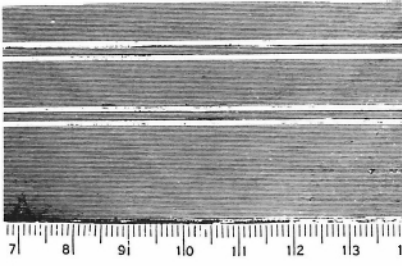


Progressive folding of parallel specimen containing annealed copper layer laterally loaded at 2,275 kg.

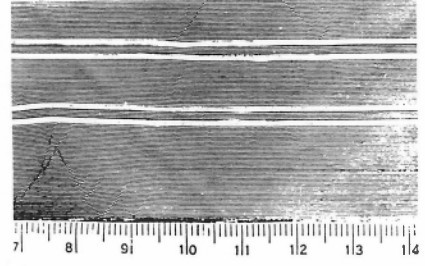




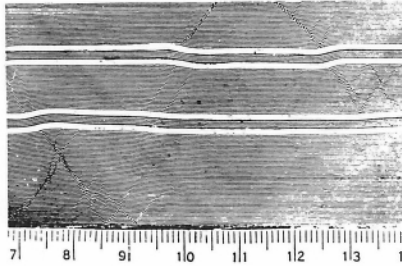
Progressive folding of parallel specimen containing annealed copper layers:
A to F; laterally loaded at 3,625 kg. P to T; laterally loaded at 4,550 kg.



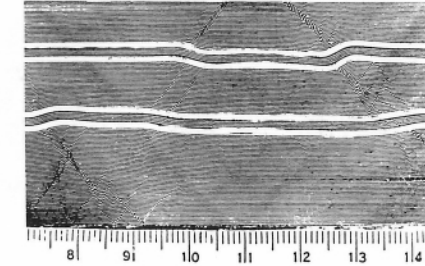
A



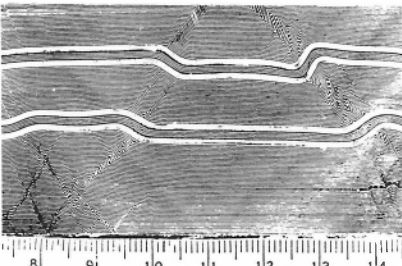
B



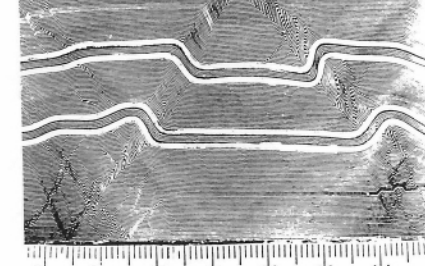
C



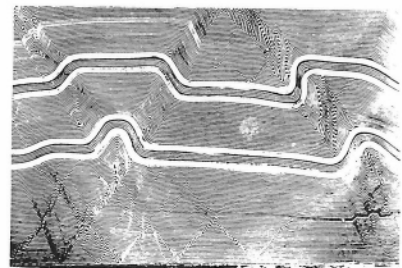
D



E



F



G



H



I



J



K



L

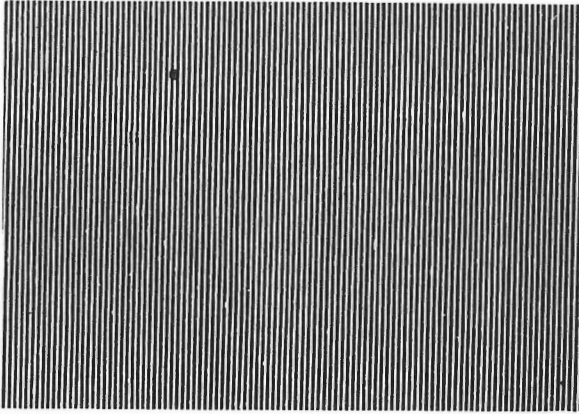


M

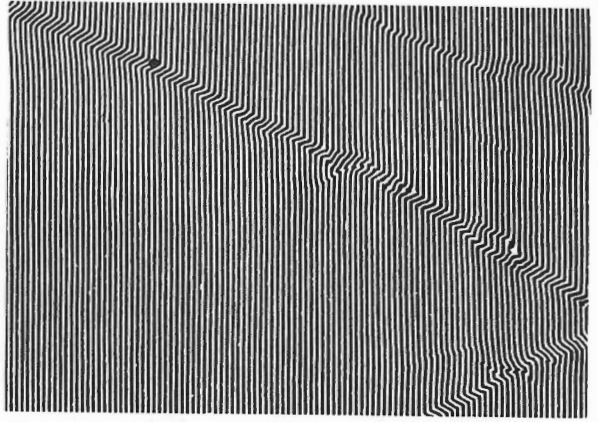


N

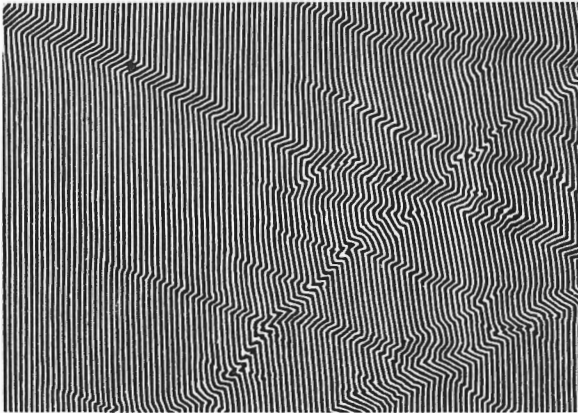
Progressive deformation of part of a specimen containing four annealed copper layers laterally loaded at 2,275 kg. (in this plate direction of deforming load is horizontal instead of vertical).



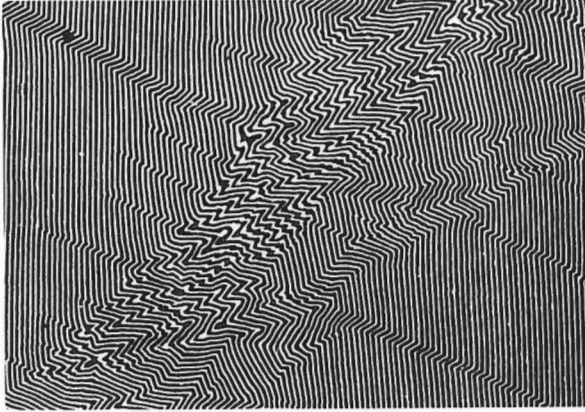
A



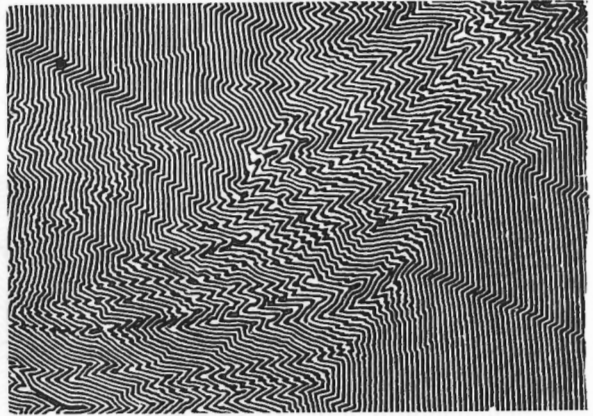
B



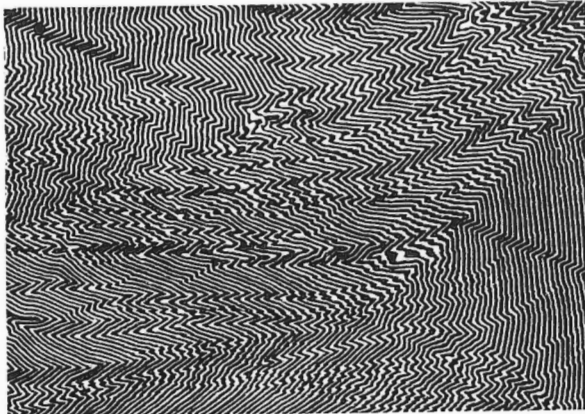
C



D



E

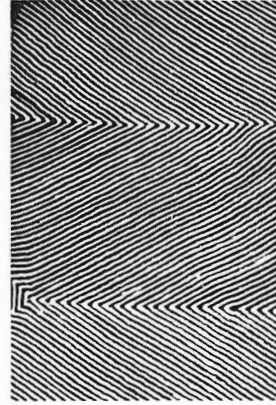


F

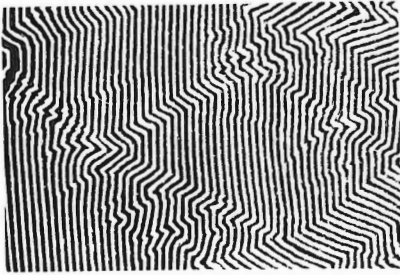
Progressive development of late stage major kink (left handed) showing internal rotation of small right-handed kink layers. The black dot identifies the same point at each stage.



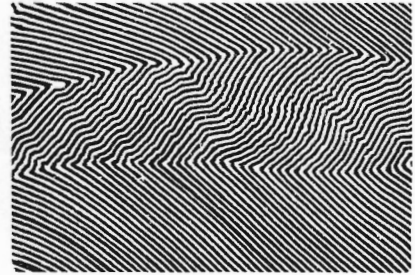
A



B



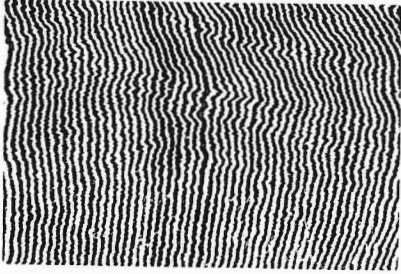
C



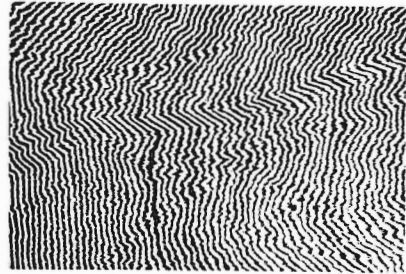
D

Details of deformed specimens (scale given by card thickness):

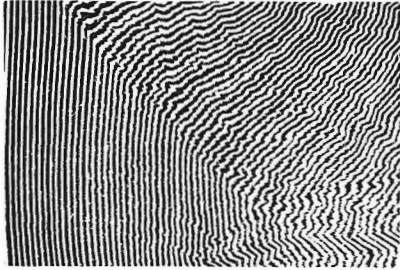
- A. Close up of very small scale kinking and chevron folding within cards at high lateral loads.
- B. Very regular symmetric chevron folds in the centre of a group 1 specimen.
- C. Nucleation of a network of smaller conjugate kinks in an undeformed domain surrounded by larger kinks.
- D. Oblique kinks formed on limbs of regular chevron folds of type shown in B, above, formed by further deformation.



A



B



C



D

Details of deformed specimens (scale given by card thickness):

- A. Very small scale chevron folding in parallel specimen laterally loaded at 4,550 kg. involving kinking by slip within cards.
- B. An early large left handed kink partially internally rotated by small scale chevron folding in the surrounding material.
- C. Migration of a late major kink boundary across a domain with a fine network of very small scale conjugate kinks.
- D. Late stage in deformation of an oblique specimen showing folds with alternating planar and folded limbs.

DISCUSSION

W.M. Schwerdtner asked if the author had obtained box folds at high confining pressures, and if he had tried to vary the thickness of the individual cards. The author said that at very high confining pressures he had not observed formation of box folds. Where box folds formed in experiments in which copper sheets were incorporated in the pack of cards, the behaviour of the copper layer was controlled by the cards, except that at very high loads the copper layers formed sinusoidal buckles. The author had tried using many materials, such as mylar sheets and telephone directories, but he did not get any essentially different results.

In answer to a question concerning variations of the boundary conditions Dr. Weiss said he had also experimented with thick layers of soft rubber placed between the platens and the cards. In such cases, kink bands would form in much the same way, but they would have rounded forms at the margins because they would be more free to buckle out. At low loads, this would permit formation of concentric folds.

F.A. Donath remarked that from field evidence, concentric folds form under relatively low confining pressure.

The author agreed, but said that under constraint (distinct from confining pressure) the box shape would be preferred because it can be propagated, whereas the concentric shape cannot.

M.B. Stauffer asked if the author had tried to vary the vertical loading rate and if an extremely slow loading rate would tend to create concentric folds.

The author said he tried to run experiments as fast as possible because of creep in the cards. He wanted the cards to be discrete layers, or if disseminated shear occurred, he wanted to keep it in the range of 5 per cent. If he had run experiments more slowly, the mechanism would have been entirely different from the one he was attempting to investigate.

M.R. Stauffer asked then if the cards, being fairly strong in respect to the rate of loading, might represent a sequence of sandstones and shales under natural geological conditions of loading.

The author thought this to be possible. No matter how slow cards were loaded, they would eventually deform in the same way. Had they been stronger, they would not have deformed by flexural-slip anyway. He had observed cherts of the Franciscan Formation along the San Andreas Fault, that contained abundant similar structures, chevrons and kinks.

Although these rocks would presumably have deformed a little more slowly, they certainly seemed to behave in a way similar to the cards in the experiments.

G. R. Stevens remarked that in that case, about 90 per cent of the grains in the rock must be warped and bent by as much as 90 degrees, be 'unrolled' and bent again as kink boundaries migrate through the rock. After boundaries have migrated throughout the rock, all grains must be fractured.

The author agreed and confirmed that in experimental work on phyllites he had noticed exactly that phenomenon. All quartz grains inside large kink bands would be fractured, whereas those outside the bands would not be. He suggested this proved the migration of the kink bands.

W. F. Brace asked what type of rock the model would represent, and if this kinking process would be similar in other types. He thought that an abundance of mica was essential to the formation of the kink bands. The author said that the model was chosen to represent a chlorite-sericite phyllite, but he could imagine folds might form in other rock types. The difficulty would be to see such structures, because of their large size. He also pointed out that as soon as the initial stage of kinking is over, the box shape disappears. Many folds in laminated shales might in fact nucleate as indicated, but by the time they became tight folds with a slaty cleavage, their early history had entirely disappeared. The only way of establishing this history was to try to find internally rotated layers on the limbs of the folds, but this was hardly possible. The author, however, did not imagine that a sequence of massive limestone 2,000 feet thick could deform in the described manner. He also mentioned a paper by R. T. Faill, where this author suggested that some folds of the Appalachians had formed like kink bands¹.

F. A. Donath said that kinks occur in limestones and sandstones, but that in these cases, there was always some evidence of cataclasis and fracturing.

¹ Faill, R. T. Valley and ridge structure in Pennsylvania, folds or macro kink bands; Am. Geophys. Union. Trans., vol. 48, No. 1, p. 214 (abstract), 1967.

GENERAL SESSION

DISCUSSION

R. L. Brown discussed some of the work he has done in the Moines of the southwestern Highlands of Scotland. There are four phases of deformation, the third phase possibly being important from the point of view of kink bands. The region has been mapped at a scale of 6 inches to the mile, and a systematic fanning of the third phase axial planes is apparent throughout the area, from north-northeast, to north, to north-northwest. Many of the minor folds are conjugate folds. Individual folds have the geometry of flexural flow folds, and they developed in conditions where sillimanite could locally recrystallize. Conjugate folds occur where thin psammities and pelites are interlayered. In spite of the flowage these are conjugate structures, and in some cases, the symmetry is perfectly orthorhombic. Tight, symmetrical folds with single closures may well have evolved by the anastomosing of kink bands rather than by buckling.

J. W. H. Monger described features he had observed in southwestern British Columbia. Rocks were very coarse-grained volcanic sandstones with a rather crude foliation, interbedded with pelitic rocks. In the sandstones kink bands form at approximately 90 degrees to the foliation, whereas in contiguous pelites, microfolds and microfractures develop. This second structure is quite similar to a slip cleavage. Both kink bands and folds appear to be synchronous, late in tectonic development of the area. No transition has been observed between the two types.

D. H. Underhill discussed some kink bands from the Labrador trough (northeastern Quebec, Canada). The rock is a quartz-sericite schist or phyllite, where micas underline a coarse foliation between more quartz-rich layers. The foliation dips approximately 30 degrees east. Thickness of foliation laminae is 2 to 4 millimetres apart, and fold axes generally trend due north. Kink band axes dip gently so that distinction between dextral and sinistral sets is important. Poles to the planes of the kink bands lie on a vague girdle in a stereographic plot. The deformation appears to be of the brittle type and some cataclastic deformation might have taken place along kink boundaries. All observed kink bands show the same relative sense of movement, the south side being displaced downwards, so that the kink bands are dextral when viewed from west to east. Where it has been measured, the angle formed by the kink boundaries and the foliation is in the range of 80 degrees to 90 degrees. Results obtained by Paterson and Weiss (1966) do not appear to apply exactly to evidence found in this case, possibly because of a slight difference in the behaviour of the rock.

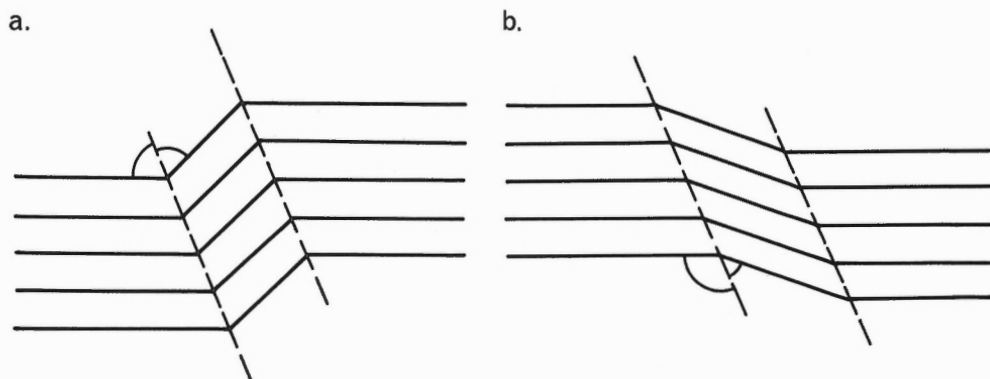


Figure 1. 1a. is a kink because the angles are equal,
1b. is not a kink, according to L.E. Weiss

An error in a drawing of D.H. Underhill on the blackboard prompted a discussion as to what can be called a kink band and what cannot. Taking part in the discussion were L.E. Weiss, M.R. Stauffer, T.B. Anderson, J. Handin and W.K. Fyson (see Fig. 1).

M.L. Stauffer indicated that the pattern of Figure 1b might be called a kink band too. It would simply form when the direction of maximum stress is at a high angle to the foliation. He knew that such features did exist in nature.

L.E. Weiss objected that although such structures are common with strain-slip cleavage they are not kink bands, and that in fact, the thickness of the laminae has to decrease in the shear zone. He suggested that they might represent some other type of plastic deformation. In experimental deformation of phyllites, no kink bands would form by the process suggested by M.L. Stauffer, only ductile folds would. L.E. Weiss insisted that the term 'kink' should be reserved for an object that has roughly the geometry of a kink.

W.K. Fyson remarked that some of the curved kink bands he had described were by this definition true kinks at one extremity, but not at the other. He suggested that such curvature is due to a change in the orientation of the local stresses influenced by variations in the physical properties of the rock.

COMMENTS BY P. CLIFFORD ON PAPERS BY
T.B. ANDERSON, P. CLIFFORD, F.A. DONATH AND W.K. FYSON

The notion behind the conference was to attempt an integration of field and laboratory data. These papers on kink folds so exactly that, if read together.

Anderson and Clifford both present graphs of the relation of the angles between kink band boundary and the foliation outside and inside the band¹. They demonstrate wide variability of the latter angle, together with a more restricted range in the former. The same graph is produced for experimental results, and Donath shows, in particular, that the angle between kink band boundary and foliation outside the band is constant, a point implicit in the marked vertical distribution of points in the plots of these angles.

All four authors also conclude that if the angle between kink band boundary and foliation outside the band is greater than the corresponding angle inside, some mechanism other than rotation gliding must have occurred. For such a situation, the width of the kink band as defined by Donath increases. This suggests that kink band width measurements are likely to be useful only where the outside angle is equal to or less than that inside.

No author has yet provided a reason for the high variability of the outside angle, though both Anderson and Donath use relatively restricted values on which to base an hypothesis. For the experimental data, the range of values is small (20°), but the mean values from field data range from 65 degrees (Anderson), to 52 degrees (Clifford) to 43 degrees (Fyson). Presumably some of this variation is the result of local inhomogeneities in the natural samples, or of some erratic behavior during deformation. It seems premature at this point to use only a mean value derived from field data as the starting point for an hypothesis, particularly in the light of experimental data, which themselves do not produce correlatable values.

However, the agreement between these papers is remarkable. The sorts of folds observed appear to be the same type - brittle kink folds - and these authors have arrived at substantially similar conclusions on the kinematics involved.

¹ For comparative terminology see Appendix I.

ON THE NUCLEATION OF KINK BANDS

H. E. Rondeel

Two notions have been advanced for the attitude of kink planes during kink band generation. Anderson (1968), Clifford (1968) and Donath (1968) suggest that as the foliation in a developing kink band rotates, the attitude of the kink planes remains fixed with respect to the foliation outside the kink zone or that these planes are composed of the same material points in every stage. Paterson and Weiss (1966) and Weiss (1968) have the opinion that kink boundaries rotate when the foliation in the kink band changes orientation.

It is generally assumed that in the generation of kinks - certainly when the principal stress axes are symmetrically arranged with respect to the foliation - deformation is restricted to the material in the kink bands. Moreover, material points which have once become involved in a forming kink cannot return to the undeformed domain situated outside the kink zone. The assumption implies, in the case in which the orientation of the kink planes is fixed, disruption or discontinuity in material properties along these planes and dilation in the kink band during its generation. Anderson (1964; 1968) and Clifford (1968) accept this dilation, the magnitude of which generally reaches high values (see Clifford, 1968, Fig. 8). Therefore, kink band formation with kink plane orientation remaining constant, can only occur in brittle materials. Donath (1968) mentions both dilation and loss of cohesion along the kink boundaries. He uses the term 'brittle' kink bands for the structures formed in his experiments. If, under the conditions mentioned before, the material of the body being deformed behaves in a ductile manner and dilation cannot occur, the kink planes have to change orientation while the foliation in the forming kink band rotates. The geometry that these conditions impose is very strict. The kink planes must bisect the angle between the foliation within and without the kink band, as a result of which the folia remain continuous across the kink boundaries. Furthermore, the amount of material involved in the forming kink has to increase. Figure 1 shows a narrow section of a developing kink band perpendicular to the foliation in which this volume increment, here increment in area, has been kept at its minimum, i. e. $l/2t \cdot \sec^2 4/2$; Figure 1b portrays the kink band at different moments of its generation and Figure 1a the undeformed body with the position of the material points forming the kink boundaries in the finite stages of Figure 1b.

From the papers of Paterson and Weiss (1966), Donath (1968) and Weiss (1968) on kink bands generated experimentally, it is clear that these structures can be initiated under strongly varying conditions. They might form in the same material under rheologically different behavior. It is suggested that in ductile behavior kink bands are produced in which the foliation is continuous across the kink boundaries, whereas in 'brittle' kinks disruption of the laminae seems to occur.

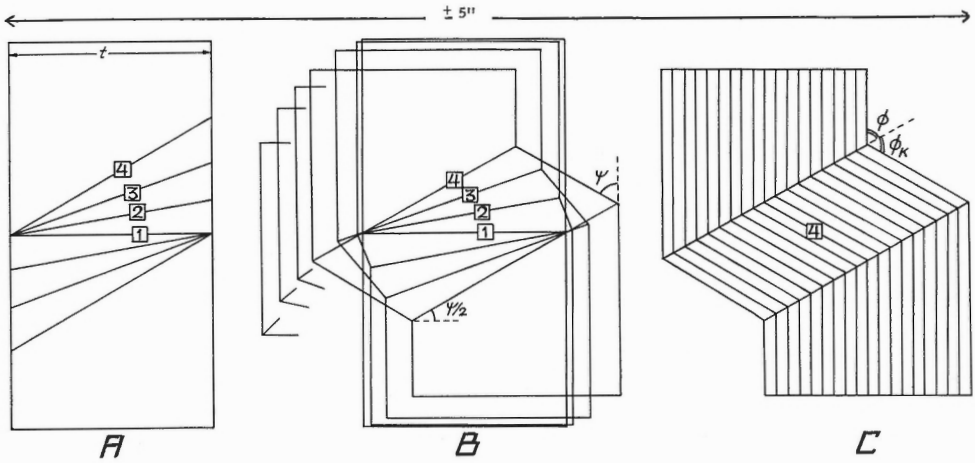


Figure 1. Kink band nucleation without dilation and with a minimum area of the deformed domain; $\phi = \phi_k = 90^\circ - 4/2$ (see text).

Experimental evidence provided by Weiss (1968) and Paterson and Weiss (1966) is that kink layers lengthen by propagation while maintaining a constant orientation, from which one might conclude that the attitude of the kink planes is determined at the moment a kink nucleus is formed and that successive stages in kink nucleation are preserved where kink bands terminate. The ends of most kink layers - at least in these experiments - are wedge-shaped. It is therefore reasonable to infer that the orientation of the kink planes changes and that progressively more material is involved in a kink nucleus. This is one of the reasons the writer does not believe Ramsay's (1967) explanation for the angular relations in kink bands to be valid (his t/l ratio decreases during nucleation).

If the orientation of kink boundaries is defined at the onset of kink band formation or kink nucleation, there is no reason why the values of kink angles - in nature and in experiments - are restricted to a narrow range and why frequency distribution diagrams prepared for these angles exhibit significant maxima. One would then expect the values of the kink angles to vary at random.

It is most likely that 'brittle' and 'ductile' kink bands are initiated in a nucleus and that the kink planes rotate while the foliation in the nucleus rotates. Under 'ductile' conditions a rotation over 4 degrees of the foliation implies a $4/2$ degree rotation of the kink boundaries; under 'brittle' conditions the ratio of these angles of rotation might not be equal to $1/2$. Once a certain configuration is reached, the kink band can propagate. Though the overall orientation of the kink boundaries will remain the same during propagation, the kink planes limiting each volume added to the lengthening kink band in ductile materials rotate into their final position. In brittle materials

the same sequence of events might take place until the moment that the shear stress acting along the kink boundaries causes displacements and 'kink propagation' by rotation of the foliation between two propagating shear planes might continue the deformation.

The model outlined here stands only for the initiation of a kink nucleus and for its longitudinal propagation in an ideally foliated, homogeneous body, in which the material outside a kink band remains undeformed. In many experiments, however, deformation takes place within this latter domain; the foliation usually becomes rotated, an event which seems to depend on the conditions of confinement and constraint. Still, the process of nucleation of a kink band can hardly be imagined to alter since the accompanying deformations are very small.

References

1. Anderson, T.B. Kink-bands and related geological structures; Nature, 202, pp. 272-274, 1964.
 2. Anderson, T.B. The geometry of a natural orthorhombic system of kink-bands; this conference, 1968.
 3. Clifford, P.M. Kink band development in the Lake St. Joseph area, northwestern Ontario; this conference, 1968.
 4. Donath, F.A. Experimental study of kink-band development in Martinsburg slate; this conference, 1968.
 5. Paterson, M.S. and Weiss, L.E. Experimental deformation and folding in phyllite; Geol. Soc. Am. Bull. 77, pp. 343-374, 1966.
 6. Ramsay, J.G. Folding and fracturing of rocks; Mc-Graw Hill Book Co., New York, 1967.
 7. Weiss, L.E. Flexural-slip folding of foliated model materials; this conference, 1968.
- P.S. The writer is much indebted to the Organization for Pure Scientific Research (Z. W. O.) for a grant enabling him to visit the Tectonic Research Conference in Ottawa.
-

At the close of the Conference, P. Clifford suggested that similar meetings take place in the future, a suggestion approved by all participants. He offered the hospitality of McMaster University in Hamilton for the next meeting.

APPENDIX I

Nomenclature of kink band angles

From the papers on kink bands included in this report it appears that different symbols are being used by the several authors to identify angles of kink bands. Such a lack of concensus makes the comparison of papers a slow and tedious process. For the convenience of the reader the following table lists the various nomenclatures used:

<u>Author</u>	<u>Figure</u>	<u>Angles</u>				
Anderson	5	α	β	γ	-	-
Clifford	4	ϕ	γ	ω	α	θ
Donath	3	α	α_k	ρ	β	θ_{kp}
Fyson	2	ϕ	ϕ_k	Δ	-	-
Weiss	5a, 7	ϕ	ϕ_k	Ψ	α	-

APPENDIX II

List of participants

- F. D. Anderson,
Geological Survey of Canada,
601 Booth Street,
Ottawa, Ontario.
- *T. B. Anderson,
Department of Geology,
The Queen's University of Belfast,
Belfast 7, North Ireland.
- E. C. Appleyard,
Department of Earth Sciences,
University of Waterloo,
Waterloo, Ontario.
- A. J. Baer,
Geological Survey of Canada,
601 Booth Street,
Ottawa, Ontario.
- *K. Barron,
Mining Research Centre,
30 Lydia Street,
Ottawa, Ontario.
- A. R. Berger,
Department of Geology,
University of Toronto,
Toronto 5, Ontario.
- H. U. Bielenstein,
Geological Survey of Canada,
601 Booth Street,
Ottawa, Ontario.
- *W. F. Brace,
Department of Geology and
Geophysics,
Massachusetts Institute of
Technology,
Cambridge, Massachusetts 02139,
U. S. A.
- *W. C. Brisbin,
Department of Geology,
University of Manitoba,
Winnipeg, Manitoba.
- *A. Brown,
Department of Geological Sciences,
Queen's University,
Kingston, Ontario.
- *R. L. Brown,
Department of Geology,
University of New Brunswick,
Fredericton, New Brunswick.
- F. H. A. Campbell,
Geology Department,
University of Manitoba,
Winnipeg, Manitoba.
- R. B. Campbell,
Geological Survey of Canada,
326 Howe Street,
Vancouver 1, British Columbia.
- *D. M. Carmichael,
Department of Geological Sciences,
McGill University,
Montreal 2, P. Q.
- A. Carrara,
Department of Geology,
Ottawa University,
Ottawa, Ontario.
- *H. A. K. Charlesworth,
Department of Geology,
The University of Alberta,
Edmonton, Alberta.
- *P. Clifford,
Department of Geology,
McMaster University,
Hamilton, Ontario.
- * Speaker or discussant.

*D. F. Coates, Head,
Mining Research Centre,
30 Lydia Street,
Ottawa, Ontario.

D. G. Cook,
Institute of Sedimentary and
Petroleum Geology,
3303 - 33rd Street N.W.,
Calgary, Alberta.

*J. B. Currie,
Department of Geology,
University of Toronto,
Toronto 5, Ontario.

*C. Dahlstrom,
Geological Department,
Chevron Standard Ltd.,
400 Fifth Avenue S.W.,
Calgary, Alberta.

E. Dimroth,
Quebec Department of Natural
Resources,
Quebec City, Quebec.

*F. A. Donath, Head,
Department of Geology,
University of Illinois,
Urbana, Illinois 61801,
U.S.A.

*Y. O. Fortier, Director,
Geological Survey of Canada,
601 Booth Street,
Ottawa, Ontario.

*W. K. Fyson,
Department of Geology,
University of Ottawa,
Ottawa, Ontario.

H. Gabrielse,
Geological Survey of Canada,
601 Booth Street,
Ottawa, Ontario.

*J. Handin, Director,
Center for Tectonophysics,
College of Geosciences,
Texas A & M University,
College Station, Texas 77843,
U.S.A.

Z. Hason,
Department of Geology,
Queen's University,
Kingston, Ontario.

J. F. Henderson,
Geological Survey of Canada,
601 Booth Street,
Ottawa, Ontario.

J. R. Henderson,
Department of Geology,
McMaster University,
Hamilton, Ontario.

P. Hill,
Department of Geology,
Carleton University,
Ottawa, Ontario.

J. Holubec,
Geological Survey of Canada,
601 Booth Street,
Ottawa, Ontario.

M. Y. Hsu,
Department of Geology,
McMaster University,
Hamilton, Ontario.

M. Kennedy,
Department of Geology,
Memorial University,
St. John's, Newfoundland.

P. Kostak,
Mines Branch Laboratory,
Elliot Lake, Ontario.

- *E. Z. Lajtai,
Department of Geology,
University of New Brunswick,
Fredericton, New Brunswick.
- M. B. Lambert,
Department of Geology,
Carleton University,
Ottawa, Ontario.
- K. D. Lyall,
Mines Branch,
Mining Research Centre,
Ottawa, Ontario.
- *J. W. H. Monger,
Geological Survey of Canada,
326 Howe Street,
Vancouver 1, British Columbia.
- H. Morris,
Cominco Ltd.,
Kimberly, British Columbia.
- W. J. McMillan,
Department of Geology,
Carleton University,
Ottawa, Ontario.
- *D. K. Norris,
Institute of Sedimentary and
Petroleum Geology,
3303 - 33rd Street N.W.,
Calgary, Alberta.
- G. E. Paulus,
Department of Geology,
University of Manitoba,
Winnipeg, Manitoba.
- R. R. Potter,
New Brunswick Mines Branch,
Department of Natural Resources,
Fredericton, New Brunswick.
- *N. J. Price,
Department of Geology,
Imperial College of Science and
Technology,
University of London,
London, England.
- *R. A. Price,
Geological Survey of Canada,
601 Booth Street,
Ottawa, Ontario.
- *J. J. Prucha,
Department of Geology,
Syracuse University,
Syracuse, New York 13210,
U. S. A.
- R. J. Rector,
Department of Geology,
McMaster University,
Hamilton, Ontario.
- J. E. Reesor,
Geological Survey of Canada,
601 Booth Street,
Ottawa, Ontario.
- G. A. Reik,
Department of Geology,
University of Toronto,
Toronto, Ontario.
- E. W. Reinhardt,
Geological Survey of Canada,
601 Booth Street,
Ottawa, Ontario.
- Rao Divi,
Geology Department,
Ottawa University,
Ottawa, Ontario.
- P. Y. Robin,
Department of Geology,
University of Toronto,
Toronto, Ontario.

*H. E. Rondeel,
Geological Institute,
Nwe. Prinsengracht 130,
Amsterdam,
The Netherland.

B. Rurk,
Geology Department,
Ottawa University,
Ottawa, Ontario.

R. D. Russell,
Department of Geophysics,
University of British Columbia,
Vancouver, British Columbia.

*W. M. Schwerdtner,
Department of Geology,
University of Toronto,
Toronto 5, Ontario.

*D. T. Secor, Jr.,
Department of Geology,
University of South Carolina,
Columbia, South Carolina 29208,
U. S. A.

K. Sharma,
Department of Geology,
Queen's University,
Kingston, Ontario.

*P. S. Simony,
Department of Geology,
University of Calgary,
Calgary, Alberta.

*M. R. Stauffer,
Department of Geology,
University of Saskatchewan,
Saskatoon, Saskatchewan.

*D. W. Stearns,
Center for Tectonophysics,
College of Geosciences,
Texas A & M University,
College Station, Texas 77843,
U. S. A.

J. E. Stephenson,
Department of Geology,
University of Manitoba,
Winnipeg, Manitoba.

*G. R. Stevens, Chairman,
Department of Geology,
Acadia University,
Wolfville, Nova Scotia.

G. C. Taylor,
Institute of Sedimentary and
Petroleum Geology,
3303 - 33rd Street N. W.,
Calgary, Alberta.

*D. H. Underhill,
Department of Geology,
McMaster University,
Hamilton, Ontario.

C. S. Venkitasubramanian,
Department of Geology,
Queen's University,
Kingston, Ontario.

J. Wallach,
Department of Geology,
Queen's University,
Kingston, Ontario.

*L. E. Weiss,
Department of Geology and
Geophysics,
University of California,
Berkeley, California 94720,
U. S. A.

J. O. Wheeler,
Geological Survey of Canada,
Vancouver, British Columbia.

*D. U. Wise,
Department of Geology,
Franklin and Marshall College,
Lancaster, Pennsylvania 17604,
U. S. A.

D. S. Wood,
Department of Geology,
University of Illinois,
Urbana, Illinois 61801,
U. S. A.

*H. R. Wynne-Edwards,
Department of Geological Sciences,
Queen's University,
Kingston, Ontario.

H. V. Zwanzeg,
Department of Geology,
University of Manitoba,
Winnipeg, Manitoba.

APPENDIX III

Program of the conference

Location of all sessions: Seminar Room, Physics Building,
Science Campus, University of Ottawa.

Thursday, March 14, 1968.

Theme: Brittle Deformation

Morning session, Chairman J. J. Prucha, Syracuse University,
Syracuse, New York.

- 9:30 Introduction and welcome, Y. O. Fortier, Director,
Geological Survey of Canada
- 9:50 D. T. Secor
- 10:25 N. J. Price
- 11:00 coffee break
- 11:15 D. W. Stearns
- 11:50 E. Z. Lajtai
- 12:25 luncheon for speakers, University of Ottawa

Afternoon session, Chairman D. F. Coates, Mining Research Centre,
Ottawa, Ontario.

- 2:00 W. F. Brace
- 2:35 H. A. K. Charlesworth
- 3:10 coffee break
- 3:25 D. K. Norris and K. Barron
- 4:00 D. U. Wise
- 4:35 general discussion

Friday, March 15, 1968.

Theme: Kink Bands

Morning session, Chairman J. W. Handin, Center for Tectonophysics,
Texas A & M University,
College Station, Texas.

Friday, March 15, 1968. (cont'd)

9:15 T.B. Anderson

9:50 P.M. Clifford

10:25 W.R. Fyson

11:00 coffee break

11:15 F.A. Donath

11:50 L.E. Weiss

1:00 luncheon for speakers, University of Ottawa

Afternoon session, Chairman D.K. Norris, Geological Survey of Canada,
Calgary, Alberta.

General discussion

